THÈSE

présentée pour l'obtention du titre de

DOCTEUR DE L'ÉCOLE NATIONALE DES PONTS ET CHAUSSÉES

Spécialité : Mathématiques appliquées

par

Tony LELIEVRE

Sujet : *Modèles multi-échelles pour les fluides viscoélastiques.*

Soutenance le 21 juin 2004 devant le jury composé de :

Président :	Patrick LE TALLEC
Rapporteurs :	Arnaud DEBUSSCHE
	Benoît PERTHAME
Examinateurs :	Félix OTTO
	Jean-Michel VACHERAND
Direction de thèse :	Benjamin JOURDAIN
	Claude LE BRIS

À Marion,

À mes parents.

Remerciements

Je voudrais tout d'abord remercier Claude Le Bris et Benjamin Jourdain qui ont assuré la direction de ma thèse, avec beaucoup de disponibilité. La complémentarité de leurs compétences et de leur exigence ainsi que leurs qualités humaines m'ont beaucoup apporté. Je suis également redevable à Jean-Frédéric Gerbeau pour le temps qu'il m'a consacré à me faire part de son expérience en calcul scientifique.

Ce travail de thèse n'aurait pas pu aboutir sans les nombreuses discussions que j'ai pu avoir avec plusieurs chercheurs. Je tiens à remercier Roland Keunings qui a su nous introduire au sujet des fluides polymériques en posant les bonnes questions, Hans Christian Öttinger, Denis Talay, Mireille Bossy, Marco Picasso et Christoph Schwab pour des rencontres très enrichissantes. Merci également à Eric Cancès pour ses idées originales, son "sens physique" et sa disponibilité.

Je tiens à remercier Patrick Le Tallec d'avoir accepté de présider mon jury de thèse, Arnaud Debussche et Benoît Perthame d'avoir bien voulu rapporter sur ce travail, Félix Otto et Jean-Michel Vacherand d'avoir accepté de faire partie de mon jury.

J'aimerais remercier également l'entreprise Pechiney et plus particulièrement le Laboratoire de Recherche des Fabrications ainsi que le Centre de Recherche de Voreppe pour une collaboration très enrichissante. Merci à Claude Vanvoren de m'avoir accepté au sein de son équipe pendant un an, Jean-Marie Gaillard, Nicolas Ligonesche, Morgan Hervet et Thierry Tomasino pour son travail sur le code Mistral.

Je tiens à remercier les personnes qui m'ont encouragé à faire de la recherche ou permis de réaliser cette thèse : Henri Berestycki, Gilles Lebeau, François Laudenbach, Pierre Arnoux, Pierre-Emmanuel Chaput, Nicolas Bouleau et Alain Neveu.

Le CERMICS est un endroit exceptionnel pour mener à bien un travail de thèse, notamment par la compétence, la complémentarité et la disponibilité de tous ses chercheurs. Je remercie Bernard Lapeyre pour son accueil et ses conseils. Merci à Alexandre Ern pour nos discussions sur la méthode des éléments finis, et sur tellement d'autres sujets. Je tiens également à remercier Jean-François Delmas et ses "exos rigolos" et Jean-Philippe Chancelier pour son aide sur Scilab. L'enseignement à l'ENPC m'a été très profitable et je remercie Benjamin Jourdain et Alexandre Ern de m'avoir confié des cours. Merci enfin à tous les autres chercheurs pour des discussions enrichissantes : Michel de Lara et ses forêts, Gilbert Caplain et ses énigmes mathématiques, Régis Monneau. J'ai également beaucoup apprécié les échanges avec plusieurs chercheurs de passage au CERMICS : Robert Eymard, Jean-Luc Guer-

Titre : Modèles multi-échelles pour les fluides viscoélastiques.

Résumé : Ce travail porte principalement sur l'analyse mathématique de modèles multi-échelles pour la simulation de fluides polymériques. Ces modèles couplent, au niveau microscopique, une description moléculaire de l'évolution des chaînes de polymère (sous forme d'une équation différentielle stochastique) avec, au niveau macroscopique, les équations de conservation de la masse et de la quantité de mouvement pour le solvant (sous forme d'équations aux dérivées partielles). Le chapitre 1 introduit les modèles et donne les principaux résultats obtenus. Dans les chapitres 2, 4, 5 et 7 on montre en quel sens les équations sont bien posées pour divers modèles de polymère, en considérant soit des écoulements homogènes, soit des écoulements cisaillés plans. Dans les chapitres 2, 3, 6 et 7, on analyse et on prouve la convergence de méthodes numériques pour ces modèles. Enfin, le chapitre 8 concerne le comportement en temps long du système. Une deuxième partie de ce document est constituée de trois chapitres portant sur un travail en magnétohydrodynamique (MHD), en collaboration avec l'industrie. Le chapitre 9 est une introduction à la problématique ainsi qu'aux méthodes numériques utilisées. Le chapitre 10 décrit un nouveau cas-test en MHD. Enfin, le chapitre 11 donne une analyse de la stabilité du schéma numérique utilisé.

Mots clés : équations différentielles stochastiques, équations aux dérivées partielles, système couplé, méthode de Monte Carlo, techniques de réduction de variance, problème multi-échelles, fluide polymérique, magnétohydrodynamique.

Title : Multiscale models for viscoelastic fluids.

Abstract : The most important part of this work deals with the mathematical analysis of multiscale models of polymeric fluids. These models couple, at the microscopic level, a molecular description of the evolution of the polymer chains (in terms of stochastic differential equations) and, at the macroscopic level, the mass conservation and momentum equations for the solvent (which are partial differential equations). In Chapter 1, we introduce the models and give the main results obtained. In Chapters 2, 4, 5 and 7 we make precise the mathematical meaning and the well-posedness of the equations in either homogeneous flows or plane shear flows for some specific models of polymer chains. In Chapters 2, 3, 6 and 7, we analyse and prove convergence of some numerical schemes. Finally, in Chapter 8, we deal with the longtime behaviour of the coupled system. A second part of this document concerns a magnetohydrodynamic (MHD) problem coming from industry. In Chapter 9, we introduce the problem and the numerical methods used. We present a new test-case in MHD in Chapter 10. Finally, we give a stability analysis of the scheme in Chapter 11.

Key words : stochastic differential equations, partial differential equations, coupled system, Monte Carlo method, variance reduction techniques, multiscale problem, polymeric fluid, magnetohydrodynamic.

Mathematical Subject Classification (2000) : 35Q35, 60H35, 60K35, 65C05, 65C30, 65C35, 65M12, 76A10, 76M10, 76W05, 82C22, 82C31, 82C80, 82D60.

Sommaire

Introduction générale

Le travail de thèse a porté principalement sur l'étude mathématique de modèles micro-macro de fluides polymériques. Il s'agit d'étudier des systèmes couplant équations aux dérivées partielles (au niveau macroscopique) et équations différentielles stochastiques (au niveau microscopique). Ces systèmes ont été assez récemment introduits pour construire des lois de comportement à partir de modèles microscopiques décrivant l'évolution des microstructures (les molécules de polymères) dans le fluide.

Précisons les contributions originales de ce travail :
- Mathématiquement, on a pu démontrer que les modèles micro-macro de fluides polymériques les plus courants sont bien posés (les équations admettent une solution et une seule) (modèles des *dumbbells* hookéens et FENE pour le système couplé dans un écoulement cisaillé, ainsi que les équations différentielles stochastiques FENE et FENE-P dans le cas d'un écoulement homogène) ; on a également analysé le comportement en temps long du système.
- Numériquement, on a pu démontrer la convergence de méthodes numériques dans certains cas (modèles des *dumbbells* hookéens et FENE-P) et analyser la manière dont la dépendance en espace du mouvement brownien interagit avec les opérateurs différentiels pour influencer la variance des résultats.

La première partie de la thèse est donc consacrée à la présentation de ces travaux. Le premier chapitre est une introduction générale aux fluides viscoélastiques et précise les modèles utilisés ainsi que les résultats que nous avons obtenus, en essayant de les positionner parmi les analyses mathématiques développées depuis plus de trente ans sur les modèles macroscopiques, pour lesquels les lois de comportement sont données par des équations aux dérivées partielles ou des équations intégrales (et non pas *via* des équations différentielles stochastiques). Les chapitres suivants donnent les détails de chacun des résultats évoqués dans le chapitre 1. Les chapitres 2 et 3 sont essentiellement consacrés à l'étude de la convergence d'un algorithme classiquement utilisé pour discrétiser le système micro-macro, dans le cas du modèle des *dumbbells* hookéens. Dans le chapitre 4, on étudie le système couplé pour le modèle des *dumbbells* FENE tenant compte de l'extensibilité finie de la molécule, tandis que le chapitre 5 s'intéresse plus spécifiquement à l'équation différentielle stochastique régissant l'évolution du polymère pour ce modèle. Dans le chapitre 6, on s'intéresse à la variance des résultats, une fois le système discrétisé, en fonction des paramètres numériques. Le chapitre 7 est consacré à l'étude d'une

équation différentielle stochastique non-linéaire au sens de Mc Kean qui apparaît dans un modèle où intervient une approximation de fermeture. Le chapitre 8 donne des résultats partiels sur un travail en cours concernant les propriétés du système en temps long.

Une grande partie de ces trois années a également été consacrée à des sujets liés à des contrats industriels. On a inclu dans une deuxième partie de ce document les travaux effectués en partenariat avec la société Aluminium Pechiney.

Pour une introduction à la modélisation des cuves d'électrolyse d'aluminium, on renvoie à la thèse de Jean-Frédéric Gerbeau (cf. [52]), et aux deux premières sections du chapitre 9. Disons simplement et succinctement qu'il s'agit de résoudre un problème de magnéto-hydrodynamique (MHD) avec deux fluides séparés par une interface.

Suite aux travaux réalisés par Jean-Frédéric Gerbeau et Claude Le Bris dans les années 1995-2000, un code d'éléments finis développé en C++ permettait de simuler des écoulements MHD avec interface libre en utilisant une formulation Arbitrary Lagrangian Eulerian (ALE). Plusieurs questions restaient en suspens :
- Analyse numérique de la stabilité du schéma dans le cas de l'interface libre,
- Prise en compte de la tension de surface,
- Validation du code dans des configurations complexes.

Nous avons pu répondre à chacun de ces points et les chapitres suivants décrivent ces résultats. Plus précisément, le chapitre 9 est une introduction aux problèmes posés par la simulation des cuves d'électrolyse de l'aluminium et présente succinctement la stratégie numérique qui a été adoptée ainsi que les simulations numériques les plus représentatives. Le chapitre 10 décrit plus en détail un cas test pertinent du point de vue industriel qui permet de comparer notre approche numérique avec d'autres. Enfin, le chapitre 11 donne les détails de l'implémentation numérique, ainsi que de l'analyse de la stabilité du schéma.

La plupart des chapitres sont des reproductions d'articles parus ou acceptés pour publication (2, 3, 4, 6, 9, 11) ou soumis (7) ou bien encore d'actes de conférences (5, 10), et l'ensemble présente donc quelques redondances.

Liste des publications parues ou acceptées dans des revues à comité de lecture

[P1] B. Jourdain, T. Lelièvre, and C. Le Bris. Existence of solution for a micro-macro model of polymeric fluid : the FENE model. *Journal of Functional Analysis*, 209 :162–193, 2004.

[P2] B. Jourdain, C. Le Bris, and T. Lelièvre. On a variance reduction technique for micro-macro simulations of polymeric fluids. *J. Non-Newtonian Fluid Mech.*, 2003. To appear.

[P3] B. Jourdain, T. Lelièvre, and C. Le Bris. Numerical analysis of micro-macro simulations of polymeric fluid flows : a simple case. *Math. Models and Methods in Applied Sciences*, 12(9) :1205–1243, 2002.

[P4] T. Lelièvre. Optimal error estimate for the CONNFFESSIT approach in a simple case. *Computers and Fluids*, 33 :815–820, 2004.

[P5] J.-F. Gerbeau, C. Le Bris, and T. Lelièvre. Simulations of MHD flows with moving interfaces. *Journal of Computational Physics*, 184 :163–191, 2003.

[P6] J.-F. Gerbeau, C. Le Bris, and T. Lelièvre. Modelling and simulation of the industrial production of aluminium : the nonlinear approach. *Computers and Fluids*, 33 :801–814, 2004.

Liste des articles soumis et des actes de conférences

[PR1] B. Jourdain and T. Lelièvre. Mathematical analysis of a stochastic differential equation arising in the micro-macro modelling of polymeric fluids. In I.M. Davies, N. Jacob, A. Truman, O. Hassan, K. Morgan, and N.P. Weatherill, editors, *Probabilisitic Methods in Fluids Proceedings of the Swansea 2002 Workshop*, pages 205–223. World Scientific, 2003.

[PR2] J.-F. Gerbeau, T. Lelièvre, C. Le Bris, and N. Ligonesche. Metal pad roll instabilities. *Light Metal*, pages 483–487, 2002. proceeding of the 2002 TMS Annual Meeting and Exhibition.

[PR3] J.-F. Gerbeau, T. Lelièvre, and C. Le Bris. Numerical simulations of two-fluids MHD flows. In *Fundamental and Applied MHD. Proceedings of the Fifth international PAMIR Conference*, pages I.101–I.105, 2002.

[PR4] F. Dubois and T. Lelièvre. Efficient pricing of Asian options by the PDE approach, 2004. Rapport CERMICS 2004-259, submitted to Journal of Computational Finance.

[PR5] J.P. Croisille, A. Ern, T. Lelièvre, and J. Proft. Analysis and simulation of a coupled hyperbolic/parabolic model problem, 2004. Rapport CERMICS 2004-262, submitted to Journal of Numerical Mathematics.

[PR6] B. Jourdain and T. Lelièvre. Convergence of a stochastic particle approximation of the stress tensor for the FENE-P model, 2004. Rapport CERMICS 2004-263, submitted to Stochastic Processes and their Applications.

Première partie

Modèles micro-macro de fluides polymériques

Chapitre 1

Modélisation micro-macro des solutions de polymères : contexte et résultats mathématiques

Les modèles et les techniques micro-macro (ou multi-échelles) se sont beaucoup développés ces dernières années, aussi bien d'un point de vue numérique que mathématique. Le qualificatif micro-macro indique l'existence de deux échelles distinctes (en espace ou en temps) s'influençant l'une l'autre et sous-tend donc l'existence d'un couplage entre des équations à chacun des niveaux.

A l'origine de cette explosion, on trouve bien sûr l'évolution informatique et notamment la parallélisation, les méthodes micro-macro conduisant souvent à un grand nombre de petits problèmes indépendants pouvant être traités en parallèle. Par ailleurs, un certain nombre de méthodes mathématiques (la stabilisation, l'homogénéisation, la réduction de systèmes) peuvent s'interpréter comme des méthodes micro-macro, car elles reposent sur l'existence de deux échelles (en espace ou en temps).

Les techniques micro-macro ont notamment été introduites en rhéologie pour simuler les fluides polymériques. Pour prévoir et mieux comprendre le comportement d'un fluide complexe, on modélise la manière dont le champ de vitesse dans le fluide influence les microstructures, le couplage se faisant *via* le tenseur des contraintes qui dépend de la configuration des microstructures.

On se propose dans un premier temps de décrire précisément les modèles micro-macro de fluides polymériques, et plus précisément des solutions infiniment diluées de polymères, en montrant leurs liens avec les modèles macroscopiques plus traditionnels de fluides viscoélastiques. On indiquera ensuite les principaux résultats mathématiques et numériques obtenus ainsi que quelques perspectives. Par ailleurs, on détaille en annexe quelques caractéristiques communes des modèles et méthodes multi-échelles.

1.1 Modèles micro-macro pour les fluides polymériques

Nous nous proposons dans cette section d'introduire les modèles micro-macro de fluides polymériques, et particulièrement les modèles de solutions diluées de polymères. On s'appuie ici sur les ouvrages de référence [12, 13, 39, 120, 122], ainsi que sur les notes de cours [10, 11]. Les deux livres [6, 38] sont des introductions plus courtes et très accessibles à la rhéologie (la science qui étudie les déformations et l'écoulement de la matière) et en particulier à la rhéologie des fluides polymériques.

Dans la suite, on entendra par polymère une macromolécule (c'est-à-dire une molécule formée de plusieurs milliers d'atomes) constituée de la répétition d'une petite unité chimique appelée monomère. L'exemple typique est une chaîne de polyéthylène de formule $CH_3 - (CH_2)_n - CH_3$, avec n grand (plusieurs milliers). On peut penser à cette molécule comme à un spaghetti.

On appelle fluide tout matériau presque incompressible qui coule, c'est-à-dire qui prend la forme du récipient qui le contient, éventuellement en un temps long. Cette notion dépend bien sûr de l'échelle spatiale et de l'échelle de temps d'observation. En mécanique des fluides comme en mécanique des solides, on cherche à comprendre les relations entre les sollicitations (contrainte ou déformation appliquées au bord) et la réponse du matériau (contrainte ou déformation obtenues dans l'échantillon), soit dans un régime transitoire, soit dans un état stationnaire. Dans le cas de la mécanique des solides, on mesure en général la déformation en fonction de la contrainte (*solides élastiques*). Pour un fluide visqueux (*fluide newtonien*), c'est en fait le taux de déformation (autrement dit la vitesse de déformation) qui est proportionnel à la contrainte (cf. la formule (1.5) ci-dessous). Pour les fluides qui nous intéressent et que l'on appelle *fluides viscoélastiques*, le comportement est une combinaison de ces deux cas et leur modélisation reste un sujet difficile et d'actualité. Les fluides viscoélastiques font partie d'une classe plus importante de fluides appelés *fluides non-newtoniens* dont on ne sait pas décrire simplement le comportement. L'étude de ce comportement sous écoulement est important car ces fluides interviennent dans de nombreuses applications (industrie alimentaire, peinture, industrie plastique,...).

Les fluides non-newtoniens (c'est-à-dire tels que le taux de déformation n'est pas proportionnel à la contrainte) sont très courants dans la nature et dans l'industrie. Les boues, le sang sont des fluides non-newtoniens. De même, dans le domaine alimentaire, le blanc d'oeuf, la mayonnaise, le fromage ou le chocolat fondu. Dans l'industrie, on ajoute souvent des polymères à des fluides pour leur conférer certaines propriétés. De tels fluides où de longues molécules baignent dans un solvant sont appelés des fluides polymériques. C'est le cas des shampooings, des gels ou des détergents. On épaissit des peintures, des dentifrices, des soupes ou des sauces en ajoutant des polymères inélastiques. On trouve également des applications dans le domaine de l'automobile où on ajoute des polymères pour modifier le comportement des carburants sous des conditions particulières de température et de pression, ou encore dans le domaine de l'industrie pétrolière pour stabiliser l'interface eau /

pétrole afin d'extraire plus de pétrole. Enfin, signalons une dernière propriété très utile des fluides polymériques et encore mal comprise : en ajoutant très peu de polymères à un solvant (comme de l'eau), on réduit la chute de pression pour un écoulement dans un tuyau jusqu'à 50% (ce phénomène est appelé *drag reduction*). Ceci trouve des applications dans tout procédé nécessitant le transport d'un liquide (lance à incendie,...).

Les fluides polymériques constituent une part très importante de la recherche en rhéologie, de par leur intérêt industriel d'une part, et aussi parce qu'on peut jouer sur leurs propriétés de manière simple, par exemple en changeant la concentration ou les propriétés des polymères ajoutés au solvant. Parmi les fluides polymériques, on distingue les solutions diluées de polymères pour lesquelles on peut négliger les interactions entre les chaînes de polymères, des polymères fondus ou solutions concentrées pour lesquelles ces interactions jouent un rôle important. Dans la suite, nous allons nous concentrer sur l'étude mathématique des modèles pour les solutions diluées.

Nous nous proposons maintenant de montrer comment on peut décrire mathématiquement le comportement des fluides polymériques, en développant particulièrement les approches basées sur le couplage entre équations macroscopiques et modèles moléculaires, du type équations de Langevin.

1.1.1 Equations de la dynamique des fluides, rhéologie

On s'intéresse à des fluides incompressibles, ce qui se traduit par :

$$\text{div}\,(\boldsymbol{u}) = 0, \tag{1.1}$$

où $(\boldsymbol{u}(t,\boldsymbol{x}))$ désigne le champ de vitesse, $t \geq 0$ le temps, et $\boldsymbol{x}$ la variable d'espace. On suppose que $\boldsymbol{x} \in \mathcal{D}$ où $\mathcal{D}$ est un domaine borné de $\mathbb{R}^d$ ($d=2$ ou $d=3$).

L'équation de conservation de la quantité de mouvement (*momentum equation* en anglais) pour un fluide incompressible s'écrit :

$$\rho\,(\partial_t \boldsymbol{u} + \boldsymbol{u}.\nabla \boldsymbol{u}) = \text{div}\,(\boldsymbol{\sigma}) + \boldsymbol{f} \tag{1.2}$$

où ρ désigne la densité du fluide (constante par hypothèse d'incompressibilité), $(\boldsymbol{f}(t,\boldsymbol{x}))$ une force volumique extérieure et $(\boldsymbol{\sigma}(t,\boldsymbol{x}))$ le tenseur des contraintes. Ce tenseur est tel que $\boldsymbol{\sigma}(t,\boldsymbol{x}).\boldsymbol{n}(\boldsymbol{x})$ représente la force surfacique élémentaire qui s'exerce au temps t sur l'élément de surface situé au point $\boldsymbol{x}$ et de normale $\boldsymbol{n}(\boldsymbol{x})$. Par des raisonnements classiques, on montre que le tenseur $\boldsymbol{\sigma}$ doit être symétrique. L'expression de $\boldsymbol{\sigma}$ est la suivante :

$$\boldsymbol{\sigma} = -p\text{Id} + \boldsymbol{\tau}, \tag{1.3}$$

où $(p(t,\boldsymbol{x}))$ est le champ de pression dans le fluide, Id désigne la matrice identité de taille $d \times d$ et $(\boldsymbol{\tau}(t,\boldsymbol{x}))$ désigne le tenseur des extra-contraintes (*extra-stress tensor*). Pour fermer le système, il reste à préciser une relation entre $\boldsymbol{\tau}$ et $\boldsymbol{u}$, relation appelée loi de comportement.

Remarque 1 *Dans plusieurs livres de physique anglo-saxons (cf. par exemple [12, 13, 120]), la convention de signe pour le tenseur des contraintes $\boldsymbol{\sigma}$ est l'opposée de la convention choisie ici.*

1.1.1.1 Fluides newtoniens

Pour un fluide newtonien, on postule une relation linéaire entre $\boldsymbol{\tau}$ et le tenseur taux de déformation $\dot{\boldsymbol{\gamma}}$ défini par :

$$\dot{\boldsymbol{\gamma}} = \nabla \boldsymbol{u} + (\nabla \boldsymbol{u})^T. \tag{1.4}$$

Remarquer que par hypothèse d'incompressibilité, $\dot{\boldsymbol{\gamma}}$ est de trace nulle. La constante de proportionnalité entre $\boldsymbol{\tau}$ et $\dot{\boldsymbol{\gamma}}$ s'appelle la viscosité (dynamique) et est notée η. On obtient alors l'expression suivante pour $\boldsymbol{\sigma}$:

$$\boldsymbol{\sigma} = -p\mathrm{Id} + \eta \left(\nabla \boldsymbol{u} + (\nabla \boldsymbol{u})^T \right), \tag{1.5}$$

et en injectant cette relation dans (1.2) et en utilisant la relation d'incompressibilité (1.1), on obtient les équations de Navier-Stokes :

$$\begin{cases} \rho \left(\partial_t \boldsymbol{u} + \boldsymbol{u}.\nabla \boldsymbol{u} \right) - \eta \Delta \boldsymbol{u} + \nabla p = \boldsymbol{f}, \\ \mathrm{div}\left(\boldsymbol{u} \right) = 0. \end{cases} \tag{1.6}$$

Il est important de noter qu'en dépit de la simplicité de la relation de comportement postulée, ces équations permettent de simuler un grand nombre de fluides (l'eau, le miel,...) et fournissent des résultats qui se comparent très bien à l'expérience, même dans des conditions extrêmes (nombre de Reynolds élevé, géométrie complexe).

1.1.1.2 Fluides viscoélastiques et écoulements simples

Les fluides viscoélastiques sont caractérisés par le fait que la réponse à une déformation présente à la fois un caractère visqueux (contrainte proportionnelle au taux de déformation) et un caractère élastique (contrainte proportionnelle à la déformation). Les fluides polymériques sont des fluides viscoélastiques.

Pour explorer le comportement des fluides viscoélastiques et plus généralement des fluides non-newtoniens, et pour comparer les modèles et les expériences, on étudie la réponse de ces fluides dans des écoulements dit simples pour lesquels le champ de vitesse est connu explicitement et pour lesquels il est facile de calculer les contraintes prédites par les modèles. Le fait que le champ de vitesse puisse être donné *a priori* provient du fait que ces écoulements sont homogènes (cf. section 1.1.3.3 pour une définition et une explication de ce fait). Citons deux exemples particulièrement importants : l'écoulement cisaillé simple et les écoulements élongationnels (cf. notamment le chapitre 3 de [12]).

Un écoulement cisaillé simple est un écoulement pour lequel la vitesse $\boldsymbol{u}$ est donnée par

$$\boldsymbol{u}(t, \boldsymbol{x}) = (\dot{\gamma}(t)y, 0, 0),$$
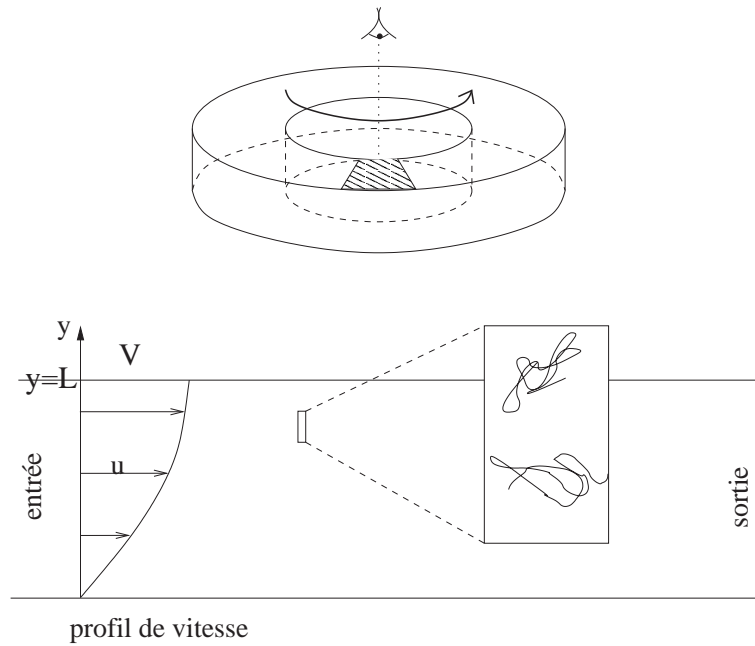
FIG. 1.1 – Représentation schématique d'un rhéomètre (ou viscosimètre) cylindrique. Sur une portion infinitésimale, on réalise un écoulement cisaillé, appelé écoulement de Couette, caractérisé par le profil de vitesse $(u(t,y), 0, 0)$. La vitesse en $y = L$ est $(V, 0, 0)$. On a également représenté quelques chaînes de polymère à l'échelle microscopique qui sont déformées par l'écoulement. Dans le cas où $u(t,y) = \dot{\gamma}(t)y$ on parle d'écoulement cisaillé simple.

où $\boldsymbol{x} = (x, y, z)$ et où $\dot{\gamma}$ est un scalaire appelé taux de cisaillement. Dans de tels écoulements, on est notamment intéressé par la viscosité de cisaillement η (*shear viscosity*) définie par :

$$\eta(t) = \frac{\boldsymbol{\sigma}_{x,y}(t)}{\dot{\boldsymbol{\gamma}}_{x,y}(t)} = \frac{\boldsymbol{\tau}_{x,y}(t)}{\dot{\gamma}(t)}, \tag{1.7}$$

et par les première et seconde différences des contraintes normales (i.e. des composantes diagonales du tenseur des contraintes) :

$$N_1(t) = \boldsymbol{\sigma}_{x,x}(t) - \boldsymbol{\sigma}_{y,y}(t), \tag{1.8}$$

$$N_2(t) = \boldsymbol{\sigma}_{y,y}(t) - \boldsymbol{\sigma}_{z,z}(t). \tag{1.9}$$

Ces quantités sont intéressantes car mesurables en pratique. Pour des fluides newtoniens, la viscosité de cisaillement est constante (égale à la viscosité dynamique η) et les différences des contraintes normales sont nulles, d'après la relation (1.5), puisque les termes diagonaux de $\nabla \boldsymbol{u}$ sont nuls. Une des caractéristiques des fluides non-newtoniens est que η n'est pas constant. En pratique, on étudie ce type d'écoulement dans des rhéomètres où le fluide est placé entre deux cylindres, l'un fixe et l'autre étant en rotation (cf. figure 1.1). Il s'agit en fait dans ce cas d'un écoulement qui est localement un écoulement cisaillé : on parle d'écoulement viscométrique (cf. [11] section 2.2, ou [133] section 3.2).

En effectuant des mesures sur des écoulements stationnaires, on peut construire pour un fluide donné les fonctions $\eta(\dot{\gamma})$, $N_1(\dot{\gamma})$ et $N_2(\dot{\gamma})$ où $\dot{\gamma} = \frac{V}{L}$ est le taux de cisaillement à l'état stationnaire (cf. figure 1.1). Pour la plupart des fluides non-newtoniens, on observe que η est une fonction décroissante de $\dot{\gamma}$ (on parle de *shear-thinning viscosity* et de fluide rhéofluidifiant) qui tend vers une constante η_∞ quand $\dot{\gamma}$ tend vers l'infini, et vers une valeur η_0 appelée *zero-shear rate viscosity* quand $\dot{\gamma}$ tend vers zéro. Par ailleurs, les expériences suggèrent que des valeurs non nulles pour $N_1(\dot{\gamma})$ et $N_2(\dot{\gamma})$ caractérisent des fluides viscoélastiques. Le fait qu'un cisaillement introduise des différences dans les contraintes normales est lié au fait que l'écoulement de cisaillement introduit des anisotropies dans la microstructure du fluide.

L'écoulement cisaillé simple est également utilisé pour étudier des comportements dynamiques. On peut par exemple étudier la réponse à une sollicitation périodique sinusoïdale de faible amplitude : $\dot{\gamma}(t) = \gamma_0 \cos(\omega t)$. Cette expérience permet notamment de distinguer la réponse élastique du fluide, qui correspond à une contrainte en phase avec la déformation, de la réponse visqueuse, qui correspond à une contrainte en quadrature de phase avec la déformation (cf. le modèle de Maxwell unidimensionnel et l'analogie avec un circuit électrique RC, figure 1.6).

Les écoulements élongationnels (appelés aussi *shear-free flows*) interviennent souvent dans les procédés industriels (filage, soufflage ou étirage de film, cf. [6] section 5). A l'état stationnaire, un écoulement élongationnel est caractérisé par le fait que le champ de vitesse s'écrit :

$$\boldsymbol{u}(\boldsymbol{x}) = (\dot{\epsilon}x, m\dot{\epsilon}y, -(1+m)\dot{\epsilon}z)$$
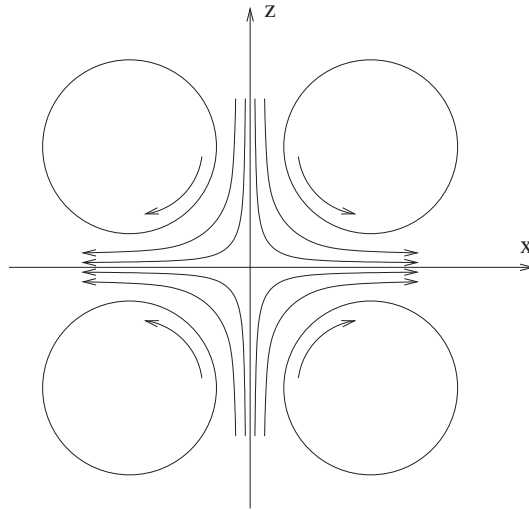
FIG. 1.2 – Représentation schématique d'un appareil à quatre rouleaux pour produire un écoulement élongationnel plan.

où $\dot{\epsilon}$ est appelé taux élongationnel et $m \in \{-0.5, 0, 1\}$ pour les écoulements élongationnels classiquement étudiés (cf. figure 1.2 pour le cas $m = 0$ correspondant à un écoulement élongationnel plan). Là encore, on définit des quantités, fonctions du taux de déformation $\dot{\epsilon}$, que l'on peut estimer dans des expériences. Ce sont les viscosités élongationnelles μ_1 et μ_2 définies par :

$$\mu_1(\dot{\epsilon}) = \frac{\boldsymbol{\sigma}_{x,x} - \boldsymbol{\sigma}_{z,z}}{2(2+m)\dot{\epsilon}}, \tag{1.10}$$

$$\mu_2(\dot{\epsilon}) = \frac{\boldsymbol{\sigma}_{y,y} - \boldsymbol{\sigma}_{z,z}}{2(1+2m)\dot{\epsilon}}. \tag{1.11}$$

Pour un fluide newtonien, on vérifie que $\mu_1 = \mu_2 = \eta$, où η est la viscosité dynamique définie dans (1.5). Pour des fluides non-newtoniens, ces coefficients dépendent généralement de $\dot{\epsilon}$.

1.1.1.3 Quelques expériences de rhéologie

Les fluides non-newtoniens ont des comportements qui permettent de les différencier nettement des fluides newtoniens. Nous décrivons ici plusieurs comportements typiquement non-newtoniens des fluides visco-élastiques, en essayant de les éclairer à partir des propriétés exhibées dans les écoulements simples décrits dans la section précédente.

Une première expérience surprenante est le *rod-climbing effect* (cf. figure 1.3 ou figure 1.9 p. 13 dans [122]) : on plonge une barre dans un fluide et on la fait tourner. Pour un fluide newtonien, la surface libre à tendance à se creuser autour de la barre. Pour certains fluides viscoélastiques, on observe que le fluide grimpe le long de la

FIG. 1.3 – Représentation schématique de deux comportements surprenants des fluides polymériques : le *rod-climbing effect* (à gauche) et le *open syphon effect* (à droite).

barre (on parle de l'effet Weissenberg). On peut montrer par des raisonnements simples que ce phénomène est lié au fait que les différences des contraintes normales (cf. (1.8)) ne sont pas nulles dans un écoulement cisaillé (cf. [11] p. 49-51 qui cite A.S. Lodge [107]).

Une seconde expérience est le *open syphon effect* (cf. figure 1.3 ou figure 1.11 p. 16 dans [122]). On observe que pour certains fluides visco-élastiques, on peut vider complètement un récipient simplement en amorçant l'écoulement en dehors du récipient (et sans tuyau !). Ce phénomène est relié à l'existence de viscosité élongationnelle importante.

Une troisième expérience, plus simple, consiste à considérer l'évolution en temps d'un fluide initialement au repos, puis cisaillé (*start-up of shear flow*) (cf. les figures 1.1 et 1.4). Pour un fluide newtonien, on observe un profil de vitesse qui atteint progressivement et de manière monotone en temps l'état stationnaire. Pour des fluides polymériques, on observe un comportement différent (cf. [97]) : la vitesse, avant d'atteindre son état stationnaire, passe localement au-delà de sa valeur à l'état stationnaire (phénomène d'*overshoot* sur la vitesse).

Signalons enfin deux cas tests sur des écoulements complexes qui sont utilisés dans la littérature : calculer l'écoulement autour d'un cylindre, et l'écoulement dans une contraction 4 :1 (cf. figure 1.5). On dispose pour ces écoulements de mesures et ils constituent donc des bons cas tests pour valider des modèles de loi de comportement.

1.1.1.4   Loi de comportement

On s'intéresse dans la suite à décrire mathématiquement le comportement des fluides polymériques. Pour cela, on décompose le tenseur $\boldsymbol{\tau}$ des extra-contraintes défini par (1.3) en une contribution newtonienne du solvant et une contribution due aux polymères :

$$\boldsymbol{\tau} = \eta_s \dot{\boldsymbol{\gamma}} + \boldsymbol{\tau}_p, \tag{1.12}$$

où η_s désigne la viscosité du solvant et $\dot{\boldsymbol{\gamma}}$ est défini par (1.4). Le tenseur $\boldsymbol{\tau}_p$ est la partie du tenseur des extra-contraintes dues aux polymères. L'objectif des modèles
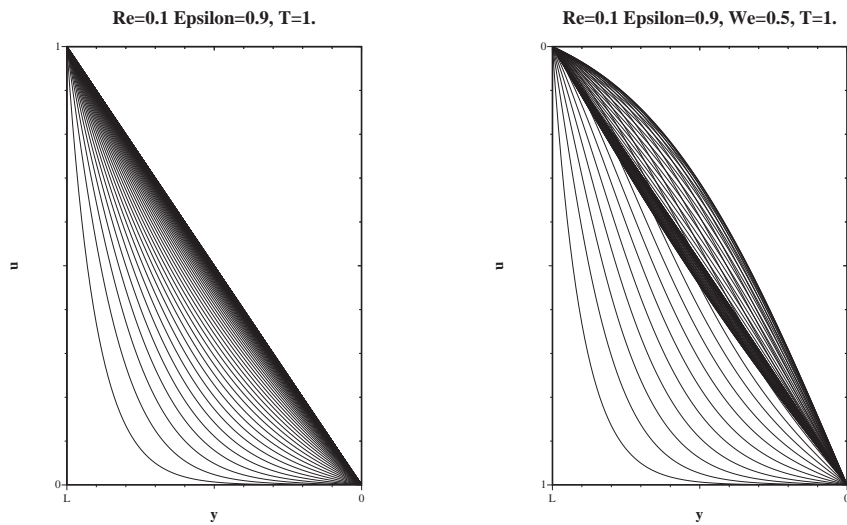
Fig. 1.4 – Représentation du profil de vitesse au cours du temps dans l'expérience du *start-up of shear flow.* On représente le profil de vitesse (u fonction de la position y, cf. figure 1.1) à différents instants de l'intervalle $[0, 1]$: à gauche pour un fluide newtonien, et à droite, pour ce même fluide auquel on a ajouté des polymères (modèle des *dumbbells* hookéens). On observe un phénomène d'*overshoot* sur la vitesse. Pour la définition des paramètres adimensionnels Re , ϵ, We , cf. (1.49).
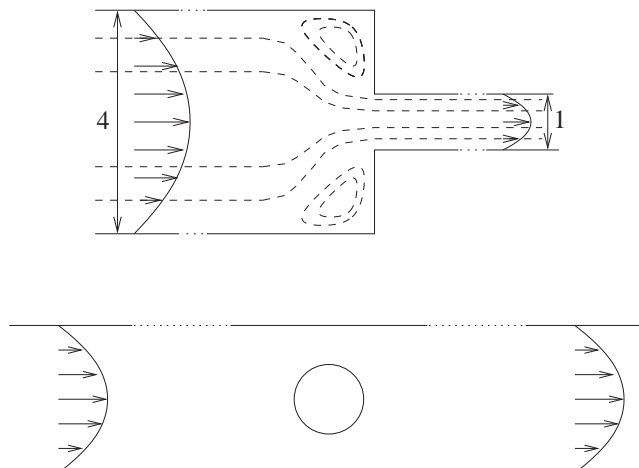
FIG. 1.5 – Représentation schématique de deux cas tests types : la contraction 4 :1 (en haut) et l'écoulement autour d'un cylindre (en bas). On calcule pour ces cas tests les solutions stationnaires. On a indiqué les profils de vitesse en entrée et en sortie ainsi que les lignes de courant, en pointillé pour la contraction 4 :1. Sur la contraction 4 :1, la taille et la forme de la zone de recirculation à l'entrée de la contraction dépend typiquement du fluide polymérique considéré (cf. figure 1.6 dans [133]).

mathématiques est de trouver une formule donnant le tenseur $\boldsymbol{\tau}_p$ en fonction de l'histoire de la déformation du fluide. Cette relation s'appelle une loi de comportement, et peut prendre des formes très différentes, parfois équivalentes : différentielle ou intégrale (cf. section 1.1.2) ou moyenne d'une fonctionnelle décrivant les microstructures du fluide (cf. section 1.1.3).

La simulation d'un écoulement complet nécessite donc la résolution du système constitué des équations aux dérivées partielles (1.1)–(1.2) (avec $\boldsymbol{\sigma}$ et $\boldsymbol{\tau}$ respectivement définis par (1.3) et (1.12)) et d'une formule donnant $\boldsymbol{\tau}_p$ du type (1.16), (1.26) ou encore (1.41)–(1.43) (cf. ci-dessous). C'est un problème posé sur trois inconnues (on parle de problème à trois champs) : la vitesse $\boldsymbol{u}(t, \boldsymbol{x})$, la pression $p(t, \boldsymbol{x})$ et le tenseur des contraintes dues aux polymères $\boldsymbol{\tau}_p(t, \boldsymbol{x})$. Quand l'équation sur $\boldsymbol{\tau}_p$ est une équation différentielle ou intégrale, on parle de modèles macroscopiques (ou modèles macro-macro). Quand l'expression de $\boldsymbol{\tau}_p$ implique des variables microscopiques dont on modélise l'évolution dans le fluide, on parle de modèles micro-macro.

1.1.2 Modèles macroscopiques pour les fluides polymériques

Historiquement, les premiers modèles qui ont été bâtis pour construire des lois de comportement pour les fluides viscoélastiques étaient des modèles macroscopiques, dans le sens où ces modèles cherchaient à donner directement une relation entre le tenseur $\boldsymbol{\tau}_p$ et le tenseur du taux de déformation $\dot{\boldsymbol{\gamma}}$ (ou d'autres tenseurs construits à
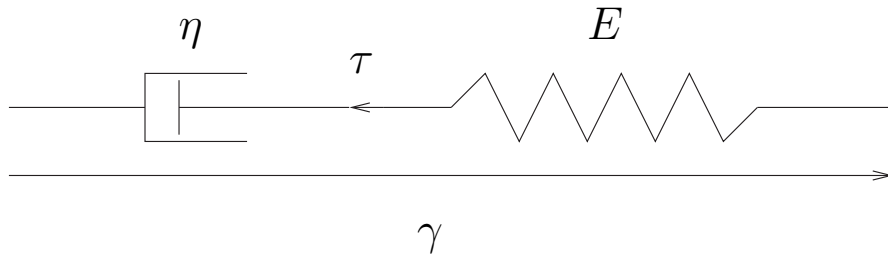
FIG. 1.6 – Schéma unidimensionnel du modèle de Maxwell. L'analogie avec un circuit électrique est évidente, la déformation γ jouant le rôle d'une tension, la contrainte τ jouant le rôle de l'intensité, et η et E se comparant respectivement à la capacité d'un condensateur et à la conductivité d'une résistance.

partir de l'histoire de la déformation, cf. section 1.1.2.2), sans introduire de variables supplémentaires microscopiques. Ces lois macroscopiques peuvent s'écrire soit sous la forme d'une équation différentielle (qui devient en fait une équation aux dérivées partielles une fois introduite l'advection), soit sous la forme d'une intégrale (qui s'écrit le long des lignes de courant une fois considérée l'advection). Dans tous les cas, ces équations traduisent le fait que $\boldsymbol{\tau}_p$ dépend de l'histoire de la déformation.

1.1.2.1 Modèles différentiels

Le modèle de base pour les fluides viscoélastiques est le modèle de Maxwell. Il consiste à combiner un modèle d'élasticité linéaire, et un modèle de viscosité linéaire. Pour le modèle d'élasticité linéaire, on postule que la contrainte est proportionnelle à la déformation (loi de Hooke), le coefficient de proportionalité étant le module d'Young E : on associe naturellement à ce modèle un ressort hookéen. Pour les fluides newtoniens, on postule que la contrainte est proportionnelle à la vitesse de déformation, le coefficient de proportionalité étant la viscosité η : on associe à ce modèle un piston. En mettant en série un ressort hookéen et un piston, on obtient le principe unidimensionnel du modèle de Maxwell (cf. figure 1.6). Dans le cas unidimensionnel, si on note τ la contrainte et $\dot{\gamma}$ la vitesse de déformation, on obtient l'équation différentielle ordinaire suivante :

$$\dot{\gamma} = \frac{1}{E}\frac{d\tau}{dt} + \frac{\tau}{\eta}. \tag{1.13}$$

On peut réécrire cette équation sous la forme

$$\lambda\frac{d\tau}{dt} + \tau = \eta\dot{\gamma}, \tag{1.14}$$

où $\lambda = \dfrac{\eta}{E}$ est un temps de relaxation du système.

Pour passer au modèle de Maxwell tensoriel, il faut remplacer la dérivée temporelle dans (1.14) par une dérivée convective sur un tenseur. Par des arguments

d'invariance par changement de référentiel (on parle aussi de dérivées objectives), on montre qu'un modèle possible est le suivant :

$$\lambda \left(\partial_t \boldsymbol{\tau}_p + \boldsymbol{u}.\nabla \boldsymbol{\tau}_p - \nabla \boldsymbol{u} \boldsymbol{\tau}_p - \boldsymbol{\tau}_p (\nabla \boldsymbol{u})^T \right) + \boldsymbol{\tau}_p = \eta_p \dot{\boldsymbol{\gamma}}, \qquad (1.15)$$

où λ est un temps de relaxation, et η_p une viscosité due aux polymères. On rappelle que le tenseur des extra-contraintes $\boldsymbol{\tau}$ est ensuite donné par (1.12). Dans le cas où $\eta_s = 0$, on parle du modèle *Upper Convected Maxwell* (UCM). Dans le cas où $\eta_s \neq 0$, on parle du modèle Oldroyd-B (ou modèle de Jeffreys).

Remarque 2 *Dans (1.15) ainsi que dans tout ce qui suit, on choisit comme convention $(\nabla \boldsymbol{u})_{i,j} = \dfrac{\partial u_i}{\partial x_j}$. Cette notation est consistante avec le fait que la différentielle de $\boldsymbol{u}$ en un point $\boldsymbol{x}$ appliquée à un vecteur (colonne) $\boldsymbol{h}$ s'exprime comme le produit matrice vecteur $\nabla \boldsymbol{u}(x) \, \boldsymbol{h}$. Noter que dans beaucoup de livres de physique anglo-saxons (cf. par exemple [12, 13, 120, 122]), la convention est $(\nabla \boldsymbol{u})_{i,j} = \dfrac{\partial u_j}{\partial x_i}$, ce qui entraîne des modifications des positions des transposées dans les équations.*

Remarque 3 *La dérivée convective apparaissant dans (1.15) (cf. le terme entre parenthèses) s'appelle la upper-convected derivative ou dérivée sur-convectée. Il existe d'autres dérivées convectives pour les tenseurs qui satisfont l'invariance par changement de référentiel (notamment la lower-convected derivative ou dérivée sous-convectée et la dérivée corotationnelle, appelée aussi dérivée de Jaumann et qui est la moyenne des deux dérivées sur et sous-convectées). Nous emploierons dans la suite exclusivement la dérivée sur-convectée, car c'est celle qui apparaît naturellement quand on relie les modèles cinétiques (modèles que nous allons considérer par la suite) aux modèles macroscopiques (cf. section 1.1.4.1). C'est d'ailleurs ce type de dérivée convective qui est utilisé dans la plupart des modèles macroscopiques (cf. par exemple ci-dessous les modèles de Phan-Thien Tanner, de Giesekus ou FENE-P). Pour une discussion de la pertinence physique du choix de la dérivée convective, on renvoie également au chapitre 3 de [11].*

Le modèle Oldroyd-B présente plusieurs défauts. En effet, avec ce modèle, on observe que (cf. section 1.1.1.2) :
- dans les écoulements cisaillés simples stationnaires, la viscosité de cisaillement η ne dépend pas du cisaillement $\dot{\gamma}$ (pas de *shear-thinning effect*),
- dans les écoulements cisaillés simples stationnaires, la seconde différence de contraintes normales N_2 est nulle,
- et surtout, dans les écoulements élongationnels stationnaires, les viscosités élongationnelles μ_1 et μ_2 explosent pour un taux élongationnel $\dot{\epsilon}$ fini.

Toutes ces prédictions sont en contradiction avec les résultats d'expériences menées sur la plupart des fluides polymériques. Notons que ces résultats sont très simplement obtenus en injectant dans (1.15) l'expression de la vitesse $\boldsymbol{u}(t, \boldsymbol{x}) = (\dot{\gamma} y, 0, 0)$ pour l'écoulement cisaillé simple, ou $\boldsymbol{u}(t, \boldsymbol{x}) = (\dot{\epsilon} x, -\dot{\epsilon} y/2, -\dot{\epsilon} z/2)$ pour l'écoulement

élongationnel (cf. [122] p. 38-39 ou [13] p. 73-74). Dans ces deux cas, le tenseur $\boldsymbol{\tau}_p$ ne dépend pas de l'espace et est donc à divergence nulle, ce qui implique que l'équation sur $\boldsymbol{\tau}_p$ est découplée de l'équation (1.2) sur $\boldsymbol{u}$ (cf. le paragraphe sur les écoulements homogènes dans la section 1.1.3.3, page 34).

Des modèles macroscopiques permettant d'obtenir des résultats qualitativement plus en accord avec les expériences ont alors été développés. De manière générale, ces modèles s'écrivent :

$$\lambda \left(\partial_t \boldsymbol{\tau}_p + \boldsymbol{u}.\nabla \boldsymbol{\tau}_p - \nabla \boldsymbol{u} \boldsymbol{\tau}_p - \boldsymbol{\tau}_p (\nabla \boldsymbol{u})^T \right) + \boldsymbol{T}(\boldsymbol{\tau}_p, \dot{\boldsymbol{\gamma}}) = \eta_p \dot{\boldsymbol{\gamma}}, \qquad (1.16)$$

où $\boldsymbol{T}(\boldsymbol{\tau}_p, \dot{\boldsymbol{\gamma}})$ dépend typiquement de manière non-linéaire de $\boldsymbol{\tau}_p$. Citons simplement trois modèles parmi les plus utilisés.

Le modèle de Giesekus (cf. [64]) introduit un terme quadratique :

$$\lambda \left(\partial_t \boldsymbol{\tau}_p + \boldsymbol{u}.\nabla \boldsymbol{\tau}_p - \nabla \boldsymbol{u} \boldsymbol{\tau}_p - \boldsymbol{\tau}_p (\nabla \boldsymbol{u})^T \right) + \boldsymbol{\tau}_p + \alpha \frac{\lambda}{\eta_p} \boldsymbol{\tau}_p \boldsymbol{\tau}_p = \eta_p \dot{\boldsymbol{\gamma}}. \qquad (1.17)$$

où α est une constante.

Le modèle de Phan-Thien Tanner (PTT) est dérivé d'un modèle sur réseau (cf. [124]) et s'écrit :

$$\lambda \left(\partial_t \boldsymbol{\tau}_p + \boldsymbol{u}.\nabla \boldsymbol{\tau}_p - \nabla \boldsymbol{u} \boldsymbol{\tau}_p - \boldsymbol{\tau}_p (\nabla \boldsymbol{u})^T \right) + Z(\text{tr}(\boldsymbol{\tau}_p))\boldsymbol{\tau}_p + \frac{\xi}{2} \lambda \left(\dot{\boldsymbol{\gamma}} \boldsymbol{\tau}_p + \boldsymbol{\tau}_p \dot{\boldsymbol{\gamma}} \right) = \eta_p \dot{\boldsymbol{\gamma}},$$
$$(1.18)$$

avec deux choix possibles pour la fonction Z :

$$Z(\text{tr}(\boldsymbol{\tau}_p)) = \left| \begin{array}{l} 1 + \epsilon\lambda \dfrac{\text{tr}(\boldsymbol{\tau}_p)}{\eta_p} \\[2mm] \exp\left(\epsilon\lambda \dfrac{\text{tr}(\boldsymbol{\tau}_p)}{\eta_p} \right) \end{array} \right. , \qquad (1.19)$$

où ξ et ϵ sont des constantes.

Citons enfin le modèle FENE-P, que l'on retrouvera par la suite car il peut être dérivé à partir d'un modèle cinétique. Suivant les idées de Peterlin (cf. [123]), Bird et al. (cf. [14]) on introduit le modèle suivant :

$$\lambda \left(\partial_t \boldsymbol{\tau}_p + \boldsymbol{u}.\nabla \boldsymbol{\tau}_p - \nabla \boldsymbol{u} \boldsymbol{\tau}_p - \boldsymbol{\tau}_p (\nabla \boldsymbol{u})^T \right) + Z(\text{tr}(\boldsymbol{\tau}_p))\boldsymbol{\tau}_p$$
$$- \lambda \left(\boldsymbol{\tau}_p + \frac{\eta_p}{\lambda} \text{Id} \right) \left((\partial_t + \boldsymbol{u}.\nabla) \ln \left(Z(\text{tr}(\boldsymbol{\tau}_p)) \right) \right) = \eta_p \dot{\boldsymbol{\gamma}}, \qquad (1.20)$$

avec

$$Z(\text{tr}(\boldsymbol{\tau}_p)) = 1 + \frac{d}{b} \left(1 + \lambda \frac{\text{tr}(\boldsymbol{\tau}_p)}{d \, \eta_p} \right), \qquad (1.21)$$

où d est la dimension de l'espace et b est une constante que l'on interprétera dans la suite comme étant proportionnelle au carré de l'extensibilité maximale des polymères.

Chacun de ces modèles non-linéaires donnent lieu à des comportements qualitativement corrects dans les écoulements simples décrits dans la section 1.1.1.2. On retiendra que les modèles macroscopiques sont dérivés de telle sorte qu'ils vérifient des principes d'invariance par changement de référentiel et que leur comportement qualitatif dans des écoulements simples soit bon. De plus beaucoup de modèles macroscopiques différentiels ont en fait été dérivés à partir de considérations microscopiques (cf. section 1.1.3).

On peut généraliser ces modèles en considérant plusieurs temps de relaxation λ_i et plusieurs viscosités $\eta_{p,i}$ et en posant $\boldsymbol{\tau}_p = \sum_{i=1}^{i_{max}} \boldsymbol{\tau}_{p,i}$ où $\boldsymbol{\tau}_{p,i}$ vérifie par exemple (1.15) ou (1.18)–(1.19) avec $\lambda = \lambda_i$ et $\eta_p = \eta_{p,i}$.

1.1.2.2   Modèles intégraux

Considérons à nouveau le modèle de Maxwell unidimensionnel (1.14). La solution peut s'écrire sous forme intégrale :

$$\tau(t) = \tau(t_0) \exp\left(-\frac{t-t_0}{\lambda}\right) + \int_{t_0}^{t} \frac{\eta}{\lambda} \exp\left(-\frac{t-s}{\lambda}\right) \dot{\gamma}(s)\,ds. \qquad (1.22)$$

En faisant tendre t_0 vers $-\infty$ et en supposant que τ reste borné si $\dot{\gamma}$ l'est, on obtient la forme suivante :

$$\tau(t) = \int_{-\infty}^{t} \frac{\eta}{\lambda} \exp\left(-\frac{t-s}{\lambda}\right) \dot{\gamma}(s)\,ds. \qquad (1.23)$$

En introduisant $\gamma(t_0, t)$ défini par :

$$\begin{cases} \frac{d}{dt}\gamma(t_0, t) = \dot{\gamma}(t) \\ \gamma(t_0, t_0) = 0 \end{cases}, \qquad (1.24)$$

on obtient par intégration par partie une relation équivalente à (1.23) :

$$\tau(t) = \int_{-\infty}^{t} \frac{\eta}{\lambda^2} \exp\left(-\frac{t-s}{\lambda}\right) \gamma(t, s)\,ds. \qquad (1.25)$$

Sous cette forme, on voit que la contrainte à l'instant t dépend de l'histoire de la déformation. La fonction $\frac{\eta}{\lambda^2} \exp\left(-\frac{t-s}{\lambda}\right)$ est appelée fonction mémoire.

Ce calcul unidimensionnel et homogène en espace se généralise en la formule suivante :

$$\boldsymbol{\tau}_p(t, \boldsymbol{x}) = -\int_{-\infty}^{t} M(t-s) f\left(\boldsymbol{C}_t^{-1}(s, \boldsymbol{x})\right) (\mathrm{Id} - \boldsymbol{C}_t^{-1}(s, \boldsymbol{x}))\,ds. \qquad (1.26)$$

où M est une fonction mémoire, f une fonction à valeur réelle, et $\boldsymbol{C}_t^{-1}(s, \boldsymbol{x})$ désigne le tenseur des déformations de Finger (relatif à la configuration au temps t). Le tenseur de Finger $\boldsymbol{C}_t^{-1}(s, \boldsymbol{x})$ est l'inverse (matriciel) du tenseur des déformations de Cauchy (relatif à la configuration au temps t) $\boldsymbol{C}_t(s, \boldsymbol{x})$ qui est défini par :

$$\boldsymbol{C}_t(s, \boldsymbol{x}) = \boldsymbol{F}_t(s, \boldsymbol{x})^T\,\boldsymbol{F}_t(s, \boldsymbol{x}) \qquad (1.27)$$

où $\boldsymbol{F}_t(s, \boldsymbol{x})$ est le gradient de déformation (relatif à la configuration au temps t) :

$$\boldsymbol{F}_t(s, \boldsymbol{x}) = \nabla(\boldsymbol{\chi}_t(s))(\boldsymbol{x}) \tag{1.28}$$

où $\boldsymbol{\chi}_t(s)$ désigne l'application qui envoie les particules de leur position à l'instant t à leur position à l'instant s. Noter qu'il est naturel de faire apparaître le tenseur $\boldsymbol{C}_t^{-1}$ pour définir une contrainte, car c'est celui qui caractérise la déformation des surfaces (cf. [10] p. 32), et qu'il est logique de penser que les contraintes surfaciques dépendent de la déformation passée des éléments de surface sur lesquels elles agissent (cf. [11] p. 84).

On peut vérifier que la dérivée sur-convectée (par rapport à t) du tenseur de Finger $\boldsymbol{C}_t^{-1}$ est nulle. Dans le cas $M(t-s) = \dfrac{\eta_p}{\lambda^2} \exp\left(-\dfrac{t-s}{\lambda}\right)$ et $f = 1$, on vérifie ainsi par simple dérivation de la formule (1.26) que le tenseur $\boldsymbol{\tau}_p$ défini par (1.26) vérifie l'équation différentielle dérivée du modèle de Maxwell (1.15). Le paramètre λ s'interprète donc facilement sous cette forme comme le temps caractéristique qu'il faut au système pour oublier l'histoire de la déformation. De même que dans le cas des modèles différentiels, on peut généraliser ce modèle en considérant plusieurs temps de relaxation λ_i et plusieurs viscosités $\eta_{p,i}$ et en posant $M(t-s) = \displaystyle\sum_{i=1}^{i_{max}} \dfrac{\eta_{p,i}}{\lambda_i^2} \exp\left(-\dfrac{t-s}{\lambda_i}\right)$. On retrouve dans ce cas le modèle de Maxwell généralisé évoqué à la fin de la section précédente.

Noter qu'il existe des modèles intégraux qui n'ont pas d'équivalent simple sous forme différentielle. On renvoie au chapitre 8 de [12] pour des exemples.

Remarque 4 *De même qu'on pouvait choisir différentes dérivées convectives pour les modèles différentiels (cf. Remarque 3), il existe également d'autres choix "naturels" que le tenseur de Finger pour exprimer le tenseur des contraintes sous forme intégrale. Comme on l'a vu ci-dessus, le tenseur de Finger est associé au choix d'une dérivée sur-convectée. Au contraire, choisir une dérivée sous-convectée revient à choisir une expression pour $\boldsymbol{\tau}_p$ de la forme :*

$$\boldsymbol{\tau}_p(t, \boldsymbol{x}) = -\int_{-\infty}^{t} M(t-s) g\left(\boldsymbol{C}_t(s, \boldsymbol{x})\right) \left(\boldsymbol{C}_t(s, \boldsymbol{x}) - Id\right) ds. \tag{1.29}$$

On renvoie à [11, 12] pour des détails.

1.1.3 Modèles microscopiques pour les fluides polymériques

Dans la section 1.1.2, on a cherché à établir une relation entre le tenseur $\boldsymbol{\tau}_p$ donnant la contribution des polymères au tenseur des extra-contraintes (cf. (1.12)) et l'histoire de la déformation au travers de formules ne faisant intervenir que des grandeurs macroscopiques (cf. (1.16) et (1.26)).

On s'intéresse maintenant à écrire une loi de comportement en partant d'un autre point de vue : on cherche à décrire la manière dont évoluent les polymères au niveau microscopique dans le champ de vitesse du solvant puis, ensuite, comment les polymères influencent le tenseur des contraintes et donc l'écoulement macroscopique. Nous allons donc introduire des variables supplémentaires dans le problème pour modéliser les microstructures. Nous ne pouvons pas nous permettre de décrire très finement les molécules de polymère dans le fluide, en utilisant par exemple la mécanique quantique ou la dynamique moléculaire, pour des raisons de coût calcul, puisque l'on cherche à simuler des écoulements à l'échelle du centimètre et de la seconde. Nous allons plutôt utiliser des modèles cinétiques, type équation de Langevin, pour simuler l'évolution de la conformation des polymères (on parle parfois de modèles mésoscopiques, pour les distinguer des modèles plus fins qui décriraient l'évolution des molécules elles-mêmes). Ces modèles ont été développés depuis les années 1930 mais ont surtout été améliorés durant les trente dernières années (cf. [12, 13, 33, 39]) et l'idée de coupler ces modèles avec les équations macroscopiques sur la vitesse pour simuler des écoulements complexes date des années 1990 (cf. [97] et les thèses récentes [16, 108, 148]).

1.1.3.1 Evolution d'une chaîne de polymère dans un champ de vitesse fixé

Nous nous intéressons dans un premier temps à la description de l'évolution d'un polymère dans un champ de vitesse donné. L'hypothèse fondamentale que nous ferons par la suite (cf. une discussion de ces hypothèses dans la section 1.1.3.5) est que *les chaînes de polymère n'interagissent pas entre elles*. Nous nous limiterons donc à la modélisation des fluides polymériques *infiniment dilués*.

Introduction du modèle du dumbbell.

Un des modèles les plus simples qui permettent de décrire la conformation d'un polymère dans un solvant est la chaîne de Kramers (cf. figure 1.7). On représente le polymère par une chaîne de N billes reliées par $N-1$ tiges rigides de longueur a. Dans ce modèle, les billes représentent des portions de 10 à 20 monomères. On suppose par ailleurs que les angles entre tiges sont libres, c'est-à-dire que les positions des tiges sont représentées par des variables aléatoires indépendantes uniformément distribuées sur la sphère (on parle de "chaîne libre"). Cette hypothèse d'absence de corrélation entre les tiges est d'ailleurs ce qui détermine la longueur des tiges (on parle de segment statistique de Kuhn). Ce modèle présente plusieurs caractéristiques d'une "vraie" chaîne de polymère :
  – la chaîne possède un grand nombre de degrés de liberté internes,
  – elle peut être étirée ou orientée,
  – elle possède une longueur maximale : $(N-1)a$.
Dans la limite N grand, en utilisant le théorème de la limite centrale (cf. [39] p. 12-13 ou [13] p. 14), on peut montrer qu'une très bonne approximation de la densité de
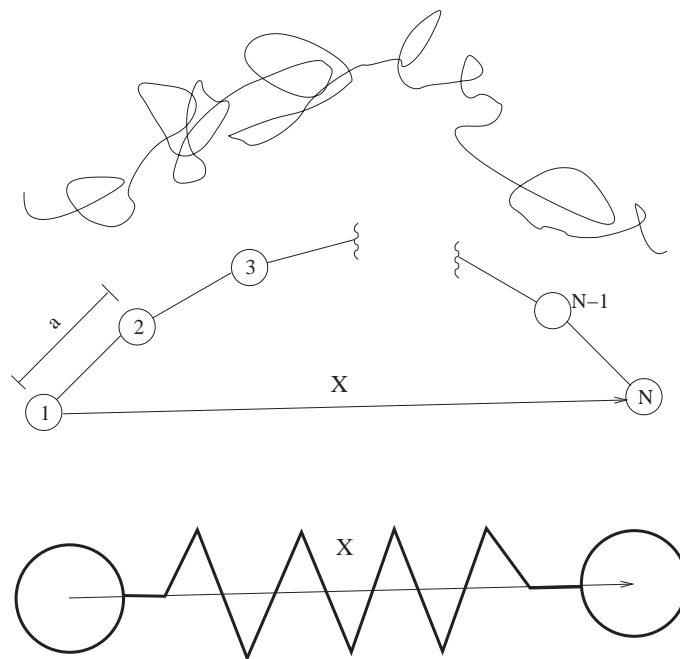
FIG. 1.7 – Modélisation d'un polymère : de la molécule au modèle du *dumbbell* en passant par le modèle de la chaîne libre de billes et de tiges (appelée chaîne de Kramers). On désigne par $\boldsymbol{X}$ le vecteur qui joint une extrémité à l'autre.

probabilité pour le vecteur bout-à-bout $\boldsymbol{X}$ joignant les deux extrémités du polymère (cf. figure 1.7), dans un champ de vitesse nulle, est :

$$\phi_{\text{eq}}(\boldsymbol{X}) = Z^{-1} \exp\left(-\frac{3\|\boldsymbol{X}\|^2}{2(N-1)a^2}\right) \tag{1.30}$$

où Z est une constante de normalisation. L'énergie libre du système étant donnée, à une constante additive près, par $A(\boldsymbol{X}) = -kT\ln(\phi_{\text{eq}}(\boldsymbol{X}))$, où k désigne la constante de Boltzmann et T la température (supposée constante dans toute la suite), on peut introduire une force qui est reliée aux variations de l'énergie libre et définie par $dA = \boldsymbol{F}(\boldsymbol{X}).d\boldsymbol{X}$ (ce qui oriente la force $\boldsymbol{F}$). On obtient alors une force linéaire, correspondant à un ressort hookéen :

$$\boldsymbol{F}_{\text{Hook}}(\boldsymbol{X}) = H\boldsymbol{X} \tag{1.31}$$

où $H = \dfrac{3kT}{(N-1)a^2}$ désigne la constante de raideur du ressort. On aboutit donc à un modèle très simple dans lequel un polymère est modélisé par deux billes reliées par un ressort hookéen (cf. figure 1.7) : ce modèle s'appelle modèle du *dumbbell* hookéen. On appellera par la suite modèle de *dumbbell* (haltère en français) tout modèle de la chaîne de polymère par deux billes reliées par un ressort. Noter que la force reliant les deux billes dans ces modèles est purement d'origine entropique. L'hypothèse fondamentale derrière cette modélisation est que l'échelle de temps à laquelle on regarde évoluer le polymère dans le fluide est suffisamment grande pour que la molécule ait le temps d'échantillonner l'espace des configurations possibles (équilibre statistique).

L'approximation précédente (appelée approximation gaussienne) peut être affinée pour prendre en compte l'extensibilité finie de la chaîne. Par des arguments de physique statistique, on peut montrer (cf. chapitre 6 de [147]) qu'une bonne approximation de la force qui s'exerce entre les deux extrémités de la chaîne est :

$$\boldsymbol{F}_{\text{Lang}}(\boldsymbol{X}) = \frac{kT}{a}\mathcal{L}^{-1}\left(\frac{\|\boldsymbol{X}\|}{(N-1)a}\right)\frac{\boldsymbol{X}}{\|\boldsymbol{X}\|} \tag{1.32}$$

où $\mathcal{L}^{-1}$ désigne la réciproque de la fonction de Langevin définie par :

$$\mathcal{L}(x) = \coth(x) - \frac{1}{x}. \tag{1.33}$$

Cette expression est difficilement manipulable en pratique, et on lui préfère souvent son approximation introduite par Warner [151] :

$$\boldsymbol{F}_{\text{FENE}}(\boldsymbol{X}) = \frac{H\boldsymbol{X}}{1 - \frac{\|\boldsymbol{X}\|^2}{b\,kT/H}} \tag{1.34}$$

où $H = \frac{3kT}{(N-1)a^2}$ et $b = 3(N-1)$. On appelle ce modèle le modèle des *dumbbells* FENE (*Finite Extensible Nonlinear Elastic dumbbells*), car la force $\boldsymbol{F}_{\text{FENE}}$ dans le ressort explose quand $\|\boldsymbol{X}\|$ tend vers $(N-1)a$. Noter que dans les limites $\|\boldsymbol{X}\|$ tend vers 0 ou bien b tend vers ∞, on retrouve bien la force hookéenne (1.31).

Remarque 5 *Les valeurs* $H = \dfrac{3kT}{(N-1)a^2}$ *et* $b = 3(N-1)$ *sont valables en dimension* $d = 3$.

Evolution du dumbbell dans un champ de vitesse donné.

Supposons un instant que le solvant soit au repos et considérons simplement le mouvement d'une bille dans le fluide (cf. [120] p. 82-83). On décompose la force que le solvant exerce sur la bille en deux types de force (approche de Langevin) :

- une force de friction, proportionnelle à la vitesse relative de la bille par rapport au solvant, (le coefficient de friction est noté ζ et peut être estimé, par exemple en utilisant la loi de Stokes, cf. [12] p. 23),
- une force brownienne, provenant des nombreux impacts aléatoires des petites molécules du solvant sur la bille représentant une "grosse" molécule.

L'hypothèse du caractère brownien de la force exercée par le solvant sur la bille provient du fait qu'on suppose que la corrélation en temps pour cette force est très petite devant le temps d'observation du mouvement de la bille. En notant m la masse de la bille et $\boldsymbol{V}_t$ son vecteur vitesse, on obtient donc l'équation du mouvement suivante (équation de Langevin) :

$$m\, d\boldsymbol{V}_t = -\zeta \boldsymbol{V}_t\, dt + D\, d\boldsymbol{B}_t, \tag{1.35}$$

où $\boldsymbol{B}_t$ désigne un mouvement brownien standard d-dimensionnel, et D un paramètre scalaire que l'on veut déterminer. La solution est un processus d'Ornstein-Uhlenbeck :

$$\boldsymbol{V}_t = \boldsymbol{V}_0 \exp\left(-\frac{\zeta}{m}t\right) + \frac{D}{m}\int_0^t \exp\left(-\frac{\zeta}{m}(t-s)\right) d\boldsymbol{B}_s,$$

où $\boldsymbol{V}_0$ désigne la vitesse initiale que l'on suppose indépendante de $\boldsymbol{B}_t$. Le processus $\boldsymbol{V}_t$ est donc un processus gaussien de moyenne

$$\mathbb{E}(\boldsymbol{V}_t) = \mathbb{E}(\boldsymbol{V}_0)\exp\left(-\frac{\zeta}{m}t\right),$$

et de matrice de variance-covariance

$$\mathbb{E}\left((\boldsymbol{V}_t - \mathbb{E}(\boldsymbol{V}_t)) \otimes (\boldsymbol{V}_t - \mathbb{E}(\boldsymbol{V}_t))\right)$$
$$= \mathbb{E}\left((\boldsymbol{V}_0 - \mathbb{E}(\boldsymbol{V}_0)) \otimes (\boldsymbol{V}_0 - \mathbb{E}(\boldsymbol{V}_0))\right)\exp\left(-\frac{2\zeta}{m}t\right)$$
$$+ \frac{D^2}{2\zeta m}\left(1 - \exp\left(-\frac{2\zeta}{m}t\right)\right)\mathrm{Id}.$$

On a supposé que le fluide était au repos, et on s'attend donc à ce que le processus $\boldsymbol{V}_t$ soit stationnaire, ce qui impose :

$$\begin{cases} \mathbb{E}(\boldsymbol{V}_t) = \mathbb{E}(\boldsymbol{V}_0) = 0, \\ \mathbb{E}(\boldsymbol{V}_t \otimes \boldsymbol{V}_t) = \mathbb{E}(\boldsymbol{V}_0 \otimes \boldsymbol{V}_0) = \dfrac{D^2}{2\zeta m}\mathrm{Id}. \end{cases} \tag{1.36}$$
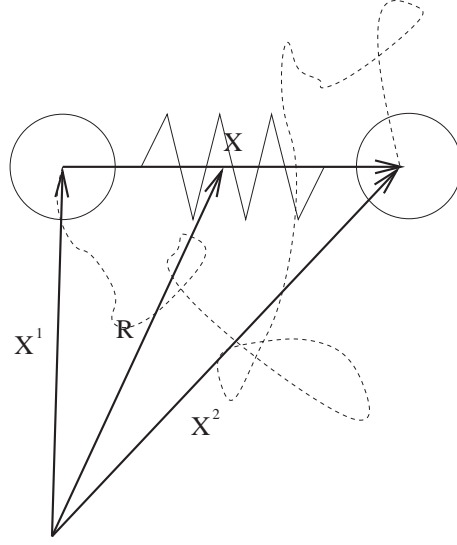
FIG. 1.8 – Modèle du *dumbbell*. Le vecteur bout-à-bout $\boldsymbol{X}$ est la différence des vecteurs positions de la bille 2 et de la bille 1. Le vecteur $\boldsymbol{R}$ donne la position du centre de masse du *dumbbell*.

En utilisant le principe d'équipartition de l'énergie, on sait que l'énergie cinétique moyenne $\frac{1}{2}m\,\mathbb{E}(||\boldsymbol{V}_t||^2)$ doit être égale à $\frac{d}{2}kT$ d'où la relation de Nernst-Einstein :

$$D = \sqrt{2kT\zeta}. \tag{1.37}$$

Ce raisonnement est lié au théorème de fluctuation-dissipation.

Intéressons-nous maintenant à une bille d'un *dumbbell* dans un champ de vitesse fixé $\boldsymbol{u}(t,\boldsymbol{x})$ (on rappelle que t désigne la variable de temps et $\boldsymbol{x}$ la variable d'espace). Aux deux forces précédemment évoquées s'ajoute la force dans le ressort, que nous notons génériquement $\boldsymbol{F}(\boldsymbol{X})$ (cf. (1.31), (1.32) ou (1.34)). On note $\boldsymbol{X}_t^i$ le vecteur position de la bille i ($i = 1$ ou 2) de sorte que $\boldsymbol{X} = \boldsymbol{X}^2 - \boldsymbol{X}^1$ (cf. figure 1.8). On introduit également $\boldsymbol{R} = \frac{1}{2}\left(\boldsymbol{X}^1 + \boldsymbol{X}^2\right)$ la position du centre de masse du *dumbbell*. On a (cf. l'équation de Langevin (1.35)) :

$$\begin{cases} m\,d\left(\dfrac{d\boldsymbol{X}_t^1}{dt}\right) = -\zeta\left(\dfrac{d\boldsymbol{X}_t^1}{dt} - \boldsymbol{u}(t,\boldsymbol{X}_t^1)\right)\,dt + \boldsymbol{F}(\boldsymbol{X}_t)\,dt + \sqrt{2kT\zeta}\,d\boldsymbol{B}_t^1, \\[2ex] m\,d\left(\dfrac{d\boldsymbol{X}_t^2}{dt}\right) = -\zeta\left(\dfrac{d\boldsymbol{X}_t^2}{dt} - \boldsymbol{u}(t,\boldsymbol{X}_t^2)\right)\,dt - \boldsymbol{F}(\boldsymbol{X}_t)\,dt + \sqrt{2kT\zeta}\,d\boldsymbol{B}_t^2, \end{cases} \tag{1.38}$$

où $\boldsymbol{B}_t^1$ et $\boldsymbol{B}_t^2$ désignent deux mouvements browniens d-dimensionnels indépendants. Dans la limite où $\frac{m}{\zeta}$ tend vers 0 (c'est-à-dire si l'échelle de temps à laquelle on regarde le mouvement du polymère est très grande devant le temps caractéristique

$\frac{m}{\zeta}$), par combinaison linéaire des deux équations de (1.38), on obtient donc :

$$\begin{cases} d\boldsymbol{X}_t = \left(\boldsymbol{u}(t, \boldsymbol{X}_t^2) - \boldsymbol{u}(t, \boldsymbol{X}_t^1)\right) dt - \dfrac{2}{\zeta}\boldsymbol{F}(\boldsymbol{X}_t)\, dt + 2\sqrt{\dfrac{kT}{\zeta}}d\boldsymbol{W}_t^1, \\[4mm] d\boldsymbol{R}_t = \dfrac{1}{2}\left(\boldsymbol{u}(t, \boldsymbol{X}_t^1) + \boldsymbol{u}(t, \boldsymbol{X}_t^2)\right) dt + \sqrt{\dfrac{kT}{\zeta}}d\boldsymbol{W}_t^2, \end{cases} \quad (1.39)$$

où $\boldsymbol{W}_t^1 = \frac{1}{\sqrt{2}}\left(\boldsymbol{B}_t^2 - \boldsymbol{B}_t^1\right)$ et $\boldsymbol{W}_t^2 = \frac{1}{\sqrt{2}}\left(\boldsymbol{B}_t^1 + \boldsymbol{B}_t^2\right)$ sont deux mouvements browniens d-dimensionnels indépendants.

On fait maintenant les approximations suivantes :
– on effectue les développements limités

$$\boldsymbol{u}(t, \boldsymbol{X}_t^i) \simeq \boldsymbol{u}(t, \boldsymbol{R}_t) + \nabla\boldsymbol{u}(t, \boldsymbol{R}_t)(\boldsymbol{X}_t^i - \boldsymbol{R}_t)$$

pour $i = 1, 2$, cette approximation étant justifiée par le fait que la taille du po-lymère est petite par rapport aux variations spatiales de la vitesse du solvant,
– on supprime le bruit dans l'équation sur $\boldsymbol{R}_t$ ($\boldsymbol{W}_t^2 = 0$), cette approximation étant justifiée par le fait que le terme $\frac{1}{2}\left(\boldsymbol{u}(t, \boldsymbol{X}_t^1) + \boldsymbol{u}(t, \boldsymbol{X}_t^2)\right) dt$ est de taille "macroscopique" par rapport à une variation $\sqrt{\frac{kT}{\zeta}}d\boldsymbol{W}_t^2$ "microscopique".

On obtient alors (en notant $\boldsymbol{W} = \boldsymbol{W}^1$) :

$$\begin{cases} d\boldsymbol{X}_t = \nabla\boldsymbol{u}(t, \boldsymbol{R}_t)\boldsymbol{X}_t\, dt - \dfrac{2}{\zeta}\boldsymbol{F}(\boldsymbol{X}_t)\, dt + 2\sqrt{\dfrac{kT}{\zeta}}d\boldsymbol{W}_t, \\[4mm] d\boldsymbol{R}_t = \boldsymbol{u}(t, \boldsymbol{R}_t)\, dt. \end{cases} \quad (1.40)$$

On adjoint à ce système d'équations des conditions initiales : $\boldsymbol{X}_0$ (la conformation initiale du vecteur bout-à-bout) et $\boldsymbol{R}_0$ (la position initiale du polymère). On voit donc que les processus $\boldsymbol{X}_t$ (et donc les mouvements browniens $\boldsymbol{W}_t$) sont naturel-lement indexés par les trajectoires des particules (disons par exemple par $\boldsymbol{R}_0$), du moins dans la mesure où le champ de vecteur $\boldsymbol{u}(t, \boldsymbol{x})$ est suffisamment régulier pour pouvoir être intégré. Si on introduit une description eulérienne du vecteur bout-à-bout, $\boldsymbol{X}_t(\boldsymbol{x})$ représentant la conformation "type" d'un polymère situé au point $\boldsymbol{x}$ à l'instant t, on obtient l'équation aux dérivées partielles stochastique (EDPS) suivante sur $\boldsymbol{X}_t(\boldsymbol{x})$:

$$d\boldsymbol{X}_t(\boldsymbol{x}) + \boldsymbol{u}(t, \boldsymbol{x}).\nabla\boldsymbol{X}_t(\boldsymbol{x})\, dt = \nabla\boldsymbol{u}(t, \boldsymbol{x})\boldsymbol{X}_t(\boldsymbol{x})\, dt - \dfrac{2}{\zeta}\boldsymbol{F}(\boldsymbol{X}_t(\boldsymbol{x}))\, dt + 2\sqrt{\dfrac{kT}{\zeta}}d\boldsymbol{W}_t.$$
$$(1.41)$$

Noter que l'on a ici supposé que le mouvement brownien $\boldsymbol{W}$ ne dépend pas de l'espace (cf. section 1.2.2.2 et chapitre 6 pour une discussion des descriptions eulériennes et lagrangiennes).

Le modèle que nous considérerons dans la suite est donc (1.40) ou (1.41) avec pour la force entropique $\boldsymbol{F}$, soit le modèle linéaire ($\boldsymbol{F} = \boldsymbol{F}_{\text{Hook}}$, cf. (1.31)), soit le
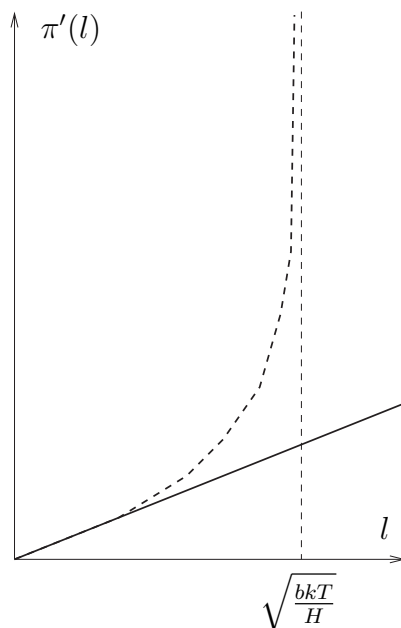
FIG. 1.9 – Représentation de la force en fonction de la longueur pour le modèle hookéen (en trait plein) et pour le modèle FENE (en trait pointillé).

modèle FENE tenant compte de l'extensibilité finie des polymères ($\boldsymbol{F} = \boldsymbol{F}_{\text{FENE}}$, cf. (1.34)).

De manière générale, la force $\boldsymbol{F}(\boldsymbol{X})$ dérive toujours d'un potentiel convexe $\Pi(\boldsymbol{X})$ qui peut s'écrire sous la forme $\Pi(\boldsymbol{X}) = \pi(||\boldsymbol{X}||)$ (potentiel radial). Ainsi,

$$\boldsymbol{F}(\boldsymbol{X}) = \pi'(||\boldsymbol{X}||)\frac{\boldsymbol{X}}{||\boldsymbol{X}||}. \tag{1.42}$$

Voici quelques exemples de potentiels utilisés en pratique (cf. figure 1.9) :

- le potentiel hookéen (cf. (1.31)) : $\pi_{\text{Hook}}(l) = H\dfrac{l^2}{2}$,
- le potentiel FENE (cf. (1.34)) : $\pi_{\text{FENE}}(l) = -\dfrac{bkT}{2}\ln\left(1 - \dfrac{l^2}{bkT/H}\right)$.

On peut également citer le potentiel de la force de Langevin (cf. (1.32)) ou un potentiel tenant compte des effets de volume exclu (cf. [120] p. 215) : $\pi_{\text{ev}}(l) = H(1-\nu)l^{1/(1-\nu)}$ avec typiquement $\nu = 0.6$ en dimension 3. Certains auteurs utilisent aussi la somme d'un potentiel hookéen quadratique et d'un terme en puissance quatre (cf. [78]).

Remarque 6 *On peut vérifier qu'une condition nécessaire et suffisante pour que Π soit une fonction convexe (resp. α-convexe) est que π soit une fonction convexe (resp. α-convexe) telle que $\pi'(0) \geq 0$.*

1.1.3.2   Contribution des polymères au tenseur des contraintes

On dispose maintenant d'un modèle décrivant l'évolution d'un polymère dans un champ de vitesse $\boldsymbol{u}(t, \boldsymbol{x})$ du solvant donné. Pour pouvoir fermer le système, il faut calculer la contribution $\boldsymbol{\tau}_p$ des polymères au tenseur des extra-contraintes $\boldsymbol{\tau}$.

Expressions du tenseur des contraintes $\boldsymbol{\tau}_p$.

En utilisant le fait que le tenseur des contraintes testé contre un vecteur unitaire $\boldsymbol{n}$ donne la force qui s'exerce sur l'élément de surface de normale $\boldsymbol{n}$, on montre que $\boldsymbol{\tau}_p$ s'exprime de la façon suivante en fonction de $\boldsymbol{X}_t$ (cf. [120] p. 158–159, [39] section 3.7.4, ou [13] section 13.3) :

$$\boldsymbol{\tau}_p(t) = n_p\Big(\mathbb{E}(\boldsymbol{X}_t \otimes \boldsymbol{F}(\boldsymbol{X}_t)) - kT\mathrm{Id}\Big), \tag{1.43}$$

où $\otimes$ désigne le produit tensoriel et n_p la concentration en chaînes de polymère. Cette expression est obtenue en écrivant que la force qui s'exerce sur l'élément de surface de normale $\boldsymbol{n}$ est égale aux forces cumulées des ressorts des *dumbbells* coupés par l'élément de surface. La formule (1.43) s'appelle la formule de Kramers. Noter que cette formule est telle que $\boldsymbol{\tau}_p$ est un tenseur symétrique, d'après l'expression générale de la force (1.42).

Remarque 7 *Nous n'avons pas indiqué de dépendance en la variable de position macroscopique $\boldsymbol{x}$ dans (1.43), mais celle-ci est sous-entendue : dans le cas lagrangien (1.40), $\boldsymbol{\tau}_p$ dépend de la trajectoire, de la même façon que $\boldsymbol{X}_t$, et dans le cas eulérien (1.41), $\boldsymbol{\tau}_p$ dépend de la position $\boldsymbol{x}$ occupée à l'instant t par le polymère de conformation "type" $\boldsymbol{X}_t(\boldsymbol{x})$.*

Par un calcul d'Itô sur le tenseur de structure $(\boldsymbol{X}_t(\boldsymbol{x}) \otimes \boldsymbol{X}_t(\boldsymbol{x}))$, en utilisant (1.41), on obtient :

$$\begin{aligned}
d(\boldsymbol{X}_t(\boldsymbol{x}) \otimes \boldsymbol{X}_t(\boldsymbol{x})) &= (d\boldsymbol{X}_t(\boldsymbol{x})) \otimes \boldsymbol{X}_t(\boldsymbol{x}) + \boldsymbol{X}_t(\boldsymbol{x}) \otimes (d\boldsymbol{X}_t(\boldsymbol{x})) + \frac{4kT}{\zeta}\mathrm{Id}\,dt \\
&= \Big(-\boldsymbol{u}(t, \boldsymbol{x}).\nabla\left(\boldsymbol{X}_t(\boldsymbol{x}) \otimes \boldsymbol{X}_t(\boldsymbol{x})\right) \\
&\quad +\nabla\boldsymbol{u}(t, \boldsymbol{x})(\boldsymbol{X}_t(\boldsymbol{x}) \otimes \boldsymbol{X}_t(\boldsymbol{x})) + (\boldsymbol{X}_t(\boldsymbol{x}) \otimes \boldsymbol{X}_t(\boldsymbol{x}))(\nabla\boldsymbol{u}(t, \boldsymbol{x}))^T \\
&\quad -\frac{2}{\zeta}\boldsymbol{F}(\boldsymbol{X}_t) \otimes \boldsymbol{X}_t - \frac{2}{\zeta}\boldsymbol{X}_t \otimes \boldsymbol{F}(\boldsymbol{X}_t) + \frac{4kT}{\zeta}\mathrm{Id}\Big)\,dt \\
&\quad +2\sqrt{\frac{kT}{\zeta}}\left((\boldsymbol{X}_t(\boldsymbol{x}) \otimes d\boldsymbol{W}_t) + (d\boldsymbol{W}_t \otimes \boldsymbol{X}_t(\boldsymbol{x}))\right).
\end{aligned}$$

On note $\boldsymbol{A}(t, \boldsymbol{x})$ la moyenne du tenseur de structure :

$$\boldsymbol{A}(t, \boldsymbol{x}) = \mathbb{E}(\boldsymbol{X}_t(\boldsymbol{x}) \otimes \boldsymbol{X}_t(\boldsymbol{x})). \tag{1.44}$$

En supposant que le processus $\boldsymbol{X}_t$ est tel que, pour tout $t \geq 0$, $\int_0^t \boldsymbol{X}_t(\boldsymbol{x}) \otimes d\boldsymbol{W}_s$ est une martingale (par exemple, $\boldsymbol{X}_t$ est un processus tel que $\int_0^t \mathbb{E}(\|\boldsymbol{X}_s\|^2)\, ds < \infty$), on obtient l'équation suivante sur $\boldsymbol{A}(t, \boldsymbol{x})$:

$$\partial_t \boldsymbol{A}(t, \boldsymbol{x}) + \boldsymbol{u}(t, \boldsymbol{x}).\nabla \boldsymbol{A}(t, \boldsymbol{x}) - \nabla \boldsymbol{u}(t, \boldsymbol{x})\boldsymbol{A}(t, \boldsymbol{x}) - \boldsymbol{A}(t, \boldsymbol{x})(\nabla \boldsymbol{u}(t, \boldsymbol{x}))^T$$
$$= -\frac{4}{\zeta}\mathbb{E}(\boldsymbol{X}_t \otimes \boldsymbol{F}(\boldsymbol{X}_t)) + \frac{4kT}{\zeta}\mathrm{Id}.$$

En utilisant (1.43), on obtient alors une expression pour $\boldsymbol{\tau}_p$ appelée expression de Giesekus qui est équivalente à celle de Kramers, mais qui ne fait intervenir que des moments d'ordre deux du processus $\boldsymbol{X}_t$:

$$\boldsymbol{\tau}_p(t, \boldsymbol{x}) = \hspace{8cm} (1.45)$$
$$-\frac{\zeta}{4}n_p\left(\partial_t \boldsymbol{A}(t, \boldsymbol{x}) + \boldsymbol{u}(t, \boldsymbol{x}).\nabla \boldsymbol{A}(t, \boldsymbol{x}) - \nabla \boldsymbol{u}(t, \boldsymbol{x})\boldsymbol{A}(t, \boldsymbol{x}) - \boldsymbol{A}(t, \boldsymbol{x})(\nabla \boldsymbol{u}(t, \boldsymbol{x}))^T\right).$$

Autrement dit, $\boldsymbol{\tau}_p$ est proportionnel à la dérivée sur-convectée de $\boldsymbol{A}$ (cf. remarque 3). Noter qu'avec cette expression, on a bien $\boldsymbol{\tau}_p = 0$ à l'équilibre (une quantité est dite "à l'équilibre" quand c'est la solution du problème stationnaire avec $\boldsymbol{u} = 0$).

Remarque 8 *La trace de $\boldsymbol{A}$ qui donne la moyenne du carré de l'extensibilité du dumbbell est une information importante en pratique car il existe des moyens pour mesurer la taille moyenne des polymères dans le fluide (cf. [13] p. 72). Dans le cas du dumbbell hookéen, à l'équilibre, on voit facilement que la racine carrée de* $\mathrm{tr}(\boldsymbol{A})$ *vaut* $\sqrt{\frac{dkT}{H}}$. *Compte tenu de l'expression de* $H = \frac{3kT}{(N-1)a^2}$ *(cf. remarque 5), on obtient donc la valeur suivante de la taille moyenne du polymère en dimension* $d = 3 : a\sqrt{N-1}$.

1.1.3.3 Le système micro-macro

On dispose à ce stade de toutes les équations pour pouvoir écrire un système micro-macro décrivant l'évolution d'un fluide polymérique. En regroupant (1.1)–(1.2)–(1.3)–(1.12)–(1.41)–(1.43), on obtient le système suivant :

$$\begin{cases} \rho\left(\partial_t \boldsymbol{u}(t, \boldsymbol{x}) + \boldsymbol{u}(t, \boldsymbol{x}).\nabla \boldsymbol{u}(t, \boldsymbol{x})\right) - \eta_s \Delta \boldsymbol{u}(t, \boldsymbol{x}) + \nabla p(t, \boldsymbol{x}) \\ \qquad = \mathrm{div}\left(\boldsymbol{\tau}_p(t, \boldsymbol{x})\right) + \boldsymbol{f}(t, \boldsymbol{x}), \\ \mathrm{div}\left(\boldsymbol{u}(t, \boldsymbol{x})\right) = 0, \\ \boldsymbol{\tau}_p(t, \boldsymbol{x}) = n_p\left(\mathbb{E}(\boldsymbol{X}_t(\boldsymbol{x}) \otimes \boldsymbol{F}(\boldsymbol{X}_t(\boldsymbol{x}))) - kT\mathrm{Id}\right), \\ d\boldsymbol{X}_t(\boldsymbol{x}) + \boldsymbol{u}(t, \boldsymbol{x}).\nabla \boldsymbol{X}_t(\boldsymbol{x})\, dt \\ \qquad = \nabla \boldsymbol{u}(t, \boldsymbol{x})\boldsymbol{X}_t(\boldsymbol{x})\, dt - \frac{2}{\zeta}\boldsymbol{F}(\boldsymbol{X}_t(\boldsymbol{x}))\, dt + 2\sqrt{\frac{kT}{\zeta}}d\boldsymbol{W}_t. \end{cases} \quad (1.46)$$

Noter que les EDS doivent être résolues en chaque point de l'écoulement. Le processus $\boldsymbol{X}_t$ dépend donc de t, de $\boldsymbol{x}$ et de la variable de probabilité que l'on note ω. Ce

type de modèle micro-macro relève de la classe générale de modèles évoquée dans la section 1.A.3.

On se propose de réécrire ce système avec des variables adimensionnelles. On introduit donc une vitesse caractéristique U et une longueur caractéristique L. Le temps est alors adimensionné par L/U et $\boldsymbol{X}_t$ par L. Par ailleurs, on introduit un temps caractéristique de relaxation des polymères λ (qui se mesure en seconde) et la viscosité due au polymère η_p (qui se mesure en Pascal.seconde) définis par :

$$\lambda = \frac{\zeta}{4H}, \tag{1.47}$$

$$\eta_p = n_p kT\lambda. \tag{1.48}$$

Ces expressions sont définies pour les forces hookéennes et FENE et seront justifiées dans la section 1.1.4.1. Dans le cas d'autres forces, H est plus généralement la dérivée seconde du potentiel π en 0. On note $\eta = \eta_s + \eta_p$ la viscosité totale et on adimensionne $\boldsymbol{\tau}_p$ et p par $\eta U/L$. On adimensionne $\boldsymbol{f}$ par $\eta U/L^2$. On introduit maintenant les nombres adimensionnels suivants :

$$\begin{cases} \mathrm{Re} = \dfrac{\rho U L}{\eta}, & \epsilon = \dfrac{\eta_p}{\eta}, \\ \mathrm{We} = \dfrac{\lambda U}{L}, & \mu = \dfrac{L^2 H}{kT}. \end{cases} \tag{1.49}$$

Le premier nombre adimensionnel Re est le nombre de Reynolds qui mesure le rapport des effets d'inertie sur la viscosité ; $\epsilon \in (0,1]$ mesure l'influence relative de la viscosité introduite par les polymères par rapport à la viscosité totale ; We est le nombre de Weissenberg (aussi appelé nombre de Deborah) et est égal au rapport d'un temps caractéristique de relaxation pour les polymères et d'un temps caractéristique de l'écoulement ; μ mesure le carré du rapport entre la longueur caractéristique choisie L et la taille caractéristique des polymères $\sqrt{\frac{kT}{H}}$ (cf. remarque 8). Le système (1.46) se réécrit alors, en surlignant les variables adimensionnées, et en omettant ici les dépendances en temps et en espace :

$$\begin{cases} \mathrm{Re}\left(\partial_{\bar{t}}\overline{\boldsymbol{u}} + \overline{\boldsymbol{u}}.\overline{\nabla}\overline{\boldsymbol{u}}\right) - (1-\epsilon)\overline{\Delta}\overline{\boldsymbol{u}} + \overline{\nabla}\overline{p} = \overline{\mathrm{div}}\left(\overline{\boldsymbol{\tau}_p}\right) + \overline{\boldsymbol{f}}, \\ \overline{\mathrm{div}}\left(\overline{\boldsymbol{u}}\right) = 0, \\ \overline{\boldsymbol{\tau}_p} = \dfrac{\epsilon}{\mathrm{We}}\left(\mu\mathbb{E}(\overline{\boldsymbol{X}} \otimes \overline{\boldsymbol{F}}(\overline{\boldsymbol{X}})) - \mathrm{Id}\right), \\ d\overline{\boldsymbol{X}} + \overline{\boldsymbol{u}}.\overline{\nabla}\,\overline{\boldsymbol{X}}\,d\bar{t} = \overline{\nabla}\overline{\boldsymbol{u}}\overline{\boldsymbol{X}}\,d\bar{t} - \dfrac{1}{2\mathrm{We}}\overline{\boldsymbol{F}}(\overline{\boldsymbol{X}})\,d\bar{t} + \dfrac{1}{\sqrt{\mathrm{We}\,\mu}}d\overline{\boldsymbol{W}}_{\bar{t}}. \end{cases} \tag{1.50}$$

où les opérateurs surlignés indiquent qu'ils agissent sur des variables adimensionnées, $\overline{\boldsymbol{W}}_{\bar{t}} = \sqrt{U/L}\boldsymbol{W}_{\bar{t}L/U}$ est un mouvement brownien et la force adimensionnée $\overline{\boldsymbol{F}}$ définie par :

$$\overline{\boldsymbol{F}}(\overline{\boldsymbol{X}}) = \frac{\boldsymbol{F}(L\overline{\boldsymbol{X}})}{HL}$$

a pour potentiel $\overline{\Pi}(\overline{\boldsymbol{X}}) = \overline{\pi}(||\overline{\boldsymbol{X}}||)$, avec :

$$\overline{\pi}(\overline{l}) = \frac{\pi(L\overline{l})}{HL^2}.$$

Dans la suite, comme cela est très souvent le cas dans les articles et les ouvrages de référence, on prend

$$\mu = 1,$$

c'est-à-dire qu'on choisit pour longueur caractéristique du système L la taille caractéristique des polymères $\sqrt{\frac{kT}{H}}$, et on se place désormais dans le cadre des équations adimensionnées (1.50). En omettant désormais et pour plus de clarté les barres surlignant les variables adimensionnées, le problème qui nous intérese est donc finalement :

$$\begin{cases} \text{Re} \left(\partial_t \boldsymbol{u} + \boldsymbol{u}.\nabla\boldsymbol{u}\right) - (1-\epsilon)\Delta\boldsymbol{u} + \nabla p = \text{div}\left(\boldsymbol{\tau}_p\right) + \boldsymbol{f}, \\ \text{div}\left(\boldsymbol{u}\right) = 0, \\ \boldsymbol{\tau}_p = \frac{\epsilon}{\text{We}}\left(\mathbb{E}(\boldsymbol{X} \otimes \boldsymbol{F}(\boldsymbol{X})) - \text{Id}\right), \\ d\boldsymbol{X} + \boldsymbol{u}.\nabla\boldsymbol{X}\,dt = \nabla\boldsymbol{u}\boldsymbol{X}\,dt - \frac{1}{2\text{We}}\boldsymbol{F}(\boldsymbol{X})\,dt + \frac{1}{\sqrt{\text{We}}}d\boldsymbol{W}_t. \end{cases} \qquad (1.51)$$

avec, typiquement, $\boldsymbol{F}(\boldsymbol{X}) = \boldsymbol{X}$ dans le cas des *dumbbells* hookéens et $\boldsymbol{F}(\boldsymbol{X}) = \frac{\boldsymbol{X}}{1-||\boldsymbol{X}||^2/b}$ dans le cas des *dumbbells* FENE.

Remarque 9 *Dans la plupart des publications, on observe des valeurs du nombre de Weissenberg entre 0.1 et 10, du nombre de Reynolds entre 0 et 10, et de ϵ de l'ordre de 0.1 (cf. [3] par exemple). Pour le modèle FENE, b varie typiquement entre 10 et 100 (cf [120] p. 217 ou [13] p. 81). En particulier, les difficultés numériques qui se posent pour la simulation de ces modèles ne sont pas dues au fait que l'on travaille avec des nombres de Reynolds importants, mais plutôt de difficultés de convergence quand le nombre de Weissenberg devient trop grand (cf. section 1.2.1.2).*

Etude des modèles cinétiques dans un champ de vitesse homogène.

Pour analyser la qualité de ces modèles, on peut commencer par calculer $\boldsymbol{\tau}_p$ pour des champs de vitesse donnés et homogènes c'est-à-dire de la forme :

$$\boldsymbol{u}(t, \boldsymbol{x}) = \boldsymbol{\kappa}(t)\boldsymbol{x},$$

où $\boldsymbol{\kappa}(t)$ est une matrice de dimension $d \times d$ de trace nulle. Noter que dans ce cas, $\nabla\boldsymbol{u} = \boldsymbol{\kappa}(t)$ ne dépend pas de la position $\boldsymbol{x}$ et que l'on peut donc chercher des solutions de (1.41) qui ne dépendent pas de la variable d'espace $\boldsymbol{x}$. Ceci permet en particulier d'éliminer le terme $\boldsymbol{u}.\nabla$ dans (1.41), et conduit donc (*via* (1.43)) à un tenseur des contraintes $\boldsymbol{\tau}_p$ indépendant de $\boldsymbol{x}$. Dans la mesure où il existe une pression p et une force extérieure $\boldsymbol{f}$ telle que $(\boldsymbol{u}(t, \boldsymbol{x}), p(t, \boldsymbol{x}))$ est solution des équations de

Navier-Stokes (les deux premières équations de (1.51) avec div $(\boldsymbol{\tau}_p) = 0$), le triplet $(\boldsymbol{u}, p, \boldsymbol{\tau}_p)$ constitue bien une solution du système (1.51) tout entier puisque $\boldsymbol{\tau}_p$ ne dépend pas de l'espace. Le problème est donc dans ce cas partiellement découplé : le champ de vitesse influe sur $\boldsymbol{X}$ et donc sur $\boldsymbol{\tau}_p$, mais $\boldsymbol{\tau}_p$ n'intervient pas dans les équations sur le couple $(\boldsymbol{u}, p)$. La mesure des contraintes dans de tels écoulements permet alors de donner des caractéristiques du fluide et de vérifier la validité des lois de comportement de manière simple (cf. la section 1.1.1.2).

Nous avons déjà rencontré dans la section 1.1.1.2 deux types d'écoulement homogènes : les écoulements cisaillés simples et les écoulements élongationnels. Observons le comportement du modèle des *dumbbells* hookéens et FENE dans ces écoulements. On montrera dans la suite (cf. section 1.1.4.1) que le modèle des *dumbbells* hookéens est en fait équivalent au modèle de Maxwell (cf. (1.15)). En particulier, il présente les mêmes inconvénients (une viscosité de cisaillement indépendante du taux de cisaillement, une seconde différence des contraintes normales nulle et des viscosités élongationnelles qui peuvent exploser pour des taux élongationnels finis, cf. section 1.1.2.1). En introduisant une extensibilité maximale pour le *dumbbell*, le modèle FENE permet de corriger ces problèmes et d'obtenir un comportement qualitatif correct pour les solutions stationnaires d'écoulements homogènes simples (en particulier la propriété de *shear-thinning* cf. [13] p. 82-83).

Le cas d'un écoulement cisaillé général.

Dans la suite, nous considérerons très souvent le cas d'un écoulement cisaillé (cf. figure 1.1) en dimension $d = 2$. Dans un écoulement cisaillé, on suppose que la vitesse s'écrit sous la forme $\boldsymbol{u}(t, \boldsymbol{x}) = (u(t, y), 0)$ et que toutes les quantités ne dépendent que de y (l'écoulement cisaillé simple introduit dans la section 1.1.1.2 correspond au cas $u(t, y) = \dot{\gamma}(t)y$). On note $\tau(t, y)$ la composante (x, y) du tenseur $\boldsymbol{\tau}_p$ et $f(t, y)$ la première composante de la force extérieure $\boldsymbol{f}(t, \boldsymbol{x})$. On montre alors facilement que le système (1.51) se simplifie en :

$$\begin{cases} \text{Re}\,\partial_t u(t, y) - (1 - \epsilon)\partial_{y,y} u(t, y) = \partial_y \tau(t, y) + f(t, y), \\ \tau(t, y) = \dfrac{\epsilon}{\text{We}}\mathbb{E}\Big(X_t(y)F_Y(\boldsymbol{X}_t(y))\Big), \\ dX_t(y) = \partial_y u(t, y)Y_t(y)\,dt - \dfrac{1}{2\text{We}}F_X(\boldsymbol{X}_t(y))\,dt + \dfrac{1}{\sqrt{\text{We}}}dV_t, \\ dY_t(y) = -\dfrac{1}{2\text{We}}F_Y(\boldsymbol{X}_t(y))\,dt + \dfrac{1}{\sqrt{\text{We}}}dW_t, \end{cases} \quad (1.52)$$

où on a noté $(X_t(y), Y_t(y))$ les composantes du processus $\boldsymbol{X}_t(y)$, (V_t, W_t) les composantes du mouvement brownien $\boldsymbol{W}_t$ et $(F_X(\boldsymbol{X}), F_Y(\boldsymbol{X}))$ les composantes de la force $\boldsymbol{F}(\boldsymbol{X})$. On rappelle que d'après l'expression générale (1.42) de $\boldsymbol{F}$, le tenseur $\boldsymbol{\tau}_p$ est symétrique et donc, on a aussi

$$\tau(t, y) = \frac{\epsilon}{\text{We}}\mathbb{E}\Big(Y_t(y)F_X(\boldsymbol{X}_t(y))\Big).$$

On distingue en particulier deux types d'écoulement cisaillé : l'écoulement de Poiseuille, pour lesquels $f \neq 0$ et u est nul sur les parois (penser à un écoulement

sous pression dans un tuyau), et l'écoulement de Couette, pour lequel $f = 0$ et $u(t, y = 0) = 0$, $u(t, y = L) = V$ (cf. figure 1.1). Noter que dans le cas d'un écoulement cisaillé général, on a bien un vrai système couplé : u intervient dans les EDS sur (X, Y) et (X, Y) dépend *a priori* de l'espace, donc intervient dans l'EDP sur u *via* $\partial_y \tau$.

1.1.3.4 Avantages et inconvénients des modèles microscopiques

Les modèles microscopiques ont d'abord été développés dans le but de comprendre quelle est l'influence des polymères sur le tenseur des contraintes et de construire des modèles macroscopiques sur $\boldsymbol{\tau}_p$: en travaillant dans un champ de vitesse homogène, on cherche à comprendre les interactions entre le solvant et les polymères, et l'influence qu'ont les polymères sur une quantité macroscopique, le tenseur des contraintes. L'idée d'utiliser directement ces modèles pour simuler des écoulements complexes est venue ensuite (cf. la méthode CONNFFESSIT [97, 98]). Dans ce cas, on résout donc directement (1.51).

Les avantages de cette approche micro-macro par rapport à une approche macroscopique plus traditionnelle qui consiste à coupler les équations sur la vitesse avec une équation macroscopique sur $\boldsymbol{\tau}_p$ sont les suivants :
- ces modèles semblent "plus sûrs" car ils reposent sur une approche cinétique dont on connaît *a priori* les limites et les hypothèses,
- les constantes introduites dans ces modèles (H, b, k, T, ζ) ont une signification physique claire et peuvent être estimées à partir des propriétés des polymères et du solvant,
- ces modèles permettent d'explorer "numériquement" les rapports entre comportement macroscopique et caractéristiques microscopiques des microstructures et ouvrent par conséquent de nouveaux champs de modélisation possibles,
- il semble que dans des écoulements complexes, les méthodes numériques bâties à partir des modèles micro-macro soient plus robustes que celles construites pour résoudre des modèles macroscopiques (cf. [148] p. 38 pour le calcul d'un écoulement autour d'un cylindre par exemple ou [16] p. 115 et [28] pour le calcul d'un écoulement sur une contraction 4 :1).

L'inconvénient principal de l'approche micro-macro est qu'elle reste extrêmement coûteuse par rapport à une approche macroscopique, puisqu'elle nécessite la résolution d'une équation différentielle stochastique pour chaque position $\boldsymbol{x}$ (disons pour chaque point de Gauss du maillage pour une discrétisation par éléments finis). Quelle que soit la méthode de résolution de cette EDS (schéma d'Euler sur l'EDS ou résolution de l'équation de Fokker-Planck associée, cf. section 1.1.4.2), le modèle nécessite donc le calcul de plus de quantités (des variables microscopiques ont été introduites) qu'un modèle macroscopique, ce qui a des conséquences en termes de coût de calcul et de stockage en mémoire. Il faut cependant remarquer que les EDS sont indexées par les trajectoires, et qu'on peut, pour un champ de vitesse donné sur un intervalle de temps $[t_n, t_{n+1}]$, les résoudre séparément : la parallélisation du
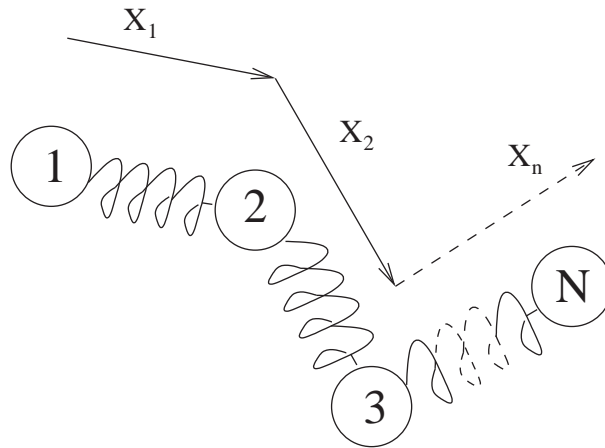
F<small>IG</small>. 1.10 – Modélisation du polymère par une chaîne de N billes et $n = N - 1$ ressorts. Les vecteurs $\boldsymbol{X}_i$ s'appellent les vecteurs connecteurs. Le modèle des *dumbbells* correspond au cas $N = 2$.

schéma numérique est immédiate ! Actuellement, l'approche micro-macro est une piste validée par les laboratoires académiques et qui semble prometteuse, mais n'est pas encore utilisée par les codes commerciaux employés par les industries.

Par ailleurs, l'approche micro-macro ne permet pas de résoudre toutes les difficultés rencontrées dans la modélisation des fluides polymériques. En particulier, même pour des modèles sophistiqués (cf. section 1.1.3.5), il reste en général difficile de retrouver quantitativement les résultats des expériences.

1.1.3.5 Raffinements et autres modèles

Le modèle des *dumbbells* décrit dans les sections précédentes et sur lequel nous allons nous concentrer dans la suite, est un modèle trop grossier pour pouvoir modéliser quantitativement le comportement des polymères. En particulier, on observe en pratique que plusieurs temps de relaxation régissent le comportement des polymères. Pour remédier à ce problème, on peut introduire une chaîne (cf. figure 1.10) de N billes reliées par $n = (N - 1)$ ressorts (et non pas $(N - 1)$ tiges rigides comme dans le modèle de la chaîne de Kramers, cf. section 1.1.3.1). Dans le cas où ces ressorts sont tous des ressorts hookéens, on parle du modèle de Rouse. En suivant la même démarche que pour le modèle des *dumbbells* (cf. section 1.1.3.1), on montre dans ce cas que les équations (1.40) deviennent :

$$\begin{cases} d\boldsymbol{X}_{i,t} = \nabla\boldsymbol{u}(t, \boldsymbol{R}_t)\boldsymbol{X}_{i,t}\,dt - \dfrac{1}{\zeta}\sum_{k=1}^{n} A_{i,k}\boldsymbol{F}(\boldsymbol{X}_{k,t})\,dt + \sqrt{\dfrac{2kT}{\zeta}}\,d\left(\sum_{l=1}^{N} S_{i,l}\boldsymbol{B}_{l,t}\right), \\ d\boldsymbol{R}_t = \boldsymbol{u}(t, \boldsymbol{R}_t)\,dt. \end{cases}$$

$$(1.53)$$

où le vecteur $\boldsymbol{X}_{k,t}$ représente l'état d'étirement du k-ième ressort ($1 \leq k \leq n$), les $(\boldsymbol{B}_{l,t})_{1 \leq l \leq N}$ sont N mouvements browniens d-dimensionnels indépendants, et les matrices A et S sont définies par :

$$
A = \begin{bmatrix}
2 & -1 & 0 & & & \cdots & 0 \\
-1 & 2 & -1 & 0 & & \cdots & 0 \\
0 & -1 & 2 & -1 & 0 & \cdots & 0 \\
\vdots & 0 & \ddots & \ddots & \ddots & 0 & \vdots \\
0 & \cdots & 0 & -1 & 2 & -1 & 0 \\
0 & \cdots & & 0 & -1 & 2 & -1 \\
0 & \cdots & & & 0 & -1 & 2
\end{bmatrix},
$$

$$
S = \begin{bmatrix}
-1 & 1 & 0 & & \cdots & 0 \\
0 & -1 & 1 & 0 & \cdots & 0 \\
\vdots & 0 & \ddots & \ddots & 0 & \vdots \\
0 & \cdots & 0 & -1 & 1 & 0 \\
0 & \cdots & & 0 & -1 & 1
\end{bmatrix}.
$$

Par ailleurs, la formule (1.43) donnant le tenseur des contraintes $\boldsymbol{\tau}_p$ devient :

$$
\boldsymbol{\tau}_p(t) = n_p \left(\sum_{k=1}^{n} \mathbb{E}(\boldsymbol{X}_{k,t} \otimes \boldsymbol{F}(\boldsymbol{X}_{k,t})) - nkT\mathrm{Id} \right). \tag{1.54}
$$

De même qu'on montrera dans la section 1.1.4.1 que le modèle du *dumbbell* hookéen est équivalent à un modèle de Maxwell (cf. (1.15) et section 1.1.2.1), on peut montrer en diagonalisant A et en utilisant le fait que $A = SS^T$ (cf. [120] section 4.1) que le modèle de Rouse est équivalent à un modèle de Maxwell différentiel généralisé avec des temps de relaxation $\lambda_i = \frac{\zeta}{2Ha_i}$ où $(a_i)_{1 \leq i \leq N-1}$ désignent les valeurs propres de la matrice A.

Par ailleurs, les principaux effets qui manquent au modèle décrit dans les sections précédentes sont la modélisation des interactions hydrodynamiques et des effets de volume exclu. On appelle "interactions hydrodynamiques" les interactions qui existent entre les billes d'une chaîne bille-ressort du fait que le mouvement d'une bille influe le mouvement d'une autre *via* la perturbation du champ de vitesse du solvant autour de la chaîne. On peut prendre en compte ces interactions on ajoutant un terme supplémentaire dans le système d'EDS (1.53) réécrit sur la position des billes (cf. formule (4.64) dans [120]). En tenant compte de ces interactions sous forme d'une approximation du type champ moyen (du même type que l'approximation FENE-P, cf. section 1.1.4.1), on arrive au modèle de Zimm. On appelle "effets de volume exclu" le fait que certaines configurations des vecteurs connecteurs $(\boldsymbol{X}_k)_{1 \leq k \leq n}$ sont interdites puisque deux billes de la chaîne ne peuvent pas occuper le même point. Ces effets peuvent être pris en compte en modifiant la force $\boldsymbol{F}$ (cf. section 1.1.3.1 et [120] section 4.3.1).

Rappelons enfin que les modèles développés ci-dessus ne s'appliquent qu'à des solutions diluées de polymères. En effet, ils ne tiennent pas compte des interactions entre chaînes de polymères. Dans le cas des polymères souples, la modélisation des interactions utilise le concept de reptation (cf. [32] et la théorie de Doi-Edwards [39]). Ces théories s'appliquent typiquement aux polymères fondus. Dans le cas de polymères rigides, la modélisation des interactions peut se faire *via* des approximations type champ moyen (cf. chapitre 10 de [39]). Ce type de modèle s'applique notamment aux cristaux liquides.

1.1.4 Modèles microscopiques et équations aux dérivées partielles

Il est bien connu que processus stochastiques et équations aux dérivées partielles entretiennent des liens étroits. Il y a au moins deux façons très naturelles d'associer une EDP à une EDS. La première consiste à écrire l'EDP vérifiée par la densité de probabilité du processus (cf. section 1.1.4.2). Cette EDP s'appelle l'équation de Fokker-Planck (ou équation de Kolmogorov forward, ou encore équation maîtresse). La deuxième consiste à écrire l'EDP vérifiée par l'espérance d'une fonctionnelle du processus (cf. section 1.1.4.3). Cette EDP s'appelle équation de Feynman-Kac (ou équation de Kolmogorov backward). Enfin, il est également possible dans certains cas d'obtenir des équations fermées sur les moments du processus (cf. section 1.1.4.1). Nous nous proposons dans cette section d'explorer les liens entre EDP et EDS dans le cas du modèle micro-macro de fluides polymériques exposé ci-dessus.

1.1.4.1 *Dumbbells* hookéens, approximations de fermeture

En observant les deux expressions équivalentes de $\boldsymbol{\tau}_p$ (expression de Kramers (1.43) et expression de Giesekus (1.45)), on voit que si $\mathbb{E}(\boldsymbol{X} \otimes \boldsymbol{F}(\boldsymbol{X}))$ s'exprime en fonction de la moyenne du tenseur de structure $\boldsymbol{A} = \mathbb{E}(\boldsymbol{X} \otimes \boldsymbol{X})$, on peut obtenir une équation aux dérivées partielles sur $\boldsymbol{A}$ et donc sur $\boldsymbol{\tau}_p$.

Dans le cas des *dumbbells* hookéens, on a $\mathbb{E}(\boldsymbol{X} \otimes \boldsymbol{F}(\boldsymbol{X})) = H\mathbb{E}(\boldsymbol{X} \otimes \boldsymbol{X})$, et on obtient donc facilement l'EDP suivante sur $\boldsymbol{A}$:

$$\partial_t \boldsymbol{A}(t, \boldsymbol{x}) + \boldsymbol{u}(t, \boldsymbol{x}).\nabla \boldsymbol{A}(t, \boldsymbol{x}) - \nabla \boldsymbol{u}(t, \boldsymbol{x})\boldsymbol{A}(t, \boldsymbol{x}) - \boldsymbol{A}(t, \boldsymbol{x})(\nabla \boldsymbol{u}(t, \boldsymbol{x}))^T$$
$$= -\frac{4H}{\zeta}\boldsymbol{A}(t, \boldsymbol{x}) + \frac{4kT}{\zeta}\mathrm{Id},$$

qui se réécrit sous la forme suivante sur $\boldsymbol{\tau}_p$:

$$\frac{\zeta}{4H}\left(\partial_t \boldsymbol{\tau}_p(t, \boldsymbol{x}) + \boldsymbol{u}(t, \boldsymbol{x}).\nabla \boldsymbol{\tau}_p(t, \boldsymbol{x}) - \nabla \boldsymbol{u}(t, \boldsymbol{x})\boldsymbol{\tau}_p(t, \boldsymbol{x}) - \boldsymbol{\tau}_p(t, \boldsymbol{x})(\nabla \boldsymbol{u}(t, \boldsymbol{x}))^T\right)$$
$$= -\boldsymbol{\tau}_p(t, \boldsymbol{x}) + n_p kT\frac{\zeta}{4H}\left(\nabla \boldsymbol{u}(t, \boldsymbol{x}) + (\nabla \boldsymbol{u}(t, \boldsymbol{x}))^T\right).$$

En introduisant le temps de relaxation λ défini par (1.47) et la viscosité η_p définie par (1.48), on retrouve donc exactement le modèle macroscopique de Maxwell (1.15). Ceci justifie les expressions (1.47) et (1.48).

On voit donc que certains modèles microscopiques sont équivalents à des modèles macroscopiques. On remarque que c'est bien la dérivée sur-convectée qui apparaît naturellement à partir de modèles cinétiques (cf. remarque 3). Le fait que l'on retrouve des modèles macroscopiques à partir de modèles cinétiques permet de conforter l'une et l'autre approches. Remarquons également que le modèle microscopique contient beaucoup plus d'informations puisque l'on modélise la chaîne de polymère elle-même, et non pas seulement une espérance d'une fonctionnelle de la conformation du polymère.

En dehors du modèle des *dumbbells* hookéens, on ne sait pas exprimer $\boldsymbol{\tau}_p$ en fonction de $\boldsymbol{A}$ pour obtenir une équation aux dérivées partielles sur $\boldsymbol{A}$ et donc sur $\boldsymbol{\tau}_p$. Or, de telles équations macroscopiques sont intéressantes d'un point de vue numérique car leur résolution nécessite moins de temps CPU et de mémoire. Afin de se ramener à une EDP, on peut alors faire des approximations (appelées approximations de fermeture). Prenons l'exemple du modèle FENE, pour lequel on ne connaît pas à ce jour de modèle macroscopique équivalent. En suivant les idées de Peterlin (cf. [123]), Bird et al. (cf. [14]) ont proposé de remplacer la force FENE (1.34) par une force avec une valeur moyenne de l'élongation au dénominateur :

$$\boldsymbol{F}_{\text{FENE--P}}(\boldsymbol{X}_t) = \frac{H\boldsymbol{X}_t}{1 - \frac{\mathbb{E}(||\boldsymbol{X}_t||^2)}{bkT/H}}. \tag{1.55}$$

Sur le système (1.46), on obtient donc pour les deux dernières équations :

$$\begin{cases} \boldsymbol{\tau}_p = n_p \left(\dfrac{H\mathbb{E}\left(\boldsymbol{X}_t \otimes \boldsymbol{X}_t\right)}{1 - \mathbb{E}\left(||\boldsymbol{X}_t||^2\right)/(bkT/H)} - kT\mathrm{Id} \right), \\[4mm] d\boldsymbol{X}_t + \boldsymbol{u}.\nabla\boldsymbol{X}_t\,dt = \left(\nabla\boldsymbol{u}\boldsymbol{X}_t - \dfrac{2H}{\zeta}\dfrac{\boldsymbol{X}_t}{1 - \mathbb{E}\left(||\boldsymbol{X}_t||^2\right)/(bkT/H)} \right) dt + 2\sqrt{\dfrac{kT}{\zeta}}d\boldsymbol{W}_t. \end{cases} \tag{1.56}$$

En utilisant l'expression de $\boldsymbol{\tau}_p$, on obtient alors à partir de (1.43) et de (1.45) l'EDP suivante sur $\boldsymbol{A}$:

$$\partial_t \boldsymbol{A}(t,\boldsymbol{x}) + \boldsymbol{u}(t,\boldsymbol{x}).\nabla\boldsymbol{A}(t,\boldsymbol{x}) - \nabla\boldsymbol{u}(t,\boldsymbol{x})\boldsymbol{A}(t,\boldsymbol{x}) - \boldsymbol{A}(t,\boldsymbol{x})(\nabla\boldsymbol{u}(t,\boldsymbol{x}))^T$$
$$= -\frac{4H}{\zeta}\frac{\boldsymbol{A}(t)}{1 - \mathrm{tr}(\boldsymbol{A}(t))/(bkt/H)} + \frac{4kT}{\zeta}\mathrm{Id}.$$

En injectant alors dans cette EDP l'expression suivante de $\boldsymbol{A}$ obtenue à partir de l'expression de $\boldsymbol{\tau}_p$:

$$\boldsymbol{A} = \frac{1}{HZ(\mathrm{tr}(\boldsymbol{\tau}_p))}\left(\frac{\boldsymbol{\tau}_p}{n_p} + kT\mathrm{Id} \right),$$

où Z est défini par (1.21), on obtient l'équation suivante sur $\boldsymbol{\tau}_p$:

$$\frac{\zeta}{4H} \left(\partial_t \boldsymbol{\tau}_p(t, \boldsymbol{x}) + \boldsymbol{u}(t, \boldsymbol{x}).\nabla \boldsymbol{\tau}_p(t, \boldsymbol{x}) - \nabla \boldsymbol{u}(t, \boldsymbol{x}) \boldsymbol{\tau}_p(t, \boldsymbol{x}) - \boldsymbol{\tau}_p(t, \boldsymbol{x})(\nabla \boldsymbol{u}(t, \boldsymbol{x}))^T \right)$$

$$+ Z(\mathrm{tr}(\boldsymbol{\tau}_p)) \boldsymbol{\tau}_p - \frac{\zeta}{4H} \left(\boldsymbol{\tau}_p + n_p kT \mathrm{Id} \right) (\partial_t + \boldsymbol{u}.\nabla) \ln(Z(\mathrm{tr}(\boldsymbol{\tau}_p)))$$

$$= n_p kT \frac{\zeta}{4H} \left(\nabla \boldsymbol{u}(t, \boldsymbol{x}) + (\nabla \boldsymbol{u}(t, \boldsymbol{x}))^T \right),$$

qui est exactement le modèle FENE-P (1.20) introduit précédemment, en prenant toujours pour λ et η_p les expressions (1.47) et (1.48).

Le modèle FENE-P n'est qu'une approximation du modèle FENE, faite pour obtenir un modèle macroscopique. On observe des différences qualitatives importantes entre ces deux modèles notamment dans des écoulements transitoires (cf. [89]). On renvoie également à [44] pour une discussion des effets de ce type d'approximation pour des écoulements élongationnels. Plusieurs améliorations du modèle FENE-P ont d'ailleurs été proposées (cf. [13] page 89, [29] et le modèle FENE-CR, ou [104] et le modèle FENE-L(S)).

Notons que ces approximations de fermeture peuvent avoir un intérêt dans le cadre des simulations micro-macro car les solutions des EDP obtenues peuvent servir de variable de contrôle pour réduire la variance des résultats (cf. section 1.2.2.2).

1.1.4.2   L'équation de Fokker Planck

Il n'est pas nécessaire de connaître la loi du processus $(\boldsymbol{X}_t)_{t \geq 0}$ pour calculer le tenseur des contraintes $\boldsymbol{\tau}_p$: seules suffisent les lois marginales (c'est-à-dire les lois des variables aléatoires $\boldsymbol{X}_t$, pour $t \geq 0$). Or, on sait que ces lois sont solutions de l'équation de Fokker Planck associée à l'EDS. Ainsi, on peut réécrire le problème (1.51) sous la forme :

$$\begin{cases} \mathrm{Re} \left(\partial_t \boldsymbol{u}(t, \boldsymbol{x}) + \boldsymbol{u}(t, \boldsymbol{x}).\nabla \boldsymbol{u}(t, \boldsymbol{x}) \right) - (1 - \epsilon)\Delta \boldsymbol{u}(t, \boldsymbol{x}) + \nabla p(t, \boldsymbol{x}) \\ \qquad = \mathrm{div} \left(\boldsymbol{\tau}_p(t, \boldsymbol{x}) \right) + \boldsymbol{f}(t, \boldsymbol{x}), \\ \mathrm{div} \left(\boldsymbol{u}(t, \boldsymbol{x}) \right) = 0, \\ \boldsymbol{\tau}_p(t, \boldsymbol{x}) = \dfrac{\epsilon}{\mathrm{We}} \left(\displaystyle\int_{\boldsymbol{X}} (\boldsymbol{X} \otimes \boldsymbol{F}(\boldsymbol{X})) \psi(t, \boldsymbol{x}, \boldsymbol{X}) \, d\boldsymbol{X} - \mathrm{Id} \right), \\ \partial_t \psi(t, \boldsymbol{x}, \boldsymbol{X}) + \boldsymbol{u}.\nabla_{\boldsymbol{x}} \psi(t, \boldsymbol{x}, \boldsymbol{X}) \\ \qquad = -\mathrm{div}_{\boldsymbol{X}} \left(\left(\nabla \boldsymbol{u}(t, \boldsymbol{x}) \boldsymbol{X} - \dfrac{1}{2\mathrm{We}} \boldsymbol{F}(\boldsymbol{X}) \right) \psi(t, \boldsymbol{x}, \boldsymbol{X}) \right) + \dfrac{1}{2\mathrm{We}} \Delta_{\boldsymbol{X}} \psi(t, \boldsymbol{x}, \boldsymbol{X}). \end{cases}$$
$$(1.57)$$

On sait que si $(\boldsymbol{u}(t, \boldsymbol{x}), p(t, \boldsymbol{x}), \boldsymbol{X}_t(\boldsymbol{x}))$ est solution de (1.51) et que $\boldsymbol{X}_t(\boldsymbol{x})$ admet une densité de probabilité $\psi(t, \boldsymbol{x}, \boldsymbol{X})$, alors $(\boldsymbol{u}(t, \boldsymbol{x}), p(t, \boldsymbol{x}), \psi(t, \boldsymbol{x}, \boldsymbol{X}))$ est solution de (1.57). La réciproque n'est pas aussi évidente, étant donné que l'information contenue dans la fonction ψ est moins importante que l'information contenue dans le processus $(\boldsymbol{X}_t)_{t \geq 0}$.

Si on est intéressé par la densité de probabilité à l'équilibre, c'est-à-dire par la solution stationnaire de l'équation de Fokker-Planck pour $\boldsymbol{u} = 0$, il faut se souvenir que la force $\boldsymbol{F}$ dérive d'un potentiel Π (cf. (1.42)). Il est alors facile de vérifier qu'une solution stationnaire est donnée par

$$\psi_{\text{eq}}(\boldsymbol{X}) = C \exp(-\Pi(\boldsymbol{X})) \tag{1.58}$$

où $C = \left(\int_{\boldsymbol{X}} \exp(-\Pi(\boldsymbol{X})) \, d\boldsymbol{X} \right)^{-1}$ est une constante de normalisation. Noter que cette solution stationnaire est bien en accord avec la densité de probabilité à l'équilibre ϕ_{eq} (définie par (1.30) dans le cas hookéen) qui était à l'origine de l'expression de la force $\boldsymbol{F}$. En fait cette solution est mieux que stationnaire : elle est réversible (on dit aussi symétrique). Cela signifie qu'elle vérifie la relation d'équilibre détaillé :

$$-\boldsymbol{F}(\boldsymbol{X})\psi_{\text{eq}}(\boldsymbol{X}) + \nabla_{\boldsymbol{X}} \psi_{\text{eq}}(\boldsymbol{X}) = 0. \tag{1.59}$$

Le fait que l'on qualifie cette solution de réversible provient du fait que si le processus $\boldsymbol{X}_t$ solution de l'EDS associée à l'équation de Fokker-Planck a pour condition initiale une variable aléatoire de densité ψ_{eq}, alors la loi de $(\boldsymbol{X}_t, \boldsymbol{X}_{t+\delta})$ est égale à la loi de $(\boldsymbol{X}_t, \boldsymbol{X}_{t-\delta})$. Ceci peut se démontrer facilement en suivant, par exemple, les arguments de Rogers dans [135] (cf. aussi [84]). On comprend également que cette densité stationnaire soit associée à l'idée d'équilibre car il est naturel qu'à l'équilibre, on ne voie pas la flèche du temps.

Remarquons que l'on peut encore identifier une solution stationnaire réversible dans le cas d'un écoulement stationnaire homogène potentiel (on dit qu'un écoulement est potentiel si le champ de vitesse s'écrit $\boldsymbol{u}(t,\boldsymbol{x}) = \nabla\phi(t,\boldsymbol{x})$ où $\phi : \mathbb{R}^+ \times \mathcal{D} \to \mathbb{R}$), c'est-à-dire si

$$\boldsymbol{u}(t,\boldsymbol{x}) = \boldsymbol{\kappa}\boldsymbol{x},$$

avec $\boldsymbol{\kappa}$ une matrice symétrique. En effet, dans ce cas, le terme de dérive dans l'EDS $\left(\boldsymbol{\kappa}\boldsymbol{X} - \frac{1}{2\text{We}}\boldsymbol{F}(\boldsymbol{X}) \right)$ dérive du potentiel $\widetilde{\Pi}(\boldsymbol{X}) = \frac{1}{2}(\boldsymbol{\kappa}\boldsymbol{X}.\boldsymbol{X}) - \frac{1}{2\text{We}}\Pi(\boldsymbol{X})$ et la solution stationnaire réversible est donc donnée par :

$$\widetilde{\psi_{\text{eq}}}(\boldsymbol{X}) = C \exp(-\Pi(\boldsymbol{X})) \exp(\text{We}\,(\boldsymbol{\kappa}\boldsymbol{X}.\boldsymbol{X})) \tag{1.60}$$

où C est une constante de normalisation. On a rencontré un exemple d'écoulement homogène potentiel stationnaire dans la section 1.1.1.2 avec les écoulements élongationnels stationnaires.

Par contre, dans le cas d'un écoulement stationnaire quelconque (non homogène potentiel), la solution stationnaire n'est pas *a priori* réversible, ce qui a des implications sur des propriétés du type convergence vers l'équilibre (cf. section 1.2.2.1).

1.1.4.3   L'équation de Feynman-Kac

Une dernière manière naturelle d'essayer de résoudre le problème (1.51) par des méthodes de type EDP est de chercher l'équation de Feynman-Kac vérifiée par le

tenseur des contraintes. On peut vérifier que

$$\boldsymbol{\tau}_p(t, \boldsymbol{x}) = \frac{\epsilon}{\mathrm{We}} \left(\mathbb{E}(\boldsymbol{T}^t(t, \boldsymbol{x}, \boldsymbol{X}_0)) - \mathrm{Id} \right)$$

où $\boldsymbol{T}^t(s, \boldsymbol{x}, \boldsymbol{X})$ (à valeurs dans $\mathbb{R}^{d \times d}$) vérifie l'EDP suivante, pour tout $0 \leq s \leq t$:

$$\begin{cases} \partial_s \boldsymbol{T}^t(s, \boldsymbol{x}, \boldsymbol{X}) - \boldsymbol{u}(t-s, \boldsymbol{x}).\nabla_{\boldsymbol{x}} \boldsymbol{T}^t(s, \boldsymbol{x}, \boldsymbol{X}) \\ \qquad = \left(\nabla \boldsymbol{u}(t-s, \boldsymbol{x}) \boldsymbol{X} - \frac{1}{2We} \boldsymbol{F}(\boldsymbol{X}) \right) . \nabla_{\boldsymbol{X}} \boldsymbol{T}^t(s, \boldsymbol{x}, \boldsymbol{X}) + \frac{1}{2We} \Delta_{\boldsymbol{X}} \boldsymbol{T}^t(s, \boldsymbol{x}, \boldsymbol{X}), \\ \boldsymbol{T}^t(0, \boldsymbol{x}, \boldsymbol{X}) = \boldsymbol{X} \otimes \boldsymbol{F}(\boldsymbol{X}). \end{cases}$$

$$(1.61)$$

Cette méthode n'est pas utilisable en pratique, car elle ne permet pas complètement d'éliminer des espérances (il reste à moyenner sur les conditions initiales) et car elle nécessiterait à chaque pas de temps un nouveau calcul complet (pour $0 \leq s \leq t$) de la fonction $\boldsymbol{T}^t$ (sauf dans le cas d'écoulements homogènes, pour lesquels $\boldsymbol{T}^t$ ne dépend pas de la variable de position $\boldsymbol{x}$). Elle a cependant le mérite de mettre à nouveau en évidence le fait que la valeur du tenseur des contraintes à l'instant t au point $\boldsymbol{x}$ dépend de toute l'histoire de la déformation du fluide le long des trajectoires aboutissant en $\boldsymbol{x}$ à l'instant t (cf. les termes contenant $\boldsymbol{u}(t-s, \boldsymbol{x})$ dans (1.61)).

Nous terminons cette section de présentation des modèles pour les fluides polymériques par un schéma récapitulant les interactions entre modèles macroscopiques et modèles microscopiques (cf. figure 1.11), et en donnant des indications sur les méthodes numériques employées pour les discrétiser, ce qui sera développé dans la section suivante.
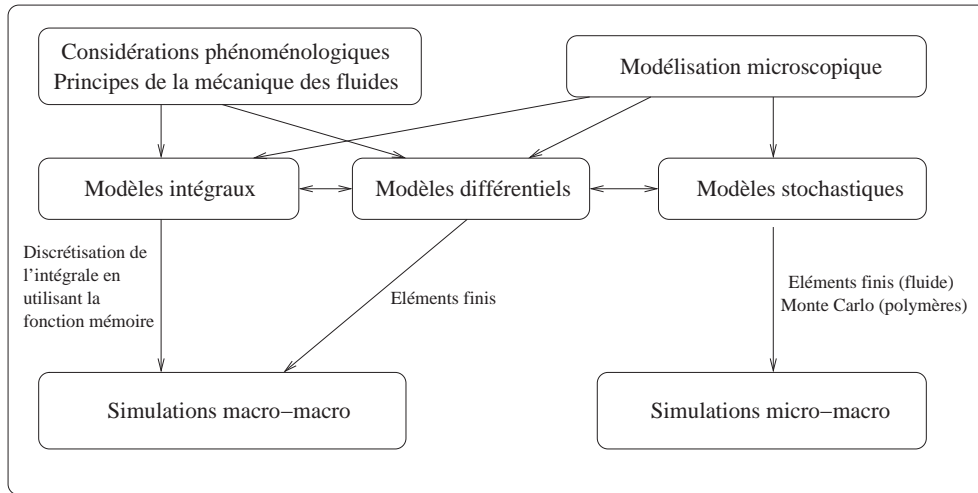
FIG. 1.11 – Les simulations macroscopiques (ou simulations macro-macro) couplent un modèle différentiel ou intégral sur $\boldsymbol{\tau}_p$ avec l'équation sur la vitesse. Les simulations micro-macro couplent des modèles moléculaires pour calculer $\boldsymbol{\tau}_p$ avec l'équation sur la vitesse.

1.2 Résultats mathématiques et numériques

Dans cette section, nous nous intéressons aux résultats mathématiques obtenus sur les modèles de fluides viscoélastiques présentés précédemment. Nous nous concentrerons sur les modèles différentiels (cf. section 1.1.2.1), et les modèles micro-macro (cf. section 1.1.3), les modèles intégraux (cf. section 1.1.2.2) ayant été beaucoup moins étudiés, aussi bien du point de vue numérique que mathématique, étant données les difficultés posées par leur implémentation (cf. chapitre 6 de [122]). Signalons simplement que certaines méthodes numériques sont basées sur une discrétisation de l'intégrale en temps du type méthode des trapèzes en tenant compte du fait que la fonction mémoire $M(t)$ tend exponentiellement vite vers zéro quand $t \to \infty$ et un calcul du tenseur de Finger $\boldsymbol{C}_t^{-1}$ pour différents instants t en utilisant le fait que la dérivée sur-convectée (par rapport à t) de ce tenseur est nulle (cf. section 1.1.2.2).

Nous nous proposons tout d'abord de résumer les difficultés mathématiques communes à ces modèles (micro-macro ou macroscopiques). Tout d'abord, ces systèmes contiennent les équations de Navier-Stokes (du moins si $\eta_s \neq 0$), avec un terme de force supplémentaire (div $(\boldsymbol{\tau}_p)$) (cf. les équations (1.2)–(1.3)–(1.12)). L'équation sur $\boldsymbol{\tau}_p$ est essentiellement une équation de transport et, formellement, $\boldsymbol{\tau}_p$ a la régularité de $\nabla \boldsymbol{u}$, ce qui fait que le terme div $(\boldsymbol{\tau}_p)$ au second membre de l'équation sur la vitesse apporte au mieux un peu plus de viscosité (le fait que $\boldsymbol{\tau}_p$ a la régularité de $\nabla \boldsymbol{u}$ se retrouvera à la fois dans les espaces fonctionnels utilisés dans les preuves d'existence-unicité, et dans le choix des espaces d'approximations). On s'attend donc à rencontrer au moins autant de difficultés dans l'étude de ces systèmes d'équations que pour *les équations de Navier-Stokes*, pour lesquelles on sait prouver l'existence de solutions faibles globales, mais les questions de l'unicité des solutions faibles et de l'existence de solutions fortes globales restent ouvertes. Aux difficultés inhérentes aux équations de Navier-Stokes (c'est-à-dire essentiellement au terme $\boldsymbol{u}.\nabla \boldsymbol{u}$) s'ajoutent des problèmes posés par les équations sur $\boldsymbol{\tau}_p$ ((1.16) pour les modèles différentiels et (1.41)–(1.43) pour les modèles moléculaires). Tout d'abord, ces équations contiennent *un terme de transport* ($\boldsymbol{u}.\nabla \boldsymbol{\tau}_p$ dans les modèles différentiels, $\boldsymbol{u}.\nabla \boldsymbol{X}_t$ dans les modèles moléculaires) sans terme de diffusion. Par ailleurs, les équations donnant $\boldsymbol{\tau}_p$ contiennent *un terme multiplicatif contenant* $\nabla \boldsymbol{u}$ ($\nabla \boldsymbol{u} \boldsymbol{\tau}_p$ pour les modèles différentiels, ou $\nabla \boldsymbol{u} \boldsymbol{X}_t$ pour les modèles moléculaires) dont la non-linéarité est difficile à traiter. Signalons enfin que les modèles qui permettent de décrire qualitativement les propriétés des fluides polymériques contiennent *des non-linéarités supplémentaires* dans les équations définissant $\boldsymbol{\tau}_p$ (la fonction $\boldsymbol{T}$ dans (1.16) pour les modèles différentiels ou la force $\boldsymbol{F}$ dans (1.41) pour les modèles moléculaires).

En résumé, les difficultés mathématiques sont de quatre types :

(i) terme de Navier $\boldsymbol{u}.\nabla \boldsymbol{u}$ dans l'équation sur $\boldsymbol{u}$,

(ii) terme de transport dans les équations définissant $\boldsymbol{\tau}_p$,

(iii) terme multiplicatif du type $\nabla \boldsymbol{u} \boldsymbol{\tau}_p$ ou $\nabla \boldsymbol{u} \boldsymbol{X}_t$ dans les équations définissant $\boldsymbol{\tau}_p$,

(iv) non-linéarité "interne" dans les équations définissant $\boldsymbol{\tau}_p$.

Ces quatre difficultés conduisent en général, sur les problèmes dépendant du temps, à des résultats d'existence partiels du type existence de solutions fortes (voire à régularité $\mathcal{C}^k$) en temps petit. Par ailleurs, elles ont également des implications numériques (difficultés de convergence, choix d'espaces de discrétisation,...).

Nous résumerons tout d'abord rapidement les principaux résultats mathématiques et numériques obtenus sur les modèles macroscopiques. Nous présenterons ensuite les travaux numériques de diverses équipes sur les modèles moléculaires, ainsi que notre travail d'analyse mathématique de ces modèles et des méthodes numériques, et notamment les questions spécifiques qu'ils posent (existence de solutions à des EDS avec des termes de dérive explosifs, analyse de la variance des résultats,...).

1.2.1 Modèles macroscopiques

Concernant l'analyse mathématique des modèles macroscopiques, nous renvoyons à l'ouvrage de M. Renardy [133]. Pour les méthodes numériques, nous renvoyons aux articles de revue [4,88] et à l'ouvrage de R.G. Owens et T.N. Phillips [122] pour les développements les plus récents.

Pour plus de clarté, on rappelle ici le modèle macroscopique le plus simple, à savoir le modèle du type sur-convecté (écrit ici sous forme adimensionnée, cf. (1.2)–(1.3)–(1.12)–(1.15)) :

$$
\begin{cases}
\text{Re}\,(\partial_t \boldsymbol{u} + \boldsymbol{u}.\nabla \boldsymbol{u}) - (1-\epsilon)\Delta \boldsymbol{u} + \nabla p = \text{div}\,(\boldsymbol{\tau}_p) + \boldsymbol{f}, \\
\text{div}\,(\boldsymbol{u}) = 0, \\
\text{We}\,\left(\partial_t \boldsymbol{\tau}_p + \boldsymbol{u}.\nabla \boldsymbol{\tau}_p - \nabla \boldsymbol{u} \boldsymbol{\tau}_p - \boldsymbol{\tau}_p (\nabla \boldsymbol{u})^T\right) + \boldsymbol{\tau}_p = \epsilon \dot{\boldsymbol{\gamma}},
\end{cases}
\tag{1.62}
$$

où $\dot{\boldsymbol{\gamma}}$ est défini par (1.4). Pour la définition des nombres adimensionnels, on renvoie à (1.49). On rappelle que $\epsilon \in (0,1]$, le cas $\epsilon = 1$ correspondant au modèle de Maxwell, et $\epsilon \in (0,1)$ au modèle de Oldroyd-B.

1.2.1.1 Résultats mathématiques

Concernant l'existence de solutions pour les modèles macroscopiques différentiels, on trouve dans la littérature essentiellement quatre types de résultats sur le problème couplé :
- des résultats en temps petits (perturbations de la condition initiale),
- des résultats en temps long avec données petites (perturbation de l'équilibre),
- des résultats d'existence de solutions stationnaires perturbations de l'équilibre,
- des résultats d'existence de solutions stationnaires perturbations de solutions des équations de Navier-Stokes stationnaires.

A titre d'exemple, citons simplement le résultat obtenu par M. Renardy dans [130]. L'auteur considère le problème couplé suivant, posé dans un domaine $\mathcal{D}$ borné de $\mathbb{R}^3$:

$$\begin{cases} \rho\left(\partial_t \boldsymbol{u} + \boldsymbol{u}.\nabla \boldsymbol{u}\right) = \operatorname{div} \boldsymbol{\tau}_p - \nabla p + \boldsymbol{f}, \\ \operatorname{div}\left(\boldsymbol{u}\right) = 0, \\ \left(\partial_t + \boldsymbol{u}.\nabla\right)\left(\boldsymbol{\tau}_p\right)_{i,j} = \boldsymbol{A}_{i,j,k,l}(\boldsymbol{\tau}_p)\dfrac{\partial \boldsymbol{u}_k}{\partial \boldsymbol{x}_l} + \boldsymbol{g}_{i,j}(\boldsymbol{\tau}_p), \end{cases} \tag{1.63}$$

où on utilise la convention de sommation sur les indices répétés dans la dernière équation. Noter qu'on considère ici un fluide sans viscosité ($\eta_s = 0$). Le système est complété de conditions aux limites de Dirichlet homogènes sur la vitesse $\boldsymbol{u}$, ainsi que de conditions initiales. Noter que les modèles différentiels rencontrés dans la section 1.1.2.1 rentrent bien dans ce cadre général. L'auteur introduit ensuite le tenseur d'ordre 4 :

$$\boldsymbol{C}_{i,j,k,l} = \boldsymbol{A}_{i,j,k,l} - (\boldsymbol{\tau}_p)_{i,l}\delta_{k,j}, \tag{1.64}$$

où δ désigne le symbole de Kronecker, et fait l'hypothèse d'ellipticité forte suivante sur $\boldsymbol{C}$: $\forall \zeta, \eta \in \mathbb{R}^3$

$$\boldsymbol{C}_{i,j,k,l}(\boldsymbol{\tau}_p)\zeta_i\zeta_k\eta_j\eta_l \geq \kappa|\zeta|^2|\eta|^2 \tag{1.65}$$

avec $\kappa > 0$ une constante ne dépendant pas de $\boldsymbol{\tau}_p$. Sous des hypothèses supplémentaires de symétrie sur le tenseur $\boldsymbol{A}$ et de régularité ou compatibilité sur les conditions initiales, l'auteur montre :

Théorème 1 (M. Renardy [130]) *Il existe un temps $T' > 0$, tel que le système (1.63) admette une unique solution de régularité :*

$$\boldsymbol{u} \in \bigcap_{k=0}^{4} \mathcal{C}^k([0, T'], H^{4-k}(\mathcal{D}), \; \boldsymbol{\tau}_p \in \bigcap_{k=0}^{3} \mathcal{C}^k([0, T'], H^{3-k}(\mathcal{D}).$$

Nous renvoyons également aux travaux de C. Guillopé et J.C. Saut [71, 72] notamment pour l'analyse du cas où $\eta_s \neq 0$, qui permet d'obtenir des résultats dans des espaces un peu moins réguliers que dans le théorème précédent.

Signalons qu'il existe par ailleurs une littérature importante sur les questions de stabilité des écoulements de fluides viscoélastiques, et du changement de type des équations. Nous renvoyons à [133] et à [122] pour les détails et une bibliographie sur ces sujets. Voir aussi l'article de revue [45].

1.2.1.2 Méthodes numériques

La plupart des méthodes numériques qui ont été développées sur le problème couplé macroscopique dépendant du temps sont de type éléments finis (cf. cependant [122] pour des méthodes spectrales) et consistent, à chaque pas de temps, à résoudre d'abord le problème sur la vitesse, à contrainte fixée, puis à résoudre le problème sur la contrainte, à vitesse fixée. Donnons les principales difficultés posées par la discrétisation d'un système du type (1.62).

Une première difficulté numérique provient de *la condition du type inf-sup* qui doit être vérifiée entre les trois espaces où l'on discrétise respectivement la vitesse, la pression et le tenseur des contraintes (cf. [16]). Plus précisément, à la condition de compatibilité classique entre l'espace en vitesse et l'espace en pression s'ajoute une condition de compatibilité supplémentaire entre l'espace en vitesse et l'espace en contraintes, cette condition provenant du fait que l'on veut une propriété de stabilité même dans la limite η_s petit par rapport à η_p (c'est-à-dire ϵ tend vers 1). Cette compatibilité nécessaire entre les trois espaces d'approximation a été analysée sur le système de Stokes à trois champs :

$$\begin{cases} -\eta_s \Delta \boldsymbol{u} + \nabla p - \text{div} (\boldsymbol{\tau}_p) = \boldsymbol{f}, \\ \text{div} (\boldsymbol{u}) = 0, \\ \boldsymbol{\tau}_p - \eta_p \dot{\boldsymbol{\gamma}} = \boldsymbol{g}, \end{cases} \tag{1.66}$$

où les inconnues sont $(\boldsymbol{u}, p, \boldsymbol{\tau}_p)$ et où $\eta_s \geq 0$ et $\eta_p > 0$. Plusieurs méthodes ont été proposées pour approximer ce problème correctement :

- Utiliser des espaces qui vérifient les conditions inf-sup. Ces espaces sont en général assez compliqués à implémenter (cf. par exemple [110]),
- Introduire une inconnue supplémentaire pour éviter la condition de compatibilité entre l'espace d'approximation de la vitesse et l'espace d'approximation du tenseur des contraintes (cf. la méthode EVSS dans [68]),
- Utiliser une méthode type *Galerkin Least Square* (cf. section 1.A.1) pour pouvoir choisir des espaces de discrétisation quelconques pour les trois inconnues (cf. [16]).

Si $\eta_s > 0$, il n'est pas *a priori* nécessaire d'ajouter une relation de compatibilité entre l'espace d'approximation de la vitesse et l'espace d'approximation du tenseur des contraintes. Ceci dit, dès que η_s est petit par rapport à η_p, on rencontre des difficultés numériques, qui nécessitent de vérifier ces relations de compatibilité.

Une deuxième difficulté numérique provient *des termes d'advection*, à la fois dans l'équation en vitesse et dans l'équation sur $\boldsymbol{\tau}_p$. Plusieurs techniques permettent de traiter cette difficulté : utilisation de méthodes de stabilisation type SUPG, utilisation d'une méthode type *Discontinuous Galerkin* (cf. [49]), ou encore utilisation de la méthode des caractéristiques (cf. [16] ou la méthode *Backward-tracking Lagrangian Particle Method* [150]). On renvoie au chapitre 7 de [122] et à [90] pour des références sur ces différentes méthodes dans le cadre de la simulation des fluides viscoélastiques (cf. aussi [114] pour une comparaison de différents schémas). Cette difficulté apparaît notamment pour des grands nombres de Reynolds (une limite qui est rarement étudiée en pratique) ou pour des grands nombres de Weissenberg (qui est un cas beaucoup plus courant).

Enfin, une troisième difficulté numérique provient du *terme non-linéaire* $\nabla \boldsymbol{u} \boldsymbol{\tau}_p + \boldsymbol{\tau}_p (\nabla \boldsymbol{u})^T$ dans la dérivée convective de $\boldsymbol{\tau}_p$. Dans la plupart des schémas numériques, il semble que ce terme est rendu explicite en prenant sa valeur en temps précédent. Linéariser ce terme en explicitant la vitesse et en implicitant la contrainte conduit d'ailleurs à un problème mal posé si le nombre de Weissenberg n'est pas suffisamment

petit ([125]).

En résumé, la discrétisation d'une équation du type (1.62) pose trois difficultés, qui sont reliées aux difficultés mathématiques des modèles (cf. page 44) :

(i) Compatibilité des espaces d'approximation vitesse, pression, contrainte,

(ii) Traitement des termes d'advection,

(iii) Traitement des termes non-linéaires dans l'équation sur $\boldsymbol{\tau}_p$.

En plus de ces difficultés, la simulation est assez coûteuse puisque l'on doit calculer trois champs de solution, si bien que la plupart des simulations numériques de fluides viscoélastiques ont pour le moment été faites en dimension $d = 2$.

Nous avons vu que deux de ces trois difficultés numériques sont exacerbées pour des grands nombres de Weissenberg. D'ailleurs, une littérature importante est consacrée aux *High Weissenberg Number Problem* (cf. notamment le chapitre 7 de [122]), qui se manifeste en pratique par la non-convergence des discrétisations quand le nombre de Weissenberg augmente, et dont l'origine n'est sans doute pas seulement numérique. On a en effet parfois observé sur certaines géométries que le nombre de Weissenberg maximum permettant la convergence de la discrétisation diminue avec le pas du maillage (cf. [90]), ce qui semblerait indiquer un défaut de régularité de la solution continue elle-même (cf. [136] à ce sujet). Il est donc possible que certaines difficultés pour les grands nombres de Weissenberg proviennent du modèle lui-même, qui induit des phénomènes de couches limites, ou des singularités au voisinage des coins rentrants. Ces aspects ont notamment été étudiés numériquement dans des écoulements autour d'un cylindre ou dans une contraction (cf. figure 1.5). Concernant l'étude de l'asymptotique We $\rightarrow \infty$, on renvoie au chapitre 6 de [133].

En guise de transition avec la section suivante, signalons que les modèles micro-macro n'apportent pas *a priori* de solutions aux difficultés évoquées ci-dessus. En particulier, le traitement des termes d'advection reste problématique, de même que la discrétisation des non-linéarités dans l'EDS. Par ailleurs, on sait que certains modèles micro-macro sont équivalents à des modèles macroscopiques (cf. section 1.1.4.1), et comme certaines des difficultés mentionnées ci-dessus semblent liées aux propriétés des solutions du problème continu, on ne s'attend pas à ce qu'elles soient résolues par l'approche micro-macro. Signalons toutefois que dans certains cas, il semble que les méthodes numériques basées sur des modèles micro-macro ont permis d'obtenir des résultats avec des nombres de Weissenberg plus grands que les méthodes construites pour des modèles macroscopiques (cf. [16,28,148]). Ceci dit, comme expliqué dans la section 1.1.3.4, l'avantage principal de l'approche micro-macro reste les possibilités supplémentaires de modélisation qu'elle offre.

1.2.2 Modèles microscopiques

Les questions d'existence de solutions, de convergence des schémas numériques et de propriétés qualitatives des solutions du problème micro-macro (1.51) ont été relativement peu explorées avant ce travail. On peut néammoins citer l'article de M. Renardy [131] s'intéressant au problème formulé avec l'équation de Fokker-Planck

(cf. (1.57)) pour une certaine classe de forces $\boldsymbol{F}$. On peut également indiquer le travail de P. Degond, M. Lemou et M. Picasso [34] qui se sont intéressés à des développements asymptotiques du modèle FENE pour obtenir des modèles macroscopiques. On renvoie également à l'article de revue [93] et à [17].

La plupart des publications autour des modèles micro-macro de fluides polymériques concerne plutôt des problèmes numériques : quelles méthodes utiliser pour discrétiser le système (1.51) ? Quelles sont les résultats numériques obtenus et comment se comparent-ils à l'expérience ? L'idée de discrétiser le système par une méthode d'éléments finis pour l'équation en vitesse et pression, couplée à une méthode stochastique (Monte Carlo pour approximer l'espérance et schéma d'Euler pour l'EDS) a été proposée au début des années 1990 par M. Laso et H.C. Öttinger [97]. Cette méthode s'appelle *Calculation Of Non-Newtonian Flow : Finite Elements and Stochastic SImulation Technique* (CONNFFESSIT). Elle a au départ été utilisée avec une méthode lagrangienne sur l'EDS et *des mouvements browniens indépendants d'une trajectoire à l'autre* (cf. [98]). Typiquement, pour chaque pas de temps, l'algorithme se décompose en quatre étapes : on commence par résoudre l'équation sur $(\boldsymbol{u}, p)$, puis on calcule les mouvements macroscopiques des *dumbbells*, ensuite on intègre l'EDS le long de la trajectoire, et enfin on calcule le tenseur des contraintes $\boldsymbol{\tau}_p$ par une moyenne empirique locale sur les *dumbbells* présents dans chaque élément fini. Cette approche lagrangienne est la plus naturelle puisque c'est celle à laquelle on arrive quand on dérive le modèle (cf. section 1.1.3). Cependant, du fait du terme div $(\boldsymbol{\tau}_p)$, les résultats numériques sont alors très bruités sur la vitesse quand on utilise des mouvements browniens indépendants d'une trajectoire à l'autre. De plus, il est difficile numériquement de suivre les trajectoires de chaque *dumbbell*, et de s'assurer à chaque pas de temps qu'il y a suffisemment de *dumbbells* dans chaque élément du maillage. L'idée est ensuite apparue d'utiliser la version eulérienne de l'EDS et d'introduire des champs de vecteurs bout-à-bout : $\boldsymbol{X}_t(\boldsymbol{x})$ (cf. le concept de *Brownian Configuration Field* introduit par M.A. Hulsen, A.P.G. van Heel et B.H.A.A. van den Brule [82]). Dans cette description eulérienne, le choix le plus naturel et le plus simple est de prendre *le même mouvement brownien* en chaque point de l'espace (nous reviendrons sur ce point dans la section 1.2.2.2). Ceci a permis de réduire la variance sur la vitesse (mais curieusement pas sur la contrainte, cf. chapitre 6). La discrétisation du terme de transport peut alors être faite par une méthode *Discontinuous Galerkin* (cf. [82]) ou une méthode des caractéristiques (cf. la méthode employée par J.C. Bonvin et M. Picasso [16] ou la *Backward-Tracking Lagrangian Particle Method* de P. Wapperom, R. Keunings et V. Legat [150]). Noter que nous n'évoquons ici que les méthodes probabilistes. Il existe également des méthodes numériques basées sur la résolution de l'équation de Fokker-Planck (cf. section 1.2.2.3).

L'objectif de ce travail est d'explorer les interactions entre équations déterministes et équations stochastiques posées par l'analyse mathématique et la discrétisation d'un système du type (1.51). Plus précisément, nous nous sommes posés trois types de questions : sens, existence et propriétés mathématiques des solutions des modèles moléculaires ; convergence des méthodes numériques ; propriétés des

schémas numériques (notamment variance des solutions).

Pour plus de clarté, on rappelle ici le système micro-macro auquel on s'intéresse (cf. (1.51)) :

$$\begin{cases} \text{Re} \left(\partial_t \boldsymbol{u} + \boldsymbol{u}.\nabla \boldsymbol{u}\right) - (1-\epsilon)\Delta \boldsymbol{u} + \nabla p = \text{div}\left(\boldsymbol{\tau}_p\right) + \boldsymbol{f}, \\ \text{div}\left(\boldsymbol{u}\right) = 0, \\ \boldsymbol{\tau}_p = \dfrac{\epsilon}{\text{We}}\left(\mathbb{E}(\boldsymbol{X} \otimes \boldsymbol{F}(\boldsymbol{X})) - \text{Id}\right), \\ d\boldsymbol{X} + \boldsymbol{u}.\nabla \boldsymbol{X}\, dt = \nabla \boldsymbol{u} \boldsymbol{X}\, dt - \dfrac{1}{2\text{We}} \boldsymbol{F}(\boldsymbol{X})\, dt + \dfrac{1}{\sqrt{\text{We}}} d\boldsymbol{W}_t. \end{cases} \quad (1.67)$$

avec, $\boldsymbol{F}(\boldsymbol{X}) = \boldsymbol{X}$ dans le cas des *dumbbells* hookéens, $\boldsymbol{F}(\boldsymbol{X}) = \frac{\boldsymbol{X}}{1-||\boldsymbol{X}||^2/b}$ dans le cas des *dumbbells* FENE ou encore $\boldsymbol{F}(\boldsymbol{X}) = \frac{\boldsymbol{X}}{1-\mathbb{E}(||\boldsymbol{X}||^2)/b}$ dans le cas des *dumbbells* FENE-P. On rappelle que $\boldsymbol{x} \in \mathcal{D}$, où $\mathcal{D}$ est un domaine borné de $\mathbb{R}^d$ et on suppose dans la suite que ce système est complété de conditions aux limites sur la vitesse et de conditions initiales sur la vitesse et les processus stochastiques. Dans la suite, nous supposerons $\epsilon \in (0,1)$.

Bien que plusieurs analyses présentées dans la suite soient valables pour ce système général (cf. chapitres 6, 8), nous avons surtout étudié des simplifications de ce système : le cas des écoulements homogènes et le cas des écoulements cisaillés.

Tout d'abord, pour se concentrer sur les aspects stochastiques, nous avons étudié les équations différentielles stochastiques pour FENE et FENE-P dans le cas d'un *écoulement homogène* (cf. section 1.1.3.3). Ceci concerne les chapitres 5 et 7. On rappelle que dans ce cas, $\boldsymbol{X}$ et donc $\boldsymbol{\tau}_p$ ne dépendent pas de l'espace, si bien que résoudre le système revient en fait à résoudre l'équation différentielle stochastique sans terme de transport, pour un champ de vitesse donné $\boldsymbol{u}(t,x) = \boldsymbol{\kappa}(t)\boldsymbol{x}$ que l'on suppose solution de l'équation de Navier-Stokes. Le système qui nous intéresse dans ce cas est donc :

$$\begin{cases} \boldsymbol{\tau}_p = \dfrac{\epsilon}{\text{We}}\left(\mathbb{E}(\boldsymbol{X} \otimes \boldsymbol{F}(\boldsymbol{X})) - \text{Id}\right), \\ d\boldsymbol{X} = \boldsymbol{\kappa}(t)\boldsymbol{X}\, dt - \dfrac{1}{2\text{We}} \boldsymbol{F}(\boldsymbol{X})\, dt + \dfrac{1}{\sqrt{\text{We}}} d\boldsymbol{W}_t. \end{cases} \quad (1.68)$$

Par ailleurs, nous avons étudié le système couplé dans le cas particulier d'un *écoulement cisaillé* (cf. figure 1.1, les chapitres 2, 3, 4 et 6). Dans cette géométrie particulière, on rappelle que le système s'écrit (cf. (1.52)) :

$$\begin{cases} \text{Re}\, \partial_t u(t,y) - (1-\epsilon)\partial_{y,y} u(t,y) = \partial_y \tau(t,y) + f(t,y), \\ \tau(t,y) = \dfrac{\epsilon}{\text{We}}\mathbb{E}(X_t(y)F_Y(\boldsymbol{X}_t(y))), \\ dX_t(y) = \partial_y u(t,y) Y_t(y)\, dt - \dfrac{1}{2\text{We}} F_X(\boldsymbol{X}_t(y))\, dt + \dfrac{1}{\sqrt{\text{We}}} dV_t, \\ dY_t(y) = -\dfrac{1}{2\text{We}} F_Y(\boldsymbol{X}_t(y))\, dt + \dfrac{1}{\sqrt{\text{We}}} dW_t, \end{cases} \quad (1.69)$$

où on a noté $(X_t(y), Y_t(y))$ les composantes du processus $\boldsymbol{X}_t(y)$, (V_t, W_t) deux mouvements browniens indépendants et $(F_X(\boldsymbol{X}), F_Y(\boldsymbol{X}))$ les composantes de la force

$\boldsymbol{F}(\boldsymbol{X})$. Dans ce cas, $y \in (0, 1)$, et on suppose des conditions aux limites de Dirichlet sur la vitesse en $y = 0$ et en $y = 1$. Les conditions initiales (X_0, Y_0) sont supposées indépendantes entre elles, et indépendantes des mouvements browniens.

Remarque 10 *On suppose dans la suite que toutes les variables aléatoires sont définies sur un espace de probabilité $(\Omega, \mathcal{F}, \mathbb{P})$ muni d'une filtration $(\mathcal{F}_t)_{t \geq 0}$ vérifiant les conditions habituelles. On suppose que tous les processus sont $(\mathcal{F}_t)$-adaptés, et on note ω la variable de probabilité.*

Précisons tout de suite pourquoi il est pertinent d'étudier le modèle dans cette géométrie particulière. L'avantage principal est bien sûr que l'on fait ainsi disparaître les termes d'advection qui sont problématiques, même pour donner un sens à l'EDS (qui est en fait une EDPS dans le cas général) (cf. [100] et chapitre 6 à ce sujet). Dans la liste des difficultés associées aux modèles mathématiques des fluides polymériques, ceci fait donc disparaître les deux premiers items (cf. page 44). Cette simplification nous permet alors de nous concentrer sur les questions soulevées par le couplage entre les deux équations, une déterministe et l'autre stochastique. En particulier, nous verrons les problèmes posés par le terme $\partial_y u(t, y) Y_t(y)$ dans l'équation sur $X_t(y)$, ou encore sur l'interaction entre la variance des résultats et les matrices obtenues par discrétisation des opérateurs différentiels dans l'équation sur $u(t, y)$. Nous discuterons également l'influence d'une force explosive $\boldsymbol{F}$ du type FENE dans l'EDS. Noter que cette géométrie particulière correspond par ailleurs à un écoulement qui est souvent rencontré en pratique, et qui est utilisé expérimentalement pour caractériser les fluides (cf. figure 1.1). D'ailleurs, ce cadre d'un écoulement cisaillé a été choisi par plusieurs auteurs pour des études mathématiques et numériques (cf. [15, 72, 97] par exemple).

Signalons enfin que l'objectif de cette section n'est pas de rentrer dans les détails techniques des preuves (on renvoie aux chapitres suivants pour cela) mais plutôt de donner les principaux résultats de manière formelle.

1.2.2.1 Analyse mathématique

Pour étudier ces systèmes micro-macro, nous avons adopté une démarche variationnelle, en cherchant des estimées *a priori* sur le système et en utilisant ensuite une méthode de Galerkin. Cette approche présente l'avantage de permettre de traiter à la fois des questions théoriques d'existence de solution et des questions plus pratiques de convergence des schémas numériques du type éléments finis.

Signalons par ailleurs que nous cherchons des solutions telles que l'EDP sur u dans (1.69) soit vérifiée au moins au sens des distributions, et telles que les EDS soient vérifiées *presque partout en espace* (ainsi que pour presque tout temps et presque sûrement). Ceci implique que nous demandons une régularité minimale sur u telle que d'une part, le terme $\partial_y u$ dans l'EDS ait un sens presque partout en espace et pour presque tout temps, et telle que d'autre part, la contrainte τ construite à partir des solutions de l'EDS s'identifie bien à une distribution (ce qui revient

essentiellement à demander de l'intégrabilité locale en espace et en temps sur τ).
Ces hypothèses sont bien vérifiées dans les cas hookéens et FENE.

Une estimée d'énergie fondamentale

Toutes les analyses que nous avons conduites reposent sur une estimée d'énergie qui est obtenue (formellement du moins) d'une part en multipliant l'équation sur $\boldsymbol{u}$ dans (1.67) par $\boldsymbol{u}$ puis en intégrant en espace et en temps, et d'autre part en faisant un calcul d'Itô sur $\Pi(\boldsymbol{X}_t)$, en intégrant en espace et en temps puis en prenant l'espérance (on rappelle que Π est le potentiel de la force $\boldsymbol{F}$). Formellement, en supposant des conditions aux limites de Dirichlet homogène sur $\boldsymbol{u}$ et une force extérieure $\boldsymbol{f}$ nulle, on obtient pour l'estimation associée à la vitesse :

$$\frac{\mathrm{Re}}{2} \int_{\mathcal{D}} |\boldsymbol{u}|^2(t,\boldsymbol{x}) + (1-\epsilon) \int_0^t \int_{\mathcal{D}} |\nabla\boldsymbol{u}|^2(s,\boldsymbol{x})$$
$$= \frac{\mathrm{Re}}{2} \int_{\mathcal{D}} |\boldsymbol{u}|^2(0,\boldsymbol{x}) - \frac{\epsilon}{\mathrm{We}} \int_0^t \int_{\mathcal{D}} \mathbb{E}(\boldsymbol{X}_s(\boldsymbol{x}) \otimes \boldsymbol{F}(\boldsymbol{X}_s(\boldsymbol{x}))) : \nabla\boldsymbol{u}(s,\boldsymbol{x}). \quad (1.70)$$

Par ailleurs, un calcul d'Itô permet d'obtenir (toujours formellement) :

$$\int_{\mathcal{D}} \mathbb{E}(\Pi(\boldsymbol{X}_t(\boldsymbol{x}))) + \frac{1}{2\mathrm{We}} \int_0^t \int_{\mathcal{D}} \mathbb{E}(||\boldsymbol{F}(\boldsymbol{X}_s(\boldsymbol{x}))||^2)$$
$$= \int_{\mathcal{D}} \mathbb{E}(\Pi(\boldsymbol{X}_0(\boldsymbol{x}))) + \int_0^t \int_{\mathcal{D}} \mathbb{E}(\boldsymbol{F}(\boldsymbol{X}_s(\boldsymbol{x})).\nabla\boldsymbol{u}(s,\boldsymbol{x})\boldsymbol{X}_s(\boldsymbol{x})) + \frac{1}{2\mathrm{We}} \int_0^t \int_{\mathcal{D}} \Delta\Pi(\boldsymbol{X}_s(\boldsymbol{x})).$$

En additionnant ces deux égalités et utilisant le fait que

$$\mathbb{E}(\boldsymbol{X}_s(\boldsymbol{x}) \otimes \boldsymbol{F}(\boldsymbol{X}_s(\boldsymbol{x}))) : \nabla\boldsymbol{u}(s,\boldsymbol{x}) = \mathbb{E}(\boldsymbol{F}(\boldsymbol{X}_s(\boldsymbol{x})).\nabla\boldsymbol{u}(s,\boldsymbol{x})\boldsymbol{X}_s(\boldsymbol{x})), \quad (1.71)$$

on obtient alors, après dérivation en temps :

$$\frac{\mathrm{Re}}{2} \frac{d}{dt} \int_{\mathcal{D}} |\boldsymbol{u}|^2(t,\boldsymbol{x}) + (1-\epsilon) \int_{\mathcal{D}} |\nabla\boldsymbol{u}|^2(t,\boldsymbol{x}) + \frac{\epsilon}{\mathrm{We}} \frac{d}{dt} \int_{\mathcal{D}} \mathbb{E}(\Pi(\boldsymbol{X}_t(\boldsymbol{x})))$$
$$+ \frac{\epsilon}{2\mathrm{We}^2} \int_{\mathcal{D}} \mathbb{E}(||\boldsymbol{F}(\boldsymbol{X}_t(\boldsymbol{x}))||^2) = \frac{\epsilon}{2\mathrm{We}^2} \int_{\mathcal{D}} \Delta\Pi(\boldsymbol{X}_t(\boldsymbol{x})). \quad (1.72)$$

Le principal inconvénient de cette estimée est la présence du terme (positif du fait de la convexité de Π) dans le membre de droite, et qui interdit par exemple toute étude du comportement en temps long (cf. le paragraphe consacré à cette question ci-dessous). Noter par ailleurs que cette estimée permet seulement de contrôler la norme $H_{\boldsymbol{x}}^1$ de $\boldsymbol{u}$ et on peut donc s'attendre à des difficultés pour passer à la limite dans le terme non-linéaire $\nabla\boldsymbol{u}\boldsymbol{X}$ dans l'EDS. Nous avons utilisé cette estimée dans le cas des *dumbbells* hookéens et des *dumbbells* FENE pour étudier l'existence et l'unicité des solutions au problème couplé, ainsi que la convergence du schéma numérique, dans le cas de l'écoulement cisaillé pour le modèle hookéen.

Le cas des dumbbells hookéens dans un écoulement cisaillé (cf. chapitre 2)

Dans le cas des *dumbbells* hookéens dans un écoulement cisaillé, on obtient en fait l'existence et l'unicité de solution au système (1.69) sur un intervalle de temps $[0, T]$ avec T arbitraire et pour toute donnée. La solution est une solution faible : $u \in L_t^\infty(L_y^2) \cap L_t^2(H_{0,y}^1)$. Ce résultat peut surprendre quand on le compare à tous les résultats en temps petit habituellement obtenus, par exemple sur les modèles type Oldroyd-B. Il est en fait dû à une spécificité du modèle hookéen dans cette géométrie : pour une force linéaire, la composante Y_t ne dépend pas de X_t (car $F_Y(\boldsymbol{X}_t) = Y_t$, cf. (1.69)) et donc, le terme $\partial_y u(t, y) Y_t$ dans l'EDS sur X_t est un terme linéaire. Un corollaire de cette propriété est que le processus Y_t est un processus d'Ornstein-Uhlenbeck indépendant de la variable d'espace y et non couplé aux équations sur u et X. De plus, nous savons que le modèle hookéen a un équivalent macroscopique ce qui se traduit ici par le fait que l'on peut donner une formule explicite reliant τ à u (cf. la relation (2.23) dans le chapitre 2). La preuve d'existence et d'unicité de la solution dans ce cas est donc très simple. Par ailleurs, du fait de la linéarité du système, on obtient des solutions plus régulières dès que les données sont plus régulières.

L'EDS pour les dumbbells FENE (cf. chapitre 5)

Nous nous sommes ensuite intéressés au modèle FENE. Une première question concerne l'existence de solutions à l'équation différentielle stochastique pour un champ de vitesse donné (cf. (1.68)). Nous avons vu que la force FENE ($\boldsymbol{F}(\boldsymbol{X}) = \frac{\boldsymbol{X}}{1 - \|\boldsymbol{X}\|^2/b}$) a été introduite pour tenir compte de l'extensibilité finie des chaînes de polymère. Nous avons effectivement montré que dès que $b > 0$ et $\boldsymbol{\kappa} \in L_{\text{loc}}^1(\mathbb{R}_+)$, il existe une unique solution $\boldsymbol{X}_t$ à valeur dans la boule fermée $\overline{\mathcal{B}}(0, \sqrt{b})$ et que le processus $\boldsymbol{X}_t$ ne touche pas la frontière de la boule $\mathcal{B}(0, \sqrt{b})$ si et seulement si $b \geq 2$, ce qui est une hypothèse vérifiée en pratique (cf. remarque 9). Ces résultats découlent de travaux de E. Cépa [25–27] sur les EDS multivoques.

Le cas des dumbbells FENE dans un écoulement cisaillé (cf. chapitre 4)

En passant du modèle des *dumbbells* hookéens au modèle des *dumbbells* FENE dans le problème couplé, deux nouvelles difficultés apparaissent :
- tout d'abord, la force non-linéaire conduit à des difficultés pour construire une solution à l'EDS elle-même (cf. paragraphe précédent),
- ensuite, et surtout, la composante Y_t dépend de X_t (au travers du terme $F_Y(\boldsymbol{X}_t(y))$) et on a donc une véritable non linéarité dans l'EDS sur X_t *via* le terme $\partial_y u(t, y) Y_t$.

La question qui est donc posée dans ce cas est : pour une régularité donnée de u, quelle est la régularité de τ ? Plus précisément, si on considère l'estimée fondamentale donnée ci-dessus, pour $u \in L_t^\infty(L_y^2) \cap L_t^2(H_{0,y}^1)$, quelle est la régularité de τ ?

Nous n'avons pas pu répondre à cette question telle quelle. En fait, formellement, du fait du terme non linéaire $\nabla \boldsymbol{u} \boldsymbol{X}_t$ dans l'EDS, τ a la régularité de $\exp(\int_0^t \partial_y u)$, ce qui n'est pas suffisant pour identifier τ à une distribution par exemple. Nous avons donc été conduits à demander plus de régularité sur la vitesse u, et à considérer des

solutions fortes de l'EDP : $u \in L_t^\infty(H_{0,y}^1) \cap L_t^2(H_y^2)$. Malheureusement, l'estimée *a priori* donnant cette estimée ne peut être obtenue qu'en temps petit, en multipliant l'équation sur u dans (1.69) par $-\partial_{y,y}u$ et en utilisant le théorème de Girsanov pour expliciter la dépendance de la contrainte τ en la variable d'espace y sous la forme :

$$
\begin{aligned}
\tau(t,y) &= \mathbb{E}\left(\frac{X_t(y)Y_t(y)}{1 - \frac{(X_t(y))^2 + (Y_t(y))^2}{b}}\right), \\
&= \mathbb{E}\left(\left(\frac{\tilde{X}_t\tilde{Y}_t}{1 - \frac{\tilde{X}_t^2 + \tilde{Y}_t^2}{b}}\right)\mathcal{E}\left(\frac{1}{\sqrt{\mathrm{We}}}\int_0^\bullet \partial_y u(y)\tilde{Y}_s \, dV_s\right)_T\right), \quad (1.73)
\end{aligned}
$$

où $\widetilde{\boldsymbol{X}}_t = (\tilde{X}_t, \tilde{Y}_t)$ est le processus solution de l'EDS pour le modèle FENE avec $\partial_y u = 0$:

$$
d\widetilde{\boldsymbol{X}}_t = -\frac{1}{2\mathrm{We}}\frac{\widetilde{\boldsymbol{X}}_t}{1 - ||\widetilde{\boldsymbol{X}}_t||^2/b} \, dt + \frac{1}{\sqrt{\mathrm{We}}}d\boldsymbol{W}_t,
$$

et $\mathcal{E}$ désigne l'exponentielle martingale :

$$
\mathcal{E}\left(\frac{1}{\sqrt{\mathrm{We}}}\int_0^\bullet \partial_y u\tilde{Y}_s \, dV_s\right)_t = \exp\left(\frac{1}{\sqrt{\mathrm{We}}}\int_0^t \partial_y u\tilde{Y}_s \, dV_s - \frac{1}{2\mathrm{We}}\int_0^t \left(\partial_y u\tilde{Y}_s\right)^2 \, ds\right).
$$

Noter que dans (1.73), la dépendance de τ en y ne provient que du terme exponentielle martingale. L'utilisation du théorème de Girsanov permet donc d'expliciter de manière rigoureuse la dépendance exponentielle de τ en fonction de $\partial_y u$ évoquée précédemment. Par ailleurs, en utilisant le fait que $\partial_y u \in H_y^1$ (pour presque tout temps) et est donc borné, on obtient des estimations en norme L_y^∞ sur τ (pour presque tout temps). Le théorème de Girsanov permet donc à la fois de définir τ comme une distribution, et d'expliciter la régularité de τ en fonction de la régularité de u. Ces estimations sont en temps petit car on obtient finalement un contrôle sur une fonctionnelle d'énergie du type : $R(t) \leq A + C\int_0^t \exp(\gamma R(s)) \, ds$ (cf. section 4.3.2.2 dans le chapitre 4 pour les détails).

En conclusion, la non-linéarité $\nabla\boldsymbol{u}\boldsymbol{X}_t$ dans l'EDS a limité le résultat à une existence de solutions fortes en temps petit. De plus, la preuve donnée pour l'écoulement cisaillé n'est pas directement généralisable pour des écoulements en dimension 2 car elle utilise l'inclusion de H^1 dans L^∞ pour contrôler les termes du type $\exp(\int_0^t \partial_y u)$.

Comportement en temps long du système (cf. chapitre 8)

Nous avons vu que l'estimée fondamentale (1.72) n'était pas utilisable en temps long à cause d'un terme de "production d'énergie" provenant du calcul d'Itô. En fait, pour éliminer ce terme, il faut considérer un terme supplémentaire d'entropie : il semble que la bonne fonctionnelle pour étudier le comportement en temps ne soit pas l'énergie mais *l'énergie libre*.

Pour introduire l'entropie, on doit considérer la densité du processus $\boldsymbol{X}_t$, et donc le système couplant l'EDP sur la vitesse avec l'équation de Fokker-Planck

(cf. (1.57)) Les calculs présentés dans la suite supposent *des conditions homogènes de Dirichlet sur la vitesse*, une force extérieure $\boldsymbol{f}$ nulle et l'existence d'une solution au problème (1.57) pour $t \in \mathbb{R}_+$. Etant données les conditions aux limites sur $\boldsymbol{u}$, la solution stationnaire "attendue" est :

$$\boldsymbol{u}(\infty, \boldsymbol{x}) = 0,$$

$$\psi(\infty, \boldsymbol{x}, \boldsymbol{X}) = \psi_{\text{eq}}(\boldsymbol{X}) = C \exp(-\Pi(\boldsymbol{X})),$$

où C est un facteur de normalisation. Nous allons montrer formellement pourquoi on obtient une convergence exponentielle vers ces solutions stationnaires. On renvoie ici à [1, 2, 109].

Nous introduisons l'énergie cinétique :

$$E(t) = \frac{\text{Re}}{2} \int_{\mathcal{D}} |\boldsymbol{u}|^2(t, \boldsymbol{x}). \tag{1.74}$$

On a comme précédemment (cf. (1.70)) :

$$\frac{dE}{dt} = -(1-\epsilon) \int_{\mathcal{D}} |\nabla \boldsymbol{u}|^2(t, \boldsymbol{x}) - \frac{\epsilon}{\text{We}} \int_{\mathcal{D}} \int_{\mathbb{R}^d} (\boldsymbol{X} \otimes \nabla\Pi(\boldsymbol{X})) : \nabla \boldsymbol{u}(t, \boldsymbol{x}) \psi(t, \boldsymbol{x}, \boldsymbol{X}).$$

Nous introduisons l'entropie :

$$\begin{aligned} H(t) &= \int_{\mathcal{D}} \int_{\mathbb{R}^d} \Pi(\boldsymbol{X}) \psi(t, \boldsymbol{x}, \boldsymbol{X}) + \int_{\mathcal{D}} \int_{\mathbb{R}^d} \psi(t, \boldsymbol{x}, \boldsymbol{X}) \ln(\psi(t, \boldsymbol{x}, \boldsymbol{X})) - |\mathcal{D}| \ln C, \\ &= \int_{\mathcal{D}} \int_{\mathbb{R}^d} \psi(t, \boldsymbol{x}, \boldsymbol{X}) \ln\left(\frac{\psi(t, \boldsymbol{x}, \boldsymbol{X})}{\psi_{\text{eq}}(\boldsymbol{X})}\right). \end{aligned} \tag{1.75}$$

Noter que l'on montre facilement que $H(t) \geq 0$ en utilisant le fait que $x \ln(x) \geq x - 1$ avec $x = \dfrac{\psi}{\psi_{\text{eq}}}$, et en multipliant l'inégalité par ψ_{eq}. Après quelques calculs (en utilisant (1.71) et le fait que div $(\boldsymbol{u}) = 0$), on obtient :

$$\begin{aligned} \frac{dH}{dt} = &-\frac{1}{2\text{We}} \int_{\mathcal{D}} \int_{\mathbb{R}^d} \psi(t, \boldsymbol{x}, \boldsymbol{X}) \left| \nabla_{\boldsymbol{X}} \ln\left(\frac{\psi(t, \boldsymbol{x}, \boldsymbol{X})}{\psi_{\text{eq}}(\boldsymbol{X})}\right) \right|^2 \\ &+ \int_{\mathcal{D}} \int_{\mathbb{R}^d} (\boldsymbol{X} \otimes \nabla\Pi(\boldsymbol{X})) : \nabla \boldsymbol{u}(t, \boldsymbol{x}) \psi(t, \boldsymbol{x}, \boldsymbol{X}). \end{aligned}$$

D'où, si on pose $F(t) = E(t) + \dfrac{\epsilon}{\text{We}} H(t)$, ($F$ est de signe positif et correspond à une énergie libre) :

$$\frac{dF}{dt} = -(1-\epsilon) \int_{\mathcal{D}} |\nabla \boldsymbol{u}|^2(t, \boldsymbol{x}) - \frac{\epsilon}{2\text{We}^2} \int_{\mathcal{D}} \int_{\mathbb{R}^d} \psi(t, \boldsymbol{x}, \boldsymbol{X}) \left| \nabla_{\boldsymbol{X}} \ln\left(\frac{\psi(t, \boldsymbol{x}, \boldsymbol{X})}{\psi_{\text{eq}}(\boldsymbol{X})}\right) \right|^2. \tag{1.76}$$

On voit donc que l'introduction de l'entropie a permis d'éliminer le terme d'Itô au membre de droite de (1.72). De cette égalité on peut déduire que les solutions stationnaires du système couplé sont bien $\boldsymbol{u} = 0$ et $\psi = \psi_{\text{eq}}$. Par ailleurs, en utilisant l'hypothèse $\epsilon \in (0, 1)$, une inégalité de Poincaré sur $\boldsymbol{u}$ et une inégalité de Sobolev logarithmique sur ψ_{eq}, on déduit de cette inégalité la décroissance exponentielle de F (et donc de $\boldsymbol{u}$) vers 0. L'inégalité de Csiszar-Kullback permet alors d'en déduire que ψ tend vers ψ_{eq} exponentiellement vite en norme $L^2_{\boldsymbol{x}}(L^1_{\boldsymbol{X}})$.

Remarque 11 *L'inégalité de Sobolev logarithmique pour ψ_{eq} entraîne :*

$$\int_{\mathbb{R}^d} \psi \ln\left(\frac{\psi}{\psi_{\text{eq}}}\right) \leq C \int_{\mathbb{R}^d} \psi \left|\nabla \ln\left(\frac{\psi}{\psi_{\text{eq}}}\right)\right|^2$$

et est vérifiée dès que, par exemple, on suppose Π α-convexe.

Faisons quelques remarques sur ces calculs.

Tout d'abord, il est important de noter que nous n'avons pas pu généraliser ces calculs au cas $\boldsymbol{u}(\infty, \boldsymbol{x}) \neq 0$.

Par ailleurs, le choix de l'entropie H semble important dans le calcul : si on choisit une entropie plus générale

$$H(t) = \int_{\mathcal{D}} \int_{\mathbb{R}^d} h\left(\frac{\psi}{\psi_{\text{eq}}}\right) \psi_{\text{eq}}$$

avec $h : \mathbb{R} \to \mathbb{R}^*_+$ de classe $\mathcal{C}^2$, convexe et telle que $h(1) = 0$ (cf. [2]), les termes contenant (1.71) ne s'éliminent que pour l'entropie "physique" $h(x) = x\ln(x) - (x - 1)$. Ceci peut sembler étonnant car quand on considère l'équation de Fokker-Planck seule (avec $\boldsymbol{u} = 0$), on peut par exemple prendre $h(x) = (x - 1)^2$ et une inégalité de Poincaré sur ψ_{eq} suffit alors pour prouver la convergence exponentielle de ψ vers ψ_{eq} en norme $L^2_{\boldsymbol{X}}$.

Enfin, on peut noter que la convergence de F vers 0 ne suffit pas en général à obtenir la convergence du tenseur des contraintes.

Importance des hypothèses sur la force $\boldsymbol{F}$

Nous pouvons à ce stade faire quelques remarques sur l'importance des hypothèses faites sur $\boldsymbol{F}$. On rappelle que l'on a supposé que $\boldsymbol{F}$ dérivait d'un potentiel Π radial (i.e. qui s'écrit $\Pi(\boldsymbol{X}) = \pi(||\boldsymbol{X}||)$ (cf. 1.42)). Voici les hypothèses que nous avons utilisées jusqu'à maintenant :
- Le fait que la force dérive d'un potentiel Π intervient dans le fait qu'il existe une densité de probabilité stationnaire et *réversible* à l'équilibre.
- Le fait que le potentiel Π soit radial intervient de manière cruciale pour assurer la symétrie du tenseur des contraintes. Cette symétrie est importante d'un point de vue physique, et intervient dans les estimées (cf. (1.71)).
- L'hypothèse de convexité du potentiel Π (cf. remarque 6) est importante pour l'analyse des EDS (unicité des solutions, interprétation en EDS multivoque).

– L'α-convexité du potentiel Π est utile quand on s'intéresse au comportement en temps long, puisqu'elle permet d'obtenir l'inégalité de Sobolev logarithmique sur ψ_{eq}, et donc la convergence exponentielle vers l'état stationnaire.

1.2.2.2 Analyse des méthodes numériques type CONNFFESSIT

Dans cette section, nous nous intéressons à la discrétisation du système (1.67) par des méthodes probabilistes.

La méthode CONNFFESSIT dans le cas d'un écoulement cisaillé

Dans nos travaux, nous nous sommes consacrés à l'étude de la méthode CONNF-FESSIT dans le cas d'un écoulement cisaillé (cf. (1.69)). Dans ce cas, les approches eulériennes et lagrangiennes aboutissent au même système, et le système discrétisé s'écrit : supposons que u_h^n, $X_{h,n}^j$ et $Y_{h,n}^j$ sont connus, trouver $u_h^{n+1} \in V_h$ tel que, pour tout $v \in V_h$,

$$
\begin{aligned}
\frac{\text{Re}}{\delta t} \int_y (u_h^{n+1} - u_h^n)v &= -(1-\epsilon)\int_y \partial_y u_h^{n+1}\partial_y v - \int_y \tau_{h,n}\partial_y v + \int_y fv, \\
\tau_{h,n} &= \frac{\epsilon}{\text{We}}\frac{1}{R}\sum_{j=1}^R X_{h,n}^j F_Y(X_{h,n}^j Y_{h,n}^j), \\
X_{h,n+1}^j - X_{h,n}^j &= \left(\partial_y u_h^{n+1} Y_{h,n}^j - \frac{1}{2\text{We}}F_X(X_{h,n}^j, Y_{h,n}^j)\right)\delta t \\
&\quad + \frac{1}{\sqrt{\text{We}}}\left(V_{h,t_{n+1}}^j - V_{h,t_n}^j\right), \\
Y_{h,n+1}^j - Y_{h,n}^j &= -\frac{1}{2\text{We}}F_Y(X_{h,n}^j, Y_{h,n}^j)\delta t + \frac{1}{\sqrt{\text{We}}}\left(W_{h,t_{n+1}}^j - W_{h,t_n}^j\right).
\end{aligned}
$$

L'indice n désigne le numéro du pas de temps et l'indice j le numéro de la réalisation de l'EDS : on considère R trajectoires des variables aléatoires $(X_{h,n}, Y_{h,n})$. Enfin, V_h désigne un espace d'éléments finis, que nous prenons dans la suite égal à $\mathbb{P}1$, de sorte que $X_{h,n}$, $Y_{h,n}$ et $\tau_{h,n}$ appartiennent à $\mathbb{P}0$ (cf. figure 1.12).

La convergence de la méthode CONNFFESSIT dans le cas des dumbbells hookéens (cf. chapitres 2 et 3)

La première question naturelle est d'étudier la convergence de l'algorithme CONNF-FESSIT dans la limite $\delta t \to 0$, $h \to 0$ et $R \to \infty$. Nous avons pu effectivement montré la convergence de l'algorithme dans le cas de l'écoulement cisaillé et pour des *dumbbells* hookéens. Dans ce cas, la composante $Y_{h,n}^j$ ne dépend pas de l'espace et est donc notée Y_n^j. Si on mesure l'erreur en norme $L_t^\infty(L_y^2(L_\omega^2))$ pour la vitesse, et en norme $L_t^\infty(L_y^1(L_\omega^1))$ pour la contrainte, on peut montrer que l'erreur est majorée par $C\left(\delta t + h^2 + \frac{1}{\sqrt{R}}\right)$ pour la vitesse et par $C\left(\delta t + h + \frac{1}{\sqrt{R}}\right)$ pour la contrainte. Les principales difficultés proviennent du fait que la vitesse u_h^n est devenue une variable

$$U_I = 0$$
$$y_I = 1$$
$$u : \mathbb{P}1$$
$$\tau : \mathbb{P}0$$
$$\tau_{h,n} = \frac{\epsilon}{\text{We}} \frac{1}{R} \sum_{j=1}^{R} (X_{h,n}^j F_Y(X_{h,n}^j, Y_{h,n}^j))$$
$$h$$
$$u$$
$$\tau$$
$$y_0 = 0$$
$$U_0 = 1$$
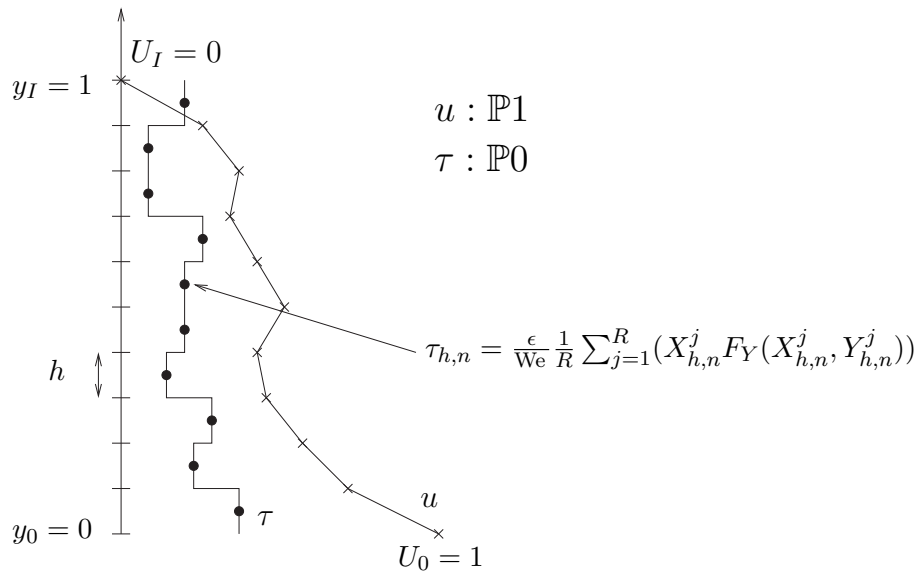
FIG. 1.12 – La méthode CONNFFESSIT dans le cas d'un écoulement cisaillé.

aléatoire (et que certaines estimées faites au niveau continu ne se traduisent donc pas directement au niveau discret), que toutes les trajectoires sont couplées *via* la vitesse et que pour prouver la stabilité du schéma, on a besoin d'une estimée sur la moyenne empirique du carré de Y_n^j :

$$\delta t \frac{1}{R} \sum_{j=1}^{R} (Y_n^j)^2 < 1.$$

Pour prouver la convergence, nous avons donc proposé d'utiliser un cut-off sur Y_n^j, puis montré que ce cut-off n'était utilisé qu'avec une probabilité extrêmement faible quand δt est suffisamment petit ou R suffisamment grand. Nous avons montré que ce résultat de convergence était valable quelle que soit la dépendance en espace des mouvements browniens $(W_{h,t}^j)_{1 \leq j \leq R}$.

Au sujet de la variance des résultats et de la dépendance en espace des mouvements browniens (cf. chapitre 6)

Nous avons également réfléchi sur l'influence de la dépendance des mouvements browniens en espace (cf. notamment la section 6.2 dans le chapitre 6). On peut se convaincre, du moins dans le cas de solutions régulières, que la dépendance du mouvement brownien en la trajectoire n'a pas d'influence sur le résultat continu. On a pu en tout cas le démontrer dans le cas des *dumbbells* hookéens dans un écoulement cisaillé. Par contre, cette dépendance a une influence sur la variance des résultats, une fois le problème discrétisé : on observe que choisir des mouvements browniens décorrélés en espace plutôt que ne dépendant pas de l'espace augmente la variance sur la vitesse mais la diminue sur la contrainte. Cette observation a été faite par plusieurs auteurs (cf. [15, 74]).

Nous avons analysé la variance des résultats en fonction des différents paramètres numériques et notamment de la matrice de corrélation en espace des mouvements browniens $(W_{h,t}^j)_{1 \le j \le R}$. Nous avons ainsi pu démontrer, toujours dans le cas des *dumbbells* hookéens dans un écoulement cisaillé, que :

a) La variance sur la vitesse est minimum pour un mouvement brownien constant en espace,

b) Utiliser des mouvements browniens complètement décorrélés n'est pas le meilleur moyen de réduire la variance sur τ ; l'utilisation d'un brownien multiplié alternativement par $+1$ ou -1 dans les cellules est optimal pour ce qui est de la variance sur τ,

c) Il est possible de réduire la variance sur τ, en comparaison du cas d'un mouvement brownien constant en espace, et ce à coût calcul constant.

Pour le détail, nous renvoyons au chapitre 6 et notamment aux tableaux récapitulatifs 6.10 et 6.11.

Méthode particulaire pour le modèle FENE-P (cf. chapitre 7)

Nous nous sommes finalement intéressés au modèle FENE-P. On rappelle que pour ce modèle, on remplace le carré de la norme du vecteur bout-à-bout dans le dénominateur par sa moyenne. Il s'agit donc d'une approximation type champ moyen qui a pour but d'obtenir une équation fermée sur le tenseur des contraintes (cf. section 1.1.4.1).

Nous avons analysé l'EDS associée au modèle FENE-P, qui est non-linéaire au sens de Mc Kean. Nous nous sommes pour cela placés dans le cadre d'un écoulement de vitesse connu (cf. (1.68)). Nous avons montré que l'EDS non-linéaire admettait une unique solution. Une fois le problème discrétisé, on peut utiliser une approximation particulaire de l'EDS sous la forme (cf. [89]) : $\forall 1 \le i \le M$,

$$d\boldsymbol{X}_t^{i,M} = \left(\boldsymbol{\kappa}(t)\boldsymbol{X}_t^{i,M} - \frac{1}{2\mathrm{We}} \frac{\boldsymbol{X}_t^{i,M}}{1 - \frac{1}{M}\sum_{i=1}^{M} ||\boldsymbol{X}_t^{i,M}||^2/b} \right) dt + \frac{1}{\sqrt{\mathrm{We}}} d\boldsymbol{W}_t^i \quad (1.77)$$

où $(\boldsymbol{W}^i)_{1 \le i \le M}$ désigne une collection de M mouvements browniens indépendants. Le tenseur des contraintes est alors estimé par la moyenne empirique :

$$\boldsymbol{\tau}_p^M = \frac{\varepsilon}{\mathrm{We}} \left(\frac{\frac{1}{M}\sum_{i=1}^{M} \left(\boldsymbol{X}_t^{i,M} \otimes \boldsymbol{X}_t^{i,M} \right)}{1 - \frac{1}{M}\sum_{i=1}^{M} ||\boldsymbol{X}_t^{i,M}||^2/b} - \mathrm{Id} \right).$$

Nous avons montré l'existence d'une solution au problème particulaire (1.77) et la convergence du tenseur des contraintes dans la limite $M \to \infty$. La preuve est basée sur la démonstration de la tension de la suite des mesures empiriques, puis sur l'identification de la mesure limite *via* un problème de martingale.

1.2.2.3 Autres méthodes numériques

Dans cette section, nous présentons d'autres aspects numériques de la discrétisation de (1.67).

Réduction de variance

Un aspect important de la simulation de (1.67) par la méthode CONNFFESSIT est la réduction de variance. Nous renvoyons à [15] pour des techniques de variables de contrôle. Il s'agit de réécrire l'équation sur $\boldsymbol{\tau}_p$ dans (1.67) sous la forme :

$$\boldsymbol{\tau}_p = \frac{\epsilon}{\text{We}} \left(\mathbb{E}(\boldsymbol{X} \otimes \boldsymbol{F}(\boldsymbol{X}) - \overline{\boldsymbol{X}} \otimes \boldsymbol{F}(\overline{\boldsymbol{X}})) + \mathbb{E}(\overline{\boldsymbol{X}} \otimes \boldsymbol{F}(\overline{\boldsymbol{X}})) - \text{Id} \right)$$

où $\overline{\boldsymbol{X}}$ désigne un processus solution d'une EDS "proche" de celle vérifiée par $\boldsymbol{X}$ (pour que la variance de la variable aléatoire $(\boldsymbol{X} \otimes \boldsymbol{F}(\boldsymbol{X}) - \overline{\boldsymbol{X}} \otimes \boldsymbol{F}(\overline{\boldsymbol{X}}))$ soit plus petite que la variance de $(\boldsymbol{X} \otimes \boldsymbol{F}(\boldsymbol{X}))$) et telle que la quantité $\mathbb{E}(\overline{\boldsymbol{X}} \otimes \boldsymbol{F}(\overline{\boldsymbol{X}}))$ peut être calculée de manière indépendante et précise (solution analytique, solution d'une EDP). Il faut bien noter que les approximations de fermeture (cf. section 1.1.4.1) qui permettent d'obtenir des modèles macroscopiques équivalents jouent un rôle important dans ce domaine, car on peut ensuite utiliser ces modèles pour bâtir des variables de contrôle. Ainsi, on peut choisir comme variable de contrôle pour le modèle FENE, soit le processus à l'équilibre ($\partial_y u = 0$ dans l'EDS), soit le processus avec la force hookéenne, soit le processus avec la force FENE-P. Dans le premier cas, on connaît analytiquement la valeur de $\mathbb{E}(\overline{\boldsymbol{X}} \otimes \boldsymbol{F}(\overline{\boldsymbol{X}}))$, tandis que dans les deux derniers cas, on peut la calculer en résolvant une EDP (cf. section 1.1.4.1).

Résolution de l'équation de Fokker-Planck

Plusieurs équipes se sont également intéressées à la résolution du système (1.57). Signalons en particulier la thèse récente de A. Lozinski [108] ainsi que [143]. Les méthodes spectrales sont en général privilégiées pour résoudre l'équation de Fokker-Planck et sont couplées à une méthode d'éléments finis pour l'équation sur la vitesse. Le problème principal de cette approche est qu'elle est *a priori* limitée au *dumbbell* et difficilement généralisable à une chaîne de ressorts, qui est un modèle plus réaliste (cf. section 1.1.3.5). Nous avons cependant commencé à tester des techniques pour pouvoir résoudre l'équation de Fokker-Planck en grande dimension, et les premiers résultats semblent prometteurs (travail en cours en collaboration avec C. Schwab).

1.3 Conclusions et perspectives

Nous avons dans ce chapitre introduit les modèles moléculaires pour les fluides polymériques et montré comment ces modèles étaient liés aux modèles macroscopiques. Nous avons ensuite analysé les modèles micro-macro, qui couplent les modèles moléculaires aux équations macroscopiques de conservation du moment et d'incompressibilité sur la vitesse.

Du point de vue de l'analyse mathématique du problème couplé, nous avons, dans le cadre d'un écoulement cisaillé, retrouvé les difficultés mathématiques déjà rencontrées par plusieurs auteurs dans l'analyse des modèles macroscopiques. Les non-linéarités dans le modèle conduisent à des résultats d'existence et unicité partiels. Nous avons par ailleurs montré, à écoulement donné, l'existence de solutions

aux EDS régissant l'évolution du *dumbbell* (pour les modèles hookéen, FENE et FENE-P).

Du point de vue de l'analyse numérique des modèles, nous avons pu, dans certains cas simplifiés, montrer la convergence des méthodes numériques employées (CONNFFESSIT). De plus, nous avons analysé la manière dont la variance des résultats dépendait des paramètres numériques, et notamment de la manière dont le mouvement brownien modélisant le bombardement du solvant sur le *dumbbell* dépend de l'espace. Enfin, nous avons également montré la convergence d'une approximation particulaire dans le cas du modèle FENE-P.

Plusieurs questions restent à ce jour ouvertes. Du point de vue de l'analyse mathématique, il reste à généraliser les résultats obtenus pour des écoulements cisaillés à des écoulements quelconques. Nous pensons que l'extrapolation de nos résultats d'existence en temps petit sur le système couplé en dimension supérieure ($d = 2$ ou $d = 3$) doit être possible, mais en invoquant parfois d'autres arguments et en demandant sans doute plus de régularité sur les solutions (cf. les résultats typiquement obtenus sur les modèles macroscopiques). Cependant, la véritable question reste l'existence de solutions en temps long. En particulier, nous n'avons pas encore pu exploiter l'estimée faisant intervenir l'entropie (1.76) qui contient *a priori* plus d'informations que la première estimée d'énergie (1.72) que nous avons utilisée. De même, la question de l'analyse des modèles micro-macro dans le cas $\epsilon = 1$ (c'est-à-dire pas de viscosité dans le solvant) n'a pas été abordée et semble difficile. Nous avons également soulevé plusieurs questions sur le comportement en temps long de ces modèles, qui semble un aspect plus spécifique aux modèles micro-macro. Nous avons par ailleurs l'intention de généraliser les résultats obtenus à d'autres modèles de fluides complexes (cf. section 1.1.3.5).

Du point de vue de l'analyse numérique, nous travaillons actuellement sur la résolution de l'équation de Fokker-Planck en grande dimension. Par ailleurs, la question de l'analyse de convergence du tenseur des contraintes dans le cas du modèle FENE en utilisant un schéma numérique adapté pour discrétiser l'EDS reste un problème ouvert. Plus précisément, il s'agit de prouver la convergence de l'espérance d'une fonction singulière (le tenseur des contraintes) de la solution d'un schéma d'Euler associée à une EDS dont le terme de dérive présente la même singularité. En outre, il serait intéressant de comprendre si les propriétés en temps long des équations au niveau continu se traduisent par des propriétés similaires sur le problème discrétisé. Les schémas numériques couplant méthodes d'éléments finis et méthodes de Monte Carlo sont certainement encore très riches de questions intéressantes et originales (réduction de variance, convergence, schémas en temps).

1.A Modèles multi-échelles et méthodes multi-échelles

Afin de présenter le contexte des modèles micro-macro pour les fluides polymériques, on se propose de dresser un rapide panorama des modèles multi-échelles, en rappelant leurs principales caractéristiques et leur utilisation. On ne prétend ici à aucune originalité ni exhaustivité. Pour une présentation plus complète d'autres problèmes multi-échelles, on renvoie à [99].

Le qualificatif multi-échelles s'applique à tout modèle ou méthode faisant intervenir au moins deux échelles (de temps ou d'espace) différentes. Les objectifs de ces modèles peuvent être :
- de stabiliser une méthode numérique,
- d'améliorer une discrétisation et de réduire l'erreur,
- de modéliser plus finement des phénomènes en décrivant les petites échelles avec des équations spécifiques.

Développons chacun des points évoqués ci-dessus.

1.A.1 Modèles multi-échelles et stabilisation

En ce qui concerne la stabilisation, on peut interpréter les méthodes du type "bulle" (cf. [21, 22]) ou SUPG (cf. [23, 50, 80]) comme des méthodes multi-échelles de la manière suivante. On considère un problème d'advection-diffusion sur un domaine $\mathcal{D} \subset \mathbb{R}^d$, posé sur une fonction $u : \mathcal{D} \to \mathbb{R}$:

$$\begin{cases} -k\Delta u + c.\nabla u = f & \text{sur } \mathcal{D}, \\ u = 0 & \text{sur } \partial\mathcal{D}. \end{cases}$$

On suppose que k est un scalaire positif et, pour simplifier, que c est un champ à divergence nulle. On note L l'opérateur défini par $Lu = -k\Delta u + c.\nabla u$. Une formulation variationnelle de ce problème s'écrit : trouver $u \in H_0^1(\mathcal{D})$ tel que $\forall v \in H_0^1(\mathcal{D})$, $a(u,v) = l(v)$ avec

$$a(u,v) = \int k\nabla u.\nabla v + \int c.\nabla u \, v$$

et

$$l(v) = \int fv.$$

On suppose, pour fixer les idées, que $c \in L^\infty(\mathcal{D})$ et $f \in L^2(\mathcal{D})$. Il est bien connu qu'une méthode d'éléments finis standards sur ce problème donne de mauvais résultats quand l'advection domine la diffusion ($||c||_{L^\infty} h \gg k$ où h désigne le pas du maillage) : les estimations d'erreurs en norme d'énergie se dégradent et on observe une oscillation des solutions si les couches limites ne sont pas résolues (c'est-à-dire suffisamment finement maillées).

L'idée est alors de décomposer la solution u en une partie grossière $\overline{u}$ et une partie plus fine u'. On peut aussi interpréter $\overline{u}$ comme une moyenne et u' comme une

variation autour de cette moyenne. Typiquement on fait l'hypothèse que $\overline{u} \in V_h$ où V_h est un espace d'éléments finis lagrangiens sur un maillage $\mathcal{T}_h = \bigcup K_h$ (où K_h désigne les éléments du maillage) et que u' appartient à un espace V' supplémentaire de V_h dans H_0^1. On se propose alors de résoudre la formulation variationnelle suivante : trouver $\overline{u} \in V_h$ et $u' \in V'$ tel que

$$
\begin{cases}
a(\overline{u}, \overline{v}) + a(u', \overline{v}) = l(\overline{v}), & \forall \overline{v} \in V_h, \\
a(u', v') = l(v') - a(\overline{u}, v'), & \forall v' \in V'.
\end{cases}
$$

Tel quel, ce problème est équivalent à résoudre le problème continu. L'hypothèse fondamentale qui permet de résoudre de manière simple le problème sur u' à l'échelle fine consiste à se restreindre à un ensemble V' de fonctions qui s'annulent sur les bords des éléments (on n'a alors évidemment plus $V_h \oplus V' = H_0^1(\mathcal{D})$). Le problème sur u' devient alors une collection de problèmes découplés et posés sur chaque maille (on parle de problèmes sous-maille, cf. aussi [69]). La fonction u' (qui dépend de $\overline{u}$) est donc construite à partir d'une collection de petits problèmes indépendants puis réinjectée dans l'équation sur $\overline{u}$. On peut par exemple prendre pour V' des fonctions bulles dans chaque élément et on obtient alors une première méthode numérique.

Une autre idée consiste à résoudre de manière approchée et analytiquement les problèmes sous-maille, qui constituent une collection de problèmes linéaires indépendants. Le second membre d'un problème sous-maille contient le résidu du problème sur $\overline{u}$ car $l(v') - a(\overline{u}, v') = \sum_{K_h} \int_{K_h} (f + k\Delta\overline{u} - c.\nabla\overline{u})v'$ (on a utilisé le fait que v' s'annule au bord des éléments). On peut donc écrire de manière symbolique la solution u' aux problèmes sous-maille sous la forme $u' = M(f + k\Delta\overline{u} - c.\nabla\overline{u})$ où M désigne un opérateur linéaire à valeur dans V'. En injectant cette relation dans l'équation sur $\overline{u}$, on obtient après une intégration par partie la formulation variationnelle : trouver $\overline{u} \in V_h$ tel que $\forall \overline{v} \in V_h$,

$$
a(\overline{u}, \overline{v}) - \int M(-k\Delta\overline{u} + c.\nabla\overline{u} - f)L'(\overline{v}) = l(\overline{v}),
$$

où $L' = -k\Delta - c.\nabla$ désigne l'opérateur transposé de L. Typiquement, on approxime ensuite M par la multiplication par une constante $\tau(K_h)$ sur chacun des éléments K_h et le terme de stabilisation s'écrit donc :

$$
-\int M(-k\Delta\overline{u} + c.\nabla\overline{u} - f)L'(\overline{v}) = \sum_{K_h} \tau(K_h) \int_{K_h} (-k\Delta\overline{u} + c.\nabla\overline{u} - f)S(\overline{v}),
$$

avec $S(\overline{v}) = -L'(\overline{v})$. Ce choix pour l'opérateur S, justifié par cette approche multi-échelle, correspond à la *Subgrid Scale Method* (SSM). Le choix $S = L$ correspond à la méthode *Galerkin Least Square* (GLS). Le choix $S = c.\nabla\overline{v}$ correspond à la méthode *Streamline Upwind Petrov Galerkin* (SUPG) (cf. [30] pour une comparaison de ces méthodes). Ces méthodes sont équivalentes dans le cas d'éléments finis du premier degré. Il est important de signaler que ces méthodes permettent aussi de s'affranchir de la condition inf-sup dans la résolution du problème de Stokes. Bien

que ces méthodes reposent sur une hypothèse difficilement justifiable (la nullité des fonctions de V' à l'échelle fine sur les arêtes du maillage), elles permettent en pratique d'améliorer les résultats obtenus par une méthode d'éléments finis standards dans des cas où cette dernière s'avère déficiente. Ces méthodes de stabilisation sont largement utilisées aujourd'hui, notamment dans le cadre de la mécanique des fluides, pour faire des calculs à des nombres de Reynolds plus élevés que ce que permettent les méthodes basées sur des éléments finis standards.

1.A.2   Modèles multi-échelles pour améliorer la discrétisation

Pour des équations dont la discrétisation ne pose pas de problèmes de stabilité, les méthodes multi-échelles peuvent également permettre d'améliorer la discrétisation et de réduire l'erreur d'approximation. L'exemple typique est l'homogénéisation (cf. [8]). On considère un milieu très hétérogène dans lequel on veut par exemple calculer un champ de température. Le problème s'écrit : trouver $u^\epsilon \in H_0^1(\mathcal{D})$ tel que

$$-\text{div}\,(A(x/\epsilon)\nabla u^\epsilon) = f(x),$$

où $\mathcal{D}$ est un domaine de $\mathbb{R}^d$, $A(x/\epsilon)$ désigne la matrice de conductivité thermique, qui varie typiquement sur une échelle de ϵ (ϵ désigne la taille typique d'une micro-structure dans le matériau). La résolution de ce problème nécessiterait normalement un maillage qui capture l'échelle ϵ des microstructures : ceci est bien souvent impossible en pratique, et on cherche donc un problème équivalent, posé à l'échelle macroscopique, mais tenant compte des microstructures du matériau.

L'hypothèse fondamentale pour pouvoir séparer les problèmes au niveau microscopique est dans ce cadre une condition de périodicité sur A (on suppose ici A périodique de maille élémentaire $Q = (0,1)^d$). En passant à la limite $\epsilon \to 0$, les problèmes microscopiques posés en chaque point macroscopique x vont se découpler. Indiquons simplement une méthode pour calculer le problème homogénéisé, sans rentrer dans les détails mathématiques justifiant la méthode. Le principe consiste à postuler un développement limité à double échelle de la forme :

$$u^\epsilon(x) = u_0(x) + \epsilon u_1(x, x/\epsilon) + \epsilon^2 u_2(x, x/\epsilon) + ...$$

où on suppose que les $(u_i(x,y))_{i\geq 1}$ sont périodiques en la variable y (que l'on appelle "variable rapide" car elle oscille avec une période à l'échelle de la microstructure). En injectant ce développement limité dans l'équation sur u et en identifiant les termes aux différents ordres en ϵ, on obtient successivement (en facteur de ϵ^{-1}, puis de ϵ^0) :

$$-\text{div}\,_y(A(y)(\nabla_x u_0(x) + \nabla_y u_1(x,y))(x,x/\epsilon) = 0,$$
$$-\text{div}\,_x(A(y)(\nabla_x u_0(x) + \nabla_y u_1(x,y)))(x,x/\epsilon)$$
$$-\text{div}\,_y(A(y)(\nabla_x u_1(x,y) + \nabla_y u_2(x,y)))(x,x/\epsilon) = f(x).$$

De la première équation complétée par les conditions aux limites de périodicité en y sur u_1, on déduit

$$u_1(x,y) = U(y).\nabla u_0(x) \tag{1.78}$$

où, par définition, la i-ème composante $U_i(y)$ de U est solution périodique et de moyenne nulle sur Q de :

$$-\text{div }_y(A(y)(e_i + \nabla_y U_i(y))) = 0,$$

où e_i désigne le i-ème vecteur de la base canonique. L'hypothèse de périodicité intervient ici de manière cruciale pour pouvoir résoudre séparément les problèmes de cellules (c'est-à-dire les problèmes posés sur Q). Pour des problèmes plus compliqués (par exemple en dimension 2 ou 3), on peut résoudre ces problèmes posés à l'échelle microscopique de manière numérique (cf. à ce sujet [111]).

En posant ensuite $< \phi >= \frac{1}{|Q|} \int_Q \phi(y)\, dy$ et en prenant la moyenne de la deuxième équation (en utilisant le fait que $< \partial_y \psi >= 0$ pour toute fonction ψ Q-périodique), on obtient :

$$-\text{div }_x < A(y)(\nabla_x u_0(x) + \nabla_y u_1(x,y)) >= f.$$

En injectant la relation (1.78) dans cette équation, on obtient finalement que u_0 est solution du problème homogénéisé :

$$-\text{div }_x < A^* \nabla_x u_0(x) >= f.$$

avec A^* défini par : pour tout vecteur p,

$$A^* p =< A(y)p + A(y)\nabla_y(U(y).p) > .$$

Dans cette exemple, on voit donc comment on peut déduire de l'équation initiale un problème sous-maille dont la solution, une fois réinjectée dans l'équation initiale, permet de poser un problème macroscopique "équivalent" tenant compte des échelles fines du problème.

1.A.3 Modélisation multi-échelles de phénomènes physiques

Dans les exemples présentés précédemment, une échelle fine est présente dans les équations que l'on cherche à discrétiser, et cette échelle fine doit être prise en compte si on veut obtenir des résultats satisfaisants. Il existe également des cas où l'on est intéressé par modéliser l'échelle fine par *des équations différentes des équations décrivant l'échelle macroscopique*. On pense évidemment ici aux sciences des matériaux, où les lois de constitutions (donnant la relation entre le tenseur des contraintes et, la déformation dans le cas de la mécanique des solides ou le taux de déformation dans le cas de la mécanique des fluides) nécessitent souvent de modéliser les échelles microscopiques pour comprendre la réponse à une sollicitation. Plutôt que de postuler des lois empiriques, on préfère alors décrire, éventuellement d'une manière approchée, les échelles microscopiques et traduire ensuite l'influence des échelles microscopiques sur les variables macroscopiques.

On peut citer dans cette classe de modèles la *quasicontinuum method* (QCM) dans laquelle l'énergie mécanique est calculée à partir de potentiels moléculaires

(cf. [144]) ou alors les modèles cinétiques de fluides complexes dans lesquels une équation du type Langevin décrit la conformation des macromolécules dans le fluide (cf. [12,13,39,120] pour les fluides polymériques ou [75] pour les suspensions concentrées, par exemple). Cette thèse porte sur de tels modèles rhéologiques pour les fluides polymériques. On renvoie à la section 1.1 pour le détail de ces modèles.

De manière générale, on peut décrire les phénomènes à l'échelle microscopique, suivant la précision requise, par les équations de la mécanique quantique (équation de Schrödinger), les équations de la dynamique moléculaire, ou des équations cinétiques (équations de Langevin, équations de Fokker-Planck). A l'échelle macroscopique, ce sont habituellement les classiques équations de conservation (de la quantité de mouvement, du moment cinétique, de la masse, de l'énergie, ...) qui sont utilisées (penser aux équations de la dynamique des fluides ou de l'élasticité). Outre la difficulté du couplage des échelles en espace se pose également ici la question du couplage des échelles en temps : les phénomènes microscopiques ont en effet souvent des temps caractéristiques beaucoup plus petits que ceux relatifs aux phénomènes macroscopiques (cf. figure 1.13). C'est pourquoi tous les couplages ne sont pas toujours possibles en pratique, et il faut parfois avoir recours à des techniques de *coarse-graining* qui permettent de réécrire les équations microscopiques à des échelles moins fines, par exemple pour ne retenir de la dynamique à l'échelle microscopique que certains évènements rares qui influencent l'échelle macroscopique. La question du couplage des échelles reste difficile et dépend grandement du problème étudié. Cette difficulté n'est pas nouvelle : un des objectifs de la physique statistique est justement de tirer de données microscopiques des variables macroscopiques et d'étudier les relations entre ces variables macroscopiques, en fonction des lois microscopiques. Relier les lois macroscopiques à des modèles microscopiques est un chantier encore ouvert dans plusieurs cas (limite des équations de Boltzmann vers Stokes ou Navier-Stokes compressible par exemple).

On remarque qu'à l'échelle microscopique, le hasard intervient de manière très naturelle dans la modélisation : en mécanique quantique, le hasard est une composante fondamentale de la théorie imposée par le fait que le résultat d'une mesure est aléatoire ; en dynamique moléculaire, la notion de hasard et de description statistique provient d'une part de la grande sensibilité du système à des perturbations (notion de chaos) et également du grand nombre de degrés de liberté qui se superposent et dont on veut extraire des informations à l'échelle macroscopique (typiquement des informations à l'équilibre, notion qui se définit naturellement à l'échelle macroscopique) ; les équations cinétiques ont également une interprétation probabiliste. En pratique, cela signifie que l'on rencontre souvent des cas où l'échelle microscopique est décrite par des modèles aléatoires (équations différentielles stochastiques, chaînes de Markov, ...) alors que l'échelle macroscopique est décrite par des modèles déterministes (équations différentielles ordinaires, équations aux dérivées partielles, ...). L'étude mathématique de ces systèmes couplés fait donc appel à des notions en probabilités et calcul stochastique, ainsi qu'en analyse fonctionnelle, deux domaines qui ont certes pour socle commun la théorie de la mesure mais qui se sont déve-
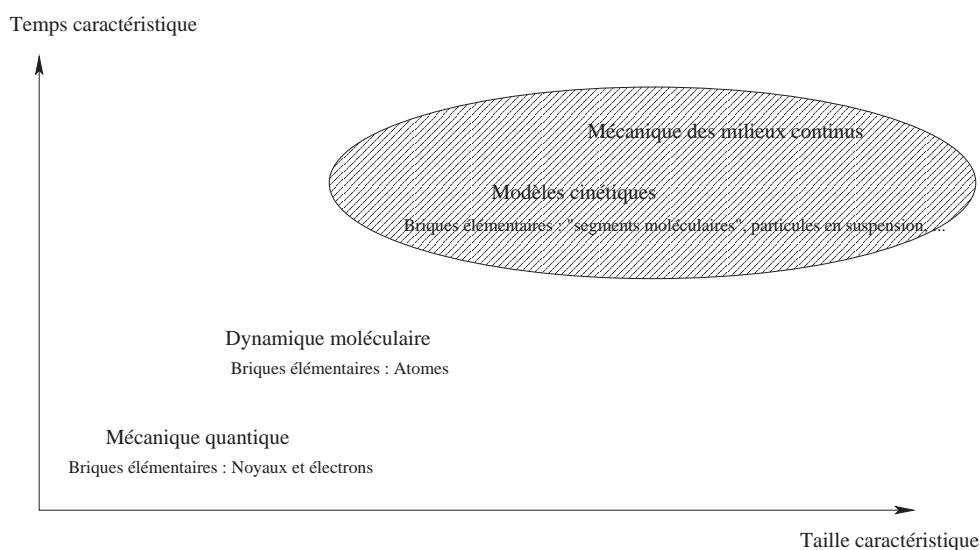
Fig. 1.13 – Champ d'application des modèles multi-échelles étudiés dans ce document (les échelles sont logarithmiques).

loppés en grande partie séparément. Typiquement, les régularités utilisées en calcul stochastique sont des régularités Höldériennes alors qu'on utilise plus volontiers des régularités Sobolev pour l'analyse mathématique des modèles issus de la physique. Ces "détails" techniques conduisent à des difficultés mathématiques quand on étudie ces modèles.

1.A.4   Hypothèse de séparation des échelles

Le point commun de tous ces modèles et de ces méthodes est qu'ils reposent sur une *hypothèse de séparation des échelles* qui permet de *découpler les calculs au niveau microscopique*. Ce découplage conduit à une collection de *petits* problèmes *indépendants*. Les équations aux échelles microscopiques sont alors résolues, de manière exacte ou approchée, soit numériquement (éventuellement en parallèle), soit analytiquement, et les solutions de ces équations interviennent dans les équations aux échelles macroscopiques. Les modélisations multi-échelles conduisent donc très généralement à des couplages entre équations qui peuvent être de natures différentes : équations aux dérivées partielles, équations différentielles ordinaires (dynamique moléculaire), équations différentielles stochastiques (rhéologie), équations intégrales (rhéologie), relations algébriques (réduction de systèmes)... Cela conduit souvent à des questions mathématiques et numériques originales.

Chapitre 2

Analyse du modèle des dumbbells hookéens : existence de solution et convergence du schéma numérique

Les résultats présentés dans ce chapitre ont fait l'objet d'un article paru dans *Mathematical Models and Methods in Applied Sciences.* On démontre un théorème d'existence et unicité en temps long pour le modèle des dumbbell Hookéens, et surtout un résultat de convergence d'une méthode utilisée pour discrétiser le système couplant Navier-Stokes avec une équation différentielle stochastique : la méthode CONNFFESSIT. Tous ces résultats sont établis dans le cadre d'un écoulement cisaillé.

<div style="text-align:center">

**Numerical analysis of micro-macro simulations
of polymeric fluid flows : a simple case.**

</div>

<div style="text-align:center">

Benjamin Jourdain, Tony Lelièvre, Claude Le Bris

CERMICS, Ecole Nationale des Ponts et Chaussées,

6 & 8 Av. Pascal, 77455 Champs-sur-Marne, France.
{jourdain, lelievre, lebris}@cermics.enpc.fr

</div>

We present in this article the numerical analysis of a simple micro-macro simulation of a polymeric fluid flow, namely the shear flow for the Hookean dumbbells model. Although restricted to this academic case (which is however used in practice as a test problem for new numerical strategies to be applied to more sophisticated cases), our study can be considered as a first step towards that of more complicated models. Our main result states the convergence of the fully discretized scheme (finite element in space, finite difference in time, plus Monte Carlo realizations) towards the coupled solution of a partial differential equation / stochastic differential equation system.

2.1   Introduction.

We are concerned here with the numerical analysis of a simple micro-macro simulation of a polymeric fluid flow. More precisely, we deal with the situation where the polymeric liquid, which is here supposed to be an infinitely diluted solution of polymers, experiences a pure shear flow and is modeled at the microscopic scale by the dynamics of stochastic Hookean dumbbells. To the best of our knowledge, such a study is new. We shall explain below why, despite the simplicity of the underlying model, our work can be seen as a first step towards the treatment of the more sophisticated models that are commonly used in the context of the so-called micro-macro approach in computational rheology.

Numerical simulations of the flow of complex fluids such as polymeric liquids is a long lasting challenge. The central difficulty is the rheology of these fluids, highly non Newtonian in nature : there is no simple linear relation linking the stress tensor $\boldsymbol{\tau}$ and the deformation tensor $\frac{1}{2}\left(\nabla\boldsymbol{u} +^t \nabla\boldsymbol{u}\right)$ as in the case of Newtonian fluids. This algebraic relation, the so-called constitutive equation of the fluid, is replaced in such fluid by a partial differential equation (abbreviated in PDE in the sequel) of the form

$$\frac{D\boldsymbol{\tau}}{Dt} = \boldsymbol{f}(\boldsymbol{\tau}, \nabla\boldsymbol{u}), \qquad (2.1)$$

to be integrated along the Lagrangian trajectories of the particles, or by an integro-

differential equation (the integral is taken along the trajectories)

$$\boldsymbol{\tau} = \int_{-\infty}^{t} m(t-s)\boldsymbol{S}_t(s)\,ds, \tag{2.2}$$

where m is a memory function (typically a decreasing exponential) and $\boldsymbol{S}_t(s)$ is a deformation-dependent tensor (typically a function of the Finger strain tensor).

The standard ("macroscopic") approach to simulate an incompressible flow of such polymeric liquids therefore consists in approximating the solution to a coupled system of the form

$$\rho\frac{D\boldsymbol{u}}{Dt} = -\nabla p + \eta\Delta\boldsymbol{u} + \operatorname{div}\boldsymbol{\tau}, \tag{2.3}$$

$$\operatorname{div}\boldsymbol{u} = 0, \tag{2.4}$$

$$\begin{cases} \frac{D\boldsymbol{\tau}}{Dt} & = & \boldsymbol{f}(\boldsymbol{\tau}, \nabla\boldsymbol{u}), \\ & \text{or} & \\ \boldsymbol{\tau} & = & \int_{-\infty}^{t} m(t-s)\boldsymbol{S}_t(s)\,ds, \end{cases} \tag{2.5}$$

together with convenient initial and boundary conditions. The derivative $\frac{D}{Dt}$ denotes the convective derivative $\frac{\partial}{\partial t} + \boldsymbol{u}.\nabla$, the vector $\boldsymbol{u}$ denotes the fluid velocity, p denotes the pressure. The two constants ρ and η denote respectively the density and the Newtonian viscosity of the solvent. We refer the reader to Refs. [88, 90, 91, 143] for a general introduction to the subject, and to Refs. [71, 72, 129, 132, 136] for examples of the numerous mathematical studies that have been devoted to such models. In this field, the most recent contribution is due to P.L. Lions and N. Masmoudi in Ref. [106].

Although very efficient, this purely macroscopic approach is now being questioned. The main concerns are indeed to find good constitutive equations (2.1) or (2.2) that could apply to the ever increasing number of non Newtonian fluids of interest in today's technology, and also to evaluate the impact of some closure hypothesis made to build these constitutive equations on the quality / validity of the final result. An alternative approach, which circumvents the bottleneck of making those closure hypothesis, has therefore been developed on the basis of kinetic theory. In a nutshell, this approach consists in finding an expression of the macroscopic stress tensor in terms of the microscopic dynamics of the polymer chains and in treating *explicitly* both scales in the simulation. On the contrary, constitutive laws are derived in a more or less rigorous way from the kinetic theory with the help of closure approximations, the kinetic foundation being next forgotten. Instead of (2.5), the system that has therefore to be treated is (2.3)-(2.4) together with the Fokker Planck equation describing the microscopic dynamics

$$\frac{\partial\psi}{\partial t} + \boldsymbol{u}.\nabla_{\boldsymbol{x}}\psi = -\operatorname{div}_{\boldsymbol{Q}}\left((\nabla_x\boldsymbol{u}\boldsymbol{Q} - \frac{2}{\zeta}\boldsymbol{F}(\boldsymbol{Q}))\psi\right) + \frac{\sigma^2}{\zeta^2}\Delta_{\boldsymbol{Q}}\psi, \tag{2.6}$$

and the expression of the stress tensor as the average

$$\boldsymbol{\tau} = n\int(\boldsymbol{Q}\otimes\boldsymbol{F}(\boldsymbol{Q}))\psi(t,\boldsymbol{x},\boldsymbol{Q})\,d\boldsymbol{Q} - nk_BT\mathrm{Id}. \tag{2.7}$$

The function $\psi(t, \boldsymbol{x}, \boldsymbol{Q})$ is the probability density function of the end-to-end vector $\boldsymbol{Q}$ of the polymer at time t and at position $\boldsymbol{x}$. The function $\boldsymbol{F}(\boldsymbol{Q})$ denotes the force within the spring which models the polymer, ζ denotes the friction, n is the number density of polymers and σ is defined by $\sigma^2 = 2k_B T\zeta$, where T is the temperature. We refer to Refs. [12, 13, 39, 120] for more details about the derivation of such equations.

From the theoretical standpoint, this approach is clearly more satisfactory than the previous one. It is however not perfect : current research in the modeling of complex flows aims at going further the simple setting of "thermodynamics at equilibrium" upon which this approach is based (see Refs. [9, 66, 67]). From the mathematical standpoint, systems of the type (2.3), (2.4), (2.6) and (2.7) have been studied for instance in Refs. [34, 131], and are therefore rather well known. However, this approach, as such, suffers from a severe drawback as far as numerical simulations are concerned : the Fokker Planck equation is to date only tractable numerically in spaces of small dimension N, far smaller than the typical N required in practice (say $N = 100$). However, huge efforts, with promising results, are devoted to such a technic (see Ref. [143]). The idea has emerged in the early 90's to simulate the underlying stochastic differential equation (abbreviated in SDE in the sequel) rather than the Fokker Planck equation itself. This approach has been called CONNFFES-SIT [97] which means Calculation of Non-Newtonian Fluids : Finite Elements and Stochastic Simulation Techniques.

The "modern" way of simulating an incompressible flow of an infinitely diluted solution of polymer is therefore to approximate

$$
\begin{cases}
\rho(\frac{\partial \boldsymbol{u}}{\partial t} + \boldsymbol{u}.\nabla\boldsymbol{u}) = -\nabla p + \eta\Delta\boldsymbol{u} + \operatorname{div}(\boldsymbol{\tau}), \\
\operatorname{div}(\boldsymbol{u}) = 0, \\
\boldsymbol{\tau} = n\mathbb{E}(\boldsymbol{Q} \otimes \boldsymbol{F}(\boldsymbol{Q})) - nk_B T\operatorname{Id}, \\
d\boldsymbol{Q} + \boldsymbol{u}.\nabla\boldsymbol{Q}dt = \left(\nabla\boldsymbol{u}\boldsymbol{Q} - \frac{2}{\zeta}\boldsymbol{F}(\boldsymbol{Q})\right)dt + \frac{\sqrt{2}\sigma}{\zeta}d\boldsymbol{W}_t,
\end{cases}
\tag{2.8}
$$

where $\mathbb{E}$ denotes the expectation and $\boldsymbol{W}_t$ is a standard (multidimensional) Brownian motion. This very lively field of numerical simulation can be approached by the reading of works such as Refs. [15, 17, 97, 120, 148] (see other references therein). It should be already clear in the reader's mind that such an approach raises hundreds of interesting questions, both theoretical and numerical, and all lying at the intersection of the world of PDEs and SDEs (or even SPDEs i.e. stochastic partial differential equations). So far as we know, no existing study deals with the existence of solution $(\boldsymbol{u}, \boldsymbol{\tau}, \boldsymbol{Q}_t)$ to the above system (2.8) or any system of the same family. Moreover, despite the numerous simulations done, no proof of convergence of a numerical scheme towards the "continuous" solution has ever been established.

Our present work aims at giving a complete mathematical and numerical analysis of a system such as (2.8). For reasons that will be clear below, we are bound to restrict ourselves to a very simple case, that we hope however to be instructive enough to motivate further studies.

2.2 The model and our main result.

The system we study here is the following

$$
\frac{\partial u}{\partial t}(t,x) - \partial_{x,x}^2 u(t,x) = \partial_x \tau(t,x) + f_{ext}(t,x), \tag{2.9}
$$

$$
\tau(t,x) = \mathbb{E}(P(t)Q(t,x)), \tag{2.10}
$$

$$
dP(t) = -\frac{P(t)}{2}dt + dV_t, \tag{2.11}
$$

$$
dQ(t,x) = \left(\partial_x u(t,x)P(t) - \frac{Q(t,x)}{2}\right)dt + dW_t, \tag{2.12}
$$

complemented with *ad hoc* boundary and initial conditions, which will be both made precise below. It is obtained from (2.8) by making the following assumptions :

 – (H1) We consider a shear flow in 2D : $\boldsymbol{u} = u_y(x)\boldsymbol{e}_y$ (see Figure 2.1). The function u_y is henceforth denoted by u. Consequently, the divergence free condition (2.4) is automatically fulfilled. Another striking consequence of this geometrical assumption is that the Navier term $\boldsymbol{u}.\nabla\boldsymbol{u}$ in (2.3) and the transport term $\boldsymbol{u}.\nabla$ in the stochastic equations both vanish. In equation (2.10), τ denotes the (x,y) components of the stress tensor $\boldsymbol{\tau}$. In equations (2.11) and (2.12), $(P(t), Q(t,x))$ (resp. (V_t, W_t)) are the two components of the end-to-end vector $\boldsymbol{Q}(t)$ (resp. the Brownian motion $\boldsymbol{W}_t$). In equation (2.9), f_{ext} denotes an external force.

 – (H2) The force $\boldsymbol{F}(\boldsymbol{Q})$ in (2.8) is chosen to be a simple linear force $\boldsymbol{F}(\boldsymbol{Q}) = H\boldsymbol{Q}$ with H the coefficient of the Hookean spring which models the polymer (let us incidentally mention that such a force has nothing to do with the modeling of intra-molecular forces inside the polymer chain : it is only entropic in nature, and models the simple property stating that when the polymer chain stretches, the volume of the region of the configurations space visited by the polymer gets smaller). A consequence of this "Hookean dumbbell" assumption is that the model (2.8) is indeed equivalent (at least formally, but more can be said than that) to a purely macroscopic model of the type (2.1), namely the famous Oldroyd B model written here in its differential form :

$$
\boldsymbol{\tau} + \lambda\frac{\delta\boldsymbol{\tau}}{\delta t} = nk_B T\lambda(\nabla\boldsymbol{u} +^t \nabla\boldsymbol{u}), \tag{2.13}
$$

with the upper convected derivative $\frac{\delta}{\delta t}$ defined by

$$
\frac{\delta\boldsymbol{\tau}}{\delta t} = \frac{\partial\boldsymbol{\tau}}{\partial t} + \boldsymbol{u}.\nabla\boldsymbol{\tau} - \boldsymbol{\tau}^t\nabla\boldsymbol{u} - \nabla\boldsymbol{u}\boldsymbol{\tau},
$$

where $\lambda = \frac{\zeta}{4H}$ is a characteristic time. In our simple case, (2.13) reduces to :

$$
\frac{\partial\tau}{\partial t} + \tau = \partial_x u. \tag{2.14}
$$
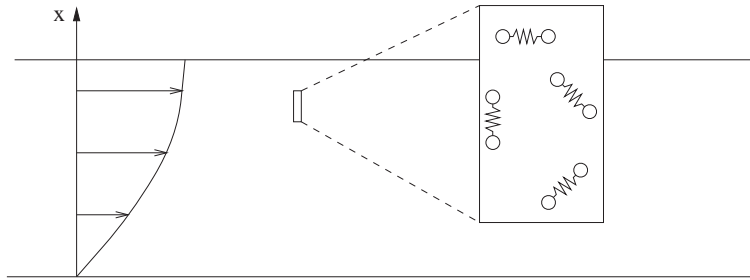
FIG. 2.1 – Velocity profile in a shear flow of a dilute solution of polymers.

Let also notice that we have chosen units of time and length such that $\lambda = 1$ and $d = \sqrt{\frac{k_B T}{H}} = 1$. Moreover, we have taken the physical parameters in order to simplify the equations. All the results we give are of course also valid with different conventions.

The main two results of our work, which are respectively stated in Theorem 1 and Theorem 3 in a very precise way show :

(a) that there exists a solution (u, Q_t) to the system in the natural energy spaces associated to the problem,

(b) that the fully discretized solution $(\overline{u}_h^n, \frac{1}{M} \sum_{j=1}^{M} \overline{P}_n^j \overline{Q}_{h,n}^j)$ (the velocity being discretized over P1 finite elements in space, and by finite differences in time while the SDE being discretized by an Euler scheme in time and the stress tensor approximated by Monte Carlo realizations) converges up to a slight technical modification, which is linked to the stability of the SDE and that will be made precise in subsection 2.4.34.3, to the continuous solution at the order $O\left(h + \delta t + \frac{1}{\sqrt{M}}\right)$, where h is the space step, δt is the time step and M is the number of realizations of the SDEs (i.e. the number of dumbbells per cell).

The sequel of this paper is devoted to the proof of these two assertions. However, before we get to the heart of the matter, let us emphasize our goal, and also give some comments that we believe such results deserve.

The proof of the existence (and in fact uniqueness and regularity) of the continuous problem is reproduced here mainly for the sake of consistency. Although it does not appear as such in the literature, it could be derived in a rather straightforward way from the observation that our model is, as mentioned above, in fact equivalent to an Oldroyd B type model. The only (slight) novelty is that, with a view to tackle next the Galerkin approximation, we deliberately work in the natural energy (Sobolev) spaces. On the contrary, studies such as Ref. [131] take a much more regular setting and the study Ref. [106] considers another type of convective derivative (for details about convective derivatives and frame indifference, see for example Ref. [137]). On the other hand, the "numerical analysis" part of our work seems completely new. We are aware that the case we deal with, precisely because of its simplicity and its formal equivalence with a purely macroscopic model

(hypotheses (H1) and (H2)) cannot be considered as a prototype (in terms of the mathematical difficulty) of all models of type (2.8). However,

(a) the simple model (2.9)-(2.12) embodies many, if not all, difficulties of model of type (2.8) : the coupling between the stochastic part and the macroscopic flow part, the fact that at any fixed number of dumbbells the (apparently determininistic) flow velocity is actually a stochastic variable. It is therefore expected that the mathematical toolbox used for its study will be useful and instructive for the analysis of the other cases. At least it is a preliminary matter for them.

(b) the simple model (2.9)-(2.12) is indeed used in the numerical practice (and coded as such) in order to serve as a test case for advanced numerical techniques that will be then extended to more sophisticated cases. This justifies (to our opinion at least) the need for the numerical analysis of this model *per se*.

Remark 1 *When the microscopic model is not that of Hookean dumbbells, the force* $\boldsymbol{F}(\boldsymbol{Q})$ *is no longer linear but can be*

$$\boldsymbol{F}(\boldsymbol{Q}) = \frac{H\boldsymbol{Q}}{1 - |\boldsymbol{Q}|^2/b},$$

or

$$\boldsymbol{F}(\boldsymbol{Q}) = \frac{H\boldsymbol{Q}}{1 - \mathbb{E}(|\boldsymbol{Q}|^2)/b},$$

which are respectively the case for the so-called FENE and FENE-P dumbbells case. The FENE-P model is derived from the FENE model via a closure approximation (the so-called Peterlin approximation), which enables to obtain a purely macroscopic equivalent of the microscopic model. In these models, b is a positive parameter which is the square of the maximum elongation of the dumbbells. The mathematical difficulty is then to ensure that $\boldsymbol{Q}$ *does not leave the region* $|\boldsymbol{Q}| \leq \sqrt{b}$ *and does not even reach its boundary. Current research (cf. Ref. [86]) is directed towards trying to extend the present analysis to this case.*

Remark 2 *When the macroscopic flow is no longer a pure shear flow, (at least) four new difficulties arise :*

(*i*) *the divergence free constraint (2.4) has to be accounted for,*

(*ii*) *the Navier term has to be treated,*

(*iii*) *the term* $\boldsymbol{u}.\nabla\boldsymbol{Q}_t$ *in the left hand side of the SDE of (2.8) has to be dealt with,*

(*iv*) *product of two non autonomous stochastic processes arises in the definition of* $\boldsymbol{\tau}$. *(Note that in (2.10),* P_t *is autonomous, i.e. does not depend on the flow.)*

Of these four difficulties, difficulties (iii) and (iv) are so far as we understand the most embarrassing ones. Difficulty (i) is standard, and (ii) is a classical well-known difficulty of the mathematical analysis of incompressible (Newtonian) Navier-Stokes equation (and we cannot hope to go further in the analysis of the present models than in that of the Navier Stokes equation). Difficulty (iii), namely the appearance of a transport term in the SDE (which ipso facto becomes a SPDE), creates at once an interesting question : in what sense can we consider the SDE of the system (2.8) ?

A way to circumvent the difficulty is to set the SDE in the Lagrangian setting, i.e. follow the characteristics of the flow and write the SDE along them. But as we have in mind to deal with a weak solution $\boldsymbol{u}$ of the macroscopic flow equations (think of the 3d case), it is not an easy task to define these characteristics, and also to give a rigorous foundation to the Lagrangian form (because of the term $\nabla \boldsymbol{u} \boldsymbol{Q}$ in the right-hand-side which lacks of regularity with respect to $\boldsymbol{Q}$ if $\boldsymbol{u}$ is only H^1). We refer the interested reader to Ref. [100] where it is shown that one can adapt and complete the Di Perna-Lions theory of almost everywhere flows to accommodate for this new situation.

Remark 3 *When the solution is no longer infinitely diluted, other models arise. For high densities, models like those issued from the theory of reptation (Doi-Edwards models) appear. Then again, macroscopic models and micro-macro models are two alternatives. Questions like those of simulation of reflected Brownian processes then come into the picture (see Ref. [120]), giving also rise to questions of interest for the numerical analysist. Let us also mention that what is expected to be the most challenging case with respect to the difficulty of its modeling is neither the infinitely dilute case, nor the polymer melt case, but the case in between!*

Let us end this section saying that we hope to complement the results of the present work at least in two directions :

(a) evaluate on the same toy-model both by numerical analysis and computational experiments the validity of well known and commonly used techniques of this field of computational rheology such as variance reduction methods,

(b) do the same analysis as that of the present paper for some of the more difficult cases mentioned in the above remarks.

We refer the reader to Refs. [83] for (a) and to Refs. [86] for (b).

2.3 Brief mathematical analysis of the continuous problem.

2.3.1 Precise setting of the equations and definition of solutions.

As announced above, we complement system (2.9)-(2.12) with the following boundary conditions :

$$\begin{cases} u(t,0) = f_0(t), \\ u(t,1) = f_1(t), \end{cases} \qquad (2.15)$$

together with the initial data :

$$\begin{cases} u(0,x) &= u_0(x), \\ Q(0,x) &= Q_0, \\ P(0) &= P_0. \end{cases} \qquad (2.16)$$

Let us also make precise the notations : P_0 and Q_0 denote two independent normal random variables (because we suppose that the polymers are initially at equilibrium),

also independent of V_t and W_t which denote two standard independent Brownian motions. Notice that, as function of the space variable x, (V_t, W_t) is constant. In the following, we have $(t, x) \in (0, T) \times \mathcal{O}$ with $\mathcal{O} = (0, 1)$.

The following regularity for the external forces and the initial velocity are supposed :

$$\begin{cases} f_{ext} \in L^1_t(H^1_x) \cap W^{1,1}_t(L^2_x), \\ f_{ext}(0, x) \in L^2_x, \\ u_0 \in H^2. \end{cases} \tag{2.17}$$

It is to be remarked that although the regularities (2.17) have been chosen for simplicity and because they are necessary for our result of convergence (Theorem 3), some parts of the arguments below may be done under less regular requirements. Let us also notice that all the results we give are also valid with other assumptions of regularity on f_{ext}.

We restrict ourselves to the case of homogeneous boundary conditions ($f_0 = f_1 = 0$), the modifications to deal with the other cases being only a technical matter. In the following, t, x and ω denote respectively the variable in time, space and probability. For example, $Q_t \in L^\infty_t(L^2_x(L^2_\omega))$ means that $\mathrm{supess}_{t \in (0,T)}\{\int_{\mathcal{O}} \mathbb{E}(Q_t^2)\, dx\} < \infty$.

We are now in position to define the notion of solution we shall deal with.

We say that (u, Q) is a weak solution of the homogeneous problem if $u \in L^\infty_t(L^2_x) \cap L^2_t(H^1_{0,x})$ and $Q_t \in L^\infty_t(L^2_x(L^2_\omega))$ satisfy that for all $v \in H^1_0(\mathcal{O})$,

$$\frac{d}{dt} \int_{\mathcal{O}} uv + \int_{\mathcal{O}} \partial_x u \partial_x v = -\int_{\mathcal{O}} \mathbb{E}(P_t Q_t(x)) \partial_x v + \int_{\mathcal{O}} f_{ext}(t, x) v, \tag{2.18}$$

for a.e. (x, ω), $\forall t \in (0, T)$, $Q_t(x) = e^{-\frac{t}{2}} Q_0 + \int_0^t e^{\frac{s-t}{2}}\, dW_s + \int_0^t e^{\frac{s-t}{2}} \partial_x u P_s\, ds$, (2.19)

with

$$P_t = e^{-\frac{t}{2}} P_0 + \int_0^t e^{\frac{s-t}{2}}\, dV_s. \tag{2.20}$$

Equation (2.18) holds in the sense of distributions in time. As usual, one may equivalently use time dependent test functions $v \in L^\infty_t(L^2_x) \cap L^2_t(H^1_{0,x})$.

2.3.2 Formal *a priori* estimates.

We now establish formal *a priori* estimates on the solution (u, Q). These estimates will be made rigorous at the discrete level in the next subsection.

Multiplying (2.9) by u, next integrating over the domain and in time, we obtain

$$\frac{1}{2} \int_{\mathcal{O}} u(t, x)^2 - \frac{1}{2} \int_{\mathcal{O}} u_0(x)^2 + \int_0^t \int_{\mathcal{O}} (\partial_x u)^2 = -\int_0^t \int_{\mathcal{O}} \mathbb{E}(P_s Q_s(x)) \partial_x u(s, x)$$
$$+ \int_0^t \int_{\mathcal{O}} f_{ext}(s, x) u(s, x).$$

Next we compute Q_t^2 by Itô's formula using (2.12), take expectations and integrate again on $\mathcal{O}$ and in time to obtain

$$\frac{1}{2}\int_{\mathcal{O}}\mathbb{E}(Q_t^2) - \frac{1}{2} = \int_0^t\int_{\mathcal{O}}\mathbb{E}(P_sQ_s(x))\partial_x u(s,x) - \frac{1}{2}\int_0^t\int_{\mathcal{O}}\mathbb{E}(Q_s^2) + \frac{1}{2}t.$$

Summing up these two equalities, we obtain

$$\frac{1}{2}||u||_{L_x^2}^2(t) + \int_0^t||\partial_x u||_{L_x^2}^2 + \frac{1}{2}\int_{\mathcal{O}}\mathbb{E}(Q_t^2) + \frac{1}{2}\int_0^t\int_{\mathcal{O}}\mathbb{E}(Q_s^2)\,ds = \frac{1}{2}||u_0||_{L_x^2}^2$$
$$+\frac{1}{2}(1+t) + \int_0^t\int_{\mathcal{O}}f_{ext}u, \quad (2.21)$$

which yields *the first energy inequality* :

$$||u||_{L_t^\infty(L_x^2)}^2 + ||u||_{L_t^2(H_{0,x}^1)}^2 + ||Q_t||_{L_t^\infty(L_x^2(L_\omega^2))}^2 + ||Q_t||_{L_t^2(L_x^2(L_\omega^2))}^2$$
$$\leq C\left(1 + ||u_0||_{L_x^2}^2 + T + ||f_{ext}||_{L_t^1(L_x^2)}^2\right), \quad (2.22)$$

with C a constant independent of the data of the problem.

At this stage, it is to be remarked that using the same arguments as in the derivation of (2.21) or (2.22) with $u = u_1 - u_2$ and $Q = Q_1 - Q_2$, one can show the uniqueness of solution. This point should be not surprising for the reader as the system (2.9)-(2.12) (once written in terms of u only, using equation (2.10) on τ and equation (2.12)) on Q_t is indeed a linear system with respect to the variable u. This is obviously a consequence of our simplifying assumptions (H1) and (H2).

We must also notice that this energy estimate shows that the regularity of the solution is at least : $u \in L_t^2(H_x^1)$ and $\frac{\partial u}{\partial t} \in L_t^2(H_x^{-1})$. This shows in fact that $u \in \mathcal{C}([0,T], L^2(\mathcal{O}))$ which allows us to define $u(0)$ (see Ref. [145] Chapter III, Lemma 1.2).

Let us now turn to the second energy inequality. This time, we multiply (2.9) by $-\partial_{x,x}^2 u$ and integrate over the domain to obtain

$$\frac{d}{dt}\int_{\mathcal{O}}(\partial_x u)^2 + \int_{\mathcal{O}}(\partial_{x,x}^2 u)^2 = -\int_{\mathcal{O}}\partial_x\mathbb{E}(P_tQ_t)\partial_{x,x}^2 u - \int_{\mathcal{O}}f_{ext}\partial_{x,x}^2 u.$$

We need to control the first term in the right-hand side. Computing $d(P_tQ_t)$ from (2.11) and (2.12) and taking expectations, we get the following equation (equivalent to (2.14)) :

$$\frac{\partial}{\partial t}\mathbb{E}(P_tQ_t) = -\mathbb{E}(P_tQ_t) + \partial_x u\,\mathbb{E}(P_t^2). \quad (2.23)$$

By a standard application of Gronwall's lemma, this yields the following bound

$$||\partial_x\mathbb{E}(P_tQ_t)||_{L_x^2}^2 \leq \int_0^t||\partial_{x,x}^2 u||_{L_x^2}^2,$$

which we use to finally obtain (using again Gronwall's lemma) *the second energy inequality* :

$$||u||_{L_t^\infty(H_x^1)\cap L_t^2(H_x^2)} \leq C\left(||u_0||_{H_x^1} + ||f_{ext}||_{L_t^1(H_x^1)}\right), \quad (2.24)$$

where C only depends on T.

Likewise, we multiply (2.9) by $\frac{\partial u}{\partial t}$ after derivating it in time (all this is done formally we recall), and we integrate over $\mathcal{O}$ to obtain

$$\left\|\frac{\partial u}{\partial t}\right\|^2_{L^\infty_t(L^2_x)} + \left\|\frac{\partial \partial_x u}{\partial t}\right\|^2_{L^2_t(L^2_x)} \leq C \left(\left\|\frac{\partial}{\partial t}\mathbb{E}(P_t Q_t)\right\|^2_{L^2_t(L^2_x)} + \left\|\frac{\partial f_{ext}}{\partial t}\right\|^2_{L^1_t(L^2_x)} + \left\|\frac{\partial u}{\partial t}\Big|_{t=0}\right\|^2_{L^2_x} \right).$$

Using again equation (2.23), we obtain (by Gronwall inequality)

$$\left\|\frac{\partial}{\partial t}\mathbb{E}(P_t Q_t)\right\|^2_{L^2_t(L^2_x)} \leq C \left(1 + ||u_0||^2_{L^2_x} + ||f_{ext}||^2_{L^1_t(L^2_x)} \right)$$

and we then derive another *regularity in time* :

$$\left\|\frac{\partial u}{\partial t}\right\|_{L^\infty_t(L^2_x) \cap L^2_t(H^1_x)} \leq C \left(1 + ||u_0||_{H^2} + ||f_{ext}||_{W^{1,1}_t(L^2_x)} + ||f_{ext}(0,x)||_{L^2_x} \right), \quad (2.25)$$

where C only depends on T.

2.3.3 Existence.

We can now show the existence of a solution of problem (2.18)-(2.19).

2.3.3.1 Semi-discretized weak formulation.

Let us define a Riesz basis $\{v_i\}_{i=1..\infty}$ of $H^1_0(\mathcal{O})$. We set $V_m = \text{Vect}\{v_1, ..., v_m\}$. The semi-discretized problem is the following :
Find $U^m \in (L^\infty_t(\mathbb{R}))^m$ and $Q^m_t \in L^\infty_t(L^2_x(L^2_\omega))$ such that, for all $1 \leq i \leq m$, the couple $(u^m(t,x), Q^m_t(x))$, where $u^m(t,x) = \sum_i U^m_i(t)v_i(x)$, satisfies :

$$\frac{d}{dt}\int_{\mathcal{O}} u^m v_i = -\int_{\mathcal{O}} \partial_x u^m \partial_x v_i - \int_{\mathcal{O}} \mathbb{E}(P_t Q^m_t(x))\partial_x v_i + \int_{\mathcal{O}} f_{ext} v_i, \quad (2.26)$$

$$Q^m_t = e^{-\frac{t}{2}}Q_0 + \int_0^t e^{\frac{s-t}{2}}\,dW_s + \int_0^t e^{\frac{s-t}{2}}\partial_x u^m P_s\,ds, \quad (2.27)$$

with $Q^m_0 = Q_0$ and $u^m(t=0) = \Pi_m(u_0)$ where Π_m is the H^1-projection on V_m. Again, (2.27) has to make sense for a.e. (x,ω), for all $t \in (0,T)$.

2.3.3.2 Existence of a semi-discretized solution.

It is standard to find a solution to the discretized problem (2.26)-(2.27) using e.g. a fixed-point argument on the function

$$F : \begin{cases} X & \longrightarrow & X \\ \begin{pmatrix} U(t) \\ Q_t(x) \end{pmatrix} & \longmapsto & \begin{pmatrix} U_0 - A^{-1}\left(\int_0^t \left(BU(s) - \int_{\mathcal{O}} \mathbb{E}(P_s Q_s)\partial_x V + F_{ext}\right)\right) \\ e^{-\frac{t}{2}}Q_0 + \int_0^t e^{\frac{s-t}{2}}\,dW_s + \int_0^t e^{\frac{s-t}{2}}\sum_i U_i \partial_x v_i P_s \end{pmatrix} \end{cases},$$

where $X = \{(U, Q_t) \in (L_t^\infty(\mathbb{R}))^m \times L_t^\infty(L_x^2(L_\omega^2))\}$ is a Banach space for the norm $||(U, Q_t)||_X = ||U||_{L_t^\infty} + ||Q_t||_{L_t^\infty(L_x^2(L_\omega^2))}$, $A_{i,j} = \int_{\mathcal{O}} v_i v_j$, $B_{i,j} = \int_{\mathcal{O}} \partial_x v_i \partial_x v_j$, V is a field of components v_j and F_{ext} is a vector of components $\int_{\mathcal{O}} f_{ext} v_j$.

The point is the following result stating the regularity of the discretized solution.

Lemma 1 (Regularity of the space-discretized solution) *Assuming $u_0 \in L_x^2$ and $f_{ext} \in L_t^1(L_x^2)$, we have :*

$$||u^m||^2_{L_t^\infty(L_x^2)} + ||u^m||^2_{L_t^2(H_{0,x}^1)} + ||Q_t^m||^2_{L_t^\infty(L_x^2(L_\omega^2))} + ||Q_t^m||^2_{L_t^2(L_x^2(L_\omega^2))}$$

$$\leq C\left(1 + ||u_0||^2_{L_x^2} + T + ||f_{ext}||^2_{L_t^1(L_x^2)}\right), \qquad (2.28)$$

with C independent of the data of the problem.

Assuming $u_0 \in H_x^2$ and $f_{ext} \in W_t^{1,1}(L_x^2)$, we have :

$$\left\|\frac{\partial u^m}{\partial t}\right\|_{L_t^\infty(L_x^2) \cap L_t^2(H_x^1)} \leq C\left(||u_0||_{H^2} + ||f_{ext}||_{W_t^{1,1}(L_x^2)} + ||f_{ext}(0, x)||_{L_x^2}\right), \quad (2.29)$$

$$\left\|\frac{\partial^2 u^m}{\partial t^2}\right\|_{L_t^2(H_{*,x}^{-1})} \leq C\left(||u_0||_{H^2} + ||f_{ext}||_{W_t^{1,1}(L_x^2)} + ||f_{ext}(0, x)||_{L_x^2}\right), \quad (2.30)$$

where C only depends on T. By definition, $||g||_{H_{*,x}^{-1}} = \sup\limits_{w \in V^m} \dfrac{|\int_{\mathcal{O}} g w|}{||\partial_x w||_{L_x^2}}$.

Proof. To obtain the first two estimates (2.28) and (2.29) is a classical exercise : one just needs to reproduce in a more rigorous way the *a priori* estimates (2.22) and (2.25) of the former subsection. The last result (2.30) is obtained by writing the derivative in time of (2.26) and observing that $\frac{\partial}{\partial t}\mathbb{E}(P_t Q_t^m) = -\mathbb{E}(P_t Q_t^m) + \partial_x u^m \mathbb{E}(P_t^2)$ which ensures $\frac{\partial}{\partial t}\mathbb{E}(P_t Q_t^m) \in L_t^2(L_x^2)$. $\qquad\square$

2.3.3.3 Convergence towards a continuous solution.

We assume $u_0 \in L_x^2$ and $f_{ext} \in L_t^1(L_x^2)$. According to the former lemma, we have $||u^m||_{L_t^\infty(L_x^2) \cap L_t^2(H_x^1)} + ||Q^m||_{L_t^\infty(L_x^2(L_\omega^2))} \leq C$ with C independent of m. The convergence of the sequence $(u^m, Q^m)_{m \in \mathbb{N}}$ then classically derives from this estimate (notice that there are only linear terms in u^n and Q^n in the equations (2.26) and (2.27), since P_t is autonomous), following the next three steps :

Step 1 Using the estimate on $(u^m)_{m \in \mathbb{N}}$, one can define a function $u \in L_t^\infty(L_x^2) \cap L_t^2(H_{0,x}^1)$ such that u^m converges towards u weakly in $L_t^2(H_x^1)$ and for the weak-* topology of $L_t^\infty(L_x^2)$ (and therefore in $\mathcal{D}'((0, T) \times \mathcal{O})$). This function u satisfies the first energy inequality (2.22) (taking the inferior limit).

Step 2 One can then define $\tilde{Q}$ by $\tilde{Q} = e^{-\frac{t}{2}} Q_0 + \int_0^t e^{\frac{s-t}{2}} dW_s + \int_0^t e^{\frac{s-t}{2}} \partial_x u(s, x) P_s \, ds$ and check that $\tilde{Q} \in L_t^\infty(L_x^2(L_\omega^2))$.

Step 3 It remains to check the convergence of the terms of the equation (2.26) satisfied by u^m. The only non-trivial term is $\int_{\mathcal{O}} \mathbb{E}(P_t Q_t^m(x)) \partial_x v_i$. We use that for $w \in L_x^2(\mathcal{O})$,

$$\int_{\mathcal{O}} \mathbb{E}(P_t Q_t^m(x)) w = \int_{\mathcal{O}} \mathbb{E}\left(P_t \int_0^t e^{\frac{s-t}{2}} \partial_x u^m P_s \, ds\right) w = \int_{\mathcal{O}} \int_0^t \partial_x u^m e^{\frac{s-t}{2}} \mathbb{E}(P_s P_t) w \, ds \, dx,$$

and this last term goes to $\int_{\mathcal{O}} \int_0^t \partial_x u \, e^{\frac{s-t}{2}} \mathbb{E}(P_s P_t) w \, ds \, dx = \int_{\mathcal{O}} \mathbb{E}(P_t \tilde{Q}_t(x)) w$ (because $\partial_x u^m$ converges weakly towards $\partial_x u$ in $L_t^2(L_x^2)$).

We have therefore obtained a solution of the problem (2.18)-(2.19). Let us show now the convergence of Q_t^m towards $\tilde{Q}_t$ as well as the strong convergence of u^m towards u.

Lemma 2 *Assume $u_0 \in H_x^2$ and $f_{ext} \in W_t^{1,1}(L_x^2)$. Set (u, Q_t) the solution of the problem (2.18)-(2.19). Set V_m a subspace of H_0^1 and (u^m, Q_t^m) the solution of the semi-discretized problem (2.26)-(2.27) with an initial velocity u_0^m. Then, we have for all $t \in [0, T]$,*

$$||u(t) - u^m(t)||_{L_x^2}^2 + \int_0^t ||\partial_x(u - u^m)||_{L_x^2}^2 + ||Q_t - Q_t^m||_{L_x^2(L_\omega^2)}^2 + \frac{1}{2} \int_0^t ||Q_s - Q_s^m||_{L_x^2(L_\omega^2)}^2$$

$$\leq ||u_0 - u_0^m||_{L_x^2}^2 + \inf_{w \in V^m} \left(3||\partial_x(u - w)||_{L_t^2(L_x^2)}^2 + C||u - w||_{L_t^2(L_x^2)} \right),$$

with a constant C which depends on the data of the problem : u_0, f_{ext} and T.

Proof. Let w be a function in V_m. One can easily obtain, using the linearity of the variational formulations, and integrating in time :

$$\frac{1}{2} \int_{\mathcal{O}} (u - u^m)^2(t) + \int_0^t \int_{\mathcal{O}} |\partial_x(u - u^m)|^2 = \frac{1}{2} \int_{\mathcal{O}} (u_0 - u_0^m)^2$$

$$- \int_0^t \int_{\mathcal{O}} \mathbb{E}(P_s(Q_s - Q_s^m)) \partial_x(u - u^m) + \int_0^t \int_{\mathcal{O}} \mathbb{E}(P_s(Q_s - Q_s^m)) \partial_x(u - w)$$

$$+ \int_0^t \int_{\mathcal{O}} \frac{\partial}{\partial t}(u - u^m)(u - w) + \int_0^t \int_{\mathcal{O}} \partial_x(u - u^m) \partial_x(u - w). \qquad (2.31)$$

Using the equations on Q_t and Q_t^m, one can show that :

$$\frac{1}{2} \int_{\mathcal{O}} \mathbb{E}(Q_t - Q_t^m)^2 = \int_0^t \int_{\mathcal{O}} \mathbb{E}(P_s(Q_s - Q_s^m)) \partial_x(u - u^m) - \frac{1}{2} \int_0^t \int_{\mathcal{O}} \mathbb{E}(Q_s - Q_s^m)^2.$$
$$(2.32)$$

Summing up (2.31) and (2.32), we have :

$$\frac{1}{2} \int_{\mathcal{O}} (u - u^m)^2(t) + \int_0^t \int_{\mathcal{O}} |\partial_x(u - u^m)|^2 + \frac{1}{2} \int_{\mathcal{O}} \mathbb{E}(Q_t - Q_t^m)^2 + \frac{1}{2} \int_0^t \int_{\mathcal{O}} \mathbb{E}(Q_s - Q_s^m)^2$$

$$= \frac{1}{2} \int_{\mathcal{O}} (u_0 - u_0^m)^2 + \int_0^t \int_{\mathcal{O}} \mathbb{E}(P_s(Q_s - Q_s^m)) \partial_x(u - w)$$

$$+ \int_0^t \int_{\mathcal{O}} \frac{\partial}{\partial t}(u - u^m)(u - w) + \int_0^t \int_{\mathcal{O}} \partial_x(u - u^m) \partial_x(u - w). \quad (2.33)$$

Using Cauchy-Schwarz inequalities, we have

$$\int_0^t \int_{\mathcal{O}} \partial_x(u - u^m)\partial_x(u - w) \leq \frac{1}{2}\int_0^t \int_{\mathcal{O}} |\partial_x(u - u^m)|^2 + \frac{1}{2}\int_0^t \int_{\mathcal{O}} |\partial_x(u - w)|^2,$$

and (using $\mathbb{E}(P_s^2) = 1$)

$$\int_0^t \int_{\mathcal{O}} \mathbb{E}(P_s(Q_s - Q_s^m))\partial_x(u - w) \leq \frac{1}{4}\int_0^t \int_{\mathcal{O}} \mathbb{E}(Q_s - Q_s^m)^2 + \int_0^t \int_{\mathcal{O}} |\partial_x(u - w)|^2.$$

The estimation of $\left|\left|\frac{\partial u^m}{\partial t}\right|\right|_{L_t^2(L_x^2)}$ given by Lemma 1 also holds for the continuous solution u (taking the inferior limit). This yields the final estimate : $\int_0^t \int_{\mathcal{O}} \frac{\partial}{\partial t}(u - u^m)(u - w) \leq C\|u - w\|_{L_t^2(L_x^2)}$. □

In the former proof, we notice that we can assume that w also depends on the time variable. Choosing $w = \Pi_m(u)$ (we recall that Π_m is the operator of the H^1-projection on V_m), one can therefore show the strong convergence of u^m towards u in $L_t^\infty(L_x^2) \cap L_t^2(H_x^1)$ and the strong convergence of Q_t^m towards Q_t in $L_t^\infty(L_x^2(L_\omega^2))$. We have therefore proved the following result :

Theorem 1 (Existence of a continuous solution) *Let us assume $u_0 \in L_x^2$ and $f_{ext} \in L_t^1(L_x^2)$. The problem (2.18)-(2.19) admits a unique solution $u \in \mathcal{C}([0, T], L_x^2(\mathcal{O})) \cap L_t^2(H_{0,x}^1)$ and $Q_t \in L_t^\infty(L_x^2(L_\omega^2))$.*
The solution (u^m, Q_t^m) of the semi-discretized problem (2.26)-(2.27) is unique. Assuming $u_0 \in H_x^2$ and $f_{ext} \in W_t^{1,1}(L_x^2)$, (u^m, Q_t^m) converges towards (u, Q_t) in the following sense : $u^m \longrightarrow u$ strongly in $L_t^\infty(L_x^2) \cap L_t^2(H_x^1)$ and $Q_t^m \longrightarrow Q_t$ strongly in $L_t^\infty(L_x^2(L_\omega^2))$.

Remark 4 *It is clear that, under the hypothesis $u_0 \in H_x^2$ and $f_{ext} \in W_t^{1,1}(L_x^2)$, the continuous solution u is a function of $L_t^\infty(L_x^2) \cap L_t^2(H_x^1)$ which satisfies the inequality (2.25). Moreover, under the assumptions $u_0 \in H_x^1$ and $f_{ext} \in L_t^1(H_x^1)$, we can also prove that the solution satisfies the second energy estimate (2.24), what will be used in the subsection 2.4.14.1. To prove this result, one uses the uniqueness of the solution and the fact that one can construct a sequence of approximations of the solution which satisfies (2.24) by a Galerkin method on a special base (stable for the laplacian). One can then also obtain (2.24) for the solution, taking the inferior limit.*

2.4 Analysis of the numerical scheme.

In this section, we want to show the convergence of a standard discretization of the problem (2.9)-(2.12). As above, we will suppose $u_0 \in H_x^2$, $f_{ext} \in L_t^1(H_x^1)$ and $\frac{\partial f_{ext}}{\partial t} \in L_t^1(L_x^2)$, which yields, using the *a priori* estimates (2.24) and (2.25) : $u \in L_t^\infty(H_x^1) \cap L_t^2(H_x^2)$ and $\frac{\partial u}{\partial t} \in L_t^\infty(L_x^2) \cap L_t^2(H_x^1)$.

For the sake of simplicity, we also assume here homogeneous Dirichlet boundary conditions. Standard modifications of our arguments yield the same conclusions with non homogeneous Dirichlet boundary conditions (see e.g. Remark 6.2.2 in Ref. [127].)

The original problem is discretized in three steps : in space (by a Galerkin method), in time (by an Euler semi-implicit scheme) and finally using the Monte Carlo method. We choose a P1 discretization in space of the velocity : the velocity space functions V_h is the space of the piecewise polynomials of degree 1 on a mesh $\mathcal{T}_h$ where h is the space discretization step. The time interval $(0, T)$ is discretized with a constant step δt. We consider M realizations of the dumbbell processes (P_t, Q_t). The scheme we use will be made precise in the subsection 2.4.34.3 (see equations (2.48)-(2.50)).

The aim of this section is to show Theorem 3 which states that the order of convergence of this scheme is $O\left(h + \delta t + \frac{1}{\sqrt{M}}\right)$.

2.4.1   Convergence of the space-discretized problem.

We consider here the space-discretized problem which is (2.26)-(2.27) with $V^m = V_h \subset H_x^1$ (we use a Galerkin method). Notice that since the velocity u_h is a piecewise linear function (P1), the process Q_h (and therefore the stress $\tau_h = \mathbb{E}(PQ_h)$) is a discontinuous piecewise constant function (discontinuous P0). We have already shown in subsection 2.3.3.23.3 that this problem admits a unique solution. Moreover, Lemma 2, together with the standard finite elements approximation inequality $||u - \Pi_h(u)||_{L_x^2}^2 + h^2 ||\partial_x(u - \Pi_h(u))||_{L_x^2}^2 \leq Ch^4 ||u||_{H_x^2}^2$ yields :

Lemma 3 (Convergence of the space-discretized problem) *Let us assume* $u_0 \in H_x^2$, $f_{ext} \in L_t^1(H_x^1)$ *and* $\frac{\partial f_{ext}}{\partial t} \in L_t^1(L_x^2)$. *Set* (u, Q_t) *the solution of the problem (2.18)-(2.19). Let us assume a P1 space discretization for the velocity. Set* V_h *the velocity space functions and* (u_h, Q_h) *the solution of the semi-discretized problem (2.26)-(2.27) with an initial velocity* $u_{h,0} = \Pi_h(u_0) \in V_h$. *Then we have :*

$$||u(t) - u_h(t)||_{L_t^\infty(L_x^2)}^2 + ||\partial_x(u - u_h)||_{L_t^2(L_x^2)}^2 + ||Q_t - Q_{h,t}||_{L_t^\infty(L_x^2(L_\omega^2))}^2 \leq Ch^2,$$

with C *a constant which depends on the data of the problem :* u_0, f_{ext} *and* T.

2.4.2   Convergence of the time-discretized problem.

We turn now to the semi-discretized problem in time and in space. We have already compared the continuous solution (u, Q) with the space-discretized solution (u_h, Q_h) and we want to estimate the error introduced by discretizing (u_h, Q_h) by an Euler scheme in time.

More precisely, we consider the following problem :
Being given $(u_h^n, Q_{h,n}, P_n)$, *we compute* $(u_h^{n+1}, Q_{h,n+1}, P_{n+1})$ *by the following algorithm :* u_h^{n+1} *is such that* $\forall v \in V_h$,

$$\frac{1}{\delta t} \int_{\mathcal{O}} (u_h^{n+1} - u_h^n)v + \int_{\mathcal{O}} \partial_x u_h^{n+1} \partial_x v = -\int_{\mathcal{O}} \mathbb{E}(P_n Q_{h,n}(x))\partial_x v + \int_{\mathcal{O}} f_{ext}(t_n)v. \quad (2.34)$$

$Q_{h,n+1}$ *and* P_{n+1} *are then computed by :*

$$Q_{h,n+1} - Q_{h,n} = \left(\partial_x u_h^{n+1} P_n - \frac{1}{2}Q_{h,n}\right)\delta t + W_{t_{n+1}} - W_{t_n}, \quad (2.35)$$

$$P_{n+1} - P_n = -\frac{1}{2}P_n \delta t + V_{t_{n+1}} - V_{t_n}. \quad (2.36)$$

This problem is complemented with the initial data $u_{h,0}$, P_0 and Q_0.

We will first show the stability of the scheme and then the convergence.

Lemma 4 (Stability of the space-time-discretized problem) *We assume that* $f_{ext} \in L_t^\infty(L_x^2)$ *and* $u_0 \in L_x^2$. *Under the assumption* $\delta t < \frac{1}{2}$, *we have : for all* $n \leq \frac{T}{\delta t}$,

$$||u_h^n||_{L_x^2}^2 + ||Q_{h,n}||_{L_x^2(L_\omega^2)}^2 + \frac{\delta t}{2} \sum_{k=1}^n \int_{\mathcal{O}} |\partial_x u_h^k|^2 \leq 1 + ||u_{h,0}||_{L_x^2}^2 + T\left(1 + C||f_{ext}||_{L_t^\infty(L_x^2)}^2\right),$$

where C is a constant independent of the data of the problem.

Proof. In order to lighten the notations, we set $u_h^n = u_n$ and $Q_{h,n} = Q_n$. We also set $||f||_{H_*^{-1}} = \sup_{v \in V_h} \frac{\int_{\mathcal{O}} fv}{||\partial_x v||_{L_x^2}}$. If $f \in L^2$, one clearly has $||f||_{H_*^{-1}} \leq C||f||_{L^2}$. We choose $v = u_{n+1}$ in (2.34), what yields

$$\frac{1}{\delta t} \int_{\mathcal{O}} u_{n+1}^2 + \int_{\mathcal{O}} (\partial_x u_{n+1})^2 = \frac{1}{\delta t} \int_{\mathcal{O}} u_n u_{n+1} + \int_{\mathcal{O}} f_{ext}(t_n) u_{n+1} - \int_{\mathcal{O}} \mathbb{E}(P_n Q_n) \partial_x u_{n+1}$$

$$\leq \frac{1}{2\delta t}\left(\int_{\mathcal{O}} u_n^2 + \int_{\mathcal{O}} u_{n+1}^2\right) + \frac{1}{10} \int_{\mathcal{O}} (\partial_x u_{n+1})^2 + C||f_{ext}(t_n)||_{H_*^{-1}}^2 - \int_{\mathcal{O}} \mathbb{E}(P_n Q_n) \partial_x u_{n+1}.$$

One multiplies next (2.35) with Q_n and takes the expectation value :

$$\mathbb{E}(Q_{n+1} Q_n) - \mathbb{E}(Q_n^2) = \left(\mathbb{E}(\partial_x u_{n+1} P_n Q_n) - \frac{1}{2}\mathbb{E}(Q_n^2)\right)\delta t,$$

$$\frac{1}{2}\left(\mathbb{E}(Q_{n+1}^2) - \mathbb{E}(Q_n^2)\right) + \frac{1}{2}\mathbb{E}(Q_n^2)\delta t = \partial_x u_{n+1}\mathbb{E}(P_n Q_n)\delta t + \frac{1}{2}\mathbb{E}((Q_{n+1} - Q_n)^2).$$

Summing this estimate multiplied by $\frac{1}{\delta t}$ and integrated in space, and the one on u_n, we get :

$$\frac{1}{2\delta t}\left(\int_{\mathcal{O}} u_{n+1}^2 - \int_{\mathcal{O}} u_n^2\right) + \frac{1}{2\delta t}\left(\int_{\mathcal{O}}\mathbb{E}(Q_{n+1}^2) - \int_{\mathcal{O}}\mathbb{E}(Q_n^2)\right) + \frac{9}{10}\int_{\mathcal{O}}(\partial_x u_{n+1})^2$$

$$+ \frac{1}{2}\int_{\mathcal{O}}\mathbb{E}(Q_n^2) \leq C||f_{ext}(t_n)||_{H_*^{-1}}^2 + \frac{1}{2\delta t}\int_{\mathcal{O}}\mathbb{E}((Q_{n+1} - Q_n)^2). \quad (2.37)$$

It remains to estimate the last term in the right-hand side. This is done by taking the square of (2.35) and then the expectation value :

$$\mathbb{E}((Q_{n+1} - Q_n)^2) = \mathbb{E}\left(\left(\partial_x u_{n+1} P_n - \frac{1}{2}Q_n\right)^2\right)\delta t^2 + \delta t$$

$$\leq 2(\partial_x u_{n+1})^2 \mathbb{E}(P_n^2)\delta t^2 + \frac{1}{2}\mathbb{E}(Q_n^2)\delta t^2 + \delta t.$$

It is easy to show that $\mathbb{E}(P_n^2)$ is bounded by $\frac{4}{4-\delta t}$ (by induction, using $\mathbb{E}(P_{n+1}^2) = \left(1 - \frac{\delta t}{2}\right)^2 \mathbb{E}(P_n^2) + \delta t$). We obtain then :

$$\mathbb{E}((Q_{n+1} - Q_n)^2) \leq (\partial_x u_{n+1})^2 \frac{8\delta t^2}{4 - \delta t} + \frac{1}{2}\mathbb{E}(Q_n^2)\delta t^2 + \delta t. \quad (2.38)$$

Using (2.37) and (2.38), one threfore obtains :

$$\frac{1}{2\delta t}\left(\int_{\mathcal{O}}u_{n+1}^2 - \int_{\mathcal{O}}u_n^2\right) + \frac{1}{2\delta t}\left(\int_{\mathcal{O}}\mathbb{E}(Q_{n+1}^2) - \int_{\mathcal{O}}\mathbb{E}(Q_n^2)\right) + \frac{9}{10}\int_{\mathcal{O}}(\partial_x u_{n+1})^2$$

$$+\frac{1}{2}\int_{\mathcal{O}}\mathbb{E}(Q_n^2) \leq C||f_{ext}(t_n)||_{H_*^{-1}}^2 + \frac{4\delta t}{4-\delta t}\int_{\mathcal{O}}(\partial_x u_{n+1})^2 + \frac{\delta t}{4}\int_{\mathcal{O}}\mathbb{E}(Q_n^2) + \frac{1}{2}. \qquad (2.39)$$

Under the assumption $\delta t < \frac{1}{2}$, one has $\int_{\mathcal{O}}u_{n+1}^2 - \int_{\mathcal{O}}u_n^2 + \int_{\mathcal{O}}\mathbb{E}(Q_{n+1}^2) - \int_{\mathcal{O}}\mathbb{E}(Q_n^2) + A\delta t\int_{\mathcal{O}}(\partial_x u_{n+1})^2 \leq \delta t\left(2C||f_{ext}(t_n)||_{H_*^{-1}}^2 + 1\right)$ (with $A = \frac{46}{70} \geq \frac{1}{2}$). We conclude by summation over n. $\qquad\square$

We are now going to show the convergence of this scheme. We will first show the convergence of P_n towards P_{t_n} and then, reproducing the proof of the energy estimate (2.22) at the discrete level, we will show the convergence of $(u_h^n, Q_{h,n})$ towards $(u_h(t_n), Q_h(t_n))$.

Let us begin with the convergence of P_n towards P_{t_n} (we recall that P_n and P_{t_n} are defined independently of any space discretization). Since the diffusion coefficient in the SDE satisfied by P_t is constant, the Euler scheme is in fact a Milshtein scheme on P_t. The convergence is therefore in δt (see Theorem 10.3.5 in Ref. [94]) :

Lemma 5 (Convergence of the Euler-Maruyama scheme) *There exists a constant C which depends only on T such that*

$$\mathbb{E}\left((P_n - P_{t_n})^2\right) \leq C(\delta t)^2.$$

Remark 5 *We could have used a scheme exact in law for P_t. We have chosen a classical Euler scheme because this is the scheme used in more complicated cases (see Remarks 1 and 2), when P_t also depends on x.*

We can now show the following convergence theorem :

Theorem 2 (Convergence of the time-discretized problem) *Let us assume $u_0 \in H_x^2$ and $f_{ext} \in W_t^{1,1}(L_x^2)$. Under the assumption $\delta t < \frac{1}{2}$, one has :*

$$||u_h^n - u_h(t_n)||_{L_x^2}^2 + ||Q_{h,n} - Q_h(t_n)||_{L_x^2(L_\omega^2)}^2 \leq C(\delta t)^2,$$

with C independent of h and $n \leq \frac{T}{\delta t}$, but depends on the data of the problem : u_0, f_{ext} and T.

Proof. As in the former proof, we omit here the subscript h : $u_h^n = u_n$, $Q_{h,n} = Q_n$, $u = u_h$ and $Q = Q_h$. We introduce the processes $\tilde{P}$ defined by $d\tilde{P}_t = -\frac{1}{2}\tilde{P}_{\tau_t}\,dt + dV_t$ (with $\tau_t = \lfloor\frac{t}{\delta t}\rfloor\delta t$, where $\lfloor x\rfloor$ is the integer part of x, and $\tilde{P}_0 = P_0$) and $\tilde{Q}$ defined by $d\tilde{Q}_t = \left(\partial_x u_{n(t)+1}\tilde{P}_{\tau_t} - \frac{1}{2}\tilde{Q}_{\tau_t}\right)dt + dW_t$ (with $n(t) = \lfloor\frac{t}{\delta t}\rfloor$ and $\tilde{Q}_0 = Q_0$). One can check easily that $P_n = \tilde{P}_{t_n}$ and $Q_n = \tilde{Q}_{t_n}$. Moreover, we set $e_n = u_n - u(t_n)$.

The stability lemma 4 shows that $\int_{\mathcal{O}}\mathbb{E}(Q_n^2)$ is uniformly bounded (in h and n), hence $\int_{\mathcal{O}}\mathbb{E}(\tilde{Q}_s^2)$ is also uniformly bounded in s. We have also a uniform bound in n on $\mathbb{E}(P_n^2)$ and a uniform bound in s on $\mathbb{E}(\tilde{P}_s^2)$.

Equation on u :

One obtains by subtraction of the continuous formulation in time at time t_n (2.26) (we recall that $u \in \mathcal{C}([0,T], L_x^2(\mathcal{O}))$) and the discretized formulation (2.34) : for all $v \in V_h$,

$$\int_{\mathcal{O}} \left(\frac{u_{n+1} - u_n}{\delta t} - \frac{\partial u}{\partial t}(t_n) \right) v + \int_{\mathcal{O}} (\partial_x u_{n+1} - \partial_x u(t_n)) \partial_x v = - \int_{\mathcal{O}} \mathbb{E}(P_n Q_n - P_{t_n} Q_{t_n}) \partial_x v.$$

With similar computations as those used in the proof of Lemma 4, choosing $v = e_{n+1}$, we obtain :

$$\frac{1}{2\delta t} \left(||e_{n+1}||_{L_x^2}^2 - ||e_n||_{L_x^2}^2 \right) + \int_{\mathcal{O}} |\partial_x e_{n+1}|^2 \leq - \int_{\mathcal{O}} \mathbb{E}(P_n Q_n - P_{t_n} Q_{t_n}) \partial_x e_{n+1}$$

$$- \int_{t_n}^{t_{n+1}} \int_{\mathcal{O}} \frac{\partial \partial_x u}{\partial t} \partial_x e_{n+1} - \frac{1}{\delta t} \int_{t_n}^{t_{n+1}} (t_{n+1} - s) \int_{\mathcal{O}} \frac{\partial^2 u}{\partial t^2}(s) e_{n+1} \, dx \, ds. \qquad (2.40)$$

For the last two terms, using Cauchy-Schwarz and the inequality $ab \leq \delta t a^2 + \frac{1}{4\delta t} b^2$, we have

$$\int_{t_n}^{t_{n+1}} \int_{\mathcal{O}} \frac{\partial \partial_x u}{\partial t} \partial_x e_{n+1} \quad \leq \quad \delta t \int_{t_n}^{t_{n+1}} \left\Vert \frac{\partial \partial_x u}{\partial t} \right\Vert_{L_x^2}^2 + \frac{1}{4} ||\partial_x e_{n+1}||_{L_x^2}^2.$$

In the same way :

$$\int_{t_n}^{t_{n+1}} (t_{n+1} - s) \int_{\mathcal{O}} \frac{\partial^2 u}{\partial t^2}(s) e_{n+1} \, dx \, ds \leq C(\delta t)^2 \int_{t_n}^{t_{n+1}} \left\Vert \frac{\partial^2 u}{\partial t^2}(s) \right\Vert_{H_{*,x}^{-1}}^2 + \frac{\delta t}{4} ||\partial_x e_{n+1}||_{L_x^2}^2.$$

Therefore, we obtain finally :

$$\frac{1}{2} \left(||e_{n+1}||_{L_x^2}^2 - ||e_n||_{L_x^2}^2 \right) + \frac{\delta t}{2} \int_{\mathcal{O}} |\partial_x e_{n+1}|^2 \leq -\delta t \int_{\mathcal{O}} \mathbb{E}(P_n Q_n - P_{t_n} Q_{t_n}) \partial_x e_{n+1}$$

$$+ (\delta t)^2 \int_{t_n}^{t_{n+1}} \left\Vert \frac{\partial \partial_x u}{\partial t}(s) \right\Vert_{L_x^2}^2 ds + C(\delta t)^2 \int_{t_n}^{t_{n+1}} \left\Vert \frac{\partial^2 u}{\partial t^2}(s) \right\Vert_{H_{*,x}^{-1}}^2 ds. \qquad (2.41)$$

Equation on Q :

In order to estimate the first term on the right-hand side of (2.41), we reproduce the proof of the energy inequality (2.22) at the discrete level. We write the SDE satisfied by $(Q_t - \tilde{Q}_t)^2$:

$$\frac{1}{2} d((Q_t - \tilde{Q}_t)^2) = \left((Q_t - \tilde{Q}_t)(\partial_x u P_t - \partial_x u_{n(t)+1} \tilde{P}_{\tau_t}) - \frac{1}{2}(Q_t - \tilde{Q}_t)(Q_t - \tilde{Q}_{\tau_t}) \right) dt.$$

We set in the following $f_n = Q_{t_n} - Q_n$. Integrating the last equation over (t_n, t_{n+1}), we have :

$$\frac{1}{2}(f_{n+1}^2 - f_n^2) = -\frac{1}{2} \int_{t_n}^{t_{n+1}} (Q_s - \tilde{Q}_s)(Q_s - Q_n) + \int_{t_n}^{t_{n+1}} (P_s \partial_x u(s) - P_n \partial_x u_{n+1})(Q_s - \tilde{Q}_s)$$

$$= -\frac{1}{2} \int_{t_n}^{t_{n+1}} (Q_s - \tilde{Q}_s)^2 + \frac{1}{2} \int_{t_n}^{t_{n+1}} (Q_s - \tilde{Q}_s)(Q_n - \tilde{Q}_s)$$

$$+ \int_{t_n}^{t_{n+1}} (P_s \partial_x u(s) - P_n \partial_x u_{n+1})(Q_s - \tilde{Q}_s).$$

We introduce in the expectation of the last expression the term of (2.41) we want to eliminate, namely $\delta t \int_{\mathcal{O}} \mathbb{E}(P_n Q_n - P_{t_n} Q_{t_n}) \partial_x e_{n+1}$. We obtain :

$$\frac{1}{2}\mathbb{E}(f_{n+1}^2 - f_n^2) + \frac{1}{2}\int_{t_n}^{t_{n+1}} \mathbb{E}(Q_s - \tilde{Q}_s)^2 = \delta t \mathbb{E}(P_n Q_n - P_{t_n} Q_{t_n})\partial_x e_{n+1} + A, \quad (2.42)$$

with

$$A = \frac{1}{2}\int_{t_n}^{t_{n+1}} \mathbb{E}\left((Q_s - \tilde{Q}_s)(Q_n - \tilde{Q}_s)\right) + \int_{t_n}^{t_{n+1}} \mathbb{E}\left((P_s \partial_x u(s) - P_n \partial_x u_{n+1})(Q_s - \tilde{Q}_s)\right)$$
$$-\delta t \mathbb{E}(P_n Q_n - P_{t_n} Q_{t_n})\partial_x e_{n+1}.$$

We will show the following estimate on A :

Proposition 1

$$\begin{aligned}
|A| \quad \leq \quad & C\delta t^3 \left(1 + |\partial_x u_{n+1}|^2 + \frac{1}{\delta t}\int_{t_n}^{t_{n+1}} \left|\frac{\partial \partial_x u}{\partial t}\right|^2 + \frac{1}{\delta t}\int_{t_n}^{t_{n+1}} |\partial_x u|^2 + \frac{1}{\delta t}\int_{t_n}^{t_{n+1}} \mathbb{E}(Q_s^2) \right. \\
& \left. + \mathbb{E}(Q_n^2) + \frac{1}{\delta t}\int_{t_n}^{t_{n+1}} \mathbb{E}(\tilde{Q}_s^2)\right) + \epsilon \int_{t_n}^{t_{n+1}} \mathbb{E}\left((Q_s - \tilde{Q}_s)^2\right) + \epsilon\delta t|\partial_x e_{n+1}|^2,
\end{aligned}$$

with ϵ arbitrarily small and C a constant which is independent of n and δt, but depends on ϵ and on the data of the problem : u_0, f_{ext} and T.

Let us postpone the proof of Proposition 1 after the end of the proof of Theorem 2. Summing up (2.41) and (2.42) (integrated in space), using the estimation of Proposition 1, we have :

$$||e_{n+1}||_{L_x^2}^2 - ||e_n||_{L_x^2}^2 + \int_{\mathcal{O}} \mathbb{E}(f_{n+1}^2 - f_n^2) + (1-2\alpha)\int_{t_n}^{t_{n+1}} \mathbb{E}(Q_s - \tilde{Q}_s)^2 + (1-2\beta)\,\delta t \int_{\mathcal{O}} |\partial_x e_{n+1}|^2$$

$$\leq C\delta t^3 \left(1 + ||\partial_x u_{n+1}||_{L_x^2}^2 + \frac{1}{\delta t}\int_{t_n}^{t_{n+1}} ||\partial_x u||_{L_x^2}^2 + \frac{1}{\delta t}\int_{t_n}^{t_{n+1}}\int_{\mathcal{O}} \mathbb{E}(Q_s^2) + \int_{\mathcal{O}} \mathbb{E}(Q_n^2) \right.$$

$$\left. + \frac{1}{\delta t}\int_{t_n}^{t_{n+1}}\int_{\mathcal{O}} \mathbb{E}(\tilde{Q}_s^2) + \frac{1}{\delta t}\int_{t_n}^{t_{n+1}} \left|\left|\frac{\partial \partial_x u}{\partial t}(s)\right|\right|_{L_x^2}^2 ds + \frac{1}{\delta t}\int_{t_n}^{t_{n+1}} \left|\left|\frac{\partial^2 u}{\partial t^2}(s)\right|\right|_{H_{*,x}^{-1}}^2 ds\right),$$

where α and β are arbitrarily small positive constants. Summing up over n and using the regularities proved in Lemmas 1 and 4, this concludes the proof. $\quad\square$

We now have to prove Proposition 1. We will need the next two lemmas.

Lemma 6 *Set $R(t,x)$ a process (possibly deterministic). We have the following inequalities :*

$$\left|\mathbb{E}\left(\int_{t_n}^{t_{n+1}} R(s,x)(\partial_x e_{n+1})\,ds\right)\right| \leq \frac{1}{4\epsilon}\int_{t_n}^{t_{n+1}} (\mathbb{E}(R(s,x)))^2\,ds + \epsilon\delta t|\partial_x e_{n+1}|^2,$$

$$\left| \mathbb{E} \left(\int_{t_n}^{t_{n+1}} R(s,x)(Q_s - \tilde{Q}_s)\, ds \right) \right| \leq \frac{1}{4\epsilon} \int_{t_n}^{t_{n+1}} \mathbb{E}\left(R(s,x)^2 \right)\, ds + \epsilon \int_{t_n}^{t_{n+1}} \mathbb{E}\left((Q_s - \tilde{Q}_s)^2 \right)\, ds.$$

Let $S(t,x)$ be an Itô process such that $dS_t = a(x,t)\, dt + b(x,t)\, dV_t + c(x,t)\, dW_t$ with b and c square integrable in t. We also have the following inequality :

$$\left| \mathbb{E} \left(\int_{t_n}^{t_{n+1}} (S(s,x) - S(t_n,x))(\partial_x e_{n+1})\, ds \right) \right| \leq \frac{1}{4\epsilon} \delta t^2 \int_{t_n}^{t_{n+1}} (\mathbb{E}(a(x,s)))^2\, ds + \epsilon \delta t |\partial_x e_{n+1}|^2,$$

with ϵ arbitrarily small.

Proof. These results are easy to obtain by Cauchy-Schwarz inequality, noticing that $\partial_x e_{n+1}$ is deterministic and using the inequality $|ab| \leq \frac{1}{4\epsilon} a^2 + \epsilon b^2$. □

Lemma 7 *We have the following two inequalities :*

$$\left| \mathbb{E} \left(\int_{t_n}^{t_{n+1}} (Q_s - \tilde{Q}_s)(\tilde{Q}_s - \tilde{Q}_{t_n})\, ds \right) \right| \leq C\delta t^2 \left(\delta t + \delta t \mathbb{E}(Q_n^2) + \delta t |\partial_x u_{n+1}|^2 + \int_{t_n}^{t_{n+1}} \mathbb{E}(Q_s^2) \right)$$
$$+ \epsilon \int_{t_n}^{t_{n+1}} \mathbb{E}\left((Q_s - \tilde{Q}_s)^2 \right)\, ds,$$

with ϵ arbitrarily small.

$$\left| \mathbb{E} \left(\int_{t_n}^{t_{n+1}} \alpha (Q_s - \tilde{Q}_s)(\tilde{P}_s - \tilde{P}_{t_n})\, ds \right) \right| \leq C\delta t^2 \left(\delta t + \delta t \alpha^2 + \int_{t_n}^{t_{n+1}} |\partial_x u|^2 \right)$$
$$+ \epsilon \int_{t_n}^{t_{n+1}} \mathbb{E}\left((Q_s - \tilde{Q}_s)^2 \right)\, ds,$$

with α a constant, ϵ arbitrarily small and C a constant independent of α. The constant C is independent of n and δt, but depends on ϵ and on the data of the problem : u_0, f_{ext} and T.

Proof. The proof of the first inequality mimics that of the second one. Therefore, we only prove the second inequality. For all $t \in (t_n, t_{n+1})$, one can write $d\tilde{P}_t = -\frac{1}{2} P_n dt + dV_t$. We have therefore :

$$\mathbb{E} \left(\int_{t_n}^{t_{n+1}} \alpha(\tilde{P}(s,x) - \tilde{P}(t_n,x))(Q_s - \tilde{Q}_s)\, ds \right)$$
$$= \int_{t_n}^{t_{n+1}} \mathbb{E} \left(-(s - t_n)\frac{\alpha}{2} P_n (Q_s - \tilde{Q}_s) \right)\, ds + \mathbb{E} \left(\int_{t_n}^{t_{n+1}} \alpha(V_s - V_{t_n})(Q_s - \tilde{Q}_s)\, ds \right). \quad (2.43)$$

For the first term of the right-hand side of (2.43), we apply the second inequality of Lemma 6 (with $R(s,x) = -(s - t_n)\frac{\alpha}{2} P_n$) in order to obtain a bound in $C\delta t^3 \alpha^2 + \epsilon \int_{t_n}^{t_{n+1}} \mathbb{E}\left((Q_s - \tilde{Q}_s)^2 \right)\, ds$. The aim of the remainder of the proof is to show the following estimation on the second term of the right-hand side of (2.43) :

$$\left| \mathbb{E} \left(\int_{t_n}^{t_{n+1}} \alpha(V_s - V_{t_n})(Q_s - \tilde{Q}_s)\, ds \right) \right| \leq C\delta t^2 \left(\delta t + \delta t \alpha^2 + \int_{t_n}^{t_{n+1}} |\partial_x u|^2 \right). \quad (2.44)$$

In order to show (2.44), we use the SDE satisfied by $Q_s - \tilde{Q}_s$:

$$
\begin{aligned}
Q_s - \tilde{Q}_s &= Q_{t_n} - Q_n - \frac{1}{2} \int_{t_n}^s (Q_v - Q_n)\, dv + \int_{t_n}^s (\partial_x u P_v - \partial_x u_{n+1} P_n)\, dv \\
&= \left[\left(1 - \frac{s - t_n}{2} \right)(Q_{t_n} - Q_n) - (s - t_n)\partial_x u_{n+1} P_n + \int_{t_n}^s \partial_x u P_{t_n}\, dv \right] \\
&\quad - \frac{1}{2} \int_{t_n}^s (Q_v - Q_{t_n})\, dv + \int_{t_n}^s \partial_x u (P_v - P_{t_n})\, dv.
\end{aligned}
\tag{2.45}
$$

Let us denote B the term in brackets. The random variable B is independent of $(V_s - V_{t_n})$, which implies :

$$
\mathbb{E} \left(\int_{t_n}^{t_{n+1}} \alpha (V_s - V_{t_n}) B\, ds \right) = 0.
$$

We still have to estimate the contributions of the last two terms of (2.45). These contributions will be denoted respectively by T_1 and T_2.
Let us first turn to the term T_1 which is :

$$
\begin{aligned}
T_1 &= \mathbb{E} \left(\int_{t_n}^{t_{n+1}} \frac{\alpha}{2} (V_s - V_{t_n}) \int_{t_n}^s (Q_v - Q_{t_n})\, dv\, ds \right) \\
&= \frac{\alpha}{2} \int_{t_n}^{t_{n+1}} \int_{t_n}^s \mathbb{E} \left((V_s - V_{t_n})(Q_v - Q_{t_n}) \right)\, dv\, ds.
\end{aligned}
$$

It is clear that :

$$
|T_1| \leq \delta t^3 \alpha^2 + \frac{1}{\delta t^3} \left(\int_{t_n}^{t_{n+1}} \int_{t_n}^s \mathbb{E} \left((V_s - V_{t_n})(Q_v - Q_{t_n}) \right)\, dv\, ds \right)^2.
$$

Using the expression of $Q_v - Q_{t_n} = -\frac{1}{2} \int_{t_n}^v Q_w\, dw + \int_{t_n}^v \partial_x u P_w\, dw + W_v - W_{t_n}$, one obtains :

$$
\begin{aligned}
\mathbb{E} \left((V_s - V_{t_n})(Q_v - Q_{t_n}) \right) &= \frac{1}{2} \mathbb{E} \left((V_s - V_{t_n}) \int_{t_n}^v (-Q_w)\, dw \right) \\
&\quad + \mathbb{E} \left((V_s - V_{t_n}) \int_{t_n}^v \partial_x u P_w\, dw \right) \\
&\quad + \mathbb{E} \left((V_s - V_{t_n})(W_v - W_{t_n}) \right).
\end{aligned}
\tag{2.46}
$$

The third term of (2.46) is zero. For the second term of (2.46), we write (using Cauchy-Schwarz) :

$$
\begin{aligned}
&\frac{1}{\delta t^3} \left(\int_{t_n}^{t_{n+1}} \int_{t_n}^s \int_{t_n}^v \partial_x u \mathbb{E} \left((V_s - V_{t_n}) P_w \right)\, dw\, dv\, ds \right)^2 \\
&\leq \int_{t_n}^{t_{n+1}} \int_{t_n}^s \int_{t_n}^v |\partial_x u|^2 \left(\mathbb{E}((V_s - V_{t_n}) P_w) \right)^2\, dw\, dv\, ds \leq C \delta t^3 \int_{t_n}^{t_{n+1}} |\partial_x u|^2.
\end{aligned}
$$

For the first term of (2.46), we write in the same manner :

$$\frac{1}{\delta t^3} \left(\int_{t_n}^{t_{n+1}} \int_{t_n}^{s} \int_{t_n}^{v} \mathbb{E}\left((V_s - V_{t_n}) Q_w \right) dw\, dv\, ds \right)^2$$

$$\leq \int_{t_n}^{t_{n+1}} \int_{t_n}^{s} \int_{t_n}^{v} \left(\mathbb{E}\left((V_s - V_{t_n}) Q_w \right) \right)^2 dw\, dv\, ds$$

$$\leq \int_{t_n}^{t_{n+1}} \int_{t_n}^{s} \int_{t_n}^{v} (s - t_n) \mathbb{E}(Q_w^2)\, dw\, dv\, ds \leq \delta t^3 \int_{t_n}^{t_{n+1}} \mathbb{E}(Q_s^2).$$

Let us now turn to the estimation of the term T_2 :

$$T_2 = \mathbb{E}\left(\int_{t_n}^{t_{n+1}} \alpha (V_s - V_{t_n}) \int_{t_n}^{s} \partial_x u (P_v - P_{t_n})\, dv\, ds \right)$$

$$= \alpha \int_{t_n}^{t_{n+1}} \int_{t_n}^{s} \partial_x u\, \mathbb{E}\left((V_s - V_{t_n})(P_v - P_{t_n}) \right) dv\, ds.$$

It is clear that :

$$|T_2| \leq \delta t^3 \alpha^2 + \frac{1}{\delta t^3} \left(\int_{t_n}^{t_{n+1}} \int_{t_n}^{s} \partial_x u\, \mathbb{E}\left((V_s - V_{t_n})(P_v - P_{t_n}) \right) dv\, ds \right)^2.$$

Using the expression of $P_v - P_{t_n} = -\frac{1}{2} \int_{t_n}^{v} P_w\, dw + V_v - V_{t_n}$, we obtain :

$$\mathbb{E}\left((V_s - V_{t_n})(P_v - P_{t_n}) \right) = \frac{1}{2} \int_{t_n}^{v} \mathbb{E}\left(-(V_s - V_{t_n}) P_w \right) dw + \mathbb{E}\left((V_s - V_{t_n})(V_v - V_{t_n}) \right).$$

$$(2.47)$$

For the second term of (2.47), we have therefore :

$$\frac{1}{\delta t^3} \left(\int_{t_n}^{t_{n+1}} \int_{t_n}^{s} \partial_x u (v - t_n)\, dv\, ds \right)^2 \leq \frac{1}{\delta t} \int_{t_n}^{t_{n+1}} \int_{t_n}^{s} |\partial_x u|^2 (v - t_n)^2\, dv\, ds$$

$$\leq \delta t^2 \int_{t_n}^{t_{n+1}} |\partial_x u|^2.$$

For the first term of (2.47), we obtain in the same way :

$$\frac{1}{\delta t^3} \left(\int_{t_n}^{t_{n+1}} \int_{t_n}^{s} \partial_x u \int_{t_n}^{v} \mathbb{E}\left((V_s - V_{t_n}) P_w \right) dw\, dv\, ds \right)^2$$

$$\leq \frac{1}{\delta t} \int_{t_n}^{t_{n+1}} \int_{t_n}^{s} |\partial_x u|^2 \int_{t_n}^{s} \int_{t_n}^{v} \left(\mathbb{E}\left((V_s - V_{t_n}) P_w \right) \right)^2 ds \leq \delta t^3 \int_{t_n}^{t_{n+1}} |\partial_x u|^2.$$

This ends the proof. $\qquad\square$

One can now prove Proposition 1.

Proof. The first inequality of Lemma 7 shows that :

$$|A| \leq C\delta t^2 \left(\delta t + \delta t |\partial_x u_{n+1}|^2 + \int_{t_n}^{t_{n+1}} \mathbb{E}(Q_s^2) + \delta t \mathbb{E}(Q_n^2) \right) + \epsilon \int_{t_n}^{t_{n+1}} \mathbb{E}\left((Q_s - \tilde{Q}_s)^2 \right) + |A'|,$$

with

$$
\begin{aligned}
A' &= \int_{t_n}^{t_{n+1}} \mathbb{E}\left((P_s \partial_x u(s) - P_n \partial_x u_{n+1})(Q_s - \tilde{Q}_s) \right) ds \\
&\quad - \delta t \mathbb{E}(P_n Q_n - P_{t_n} Q_{t_n}) \partial_x (u_{n+1} - u(t_{n+1})) \\
&= \int_{t_n}^{t_{n+1}} \mathbb{E}\Big((P_s \partial_x u(s) - P_n \partial_x u_{n+1})(Q_s - \tilde{Q}_s) \\
&\qquad\qquad - (P_n Q_n - P_{t_n} Q_{t_n})(\partial_x u_{n+1} - \partial_x u(t_{n+1})) \Big) ds.
\end{aligned}
$$

Using Lemmas 6 and 7, we will prove the following estimate on A' :

$$
\begin{aligned}
|A'| &\leq C\delta t^3 \left(1 + |\partial_x u_{n+1}|^2 + \frac{1}{\delta t} \int_{t_n}^{t_{n+1}} \left| \frac{\partial \partial_x u}{\partial t} \right|^2 + \frac{1}{\delta t} \int_{t_n}^{t_{n+1}} |\partial_x u|^2 + \frac{1}{\delta t} \int_{t_n}^{t_{n+1}} \mathbb{E}(Q_s^2) \right. \\
&\quad \left. + \mathbb{E}(Q_n^2) + \frac{1}{\delta t} \int_{t_n}^{t_{n+1}} \mathbb{E}(\tilde{Q}_s^2) \right) + \epsilon \int_{t_n}^{t_{n+1}} \mathbb{E}\left((Q_s - \tilde{Q}_s)^2 \right) + \epsilon \delta t |\partial_x e_{n+1}|^2,
\end{aligned}
$$

with ϵ arbitrarily small.

The third inequality of Lemma 6 applied successively to $P_s Q_s$ and $\tilde{P}_s \tilde{Q}_s$ and the second inequality of Lemma 7 (applied with $\alpha = \partial_x u_{n+1}$) show that $|A'|$ is bounded by :

$$
\begin{aligned}
&\left| \int_{t_n}^{t_{n+1}} \mathbb{E}\Big((P_s \partial_x u(s) - \tilde{P}_s \partial_x u_{n+1})(Q_s - \tilde{Q}_s) - (\tilde{P}_s \tilde{Q}_s - P_s Q_s)(\partial_x u_{n+1} - \partial_x u(t_{n+1})) \Big) \right| \\
&+ C\delta t^3 \left(1 + |\partial_x u_{n+1}|^2 + \tfrac{1}{\delta t} \int_{t_n}^{t_{n+1}} |\partial_x u|^2 + \frac{1}{\delta t} \int_{t_n}^{t_{n+1}} \mathbb{E}(Q_s^2) + \mathbb{E}(Q_n^2) + \frac{1}{\delta t} \int_{t_n}^{t_{n+1}} \mathbb{E}(\tilde{Q}_s^2) \right) \\
&+ \epsilon \int_{t_n}^{t_{n+1}} \mathbb{E}\left((Q_s - \tilde{Q}_s)^2 \right) + \epsilon \delta t |\partial_x e_{n+1}|^2.
\end{aligned}
$$

Then, using the second inequality of Lemma 6 (with $R(s,x) = P_s(\partial_x u(s) - \partial_x u(t_{n+1}))$), we obtain the following bound on $|A'|$:

$$
\begin{aligned}
&\left| \int_{t_n}^{t_{n+1}} \mathbb{E}\Big((P_s \partial_x u(t_{n+1}) - \tilde{P}_s \partial_x u_{n+1})(Q_s - \tilde{Q}_s) - (\tilde{P}_s \tilde{Q}_s - P_s Q_s)(\partial_x u_{n+1} - \partial_x u(t_{n+1})) \Big) \right| \\
&+ C\delta t^3 \left(1 + |\partial_x u_{n+1}|^2 + \tfrac{1}{\delta t} \int_{t_n}^{t_{n+1}} |\partial_x u|^2 + \frac{1}{\delta t} \int_{t_n}^{t_{n+1}} \left| \frac{\partial \partial_x u}{\partial t} \right|^2 + \frac{1}{\delta t} \int_{t_n}^{t_{n+1}} \mathbb{E}(Q_s^2) + \mathbb{E}(Q_n^2) \right. \\
&\left. + \frac{1}{\delta t} \int_{t_n}^{t_{n+1}} \mathbb{E}(\tilde{Q}_s^2) \right) + \epsilon \int_{t_n}^{t_{n+1}} \mathbb{E}\left((Q_s - \tilde{Q}_s)^2 \right) + \epsilon \delta t |\partial_x e_{n+1}|^2.
\end{aligned}
$$

Then, developing the expression under the integral, we obtain the following term :

$$-\int_{t_n}^{t_{n+1}} \mathbb{E}\left(\partial_x u(t_{n+1})\tilde{Q}_s(P_s - \tilde{P}_s)\right) + \int_{t_n}^{t_{n+1}} \mathbb{E}\left(\partial_x u_{n+1}Q_s(P_s - \tilde{P}_s)\right)$$
$$= \int_{t_n}^{t_{n+1}} \mathbb{E}\left(\partial_x u_{n+1}(P_s - \tilde{P}_s)(Q_s - \tilde{Q}_s)\right) + \int_{t_n}^{t_{n+1}} \mathbb{E}\left(\tilde{Q}_s(P_s - \tilde{P}_s)\left(\partial_x u_{n+1} - \partial_x u(t_{n+1})\right)\right).$$

One can now conclude using the inequality $\mathbb{E}\left((P_s - \tilde{P}_s)^2\right) < C\delta t^2$ and applying the first two inequalities of Lemma 6 to both terms of the above expression. $\qquad\square$

2.4.3 Convergence of the Monte Carlo discretized problem.

We now turn to the last level of discretization : the Monte Carlo method. In the preceding subsections, we have shown that the space and time discretized problem $(u_h^n, Q_{h,n})$ converges towards the continuous solution at time $t_n = n\delta t : (u(t_n), Q_{t_n})$. We now want to estimate the error induced by the approximation of $\mathbb{E}(P_n Q_{h,n})$ by an empirical mean. All the results of this subsection hold under the assumption $u_0 \in L_x^2$ and $f_{ext} \in L_t^\infty(L_x^2)$.

We define the fully discretized problem :
Being given at time $t_n = n\delta t$, the velocity $\overline{u}_h^n$ and the random variables P_n^j, $\overline{P}_n^j$ and $\overline{Q}_{h,n}^j$, one finds $\overline{u}_h^{n+1} \in V_h$ such that $\forall v \in V_h$,

$$\frac{1}{\delta t}\int_{\mathcal{O}}(\overline{u}_h^{n+1} - \overline{u}_h^n)v + \int_{\mathcal{O}}\partial_x\overline{u}_h^{n+1}\partial_x v \quad = \quad -\int_{\mathcal{O}}\overline{S}_{h,n}\partial_x v + \int_{\mathcal{O}}f_{ext}(t_n)v. \quad (2.48)$$

with $\overline{S}_{h,n} = \frac{1}{M}\sum_{j=1}^{M}\overline{P}_n^j\overline{Q}_{h,n}^j$. Then, one computes P_{n+1}^j, $\overline{P}_{n+1}^j$ and $\overline{Q}_{h,n+1}^j$ using :

$$\overline{Q}_{h,n+1}^j - \overline{Q}_{h,n}^j \quad = \quad \left(\partial_x\overline{u}_h^{n+1}\overline{P}_{h,n}^j - \frac{1}{2}\overline{Q}_{h,n}^j\right)\delta t + \left(W_{t_{n+1}}^j - W_{t_n}^j\right), \quad (2.49)$$

$$\begin{cases} P_{n+1}^j - P_n^j & = \quad -\frac{1}{2}P_n^j\,\delta t + (V_{t_{n+1}}^j - V_{t_n}^j), \\ \overline{P}_{n+1}^j & = \quad \sup(-A, \inf(A, P_{n+1}^j)). \end{cases} \quad (2.50)$$

The processes $(V_t^1, \ldots, V_t^N)$ and $(W_t^1, \ldots, W_t^N)$ are standard independent M-dimensional Brownian motions. Initial conditions are $\overline{u}_{h,0} = \Pi_h(u_0)$ (with Π_h the finite elements interpolation operator), P_0^j and Q_0^j, which are independent normal variables, independent of the Brownian motion V_t^j and W_t^j.

One can see that we have modified the standard Euler scheme on P_t by introducing a cut-off constant $A > 0$. In fact, we will show two types of results : results with cut-off ($A < \infty$) and results without cut-off ($A = \infty$). In the first case, we will require $0 < A < \sqrt{\frac{3}{5\delta t}}$ (and then use a constant $\gamma > 0$ such that $A > -\gamma\ln(\delta t)$). The choice of the upper bound will be justified in the proof of Lemma 10. In the second case ($A = \infty$), we have $\overline{P}_n^j = P_n^j$ and we will state the results on a subset of the

probability space. This subset will tend to the entire probability space when $\delta t \to 0$ or $M \to \infty$. These difficulties are linked with usual stability problems encountered in the discretization of SDEs (see Ref. [126]). More precisely, let us introduce the subset $\mathcal{A}_n$ defined for all $n \leq \frac{T}{\delta t}$ by :

$$\mathcal{A}_n = \left\{ \forall k \leq n, \ \frac{1}{M} \sum_{j=1}^{M} (\overline{P}_k^j)^2 < \frac{13}{20} \frac{1}{\delta t} \right\}.$$

The value of the upper bound $\frac{13}{20} \frac{1}{\delta t}$ will be justified in the proof of the stability lemma 9. For the sake of concision, the results at time $n\delta t$ will be stated on the event $\mathcal{A}_n$ in the absence ($A = \infty$) as well as in the presence ($A < \sqrt{\frac{3}{5\delta t}}$) of the cut-off, but it is important to notice that in the latter case, the probability of $\mathcal{A}_n$ is equal to 1.

Lemma 8 (Properties of $\mathcal{A}_n$) *Let us assume $A = \infty$ (in which case $\overline{P}_n^j = P_n^j$). The sequence of sets $(\mathcal{A}_n)_{n \in \mathbb{N}}$ is decreasing. Moreover, we can estimate the probability of the event $\mathcal{A}_n$: assuming $\delta t < \frac{13}{40}$,*

$$\mathbb{P}(\mathcal{A}_n) \geq 1 - \frac{1}{\delta t} \exp\left(-\frac{M}{2} \left(\frac{13}{40\delta t} - 1 - \ln\left(\frac{13}{40\delta t} \right) \right) \right),$$

with C_1 and C_2 two constants independent of n. In particular, for any $t \in [0, T]$, $\mathbb{P}\left(\mathcal{A}_{\lfloor \frac{t}{\delta t} \rfloor} \right) \longrightarrow 1$ when $\delta t \longrightarrow 0$, or when $M \longrightarrow \infty$ with $\delta t < \frac{13}{40}$.

Proof. The first property is clear. For the second one, notice first that a simple calculation yields $\mathbb{E}(P_n^2) < 2$. Hence, if $(G_j)_{j \geq 1}$ denotes a sequence of i.i.d. normal random variables, $\mathbb{P}\left(\frac{1}{M} \sum_{j=1}^{M} (P_n^j)^2 > C \right) \leq \mathbb{P}\left(\frac{1}{M} \sum_{j=1}^{M} (G_j)^2 > \frac{C}{2} \right)$. By Chernoff inequality,

$$\mathbb{P}\left(\frac{1}{M} \sum_{j=1}^{M} (G_j)^2 > C \right) \leq \exp(-M(\lambda C - \Lambda(\lambda))),$$

for any $\lambda > 0$ where Λ denotes the Legendre transform : $\Lambda(\lambda) = \ln(\mathbb{E}(\exp(\lambda G_1^2)))$. We conclude by minimizing the right-hand side over λ using :

$$\sup_{\lambda > 0}(\lambda x - \Lambda(\lambda)) = \left\{ \begin{array}{ll} 0 & \text{if } x \leq 1, \\ \frac{1}{2}(x - 1 - \ln x) & \text{if } x > 1. \end{array} \right.$$

$\square$

In the following, we omit the subscript h in order to lighten the notations. It is important to already notice that for all n, the couples $(\overline{P}_n^j, \overline{Q}_n^j)$ are exchangeable, i.e. the law of the M-uplet $((\overline{P}_n^1, \overline{Q}_n^1), ..., (\overline{P}_n^M, \overline{Q}_n^M))$ remains the same for any permutation on the indices $(1, ..., M)$. This allows one to write e.g. $\mathbb{E}\left(\frac{1}{M} \sum_{j=1}^{M} \overline{Q}_n^j \right) =$

$\mathbb{E}\left(\overline{Q}_n^1\right)$ or $\mathbb{E}\left(\frac{1}{M}\sum_{j=1}^M (\overline{P}_n^j)^2 \partial_x \overline{u}_{n+1}^2\right) = \mathbb{E}\left((\overline{P}_n^1)^2 \partial_x \overline{u}_{n+1}^2\right)$. Let us introduce another notation, only used in the proofs. We define the function $\mathbb{E}^n$ by : for any random variable X, $\mathbb{E}^n(X) = \mathbb{E}(X 1_{\mathcal{A}_n})$. Notice that in the case $A < \sqrt{\frac{3}{5\delta t}}$ (with cut-off), one has $\mathbb{E}^n = \mathbb{E}$.

We start with the stability of the scheme.

Lemma 9 (Stability of the fully discretized problem) *We assume $\delta t < 2$. Moreover, we assume either $\delta t A^2 \leq \frac{13}{20}$, or $A = \infty$. We have then the following inequality : $\forall n \leq \frac{T}{\delta t}$,*

$$\int_{\mathcal{O}} \mathbb{E}(\overline{u}_n^2 1_{\mathcal{A}_n}) + \frac{\delta t}{2}\sum_{k=0}^{n-1}\int_{\mathcal{O}} \mathbb{E}\left((\partial_x \overline{u}_{k+1})^2 1_{\mathcal{A}_k}\right) + \int_{\mathcal{O}} \mathbb{E}\left(\frac{1}{M}\sum_{j=1}^M (\overline{Q}_n^j)^2 1_{\mathcal{A}_n}\right)$$
$$\leq 1 + ||u_0||_{L_x^2}^2 + T\left(1 + C||f_{ext}||_{L_t^\infty(L_x^2)}\right),$$

with C a constant independent of the data of the problem.

Proof. Choosing $v = \overline{u}_{n+1}$ as a test function in (2.48), we obtain (in the same way as in the preceding stability proofs) :

$$\frac{1}{2\delta t}\left(\int_{\mathcal{O}} \overline{u}_{n+1}^2 - \int_{\mathcal{O}} \overline{u}_n^2\right) + \frac{9}{10}\int_{\mathcal{O}} \partial_x \overline{u}_{n+1}^2 \quad \leq \quad -\int_{\mathcal{O}} \overline{S}_n \partial_x \overline{u}_{n+1} + C||f_{ext}(t_n)||_{L_x^2}^2.$$

Multiplying the equation (2.49) with $\overline{Q}_n^j$ and $1_{\mathcal{A}_n}$, we obtain :

$$\frac{1}{2\delta t}\left(\mathbb{E}^n((\overline{Q}_{n+1}^j)^2) - \mathbb{E}^n((\overline{Q}_n^j)^2)\right) + \frac{1}{2}\mathbb{E}^n((\overline{Q}_n^j)^2)$$
$$= \mathbb{E}^n(\partial_x \overline{u}_{n+1}\overline{P}_n^j \overline{Q}_n^j) + \frac{1}{2\delta t}\mathbb{E}^n((\overline{Q}_{n+1}^j - \overline{Q}_n^j)^2).$$

Summing up these two relations and using exchangeability, one obtains :

$$\frac{1}{2\delta t}\left(\int_{\mathcal{O}}\mathbb{E}^n(\overline{u}_{n+1}^2) - \int_{\mathcal{O}}\mathbb{E}^n(\overline{u}_n^2)\right) + \frac{1}{2\delta t}\left(\int_{\mathcal{O}}\mathbb{E}^n\left((\overline{Q}_{n+1}^1)^2\right) - \int_{\mathcal{O}}\mathbb{E}^n\left((\overline{Q}_n^1)^2\right)\right)$$
$$+\frac{9}{10}\int_{\mathcal{O}}\mathbb{E}^n(\partial_x \overline{u}_{n+1}^2) + \frac{1}{2}\int_{\mathcal{O}}\mathbb{E}^n\left((\overline{Q}_n^1)^2\right) \leq \frac{1}{2\delta t}\mathbb{E}^n\left((\overline{Q}_{n+1}^1 - \overline{Q}_n^1)^2\right) + C||f_{ext}(t_n)||_{L_x^2}^2.$$

We have now to estimate the term on the right-hand side. We use again :

$$\mathbb{E}^n((\overline{Q}_{n+1}^1 - \overline{Q}_n^1)^2) = \delta t^2 \mathbb{E}^n((\partial_x \overline{u}_{n+1}\overline{P}_n^1 - \frac{1}{2}\overline{Q}_n^1)^2) + \delta t$$
$$\leq 2\delta t^2 \mathbb{E}^n((\partial_x \overline{u}_{n+1}\overline{P}_n^1)^2) + \frac{1}{2}\delta t^2 \mathbb{E}^n((\overline{Q}_n^1)^2) + \delta t.$$

This yields :

$$\frac{1}{2\delta t}\left(\int_{\mathcal{O}}\mathbb{E}^n(\overline{u}_{n+1}^2) - \int_{\mathcal{O}}\mathbb{E}^n(\overline{u}_n^2)\right) + \int_{\mathcal{O}}\mathbb{E}^n\left(\left(\frac{9}{10} - \delta t\frac{1}{M}\sum_{j=1}^{M}(\overline{P}_n^j)^2\right)\partial_x\overline{u}_{n+1}^2\right)$$

$$+\frac{1}{2\delta t}\left(\int_{\mathcal{O}}\mathbb{E}^n((\overline{Q}_{n+1}^1)^2) - \int_{\mathcal{O}}\mathbb{E}^n((\overline{Q}_n^1)^2)\right) + \frac{1}{2}\int_{\mathcal{O}}\left(1 - \frac{\delta t}{2}\right)\mathbb{E}^n((\overline{Q}_n^1)^2)$$

$$\leq \frac{1}{2} + C||f_{ext}(t_n)||_{L_x^2}^2.$$

Using the following three properties :
$\left(\left(\frac{9}{10} - \delta t\frac{1}{M}\sum_{j=1}^{M}(\overline{P}_n^j)^2\right)\partial_x\overline{u}_{n+1}^2\right)1_{\mathcal{A}_n} \geq \frac{1}{4}\partial_x\overline{u}_{n+1}^2 1_{\mathcal{A}_n}$ (this is the inequality which defines the upper bound in the definition of $\mathcal{A}_n$), $1_{\mathcal{A}_n} \geq 1_{\mathcal{A}_{n+1}}$ and $\delta t < 2$, we get :

$$\frac{1}{2\delta t}\left(\int_{\mathcal{O}}\mathbb{E}^{n+1}(\overline{u}_{n+1}^2) - \int_{\mathcal{O}}\mathbb{E}^n(\overline{u}_n^2)\right) + \frac{1}{4}\int_{\mathcal{O}}\mathbb{E}^n\left(\partial_x\overline{u}_{n+1}^2\right)$$

$$+\frac{1}{2\delta t}\left(\int_{\mathcal{O}}\mathbb{E}^{n+1}((\overline{Q}_{n+1}^1)^2) - \int_{\mathcal{O}}\mathbb{E}^n((\overline{Q}_n^1)^2)\right) \leq \frac{1}{2} + C||f_{ext}(t_n)||_{L_x^2}^2.$$

This yields the stability, by summing up over n. $\qquad\square$

Let us now turn to the convergence of the solution of the fully discretized problem towards the solution of the problem discretized in space and time.

We need to introduce the random variables $Q_{h,n}^j$ (denoted Q_n^j in the following) :

$$Q_{h,n+1}^j - Q_{h,n}^j = \left(\partial_x u_h^{n+1}P_n^j - \frac{1}{2}Q_{h,n}^j\right)\delta t + W_{t_{n+1}}^j - W_{t_n}^j. \qquad (2.51)$$

The couples (P_n^j, Q_n^j) are independent realizations of the couples (P_n, Q_n). They also are exchangeable random variables.

The aim of this section is to prove the following lemma.

Lemma 10 (Convergence of the Monte Carlo method) *We assume $\delta t < \frac{1}{2}$. Moreover, we assume either $0 < A < \sqrt{\frac{3}{5\delta t}}$ (convergence with cut-off), or $A = \infty$ (convergence without cut-off). We have then the following inequality : $\forall n \leq \frac{T}{\delta t}$,*

$$\int_{\mathcal{O}}\mathbb{E}((u_n - \overline{u}_n)^2 1_{\mathcal{A}_n}) + \int_{\mathcal{O}}\mathbb{E}\left(\frac{1}{M}\sum_{j=1}^{M}(Q_n^j - \overline{Q}_n^j)^2 1_{\mathcal{A}_n}\right) \leq C\left(\frac{1}{M} + \delta t^2\right).$$

The constant C is independent of n, h and δt, but depends on the data of the problem : u_0, f_{ext} and T. In the case $0 < A < \sqrt{\frac{3}{5\delta t}}$, C also depends on $\gamma > 0$ such that $A > -\gamma\ln(\delta t)$. In the case $A = \infty$ the estimation is in fact of order $\frac{C}{M}$.

In the following, we will need an estimate of the variance of $P_nQ_{h,n}$.

Lemma 11 (A variance estimate) *We assume $\delta t < 1$. Then, $\exists C, \forall n \leq \frac{T}{\delta t}$,*

$$\int_{\mathcal{O}} \mathbb{E}\left((P_n Q_{h,n} - \mathbb{E}(P_n Q_{h,n}))^2\right) < C.$$

The constant C is independent of h and δt, but depends on the data of the problem : u_0, f_{ext} and T.

Proof. The proof is based on an explicit calculation of the variance. Recall that we omit the subscript h.

In the following, we set $W_{t_{n+1}} - W_{t_n} = \sqrt{\delta t}G_n$ and $V_{t_{n+1}} - V_{t_n} = \sqrt{\delta t}G'_n$. The random variables G_n, G'_n are independent normal random variables, independent of P_0 and Q_0.

We recall that P_n and Q_n are defined by :

$$P_{k+1} = \left(1 - \frac{\delta t}{2}\right) P_k + \sqrt{\delta t}G'_k \text{ and } Q_{k+1} = \left(1 - \frac{\delta t}{2}\right) Q_k + \delta t \partial_x u_{k+1} P_k + \sqrt{\delta t}G_k.$$

By induction, it is easy to show that

$$Q_n = \left(1 - \frac{\delta t}{2}\right)^n Q_0 + \sum_{k=1}^{n} \left(1 - \frac{\delta t}{2}\right)^{n-k} \sqrt{\delta t}G_{k-1} + \sum_{k=1}^{n} \left(1 - \frac{\delta t}{2}\right)^{n-k} \partial_x u_k P_{k-1}\delta t.$$
$$(2.52)$$

We set $X_n = \delta t \sum_{k=1}^{n} \left(1 - \frac{\delta t}{2}\right)^{-k} \partial_x u_k P_{k-1}P_n$. We have the following equalities :

$$P_n Q_n = \left(1 - \frac{\delta t}{2}\right)^n \left(P_n Q_0 + \sum_{k=1}^{n} \left(1 - \frac{\delta t}{2}\right)^{-k} \sqrt{\delta t}P_n G_{k-1} + X_n\right),$$

$$P_n Q_n - \mathbb{E}(P_n Q_n) = \left(1 - \frac{\delta t}{2}\right)^n \left(P_n Q_0 + \sum_{k=1}^{n} \left(1 - \frac{\delta t}{2}\right)^{-k} \sqrt{\delta t}P_n G_{k-1} + X_n - \mathbb{E}(X_n)\right).$$

Using independence properties, we find :

$\mathbb{E}\left((P_n Q_n - \mathbb{E}(P_n Q_n))^2\right)$

$$= \left(1 - \frac{\delta t}{2}\right)^{2n} \left(\mathbb{E}(P_n^2) + \sum_{k=1}^{n} \left(1 - \frac{\delta t}{2}\right)^{-2k} \delta t \mathbb{E}(P_n^2) + \mathbb{E}\left((X_n - \mathbb{E}(X_n))^2\right)\right).$$

A simple calculation yields $\mathbb{E}(P_n^2) < 2$ and therefore $\mathbb{E}(P_n P_m) < 2$. It remains now to estimate $\left(1 - \frac{\delta t}{2}\right)^{2n} \mathbb{E}\left((X_n - \mathbb{E}(X_n))^2\right)$. One can show that

$$\left(1 - \frac{\delta t}{2}\right)^{2n} (X_n - \mathbb{E}(X_n))^2 \leq \delta t^2 n \sum_{k=1}^{n} \left(1 - \frac{\delta t}{2}\right)^{2(n-k)} |\partial_x u^k|^2 (P_{k-1}P_n - \mathbb{E}(P_{k-1}P_n))^2.$$

One can check that $\mathbb{E}\left((P_{k-1}P_n - \mathbb{E}(P_{k-1}P_n))^2\right) < C$ with C independent of δt (this is deduced from $\mathbb{E}(P_k^4) < C$). We obtain then :

$$\left(1 - \frac{\delta t}{2}\right)^{2n} \mathbb{E}\left((X_n - \mathbb{E}(X_n))^2\right) \leq CT\delta t \sum_{k=1}^{n} |\partial_x u^k|^2.$$

The stability lemma 4 has shown that $\sum_{k=1}^{n} \delta t \|\partial_x u_k\|_{L_x^2}^2 < C$, which leads to the result. $\qquad\square$

In order to prove Lemma 10 in the case $A < \infty$ (convergence with cut-off), we will also use the following estimates :

Lemma 12 *We assume $\delta t < \frac{1}{2}$. Moreover, we assume that the cut-off constant is such that $-\gamma \ln(\delta t) < A < \infty$, for some positive constant γ. We have then :*

$$\mathbb{E}\left((P_n^1 - \overline{P}_n^1)^2 \right) < C\delta t^4,$$

$$\int_{\mathcal{O}} \mathbb{E}\left(\left(Q_n^1 (P_n^1 - \overline{P}_n^1) \right)^2 \right) < C\delta t^4,$$

with C a constant depending on γ and on the data of the problem : u_0, f_{ext} and T.

Proof. In the following, as in the former proof, we set $W_{t_{n+1}}^j - W_{t_n}^j = \sqrt{\delta t} G_n^j$ and $V_{t_{n+1}}^j - V_{t_n}^j = \sqrt{\delta t}(G_n^j)'$. The first estimate is deduced from an estimation on normal random variables. We know that for all n, the random variables P_n^1 are normal variables of variance less than 2. One can therefore write : for all n,

$$\mathbb{E}\left((P_n^1 - \overline{P}_n^1)^2 \right) < \frac{1}{\sqrt{\pi}} \int_A^\infty (x - A)^2 e^{-\frac{x^2}{4}} \, dx.$$

A simple calculation yields

$$\frac{1}{\sqrt{\pi}} \int_A^\infty (x - A)^2 e^{-\frac{x^2}{4}} \, dx < C \exp\left(-C' \frac{A^2}{8} \right) < C_\alpha \exp(\alpha \ln(\delta t)),$$

for any exponent $\alpha > 0$. Taking $\alpha = 4$, we obtain the first estimate. One can show in the same way the following estimate which will be used at the end of this proof :

$$\mathbb{E}\left((P_n^1 - \overline{P}_n^1)^4 \right) < C\delta t^8. \tag{2.53}$$

For the second estimate, we use the former computation (2.52) of Q_n^1. We can then write :

$$\int_{\mathcal{O}} \mathbb{E}\left(\left(Q_n^1 (P_n^1 - \overline{P}_n^1) \right)^2 \right) \leq 3 \int_{\mathcal{O}} \mathbb{E}\left(\left(\left(1 - \frac{\delta t}{2}\right)^n Q_0^1 (P_n^1 - \overline{P}_n^1) \right)^2 \right)$$

$$+ 3 \int_{\mathcal{O}} \mathbb{E}\left(\left(\sum_{k=1}^n \left(1 - \frac{\delta t}{2}\right)^{n-k} \sqrt{\delta t} G_{k-1}^1 (P_n^1 - \overline{P}_n^1) \right)^2 \right)$$

$$+ 3 \int_{\mathcal{O}} \mathbb{E}\left(\left(\sum_{k=1}^n \left(1 - \frac{\delta t}{2}\right)^{n-k} \partial_x u_k P_{k-1}^1 (P_n^1 - \overline{P}_n^1) \delta t \right)^2 \right).$$

For the first and second terms, we notice that the random variables Q_0^1, $(P_n^1 - \overline{P}_n^1)$ and G_n^1 are independent, which yields :

$$\int_{\mathcal{O}} \mathbb{E}\left(\left(\left(1 - \frac{\delta t}{2}\right) Q_0^1 (P_n^1 - \overline{P}_n^1)\right)^2\right) + \int_{\mathcal{O}} \mathbb{E}\left(\left(\sum_{k=1}^n \left(1 - \frac{\delta t}{2}\right)^{n-k} \sqrt{\delta t} G_{k-1}^1 (P_n^1 - \overline{P}_n^1)\right)^2\right)$$

$$\leq \mathbb{E}\left((Q_0^1)^2\right) \mathbb{E}\left((P_n^1 - \overline{P}_n^1)^2\right) + \sum_{k=1}^n \delta t\, \mathbb{E}\left((G_{k-1}^1)^2\right) \mathbb{E}\left((P_n^1 - \overline{P}_n^1)^2\right)$$

$$\leq (1+T)\mathbb{E}\left((P_n^1 - \overline{P}_n^1)^2\right) \leq C\delta t^4.$$

For the third term, we write :

$$\int_{\mathcal{O}} \mathbb{E}\left(\left(\sum_{k=1}^n \left(1 - \frac{\delta t}{2}\right)^{n-k} \partial_x u_k P_{k-1}^1 (P_n^1 - \overline{P}_n^1)\delta t\right)^2\right)$$

$$\leq \int_{\mathcal{O}} \mathbb{E}\left(\left(\sqrt{\sum_{k=1}^n \partial_x u_k^2}\sqrt{\sum_{k=1}^n (P_{k-1}^1)^2}(P_n^1 - \overline{P}_n^1)\delta t\right)^2\right)$$

$$\leq \delta t^2 \int_{\mathcal{O}} \sum_{k=1}^n \partial_x u_k^2 \mathbb{E}\left(\sum_{k=1}^n (P_{k-1}^1)^2 (P_n^1 - \overline{P}_n^1)^2\right).$$

We have shown in the stability lemma 4 that $\delta t \sum_{k=1}^n \int_{\mathcal{O}} \partial_x u_k^2 < C$. One last term remains :

$$\mathbb{E}\left(\sum_{k=1}^n (P_{k-1}^1)^2 (P_n^1 - \overline{P}_n^1)^2\right) \leq \sum_{k=1}^n \sqrt{\mathbb{E}\left((P_{k-1}^1)^4\right)}\sqrt{\mathbb{E}\left((P_n^1 - \overline{P}_n^1)^4\right)} \leq \frac{C}{\delta t}\delta t^4.$$

using the fact that $\mathbb{E}\left((P_k^1)^4\right) \leq C$ and (2.53). $\qquad \square$

We can now prove Lemma 10.

Proof. We set $S_n = \frac{1}{M}\sum_{j=1}^M P_n^j Q_n^j$, $g_n = u_n - \overline{u}_n$ and $R_n^j = Q_n^j - \overline{Q}_n^j$. Using the same arguments as in the former proofs, we obtain

$$\frac{1}{2\delta t}\left(\int_{\mathcal{O}} g_{n+1}^2 - \int_{\mathcal{O}} g_n^2\right) + \int_{\mathcal{O}} \partial_x g_{n+1}^2 \leq -\int_{\mathcal{O}} (\mathbb{E}(P_n Q_n) - \overline{S}_n)\partial_x g_{n+1},$$

$$\frac{1}{2\delta t}\left(\mathbb{E}^n((R_{n+1}^j)^2) - \mathbb{E}^n((R_n^j)^2)\right) + \frac{1}{2}\mathbb{E}^n((R_n^j)^2) = \mathbb{E}^n\left((\partial_x u_{n+1}P_n^j - \partial_x \overline{u}_{n+1}\overline{P}_n^j)R_n^j\right)$$

$$+ \frac{1}{2\delta t}\mathbb{E}^n((R_{n+1}^j - R_n^j)^2).$$

Summing up these two expressions, one finds :

$$\frac{1}{2\delta t}\left(\int_{\mathcal{O}}\mathbb{E}^n(g_{n+1}^2) - \int_{\mathcal{O}}\mathbb{E}^n(g_n^2)\right) + \int_{\mathcal{O}}\mathbb{E}^n(\partial_x g_{n+1}^2)$$
$$+\frac{1}{2\delta t}\left(\int_{\mathcal{O}}\mathbb{E}^n\left((R_{n+1}^1)^2\right) - \int_{\mathcal{O}}\mathbb{E}^n\left((R_n^1)^2\right)\right) + \frac{1}{2}\int_{\mathcal{O}}\mathbb{E}^n\left((R_n^1)^2\right)$$
$$\leq \frac{1}{2\delta t}\int_{\mathcal{O}}\mathbb{E}^n\left((R_{n+1}^1 - R_n^1)^2\right) + \int_{\mathcal{O}}\mathbb{E}^n\left((S_n - \mathbb{E}(P_nQ_n))\partial_x g_{n+1}\right) + \int_{\mathcal{O}}\mathbb{E}^n\left(I_n^1\right).$$

with

$$\begin{aligned}I_n^1 &= (\partial_x u_{n+1}P_n^1 - \partial_x \overline{u}_{n+1}\overline{P}_n^1)R_n^1 - (P_n^1 Q_n^1 - \overline{P}_n^1 \overline{Q}_n^1)\partial_x g_{n+1}\\ &= \partial_x u_{n+1}\overline{Q}_n^1(\overline{P}_n^1 - P_n^1) + \partial_x \overline{u}_{n+1}Q_n^1(P_n^1 - \overline{P}_n^1).\end{aligned}$$

For the second term on the right-hand side of (2.54), we use Lemma 11 :

$$\int_{\mathcal{O}}\mathbb{E}^n\left((S_n - \mathbb{E}(P_nQ_n))\partial_x g_{n+1}\right) \leq \frac{1}{10}\int_{\mathcal{O}}\mathbb{E}^n\left((\partial_x g_{n+1})^2\right) + 10\int_{\mathcal{O}}\mathbb{E}\left((S_n - \mathbb{E}(P_nQ_n))^2\right).$$

The first term is controlled on the left-hand side of (2.54), while the second term is estimated using the variance of P_nQ_n (see Lemma 11) :

$$\int_{\mathcal{O}}\mathbb{E}\left((S_n - \mathbb{E}(P_nQ_n)^2\right) = \int_{\mathcal{O}}\mathbb{E}\left(\left(\frac{1}{M}\sum_{j=1}^M(P_n^j Q_n^j - \mathbb{E}(P_n^j Q_n^j))\right)^2\right) \leq \frac{C}{M}.$$

For the first term on the right-hand side of (2.54), we write :

$$\begin{aligned}(R_{n+1}^1 - R_n^1)^2 &= \left((\partial_x u_{n+1}P_n^1 - \partial_x \overline{u}_{n+1}\overline{P}_n^1) - \frac{1}{2}R_n^1\right)^2 \delta t^2\\ &= \left(\partial_x u_{n+1}(P_n^1 - \overline{P}_n^1) + (\partial_x g_{n+1}\overline{P}_n^1) - \frac{1}{2}R_n^1\right)^2 \delta t^2.\end{aligned}$$

In the case $A = \infty$, using $P_n^j = \overline{P}_n^j$, one notices that forall j, $I_n^j = 0$ and that

$$(R_{n+1}^j - R_n^j)^2 \leq 2\left(\partial_x g_{n+1}\overline{P}_n^j\right)^2 \delta t^2 + \frac{1}{2}\left(R_n^j\right)^2 \delta t^2.$$

Using the assumption $\frac{1}{2}\delta t < 1$, the second term is controlled on the left-hand side of (2.54). It follows that :

$$\frac{1}{2\delta t}\left(\int_{\mathcal{O}}\mathbb{E}^n(g_{n+1}^2) - \int_{\mathcal{O}}\mathbb{E}^n(g_n^2)\right) + \int_{\mathcal{O}}\mathbb{E}^n\left(\left(\frac{9}{10} - \delta t \frac{1}{M}\sum_{j=1}^M(\overline{P}_n^j)^2\right)\partial_x g_{n+1}^2\right)$$
$$+\frac{1}{2\delta t}\left(\int_{\mathcal{O}}\mathbb{E}^n\left((R_{n+1}^1)^2\right) - \int_{\mathcal{O}}\mathbb{E}^n\left((R_n^1)^2\right)\right) \leq \frac{C}{M}.$$

Using the properties of $\mathcal{A}_n$, we easily derive

$$\frac{1}{2\delta t}\left(\int_{\mathcal{O}}\mathbb{E}^{n+1}(g_{n+1}^2)-\int_{\mathcal{O}}\mathbb{E}^n(g_n^2)\right)+\frac{1}{2\delta t}\left(\int_{\mathcal{O}}\mathbb{E}^{n+1}\left((R_{n+1}^1)^2\right)-\int_{\mathcal{O}}\mathbb{E}^n\left((R_n^1)^2\right)\right)\leq\frac{C}{M}.$$

Summing up (2.54) on n, we obtain an estimation in $\frac{C}{M}$, using the stability lemmas 4 and 9.

In the case $A < \infty$, we have (notice that $P_n^1 \neq \overline{P}_n^1$) :

$$(R_{n+1}^1 - R_n^1)^2 \leq 3\left(\partial_x u_{n+1}(P_n^1 - \overline{P}_n^1)\right)^2\delta t^2 + 3\left(\partial_x g_{n+1}\overline{P}_n^1\right)^2\delta t^2 + \frac{3}{4}\left(R_n^1\right)^2\delta t^2.$$

Using the assumption $\frac{3}{2}A^2\delta t < \frac{9}{10}$ (this is the inequality which defines the upper bound of A in the case $A < \infty$) and $\frac{3}{4}\delta t < 1$, the last two terms are controlled on the left-hand side of (2.54). We obtain a bound of order $C\delta t^2$ on the first term using $\delta t\sum_n\int_{\mathcal{O}}\partial_x u_{n+1}^2 < C$ (see Lemma 4) and $\mathbb{E}\left((P_n^1 - \overline{P}_n^1)^2\right) < C\delta t$ (see Lemma 12). For the third term on the right-hand side of (2.54) (which is $\mathbb{E}(I_n^1)$), we use twice Lemma 12. Indeed, for the first term of I_n^1, we write :

$$\int_{\mathcal{O}}\mathbb{E}\left(\partial_x u_{n+1}\overline{Q}_n^1(\overline{P}_n^1 - P_n^1)\right)\leq\sqrt{\int_{\mathcal{O}}(\partial_x u_{n+1})^2}\mathbb{E}\left(\sqrt{\int_{\mathcal{O}}(\overline{Q}_n^1)^2}(\overline{P}_n^1 - P_n^1)\right)$$

$$\leq\sqrt{\int_{\mathcal{O}}(\partial_x u_{n+1})^2}\sqrt{\mathbb{E}\left(\int_{\mathcal{O}}(\overline{Q}_n^1)^2\right)}\sqrt{\mathbb{E}\left((\overline{P}_n^1 - P_n^1)^2\right)},$$

which yields after summation over n an estimate of order $C\delta t^2$. For the second term of I_n^1, we write :

$$\int_{\mathcal{O}}\mathbb{E}\left(\partial_x\overline{u}_{n+1}Q_n^1(\overline{P}_n^1 - P_n^1)\right)\leq\sqrt{\int_{\mathcal{O}}\mathbb{E}\left((\partial_x\overline{u}_{n+1})^2\right)}\sqrt{\int_{\mathcal{O}}\mathbb{E}\left(\left(Q_n^1(\overline{P}_n^1 - P_n^1)\right)^2\right)},$$

which also yields after summation over n a bound in $C\delta t^2$. We can again conclude summing up over n and using the stability lemmas 4 and 9. □

Remark 6 *One can estimate, in the case $A < \infty$, the probability that the cut-off is active during a simulation. Indeed, the probability that one of the $|P_n^j|$ (with $n \leq \frac{T}{\delta t}$) goes beyond A is roughly bounded by $\frac{M}{\delta t}\left(1 - \frac{2}{\sigma\sqrt{2\pi}}\int_0^A e^{-\frac{x^2}{2\sigma^2}}\right) = \frac{M}{\delta t}\left(1 - erf\left(\frac{A}{\sigma\sqrt{2}}\right)\right)$ with σ^2 an upper bound on the variance of the P_n^j (one can take $\sigma^2 = \frac{4}{4-\delta t}$) and $erf(x) = \frac{2}{\sqrt{\pi}}\int_0^x e^{-t^2}\,dt$. Choosing $M = \frac{1}{\delta t^2}$ (which is consistent with the order of convergence $O\left(h + \delta t + \frac{1}{\sqrt{M}}\right)$) and $A = \sqrt{\frac{3}{5\delta t}}$, this probability is bounded by $\frac{1}{\delta t^3}\left(1 - erf\left(\sqrt{\frac{3(4-\delta t)}{40\delta t}}\right)\right)$. This upper bound is very close to 0 when δt is small (it is equal to 10^{-8} for $\delta t = 0.01$).*

2.4.4 Conclusion : convergence of the fully discretized problem.

We now state our main result.

Theorem 3 (Convergence of the fully discretized problem) *We assume a P1 discretization of the velocity in space. We also make the following regularity hypothesis :* $u_0 \in H_x^2$, $f_{ext} \in L_t^1(H_x^1)$ *and* $\dfrac{\partial f_{ext}}{\partial t} \in L_t^1(L_x^2)$. *We assume either* $A = \infty$ *(without cut-off), or* $0 < A < \sqrt{\dfrac{3}{5\delta t}}$ *(with cut-off, in which case* $1_{\mathcal{A}_n} = 1$). *Assuming* $\delta t < \frac{1}{2}$, *we have :* $\forall n \leq \frac{T}{\delta t}$,

$$\left\| u(t_n) - \overline{u}_h^n 1_{\mathcal{A}_n} \right\|_{L_x^2(L_\omega^2)} + \left\| \mathbb{E}(P_{t_n} Q_{t_n}) - \frac{1}{M} \sum_{j=1}^M \overline{P}_n^j \overline{Q}_{h,n}^j 1_{\mathcal{A}_n} \right\|_{L_x^1(L_\omega^1)} \leq C \left(h + \delta t + \frac{1}{\sqrt{M}} \right),$$

where C is independent of h and δt, but depends on the data of the problem : u_0, f_{ext} *and T. In the case* $0 < A < \sqrt{\dfrac{3}{5\delta t}}$, *$C$ also depends on $\gamma > 0$ such that $A > -\gamma \ln(\delta t)$.*

Proof. For the estimation on u, we write : $u(t_n) - \overline{u}_h^n 1_{\mathcal{A}_n} = (u(t_n) - u_h(t_n)) + (u_h(t_n) - u_h^n) + u_h^n (1 - 1_{\mathcal{A}_n}) + (u_h^n - \overline{u}_h^n) 1_{\mathcal{A}_n}$. We use Lemma 3 for the first term, Theorem 2 for the second term and Lemma 10 for the last term. In case $A < \sqrt{\dfrac{3}{5\delta t}}$, the third term is nul. In case $A = \infty$, we upper bound this term thanks to Lemmas 8 and 4.

For the estimation on $\mathbb{E}(P_t Q_t)$, we write : $\mathbb{E}(P_{t_n} Q_{t_n}) - \frac{1}{M} \sum_{j=1}^M \overline{P}_n^j \overline{Q}_{h,n}^j 1_{\mathcal{A}_n} = (\mathbb{E}(P_{t_n} Q_{t_n}) - \mathbb{E}(P_{t_n} Q_{h,t_n})) + (\mathbb{E}(P_{t_n} Q_{h,t_n}) - \mathbb{E}(P_n Q_{h,n})) + \mathbb{E}(P_n Q_{h,n})(1 - 1_{\mathcal{A}_n}) + \left(\mathbb{E}(P_n Q_{h,n}) - \frac{1}{M} \sum_{j=1}^M P_n^j Q_{h,n}^j \right) 1_{\mathcal{A}_n} + \left(\frac{1}{M} \sum_{j=1}^M P_n^j (Q_{h,n}^j - \overline{Q}_{h,n}^j) \right) 1_{\mathcal{A}_n} + \left(\frac{1}{M} \sum_{j=1}^M \overline{Q}_{h,n}^j (P_n^j - \overline{P}_n^j) \right) 1_{\mathcal{A}_n}$. We use then Lemma 3 for the first term, Theorem 2 for the second term, Lemma 11 for the fourth term and Lemma 10 for the fifth term. The third term is nul when $A < \sqrt{\dfrac{3}{5\delta t}}$ and is estimated by Lemmas 8 and 4 in the case $A = \infty$. The last term is zero in the case $A = \infty$ and is estimated by Lemma 12 in the case $A < \infty$. $\qquad \square$

Remark 7 *We have actually shown the following convergence result on Q_t :* $\forall j \leq M$,

$$\left\| Q_{t_n}^j - \overline{Q}_{h,n}^j \right\|_{L_x^2(L_\omega^2)} \leq C \left(h + \delta t + \frac{1}{\sqrt{M}} \right),$$

where (P_t^j, Q_t^j) are the processes defined by (2.20) and (2.19) with (V_t, W_t) replaced by (V_t^j, W_t^j).

Remark 8 *In the space-discretized problem of our model, the jth dumbbell in each cell is driven by the same Brownian motion (V^j, W^j). However, the first CONNF-FESSIT simulations were made with driving Brownian motions independent from*

one cell to another. More generally, one could choose any correlation in space for these Brownian motions. In fact, the convergence result stated in Theorem 3 holds whatever the choice of the correlation in space (the constant C in front of the rate of convergence $C\left(h + \delta t + \frac{1}{\sqrt{M}}\right)$, does not depend on the correlation). In return, the convergence on $\overline{Q}_{h,n}^j$ stated in the previous remark no longer makes sense.

Remark 9 *It can be noticed that we obtain a convergence of the $L_t^\infty(L_x^2)$ norm of $\overline{u}_h^n$ to $u(t_n)$ at the speed h (up to the L_ω^2 norm of course). As we work with $\mathbb{P}1$ finite elements, the convergence of $\overline{u}_h^n$ to $u(t_n)$ is expected at the speed h in the $L_t^2(H_x^1)$ norm (which we indeed obtain in Lemma 3 above) but also at the speed h^2 in the $L_t^\infty(L_x^2)$ norm. In our context, this h^2 convergence is indeed confirmed by numerical experiments. It is indeed possible to prove it using similar techniques as those of the standard case, but, as our emphasis here is on the stochastic side (see section 11.2 of Ref. [127] and chapter 1 of Ref. [146]), we do not want to enter such technicalities here.*

2.5 Numerical results.

In this section, we show some numerical results about the latter step of discretization : the convergence of the Monte Carlo method. It is indeed the less classical one, and the model we use is simple enough to compute exactly $(u_h^{n+1}, \mathbb{E}(P_{n+1}Q_{h,n+1}))$ being given $(u_h^n, \mathbb{E}(P_nQ_{h,n}))$. We use (2.34) to compute u_h^{n+1} and the following explicite calculation of $\mathbb{E}(P_{n+1}Q_{h,n+1})$ derived from (2.35) and (2.36) (which is just a discretization of the equivalent macroscopic model for the stress tensor) :

$$\begin{cases} \mathbb{E}(P_{n+1}Q_{h,n+1}) & = \ \left(1 - \frac{\delta t}{2}\right)^2 \mathbb{E}(P_nQ_{h,n}) + \left(1 - \frac{\delta t}{2}\right)\partial_x u_h^{n+1}\mathbb{E}(P_n^2)\delta t, \\ \mathbb{E}(P_{n+1}^2) & = \ \left(1 - \frac{\delta t}{2}\right)^2 \mathbb{E}(P_n^2) + \delta t. \end{cases}$$

This enables us to compare numerically the deterministic variables $(u_h^n, \mathbb{E}(P_nQ_{h,n}))$ (which, we recall, are an approximation in space and time of $(u(t_n), \mathbb{E}(P_{t_n}Q_{t_n}))$) with the Monte Carlo approximation $\left(\overline{u}_h^n, \frac{1}{M}\sum_{j=1}^M \overline{P}_n^j\overline{Q}_{h,n}^j\right)$. All the tests have been done with the following values for the physical parameters : $\lambda = 1$, $nk_BT = 20$ and $T = 1$. In the following, I denotes the number of space steps, N denotes the number of time steps and M denotes the number of Monte Carlo realizations (i.e. the number of dumbbells in each cell).
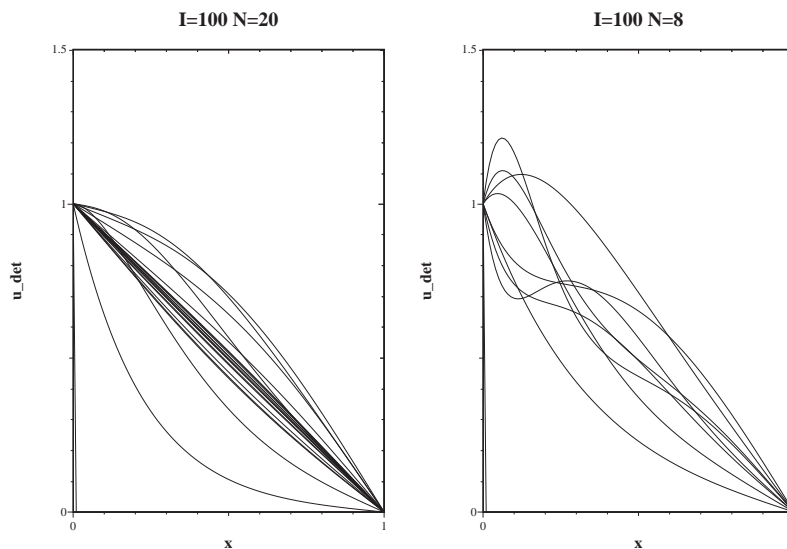
FIG. 2.2 – Deterministic computation of velocity profile as time evolves.

Tests on the stability.

First, by a deterministic calculus yielding $(u_h^n, \mathbb{E}(P_n Q_{h,n}))$, we have checked that when δt is too large, the solution oscillates (see Figure 2.2). This result is to be related to the stability lemma 4, which states that stability holds for δt small enough.

Tests on the cut-off.

In order to illustrate the effect of the cut-off on the fully discretized problem, one needs to take a δt near the upper bound of stability given in Lemma 4. In practice, we have chosen δt such that the deterministic computation begins to oscillate. We have chosen the following parameters : I = 10, N = 8 and M = 100. We have performed for each simulation (with cut-off and without cut-off) one million runs. We have then analyzed the errors (on velocity and stress) :

$$\sup_{0 \leq n \leq \frac{T}{\delta t}} ||u_h^n - \overline{u}_h^n||_{L_x^2} \text{ and } \sup_{0 \leq n \leq \frac{T}{\delta t}} \left|\left| \mathbb{E}(P_n Q_{h,n}) - \frac{1}{M} \sum_{j=1}^{M} \overline{P}_n^j \overline{Q}_{h,n}^j \right|\right|_{L_x^1} . \tag{2.54}$$

These errors are in fact relative errors since u_h^n and $\mathbb{E}(P_n Q_{h,n})$ are of order 1. For the simulation with cut-off, the value of A has been chosen "optimally" in order to obtain the best numerical distribution of errors. It is greater than the theoretical upper bound $\sqrt{\frac{3}{5\delta t}}$ that we need in our convergence result (Theorem 3).

We have noticed that the errors are clearly reduced in the simulations with cut-off : for the set of parameters given above, the mean error on the velocity goes from 1.68×10^{-1} without cut-off to 7.56×10^{-2} with cut-off and the mean error on the stress goes from 0.19 to 0.13. Moreover, the empirical probability for the error on the velocity to be smaller than 0.01 goes from 72% without cut-off to more than 88% with cut-off.

In Figure 2.3, we give a zoom of an histogram representing the empirical distribution of the error on the velocity : $\sup_{0 \leq n \leq \frac{T}{\delta t}} ||u_h^n - \overline{u}_h^n||_{L_x^2}$. On the left figure,
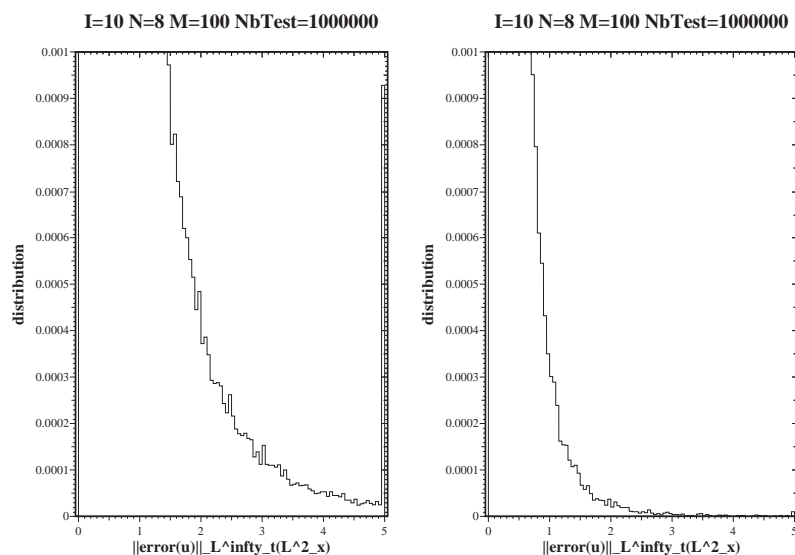
FIG. 2.3 – Distribution of the errors on velocity (zoom) : on the left-hand side, simulation without cut-off and on the right-hand side, simulation with cut-off ($A = 2.3$).

the bar on the far right contains all the simulations for which the error is greater than 4.95. One can clearly see on Figure 2.3 that the use of the cut-off reduces the empirical probability for the error to be large. This can be related to the fact that without cut-off, $\mathbb{P}(\mathcal{A}_n) < 1$ in the conclusion of the stability Lemma 9.

Tests on the space step, the number of realizations and the time step.

We have also checked that the means (computed without cut-off using 100 000 tests for each simulation) of the errors (2.54) on the velocity and the stress do not depend on the space step (at least when the solution does not oscillate, i.e. when δt is small enough for Lemma 4 to hold), which is in agreement with the result of Lemma 10. As usual in Monte Carlo methods, the error scales like $\frac{1}{\sqrt{M}}$, where M is the number of realizations, which confirms Lemma 10 (see Figure 2.4). Finally, we show the dependence of the error with repect to δt (see Figure 2.4). One can observe that there exists a bound on δt below which the error remains constant, which can be related to the result of Lemma 10.

Acknowledgments
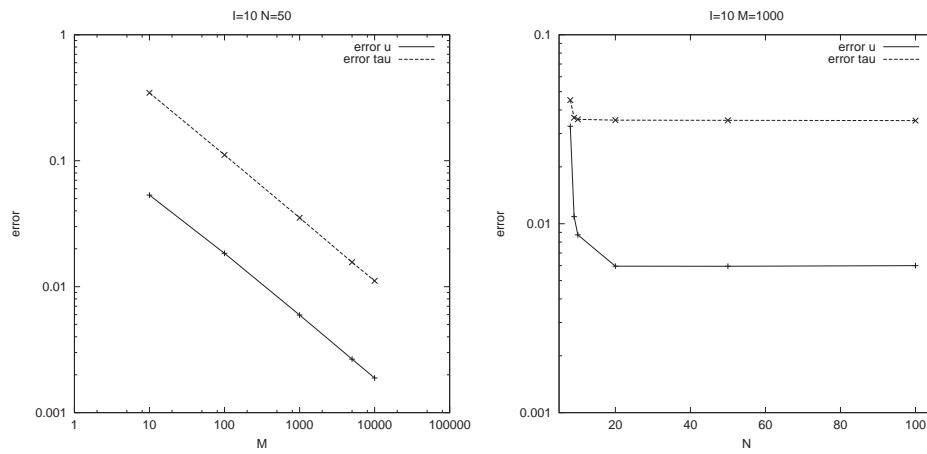
FIG. 2.4 – Errors $L_t^\infty(L_x^2(L_\omega^2))$ on u and $L_t^\infty(L_x^1(L_\omega^1))$ on τ depending on the number of Monte Carlo realizations (M) and on the number of time steps (N).

Chapitre 3

Calcul de l'erreur optimale sur la vitesse

Les résultats présentés dans ce chapitre ont fait l'objet d'un court article paru dans *Computers and Fluids*. On complète les résultats obtenus au chapitre 2 en dérivant une estimation *optimale* de l'erreur sur la vitesse pour la méthode CONNF-FESSIT.

**Optimal error estimate for the CONNFFESSIT approach
in a simple case.**

Tony Lelièvre

In this short note, we deal with a micro-macro model of polymeric fluids. We first summarize some mathematical results we have obtained so far on this model and then focus on a question about the optimality of the error estimate for the coupled finite element / Monte Carlo discretization.

3.1   Introduction

In order to understand the behavior of non-newtonian fluids, one of the current trend is to directly modelize the microstructures of the fluid and to then couple the evolution of these microstructures and the evolution of some macroscopic quantities (such as velocity or pressure). This coupling is usually performed through the expression of the stress tensor (which appears in the Navier-Stokes equation) in function of the microscopic variables.

We are here interested in dilute solutions of polymers. Such fluids consist of chains of polymers, supposedly non interacting, that evolve within a solvent. For a general introduction to these types of models, we refer to [12, 13, 39, 120]. In simple models, the polymer is modeled by two beads linked by a spring (see Figure 3.1). The evolution of this microstructure at a point x is ruled by a stochastic differential equation depending on the velocity of the fluid and its gradient at point x. The stress tensor is expressed as an expectation value built from the orientation of the polymer. This expression is then inserted in the Navier-Stokes equation.
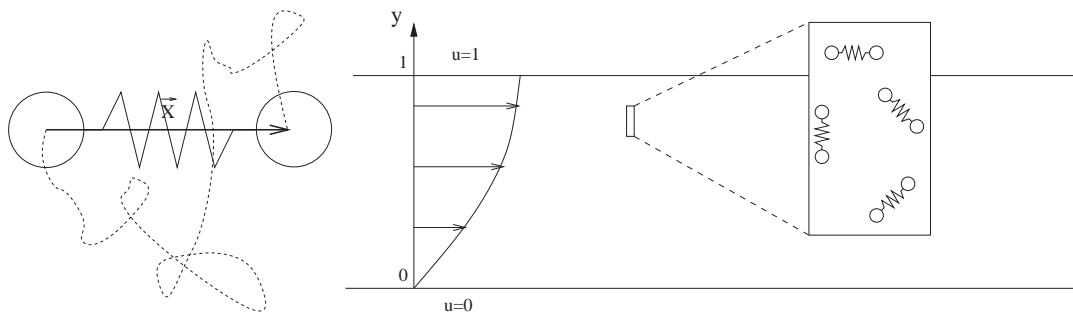
FIG. 3.1 – On the left, the polymer (in dashed line) is modelled by a "dumbbell" : two beads linked by a spring. The vector X is called the end-to-end vector. On the right, these dumbbells influence the velocity profile in a shear flow.

In [85], we have so far studied the case of a start-up of shear flow (see Figure 3.1). The focus lies on the coupling between the Stochastic Differential Equation (SDE) and the Partial Differential Equation (PDE). We have studied the case of a linear spring force (Hookean Dumbbell) in [85], where it is shown that the coupled system admits a unique solution and that the finite element method coupled with Monte Carlo converges. For the sake of consistency, we summarize these results in next

section. For an analysis of the case of a non-linear dumbbell which takes into account the finite extensibility of the polymer, we refer to [84, 86].

3.2 Some mathematical results on the coupled system

Let us precisely introduce the mathematical system we deal with. Due to the simple geometry of our problem, the velocity $u(t, y)$ is a scalar only depending on time $t \in (0, T)$ and on the one-dimensional space variable $y \in \mathcal{O} = (0, 1)$, and the end-to-end vector $\boldsymbol{X}_t = (X_t, Y_t)$ only depends on y through ist first component. The system reads :

$$\begin{cases} \partial_t u(t, y) - \partial_{yy} u(t, y) = \partial_y \tau(t, y) + f_{ext}(t, y), \\ \tau(t, y) = \mathbb{E}\left(X(t, y) Y(t) \right), \\ dX(t, y) = \left(-\frac{1}{2} X(t, y) + \partial_y u(t, y) Y(t) \right) dt + dV_t, \\ dY(t) = -\frac{1}{2} Y(t)\, dt + dW_t, \end{cases} \quad (3.1)$$

and is complemented by an initial condition $u(0, y) = u_0(y)$, and some boundary conditions $u(t, 0) = f_0(t)$ and $u(t, 1) = f_1(t)$ which we can suppose to be zero (see [85]). The stochastic process (V_t, W_t) is a standard bidimensional Brownian motion while the initial condition for $\boldsymbol{X}_t$, namely X_0 and Y_0, are independent normal random variables. Notice that one can compute Y independently of $(u, X) : Y_t = Y_0\, e^{-t/2} + \int_0^t e^{\frac{s-t}{2}}\, dW_s$.

Like in [85, 86], (u, X) is said to be a solution of (3.1) if : $u \in L_t^\infty(L_y^2) \cap L_t^2(H_{0,y}^1)$ and $X \in L_t^\infty(L_y^2(L_\omega^2))$ are s.t.,

$$\partial_t u(t, y) - \partial_{yy} u(t, y) = \partial_y \mathbb{E}\left(X(t, y) Y(t) \right) + f_{ext}(t, y), \text{ in } \mathcal{D}'([0, T) \times \mathcal{O}),$$

$$X_t(y) = e^{-\frac{t}{2}} X_0 + \int_0^t e^{\frac{s-t}{2}}\, dV_s + \int_0^t e^{\frac{s-t}{2}} \partial_y u(s, y) Y_s\, ds, \text{ for a.e. } (y, \omega),\ \forall t \in (0, T).$$

Then, we recall :

Theorem 4 (Global-in-time existence and uniqueness [85]) *Assuming $u_0 \in L_y^2$ and $f_{ext} \in L_t^1(L_y^2)$, this problem admits a unique solution (u, X). In addition, the following estimate holds :*

$$||u||^2_{L_t^\infty(L_y^2)} + ||u||^2_{L_t^2(H_{0,y}^1)} + ||X_t||^2_{L_t^\infty(L_y^2(L_\omega^2))} + ||X_t||^2_{L_t^2(L_y^2(L_\omega^2))}$$

$$\leq C \left(1 + ||u_0||^2_{L_y^2} + T + ||f_{ext}||^2_{L_t^1(L_y^2)} \right).$$

A discretization of the coupled PDE-SDE system (3.1) has been proposed by H.C. Öttinger in [97]. In our simple case, it reads : find $\overline{u}_h^n \in V_h$ such that,

$$\begin{cases} \frac{1}{\delta t} \int_{\mathcal{O}} \left(\overline{u}_h^{n+1} - \overline{u}_h^n \right) v_h + \int_{\mathcal{O}} \partial_y \overline{u}_h^{n+1} \partial_y v_h = -\int_{\mathcal{O}} \overline{\tau}_h^n \partial_y v_h + F_{ext},\ \forall v_h \in V_h, \\ \overline{\tau}_h^n = \frac{1}{M} \sum_{j=1}^M \left(\overline{X}_h^{j,n} \overline{Y}^{j,n} \right), \\ \overline{X}_h^{j,n+1} = \overline{X}_h^{j,n} + \left(-\frac{1}{2} \overline{X}_h^{j,n} + \partial_y \overline{u}_h^{n+1} \overline{Y}^{j,n} \right) \delta t + \left(V_{t_{n+1}}^j - V_{t_n}^j \right), \\ \overline{Y}^{j,n+1} = \overline{Y}^{j,n} + \left(-\frac{1}{2} \overline{Y}^{j,n} \right) \delta t + \left(W_{t_{n+1}}^j - W_{t_n}^j \right). \end{cases} \quad (3.2)$$

where V_h is the continuous $\mathbb{P}1$ finite element space, h is the spacestep, δt the timestep and M the number of realizations. Notice that for any $h > 0$, $\overline{u}_h^n \in V_h$ is a random variable (contrary to the continuous velocity u). We have proven in [85] :

Theorem 5 (Convergence of the numerical scheme [85]) *Assuming $u_0 \in H_y^2$, $f_{ext} \in L_t^1(H_y^1)$, $\partial_t f_{ext} \in L_t^1(L_y^2)$ and $\delta t < \frac{1}{2}$, we have (for $V_h = \mathbb{P}1$) : $\forall n < \frac{T}{\delta t}$,*

$$
\left\| u(t_n) - \overline{u}_h^n 1_{\mathcal{A}_n} \right\|_{L_y^2(L_\omega^2)} + \left\| \mathbb{E}(X_{t_n} Y_{t_n}) - \frac{1}{M} \sum_{j=1}^{M} \overline{X}_{h,n}^j \overline{Y}_n^j 1_{\mathcal{A}_n} \right\|_{L_y^1(L_\omega^1)} \leq C \left(h + \delta t + \frac{1}{\sqrt{M}} \right),
$$
(3.3)

with $\mathcal{A}_n = \left\{ \forall k \leq n, \; \frac{1}{M} \sum_{j=1}^{M} (\overline{Y}_k^j)^2 < \frac{13}{20} \frac{1}{\delta t} \right\}$.

The introduction of the event $\mathcal{A}_n$ is due to the fact that in the present model the dumbbell may extend to infinity (contrary to the model in [86]). However, it is to be remarked that the event $\mathcal{A}_n$ is "numerically" negligeable since its probability goes to 1 either when δt goes to 0 or when M goes to infinity.

3.3 Optimality in space

Our attention was brought by M. Picasso on the fact that the estimate (3.3) is not optimal in space for the velocity. Indeed, in a standard $\mathbb{P}1$ finite element discretization, a quadratic convergence in h is expected for the L^2 norm. Numerical experiments confirm that the h^2 convergence is indeed observed in practice. Our purpose here is to complement the results of [85] by showing that such convergence can actually be proven on the model we have considered. This result was announced in Remark 9 of [85]. We refer here to A. Quarteroni and A. Valli [127] (section 11.2) and to V. Thomée [146].

Going through the proof of Theorem 5 in [85], one can see that it is sufficient to prove that the semi-discretized problem in space enjoys a h^2 convergence. The semi-discretized problem is equivalent to : find $u \in V$ and $\mathbb{E}(X_t Y_t) \in \partial_y V$ such that,

$$
\begin{cases}
\int_{\mathcal{O}} \partial_t u v + \int_{\mathcal{O}} \partial_y u \partial_y v = - \int_{\mathcal{O}} \mathbb{E}(X_t Y_t) \partial_y v \\
\int_{\mathcal{O}} \partial_t \mathbb{E}(Y_t X_t) \sigma + \int_{\mathcal{O}} \mathbb{E}(X_t Y_t) \sigma = \int_{\mathcal{O}} \partial_y u \sigma
\end{cases}
$$

for all $v \in V$ and $\sigma \in \partial_y V$. For example, for $\mathbb{P}1$ finite elements, one chooses $V = \mathbb{P}1$ and $\partial_y V = \mathbb{P}0$. For the continuous problem, one takes $V = H_0^1$ and $\partial_y V = L^2$. Notice that the former system is equivalent to : find $u \in V$ such that,

$$
\int_{\mathcal{O}} \partial_t u v + \int_{\mathcal{O}} \partial_y u \partial_y v = - \int_{\mathcal{O}} \int_0^t e^{s-t} \partial_y u(s) \, ds \partial_y v,
$$

for all $v \in V$ and $\sigma \in \partial_y V$. Let us denote u_h the $\mathbb{P}1$ finite element solution. We suppose in the following that the solution of the continuous problem is such that : $u_0 \in H_y^2$ and $\partial_t u \in L_t^1(H_y^2)$. For any $v \in H_0^1$, we denote $\Pi_h(v)$ the H_0^1 projection of

v onto V_h defined by : $\Pi_h(v) \in V_h$ and $\forall v_h \in V_h$, $\int_{\mathcal{O}} \partial_y(v - \Pi_h(v))\partial_y v_h = 0$. We have the following standard finite element estimate (for $V_h = \mathbb{P}1$ and $v \in H^2$) :

$$||v - \Pi_h(v)||_{L_y^2} \leq Ch^2 ||v||_{H_y^2}. \tag{3.4}$$

We now want to estimate $u - u_h = (u - \Pi_h(u)) + (\Pi_h(u) - u_h)$. For the first term, we have just recalled the h^2 estimate (3.4) so that $||u - \Pi_h(u)||_{L_y^2} \leq Ch^2$, where C depends on $||u_0||_{H_y^2}$ and $||\partial_t u||_{L_t^1(H_y^2)}$. For the second term, one has :

$$
\begin{aligned}
&\int_{\mathcal{O}} \partial_t(u_h - \Pi_h(u))w_h + \int_{\mathcal{O}} \partial_y(u_h - \Pi_h(u))\partial_y w_h \\
&= \int_{\mathcal{O}} \partial_t u_h w_h + \int_{\mathcal{O}} \partial_y u_h \partial_y w_h - \int_{\mathcal{O}} \partial_t \Pi_h(u) w_h - \int_{\mathcal{O}} \partial_y \Pi_h(u) \partial_y w_h \\
&= \int_{\mathcal{O}} \partial_t u w_h + \int_{\mathcal{O}} \partial_y u \partial_y w_h + \int_{\mathcal{O}} \int_0^t e^{s-t} \partial_y(u - u_h)(s)\,ds \partial_y w_h - \int_{\mathcal{O}} \partial_t \Pi_h(u) w_h \\
&\quad - \int_{\mathcal{O}} \partial_y u \partial_y w_h \\
&= \int_{\mathcal{O}} \partial_t(u - \Pi_h(u))w_h + \int_{\mathcal{O}} \int_0^t e^{s-t}\partial_y(u - u_h)(s)\,ds \partial_y w_h \\
&= \int_{\mathcal{O}} (\partial_t u - \Pi_h(\partial_t u))w_h + \int_0^t e^{s-t} \int_{\mathcal{O}} \partial_y(u - \Pi_h(u))(s)\partial_y w_h\,ds \\
&\quad + \int_{\mathcal{O}} \int_0^t e^{s-t}\partial_y(\Pi_h(u) - u_h)\,ds \partial_y w_h \\
&= \int_{\mathcal{O}} (\partial_t u - \Pi_h(\partial_t u))w_h + \int_{\mathcal{O}} \int_0^t e^{s-t}\partial_y(\Pi_h(u) - u_h)\,ds \partial_y w_h.
\end{aligned}
$$

Choosing $w_h = (u_h - \Pi_h(u))(t)$, one obtains :

$$\frac{1}{2}\partial_t ||u_h - \Pi_h(u)||_{L_y^2}^2 + ||\partial_y(u_h - \Pi_h(u))||_{L_y^2}^2 \leq$$

$$Ch^2 ||\partial_t u||_{H_y^2}||u_h - \Pi_h(u)||_{L_y^2} + \int_0^t e^{s-t}||\partial_y(u_h - \Pi_h(u))||_{L_y^2}(s)\,ds\,||\partial_y(u_h - \Pi_h(u))||_{L_y^2}(t)$$

so that :

$$
\begin{aligned}
\partial_t ||u_h - \Pi_h(u)||_{L_y^2}^2 + ||\partial_y(u_h - \Pi_h(u))||_{L_y^2}^2 &\leq Ch^2 ||\partial_t u||_{H_y^2}||u_h - \Pi_h(u)||_{L_y^2} \\
&\quad + C\int_0^t e^{2(s-t)}||\partial_y(u_h - \Pi_h(u))||_{L_y^2}^2(s)\,ds
\end{aligned}
$$

and

$$||u_h - \Pi_h(u)||^2_{L_y^2}(t) + \int_0^t ||\partial_y(u_h - \Pi_h(u))||^2_{L_y^2}(s)\,ds \leq ||u_h - \Pi_h(u)||^2_{L_y^2}(0)$$

$$+ Ch^2 \int_0^t ||\partial_t u||_{H_y^2}(s)||u_h - \Pi_h(u)||_{L_y^2}(s)\,ds$$

$$+ C \int_0^t \int_0^s e^{2(r-s)} ||\partial_y(u_h - \Pi_h(u))||^2_{L_y^2}(r)\,dr\,ds$$

$$\leq Ch^4 + Ch^2 \int_0^t ||\partial_t u||_{H_y^2}(s)||u_h - \Pi_h(u)||_{L_y^2}(s)\,ds$$

$$+ C \int_0^t\!\!\int_0^s e^{2(r-s)} ||\partial_y(u_h - \Pi_h(u))||^2_{L_y^2}(r)\,dr\,ds.$$

One can suppose that the initial conditions are such that $||u_h - \Pi_h(u)||_{L_y^2}(0) \leq Ch^2$.
(In practice, one can even choose $u_h(0) := \Pi_h(u(0))$.)
   Let us denote $G(t)$ the right hand side. One has :

$$
\begin{aligned}
G'(t) &= Ch^2||\partial_t u||_{H_y^2}(t)||u_h - \Pi_h(u)||_{L_y^2}(t) + C\int_0^t e^{2(s-t)}||\partial_y(u_h - \Pi_h(u))||^2_{L_y^2}(s)\,ds, \\
&\leq C\left(h^2||\partial_t u||_{H_y^2}(t)\sqrt{G(t)} + G(t)\right).
\end{aligned}
$$

Let us denote $H(t) = \sqrt{G(t)}$. One has $H'(t) \leq C\left(h^2||\partial_t u||_{H_y^2}(t) + H(t)\right)$, so that $H(t) \leq Ch^2$ where C depends on $||u_0||_{H_y^2}$ and $||\partial_t u||_{L_t^1(H_y^2)}$ and therefore, for all $t \in [0, T]$:

$$||u_h - \Pi_h(u)||_{L_y^2}(t) \leq Ch^2. \tag{3.5}$$

   Collecting (3.4) and (3.5), we obtain

$$||u - u_h||_{L_y^2}(t) \leq Ch^2,$$

which completes the proof of :

Theorem 6 *Under the assumption of Theorem 5 and if moreover $\partial_t u \in L_t^1(H_y^2)$, we have (for $V_h = \mathbb{P}1$) : $\forall n < \frac{T}{\delta t}$,*

$$\left|\left| u(t_n) - \overline{u}_h^n 1_{\mathcal{A}_n} \right|\right|_{L_y^2(L_\omega^2)} \leq C\left(h^2 + \delta t + \frac{1}{\sqrt{M}}\right). \tag{3.6}$$

Chapitre 4

Analyse du modèle des dumbbells FENE : le problème couplé

Les résultats présentés dans ce chapitre ont fait l'objet d'un article paru dans *Journal of Functional Analysis*. Il s'agit d'un théorème d'existence et unicité en temps petit pour le problème couplé avec le modèle des dumbbells FENE, dans le cadre d'un écoulement cisaillé.

<center>
**Existence of solution for a micro-macro model
of polymeric fluid : the FENE model.**
</center>

Benjamin Jourdain, Tony Lelièvre, Claude Le Bris

We analyse a non-linear micro-macro model of polymeric fluids in the case
of a shear flow. More precisely, we consider the FENE dumbbell model,
which models polymers by nonlinear springs, accounting for the finite ex-
tensibility of the polymer chain. We prove the existence of a unique solution
to the stochastic differential equation which rules the evolution of a repre-
sentative polymer in the flow and next deduce a local-in-time existence and
uniqueness result on the system coupling the stochastic differential equation
and the momentum equation on the fluid.

Keywords : polymeric fluids, CONNFFESSIT method, FENE dumbbell, stochas-
tic differential equation, Cauchy problems.

4.1   Introduction and motivation

We continue here our endeavor, initiated in [85], to put the micro-macro models
for polymeric fluid flows on a mathematically sound ground.

Let us recall for consistency that these models aim at circumventing the diffi-
culty of finding a closure equation at the pure macroscopic level. In the case of non
newtonian fluids such as polymeric fluids, such an equation links the stress tensor to
the velocity field through, say, a partial differential equation or an integral relation.
In order to build a micro-macro model, one goes down to the microscopic scale and
makes use of kinetic theory to obtain a mathematical model for the evolution of the
microstructures of the fluid, here the configurations of the polymer chains. We refer
the reader to [85] or [90] for a more complete introduction to this type of models and
to [12, 13, 39, 120] for a comprehensive survey of the physical background. Contrary
to the purely macroscopic approach where the microscopic models are used to derive
macroscopic constitutive equations, most of the time through some simplifying as-
sumptions (closure assumptions) whose impact on the result is difficult to evaluate,
the so-called micro-macro approach consists in keeping explicit track of both scales.
In mathematical terms, this micro-macro approach translates into a coupled multis-
cale system of the following form (we consider here the simplest case : the so-called
dumbbell model, where the polymer is modelled by two beads linked by a spring,
see Figure 4.1) :

$$
\begin{cases}
\rho \left(\dfrac{\partial \boldsymbol{u}}{\partial t} + \boldsymbol{u}.\nabla \boldsymbol{u} \right) = -\nabla p + \eta \Delta \boldsymbol{u} + \operatorname{div} \boldsymbol{\tau}, \\[2mm]
\operatorname{div} \boldsymbol{u} = 0, \\[2mm]
\boldsymbol{\tau} = n \displaystyle\int (\boldsymbol{X} \otimes \boldsymbol{F}(\boldsymbol{X}))\psi(t,\boldsymbol{x},\boldsymbol{X})\,d\boldsymbol{X} - nk_B T \mathrm{Id}, \\[2mm]
\dfrac{\partial \psi}{\partial t} + \boldsymbol{u}.\nabla_{\boldsymbol{x}}\psi = -\operatorname{div}_{\boldsymbol{X}} \left(\left(\nabla_{\boldsymbol{x}}\boldsymbol{u}\,\boldsymbol{X} - \dfrac{2}{\zeta}\boldsymbol{F}(\boldsymbol{X}) \right)\psi \right) + \dfrac{\sigma^2}{\zeta^2}\Delta_{\boldsymbol{X}}\psi,
\end{cases}
\tag{4.1}
$$

where $\boldsymbol{u}(t,\boldsymbol{x})$ is the velocity of the fluid, $p(t,\boldsymbol{x})$ the pressure, $\boldsymbol{\tau}(t,\boldsymbol{x})$ the stress
tensor, and $\psi(t,\boldsymbol{x},\boldsymbol{X})$ denotes the probability density function of the end-to-end
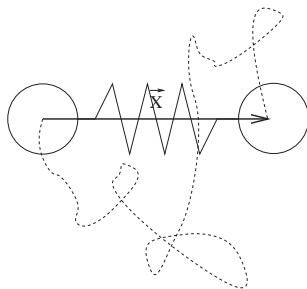
FIG. 4.1 – The polymer (in dashed line) is modelled by a "dumbbell" : two beads linked by a spring. The vector $\boldsymbol{X}$ is called the end-to-end vector.

vector $\boldsymbol{X}$ of the polymer at time t and at position $\boldsymbol{x}$. The other symbols are physical parameters : $\boldsymbol{F}(\boldsymbol{X})$ is the entropic force a representative polymer chain experiences, ρ and η respectively are the density and the viscosity of the ambiant fluid, n denotes the density of polymers, the coefficient σ is defined by $\sigma^2 = 2k_B T\zeta$ with T the temperature and ζ the friction coefficient of the beads within the fluid. It is to be noted that the Fokker-Planck equation on ψ holds at each macroscopic point $\boldsymbol{x}$.

Let us at once indicate that, from a physical point of view, the dumbbell model, for which the configuration space is $\mathbb{R}^3$ (that is, $\boldsymbol{X} \in \mathbb{R}^3$), is too crude to completely describe the evolution of the polymer chain. But this model serves as an efficient test problem for more sophisticated modelling strategies. In order to be more realistic, one has indeed to consider a model where the polymer is not just modelled by its end-to-end vector but by a chain of beads and springs, which leads to a system of the form (4.1), but with a Fokker-Planck equation set in a configuration space of dimension larger than 3. This highly complicates a direct numerical attack of the Fokker-Planck equation on ψ (there exists however such tentatives of direct attacks, see [143] and the references therein).

The main trend in the community of researchers performing numerical simulations of such complex flows is therefore to "replace" the Fokker-Planck equation by the underlying stochastic differential equation ruling the evolution of random variables whose density is ψ. Such an hybrid strategy mixing stochastic and deterministic aspects can be advantageously studied already in the setting of the simple dumbbell model. In the simple case of the dumbbell model, it indeed consists in turning (4.1) into the following mathematical system :

$$\begin{cases} \rho\left(\dfrac{\partial \boldsymbol{u}}{\partial t} + \boldsymbol{u}.\nabla \boldsymbol{u}\right) = -\nabla p + \eta\Delta\boldsymbol{u} + \mathrm{div}\,(\boldsymbol{\tau}), \\[2mm] \mathrm{div}\,(\boldsymbol{u}) = 0, \\[2mm] \boldsymbol{\tau} = n\mathbb{E}(\boldsymbol{X} \otimes \boldsymbol{F}(\boldsymbol{X})) - nk_B T\mathrm{Id}, \\[2mm] d\boldsymbol{X} + \boldsymbol{u}.\nabla\boldsymbol{X}\,dt = \left(\nabla\boldsymbol{u}\boldsymbol{X} - \dfrac{2}{\zeta}\boldsymbol{F}(\boldsymbol{X})\right)dt + \dfrac{\sqrt{2}\sigma}{\zeta}d\boldsymbol{W}_t, \end{cases} \qquad (4.2)$$

where $\boldsymbol{X}(t,\boldsymbol{x})$ is a stochastic process representing the end-to-end vector of the polymer modelled by a dumbbell (see Figure 4.1). The stochastic process $\boldsymbol{W}_t$ is a

standard (multidimensional) Brownian motion and $\mathbb{E}$ denotes the expectation.
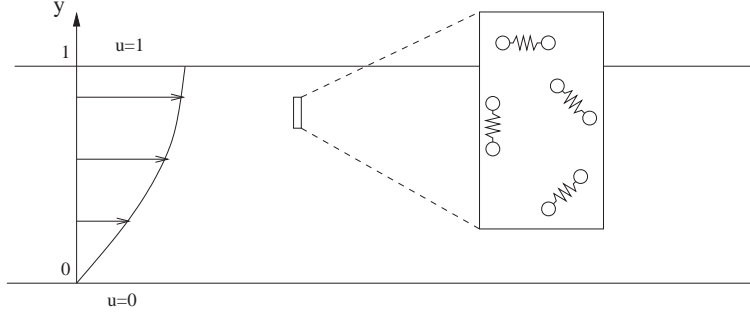
FIG. 4.2 − Velocity profile in a shear flow of a dilute solution of polymers.

In our previous work (see [85]), we have made the (simple) mathematical analysis and the (more intricate) numerical analysis of this model when applied to a simple Couette flow (see Figure 4.2) and when considering a linear force in the dumbbell (model of Hookean dumbbells : $\boldsymbol{F}(\boldsymbol{X}) = H\boldsymbol{X}$, with H a constant coefficient) (see also [72] for an other example of a mathematical analysis of a viscoelastic flow in this geometry). It then reduces to the system :

$$\begin{cases} \partial_t u - \partial_{yy} u = \partial_y \tau + f_{ext}, \\ \tau(t,y) = \mathbb{E}(X_t^y Y_t), \\ dX_t^y = \left(-\dfrac{X_t^y}{2} + \partial_y u Y_t \right) dt + dV_t, \\ dY_t = -\dfrac{Y_t}{2} dt + dW_t, \end{cases} \tag{4.3}$$

where (due to the simple geometry of the problem) $u = \boldsymbol{u}_x(y)$ and $\tau = \boldsymbol{\tau}_{xy}(y)$ are here valued in $\mathbb{R}$, while the space variable y varies in $\mathcal{O} = (0,1)$. In (4.3) and henceforth, we write all the equations in a non dimensional form and f_{ext} denotes an external force. The stochastic variables (X_t^y, Y_t) denote the components of the stochastic variable $\boldsymbol{X}_t$ introduced before. We have proved in [85] the well-posedness of the Cauchy problem by showing a global-in-time existence and uniqueness result. On the other hand, we have shown the convergence of the numerical approximation of the solution (finite difference in time, $\mathbb{P}1$ finite element in space, and Monte Carlo realizations) to the exact solution.

Despite its interest as a test problem for many mathematical and numerical techniques, the above Hookean dumbbell model is somewhat limited since it can in fact be written under the form of a purely macroscopic model, namely the Oldroyd-B model, that we recall here in its differential form :

$$\boldsymbol{\tau} + \lambda \frac{\delta \boldsymbol{\tau}}{\delta t} = nk_B T\lambda(\nabla \boldsymbol{u} +^t \nabla \boldsymbol{u}), \tag{4.4}$$

with the upper convected derivative $\frac{\delta}{\delta t}$ defined by :

$$\frac{\delta \boldsymbol{\tau}}{\delta t} = \frac{\partial \boldsymbol{\tau}}{\partial t} + \boldsymbol{u}.\nabla \boldsymbol{\tau} - \boldsymbol{\tau}^t \nabla \boldsymbol{u} - \nabla \boldsymbol{u} \boldsymbol{\tau},$$

where $\lambda = \frac{\zeta}{4H}$ is a characteristic time.

In order to address more general situations, we here want to treat the case of a micro-macro model which cannot be written under the form of a macroscopic model, and therefore is genuinely micro-macro. An instance of this model (at least to the best of our knowledge, see [89] on this subject) is the so-called FENE model where the acronym FENE stands for Finite Extensible Nonlinear Elastic. In this model, the force within the spring has the following expression : $\boldsymbol{F}(\boldsymbol{X}) = \frac{H\boldsymbol{X}}{1-\|\boldsymbol{X}\|^2/(bk_BT/H)}$ (H and b being two constant coefficients). This model is more realistic from a physical point of view than the model of Hookean dumbbell since it accounts for the finite extensibility of the real polymer. For example, this model exhibits shear-thinning or hysteretic behavior in elongational flows, contrary to the linear model of Hookean dumbbells, and accordingly to experiment.

Like in [85], we only consider in the sequel the setting of a simple Couette flow. The FENE model then reads, in a non-dimensional form :

$$\partial_t u - \partial_{yy} u = \partial_y \tau + f_{ext}, \tag{4.5}$$

$$\tau = \mathbb{E}\left(\frac{X_t^y Y_t^y}{1 - \frac{(X_t^y)^2 + (Y_t^y)^2}{b}} \right), \tag{4.6}$$

$$\begin{cases} dX_t^y = \left(-\frac{1}{2} \frac{X_t^y}{1 - \frac{(X_t^y)^2 + (Y_t^y)^2}{b}} + \partial_y u\, Y_t^y \right) dt + dV_t, \\[4mm] dY_t^y = \left(-\frac{1}{2} \frac{Y_t^y}{1 - \frac{(X_t^y)^2 + (Y_t^y)^2}{b}} \right) dt + dW_t. \end{cases} \tag{4.7}$$

where the non-dimensional parameter $b > 0$ measures the finite extensibility of the polymer and is in practice of the order of 100 (see [120] page 217). The space variable y varies in $\mathcal{O} = (0,1)$ and $t \in [0, T]$. The random variables are defined on a filtered probability space $(\Omega, \mathcal{F}, \mathcal{F}_t, \mathbb{P})$. The random process (V_t, W_t) is a $(\mathcal{F}_t)$-two-dimensional Brownian motion. For simplicity, the boundary conditions are taken homogenous : $u(t, y = 0) = u(t, y = 1) = 0$. The initial velocity is $u(t = 0, .) = u_0$, and (X_0, Y_0) is a $\mathcal{F}_0$-measurable random variable.

It is worth emphasizing the differences with respect to the Hookean dumbbell model (4.3) (which can formally be recovered from (4.5)–(4.7) by letting b go to infinity) :

 – No explicit expression of the stress in function of the velocity is known to date (the FENE model is not closed),
 – Both components X_t^y and Y_t^y of the connecting vector modelling the polymer chain depend on the space variable,
 – The drift term in (4.7) is nonlinear and singular.

Such differences make the mathematical analysis more delicate than that for the Hookean dumbbell model. The purpose of the present article is to conduct such an analysis. We hope to be able to treat the numerical analysis of such a system in the future.

To the best of our knowledge, system (4.5)–(4.7) has never been analyzed mathematically. The only result concerning a problem close to (4.5)–(4.7) is due to M. Renardy in [131] where system (4.1) is analyzed and proved to admit a local-in-time

solution in spaces of regular functions. The result applies to the case of a flow of polymeric inviscid fluid ($\eta = 0$) in $\mathbb{R}^3$ with spring forces slightly more explosive than the FENE force.

The article is organized as follows. In Section 4.2, we deal with the stochastic differential equation (4.7) (see also [84] for a more complete analysis of this stochastic differential equation). We first show the existence of a solution when $u = 0$ and then, using the Girsanov Theorem, we build a weak solution to (4.7) when the velocity u is arbitrarly given. Using Yamada-Watanabe Theorem, we next show that (4.7) admits a unique strong solution. The main difficulty in proving the existence of a solution to the stochastic differential equation comes from the singular nature of the drift. We shall however see that we can take benefit of this singular nature to obtain an *a priori* bound on the stochastic processes (which does not exist in the Hookean case and must therefore be circumvented by *ad hoc* cut-off techniques, see [85]). We next consider the coupled system (4.5)–(4.7) and show some *a priori* estimates in Section 4.3. We use these estimates in Section 4.4 to prove our main result (stated in Theorem 7), namely a local-in-time existence and uniqueness result of the solution (u, X_t^y, Y_t^y) to the coupled system (4.5)–(4.7), being understood that (X_t^y, Y_t^y) is a strong solution (in the sense of probability theory) of (4.7) and u is a regular solution giving to (4.5) an almost everywhere sense (which requires a good regularity of the data : initial condition, boundary conditions, f_{ext}). We unfortunately are unable to extend this existence result to any arbitrary large time, nor to extend it to a less regular class of data. The numerical analysis of some discretization schemes used for the simulation of stochastic differential equations of type (4.7) is currently under study.

4.2 Existence of a solution to the stochastic differential equation

In this section, we consider the stochastic differential equation (4.7) with a given velocity u. More precisely, we fix y in $\mathcal{O}$, we set $g(t) = \partial_y u(y, t)$ for conciseness, and we suppose throughout this section that

$$g \in L_t^2. \tag{4.8}$$

We are interested in solving for $t \geq 0$ the following stochastic differential equation :

$$
\begin{cases}
dX_t^g = \left(-\frac{1}{2} \dfrac{X_t^g}{1 - \frac{(X_t^g)^2 + (Y_t^g)^2}{b}} + g(t)\, Y_t^g \right) dt + dV_t, \\[3ex]
dY_t^g = \left(-\frac{1}{2} \dfrac{Y_t^g}{1 - \frac{(X_t^g)^2 + (Y_t^g)^2}{b}} \right) dt + dW_t,
\end{cases}
\tag{4.9}
$$

with initial condition (X_0, Y_0). Throughout this paper we will suppose that (X_0, Y_0) is such that $\mathbb{P}\left(X_0^2 + Y_0^2 \geq b \right) = 0$. In this section, we consider that t varies in the whole of $\mathbb{R}_+$.

4.2.1 Notion of solution

Let us begin by giving a precise mathematical meaning to (4.9).

Definition 1 *We consider a filtered probability space $(\Omega, \mathcal{F}, \mathcal{F}_t, \mathbb{P})$, a $(\mathcal{F}_t)$-two-dimensional Brownian motion (V_t, W_t) and a $\mathcal{F}_0$-measurable random variable (X_0, Y_0). We shall say that a $(\mathcal{F}_t)$-adapted process (X_t^g, Y_t^g) is a solution to (4.9) when : for $\mathbb{P}$-a.e. ω, $\forall t \geq 0$,*

$$
\begin{cases}
\displaystyle \int_0^t \left| \frac{1}{1 - \frac{(X_s^g)^2 + (Y_s^g)^2}{b}} \right| ds < \infty \text{ with the convention } \frac{1}{1 - \frac{x^2 + y^2}{b}} = +\infty \text{ if } x^2 + y^2 = b, \\[4mm]
\displaystyle X_t^g = X_0 + \int_0^t \left(-\frac{1}{2} \frac{X_s^g}{1 - \frac{(X_s^g)^2 + (Y_s^g)^2}{b}} + g(s) Y_s^g \right) ds + V_t, \\[4mm]
\displaystyle Y_t^g = Y_0 + \int_0^t -\frac{1}{2} \frac{Y_s^g}{1 - \frac{(X_s^g)^2 + (Y_s^g)^2}{b}} ds + W_t.
\end{cases}
$$

$$(4.10)$$

Our purpose in this section is to show :

Proposition 2 *Assume that $b \geq 2$ and (4.8). There exists a unique $(\mathcal{F}_t)$-adapted process (X_t^g, Y_t^g) with values in $\mathcal{C}([0, \infty[, \mathbb{R}^2)$ solution to (4.9) in the sense of Definition 1. In addition, this solution is such that $\mathbb{P}(\exists t \geq 0, (X_t^g)^2 + (Y_t^g)^2 = b) = 0$ and (X_t^g, Y_t^g) is $\sigma(X_0, Y_0, (V_s, W_s)_{s \leq t})$-adapted. Moreover, assuming $b > 4$ and $\left(\dfrac{1}{1 - \frac{X_0^2 + Y_0^2}{b}} \right)^p$ is integrable for some $p > 1$, we have the following expression of the stress (4.6) in function of the solution (X_t^g, Y_t^g) for $g = 0$ **henceforth denoted by** (X_t, Y_t) :*

$$
\mathbb{E} \left(\frac{X_t^g Y_t^g}{1 - \frac{(X_t^g)^2 + (Y_t^g)^2}{b}} \right) = \mathbb{E} \left(\left(\frac{X_t Y_t}{1 - \frac{X_t^2 + Y_t^2}{b}} \right) \mathcal{E} \left(\int_0^\bullet g(s) Y_s \, dV_s \right)_t \right), \qquad (4.11)
$$

where $\mathcal{E} \left(\displaystyle \int_0^\bullet g(s) Y_s \, dV_s \right)_t$ is the exponential martingale :

$$
\mathcal{E} \left(\int_0^\bullet g(s) Y_s \, dV_s \right)_t = \exp \left(\int_0^t g(s) Y_s \, dV_s - \frac{1}{2} \int_0^t (g(s) Y_s)^2 \, ds \right).
$$

We begin by proving the uniqueness, next show the existence when $g = 0$ and in a third step show the existence for a general g satisfying (4.8).

4.2.2   Uniqueness

Lemma 13 *Let (X^g, Y^g) and $(\tilde{X}^g, \tilde{Y}^g)$ be two solutions of (4.9) in the sense of Definition 1. Provided (X^g, Y^g) is such that $\mathbb{P}\left(\exists t \geq 0, (X_t^g, Y_t^g) \geq b \right) = 0$, then,*

$$
\mathbb{P} \left(\forall t \geq 0, (X_t^g, Y_t^g) = (\tilde{X}_t^g, \tilde{Y}_t^g) \right) = 1.
$$

Proof.
Let us consider the stopping time

$$\tau_n = \inf \left\{ t, \max \left((X_t^g)^2 + (Y_t^g)^2, (\tilde{X}_t^g)^2 + (\tilde{Y}_t^g)^2 \right) \geq b \left(1 - \frac{1}{n} \right) \right\}.$$

Let set $F_x(x,y) = -\frac{1}{2} \frac{x}{1 - \frac{x^2+y^2}{b}}$ and $F_y(x,y) = -\frac{1}{2} \frac{y}{1 - \frac{x^2+y^2}{b}}$. These functions are Lipschitz continuous with constant K_n on the ball $B_n = \left\{ (x,y), x^2 + y^2 \leq b \left(1 - \frac{1}{n} \right) \right\}$. Let us now consider $P_t = X_t^g - \tilde{X}_t^g$ and $Q_t = Y_t^g - \tilde{Y}_t^g$. We have

$$\begin{aligned}
P_t &= \int_0^t F_x(X_s^g, Y_s^g) - F_x(\tilde{X}_s^g, \tilde{Y}_s^g) \, ds + \int_0^t g(s) Q_s \, ds, \\
Q_t &= \int_0^t F_y(X_s^g, Y_s^g) - F_y(\tilde{X}_s^g, \tilde{Y}_s^g) \, ds.
\end{aligned}$$

We can therefore write, for any $t \in (0, \tau_n)$:

$$|P_t| + |Q_t| \leq \int_0^t (2 \, K_n + |g(s)|) \, (|P_s| + |Q_s|) \, ds.$$

Using Gronwall Lemma and the fact that $g \in L_t^1$, we deduce that, almost surely, for any $t \in (0, \tau_n)$, $P_t = 0$ and $Q_t = 0$. Hence (X_t^g, Y_t^g) and $(\tilde{X}_t^g, \tilde{Y}_t^g)$ coincide on $(0, \lim_{n \to \infty} \tau_n)$. As a consequence, $\tau_n = \inf \left\{ t, (X_t^g)^2 + (Y_t^g)^2 \geq b \left(1 - \frac{1}{n} \right) \right\}$ and by the assumption made on (X_t^g, Y_t^g), $\lim_{n \to \infty} \tau_n = +\infty$. $\qquad \square$

Remark 10 *The proof makes a crucial use of the fact that (4.9) only differs from a system of ordinary differential equations by the simple addition of a Brownian motion.*

4.2.3 Existence when $g = 0$

The crucial lemma which will be used in the sequel states the existence of a (strong) solution to (4.9) when $g = 0$. We recall that this solution will be denoted in the following by (X_t, Y_t).

Lemma 14 *Assume that $b \geq 2$ and $g = 0$, then there exists a unique solution (X_t, Y_t) to (4.9) in the sense of Definition 1. This solution is such that $\mathbb{P} \left(\exists t \geq 0, (X_t)^2 + (Y_t)^2 = b \right) = 0$. In addition, for any $p \geq 1$, if b is such that $b > 2(p + 1)$ and if the random variable $\left(\dfrac{1}{1 - \frac{X_0^2 + Y_0^2}{b}} \right)^p$ is integrable, then*

$$t \longmapsto \mathbb{E} \left(\frac{1}{1 - \frac{X_t^2 + Y_t^2}{b}} \right)^p \text{ is locally bounded.}$$

Proof. We consider the following approximation of the stochastic differential equation (4.9), with $g = 0$:

$$\begin{cases} dX_t^n = \left(-\frac{1}{2} \dfrac{X_t^n}{\max\left(1 - \frac{(X_t^n)^2 + (Y_t^n)^2}{b}, \frac{1}{n} \right)} \right) dt + dV_t, \\[3mm] dY_t^n = \left(-\frac{1}{2} \dfrac{Y_t^n}{\max\left(1 - \frac{(X_t^n)^2 + (Y_t^n)^2}{b}, \frac{1}{n} \right)} \right) dt + dW_t, \end{cases} \tag{4.12}$$

and the stopping time :

$$\tau_n = \inf \left\{ t, (X_t^n)^2 + (Y_t^n)^2 \geq b \left(1 - \frac{1}{n} \right) \right\}.$$

Using the fact that (4.12) has a unique strong solution (X_t^n, Y_t^n) on $[0, \tau_n)$ and setting $(X_t, Y_t) = (X_t^n, Y_t^n)$ on $[\tau_{n-1}, \tau_n)$, one obtains by continuation of the piecewise solutions a strong solution to (4.9) with $g = 0$ on $[0, \lim_{n \to \infty} \tau_n)$. Using Itô's formula, one finds that $R_t = (X_t)^2 + (Y_t)^2$ satisfies the following stochastic differential equation on $[0, \lim_{n \to \infty} \tau_n)$:

$$dR_t = \left(-\frac{R_t}{1 - \frac{R_t}{b}} + 2 \right) dt + 2 \left(X_t \, dV_t + Y_t dW_t \right).$$

Using Girsanov Theorem on (X_t^n, Y_t^n), one may next check that $\mathbb{P}(\exists t \in [0, \tau_n), (X_t^n)^2 + (Y_t^n)^2 = 0) = 0$ and therefore $\mathbb{P}(\exists t \in [0, \lim_{n \to \infty} \tau_n), R_t = 0) = 0$. The former equation may thus be written in the following form :

$$dR_t = \left(-\frac{R_t}{1 - \frac{R_t}{b}} + 2 \right) dt + 2\sqrt{R_t} dB_t, \tag{4.13}$$

where B_t is a Brownian motion by Paul Lévy characterization. Let us now consider a scale function $s : (0, b) \longrightarrow \mathbb{R}$ such that :

$$\left(-\frac{x}{1 - \frac{x}{b}} + 2 \right) s'(x) + 2 \, x \, s''(x) = 0$$

which leads to

$$s'(x) = C(b - x)^{-b/2} x^{-1}.$$

We choose a primitive function s defined on $(0, b)$. This function s is increasing and is such that $\lim_{x \to b} s(x) = +\infty$, provided $b \geq 2$. Using Itô's formula, on $[0, \lim_{n \to \infty} \tau_n)$, we have

$$s(R_t) = s(R_0) + 2 \int_0^t s'(R_s) \sqrt{R_s} dB_s. \tag{4.14}$$

Let us suppose first that $s(R_0)$ is integrable, so that $s(R_t)$ is a local martingale. Let k be a non-negative integer. We now introduce the stopping time

$$\sigma_k = \inf \left\{ t < \lim_{n \to \infty} \tau_n, R_t \leq \frac{1}{k} \right\}, \text{ with the convention } \inf\{\emptyset\} = +\infty.$$

The random process $s(R_{t \wedge \tau_n \wedge \sigma_k})$ is a martingale. Thus we have for any t and for any n,

$$\mathbb{E}(s(R_{t \wedge \tau_n \wedge \sigma_k})) = \mathbb{E}(s(R_0))$$

which leads (using the fact that s is increasing) to

$$s\left(b\left(1 - \frac{1}{n}\right)\right) \mathbb{P}(\tau_n \leq t \wedge \sigma_k) + s\left(\frac{1}{k}\right)(1 - \mathbb{P}(\tau_n \leq t \wedge \sigma_k)) \leq \mathbb{E}(s(R_0)).$$

Taking first the limit $n \to \infty$, we obtain $\mathbb{P}(\lim_{n \to \infty} \tau_n \leq t \wedge \sigma_k) = 0$. Taking then the limit $k \to \infty$, we obtain $\mathbb{P}(\lim_{n \to \infty} \tau_n \leq t \wedge \lim_{k \to \infty} \sigma_k) = 0$. We know that $\mathbb{P}(\exists t \in [0, \lim_{n \to \infty} \tau_n), R_t = 0) = 0$, which implies $\mathbb{P}(\lim_{n \to \infty} \tau_n > \lim_{k \to \infty} \sigma_k) = 0$ and finally

$$\mathbb{P}\left(\lim_{n \to \infty} \tau_n \leq t\right) \leq \mathbb{P}\left(\lim_{n \to \infty} \tau_n \leq t \wedge \lim_{k \to \infty} \sigma_k\right) + \mathbb{P}\left(\lim_{n \to \infty} \tau_n > \lim_{k \to \infty} \sigma_k\right) = 0.$$

We have shown that $\mathbb{P}(\lim_{n \to \infty} \tau_n = \infty) = 1$, and we have therefore built a strong solution (X, Y) to (4.9) with $g = 0$ on $\mathbb{R}_+$. If $s(R_0)$ is not integrable, one has to use the same arguments as before on $\{\epsilon < X_0^2 + Y_0^2 < b - \epsilon\}$ where $\epsilon > 0$ (by multiplying (4.14) by $1_{\epsilon < X_0^2 + Y_0^2 < b - \epsilon}$) and conclude by letting ϵ go to 0.

If one considers another solution $(\tilde{X}, \tilde{Y})$ of (4.9) with $g = 0$ in the sense of Definition 1, using Lemma 13, this solution is such that $\mathbb{P}\left(\forall t \geq 0, (X_t, Y_t) = (\tilde{X}_t, \tilde{Y}_t)\right) = 1$. This shows that (4.9) admits a unique strong solution.

Let us now turn to the integrability of $\left(\dfrac{1}{1 - \frac{X_t^2 + Y_t^2}{b}}\right)^p$ and let us consider first the case $p = 1$, assuming $\mathbb{E}\left(\dfrac{1}{1 - \frac{R_0}{b}}\right) < \infty$. Using Itô's formula, it is easy to derive :

$$\mathbb{E}\left(\frac{1}{1 - \frac{R_{t \wedge \tau_n}}{b}}\right) = \mathbb{E}\left(\frac{1}{1 - \frac{R_0}{b}}\right) + \mathbb{E}\left(\int_0^{t \wedge \tau_n} \frac{2/b}{\left(1 - \frac{R_s}{b}\right)^2} + \frac{(4 - b)R_s/b^2}{\left(1 - \frac{R_s}{b}\right)^3} \, ds\right).$$

Assuming $b > 4$, it is clear that $M = \sup_{x \in (0,b)} \left(\dfrac{2/b}{\left(1 - \frac{x}{b}\right)^2} + \dfrac{(4-b)x/b^2}{\left(1 - \frac{x}{b}\right)^3}\right) < \infty$ and one can then obtain

$$\mathbb{E}\left(\frac{1}{1 - \frac{R_{t \wedge \tau_n}}{b}}\right) \leq \mathbb{E}\left(\frac{1}{1 - \frac{R_0}{b}}\right) + M \, \mathbb{E}(t \wedge \tau_n).$$

This yields, for any $t > 0$,

$$\mathbb{E}\left(\frac{1}{1 - \frac{R_t}{b}}\right) \leq \mathbb{E}\left(\frac{1}{1 - \frac{R_0}{b}}\right) + M \, t.$$

For an exponent $p > 1$, the same arguments show that $\left(\dfrac{1}{1 - \frac{X_t^2 + Y_t^2}{b}} \right)^p$ is integrable,

provided $b > 2(p+1)$ and that $\left(\dfrac{1}{1 - \frac{X_0^2 + Y_0^2}{b}} \right)^p$ is integrable. $\qquad\square$

Remark 11 (On the assumption $b > 2(p+1)$.) *We assume that $b \geq 2$ as in Lemma 14. Let*

$$\Pi(x,y) = \begin{cases} -\frac{b}{2} \ln\left(1 - \frac{x^2 + y^2}{b} \right) & \text{if } x^2 + y^2 < b, \\ +\infty & \text{otherwise,} \end{cases} \tag{4.15}$$

denote a potential of the FENE force. Setting $\boldsymbol{X}_t = (X_t, Y_t)$ and $\boldsymbol{W}_t = (V_t, W_t)$, we see that the stochastic differential equation (4.9) with $g = 0$ has the following form :

$$d\boldsymbol{X}_t = -\frac{1}{2} \nabla \Pi(\boldsymbol{X}_t)\, dt + d\boldsymbol{W}_t. \tag{4.16}$$

Hence, one expects the probability measure with density

$$p_0(x,y) = \frac{\exp(-\Pi(x,y))}{\int_{\mathbb{R}^2} \exp(-\Pi(x,y))\, dx\, dy} = \frac{b+2}{2\pi b} \left(1 - \frac{x^2 + y^2}{b} \right)^{b/2} \mathbb{1}_{x^2 + y^2 < b} \tag{4.17}$$

to be invariant. One can indeed prove this property by comparing (4.16) with stochastic differential equations where the potential Π is carefully regularized and for which the symmetry properties of the transition densities given by Rogers in [135] (see remark (ii) and line 2 p.161) hold. The choice of this invariant probability measure as the law for the initial random variable (X_0, Y_0) is natural from a physical point of view, since we consider here the start up of a shear flow : the fluid is therefore initially at rest (see also [15]). Notice that for this initial distribution, we have $\tau|_{t=0} = \mathbb{E}\left(\dfrac{X_0 Y_0}{1 - \frac{X_0^2 + Y_0^2}{b}} \right) = 0$. In addition, for this initial distribution, for any $t \geq 0$, (X_t, Y_t) has the density p_0 and therefore $\left(\dfrac{1}{1 - \frac{X_t^2 + Y_t^2}{b}} \right)^p$ is integrable as soon as $b > 2(p-1)$ (and not only under the stronger assumption $b > 2(p+1)$ made in Lemma 14). See [84] for more details.

Remark 12 (On the optimality of the assumption $b \geq 2$.) *The assumption $b \geq 2$ turns out to be a necessary condition to prevent (X_t, Y_t) from touching the boundary of the ball $B = B(0, \sqrt{b}) = \{(x,y), x^2 + y^2 < b\}$ and therefore to have pathwise uniqueness of the solution to the stochastic differential equation (4.9) when $g = 0$ in the sense of Definition 1. The function $\frac{1}{2}\Pi : \mathbb{R}^2 \to]-\infty, +\infty]$, where Π is defined by (4.15), is a continuous convex function with domain B. Its subdifferential*

$\partial\left(\frac{1}{2}\Pi\right)$ *is a maximal monotone operator on* $\mathbb{R}^2$. *According to [26],* **for any** $b > 0$, *the multivalued stochastic differential equation*

$$d\boldsymbol{X}_t + \partial\left(\frac{1}{2}\Pi\right)(\boldsymbol{X}_t)\,dt \ni d\boldsymbol{W}_t$$

where $\boldsymbol{W}_t = (V_t, W_t)$ *and with* $\boldsymbol{X}_0 = (X_0, Y_0)$ *has a unique strong solution. This solution belongs to* $\mathcal{C}(\mathbb{R}_+, \overline{B})$ *and following the approach of [27] (see Lemmas 3.3, 3.4, 3.6 and 3.8), one can check that* $\boldsymbol{X}_t = (X_t, Y_t)$ *is a solution of the stochastic differential equation (4.9) when* $g = 0$ *in the sense of Definition 1. In case* $b \geq 2$, *this solution is equal to the one given in Lemma 14 and* $\mathbb{P}\left(\exists t \geq 0, X_t^2 + Y_t^2 = b\right) = 0$. *In case* $0 < b < 2$, *applying Feller's test for explosions (see [87] pages 348-350) to the semi-martingale* $R_t = ||\boldsymbol{X}_t||^2$ *which satisfies (4.13), we check that* $\mathbb{P}\left(\exists t \geq 0, X_t^2 + Y_t^2 = b\right) = 1$. *In this case, using again results concerning multivalued stochastic differential equations, one can build a solution to (4.10) outside of the ball B, with initial condition on the boundary and with* $g = 0$ *: this can be used to show that uniqueness in law and therefore pathwise uniqueness do not hold for (4.10). All these results are detailed in [84].*

4.2.4 Existence in the general case

We now turn to the proof of Proposition 2 in the general case $g \neq 0$.

Lemma 14 provides us with a weak solution to the stochastic differential equation (4.9) when $g \in L_t^2$ by the Girsanov Theorem. Indeed, let us consider the solution (X_t, Y_t) defined in Lemma 14 in the probability space $(\Omega, \mathcal{F}, \mathcal{F}_t, \mathbb{P})$. Under the probability $\mathbb{P}^g$ defined by

$$\left.\frac{d\mathbb{P}^g}{d\mathbb{P}}\right|_{\mathcal{F}_t} = \mathcal{E}\left(\int_0^\bullet g(s)Y_s\,dV_s\right)_t,$$

the process $(V_t^g, W_t^g) = (V_t - \int_0^t g(s)Y_s\,ds, W_t)$ is a Brownian motion and therefore $(X_t, Y_t, V_t^g, W_t^g, \mathbb{P}^g)$ is a weak solution of the stochastic differential equation (4.9).

By construction, this weak solution has its paths in $\mathcal{C}([0,T], B)$, where $B = B(0, \sqrt{b}) = \{(x,y), x^2 + y^2 < b\}$. On the other hand, we know that trajectorial uniqueness holds for such solutions in the ball (by Lemma 13). Therefore, by Yamada-Watanabe Theorem, we have the existence of a strong solution (X_t^g, Y_t^g) to (4.9) with its paths in $\mathcal{C}([0,T], B)$. Yamada-Watanabe Theorem also gives us uniqueness in law for the solution to (4.9).

Suppose we are now given another solution of (4.9) in the sense of Definition 1. By comparing this solution to the above strong solution (X_t^g, Y_t^g) and applying again Lemma 13, we obtain that this solution is equal to the one we have built. This also shows that any solution $(\tilde{X}^g, \tilde{Y}^g)$ of (4.9) in the sense of Definition 1 is such that $\mathbb{P}\left(\exists t \geq 0, (\tilde{X}_t^g)^2 + (\tilde{Y}_t^g)^2 = b\right) = 0$.

Let us now suppose that $b > 4$ and $\left(\dfrac{1}{1 - \frac{X_0^2 + Y_0^2}{b}}\right)^p$ is integrable for some $p > 1$.

We want to show the equality (4.11). We need the following Lemma :

Lemma 15 *If $g \in L_t^2$, then we have, for any $1 \le r < \infty$, if $b > 2(r+1)$, and provided that $\left(\dfrac{1}{1 - \frac{X_0^2 + Y_0^2}{b}}\right)^p$ is integrable for some $p > r$, for all t, $\left|\dfrac{X_t^g Y_t^g}{1 - \frac{(X_t^g)^2 + (Y_t^g)^2}{b}}\right|^r$ is integrable and, for any $\frac{b-2}{b-2(1+r)} \vee \frac{p}{p-r} < q < \infty$:*

$$\mathbb{E}\left(\left|\frac{X_t^g Y_t^g}{1 - \frac{(X_t^g)^2 + (Y_t^g)^2}{b}}\right|^r\right)^{1/r} \le C_{q,r} \exp\left(\frac{q-1}{2r} b \int_0^t |g(s)|^2 \, ds\right),$$

where $C_{q,r}$ denotes a constant depending only on q, r, b and $\mathbb{E}\left(\left(\dfrac{1}{1 - \frac{X_0^2 + Y_0^2}{b}}\right)^{\frac{rq}{q-1}}\right)$.

Proof. Using Hölder inequality and the properties of the exponential martingale, we have :

$$\mathbb{E}\left|\frac{X_t^g Y_t^g}{1 - \frac{(X_t^g)^2 + (Y_t^g)^2}{b}}\right|^r = \mathbb{E}\left(\left|\frac{X_t Y_t}{1 - \frac{X_t^2 + Y_t^2}{b}}\right|^r \mathcal{E}\left(\int_0^\bullet g(s) Y_s \, dV_s\right)_t\right)$$

$$\le \mathbb{E}\left(\left|\frac{X_t Y_t}{1 - \frac{X_t^2 + Y_t^2}{b}}\right|^{q'r}\right)^{1/q'} \mathbb{E}\left(\mathcal{E}\left(\int_0^\bullet g(s) Y_s \, dV_s\right)_t^q\right)^{1/q}$$

$$\le (C_{q,r})^r \mathbb{E}\left(\mathcal{E}\left(q \int_0^\bullet g(s) Y_s \, dV_s\right)_t \exp\left(\frac{q^2 - q}{2} \int_0^t (g(s) Y_s)^2 \, ds\right)\right)^{1/q}$$

$$\le (C_{q,r})^r \exp\left(\frac{q-1}{2} b \int_0^t |g(s)|^2 \, ds\right) \mathbb{E}\left(\mathcal{E}\left(q \int_0^\bullet g(s) Y_s \, dV_s\right)_t\right)^{1/q}$$

$$\le (C_{q,r})^r \exp\left(\frac{q-1}{2} b \int_0^t |g(s)|^2 \, ds\right)$$

with $q' = \frac{q}{q-1}$ and $C_{q,r} = \sup_{t \in [0,T]} \mathbb{E}\left(\left(\frac{X_t Y_t}{1 - \frac{X_t^2 + Y_t^2}{b}}\right)^{q'r}\right)^{1/(q'r)} < \infty$ by Lemma 14. $\square$

Using this Lemma with $r = 1$ (and a q such that $q > \frac{b-2}{b-4} \vee \frac{p}{p-1}$), one can show that $\dfrac{X_t^g Y_t^g}{1 - \frac{(X_t^g)^2 + (Y_t^g)^2}{b}}$ is integrable and therefore that the equality (4.11) holds. This concludes the proof of Proposition 2.

4.3 Notion of solution and *a priori* estimates on the coupled system

We now consider the coupled system of equations (4.5)–(4.7). From now on, we suppose that t varies in a bounded interval $[0, T]$. The space variable y varies in $\mathcal{O} = (0, 1)$. The notation $L_t^2(L_y^2)$ is a shortcut for $L^2([0, T], L^2(\mathcal{O}))$, for example.

4.3.1 Notion of solution

The notion of solution we shall deal with in the sequel is the following.

Definition 2 *Let us be given $u_0 \in H_y^1$, $f_{ext} \in L_t^2(L_y^2)$, together with a probabilized space $(\Omega, \mathcal{F}, \mathcal{F}_t, \mathbb{P})$, (X_0, Y_0) a $\mathcal{F}_0$-measurable random variable and (V_t, W_t) a $(\mathcal{F}_t)$ two-dimensional Brownian motion. We shall say that $(u(t,y), X_t^y, Y_t^y)$ is a solution on the time interval $[0, \Theta)$ if $u \in L^\infty([0, \Theta], H_{0,y}^1) \cap L^2([0, \Theta], H_y^2)$ satisfies :*

$$\partial_t u(t,y) - \partial_{yy} u(t,y) = \partial_y \mathbb{E}\left(\frac{X_t^y Y_t^y}{1 - \frac{(X_t^y)^2 + (Y_t^y)^2}{b}} \right) + f_{ext}(t,y),$$

in the sense of $\mathcal{D}'([0, \Theta) \times \mathcal{O})$ (at least), and for a.e. (y, ω), $\forall t \in (0, \Theta)$,

$$\int_0^t \left| \frac{1}{1 - \frac{(X_s^y)^2 + (Y_s^y)^2}{b}} \right| ds < \infty, \text{ with the convention } \frac{1}{1 - \frac{x^2 + y^2}{b}} = +\infty \text{ if } x^2 + y^2 = b,$$

$$X_t^y = X_0 + \int_0^t \left(-\frac{1}{2} \frac{X_s^y}{1 - \frac{(X_s^y)^2 + (Y_s^y)^2}{b}} + \partial_y u\, Y_s^y \right) ds + V_t,$$

$$Y_t^y = Y_0 + \int_0^t -\frac{1}{2} \frac{Y_s^y}{1 - \frac{(X_s^y)^2 + (Y_s^y)^2}{b}} ds + W_t.$$

Remark 13 *One can notice that we require the solution u to the partial differential equation (4.5) is strong. This is due to the fact that our technique of proof requires an estimate on $\partial_y u$ in norm H_y^1 in order to control the stress τ (see Section 4.3.2.2).*

Remark 14 *Since for a.e. $y \in \mathcal{O}$, $\partial_y u(., y)$ is in $L^2([0, \Theta])$, we see that $(X_t^y, Y_t^y) = (X_t^{\partial_y u}, Y_t^{\partial_y u})$, where $(X_t^{\partial_y u}, Y_t^{\partial_y u})$ denotes the solution to (4.10) with $g = \partial_y u(., y)$ (see Proposition 2).*

4.3.2 *A priori* estimates

In this section, we give some **formal** *a priori* estimates which will be used in the sequel to prove the existence of a solution to the coupled problem.

4.3.2.1 First energy estimate

The first *a priori* estimate expresses the conservation of the energy stored in the flow and in the dumbbells.

Lemma 16 (Global-in-time first energy estimate) *Let $(u(t,y), X_t^y, Y_t^y)$ be a solution of (4.5)–(4.7) on $[0, T)$ in the sense of Definition 2. Assume moreover $b > 6$*

and $\left(\dfrac{1}{1 - \frac{X_0^2 + Y_0^2}{b}} \right)^p$ *integrable for some $p > 2$. Then we have the following formal estimate :*

$$\frac{1}{2}\frac{d}{dt}\int_{\mathcal{O}} u^2 + \frac{d}{dt}\int_{\mathcal{O}} \mathbb{E}(\Pi(X_t^y, Y_t^y)) + \int_{\mathcal{O}} (\partial_y u)^2$$

$$+\frac{1}{2}\int_{\mathcal{O}} \mathbb{E}\left(\frac{(X_t^y)^2 + (Y_t^y)^2}{\left(1 - \frac{(X_t^y)^2 + (Y_t^y)^2}{b}\right)^2} \right) - \int_{\mathcal{O}} \mathbb{E}\left(\frac{1}{\left(1 - \frac{(X_t^y)^2 + (Y_t^y)^2}{b}\right)^2} \right) = \int_{\mathcal{O}} f_{ext} u \ (4.18)$$

where Π is the potential for the FENE force defined by (4.15). Under the additional assumptions $f_{ext} \in L_t^1(L_y^2)$ and $u_0 \in L_y^2$, this yields the following formal estimate on the solution :

$$||u||_{L_t^\infty(L_y^2)} + ||\partial_y u||_{L_t^2(L_y^2)} + ||\Pi(X^y, Y^y)||_{L_t^\infty(L_y^1(L_\omega^1))} + ||\Upsilon(X^y, Y^y)||_{L_t^2(L_y^2(L_\omega^2))} \leq C,$$
$$(4.19)$$

where $\Upsilon(x, y) = \dfrac{\sqrt{x^2 + y^2}}{1 - \frac{x^2 + y^2}{b}}$ and C is a constant depending on T, $||u_0||_{L_y^2}$, $||f_{ext}||_{L_t^1(L_y^2)}$ and $\mathbb{E}(\Pi(X_0, Y_0))$.

Proof. Multiplying the equation (4.5) by u and integrating over $\mathcal{O}$, one obtains :

$$\frac{1}{2}\int_{\mathcal{O}} u(t, y)^2 - \frac{1}{2}\int_{\mathcal{O}} u_0(y)^2 + \int_0^t \int_{\mathcal{O}} (\partial_y u)^2 = -\int_0^t \int_{\mathcal{O}} \tau \, \partial_y u + \int_0^t \int_{\mathcal{O}} f_{ext} u. \quad (4.20)$$

Notice that this is the only formal operation that will be later on justified once the problem discretized : the following of the proof is completely rigorous.

A simple calculus shows that $\nabla \Pi = \dfrac{1}{1 - \frac{x^2 + y^2}{b}}(x, y) 1_{x^2 + y^2 < b}$ and

$\Delta \Pi = \dfrac{2}{\left(1 - \frac{x^2 + y^2}{b}\right)^2} 1_{x^2 + y^2 < b}$. Therefore, using Itô's formula, we have :

$$d(\Pi(X_t^y, Y_t^y)) = -\frac{1}{2}\Upsilon(X_t^y, Y_t^y)^2 \, dt + \partial_y u \frac{X_t^y Y_t^y}{1 - \frac{(X_t^y)^2 + (Y_t^y)^2}{b}} \, dt + \frac{1}{\left(1 - \frac{(X_t^y)^2 + (Y_t^y)^2}{b}\right)^2} \, dt +$$

$$\frac{X_t^y}{1 - \frac{(X_t^y)^2 + (Y_t^y)^2}{b}} \, dV_t + \frac{Y_t^y}{1 - \frac{(X_t^y)^2 + (Y_t^y)^2}{b}} \, dW_t.$$

This calculus is justified by the fact that the random process (X_t^y, Y_t^y) does not touch the boundary of B (see Proposition 2). Integrating both in time and space and taking the expectation value, we therefore obtain :

$$\int_{\mathcal{O}} \mathbb{E}(\Pi(X_t^y, Y_t^y)) = \int_{\mathcal{O}} \mathbb{E}(\Pi(X_0, Y_0)) - \frac{1}{2}\int_0^t \int_{\mathcal{O}} \mathbb{E}(\Upsilon(X_s^y, Y_s^y)^2) \, ds +$$

$$\int_0^t \int_{\mathcal{O}} \partial_y u \, \tau + \int_0^t \int_{\mathcal{O}} \mathbb{E}\left(\frac{1}{\left(1 - \frac{(X_s^y)^2 + (Y_s^y)^2}{b}\right)^2} \right) \, ds. (4.21)$$

Notice that the expectations of the local martingales are null since we have assumed $b > 6$ and $\left(\dfrac{1}{1 - \frac{X_0^2 + Y_0^2}{b}} \right)^p$ integrable for some $p > 2$ so that, by Lemma 15, for a.e. $y \in \mathcal{O}$, $\mathbb{E} \left(\int_0^T \left(\dfrac{1}{1 - \frac{(X_s^y)^2 + (Y_s^y)^2}{b}} \right)^2 ds \right)$ has a finite value. By summing (4.20) and (4.21), one obtains the energy equality (4.18).

Estimate (4.19) is then obtained by using the energy equality. Indeed, the term $\Pi(X_t^y, Y_t^y)$ is positive and one can notice that the term $\displaystyle\int_{\mathcal{O}} \mathbb{E} \left(\dfrac{1}{\left(1 - \frac{(X_t^y)^2 + (Y_t^y)^2}{b} \right)^2} \right)$ can be bounded from above by the term $\dfrac{1}{2} \displaystyle\int_{\mathcal{O}} \mathbb{E} \left(\dfrac{(X_t^y)^2 + (Y_t^y)^2}{\left(1 - \frac{(X_t^y)^2 + (Y_t^y)^2}{b} \right)^2} \right)$ by writing :

$$
\begin{aligned}
&\frac{1}{2} \frac{(X_t^y)^2 + (Y_t^y)^2}{\left(1 - \frac{(X_t^y)^2 + (Y_t^y)^2}{b} \right)^2} - \frac{1}{\left(1 - \frac{(X_t^y)^2 + (Y_t^y)^2}{b} \right)^2} \\
&= \frac{1}{2} \frac{(X_t^y)^2 + (Y_t^y)^2}{\left(1 - \frac{(X_t^y)^2 + (Y_t^y)^2}{b} \right)^2} - \frac{\mathbf{1}_{(X_t^y)^2 + (Y_t^y)^2 > 2 + \epsilon}}{\left(1 - \frac{(X_t^y)^2 + (Y_t^y)^2}{b} \right)^2} - \frac{\mathbf{1}_{(X_t^y)^2 + (Y_t^y)^2 < 2 + \epsilon}}{\left(1 - \frac{(X_t^y)^2 + (Y_t^y)^2}{b} \right)^2} \\
&\geq \frac{\epsilon}{2(2 + \epsilon)} \frac{(X_t^y)^2 + (Y_t^y)^2}{\left(1 - \frac{(X_t^y)^2 + (Y_t^y)^2}{b} \right)^2} - \frac{b^2}{(b - (2 + \epsilon))^2}
\end{aligned}
$$

with ϵ such that $b - 2 > \epsilon$. $\qquad\qquad\square$

4.3.2.2 Second energy estimate

In order to show the second estimate, we have to use an expression of the stress τ which will give us regularity in the space variable y. In Proposition 2, we have shown that the stress τ has the following expression (assuming $b > 4$ and $\left(\dfrac{1}{1 - \frac{X_0^2 + Y_0^2}{b}} \right)^p$ is integrable for some $p > 1$, see (4.11)) :

$$
\begin{aligned}
\tau(t, y) &= \mathbb{E} \left(\frac{X_t^y Y_t^y}{1 - \frac{(X_t^y)^2 + (Y_t^y)^2}{b}} \right), \\
&= \mathbb{E} \left(\left(\frac{X_t Y_t}{1 - \frac{X_t^2 + Y_t^2}{b}} \right) \mathcal{E} \left(\int_0^{\bullet} \partial_y u(y) Y_s \, dV_s \right)_t \right). \qquad (4.22)
\end{aligned}
$$

Diffrenciating (4.22) with respect to y enables us to convert the regularity of u to the one of $\partial_y \tau$, which provides us with the following local-in-time estimate.

Lemma 17 (Local-in-time second energy estimate) *Under the assumptions $b > 6$, $f_{ext} \in L^2_t(L^2_y)$, $u_0 \in H^1_y$ and provided that $\left(\dfrac{1}{1 - \frac{X_0^2 + Y_0^2}{b}} \right)^p$ is integrable for some $p > 2$, we have the following formal estimate on $[0, T']$, with $T' \in (0, T)$ depending on $||\partial_y u_0||_{L^2_y}$, on $||f_{ext}||_{L^2_t(L^2_y)}$, on b, and on $\mathbb{E}\left(\left(\dfrac{1}{1 - \frac{X_0^2 + Y_0^2}{b}} \right)^p \right)$:*

$$||u||_{L^\infty([0,T'],H^1_y)} + ||u||_{L^2([0,T'],H^2_y)} \leq C.$$

This also yields the following formal estimate on $\partial_t u$, on $[0, T']$:

$$||\partial_t u||_{L^2([0,T'],L^2_y)} \leq C.$$

In both cases, C is a constant depending on $||\partial_y u_0||_{L^2_y}$, $||f_{ext}||_{L^2([0,T'],L^2_y)}$, on b and on
$\mathbb{E}\left(\left(\dfrac{1}{1 - \frac{X_0^2 + Y_0^2}{b}} \right)^p \right).$

Proof. Multiplying (4.5) by $-\partial_{yy}u$ and integrating over $\mathcal{O}$, one obtains :

$$\frac{1}{2} \int_{\mathcal{O}} (\partial_y u(t,y))^2 - \frac{1}{2} \int_{\mathcal{O}} (\partial_y u_0)^2 + \int_0^t \int_{\mathcal{O}} (\partial_{yy}u)^2 = -\int_0^t \int_{\mathcal{O}} \partial_y \tau \partial_{yy} u - \int_0^t \int_{\mathcal{O}} f_{ext} \partial_{yy} u.$$

This yields

$$\int_{\mathcal{O}} (\partial_y u(t,y))^2 + \int_0^t \int_{\mathcal{O}} (\partial_{yy}u)^2 \leq A + 2 \int_0^t \int_{\mathcal{O}} |\partial_y \tau| |\partial_{yy} u|,$$

with $A = ||\partial_y u_0||^2_{L^2_y} + \int_0^T \int_{\mathcal{O}} |f_{ext}|^2$. Notice that this is a formal operation that will be later on justified once the problem discretized.

Using (4.22), we can derive :

$$\partial_y \tau = \mathbb{E}\left(\left(\frac{X_t Y_t}{1 - \frac{X_t^2 + Y_t^2}{b}} \right) \left(\int_0^t \partial_{yy} u Y_s \, dV_s - \int_0^t (\partial_{yy} u)(\partial_y u) Y_s^2 \, ds \right) \mathcal{E}\left(\int_0^\bullet \partial_y u Y_s \, dV_s \right)_t \right).$$
$$\tag{4.23}$$

This can be shown in two steps, by first derivating with respect to y, for almost every ω, the random variable $\left(\dfrac{X_t Y_t}{1 - \frac{X_t^2 + Y_t^2}{b}} \right) \mathcal{E}\left(\int_0^\bullet \partial_y u(y) Y_s \, dV_s \right)_t$ and then by proving uniform integrability (in ω) on this derivative. To perform the first step, one can consider the random variable $\zeta_{t,h}$ defined by :

$$\zeta_{t,h} = \begin{cases} \dfrac{\int_0^t \partial_y u(y+h) Y_s \, dV_s - \int_0^t \partial_y u(y) Y_s \, dV_s}{h} & \text{if } h \neq 0 \\ \int_0^t \partial_{y,y} u(y) Y_s \, dV_s & \text{if } h = 0 \end{cases}$$

and prove that ζ is continuous by Kolmogorov Theorem (see Theorem 2.8 p. 53 of [87]). This is also done in a formal way, since it required regularity on u : this operation will be justified once the problem discretized. Notice that the following of the proof is now completely rigorous.

For the first term, one can obtain, by using the fact that Y_t is bounded (see Proposition 2) and Hölder inequality in ω, for any q such that $q > \frac{2(b-2)}{b-6} \vee \frac{2p}{p-2}$:

$$
\left| \mathbb{E} \left(\left(\frac{X_t Y_t}{1 - \frac{X_t^2 + Y_t^2}{b}} \right) \left(\int_0^t \partial_{yy} u Y_s \, dV_s \right) \mathcal{E} \left(\int_0^\bullet \partial_y u Y_s \, dV_s \right)_t \right) \right| \leq
$$

$$
C_q \left(\mathbb{E} \left(\int_0^t \partial_{yy} u Y_s \, dV_s \right)^2 \right)^{1/2} \exp \left(\frac{q-1}{2} b \int_0^t (\partial_y u)^2 \, ds \right) \leq
$$

$$
C_q \sqrt{b} \left(\int_0^t |\partial_{yy} u|^2 \, ds \right)^{1/2} \exp \left(\frac{q-1}{2} b \int_0^t (\partial_y u)^2 \, ds \right).
$$

For the second term, a similar argument shows :

$$
\left| \mathbb{E} \left(\left(\frac{X_t Y_t}{1 - \frac{X_t^2 + Y_t^2}{b}} \right) \left(\int_0^t (\partial_{yy} u)(\partial_y u) Y_s^2 \, ds \right) \mathcal{E} \left(\int_0^\bullet \partial_y u Y_s \, dV_s \right)_t \right) \right| \leq
$$

$$
C_q' b \left(\int_0^t |\partial_{yy} u||\partial_y u| \, ds \right) \exp \left(\frac{q-1}{2} b \int_0^t (\partial_y u)^2 \, ds \right).
$$

We thus have (using, since we are in dimension one, $\partial_y u(r, y) \leq ||\partial_y u(r, .)||_{H_y^1}$) :

$$
\int_0^t \int_{\mathcal{O}} |\partial_y \tau||\partial_{yy} u| \, ds
$$

$$
\leq \int_0^t \int_{\mathcal{O}} \exp \left(\frac{q-1}{2} b \int_0^s (\partial_y u)^2 \, dr \right)
$$

$$
* \left(C_q \sqrt{b} \left(\int_0^s |\partial_{yy} u|^2 \, dr \right)^{1/2} + C_q' b \left(\int_0^s |\partial_{yy} u||\partial_y u| \, dr \right) \right) |\partial_{yy} u|(s) \, ds
$$

$$
\leq C_q \sqrt{b} \int_0^t \exp \left(\frac{q-1}{2} b \int_0^s ||\partial_y u||_{H_y^1}^2 \, dr \right) \left(\int_{\mathcal{O}} \left(\int_0^s |\partial_{yy} u|^2(r) \, dr \right)^{1/2} |\partial_{yy} u|(s) \right) \, ds
$$

$$
+ C_q' b \int_0^t \exp \left(\frac{q-1}{2} b \int_0^s ||\partial_y u||_{H_y^1}^2 \, dr \right) \left(\int_0^s ||\partial_y u||_{H_y^1}(r) \int_{\mathcal{O}} |\partial_{yy} u|(r)|\partial_{yy} u|(s) \, dr \right) \, ds.
$$

So we obtain by the application of Cauchy Schwartz inequality (to the spatial inte-

gral) to both terms :

$$\int_0^t \int_{\mathcal{O}} |\partial_y \tau| |\partial_{yy} u| \, ds$$

$$\leq \quad C_q \sqrt{b} \int_0^t \exp\left(\frac{q-1}{2} b \int_0^s ||\partial_y u||^2_{H^1_y}(r) \, dr\right) \left(\int_0^s ||\partial_{yy} u||^2_{L^2_y}(r) \, dr\right)^{1/2} ||\partial_{yy} u||_{L^2_y}(s) \, ds$$

$$+C'_q \, b \int_0^t \exp\left(\frac{q-1}{2} b \int_0^s ||\partial_y u||^2_{H^1_y}(r) \, dr\right) \left(\int_0^s ||\partial_y u||_{H^1_y}(r) ||\partial_{yy} u||_{L^2_y}(r) \, dr\right) ||\partial_{yy} u||_{L^2_y}(s) \, ds$$

$$\leq \quad \frac{1}{4} \int_0^t ||\partial_{yy} u||^2_{L^2_y}(s) \, ds$$

$$+C(q,b) \int_0^t \exp\left((q-1)b \int_0^s ||\partial_y u||^2_{H^1_y}(r) \, dr\right) \left(\int_0^s ||\partial_{yy} u||^2_{L^2_y}(r) \, dr\right) ds$$

$$+C'(q,b) \int_0^t \exp\left((q-1)b \int_0^s ||\partial_y u||^2_{H^1_y}(r) \, dr\right) \left(\int_0^s ||\partial_y u||_{H^1_y}(r) ||\partial_{yy} u||_{L^2_y}(r) \, dr\right)^2 ds.$$

We thus have shown the following inequality :

$$||\partial_y u||^2_{L^2_y}(t) + \frac{1}{2} \int_0^t ||\partial_{yy} u||^2_{L^2_y}(s) \, ds \leq$$

$$A + 2C(q,b) \int_0^t \exp\left((q-1)b \int_0^s ||\partial_y u||^2_{H^1_y}(r) \, dr\right) \left(\int_0^s ||\partial_{yy} u||^2_{L^2_y}(r) \, dr\right) ds$$

$$+2C'(q,b) \int_0^t \exp\left((q-1)b \int_0^s ||\partial_y u||^2_{H^1_y}(r) \, dr\right) \left(\int_0^s ||\partial_y u||_{H^1_y}(r) ||\partial_{yy} u||_{L^2_y}(r) \, dr\right)^2 ds.$$

Let $f_1(t) = ||\partial_y u||^2_{L^2_y}(t)$ and $f_2(t) = \int_0^t ||\partial_{yy} u||^2_{L^2_y}(s) \, ds$. We have :

$$f_1(t) + \frac{1}{2} f_2(t) \leq A + 2C(q,b) \int_0^t \exp\left(\alpha \left(\int_0^s f_1(r) \, dr + f_2(s)\right)\right) f_2(s) \, ds$$

$$+2C'(q,b) \int_0^t \exp\left(\alpha \left(\int_0^s f_1(r) \, dr + f_2(s)\right)\right) \left(\int_0^s f_1(r) \, dr + f_2(s)\right) f_2(s) \, ds,$$

with $\alpha = (q-1)b$. Let $R(t)$ be the right hand side of the former equation. We can then write :

$$R'(t) = 2 \exp\left(\alpha \left(\int_0^t f_1(r) \, dr + f_2(t)\right)\right) \left(C(q,b) + C'(q,b) \left(\int_0^t f_1(r) \, dr + f_2(t)\right)\right) f_2(t)$$

$$\leq 4 \exp\left(\alpha \left(\int_0^t R(r) \, dr + 2R(t)\right)\right) \left(C(q,b) + C'(q,b) \left(\int_0^t R(r) \, dr + 2R(t)\right)\right) R(t).$$

By integrating in time, this leads to

$$R(t) \leq A + 4 \int_0^t \exp\left(\alpha \left(\int_0^s R(r) \, dr + 2R(s)\right)\right)$$

$$* \left(C(q,b) + C'(q,b) \left(\int_0^s R(r) \, dr + 2R(s)\right)\right) R(s) \, ds.$$

Since R is an increasing function, we have :

$$
\begin{aligned}
R(t) &\leq A + 4 \int_0^t \exp\left(\alpha\left(T+2\right)R(s)\right)\left(C(q,b) + C'(q,b)\left(T+2\right)R(s)\right)R(s)\,ds \\
&\leq A + \int_0^t \exp\left(\beta R(s)\right)\left(c + c'R(s)\right)R(s)\,ds,
\end{aligned}
$$

with $\beta = \alpha\left(T+2\right)$, $c = 4C(q,b)$ and $c' = 4\left(T+2\right)C'(q,b)$. From this one can deduce that there exists $\gamma > 0$ and $C > 0$, (both depending on q, b, $\mathbb{E}\left(\left(\frac{1}{1-\frac{X_0^2+Y_0^2}{b}}\right)^p\right)$ and T) such that :

$$
R(t) \leq A + C \int_0^t \exp(\gamma R(s))\,ds.
$$

Let $H(t)$ denote the right hand side. It is easy to derive from this inequality the following estimate : $\forall t \in \left(0, \frac{1}{\gamma C}\exp(-\gamma A)\right)$,

$$
R(t) \leq H(t) \leq \frac{1}{\gamma}\ln\left(\frac{1}{\exp(-\gamma A) - \gamma C t}\right).
$$

If we set $T' = \frac{1}{\gamma C}\left(\exp(-\gamma A) - \exp(-2\gamma A)\right)$, we have : for all $t \in (0, T')$,

$$
R(t) \leq H(t) \leq 2A.
$$

This leads to the following estimate : for all $t \in (0, T')$,

$$
||\partial_y u||_{L_y^2}^2(t) + \frac{1}{2}\int_0^t ||\partial_{yy}u||_{L_y^2}^2(s)\,ds \leq 2A. \tag{4.24}
$$

In order to obtain the estimate on $\partial_t u$, we observe that $\partial_t u = \partial_{yy}u + f_{ext} + \partial_y \tau$. We have already shown an estimation of $\partial_{yy}u$ in $L^2([0,T'], L_y^2)$ norm. Moreover, using the same argument as before, we can easily show that, for any function $v \in L^2([0,T'], L_y^2)$,

$$
\left|\int_0^t \int_{\mathcal{O}} \partial_y \tau \, v\right| \leq C||v||_{L^2([0,T'], L_y^2)},
$$

where C is a constant depending on q, b, A, $\mathbb{E}\left(\left(\frac{1}{1-\frac{X_0^2+Y_0^2}{b}}\right)^p\right)$ and T'. This yields the estimate on $\partial_t u$. $\qquad\square$

4.4 Existence of a solution to the coupled system

The aim of this section is to prove the following :

Theorem 7 (Local-in-time existence and uniqueness) *We assume that $b >$ 6, $f_{ext} \in L_t^2(L_y^2)$, $u_0 \in H_y^1$ and $\left(\dfrac{1}{1 - \frac{X_0^2 + Y_0^2}{b}} \right)^p$ is integrable for some $p > 2$. Then there exists $T' \in (0, T)$ (depending on the data) such that the system (4.5)–(4.7) admits a unique solution $(u(t, y), X_t^y, Y_t^y)$ on $[0, T']$ in the sense given in Definition 2.*

Remark 15 *If one chooses some initial random variables (X_0, Y_0) distributed with the invariant density p_0 defined by (4.17), then Theorem 7 holds under the weaker assumption $b > 2$ (see Remark 11 and Lemma 17). We recall that none of these assumptions on b is restrictive in practice since b is physically of the order of 100.*

In the following, we assume $b > 6$, $f_{ext} \in L_t^2(L_y^2)$, $u_0 \in H_y^1$ and $\left(\dfrac{1}{1 - \frac{X_0^2 + Y_0^2}{b}} \right)^p$ is integrable for some $p > 2$.

In order to show the existence of a solution to the coupled system, we introduce the following variational formulation of (4.5) :
Find $u \in L_t^\infty(H_{0,y}^1) \cap L_t^2(H_y^2)$ such that for all $v \in H_{0,y}^1$,

$$\frac{d}{dt} \int_{\mathcal{O}} u\, v \;=\; -\int_{\mathcal{O}} \partial_y u\, \partial_y v - \int_{\mathcal{O}} \tau\, \partial_y v + \int_{\mathcal{O}} f_{ext}\, v, \qquad (4.25)$$

together with

$$\tau \;=\; \mathbb{E}\left(\frac{X_t^y Y_t^y}{1 - \frac{(X_t^y)^2 + (Y_t^y)^2}{b}} \right), \qquad (4.26)$$

$$X_t^y \;=\; X_0 + \int_0^t \left(-\frac{1}{2} \frac{X_s^y}{1 - \frac{(X_s^y)^2 + (Y_s^y)^2}{b}} + \partial_y u\, Y_s^y \right) ds + V_t, \qquad (4.27)$$

$$Y_t^y \;=\; Y_0 + \int_0^t -\frac{1}{2} \frac{Y_s^y}{1 - \frac{(X_s^y)^2 + (Y_s^y)^2}{b}}\, ds + W_t. \qquad (4.28)$$

The ordinary differential equation (4.25) is to be understood in $\mathcal{D}'([0, T))$. The stochastic differential equations (4.27)–(4.28) are to be understood in the sense of Definition 1. This problem is well defined. Indeed, Proposition 2 gives a strong solution to (4.27)–(4.28). Moreover, the term $\int_{\mathcal{O}} \tau \partial_y v$ has a meaning since Lemma 15 shows that τ is in $L_t^\infty(L_y^\infty)$. A solution to this variational problem is a solution to (4.5)–(4.7) in the sense of Definition 2.

4.4.1 Definition and resolution of the discretized problem

We introduce a Galerkin approximation of the variational problem (4.25) − (4.28). Let $(v_i)_{1 \leq i \leq \infty} \in \mathcal{C}^\infty(\overline{\mathcal{O}}) \cap H_0^1(\mathcal{O})$ be such that $\{v_i\}$ is a basis of $H_0^1(\mathcal{O})$ and such that $\partial_{yy} v_i \in \mathrm{Vect}\{v_j, 1 \leq j \leq i\}$ (take e.g. the eigenvectors of the Dirichlet laplacian on $\mathcal{O}$). We set $V_m = \mathrm{Vect}\{v_j, 1 \leq j \leq m\}$. The problem we consider at the discrete

level reads :
Find $U^m \in L_t^\infty(\mathbb{R}^m)$ such that the function $u^m(t, y) = \sum_i U_i^m(t) v_i(y)$ satisfies :

$$\frac{d}{dt} \int_{\mathcal{O}} u^m \, v_i = -\int_{\mathcal{O}} \partial_y u^m \, \partial_y v_i - \int_{\mathcal{O}} \tau^m \, \partial_y v_i + \int_{\mathcal{O}} f_{ext} \, v_i, \ \text{for } 1 \leq i \leq m, (4.29)$$

$$\tau^m = \mathbb{E}\left(\frac{X_t^{y,m} Y_t^{y,m}}{1 - \frac{(X_t^{y,m})^2 + (Y_t^{y,m})^2}{b}} \right), \qquad (4.30)$$

$$X_t^{y,m} = X_0 + \int_0^t \left(-\frac{1}{2} \frac{X_s^{y,m}}{1 - \frac{(X_s^{y,m})^2 + (Y_s^{y,m})^2}{b}} + \partial_y u^m \, Y_s^{y,m} \right) ds + V_t, (4.31)$$

$$Y_t^{y,m} = Y_0 + \int_0^t -\frac{1}{2} \frac{Y_s^{y,m}}{1 - \frac{(X_s^{y,m})^2 + (Y_s^{y,m})^2}{b}} ds + W_t. \qquad (4.32)$$

The initial condition $u^m(t = 0)$ is $\Pi^m(u_0)$ where Π^m is the H^1-projection on V_m. The ordinary differential equation (4.29) is to be understood in $\mathcal{D}'([0, T))$. The stochastic differential equations (4.31)–(4.32) are to be understood in the sense of Definition 1. We know from Proposition 2 that the stress can be written in the following form :

$$\tau^m = \mathbb{E}\left(\left(\frac{X_t Y_t}{1 - \frac{X_t^2 + Y_t^2}{b}} \right) \mathcal{E}\left(\int_0^\bullet \partial_y u^m Y_s \, dV_s \right)_t \right).$$

Notice first that the formal *a priori* estimates of Lemma 16 can now be derived rigorously on the discretized problem (since one can take $v = u^m$ as a test function in (4.29)) and show that if u^m is a solution of the problem (4.29)–(4.32) on $[0, T]$, then $||u^m||_{L^\infty([0,T], L_y^2)}$ is bounded which means that $||U^m(t)||_{L^\infty[0,T]} \leq M$ (where M depends on m). Notice also that if u^m is a solution of the problem (4.29)–(4.32) on $[0, \Theta]$, with $\Theta < T$, then we also have $||U^m(t)||_{L^\infty[0,\Theta]} \leq M$ with the same upper bound M (independant of Θ).

In the following, the dimension m is fixed and we omit the superscript m.

We now want to show that the nonlinear system (4.29)–(4.32) admits a solution. We introduce the matrices $A_{i,j} = \int_{\mathcal{O}} v_i v_j$, $B_{i,j} = \int_{\mathcal{O}} \partial_y v_i \partial_y v_j$, the field $\Xi = (v_1, ..., v_m)$ and the vector F_{ext} with components $\int_{\mathcal{O}} f_{ext} v_j$. We are going to construct a fixed point U of the following mapping which associates to any function $\Phi \in \mathcal{C}([0, T], \mathbb{R}^m)$ the function $F(\Phi) \in \mathcal{C}([0, T], \mathbb{R}^m)$ defined by :

$$F(\Phi)(t) = U_0 - A^{-1}\left(\int_0^t \left(B\Phi(s) - \int_{\mathcal{O}} \mathbb{E}\left(\frac{X_s Y_s}{1 - \frac{X_s^2 + Y_s^2}{b}} Z(\Phi)_s \right) \partial_y \Xi + F_{ext}(s) \right) ds \right),$$

where

$$Z(\Phi)_s = \mathcal{E}\left(\int_0^\bullet \sum_i \Phi_i(r) \partial_y v_i Y_r \, dV_r \right)_s.$$

The initial condition U_0 is the vector with components $(\Pi^m(u_0))_j$.

First step :

First, we are going to show by the Picard fixed point theorem that the function F has a unique fixed point when restricted on $\mathcal{C}([0,\alpha], B(U_0, 1))$ endowed with the uniform convergence topology, for some $\alpha \in (0, T)$ well chosen and only depending on $||F_{ext}||_{L_t^\infty}$, $\max_{1 \leq i \leq m} ||v_i||_{W_y^{1,\infty}}$, m, b and T (see inequalities (4.34) and (4.35) below). The ball $B(U_0, 1)$ is defined by $B(U_0, 1) = \{K \in \mathbb{R}^m, ||K - U_0|| < 1\}$. Notice first that we have, for any $\Phi \in \mathcal{C}([0,\alpha], B(U_0, 1))$ and for any $t \in [0,\alpha]$:

$$
\begin{aligned}
\mathbb{E}\left((Z(\Phi)_t)^2\right) &= \mathbb{E}\left(\left(\left(\mathcal{E}\left(\int_0^\bullet \sum_i \Phi_i(r)\partial_y v_i Y_r \, dV_r\right)\right)_t\right)^2\right) \\
&= \mathbb{E}\left(\exp\left(\int_0^t \left(\sum_i \Phi_i(r)\partial_y v_i Y_r\right)^2 dr\right)\mathcal{E}\left(2\int_0^\bullet \sum_i \Phi_i(r)\partial_y v_i Y_r \, dV_r\right)_t\right) \\
&\leq \exp\left(C\alpha b\left(||\Phi||_{L^\infty[0,\alpha]}^2\right)\right)\mathbb{E}\left(\mathcal{E}\left(2\int_0^\bullet \sum_i \Phi_i(r)\partial_y v_i Y_r \, dV_r\right)_t\right) \\
&\leq \exp\left(C\alpha b\left(||\Phi||_{L^\infty[0,\alpha]}^2\right)\right),
\end{aligned}
$$

where C only depends on $\max_{1 \leq i \leq m} ||v_i||_{W_y^{1,\infty}}$. This means (since $\alpha < T$ and $\Phi \in \mathcal{C}([0,\alpha], B(U_0, 1))$) :

$$
||Z(\Phi)_t||_{L^\infty([0,\alpha], L_y^\infty(L_\omega^2))} \leq \exp\left(CTb\left(1 + ||U_0||^2\right)\right). \tag{4.33}
$$

Using this estimate (and Lemma 14), for any $\Phi \in \mathcal{C}([0,\alpha], B(U_0, 1))$, we have the following estimate on $\Phi' = F(\Phi)$:

$$
\begin{aligned}
||\Phi'(t) - U_0||_{L^\infty[0,\alpha]} &\leq |||A^{-1}|||\left(|||B|||\,\alpha(1 + ||U_0||) + C\alpha||Z(\Phi)||_{L^\infty([0,\alpha], L_y^\infty(L_\omega^2))}\right. \\
&\qquad \left. + \alpha||F_{ext}||_{L_t^\infty}\right) \\
&\leq C\alpha(1 + ||U_0||)\exp(C||U_0||^2),
\end{aligned}
$$

where C is a constant depending only on $||F_{ext}||_{L_t^\infty}$, $\max_{1 \leq i \leq m} ||v_i||_{W_y^{1,\infty}}$, m, b and T (and not on $||U_0||$). Thus, $F\left(\mathcal{C}([0,\alpha], B(U_0, 1))\right) \subset \mathcal{C}([0,\alpha], B(U_0, 1))$ if we choose α small enough to ensure that :

$$
C\alpha(1 + ||U_0||)\exp(C||U_0||^2) \leq 1. \tag{4.34}
$$

We next show that the function F restricted on $\mathcal{C}([0,\alpha], B(U_0, 1))$ (with α small enough) is contracting. Let $\Phi^{1'} = F(\Phi^1)$, $Z_t^1 = Z(\Phi^1)_t$ and $\Phi^{2'} = F(\Phi^2)$, $Z_t^2 = Z(\Phi^2)_t$ where $\Phi^1 \in B(U_0, 1)$ and $\Phi^2 \in B(U_0, 1)$. Suppose moreover that (4.34)

holds. We have

$$||\Phi^{1'}(t) - \Phi^{2'}(t)||_{L^\infty[0,\alpha]} \leq |||A^{-1}||| \left(|||B||| \, \alpha ||\Phi^1(t) - \Phi^2(t)||_{L^\infty[0,\alpha]} \right.$$
$$\left. + C\alpha ||Z_t^1 - Z_t^2||_{L^\infty([0,\alpha], L_y^\infty(L_\omega^2))}\right)$$
$$\leq C'\alpha \left(||\Phi^1(t) - \Phi^2(t)||_{L^\infty[0,\alpha]} + ||Z_t^1 - Z_t^2||_{L^\infty([0,\alpha], L_y^\infty(L_\omega^2))}\right).$$

We now want to estimate $(Z_t^1 - Z_t^2)$. We use the fact that $Z_t^k = 1 + \int_0^t \sum_i \Phi_i^k(r) \partial_y v_i \, Y_r \, Z_r^k \, dV_r$ ($k = 1$ or 2) :

$$Z_t^1 - Z_t^2 = \int_0^t \left(\sum_i \Phi_i^1(r) \partial_y v_i \, Z_r^1 - \sum_i \Phi_i^2(r) \partial_y v_i \, Z_r^2\right) Y_r \, dV_r$$
$$= \int_0^t \sum_i \left(\Phi_i^1(r) - \Phi_i^2(r)\right) \partial_y v_i \, Z_r^2 Y_r \, dV_r + \int_0^t \left(\sum_i \Phi_i^1(r) \partial_y v_i\right) \left(Z_r^1 - Z_r^2\right) Y_r \, dV_r.$$

From this and (4.33), we deduce that, $\forall t \in [0, \alpha]$,

$$\mathbb{E}\left(\left(Z_t^1 - Z_t^2\right)^2\right) \leq 2\mathbb{E}\left(\left(\int_0^t \sum_i \left(\Phi_i^1(r) - \Phi_i^2(r)\right) \partial_y v_i \, Z_r^2 Y_r \, dV_r\right)^2\right)$$
$$+ 2\mathbb{E}\left(\left(\int_0^t \left(\sum_i \Phi_i^1(r) \partial_y v_i\right) \left(Z_r^1 - Z_r^2\right) Y_r \, dV_r\right)^2\right),$$
$$\leq 2\int_0^t \mathbb{E}\left(\left(\sum_i \left(\Phi_i^1(r) - \Phi_i^2(r)\right) \partial_y v_i \, Z_r^2 Y_r\right)^2\right) dr$$
$$+ 2\int_0^t \mathbb{E}\left(\left(\left(\sum_i \Phi_i^1(r) \partial_y v_i\right) \left(Z_r^1 - Z_r^2\right) Y_r\right)^2\right) dr,$$
$$\leq 2bC'\alpha \exp\left(CTb\left(1 + ||U_0||^2\right)\right) ||\Phi^1 - \Phi^2||_{L^\infty[0,\alpha]}^2$$
$$+ 2bC'||\Phi^1||_{L^\infty[0,\alpha]}^2 \int_0^t \mathbb{E}\left(\left(Z_r^1 - Z_r^2\right)^2\right) dr.$$

Using Gronwall Lemma, this yields an estimate :

$$\left|\left|Z_t^1 - Z_t^2\right|\right|_{L^\infty([0,\alpha], L_y^\infty(L_\omega^2))} \leq C'\alpha \exp(C'||U_0||^2) ||\Phi^1 - \Phi^2||_{L^\infty[0,\alpha]},$$

where C' is a constant depending only on $||F_{ext}||_{L_t^\infty}$, $\max_{1 \leq i \leq m} ||v_i||_{W_y^{1,\infty}}$, m, b and T. We finally have an inequality of the following type :

$$||\Phi^{1'}(t) - \Phi^{2'}(t)||_{L^\infty[0,\alpha]} \leq C'\alpha \exp(C'||U_0||^2) ||\Phi^1(t) - \Phi^2(t)||_{L^\infty[0,\alpha]},$$

so that F is contracting if we have :

$$C'\alpha \exp(C'||U_0||^2) < 1. \tag{4.35}$$

At this stage, we have shown that for any initial condition U_0, there exists a solution $U \in \mathcal{C}([0,\alpha_0], \mathbb{R}^m)$ to the discrete problem on a time interval $[0,\alpha_0]$, with $\alpha_0 > 0$ such that (4.34) and (4.35) hold.

   Second step (continuation) :
We can now start again the construction of a solution to (4.29)–(4.32) from the final point $U(\alpha_0)$ and $Z_{\alpha_0} = Z(U)_{\alpha_0} = \exp\left(\int_0^{\alpha_0} \sum_i U_i(r)\partial_y v_i Y_r\, dV_r - \frac{1}{2}\int_0^{\alpha_0} \left(\sum_i U_i(r)\partial_y v_i Y_r\right)^2\, dr\right)$ using the same arguments as before. Notice that by the *a priori* estimate of Lemma 16, we have on the one hand $U(\alpha_0) \le M$ and on the other hand $||Z_{\alpha_0}||_{L_y^\infty(L_\omega^2)} \le \exp(C\alpha_0 b(1+M^2)) \le \exp(CTb(1+M^2)) = M'$ (using (4.33)), with C only depending on $\max_{1\le i\le m} ||v_i||_{W_y^{1,\infty}}$. We now consider the mapping F^{α_0} which associates to any function $\Phi \in \mathcal{C}([\alpha_0, T], \mathbb{R}^m)$ the function $F^{\alpha_0}(\Phi) \in \mathcal{C}([\alpha_0, T], \mathbb{R}^m)$ defined by :

$$F^{\alpha_0}(\Phi)(t) = U(\alpha_0) - A^{-1}\left(\int_{\alpha_0}^t \left(B\Phi(s) - \int_{\mathcal{O}} \mathbb{E}\left(\frac{X_s Y_s}{1 - \frac{X_s^2+Y_s^2}{b}} Z^{\alpha_0}(\Phi)_s\right)\partial_y \Xi + F_{ext}(s)\right) ds\right),$$

where $Z^{\alpha_0}(\Phi)_s = Z_{\alpha_0}\mathcal{E}\left(\int_{\alpha_0}^{\bullet}\sum_i \Phi_i(r)\partial_y v_i Y_r\, dV_r\right)_s$. The same arguments as before show that we can find a time interval $[\alpha_0, \alpha_0 + \alpha]$ (with $\alpha \in (0, T-\alpha_0)$) on which F^{α_0} has a fixed point. Indeed, what is important is just that $Z_{\alpha_0} \in L_y^\infty(L_\omega^2)$. This is for example the way one can estimate $Z^{\alpha_0}(\Phi)_t$, for any $t \in [\alpha_0, \alpha_0 + \alpha]$:

$$\mathbb{E}\left((Z^{\alpha_0}(\Phi)_t)^2\right) = \mathbb{E}\left(\left(Z(\alpha_0)\mathcal{E}\left(\int_{\alpha_0}^{\bullet}\sum_i \Phi_i(r)\partial_y v_i Y_r\, dV_r\right)_t\right)^2\right)$$

$$= \mathbb{E}\left(Z_{\alpha_0}^2\, \mathbb{E}\left(\left(\mathcal{E}\left(\int_{\alpha_0}^{\bullet}\sum_i \Phi_i(r)\partial_y v_i Y_r\, dV_r\right)_t\right)^2 | \mathcal{F}_{\alpha_0}\right)\right)$$

$$= \mathbb{E}\left(Z_{\alpha_0}^2\, \mathbb{E}\left(\mathcal{E}\left(2\int_{\alpha_0}^{\bullet}\sum_i \Phi_i(r)\partial_y v_i Y_r\, dV_r\right)_t \exp\left(\int_{\alpha_0}^t \left(\sum_i \Phi_i(r)\partial_y v_i Y_r\right)^2\, dr\right) | \mathcal{F}_{\alpha_0}\right)\right)$$

$$\le \exp\left(C(\alpha - \alpha_0)b||\Phi||^2_{L^\infty[\alpha_0,\alpha_0+\alpha]}\right)\mathbb{E}\left(Z_{\alpha_0}^2\, \mathbb{E}\left(\mathcal{E}\left(2\int_{\alpha_0}^{\bullet}\sum_i \Phi_i(r)\partial_y v_i Y_r\, dV_r\right)_t | \mathcal{F}_{\alpha_0}\right)\right)$$

$$\le \exp\left(C(\alpha - \alpha_0)b||\Phi||^2_{L^\infty[\alpha_0,\alpha_0+\alpha]}\right)\mathbb{E}\left(Z_{\alpha_0}^2\right).$$

Going through the same arguments as before, one can thus show that F^{α_0}, when restricted to $\mathcal{C}([\alpha_0, \alpha_0+\alpha], B(U(\alpha_0), 1))$ is such that $F^{\alpha_0}\left(\mathcal{C}([\alpha_0, \alpha_0 + \alpha], B(U(\alpha_0), 1))\right) \subset \mathcal{C}([\alpha_0, \alpha_0+\alpha], B(U(\alpha_0), 1))$ and is contracting, provided that α satisfies an inequality of the type :

$$C\alpha M'(1 + M)\exp(CM^2) \le 1$$

where C is a constant only depending on $||F_{ext}||_{L_t^\infty}$, $\max_{1 \leq i \leq m} ||v_i||_{W_y^{1,\infty}}$, m, b and T. We can choose
$$\alpha = \alpha_1 = \frac{1}{CM'(1 + M) \exp(CM^2)}.$$
We have thus built a solution $U \in \mathcal{C}([0, \alpha_0 + \alpha_1], \mathbb{R}^m)$ to the discrete problem on the interval $[0, \alpha_0 + \alpha_1]$. The final points $U(\alpha_0 + \alpha_1)$ and $Z(U)_{\alpha_0 + \alpha_1}$ are again such that $||U(\alpha_0 + \alpha_1)|| \leq M$ and $||Z(U)_{\alpha_0 + \alpha_1}||_{L_y^\infty(L_\omega^2)} \leq M'$. This means that we can, by the same arguments, extend the solution on the time interval $[\alpha_0 + \alpha_1, \alpha_0 + 2\alpha_1]$, and by a continuation argument, we can build a solution to (4.29)–(4.32) on the time interval $[0, T]$.

Remark 16 *This proves that any finite element approximation of the variational problem (4.25) – (4.28) has a solution on a time interval $[0, T]$ for any $T > 0$.*

Remark 17 *One can easily prove the uniqueness of a solution to the problem (4.25) – (4.28) on $[0, T]$, for example by adapting the proof of Lemma 18 to the finite dimensional case.*

4.4.2   Convergence of the discretized problem

We now turn to the convergence of the solution of the discretized problem. The formal *a priori* estimates of Lemma 17 can be derived rigorously on the discretized system. Indeed, one can take $v = -\partial_{y,y} u^m$ as a test function in (4.29) (see the special basis (v_i) we have chosen), and the expression (4.23) of the derivative of τ with respect to y is completely rigorous since $\forall t \in [0, T]$, $u^m(t, .) \in C^\infty(\overline{\mathcal{O}})$. Therefore, using Lemma 17, we know that there exists $T' > 0$ such that there exists a uniform bound on u^m in norm $L^\infty([0, T'], H_y^1) \cap L^2([0, T'], H_y^2)$ and on $\partial_t u^m$ in norm $L^2([0, T'], L_y^2)$.

Up to the extraction of a subsequence, we can suppose that there exists $u \in L^\infty([0, T'], H_y^1) \cap L^2([0, T'], H_y^2)$ such that :
- $u^m \rightharpoonup u$ weakly in $L^2([0, T'], H_y^2)$ and weakly-* in $L^\infty([0, T'], H_y^1)$,
- $\partial_t u^m \rightharpoonup \partial_t u$ weakly in $L^2([0, T'], L_y^2)$,
- $u^m \rightarrow u$ strongly in $L^2([0, T'], H_y^1)$.

For the third convergence, we use the standard fact that the injection $\{v \text{ s.t. } v \in L^2([0, T'], H_y^2 \cap H_{0,y}^1), \partial_t v \in L^2([0, T'], L_y^2)\} \hookrightarrow L^2([0, T'], H_{0,y}^1)$ is compact (see Theorem 5.1 p. 58 in [105]). We can also suppose that $u^m \longrightarrow u$ for almost every $(t, y) \in (0, T') \times \mathcal{O}$. We want to show the convergence of each of the terms of the following equation (for a fixed i) :

$$\frac{d}{dt} \int_{\mathcal{O}} u^m v_i + \int_{\mathcal{O}} \partial_y u^m \partial_y v_i = \int_{\mathcal{O}} \mathbb{E}\left(\left(\frac{X_t Y_t}{1 - \frac{X_t^2 + Y_t^2}{b}}\right) \mathcal{E}\left(\int_0^{\bullet} \partial_y u^m Y_s \, dV_s\right)_{T'}\right) \partial_y v_i + \int_{\mathcal{O}} f_{ext} v_i,$$
(4.36)

where we have used the following standard property of the exponential martingale : for any y fixed in $\mathcal{O}$, since $\partial_y u(t, y) \in L^2(0, T')$, we have $\forall t \in (0, T')$,

$$\tau(t, y) = \mathbb{E}\left(\left(\frac{X_t Y_t}{1 - \frac{X_t^2 + Y_t^2}{b}}\right) \mathcal{E}\left(\int_0^{\bullet} \partial_y u(y) Y_s \, dV_s\right)_{T'}\right).$$

Using the above convergences, we easily pass to the limit in all terms of (4.36) but $\int_0^{T'} \int_{\mathcal{O}} \mathbb{E}\left(\left(\dfrac{X_t Y_t}{1 - \frac{X_t^2 + Y_t^2}{b}}\right) \mathcal{E}\left(\int_0^{\bullet} \partial_y u^m Y_s \, dV_s\right)_{T'} \partial_y v_i \, w\right)$, where $w \in C_0^{\infty}(0, T')$.

Let us define the function $f^m(t, y, \omega) = \left(\dfrac{X_t Y_t}{1 - \frac{X_t^2 + Y_t^2}{b}}\right) \mathcal{E}\left(\int_0^{\bullet} \partial_y u^m Y_s \, dV_s\right)_{T'} \partial_y v_i \, w$.

It is easy to see that, $\int_0^{T'} \partial_y u^m Y_s \, dV_s$ converges in $L_y^2(L_{\omega}^2)$ to $\int_0^{T'} \partial_y u Y_s \, dV_s$ and that $\dfrac{1}{2}\int_0^{T'} (\partial_y u^m Y_s)^2 \, ds$ converges in $L_y^1(L_{\omega}^1)$ to $\dfrac{1}{2}\int_0^{T} (\partial_y u Y_s)^2 \, ds$. We can therefore (extracting a subsequence) suppose that f^m converges for almost every (t, y, ω) towards $f(t, y, \omega) = \left(\dfrac{X_t Y_t}{1 - \frac{X_t^2 + Y_t^2}{b}}\right) \mathcal{E}\left(\int_0^{\bullet} \partial_y u Y_s \, dV_s\right)_{T'} \partial_y v_i \, w$. Moreover, we can find a uniform bound on the norm $L^2([0, T'], L_y^2(L_{\omega}^2))$ of f^m (using the same techniques as in Lemma 15). This shows that the family $(f^m)_{m \geq 1}$ is uniformly integrable and therefore that $\int_0^{T'} \int_{\mathcal{O}} \mathbb{E}(f^m) \longrightarrow \int_0^{T'} \int_{\mathcal{O}} \mathbb{E}(f)$.

Finally, one can prove by standard arguments (see e.g. [145] page 260) that $u(0) = u_0$ and this concludes the "existence part" of Theorem 7.

4.4.3   Uniqueness of the solution

Lemma 18 (Uniqueness of the solution) *The system (4.5)–(4.7) admits a unique solution on $[0, T']$ in the sense given in Definition 2.*

Proof.   Let us consider two solutions (u, X, Y) and $(\tilde{u}, \tilde{X}, \tilde{Y})$. One easily obtains the following estimate on $w = u - \tilde{u}$, for any $0 < t < T'$:

$$\frac{1}{2}\int_{\mathcal{O}} w^2(t) + \int_0^t \int_{\mathcal{O}} |\partial_y w|^2 \;=\; -\int_0^t \int_{\mathcal{O}} (\tau - \tilde{\tau})\partial_y w$$
$$\leq\; \frac{1}{2}\int_0^t \int_{\mathcal{O}} |\partial_y w|^2 + \frac{1}{2}\int_0^t \int_{\mathcal{O}} |\tau - \tilde{\tau}|^2,$$

where

$$\tau - \tilde{\tau} = \mathbb{E}\left(\left(\frac{X_t Y_t}{1 - \frac{X_t^2 + Y_t^2}{b}}\right)(Z(u) - Z(\tilde{u}))\right),$$

with $Z(u)_t = \mathcal{E}\left(\int_0^{\bullet} \partial_y u(y) Y_s \, dV_s\right)_t$. We have

$$
\begin{aligned}
|\tau - \tilde{\tau}|^2 &= \mathbb{E}\left(\left(\left(\frac{X_t Y_t}{1 - \frac{X_t^2 + Y_t^2}{b}}\right)(Z(u) - Z(\tilde{u}))\right)^2\right) \\
&\leq \mathbb{E}\left(\left(\frac{X_t Y_t}{1 - \frac{X_t^2 + Y_t^2}{b}}\right)^2\right)\mathbb{E}\left((Z(u) - Z(\tilde{u}))^2\right).
\end{aligned}
$$

We know that

$$
\begin{aligned}
Z(u)_t - Z(\tilde{u})_t &= \int_0^t \left(\partial_y u(y) Z(u)_r - \partial_y \tilde{u}(y) Z(\tilde{u})_r\right) Y_r dV_r \\
&= \int_0^t \left(\partial_y u(y) - \partial_y \tilde{u}(y)\right) Z(u)_r Y_r dV_r + \int_0^t \left(Z(u)_r - Z(\tilde{u})_r\right) \partial_y \tilde{u}(y) Y_r dV_r.
\end{aligned}
$$

This yields :

$$
\begin{aligned}
\mathbb{E}\left((Z(u)_t - Z(\tilde{u})_t)^2\right) &\leq 2b \int_0^t |\partial_y w(y)|^2 \mathbb{E}(Z(u)_r^2) \, dr \\
&\quad + 2b \int_0^t |\partial_y \tilde{u}(y)|^2 \mathbb{E}\left((Z(u)_r - Z(\tilde{u})_r)^2\right) \, dr.
\end{aligned}
$$

Using Gronwall Lemma and the fact that $\mathbb{E}(Z(u)_t^2) \leq \exp\left(b\int_0^{T'} |\partial_y u|^2 \, ds\right)$, this yields an estimate :

$$
\mathbb{E}\left((Z(u)_t - Z(\tilde{u})_t)^2\right) \leq C \exp\left(C \int_0^{T'} |\partial_y \tilde{u}(y)|^2 + |\partial_y u(y)|^2\right) \int_0^t |\partial_y w(y)|^2.
$$

We have finally, using the estimates of Lemma 17 :

$$
\int_0^t \int_{\mathcal{O}} |\partial_y w|^2 \leq C \int_0^t \int_0^s \int_{\mathcal{O}} |\partial_y w|^2.
$$

which shows that $w = 0$ by Gronwall Lemma.

In order to conclude this proof of Lemma 18, and therefore of Theorem 7, it remains to recall from Proposition 2 that the stochastic differential equation (4.7) admits a unique strong solution. □

Chapitre 5

Analyse du modèle des dumbbells FENE : l'EDS

Les résultats présentés dans ce chapitre ont fait l'objet d'un proceeding paru dans *Probabilistic Methods in Fluids Proceedings of the Swansea 2002 Workshop.* Ce chapitre complète le précédent en donnant des résultats sur l'équation différentielle stochastique associée au modèle des dumbbells FENE. Les résultats qui suivent ont été écrits dans le cadre d'un écoulement cisaillé, mais sont également valables pour un écoulement 2D quelconque, régulier et fixé (cf. notamment le cas des écoulements homogènes et le Chapitre 7 pour des détails sur ce point).

**Mathematical analysis of a stochastic differential equation
arising in the micro-macro modelling of polymeric fluids**

Benjamin Jourdain, Tony Lelièvre

We analyze the properties of a stochastic differential equation (SDE) arising
in the modeling of polymeric fluids. More precisely, we focus on the so-called
FENE (Finite Extensible Nonlinear Elastic) model, for which the drift term
in the SDE is singular.

5.1   Introduction

The rheology of non-newtonian fluids is a very lively field of modern fluid mechanics. The challenge is to find a good relation linking within the fluid the stress tensor to the velocity field in order to reproduce the behavior of the fluid in some classical situations (shear flow, elongational flow) and to simulate it in some more complex cases. This relation may be complicated since the stress generally depends on the whole history of the velocity field. Many approaches consist in deriving this relation from the microscopic structure of the fluid. In some cases, it is possible to directly attack the full system coupling the evolution of these microscopic structures to the macroscopic quantities (such as velocity or pressure) : this is the so-called micro-macro approach.

We are here interested in the modeling of polymeric fluids. More precisely, we consider dilute solutions of polymers, so that the chains of polymers (the "microscopic structures") do not interact with each other. In order to describe the microscopic structure of this fluid, one can model a polymer by a chain of beads and rods (this is the Kramers model) or more simply by some beads linked by springs (see Figure 5.1). We consider here the simplest model consisting in two beads linked by one spring : this is the dumbbell model. In this model, the evolution of the end-to-end vector (which joins the two beads) is described by a SDE. We refer the interested reader to Refs [12, 13, 39, 120] for the general physical background of these models. This SDE is actually coupled to the Navier-Stokes equation through the expression of the stress tensor as an expectation value built from the end-to-end vector.

The spring force can be linear (Hookean dumbbell model) or explosive (Finite Extensible Nonlinear Elastic dumbbell model).

In the following, we consider the start-up of a Couette flow of a polymeric fluid (see Figure 5.2) : the fluid is initially at rest, and for $t > 0$, the upper plate moves with a constant velocity. For a complete analysis (existence, uniqueness, convergence of a finite element method coupled with a Monte Carlo method) of this model in the Hookean dumbbell case, we refer to Ref. [85]. This reference also contains a more detailed introduction to these types of models and the way to discretize the corresponding system of coupled PDE-SDE.

We here complement the mathematical analysis of the FENE model presented in Ref. [86] by focusing on the SDE modeling the evolution of the conformation of the polymers in the FENE case. It is proven in Ref. [86] that a solution to the coupled micro-macro system uniquely exists under natural assumptions. Our concern in the
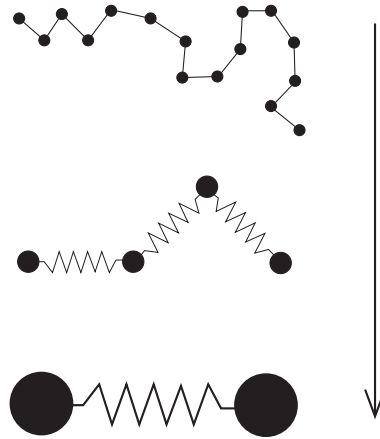
FIG. 5.1 – A hierarchy of models : from Kramers chain (top) to dumbbell (bottom).

present paper is in particular to investigate the role played by the finite extensibility coefficient b (see formulas (5.2) and (5.3) below) in the existence and uniqueness of solution of the SDE itself, the fluid velocity being considered known.
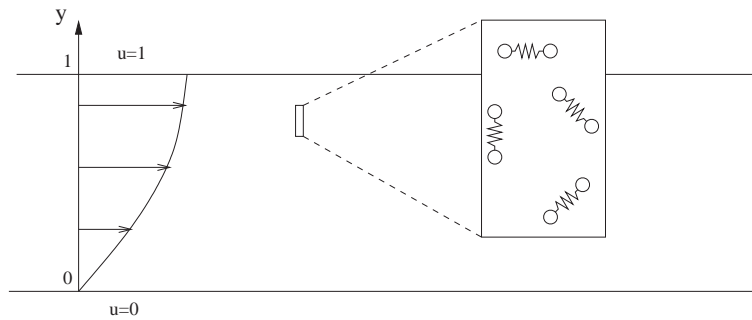
FIG. 5.2 – Velocity profile in a shear flow of a dilute solution of polymers.

Let us now introduce the equations we deal with. They read, in a non-dimensional form :

$$\partial_t u - \partial_{yy} u = \partial_y \tau + f_{ext}, \tag{5.1}$$

$$\tau = \mathbb{E}\left(\frac{X_t^y Y_t^y}{1 - \frac{(X_t^y)^2 + (Y_t^y)^2}{b}}\right), \tag{5.2}$$

$$\begin{cases} dX_t^y = \left(-\frac{1}{2}\frac{X_t^y}{1 - \frac{(X_t^y)^2 + (Y_t^y)^2}{b}} + \partial_y u\, Y_t^y\right) dt + dV_t, \\[4mm] dY_t^y = \left(-\frac{1}{2}\frac{Y_t^y}{1 - \frac{(X_t^y)^2 + (Y_t^y)^2}{b}}\right) dt + dW_t. \end{cases} \tag{5.3}$$

where the parameter $b > 0$ measures the finite extensibility of the polymer. The space variable y varies in $\mathcal{O} = (0,1)$ and t varies in the whole of $\mathbb{R}_+$. The random variables are defined on a filtered probability space $(\Omega, \mathcal{F}, \mathcal{F}_t, \mathbb{P})$. The random process

(V_t, W_t) is a $(\mathcal{F}_t)$-two-dimensional Brownian motion. We take Dirichlet boundary conditions on the velocity. The initial velocity is $u(t=0, .) = u_0$, and (X_0, Y_0) is a $\mathcal{F}_0$-measurable random variable. We will suppose that (X_0, Y_0) is either such that $\mathbb{P}\left(X_0^2 + Y_0^2 > b\right) = 0$ (Section 5.2) or such that $\mathbb{P}\left(X_0^2 + Y_0^2 \geq b\right) = 0$ (Sections 5.3 and 5.4).

We fix y in $\mathcal{O}$, set $g(t) = \partial_y u(y, t)$ and suppose throughout this paper that we have at least the following regularity on g :

$$g \in L^1_{\mathrm{loc}}\left(\mathbb{R}_+\right) \tag{5.4}$$

where $\mathbb{R}_+ = [0, +\infty)$. We are then interested in solving for $t \geq 0$ the following SDE, which is a rewriting of the SDE (5.3) of the initial coupled system :

$$\begin{cases} dX_t^g = \left(-\dfrac{1}{2}\dfrac{X_t^g}{1-\frac{(X_t^g)^2+(Y_t^g)^2}{b}} + g(t)\,Y_t^g\right) dt + dV_t, \\[4mm] dY_t^g = \left(-\dfrac{1}{2}\dfrac{Y_t^g}{1-\frac{(X_t^g)^2+(Y_t^g)^2}{b}}\right) dt + dW_t, \end{cases} \tag{5.5}$$

with initial condition (X_0, Y_0).

Let us begin by recalling from Ref. [86] the precise mathematical meaning we give to (5.5).

Definition 1 *Let $\boldsymbol{X}_0 = (X_0, Y_0)$ and $\boldsymbol{W}_t = (V_t, W_t)$. We shall say that a $(\mathcal{F}_t)$-adapted process $\boldsymbol{X}_t^g = (X_t^g, Y_t^g)$ is a solution to (5.5) when : for $\mathbb{P}$-a.e. ω, $\forall t \geq 0$,*

$$\begin{cases} \displaystyle\int_0^t \left|\dfrac{1}{1-\frac{|\boldsymbol{X}_s^g|^2}{b}}\right| ds < \infty, \\[3mm] \textit{with the convention } , \forall \boldsymbol{x} = (x, y) \in \mathbb{R}^2, \dfrac{1}{1-\frac{|\boldsymbol{x}|^2}{b}} = +\infty \textit{ if } |\boldsymbol{x}|^2 = b, \\[3mm] \boldsymbol{X}_t^g = \boldsymbol{X}_0 - \dfrac{1}{2}\displaystyle\int_0^t \dfrac{\boldsymbol{X}_s^g}{1-\frac{|\boldsymbol{X}_s^g|^2}{b}}\, ds + \displaystyle\int_0^t (g(s)Y_s^g, 0)\, ds + \boldsymbol{W}_t \end{cases} \tag{5.6}$$

Remark 1 *Because of the convention $\dfrac{1}{1-\frac{|\boldsymbol{x}|^2}{b}} = +\infty$ if $|\boldsymbol{x}|^2 = b$, we deduce that a solution to (5.6) is such that the subset of $\mathbb{R}_+$ $\{0 \leq u < \infty, |\boldsymbol{X}_u^g|^2 = b\}$ has $\mathbb{P}$-a.s. zero Lebesgue measure.*

The paper is organized as follows : in Section 5.2, we prove the existence and uniqueness of the solution to (5.6) with values in $\overline{B}$, where

$$B = B(0, \sqrt{b}) = \left\{(x, y), x^2 + y^2 < b\right\}.$$

The existence of such a solution is derived from results concerning multivalued SDEs (see Refs [25, 27]). We then focus on the probability for this solution to reach the boundary of $\overline{B}$ (see Section 5.3). When $b < 2$ and $\mathbb{P}(|\boldsymbol{X}_0|^2 < b) = 1$, this probability is equal to one. This enables us to construct (for $g = 0$) a solution to (5.6) that leaves a.s. $\overline{B}$. Hence, if $b < 2$, uniqueness of solutions does not hold for solutions to (5.6) without the additional requirement to take values in $\overline{B}$. When $b \geq 2$ and

again $\mathbb{P}(|\boldsymbol{X}_0|^2 < b) = 1$, the probability to reach the boundary is equal to zero and trajectorial uniqueness holds. We exhibit the unique invariant probability measure of the SDE (5.6) with $g = 0$ (see Section 5.4). All these results on the SDE have an impact on the analysis and the understanding of the coupled SDE-PDE system (for which we refer to Ref. [86]). They show that the assumption $b \geq 2$ adopted in Ref. [86] to prove existence and uniqueness of solution to the coupled system is in some sense "optimal".

5.2   Existence and uniqueness

In this section, we suppose that (X_0, Y_0) is such that $\mathbb{P}\left(X_0^2 + Y_0^2 > b\right) = 0$. Our aim is to prove the following :

Proposition 1 *Under assumption (5.4), for any $b > 0$ and for any initial condition (X_0, Y_0) such that $\mathbb{P}\left(X_0^2 + Y_0^2 > b\right) = 0$, there exists a unique solution to (5.6) with values in $\overline{B}$.*

We first prove the uniqueness statement (Section 5.2.1), then turn to the existence first when $g \in L_t^\infty$ (Section 5.2.2) and finally when $g \in L_{\mathrm{loc}}^1$ (Section 5.2.3). In the following, the point is to notice that the singular term in the drift derives from a convex potential $\Pi : \mathbb{R}^2 \to]-\infty, +\infty]$:

$$\Pi(x, y) = \begin{cases} -\frac{b}{4} \ln\left(1 - \frac{x^2 + y^2}{b}\right) & \text{if } x^2 + y^2 < b, \\ +\infty & \text{otherwise.} \end{cases} \qquad (5.7)$$

We have : $\forall x \in B, \nabla\Pi(\boldsymbol{x}) = \frac{1}{2}\frac{\boldsymbol{x}}{1 - \frac{|\boldsymbol{x}|^2}{b}}$. Moreover, the function Π is a continuous convex function with domain B.

5.2.1   Trajectorial uniqueness for solutions with values in $\overline{B}$

Let us begin with the uniqueness.

Proposition 2 *Let us suppose we have two solutions $\boldsymbol{X}_t^g$ and $\tilde{\boldsymbol{X}}_t^g$ to (5.6) and such that $\mathbb{P}$-a.s., $\boldsymbol{X}_0^g = \tilde{\boldsymbol{X}}_0^g$. Then these two solutions are indistiguishable until one of the processes leaves $\overline{B}$. In addition, if $\mathbb{P}(\exists t \geq 0 | \boldsymbol{X}_t^g|^2 = b) = 0$, then $\boldsymbol{X}_t^g$ and $\tilde{\boldsymbol{X}}_t^g$ are indistiguishable.*

Proof.   Let us consider $\tau = \inf\{t \geq 0, (|\tilde{\boldsymbol{X}}_t^g|^2 \vee |\boldsymbol{X}_t^g|^2) > b\}$ and $\boldsymbol{Z}_t = \left(\boldsymbol{X}_t^g - \tilde{\boldsymbol{X}}_t^g\right)$. By Itô's formula, we have :

$$\begin{aligned} d|\boldsymbol{Z}|_t^2 &= 2\boldsymbol{Z}_t.d\boldsymbol{Z}_t, \\ &= -2(\nabla\Pi(\boldsymbol{X}_t^g) - \nabla\Pi(\tilde{\boldsymbol{X}}_t^g)).\boldsymbol{Z}_t\, dt + 2g(t)(X_t^g - \tilde{X}_t^g)(Y_t^g - \tilde{Y}_t^g)dt, \end{aligned}$$

where $\boldsymbol{x}.\boldsymbol{y}$ denotes the scalar product of $\boldsymbol{x}$ and $\boldsymbol{y} \in \mathbb{R}^2$.

Using the fact that, since Π is convex, for any $\boldsymbol{x}$ and $\tilde{\boldsymbol{x}} \in B$, $(\nabla\Pi(\boldsymbol{x}) - \nabla\Pi(\tilde{\boldsymbol{x}})).(\boldsymbol{x} - \tilde{\boldsymbol{x}}) \geq 0$, we obtain, for any $t \geq 0$:

$$
\begin{aligned}
|\boldsymbol{Z}_{t \wedge \tau}|^2 &\leq 2 \int_0^{t \wedge \tau} |g(s)| \left| X_s^g - \tilde{X}_s^g \right| \left| Y_s^g - \tilde{Y}_s^g \right| ds, \\
&\leq \int_0^t |g(s)| |\boldsymbol{Z}_{s \wedge \tau}|^2 \, ds.
\end{aligned}
$$

Using Gronwall Lemma and the fact that $g \in L_{\text{loc}}^1(\mathbb{R}_+)$, we have thus shown that $\mathbb{P}$-a.s., $\forall t \geq 0$, $\boldsymbol{X}_{t \wedge \tau}^g = \tilde{\boldsymbol{X}}_{t \wedge \tau}^g$. Therefore, on $\{\tau < \infty\}$, $|\boldsymbol{X}_\tau^g|^2 = b$. We deduce that in case $\mathbb{P}(\exists t \geq 0, |\boldsymbol{X}_t^g|^2 = b) = 0$, $\tau = \infty$ $\mathbb{P}$-a.s. . $\qquad\square$

5.2.2 Existence in the case $g \in L_t^\infty$

In this section, we suppose :

$$
g \in L^\infty(\mathbb{R}_+). \tag{5.8}
$$

In order to prove an existence result, we will use a multivalued stochastic differential equation. In this section, we use the results of E. Cépa [25] and E. Cépa and D. Lépingle [27].
Since the function Π is convex on the open set B, its subdifferential $\partial\Pi$ is a simple-valued maximal monotone operator on $\mathbb{R}^2$ with domain B :

$$
\partial\Pi(\boldsymbol{x}) = \left\{ \begin{array}{ll} \{\nabla\Pi(\boldsymbol{x})\} & \text{if } \boldsymbol{x} \in B, \\ \emptyset & \text{if } \boldsymbol{x} \notin B. \end{array} \right.
$$

Let us now consider the two-dimensional process $\boldsymbol{X}_t$ solution of the following multivalued SDE :

$$
\left\{ \begin{array}{l} d\boldsymbol{X}_t^g + \partial\Pi(\boldsymbol{X}_t^g) \, dt \ni (g(t) Y_t^g, 0) \, dt + d\boldsymbol{W}_t, \\ \boldsymbol{X}_0^g = \boldsymbol{X}_0 = (X_0, Y_0), \end{array} \right. \tag{5.9}
$$

We first recall the precise meaning of a solution to (5.9).

Definition 2 *We shall say that a continuous $(\mathcal{F}_t)$-adapted process $\boldsymbol{X}_t^g = (X_t^g, Y_t^g)$ with values in $\overline{B}$ is a solution to (5.9) if and only if $\boldsymbol{X}_0^g = \boldsymbol{X}_0$ and the process $\boldsymbol{K}_t^g = \boldsymbol{W}_t + \int_0^t (g(s) Y_s^g, 0) \, ds - (\boldsymbol{X}_t^g - \boldsymbol{X}_0^g)$ is a continuous process with finite variation such that : for any continuous $(\mathcal{F}_t)$-adapted process $\boldsymbol{\alpha}_t$ with values in $\mathbb{R}^2$, for $\mathbb{P}$-a.e. ω, $\forall 0 \leq s \leq t < \infty$,*

$$
\int_s^t \Pi(\boldsymbol{X}_u^g) \, du \leq \int_s^t \Pi(\boldsymbol{\alpha}_u) \, du + \int_s^t (\boldsymbol{X}_u^g - \boldsymbol{\alpha}_u).d\boldsymbol{K}_u^g. \tag{5.10}
$$

Remark 2 *A condition equivalent to (5.10) is the following : for any continuous $(\mathcal{F}_t)$-adapted process $\boldsymbol{\alpha}_t$ with values in B, the measure on $\mathbb{R}_+$:*

$$
(\boldsymbol{X}_u^g - \alpha_u).(d\boldsymbol{K}_u^g - \nabla\Pi(\alpha_u) \, du)
$$

is $\mathbb{P}$-a.s. nonnegative.

Since (5.8) ensures that $\boldsymbol{x} = (x, y) \mapsto (g(t)y, 0)$ is (uniformly in time) Lipschitz and with linear growth, according to E. Cépa [25], we have :

Proposition 3 *Under the assumption (5.8), for any $b > 0$, the multivalued SDE (5.9) has a unique strong solution.*

We are now going to recover a solution to (5.6) from the solution of (5.9). More precisely, we follow the method of E. Cépa and D. Lépingle [27] (see Lemmas 3.3, 3.4 and 3.6) in order to identify the process $\boldsymbol{K}_t^g$.

We can thus show that for all $0 < t < \infty$, we have :

$$\mathbb{E}\left(\int_0^t |\partial\Pi(\boldsymbol{X}_u^g)|\, du\right) < \infty, \text{ with convention } |\partial\Pi(\boldsymbol{x})| = +\infty \text{ if } \boldsymbol{x} \notin B.$$

As a consequence, for any $0 < t < \infty$, $\mathbb{P}$-a.s.,

$$\int_0^t \frac{1}{1 - \frac{\left|\boldsymbol{X}_u^g\right|^2}{b}}\, du < \infty \text{ with convention } \frac{1}{1 - \frac{b}{b}} = +\infty. \qquad (5.11)$$

Moreover, the process $\boldsymbol{K}_t^g$ is $\mathbb{P}$-a.s. absolutely continuous on $\{0 \le u < \infty,\ \boldsymbol{X}_u^g \in B\}$, with density $\nabla\Pi(\boldsymbol{X}_u^g)$ so that $d\boldsymbol{K}_u^g$ has the following form :

$$d\boldsymbol{K}_u^g = \nabla\Pi(\boldsymbol{X}_u^g)\, du + d\boldsymbol{G}_u^g, \qquad (5.12)$$

where $\boldsymbol{G}^g$ is a continuous boundary process with finite variation $|\boldsymbol{G}^g|$:

$$\boldsymbol{G}_t^g = \int_0^t 1_{\{\boldsymbol{X}_u^g \in \partial B\}} d\boldsymbol{K}_u^g = \int_0^t 1_{\{\boldsymbol{X}_u^g \in \partial B\}} d\boldsymbol{G}_u^g. \qquad (5.13)$$

Finally, one can identify this process $\boldsymbol{G}_t^g$: for all $t \ge 0$,

$$\boldsymbol{G}_t^g = \int_0^t 1_{\{\boldsymbol{X}_u^g \in \partial B\}} \boldsymbol{n}(\boldsymbol{X}_u^g) d|\boldsymbol{G}^g|_u = \int_0^t \frac{\boldsymbol{X}_u^g}{\sqrt{b}} d|\boldsymbol{G}^g|_u,$$

where, for any $\boldsymbol{x} \in \partial B$, $\boldsymbol{n}(\boldsymbol{x}) = \frac{\boldsymbol{x}}{\sqrt{b}}$ is the unitary outward normal to B at the point $\boldsymbol{x}$.

Hence the process $\boldsymbol{X}_t^g$ is solution of the following SDE with normal reflexion at the boundary of B :

$$d\boldsymbol{X}_t^g = -\nabla\Pi(\boldsymbol{X}_t^g)\, dt + (g(t)Y_t^g, 0)\, dt + d\boldsymbol{W}_t - 1_{\{\boldsymbol{X}_t^g \in \partial B\}} \boldsymbol{n}(\boldsymbol{X}_t^g) d|\boldsymbol{G}^g|_t.$$

It just remains to show that $|\boldsymbol{G}^g|_u = 0$, for $u \ge 0$, in order to recover (5.6). Notice in particular that by (5.11), the property of integrability of the drift term in (5.6) holds for the solution $\boldsymbol{X}_t^g$ of the multivalued SDE (5.9).

Lemma 1 $|\boldsymbol{G}^g| = 0$.

Proof. We follow here again the ideas of E. Cépa and D. Lépingle [27] (see Lemma 3.8 p. 438) to prove that $|\boldsymbol{G}^g| = 0$. Let us consider $R_t^g = b - |\boldsymbol{X}_t^g|^2$. By Itô's formula,

$$
\begin{aligned}
dR_t^g &= -2\boldsymbol{X}_t^g.d\boldsymbol{X}_t^g - 2\,dt, \\
&= 2\nabla\Pi(\boldsymbol{X}_t^g).\boldsymbol{X}_t^g\,dt - 2g(t)X_t^g Y_t^g\,dt - 2\,dt - 2\boldsymbol{X}_t^g.d\boldsymbol{W}_t + 2\frac{|\boldsymbol{X}_t^g|^2}{\sqrt{b}}\,d|\boldsymbol{G}^g|_t, \\
&= \frac{b^2}{R_t^g}\,dt - 2g(t)X_t^g Y_t^g\,dt - (2+b)\,dt - 2\boldsymbol{X}_t^g.d\boldsymbol{W}_t + 2\sqrt{b}\,d|\boldsymbol{G}^g|_t, \quad (5.14)
\end{aligned}
$$

the last equality using the fact that $d|\boldsymbol{G}^g|_t = 1_{\{\boldsymbol{X}_t^g \in \partial B\}}d|\boldsymbol{G}^g|_t$.

We know that R_t^g is a continuous semimartingale with values in $[0, b]$. We want to prove that $dR_t^g = 1_{R_t^g > 0}dR_t^g$. Using Tanaka's formula (see Ref. [134] Theorem 1.2 p. 207),

$$
R_t^g = (R_t^g)^+ = (R_0^g)^+ + \int_0^t 1_{R_s^g > 0}\,dR_s^g + \frac{1}{2}L_t^0, \quad (5.15)
$$

where, for any $a \in [0, b]$, L_t^a denotes the local time in a of R^g. Using now the occupation times formula (see Ref. [134] Corollary 1.6 p. 209), we know (using (5.11)) that, for any fixed $t > 0$:

$$
\int_0^b \frac{1}{a}L_t^a\,da = \int_0^t \frac{1}{R_s^g}\,d<R^g>_s \le 4\int_0^t \frac{1}{1 - \frac{|\boldsymbol{X}_s^g|^2}{b}}\,ds < \infty.
$$

Since $a \mapsto L_t^a$ is a.s. cadlag (see Ref. [134] Theorem 1.7 p. 209), we deduce that for any $t > 0$, $\mathbb{P}$-a.s., $L_t^0 = 0$. Using this in (5.15), we obtain

$$
dR_t^g = 1_{R_t^g > 0}\,dR_t^g.
$$

Using this equality in (5.14), we have : $\forall t \ge 0$,

$$
\int_0^t 1_{R_s^g = 0}d|\boldsymbol{G}^g|_s =
$$
$$
\frac{1}{2\sqrt{b}}\int_0^t 1_{R_s^g = 0}\left(-\frac{b^2}{R_s^g}\,ds + 2g(s)X_s^g Y_s^g\,ds + (2+b)\,ds + 2\boldsymbol{X}_s^g.d\boldsymbol{W}_s\right).
$$

Since, according to (5.11), $\mathbb{P}$-a.s., $\{0 \le t < \infty, R_t^g = 0\}$ has zero Lebesgue measure, the right hand side is nul. We conclude by using $d|\boldsymbol{G}^g|_t = 1_{R_t^g = 0}d|\boldsymbol{G}^g|_t$. $\quad\square$

We have thus shown the following properties on the process $\boldsymbol{X}_t^g$:

– for any $0 < t < \infty$, $\mathbb{P}$-a.s., $\displaystyle\int_0^t \frac{1}{1 - \frac{|\boldsymbol{X}_u^g|^2}{b}}\,du < \infty$,

– $d\boldsymbol{X}_t^g = -\nabla\Pi(\boldsymbol{X}_t^g)\,dt + (g(t)Y_t^g, 0)\,dt + d\boldsymbol{W}_t$.

We have thus built a solution $\boldsymbol{X}_t^g = (X_t^g, Y_t^g)$ to our initial problem (5.6) in case $g \in L^\infty(\mathbb{R}_+)$. This result is not sufficient in our context since the energy estimates on the coupled system (5.1-5.3) yields less regularity on g (see Ref. [85]).

5.2.3 Existence in the case $g \in L^1_{\mathbf{loc}}(\mathbb{R}_+)$

We now want to build a solution to (5.6) using the multivalued SDE (5.9), but with a weaker assumption on g, namely (5.4). In this case, the general results of existence on multivalued SDE do not apply immediatly.

Therefore, we consider the following sequence of approximations of this problem :

$$\begin{cases} d\boldsymbol{X}_t^{g^n} + \partial\Pi(\boldsymbol{X}_t^{g^n})\, dt \ni (g^n(t)Y_t^{g^n}, 0)\, dt + d\boldsymbol{W}_t, \\ \boldsymbol{X}_0^{g^n} = \boldsymbol{X}_0, \end{cases} \tag{5.16}$$

where $n \in \mathbb{N}^*$ and $g^n(t) = (-n) \vee (n \wedge g(t))$. Since g^n is bounded, the results of the previous section apply and we obtain a unique solution $\boldsymbol{X}_t^{g^n}$ of the multivalued SDE (5.16). Moreover, these processes $\boldsymbol{X}_t^{g^n}$ are such that :

– for any $0 < t < \infty$, $\mathbb{P}$-a.s., $\displaystyle\int_0^t \frac{1}{1 - \frac{|\boldsymbol{X}_u^{g^n}|^2}{b}}\, du < \infty$,

–

$$\boldsymbol{X}_t^{g^n} = \boldsymbol{X}_0 - \int_0^t \nabla\Pi(\boldsymbol{X}_s^{g^n})\, ds + \int_0^t (g^n(s)Y_s^{g^n}, 0)\, ds + \boldsymbol{W}_t. \tag{5.17}$$

We now want to let n go to ∞ in Definition 2 (notice that by (5.17), $d\boldsymbol{K}_t^{g^n} = \nabla\Pi(\boldsymbol{X}_t^{g^n})\, dt$). In the following, we choose $T > 0$ and we work on the time interval $[0, T]$. We know that for all n, $\sup_{t \geq 0} \left|\boldsymbol{X}_t^{g^n}\right|^2 \leq b$. For any $n \geq m$, we have, by Itô's formula,

$$\begin{aligned} d\left|\boldsymbol{X}_t^{g^n} - \boldsymbol{X}_t^{g^m}\right|^2 &= -\left(\nabla\Pi(\boldsymbol{X}_t^{g^n}) - \nabla\Pi(\boldsymbol{X}_t^{g^m})\right).\left(\boldsymbol{X}_t^{g^n} - \boldsymbol{X}_t^{g^m}\right)\, dt \\ &\quad + \left(g^n(t)Y_t^{g^n} - g^m(t)Y^{g^m}(t)\right)\left(X_t^{g^n} - X_t^{g^m}\right)\, dt. \end{aligned}$$

Using the fact that, since Π is convex, for any $\boldsymbol{x}$ and $\boldsymbol{y} \in B$, $(\nabla\Pi(\boldsymbol{x}) - \nabla\Pi(\boldsymbol{y})).(\boldsymbol{x} - \boldsymbol{y}) \geq 0$, we obtain : $\forall t \in [0, T]$,

$$\left|\boldsymbol{X}_t^{g^n} - \boldsymbol{X}_t^{g^m}\right|^2 \leq \int_0^t \left(g^n(s)Y^{g^n}(s) - g^m(s)Y^{g^m}(s)\right)\left(X_s^{g^n} - X_s^{g^m}\right)\, ds$$

so that : $\forall t \in [0, T]$,

$$\begin{aligned} \left|\boldsymbol{X}_t^{g^n} - \boldsymbol{X}_t^{g^m}\right|^2 &\leq \int_0^t \left|g^n(s)Y_s^{g^n} - g^m(s)Y_s^{g^m}\right|\left|X_s^{g^n} - X_s^{g^m}\right|\, ds \\ &\leq \int_0^t \left(|g^n(s)|\left|Y_s^{g^n} - Y_s^{g^m}\right| + \left|Y_s^{g^m}\right||g^n(s) - g^m(s)|\right)\left|X_s^{g^n} - X_s^{g^m}\right|\, ds \\ &\leq \frac{1}{2}\int_0^t |g|(s)\left|\boldsymbol{X}_s^{g^n} - \boldsymbol{X}_s^{g^m}\right|^2\, ds + 2b\int_0^t |g^n(s) - g^m(s)|\, ds. \end{aligned}$$

Using Gronwall Lemma, we then obtain :

$$
\begin{aligned}
\sup_{t \in [0,T]} \left| \boldsymbol{X}_t^{g^n} - \boldsymbol{X}_t^{g^m} \right|^2 & \leq 2b \int_0^T \exp\left(\frac{1}{2} \int_s^T |g(u)|\, du \right) |g^n(s) - g^m(s)|\, ds \\
& \leq 2b \exp\left(\frac{1}{2} \|g\|_{L_t^1([0,T])} \right) \int_0^T |g^n(s) - g^m(s)|\, ds.
\end{aligned}
$$

From this inequality and the fact that $g \in L_t^1([0,T])$, we deduce that there exists a continuous adapted process $\boldsymbol{X}_t^g$ with values in $\overline{B}$ such that $\boldsymbol{X}_t^{g^n} \to \boldsymbol{X}_t^g$ in $L_\omega^\infty(L_t^\infty([0,T]))$.

One has the following estimate on the total variation of $\nabla \Pi(\boldsymbol{X}_u^{g^n})\, du$ on $[0,T]$:

$$
\int_0^T \left| \nabla \Pi(\boldsymbol{X}_t^{g^n}) \right| dt \leq \frac{\sqrt{b}}{2} \int_0^T \frac{1}{1 - \frac{|\boldsymbol{X}_s^{g^n}|^2}{b}}\, ds. \tag{5.18}
$$

By Itô's formula, we know that : $\forall t \in [0,T]$,

$$
|\boldsymbol{X}_t^{g^n}|^2 = |\boldsymbol{X}_0|^2 - \int_0^t \frac{|\boldsymbol{X}_s^{g^n}|^2}{1 - \frac{|\boldsymbol{X}_s^{g^n}|^2}{b}}\, ds + 2 \int_0^t g^n(s)\, X_s^{g^n} Y_s^{g^n}\, ds + 2t + 2 \int_0^t \boldsymbol{X}_s^{g^n}.d\boldsymbol{W}_s,
$$

which yields : $\forall t \in [0,T]$,

$$
\begin{aligned}
\int_0^t \frac{1}{1 - \frac{|\boldsymbol{X}_s^{g^n}|^2}{b}}\, ds & = \frac{1}{b}\left(-|\boldsymbol{X}_t^{g^n}|^2 + |\boldsymbol{X}_0|^2 + (2+b)t + 2\int_0^t g^n(s)\, X_s^{g^n} Y_s^{g^n}\, ds \right. \\
& \left. + 2\int_0^t \boldsymbol{X}_s^{g^n}.d\boldsymbol{W}_s \right).
\end{aligned} \tag{5.19}
$$

It is obvious that $\int_0^t \boldsymbol{X}_s^{g^n}.d\boldsymbol{W}_s \to \int_0^t \boldsymbol{X}_s.d\boldsymbol{W}_s$ in $L_\omega^2(L_t^\infty([0,T]))$-norm. Up to the extraction of a subsequence, we can suppose that this convergence holds for almost every ω. Using this property together with (5.18) and (5.19), we deduce that for a.e. ω, the measure $\nabla \Pi(\boldsymbol{X}_t^{g^n})\, dt$ on $[0,T]$ is such that $\int_0^T \left| \nabla \Pi(\boldsymbol{X}_t^{g^n}) \right| dt < C(T,\omega)$ where $C(T,\omega)$ is a constant only depending on T and ω. One can thus extract a weakly converging subsequence of $\left(\nabla \Pi(\boldsymbol{X}_t^{g^n})\, dt \right)_{n \geq 1}$. On the other hand, taking the limit $n \to \infty$ in (5.17), we see that $\int_0^t \nabla \Pi(\boldsymbol{X}_u^{g^n})\, du$ uniformly converges on $[0,T]$ to $\boldsymbol{K}_t^g$ satisfying : $\forall t \in [0,T]$,

$$
\boldsymbol{K}_t^g = \int_0^t (g(u)Y_u^g, 0)\, du + \boldsymbol{W}_t - (\boldsymbol{X}_t^g - \boldsymbol{X}_0).
$$

By identification of the limit, we have $\nabla \Pi(\boldsymbol{X}_t^{g^n})\, dt \rightharpoonup d\boldsymbol{K}_t^g$ weakly.

By Definition 2, the processes $\boldsymbol{X}_t^{g^n}$ are such that for any continuous $(\mathcal{F}_t)$-adapted process $\boldsymbol{\alpha}_t$ with values in $\mathbb{R}^2$, for $\mathbb{P}$-a.e. ω, $\forall\, 0 \leq s \leq t < \infty$,

$$
\int_s^t \Pi(\boldsymbol{X}_u^{g^n})\, du \leq \int_s^t \Pi(\boldsymbol{\alpha}_u)\, du + \int_s^t (\boldsymbol{X}_u^{g^n} - \boldsymbol{\alpha}_u).\nabla \Pi(\boldsymbol{X}_u^{g^n})\, du. \tag{5.20}
$$

One can pass to the limit $n \to \infty$ in (5.20), using the fact that $\Pi(\boldsymbol{X}_u^{g^n}) \to \Pi(\boldsymbol{X}_u^g)$ pointwise in u and that $\Pi(\boldsymbol{X}_u^{g^n})$ is uniformly integrable. Indeed, for any $A \geq \frac{b}{4}$, if we set $M_u = \left(1 - \frac{\left| \boldsymbol{X}_u^{g^n} \right|^2}{b} \right)^{-1}$, we have (since $x \mapsto \frac{\ln(x)}{x}$ is decreasing on $[e, +\infty)$) :

$$
\begin{aligned}
\int_0^T 1_{\left| \Pi(\boldsymbol{X}_u^{g^n}) \right| \geq A} \Pi(\boldsymbol{X}_u^{g^n}) \, du &= \frac{b}{4} \int_0^T 1_{M_u \geq \exp(4A/b)} \frac{\ln(M_u)}{M_u} M_u \, du \\
&\leq \frac{A}{\exp(4A/b)} C(T, \omega),
\end{aligned}
$$

so that $\displaystyle \int_0^T 1_{\left| \Pi(\boldsymbol{X}_u^{g^n}) \right| \geq A} \Pi(\boldsymbol{X}_u^{g^n}) \, du \to 0$ uniformly in n when $A \to \infty$. We have thus obtained a continuous process $\boldsymbol{X}_t^g$ on $[0, T]$ and a continuous process with finite variation $\boldsymbol{K}_t^g = \int_0^t (g(u) Y_u^g, 0) \, du + \boldsymbol{W}_t - (\boldsymbol{X}_t^g - \boldsymbol{X}_0)$ on $[0, T]$ such that for any continuous $(\mathcal{F}_t)$-adapted process $\boldsymbol{\alpha}_t$ with values in $\mathbb{R}^2$, for $\mathbb{P}$-a.e. ω, $\forall 0 \leq s \leq t < T$,

$$
\int_s^t \Pi(\boldsymbol{X}_u^g) \, du \leq \int_s^t \Pi(\boldsymbol{\alpha}_u) \, du + \int_s^t (\boldsymbol{X}_u^g - \boldsymbol{\alpha}_u) . d\boldsymbol{K}_u^g.
$$

This shows that we have built a solution to the multivalued SDE (5.9) on the time interval $[0, T]$. Since T is arbitrary, using Proposition 2, we have built a solution on $\mathbb{R}_+$. Following again the arguments of the last section it is easy to show that :
- for any $0 < t < \infty$, $\mathbb{P}$-a.s., $\displaystyle \int_0^t \frac{1}{1 - \frac{\left| \boldsymbol{X}_u^g \right|^2}{b}} \, du < \infty$,
- $d\boldsymbol{X}_t^g = -\nabla \Pi(\boldsymbol{X}_t^g) \, dt + (g(t) Y_t^g, 0) \, dt + d\boldsymbol{W}_t$.

This shows that $\boldsymbol{X}_t^g$ is a solution to (5.6) and completes the proof of Proposition 1.

5.3   Does the solution reach the boundary ?

In this section, we want to determine whether or not the process $\boldsymbol{X}_t^g$ we have built in the previous section reaches the boundary of B. Should the occasion arise, we deduce that uniqueness does not hold for (5.6), at least in the case $g = 0$. Throughout this section, we suppose that the initial condition is such that $\mathbb{P}(|\boldsymbol{X}_0|^2 < b) = 1$.

5.3.1   Necessary and sufficient conditions

In this section, we want to analyze the event $\{ \exists t > 0, |\boldsymbol{X}_t^g|^2 = b \}$. We are going to prove :

Proposition 4 *Assume*

$$
g \in L^2(\mathbb{R}_+), \tag{5.21}
$$

and that $\mathbb{P}(|\boldsymbol{X}_0|^2 < b) = 1$. Let us consider the process $\boldsymbol{X}_t^g$ solution to (5.6) built above. We have :

– *if $b \geq 2$, then $\mathbb{P}\left(\exists t > 0, |\boldsymbol{X}_t^g|^2 = b\right) = 0$,*
– *if $b < 2$, then $\mathbb{P}\left(\exists t > 0, |\boldsymbol{X}_t^g|^2 = b\right) = 1$.*

In view of Proposition 2, we deduce immediatly :

Corollary 1 *If $b \geq 2$ and $\mathbb{P}(|\boldsymbol{X}_0|^2 < b) = 1$, then trajectorial uniqueness holds for (5.6).*

   Proof. First, by Girsanov Lemma, one can suppose $g = 0$. Indeed, let us consider the process $\boldsymbol{X}_t^g$ we have built in last section. Under the probability $\mathbb{P}^g$ defined by

$$\frac{d\mathbb{P}^g}{d\mathbb{P}} = \exp\left(-\int_0^\infty g(s)Y_s^g \, dV_s - \frac{1}{2}\int_0^\infty \left(g(s)Y_s^g\right)^2 \, ds\right),$$

the process $(V_t^g, W_t^g) = (V_t + \int_0^t g(s)Y_s^g \, ds, W_t)$ is a Brownian motion and therefore $(X_t^g, Y_t^g, V_t^g, W_t^g, \mathbb{P}^g)_{t\in\mathbb{R}_+}$ is a weak solution of the SDE (5.5) with $g = 0$. Since this solution is with values in $\overline{B}$, it is also a weak solution of the multivalued SDE (5.9), with $g = 0$, for which uniqueness in law holds. Since $\mathbb{P}^g$ and $\mathbb{P}$ are equivalent on $\mathcal{F}$, we can then deduce the properties of Proposition 4 in case $g \in L^2(\mathbb{R}_+)$ from the properties of Proposition 4 in case $g = 0$.
   In the following, we focus on the solution to (5.9) with $g = 0$, which we denote by $\boldsymbol{X}_t = (X_t, Y_t)$. We fix $\boldsymbol{x} \in B$ and the superscript $\boldsymbol{x}$ means that we consider the solution to (5.9) with $g = 0$ such that $\boldsymbol{X}_0 = \boldsymbol{x}$.
   Let us first suppose that $|\boldsymbol{x}| > 0$. Let us consider the process $R_t^{\boldsymbol{x}} = b - |\boldsymbol{X}_t^{\boldsymbol{x}}|^2$. We know that :

$$dR_t^{\boldsymbol{x}} = \frac{b^2}{R_t^{\boldsymbol{x}}} \, dt - (2+b) \, dt - 2\boldsymbol{X}_t^{\boldsymbol{x}}.d\boldsymbol{W}_t. \tag{5.22}$$

Let us introduce the stopping time

$$\tau_n^{\boldsymbol{x}} = \inf\left\{t \geq 0, |\boldsymbol{X}_t^{\boldsymbol{x}}|^2 \geq b\left(1 - \frac{1}{n}\right)\right\}.$$

Let fix $t > 0$. By Girsanov Lemma, one shows that $\mathbb{P}$-a.s., $\left|\boldsymbol{X}_{t\wedge\tau_n^{\boldsymbol{x}}}^{\boldsymbol{x}}\right| \neq 0$. Indeed, by definition of $\tau_n^{\boldsymbol{x}}$,

$$\mathbb{P}(|\boldsymbol{X}_{t\wedge\tau_n^{\boldsymbol{x}}}^{\boldsymbol{x}}| = 0) = \mathbb{P}(|\boldsymbol{X}_t^{\boldsymbol{x}}| = 0 \text{ and } t < \tau_n^{\boldsymbol{x}}).$$

Let $\mathbb{P}_n^{\boldsymbol{x}}$ be defined by :

$$\frac{d\mathbb{P}_n^{\boldsymbol{x}}}{d\mathbb{P}} = \exp\left(\int_0^t \nabla\Pi(\boldsymbol{X}_{s\wedge\tau_n^{\boldsymbol{x}}}^{\boldsymbol{x}}).d\boldsymbol{W}_s - \frac{1}{2}\int_0^t \left|\nabla\Pi(\boldsymbol{X}_{s\wedge\tau_n^{\boldsymbol{x}}}^{\boldsymbol{x}})\right|^2 \, ds\right)$$

and $\mathbb{E}_n^{\boldsymbol{x}}$ denote the corresponding expectation. By Girsanov Theorem, $\left(\boldsymbol{B}_s^{\boldsymbol{x}} = \boldsymbol{x} + \boldsymbol{W}_s - \int_0^s \nabla\Pi(\boldsymbol{X}_{u\wedge\tau_n^{\boldsymbol{x}}}^{\boldsymbol{x}}) \, du\right)_{s\leq t}$ is a $\mathbb{P}_n^{\boldsymbol{x}}$-Brownian motion starting from $\boldsymbol{x}$. Since on $t \leq \tau_n^{\boldsymbol{x}}$, $\boldsymbol{X}_t^{\boldsymbol{x}} = \boldsymbol{B}_t^{\boldsymbol{x}}$,

$$
\begin{aligned}
\mathbb{P}(|\boldsymbol{X}_t^{\boldsymbol{x}}| = 0 \text{ and } t < \tau_n^{\boldsymbol{x}}) &\leq \mathbb{P}(|\boldsymbol{B}_t^{\boldsymbol{x}}| = 0) \\
&= \mathbb{E}_n^{\boldsymbol{x}}\left(1_{|\boldsymbol{B}_t^{\boldsymbol{x}}|=0}\frac{d\mathbb{P}}{d\mathbb{P}_n^{\boldsymbol{x}}}\right) \\
&= 0. \tag{5.23}
\end{aligned}
$$

One can therefore show that $|\boldsymbol{X}_t^{\boldsymbol{x}}| > 0$ on $[0, T^{\boldsymbol{x}})$, where

$$T^{\boldsymbol{x}} = \lim_{n \to \infty} \tau_n^{\boldsymbol{x}} = \inf \left\{ t \geq 0, |\boldsymbol{X}_t^{\boldsymbol{x}}|^2 = b \right\} = \inf \left\{ t \geq 0, R_t^{\boldsymbol{x}} = 0 \right\}.$$

Thus, one can write, for $t \in [0, T^{\boldsymbol{x}})$:

$$dR_t^{\boldsymbol{x}} = \frac{b^2}{R_t^{\boldsymbol{x}}} \, dt - (2 + b) \, dt + 2\sqrt{b - R_t^{\boldsymbol{x}}} \, d\beta_t, \qquad (5.24)$$

where β_t is a $\mathcal{F}_t$-adapted 1-dimensional Brownian motion.
    Let us now introduce the stopping time

$$S^{\boldsymbol{x}} = \inf \left\{ t \geq 0, R_t^{\boldsymbol{x}} \notin (0, b) \right\}.$$

We have, $\mathbb{P}$-a.s., $S^{\boldsymbol{x}} \leq T^{\boldsymbol{x}}$. We refer here to I. Karatzas and S.E. Shreve [87] (see Section 5.5 p. 342-351).
    We introduce a scale function p such that :

$$\left(\frac{b^2}{r} - (2 + b) \right) p'(r) + 2(b - r)p''(r) = 0,$$

which leads to :
$$p'(r) = C(b - r)^{-1} r^{-b/2},$$

where $C > 0$. We have therefore $p(b-) = +\infty$ and $(b < 2 \iff p(0+) > -\infty)$. Using this property of the scale function and the results of I. Karatzas and S.E. Shreve, one can conclude that :

$$\text{if } b \geq 2, \text{ then } \mathbb{P}\left(S^{\boldsymbol{x}} = +\infty \right) = \mathbb{P}\left(T^{\boldsymbol{x}} = +\infty \right) = 1, \qquad (5.25)$$

$$\text{if } b < 2, \text{ then } \mathbb{P}\left(\lim_{t \to S^{\boldsymbol{x}}} |\boldsymbol{X}_t^{\boldsymbol{x}}|^2 = b \right) = 1.$$

In case $b < 2$, we can deduce from the second item that $S^{\boldsymbol{x}} = T^{\boldsymbol{x}}$. We now want to know whether $S^{\boldsymbol{x}} = +\infty$ or not in this case. Let us introduce the speed measure m on $(0, b)$ defined by

$$m(dr) = \frac{2 \, dr}{4(b - r)p'(r)} = \frac{r^{b/2} dr}{2C},$$

and the function v such that, for any $r \in (0, b)$,

$$v(r) = \int_a^r (p(r) - p(s))m(ds) = \int_a^r (p(r) - p(s))\frac{s^{b/2}}{2C} \, ds.$$

We have $p(b-) = +\infty$ and therefore $v(b-) = +\infty$. In case $b < 2$, it is easy to check that $v(0+) < \infty$. Using again the results of I. Karatzas and S.E. Shreve, we can deduce from this that in case $b < 2$, we have

$$\mathbb{P}(S^{\boldsymbol{x}} < \infty) = \mathbb{P}(T^{\boldsymbol{x}} < \infty) = 1. \qquad (5.26)$$

In case $|\boldsymbol{x}| = 0$, the former results (5.25) and (5.26) still hold. Indeed, let us suppose that $\boldsymbol{x} = \boldsymbol{0}$ and let us introduce the stopping time $\tau = \inf \left\{ t \geq 0, |\boldsymbol{X}_t^{\boldsymbol{0}}|^2 \geq \frac{b}{2} \right\}$. Obvisouly, one has :

$$\mathbb{P}\left(\exists t > 0, |\boldsymbol{X}_t^{\boldsymbol{0}}|^2 = b\right) = \mathbb{P}\left(\exists t > 0, |\boldsymbol{X}_t^{\boldsymbol{0}}|^2 = b \text{ and } \tau < \infty\right).$$

In case $b \geq 2$, using the strong Markov property of $\boldsymbol{X}_t^{\boldsymbol{0}}$ (see E. Cépa [25] p. 86), one has :

$$
\begin{aligned}
\mathbb{P}\left(\exists t > 0, |\boldsymbol{X}_t^{\boldsymbol{0}}|^2 = b\right) &= \mathbb{P}\left(\exists t > 0, |\boldsymbol{X}_t^{\boldsymbol{0}}|^2 = b \text{ and } \tau < \infty\right), \\
&= \mathbb{E}\left(1_{\tau < \infty} \mathbb{P}\left(\exists t > 0, |\boldsymbol{X}_t^{\boldsymbol{x}}|^2 = b\right)|_{\boldsymbol{x} = \boldsymbol{X}_\tau}\right), \\
&= 0.
\end{aligned}
$$

In case $b < 2$, we use the fact that, due to the proof of (5.23), $\mathbb{P}(|\boldsymbol{X}_{1 \wedge \tau}^{\boldsymbol{0}}| = 0) = 0$. By the strong Markov property and since $\mathbb{P}$-a.s., $\sup_{t \in [0, 1 \wedge \tau]} |\boldsymbol{X}_t^{\boldsymbol{0}}|^2 < b$, we have $\mathbb{P}\left(\exists t > 0, |\boldsymbol{X}_t^{\boldsymbol{0}}|^2 = b\right) = \mathbb{E}\left(\mathbb{P}\left(\exists t > 0, |\boldsymbol{X}_t^{\boldsymbol{x}}|^2 = b\right)|_{\boldsymbol{x} = \boldsymbol{X}_{1 \wedge \tau}}\right) = 1$.

In case of a non-deterministic initial condition $\boldsymbol{X}_0$ with law μ_0, we can deduce the properties of Proposition 4 from the fact that (by uniqueness of the solution) :

$$\mathbb{P}\left(\exists t > 0, |\boldsymbol{X}_t|^2 = b\right) = \int \mathbb{P}\left(\exists t > 0, |\boldsymbol{X}_t^{\boldsymbol{x}}|^2 = b\right) \, d\mu_0(\boldsymbol{x}).$$

$\square$

Remark 3 *In case $g \in L_{loc}^2(\mathbb{R}_+)$, what we can conclude is the following :*
  – *if $b \geq 2$, then $\mathbb{P}\left(\exists t > 0, |\boldsymbol{X}_t^g|^2 = b\right) = 0$,*
  – *if $b < 2$, then $\mathbb{P}\left(\exists t > 0, |\boldsymbol{X}_t^g|^2 = b\right) > 0$.*

5.3.2 Non-uniqueness in case $b < 2$

In this section, we suppose $b < 2$ and $\mathbb{P}(|\boldsymbol{X}_0|^2 < b) = 1$. We restrict our attention to the case $g = 0$. We are going to construct another process $\tilde{\boldsymbol{X}}_t$ weak solution to (5.6) and such that $\mathbb{P}(\exists t > 0, \tilde{\boldsymbol{X}}_t \notin \overline{B}) = 1$. In other words, we will build a solution to (5.6) which, unlike $\boldsymbol{X}_t$, goes out of the ball $\overline{B}$. This will show that (5.6) admits at least two different solutions.

Let us consider the solution $\boldsymbol{X}_t$ to (5.6) we have built in Section 5.2. We know that $\mathbb{P}$-a.s., the process $\boldsymbol{X}_t$ reaches the boundary of B in finite time (see Proposition 4). Let us introduce the stopping time $T = \inf\{t \geq 0, |\boldsymbol{X}_t|^2 \geq b\}$. In polar coordinate, we write $\boldsymbol{X}_T = (\sqrt{b}, \theta_0) : (X_T, Y_T) = (\sqrt{b}\cos(\theta_0), \sqrt{b}\sin(\theta_0))$, where $\theta_0 \in [0, 2\pi)$ denotes the polar angle. We now want to construct a solution to (5.6), which takes (X_T, Y_T) as initial value, and lives outside of the ball $\overline{B}$. Let us introduce a two-dimensional standard Brownian motion (β_t, γ_t) independent of $\boldsymbol{W}_t$. We use a polar representation $(\sqrt{r_t}, \theta_t)$ of the process we want to build. We consider the solution r_t to the following multivalued SDE :

$$
\begin{cases}
dr_t + \partial f(r_t) \, dt \ni (2 + b) \, dt + 2\sqrt{r_t} d\beta_t, \\
r_0 = b,
\end{cases}
\tag{5.27}
$$

where $f : \mathbb{R} \to]-\infty, +\infty]$ is the convex function defined by :

$$f(r) = \begin{cases} -b^2 \ln(r - b) & \text{if } r > b, \\ +\infty & \text{otherwise.} \end{cases} \tag{5.28}$$

so that ∂f is a simple-valued maximal monotone operator with domain $I = (b, \infty)$ (for all $r > b$, $\partial f(r) = \{\nabla f(r)\} = \{\frac{b^2}{b-r}\}$). By E. Cépa [25], there exists a unique process r_t solution to (5.27). Following exactly the arguments of Lemma 1, one can show that this process r_t is such that :

- for any $0 < t < \infty$, $\mathbb{P}$-a.s., $\int_0^t \left| \dfrac{1}{r_u - b} \right| du < \infty$, with convention $\frac{1}{b-b} = +\infty$,
- $dr_t = -\frac{b^2}{b-r_t} dt + (2 + b) dt + 2\sqrt{r_t} d\beta_t$.

Let us now consider the process θ_t defined by :

$$\theta_t = \theta_0 + \int_0^t \frac{1}{\sqrt{r_s}} d\gamma_s, \tag{5.29}$$

and the random process $\bar{\boldsymbol{X}}_t$ in $\mathbb{R}^2$ defined by :

$$\bar{\boldsymbol{X}}_t = \left(\sqrt{r_t} \cos(\theta_t), \sqrt{r_t} \sin(\theta_t) \right).$$

By Itô's formula, we have :

$$d\bar{\boldsymbol{X}}_t = -\frac{1}{2} \frac{\bar{\boldsymbol{X}}_t}{1 - \frac{|\bar{\boldsymbol{X}}_t|^2}{b}} dt + (-\sin(\theta_t), \cos(\theta_t)) d\gamma_t + (\cos(\theta_t), \sin(\theta_t)) d\beta_t.$$

Using Paul Lévy characterisation, one can show that $(-\sin(\theta_t), \cos(\theta_t)) d\gamma_t + (\cos(\theta_t), \sin(\theta_t)) d\beta_t = d\boldsymbol{B}_t$ where $\boldsymbol{B}_t$ is a two-dimensional Brownian motion, independent of $\boldsymbol{W}_t$.

Let us now consider $\tilde{\boldsymbol{X}}_t$ defined by $\tilde{\boldsymbol{X}}_t = 1_{0 \leq t \leq T} \boldsymbol{X}_t + 1_{t > T} \bar{\boldsymbol{X}}_{t-T}$ and the process $\tilde{\boldsymbol{W}}_t$ defined by $\tilde{\boldsymbol{W}}_t = \boldsymbol{W}_{t \wedge T} + 1_{t > T} \boldsymbol{B}_{t-T}$. It is obvious (for example by Paul Lévy characterisation) that $\tilde{\boldsymbol{W}}_t$ is a Brownian motion. In addition, the process $\tilde{\boldsymbol{X}}_t$ is a solution to (5.6) with $g = 0$, such that $\mathbb{P}(\exists t > 0, \tilde{\boldsymbol{X}}_t \notin \overline{B}) = 1$. This shows that the problem (5.6) with $g = 0$ does not admit a unique solution.

Remark 4 *In case $g \in L^\infty_{loc}(\mathbb{R}_+)$, using the solution (r_t, θ_t) of the multivalued SDE : $(r_0, \theta_0) = (b, \theta_0)$ and*

$$d(r_t, \theta_t) + \partial h(r_t, \theta_t) dt \ni$$
$$\left((2 + b) + r_t \sin(\theta_t) g(t), -\sin^2(\theta_t) g(t) \right) dt + (2\sqrt{r_t}, \tfrac{1}{\sqrt{r_t}}) d(\beta_t, \gamma_t),$$

where $h : \mathbb{R}^2 \to]-\infty, +\infty]$ is the convex function defined by $h(r, \theta) = f(r)$ (see formula (5.28)), one can by the same arguments prove that there is non-uniqueness in law for the solutions to (5.6).

We have summarized in Table 5.1 some of the results we have obtained in the last two sections.

	$b < 2.$	$b \geq 2.$
$\mathbb{P}(|\boldsymbol{X}_0|^2 = b) = 0.$	Existence. $\mathbb{P}\left(\exists t \geq 0, |\boldsymbol{X}_t|^2 = b\right) = 1.$ Non-uniqueness.	Existence. $\mathbb{P}\left(\exists t \geq 0, |\boldsymbol{X}_t|^2 = b\right) = 0.$ Uniqueness.
$\mathbb{P}(|\boldsymbol{X}_0|^2 = b) > 0.$	Existence. Non-uniqueness.	Existence. Non-uniqueness

TAB. 5.1 – Properties of solutions to (5.6) when $g = 0$. We suppose $\mathbb{P}(|\boldsymbol{X}_0|^2 \leq b) = 1$. In any case, uniqueness holds for solutions with values in $\overline{B}$ according to Proposition 2. The terminology uniqueness and non uniqueness relates to a solution that is not enforced to take values in $\overline{B}$.

5.4 Invariant probability measure in case $g = 0$ and $b \geq 2$

In this section we are interested in invariant probability measures for the SDE (5.6) with $g = 0$ in case $b \geq 2$.

The motivation for this study is twofold. First, since we consider a fluid which is initially at rest, it is natural from a physical point of view to choose an invariant probability for the SDE (5.6) with $g = 0$ as law for $\boldsymbol{X}_0$. Second, in the analysis of the coupled system (5.1-5.3), we are interested in the regularity of the stress $\tau(t, y) = \mathbb{E}\left(\frac{X_t^y Y_t^y}{1 - \frac{(X_t^y)^2 + (Y_t^y)^2}{b}}\right)$ which, by Girsanov, can also be written in the following form :

$$\mathbb{E}\left(\left(\frac{X_t Y_t}{1 - \frac{X_t^2 + Y_t^2}{b}}\right) \exp\left(\int_0^t \partial_y u(s, y) Y_s \, dV_s - \frac{1}{2} \int_0^t (\partial_y u(s, y) Y_s)^2 \, ds\right)\right),$$

where $\boldsymbol{X}_t = (X_t, Y_t)$ denotes (as in last section) the solution with values in $\overline{B}$ to (5.6) with $g = 0$ (see Ref. [86]). This expression of the stress yields the following estimate (using Hölder inequality) : for almost all y and t,

$$|\tau(y, t)| \leq \mathbb{E}\left(\left(\frac{X_t Y_t}{1 - \frac{X_t^2 + Y_t^2}{b}}\right)^p\right)^{1/p} \exp\left(\frac{q-1}{2} b \int_0^t (\partial_y u(s, y))^2 \, ds\right),$$

where $p = \frac{q}{q-1}$.

It is thus important to estimate the quantities $\mathbb{E}\left(\left(\frac{X_t Y_t}{1 - \frac{X_t^2 + Y_t^2}{b}}\right)^p\right)$, which is simple if we identify and start under an invariant probability measure (see formula (5.31)).

The density p_0 defined by :

$$p_0(\boldsymbol{x}) = \frac{\exp(-2\Pi(\boldsymbol{x}))}{\int \exp(-2\Pi(\boldsymbol{x})) \, d\boldsymbol{x}} = \frac{b+2}{2\pi b}\left(1 - \frac{|\boldsymbol{x}|^2}{b}\right)^{b/2} 1_{|\boldsymbol{x}|^2 < b} \tag{5.30}$$

obviously solves div $_{\boldsymbol{x}} \left(-(\nabla_{\boldsymbol{x}} \Pi) p_0 + \frac{1}{2}(\nabla_{\boldsymbol{x}} p_0) \right) = 0$ and is therefore a natural candidate to be invariant. This is indeed the case as shown by :

Proposition 5 *For* $b \geq 2$, $p_0(\boldsymbol{x})\, d\boldsymbol{x}$ *is the unique invariant probability measure on* B *for the SDE (5.6) with* $g = 0$.

This proposition is a consequence of the following lemma :

Lemma 2 *Let* $b \geq 2$. *For any* $\boldsymbol{x} \in B$, $t > 0$, *the solution* $\boldsymbol{X}_t^{\boldsymbol{x}}$ *of the SDE (5.6) with* $g = 0$ *and* $\boldsymbol{X}_0 = \boldsymbol{x}$ *has a density* $p(t, \boldsymbol{x}, \boldsymbol{y})$ *with respect to the Lebesgue measure on* B. *In addition,* $\forall t \geq 0$,

(i) $d\boldsymbol{x}\, d\boldsymbol{y}$-*a.e.,* $\exp(-2\Pi(\boldsymbol{x})) p(t, \boldsymbol{x}, \boldsymbol{y}) = \exp(-2\Pi(\boldsymbol{y})) p(t, \boldsymbol{y}, \boldsymbol{x})$,

(ii) $\forall \boldsymbol{x} \in B$, $d\boldsymbol{y}$-*a.e.,* $p(t, \boldsymbol{x}, \boldsymbol{y}) > 0$.

Indeed, by (i), one easily checks that $p_0(\boldsymbol{x})\, d\boldsymbol{x}$ is invariant. By (ii), any invariant probability measure is equivalent to the Lebesgue measure on B which implies uniqueness (see Proposition 6.1.9 p. 188 of M. Duflo [40]).

With Proposition 5, it is then straightforward to prove that, if $\boldsymbol{X}_0$ has the density $p_0(\boldsymbol{x})$, then we have :

$$\mathbb{E}\left(\left(\frac{X_t Y_t}{1 - \frac{X_t^2 + Y_t^2}{b}} \right)^p \right) < \infty \iff b > 2(p - 1). \tag{5.31}$$

Let us now prove Lemma 2. **Proof.** In order to prove (i), we regularize the potential Π so that the results of L.C.G. Rogers [135] (see p. 161) apply. Let Π_n be defined by :

$$\Pi_n(\boldsymbol{x}) = \pi_n(|\boldsymbol{x}|^2), \tag{5.32}$$

$$\pi_n(r) = \begin{cases} -\dfrac{b}{4} \ln\left(1 - \dfrac{r}{b} \right) & \text{if } r \leq b\left(1 - \frac{1}{n} \right), \\ \sqrt{r} + \frac{b}{4} \ln(n) & \text{if } r \geq b, \end{cases} \tag{5.33}$$

and π_n is increasing and $\mathcal{C}^2(\mathbb{R}_+, \mathbb{R}_+)$, so that $\nabla \Pi_n$ is bounded with continuous derivatives of first order. Let $t > 0$ and $\boldsymbol{x} \in \mathbb{R}^2$. According to L.C.G. Rogers, the solution $\boldsymbol{X}^{n, \boldsymbol{x}}$ of the SDE :

$$\boldsymbol{X}_t^{n, \boldsymbol{x}} = \boldsymbol{x} - \int_0^t \nabla \Pi_n(\boldsymbol{X}_s^{n, \boldsymbol{x}})\, ds + \boldsymbol{W}_t, \tag{5.34}$$

has a density $p_n(t, \boldsymbol{x}, \boldsymbol{y})$ with respect to the Lebesgue measure on $\mathbb{R}^2$ which satisfies $d\boldsymbol{x}\, d\boldsymbol{y}$-a.e., $\exp(-2\Pi_n(\boldsymbol{x})) p_n(t, \boldsymbol{x}, \boldsymbol{y}) = \exp(-2\Pi_n(\boldsymbol{y})) p_n(t, \boldsymbol{y}, \boldsymbol{x})$. For $\boldsymbol{x} \in B$, let $\tau_n^{\boldsymbol{x}} = \inf \left\{ t \geq 0, |\boldsymbol{X}_t^{\boldsymbol{x}}|^2 \geq b\left(1 - \frac{1}{n} \right) \right\}$. Since $\mathbb{P}\left(\boldsymbol{X}_t^{n, \boldsymbol{x}} \neq \boldsymbol{X}_t^{\boldsymbol{x}} \right) \leq \mathbb{P}(\tau_n^{\boldsymbol{x}} < t)$, according to Proposition 4,

$$\lim_{n \to \infty} \mathbb{P}\left(\boldsymbol{X}_t^{n, \boldsymbol{x}} \neq \boldsymbol{X}_t^{\boldsymbol{x}} \right) = 0. \tag{5.35}$$

We deduce that for a fixed $\boldsymbol{x} \in B$, $p_n(t, \boldsymbol{x}, \boldsymbol{y})$ converges in $L_{\boldsymbol{y}}^1(\mathbb{R}^2)$ to $p(t, \boldsymbol{x}, \boldsymbol{y})$, which is the density of $\boldsymbol{X}_t^{\boldsymbol{x}}$.

As the non-negative potential Π_n converges pointwise to Π in B, we deduce that $\exp(-2\Pi_n(\boldsymbol{x})) p_n(t, \boldsymbol{x}, \boldsymbol{y})$ converges to $\exp(-2\Pi(\boldsymbol{x})) p(t, \boldsymbol{x}, \boldsymbol{y})$ in $L_{\boldsymbol{x}, \boldsymbol{y}}^1(B \times B)$ and conclude that (i) holds.

We are now going to check (ii) for a fixed $\boldsymbol{x} \in B$ and $t > 0$. Let A be a Borel subset of B such that $\int 1_A \, d\boldsymbol{x} > 0$. We choose $n \in \mathbb{N}^*$ such that $|\boldsymbol{x}|^2 < b \left(1 - \frac{1}{n} \right)$ and $\int 1_{A_n} \, d\boldsymbol{x} > 0$ where $A_n = A \cap B \left(0, \sqrt{b \left(1 - \frac{1}{n} \right)} \right)$. By Girsanov Theorem, under $\mathbb{P}_n^{\boldsymbol{x}}$ defined by :

$$\frac{d\mathbb{P}_n^{\boldsymbol{x}}}{d\mathbb{P}} = \exp \left(\int_0^t \nabla \Pi(\boldsymbol{X}_{s \wedge \tau_n^{\boldsymbol{x}}}^{\boldsymbol{x}}) . d\boldsymbol{W}_s - \frac{1}{2} \int_0^t \left| \nabla \Pi(\boldsymbol{X}_{s \wedge \tau_n^{\boldsymbol{x}}}^{\boldsymbol{x}}) \right|^2 ds \right),$$

where $\tau_n^{\boldsymbol{x}}$ is as above, $(\boldsymbol{X}_{s \wedge \tau_n^{\boldsymbol{x}}}^{\boldsymbol{x}})_{s \leq t}$ is a Brownian motion starting from $\boldsymbol{x}$ and stopped at the boundary of $B \left(0, \sqrt{b \left(1 - \frac{1}{n} \right)} \right)$ so that $\mathbb{P}_n^{\boldsymbol{x}} \left(\boldsymbol{X}_{t \wedge \tau_n^{\boldsymbol{x}}}^{\boldsymbol{x}} \in A_n \right) > 0$. Therefore, $\mathbb{P} \left(\boldsymbol{X}_t^{\boldsymbol{x}} \in A \right) \geq \mathbb{P} \left(\boldsymbol{X}_{t \wedge \tau_n^{\boldsymbol{x}}}^{\boldsymbol{x}} \in A_n \right) = \mathbb{E}_n^{\boldsymbol{x}} \left(1_{A_n} \left(\boldsymbol{X}_{t \wedge \tau_n^{\boldsymbol{x}}}^{\boldsymbol{x}} \right) \frac{d\mathbb{P}}{d\mathbb{P}_n^{\boldsymbol{x}}} \right) > 0$, which concludes the proof. $\qquad \square$

Acknowledgments

Chapitre 6

Analyse d'une méthode de réduction de variance

Les résultats présentés dans ce chapitre ont fait l'objet d'un article paru dans *Journal of Non-Newtonian Fluid Mechanics*. Nous analysons comment la variance des résultats obtenus par la méthode CONNFFESSIT dépend des paramètres numériques, et notamment de la manière dont le mouvement Brownien dépend de l'espace.

<div align="center">

On a variance reduction technique
for micro-macro simulations of polymeric fluids

</div>

<div align="center">

Benjamin Jourdain, Claude Le Bris, Tony Lelièvre

</div>

> The micro-macro simulations of polymeric fluids couple the mass and momentum conservation equations at the macroscopic level, with a stochastic differential equation which models the evolution of the polymer configurations at the microscopic level (Brownian dynamics simulation). Accordingly, the system is discretized by a finite element method coupled with a Monte Carlo method. All the discrete variables are random, and the accuracy of the result highly depends on the variance of these random variables. We give here some elements of numerical analysis on the crucial issue of variance reduction in order to get results of a better quality for a given computational cost. The present analytical study only deals with a one dimensional case, but nevertheless gives a track for computational strategies that may apply to the more physically relevant two and three dimensional cases.

Keywords : CONNFFESSIT, Dumbbells, FENE, Variance reduction

6.1 Introduction and motivation

6.1.1 Micro-macro models of dilute solutions

In this paper, we focus on some micro-macro models of dilute solutions of polymers. Let us introduce briefly these models which now give rise to a lively and expanding field of computational simulation for non-Newtonian fluid dynamics (we refer the reader to $[12, 13, 39, 46, 120]$ for some comprehensive surveys of the physical background). For the "macroscopic" part, the evolution of the velocity $\mathbf{u}$ and the pressure p is described by the momentum and mass conservation equations :

$$\rho \left(\frac{\partial \mathbf{u}}{\partial t} + \mathbf{u} \cdot \nabla \mathbf{u} \right) = \eta_s \Delta \mathbf{u} - \nabla p + \text{div} \left(\boldsymbol{\tau}_p \right) , \tag{6.1}$$

$$\text{div} \left(\mathbf{u} \right) = 0 , \tag{6.2}$$

where $\boldsymbol{\tau}_p$ is an extra-stress tensor, due to the contribution of polymers. In order to derive the expression of this extra-stress tensor, one can use kinetic models of polymers. We deal here with the "dumbbell" model (a particular case of the Rouse model) in which a polymer is described by two beads linked by a spring (see Figure 6.1). The expression of the entropic force $\mathbf{F}$ in the spring, in term of the so-called end-to-end vector $\boldsymbol{X}$, can have more or less complicated expression, depending on the effects taken into account (excluded volume effects, finite extensibility of the polymer,...). We deal here with two types of forces (but our method is likely to apply to other cases of forces) : a linear force : $\mathbf{F}(\boldsymbol{X}) = \mathbf{F}_{HOOK}(\boldsymbol{X}) = H\boldsymbol{X}$ (model of "Hookean dumbbells") or a non-linear force which takes into account the finite extensibility of the polymer (described by the non-dimensional parameter b) :

$\mathbf{F}(\boldsymbol{X}) = \mathbf{F}_{FENE}(\boldsymbol{X}) = H\dfrac{\boldsymbol{X}}{1-\frac{||\boldsymbol{X}||^2}{bk_BT/H}}$ (model of "FENE dumbbells"). The "microscopic" part of the model is the description of the evolution of the end-to-end vector $\boldsymbol{X}$ through a stochastic partial differential equation (Brownian dynamics simulation) :

$$dX + \mathbf{u} \cdot \nabla X \, dt = \left(\nabla \mathbf{u} X - \frac{2}{\zeta} \boldsymbol{F}(\boldsymbol{X})\right) dt + \frac{\sqrt{2}\sigma}{\zeta} d\mathbf{W}_t, \qquad (6.3)$$

where ζ is a friction coefficient, $\sigma^2 = 2k_BT\zeta$ (T is the temperature) and $\mathbf{W}_t$ is a standard (multi-dimensional) Brownian motion. The expression of this extra-stress
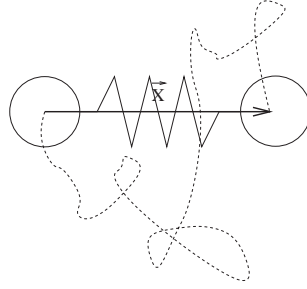

FIG. 6.1 – The polymer (in dashed line) is modeled by a "dumbbell" : two beads linked by a spring. The vector $\boldsymbol{X}$ which goes from one bead to the other is called the end-to-end vector.

tensor $\boldsymbol{\tau}_p$ is then given by an expectation of a function of the configurations of the polymers (this is the Kramers expression) :

$$\boldsymbol{\tau}_p = n\mathbb{E}(\mathbf{X} \otimes \mathbf{F}(\mathbf{X})) - nk_BT\mathrm{Id}, \qquad (6.4)$$

where n denotes the concentration of polymers.

It is to be noted that the "Hookean dumbbell" model described by equations (6.1), (6.2), (6.3) and (6.4), with $\boldsymbol{F} = \boldsymbol{F}_{HOOK}$ is equivalent to the famous Oldroyd-B model, which is usually written in a purely macroscopic differential or integral form (see [13] page 72). On the other hand, no closed differential or integral equations on $\boldsymbol{\tau}_p$ have been found to be equivalent to the more realistic FENE model. Being more general than the purely macroscopic approach, the micro-macro approach seems all the more promising.

Once the system (6.1)-(6.4) is non-dimensionalised, it has the following form :

$$\mathrm{Re}\left(\frac{\partial \mathbf{u}}{\partial t} + \mathbf{u} \cdot \nabla \mathbf{u}\right) = (1-\epsilon)\Delta \mathbf{u} - \nabla p + \mathrm{div}\,(\boldsymbol{\tau}_p), \qquad (6.5)$$

$$\mathrm{div}\,(\mathbf{u}) = 0, \qquad (6.6)$$

$$\boldsymbol{\tau}_p = \frac{\epsilon}{\mathrm{We}}(\mu\mathbb{E}(\boldsymbol{X} \otimes \boldsymbol{F}(\boldsymbol{X})) - \mathrm{Id}), \qquad (6.7)$$

$$dX + \mathbf{u} \cdot \nabla X \, dt = \left(\nabla \mathbf{u} X - \frac{1}{2\mathrm{We}} \boldsymbol{F}(\boldsymbol{X})\right) dt + \frac{1}{\sqrt{\mathrm{We}\,\mu}} d\mathbf{W}_t, \qquad (6.8)$$

with the following non-dimensional numbers :

$$\mathrm{Re} = \frac{\rho U L}{\eta} \ , \ \mathrm{We} = \frac{\lambda U}{L} \ , \ \epsilon = \frac{\eta_p}{\eta} \ , \ \mu = \frac{L^2 H}{k_b T} \ , \tag{6.9}$$

and the following non-dimensional forces :

$$\boldsymbol{F}_{HOOK}(\boldsymbol{X}) = \boldsymbol{X} \ , \ \boldsymbol{F}_{FENE}(\boldsymbol{X}) = \frac{\boldsymbol{X}}{1 - \frac{\mu \|\boldsymbol{X}\|^2}{b}} \ . \tag{6.10}$$

The numbers U and L denote the characteristic velocity and length, while λ (a relaxation time of the polymers) and η_p (the viscosity associated to the polymers) are defined by $\lambda = \frac{\zeta}{4H}$ and $\eta_p = n k_B T \lambda$. The total viscosity η is defined by $\eta = \eta_s + \eta_p$.

This problem can be discretized by the so-called CONNFFESSIT method (see [97]), coupling a finite element method to discretize equations (6.5)-(6.6), standard Euler schemes in time for (6.5) and (6.8), and a Monte Carlo method to approximate the stress $\boldsymbol{\tau}_p$ in (6.7). Compared with a deterministic approach which solves directly the Fokker-Planck equation associated to (6.8), the convergence of this stochastic approach scales efficiently with respect to the number of springs in the Rouse chain. However, the leading error in this kind of discretization is a statistical error due to the Monte Carlo method, and depends on the variance of the variables. Our aim here is to study the dependency of these variances in terms of the numerical parameters of the discretization.

More precisely, many authors (see Halin, Lielens, Keunings and Legat in [74] or Bonvin and Picasso in [15]) have observed that using a Brownian motion in (6.8) which does not depend on space, rather than a collection of Brownian motions uncorrelated from one Lagrangian trajectory to another, leads on the discretized problem to a reduction of the variance of the velocity **u** but also to an increase of the variance of the stress $\boldsymbol{\tau}_p$. After a discussion about the space-dependency of the Brownian motion in Section 6.2, we analyze in Section 6.3 this problem in the case of a pure shear flow. The momentum and mass conservation equations then reduce to a scalar heat equation (see Eq. (6.14) below). We then completely analyze the case of the long time behavior of the variances for Hookean dumbbells and recover by our analysis the observations mentioned above. We are also able to propose a strategy to reduce the variance on the stress in the shear flow case, at a given computational cost, by choosing an *ad hoc* correlation in space for the Brownian motion. In Section 6.4, we numerically test our strategy for Hookean and FENE springs in the one-dimensional case, leaving for the future numerical tests in dimensions 2 and 3. Other related issues are also addressed in this paper, such as the dependency of the variances in terms of the boundary conditions (see Remark 11) and the space step (see Section 6.5), or the dependency of the bias upon the number of realizations (see Section 6.5).

Remark 5 *Let us note that we do not consider in this paper other variance reduction methods like control variates or importance sampling, see [15, 113, 120] about these subjects. Our aim is not to compare the variance reduction obtained by using appropriate dependency on space of the Brownian motions with other variance reduction techniques, but rather to rigorously analyse in a simple case the influence of the dependency on space of the Brownian motions on the numerical results and particularly on their variances.*

6.2 The dependency of the Brownian motion in space

As mentioned above, the main subject of the present work is the dependency upon the space variable of the Brownian motion $\boldsymbol{W}_t$. Let us look at this question from different viewpoints : the modeling viewpoint, that of the numerical simulations, and the mathematical viewpoint.

6.2.1 The modeling viewpoint

We recall that the derivation of (6.8) from kinetic theory requires that the Brownian motion on one bead of the dumbbell is independent of the Brownian motion which acts on the other bead (completely uncorrelated Brownian motion in space, see e.g. [120]). The modeling step therefore pushes forward the uncorrelated framework. Note however that this simple presentation is a little bit controversial in itself, as it may also seem quite natural that some kind of correlation in space between the Brownian motions appears (see [74] page 394). Indeed, the Brownian motion seen by a particle convected on one trajectory of the flow is somewhat correlated, at least at a sufficiently small scale, to another Brownian motion seen by a particle which follows a trajectory "close to the first one" (see Figure 6.2). The notion of "trajectory dependent" Brownian motion, that we will introduce and develop later in this section, is thus likely to be relevant. In the following, we will not discuss further the modeling and physical aspects of the correlation in space of the Brownian motions used. We rather focus on the numerical counterparts of these correlations.

6.2.2 The numerical viewpoint

Historically, the first of the two currently adopted approaches for the numerical simulation of (6.5)-(6.8) namely the CONNFFESSIT method, mimicked the modeling viewpoint. This method couples the macro-scale simulation with the Lagrangian approach for the micro-scale. The first simulations (performed first on the start-up of a shear flow problem) accordingly made use of completely uncorrelated in space Brownian motions (see [97]). When the state of the art went to 2D simulations (see [98]), a Lagrangian computation of (6.8) was naturally adopted. In this framework, the authors used one Brownian motion per trajectory, all of them being independent from one another. Therefore, we may think of a collection of uncorrelated Brownian motions labelled by Lagrangian trajectories.

The second approach is the Eulerian one. It consisted in introducing the notion of configuration fields (see [82]) : the end-to-end vector $\boldsymbol{X}_t$ is seen as an Eulerian variable that explicitly depends on the space variable $\boldsymbol{x}$. Equation (6.8) may then be solved in an Eulerian setting, which greatly simplifies the numerical implementation of the CONNFFESSIT method (no dumbbell tracking, no problem of dumbbell deletion or dumbbell relocation). In this approach, it is of course easier to take Brownian motions not depending on space. Nevertheless, one can imagine to keep the Brownian motions of the Lagrangian approach (a collection of uncorrelated Brownian motions labelled by the trajectories), for example by using a characteristic method to solve (6.8) (see [74]). In fact, the use of configuration fields together with Brownian motions not depending on space has revealed to be a very efficient method

to reduce variance of the velocity $\boldsymbol{u}$. In spite of the fact that the modeling issue is not settled, the use of a Brownian motion not depending on space on the discretized system can be seen as a pure numerical trick, that leads to a reduction of the variance of the velocity $\boldsymbol{u}$. Intuitively, this fact may be understood, since in (6.5), a derivative with respect to $\boldsymbol{x}$ of the stress is involved. But the situation is not so clear either. What is indeed counterintuitive (see Halin, Lielens, Keunings and Legat in [74] page 397 or Bonvin and Picasso in [15] page 197) is the fact that, contrary to what happens for the velocity field, the variance on the stress $\boldsymbol{\tau}_p$ increases when one goes from uncorrelated Brownian motions to a Brownian not depending on $\boldsymbol{x}$. Despite the lack of a theoretical understanding of this phenomenon, experts of the field seem to agree in the numerical simulations on the use of Brownian motions not depending on space, mainly because it leads to less noisy results in space, and because it greatly reduces the variance on the velocity. The state of the art of the numerical simulations seems to stay today on this point : use a Brownian motion not depending on space (see [82, 121]).
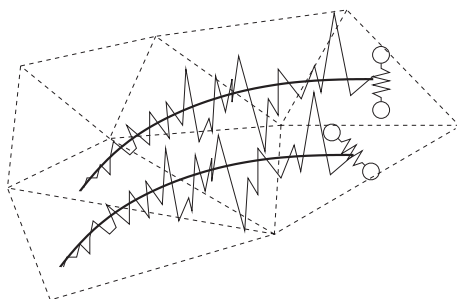
FIG. 6.2 – Trajectories of two dumbbells, ending in two different cells : does each dumbbell "sees" the same noise, as is represented on this figure ?

6.2.3   The mathematical viewpoint

Let us now turn to mathematics. It is to be made precise at once that it is not straightforward to give a sense to the Eulerian system (6.5)-(6.8) at the continuous level with a Brownian motion depending on space. There are three ways to avoid the treatment of this delicate question. The first is to stay at the continuous level and turn to the Lagrangian form of (6.8) with Brownian motions depending on the trajectory. The second is to go at the discrete level : once being discretized in space, it is easy to give a proper meaning to (6.5)-(6.8), and to play with the dependence in space of the Brownian motion. A third way is to treat the shear flow case. Let us details these three approaches.

The continuous level

Let us introduce the Lagrangian form of (6.8), namely

$$d\tilde{\boldsymbol{X}}_t(\boldsymbol{x}) = \left(\nabla \mathbf{u}(\boldsymbol{c}(0, \boldsymbol{x}, t)) \tilde{\boldsymbol{X}}_t(\boldsymbol{x}) - \frac{1}{2\mathrm{We}} \boldsymbol{F}(\tilde{\boldsymbol{X}}_t(\boldsymbol{x})) \right) dt + \frac{1}{\sqrt{\mathrm{We}\,\mu}} d\tilde{\mathbf{W}}_t^{\boldsymbol{x}}, \quad (6.11)$$

where $\tilde{\boldsymbol{X}}_t(\boldsymbol{x}) = \boldsymbol{X}_t(\boldsymbol{c}(0, \boldsymbol{x}, t))$ and

$$\begin{cases} \frac{d}{dt}\boldsymbol{c}(s, \boldsymbol{x}, t) = \mathbf{u}(t, \boldsymbol{c}(s, \boldsymbol{x}, t)), \\ \qquad\quad \boldsymbol{c}(s, \boldsymbol{x}, s) = \boldsymbol{x}. \end{cases} \tag{6.12}$$

We suppose here that the velocity field $\boldsymbol{u}(t, \boldsymbol{x})$ is smooth enough to define the characteristics. The stress $\tilde{\boldsymbol{\tau}}_p$ defined by (6.7), is then obtained by the following formula :

$$\tilde{\boldsymbol{\tau}}_p(t, \boldsymbol{x}) = \frac{\epsilon}{\mathrm{We}}\left(\mu\mathbb{E}\big(\tilde{\boldsymbol{X}}_t(\boldsymbol{c}(t, \boldsymbol{x}, 0)) \otimes \boldsymbol{F}(\tilde{\boldsymbol{X}}_t(\boldsymbol{c}(t, \boldsymbol{x}, 0)))\big) - \mathrm{Id}\right). \tag{6.13}$$

Notice that the stochastic differential equations (6.11) indexed by $\boldsymbol{x}$ are rigorously defined and are not coupled in space by (6.13).

Let us now consider a smooth solution $(\mathbf{u}, \boldsymbol{\tau}_p)$ of (6.5)-(6.8) obtained with a Brownian motion which does not depend on the space variable, and asigns to each trajectory obtained by solving (6.12) a Brownian motion. Since the law of $\tilde{\boldsymbol{X}}$ (solution of (6.11)) is not influenced by the way the Brownian motions depend on the trajectory, we have $\tilde{\boldsymbol{\tau}}_p = \boldsymbol{\tau}_p$. Therefore, $(\mathbf{u}, \boldsymbol{\tau}_p)$ will remain a solution to (6.5)-(6.8), whatever the dependency of the Brownian motions on the trajectory is. In other words, we have proved that the continuous solution $(\mathbf{u}, \boldsymbol{\tau}_p)$ does not depend on the the way the Brownian motions depend on the trajectory, provided that the solution of the problem is unique and smooth enough.

The discrete level

Once the system (6.5)-(6.8) is discretized in space (say, by a finite element method, to fix the ideas), it is easy to give a proper meaning to (6.8) with a Brownian motion depending on space being understood that we in fact deal with a Brownian motion which depends polynomialy on the space variable (i.e. a discrete-in-space Brownian motion). Then, once one approaches the expectation (6.7) by an empirical mean, the results (and in particular their variances) may depend on the way the Brownian motion depends on trajectories.

If one considers that the scheme converges in the limit of the space step h and the time step δt go to zero, and the number of realizations goes to infinity, two questions then arise : May the limit depend on the dependency in space of the Brownian motions used ? What is the "best dependency" as far as the variance of the results is concerned ?

To the best of our knowledge, the first question is open : note for instance that contrary to the shear flow case, in a general geometry, the "discrete" streamlines themselves may be influenced by the dependency in space of the Brownian motion. As was pointed out in [121] (page 259), by using Brownian motions not depending on space, "completely unphysical correlations in the random forces at different positions are introduced". This crucial point would need further investigations.

Concerning the second question about the variance of the results, we have already pointed out that using a Brownian motion not depending on space leads to a reduction of the variance of the velocity $\boldsymbol{u}$, but an increasing of that on $\boldsymbol{\tau}_p$. Thus the natural question arises to find the best correlation in space, for the discrete-in-space Brownian, that will lead *in fine* to the least variance in the result for *both* $\boldsymbol{u}$ and $\boldsymbol{\tau}_p$.

The case of the shear flow

Let us now concentrate on the shear flow case, which will be the framework of the rest of this article. In this special geometry (see Figure 6.3 below), the transport term $\boldsymbol{u} \cdot \nabla \boldsymbol{X}$ vanishes on the left hand side of (6.8). Therefore, the streamlines are fixed, and one can then rigorously define, at the continuous level, the stochastic differential equation (6.8) for Brownian motions indexed by the space variable y. A given stochastic differential equation at macro point y does not interact with another one, at point $y' \neq y$, since (6.7) is a point-wise expectation. Therefore, the continuous solution $(\boldsymbol{u}, \boldsymbol{\tau}_p)$ does not depend on the way the Brownian motions depend on the space variable y (see Remark 8 in [85]).

Once the system is discretized, in the case of a shear flow and for Hookean dumbbells, we have shown in [85] that the convergence of the CONNFFESSIT scheme towards the unique continuous solution $(\mathbf{u}, \boldsymbol{\tau}_\mathbf{p})$ holds, whatever the correlation in space of the discrete-in-space Brownian motions is.

One aim in Section 6.3 is to contribute to the understanding of all the above observations and remarks. For this purpose, we consider a simple case, namely the start-up of shear flow problem which has been considered as a test case in many papers (see [15, 97, 121]). In this simple geometry, the Lagrangian and the Eulerian formulations are the same. The classical approaches adopted in the literature therefore amount in this case to the following alternative : the Brownian motions in each cells of the space discretization are either the same or completely uncorrelated. One could imagine to use other correlations in space of the Brownian motions, and this will be investigated in Section 6.3. It would even be possible to introduce correlations in space different from one time-step to another, but we have not considered this possibility in the following.

6.3 Explicit computations of variances in a simple case

6.3.1 A simple model : the pure shear flow

In order to simplify the problem and enable explicit computations, we consider in the following a simple geometry of the flow namely a pure shear flow (see Figure 6.3). Due to this special geometry, the velocity becomes a one-dimensional variable :
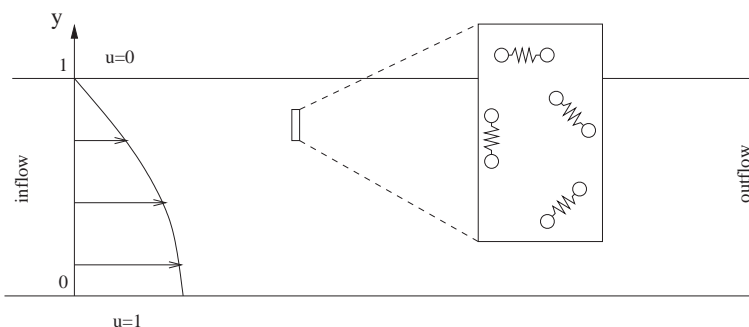

FIG. 6.3 − Velocity profile in a shear flow of a dilute solution of polymers.

$\boldsymbol{u}(t, \boldsymbol{x}) = (u(t,y), 0)$, with the notation $\boldsymbol{x} = (x, y)$, and therefore the convective derivative $\boldsymbol{u}.\nabla$ is zero. One can thus show that the mass and momentum conservation equations reduce to a scalar heat equation. In addition to the above simplification of the geometry, we consider Hookean dumbbells. In the following, in order to simplify the notation, we choose the following values for the non-dimensional numbers : Re $= 1/2$, We $= 1$, $\epsilon = 1/2$, $\mu = 1$. Thus, the system (6.5)-(6.8) can be written in the following form :

$$
\frac{\partial u}{\partial t}(t, y) = \frac{\partial^2 u}{\partial y^2}(t, y) + \frac{\partial \, \mathbb{E}(Y_t X_t(y))}{\partial y} \; , \tag{6.14}
$$

$$
dX_t(y) = \left(\frac{\partial u(t, y)}{\partial y} Y_t - \frac{X_t(y)}{2} \right) dt + dW_t(y) \; , \tag{6.15}
$$

$$
dY_t = -\frac{Y_t}{2} dt + dV_t \; , \tag{6.16}
$$

where we have adopted the following notation for the components of $\boldsymbol{X}$ and $\boldsymbol{W}_t$: $\boldsymbol{X} = (X, Y)$ and $\boldsymbol{W}_t = (W_t, V_t)$. The system of equations is supplied with the following boundary and initial conditions :

$$u(0, y) = 0, \; X_0 \sim \mathcal{N}(0, 1), \; Y_0 \sim \mathcal{N}(0, 1), \; (X_0 \text{ and } Y_0 \text{ independent}),$$

$$u(t, 0) = v(t) = v \min(1, 10 \, t/T) \; , \; u(t, 1) = 0,$$

where T denotes the final time of the simulation and v is a constant denoting the velocity on the boundary, after a transition period in time of length $T/10$.

Note that, as explained in Section 6.2, we may let the Brownian motion W_t depend on space, and more precisely (see discussion above in Section 6.2) on trajectory. In the case that we consider, namely a shear flow, one can simply label the Brownian motions by the space variable y. The question is therefore how to define a process $(W_t(y))_{t \geq 0, y \in (0,1)}$. We impose the following constraints on the process $(W_t(y))_{t \geq 0, y \in (0,1)}$:

    a) The process $(t, y) \to W_t(y)$ is a Gaussian process,
    b) For a fixed $y \in (0, 1)$, $t \to W_t(y)$ is a Brownian motion,
    c) The covariance in space $\mathbb{E}(W_t(x)W_t(y))$ does not depend on the time variable t.

Constraint b) is natural. We impose a) and c) in order to simplify and enable explicit computations. These assumptions clearly restrict the field of all possible $W_t(y)$ but we nevertheless believe they are general enough. Note that because of assumption a), the process $W_t(y)$ is completely determined by its covariance function.

We have chosen not to let the Brownian motion V_t depend on space since the process Y_t defined by (6.16) can be computed independently of the other unknowns u and X (see formula (6.24)). This point is of course specific to the Hookean case and will be modified in the FENE case (see Eq. (6.40) below).

6.3.2 The discretized problem

The CONNFFESSIT method applied to discretize system (6.14)-(6.16) can be written in the following way : assuming u_h^n, $X_{h,n}^j$ and Y_n^j are known, find $u_h^{n+1} \in V_h$

such that, for all $v \in V_h$,

$$\frac{1}{\delta t} \int_y (u_h^{n+1} - u_h^n) v \;=\; -\int_y \frac{\partial u_h^{n+1}}{\partial y} \frac{\partial v}{\partial y} - \int_y \tau_{h,n} \frac{\partial v}{\partial y}, \tag{6.17}$$

$$\tau_{h,n} \;=\; \frac{1}{R} \sum_{j=1}^R X_{h,n}^j Y_n^j, \tag{6.18}$$

$$X_{h,n+1}^j - X_{h,n}^j \;=\; \left(\frac{\partial u_h^{n+1}}{\partial y} Y_n^j - \frac{1}{2} X_{h,n}^j \right) \delta t + \left(W_{h,t_{n+1}}^j - W_{h,t_n}^j \right), \tag{6.19}$$

$$Y_{n+1}^j - Y_n^j \;=\; -\frac{1}{2} Y_n^j \delta t + \left(V_{t_{n+1}}^j - V_{t_n}^j \right). \tag{6.20}$$

The indices n and j respectively denote the time index and the realization index : we indeed consider R trajectories of the random variables $X_{h,n}$ and Y_n ($1 \leq j \leq R$). The time interval $(0,T)$ is divided into N intervals, $\delta t = T/N$ and $t_n = n\,\delta t$. The subscript h indicates that we are considering space discretized variables. The random variables $\tau_{h,n}$ (or more precisely $\frac{1}{2}\tau_{h,n}$) are approximations of the off-diagonal component of the stress $\boldsymbol{\tau}_p$. The space of discretization V_h is a finite element space. In the following, we consider $V_h = \mathbb{P}1$, the space of continuous piecewise affine functions on a mesh of I cells of the interval $(0,1)$: $(y_0 = 0, y_1, ..., y_I = 1)$. The random variables $X_{h,n}^j$, $\tau_{h,n}$ and $\left(W_{h,t_{n+1}}^j - W_{h,t_n}^j \right)_{j,n}$ belong therefore naturally to the space $\partial_y V_h$ (in our case, $\partial_y \mathbb{P}1 = \mathbb{P}0$, see Figure 6.4). We can therefore associate to the piecewise constant in space functions $X_{h,n}^j$ and $\left(W_{h,t_{n+1}}^j - W_{h,t_n}^j \right)_{j,n}$ two vectors whose components are the values of these random variables on each cell (y_{i-1}, y_i) of the mesh : $\left(X_{i,n}^j \right)_{1 \leq i \leq I}$ and $\left(W_{i,t_{n+1}}^j - W_{i,t_n}^j \right)_{1 \leq i \leq I}$. Let us make precise that for $1 \leq j \leq R$, the processes $\left(W_{1,t}^j, ..., W_{I,t}^j, V_t^j \right)_{0 \leq t \leq T}$ are independent and identically distributed Gaussian processes whose components are standard Brownian motions, the last one being independent from the first I ones. For a mathematical analysis of the system (6.14)-(6.16), and the convergence of the CONNFFESSIT method in this case, we refer to [41, 85, 102].

We now want to introduce some notation to make precise the dependency on space of the space-discretized Brownian motion $W_{h,t}^j$. Throughout this section, we will omit the superscript j which denotes the realization index, since the law of $W_{h,t}^j$ does not depend on j.

Since we choose a correlation in space which does not depend on time, the parameter we will consider in the following is the correlation matrix in space K defined by

$$K_{l,m} = \frac{1}{t} \mathbb{E}(W_{l,t} W_{m,t}), \tag{6.21}$$

where $1 \leq l \leq I$ and $1 \leq m \leq I$ denote two cell indices. With a slight abuse of notation, we denote by $\bar{W}_t$ the I-dimensional process whose components are $W_{i,t}$: $\bar{W}_t = (W_{1,t}, ..., W_{I,t})$, and thus, $K = \frac{1}{t}\text{Cov}(\bar{W}_t) = \frac{1}{t}\mathbb{E}(\bar{W}_t \otimes \bar{W}_t)$, where $\otimes$ denotes the tensorial product (for two vectors a and b in $\mathbb{R}^d$, $a \otimes b$ is the $d \times d$ matrix whose components are $(a_i \, b_j)_{1 \leq i \leq d, \, 1 \leq j \leq d}$).
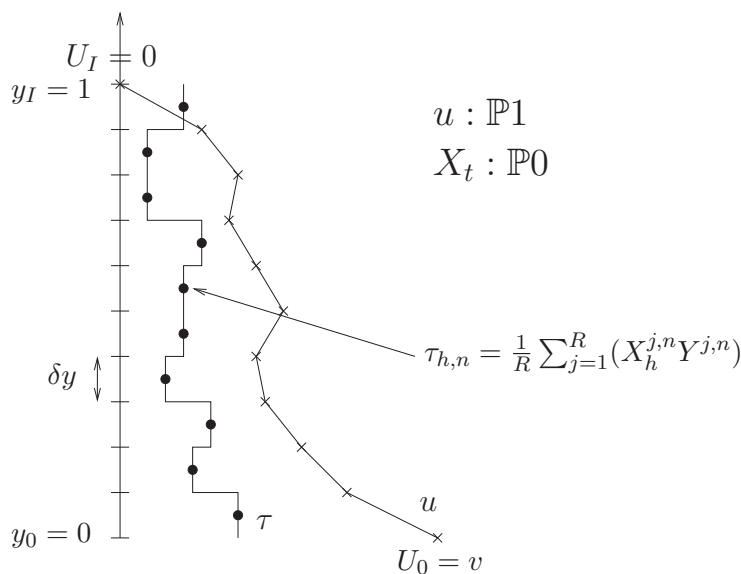
$$u : \mathbb{P}1$$
$$X_t : \mathbb{P}0$$
$$\tau_{h,n} = \frac{1}{R} \sum_{j=1}^{R} (X_h^{j,n} Y^{j,n})$$

FIG. 6.4 – Discretization of u and τ.

If the components of W_t are independent, then $K = \mathrm{Id}$ and if the components of W_t are the same (W_t is not depending on space), then $K = J$, where J henceforth denotes the matrix with all components equal to 1.

In practice, in order to build the Brownian motion $W_t = (W_{1,t}, ..., W_{I,t})$, we consider a I-dimensional Brownian motion $\overline{W}_t$ (whose components are independent 1-dimensional Brownian motions) and compute W as an image by a linear application of $\overline{W}$: $W_t = N\overline{W}_t$ (N is a $I \times I$ matrix such that each line has an Euclidean norm equal to one). Therefore, $K = N(^t N)$. To construct a Brownian motion not depending on space, one can take N such that $N_{i,j} = \delta_{1,j}$ and thus $K = J$ (δ denotes the Kronecker function). To build uncorrelated Brownian motions in space, one can consider $N = \mathrm{Id}$ and thus $K = \mathrm{Id}$.

In our simple case, one can consider that the correlation in space matrix K is just a numerical parameter. Indeed, we have shown (see Remark 8 in [85]) that whatever the correlation in space is, the scheme converges towards a unique solution $(u(t, y), \mathbb{E}(Y_t X_t(y)))$. Therefore, the matrix K (or N) can be seen as another numerical parameter, that can be used to reduce the prefactor in the error $O(1/\sqrt{R})$ due to the Monte Carlo discretization (R denotes the number of realizations).

Note that in our numerical simulations (see Section 6.4), the spatial correlation of the initial variables is the same as the spatial correlation of the Brownian motions.

This simple problem presents the behavior already noticed in more complicated geometry : when one goes from $K = \mathrm{Id}$ (uncorrelated Brownian motions in space) to $K = J$ (a Brownian motion not depending on space), the variance on the velocity u_h^n decreases but the variance on the stress $\tau_{h,n}$ increases (see Section 6.4 and the curves labelled 'Wt(y)' and 'Wt' on Figure 6.6).

Remark 6 *One important remark is that the counterintuitive reduction of variance on the stress when one takes Brownian motions completely uncorrelated in space*

is intimately due to the coupling (in a probabilistic sense) between the variables u and X, or in other terms to the nonlinearity of the problem. If one performs the same simulation, but uses a pre-computed deterministic velocity u in (6.15), then the variance on τ is not reduced, which was indeed knwon (see [92]). Let us make precise this point. First observe that one can compute explicitly the expectations $\mathbb{E}(X_{h,n}Y_n)$ in the simple case of a shear flow, and use this deterministic computations to obtain a deterministic velocity u_h^n. One can then use this deterministic velocity in the computation of the stress with a Monte Carlo method in (6.18)-(6.20) and check that, whatever the correlation in space is, the variance obtained on τ for long time is about 0.058, which is what we obtained in the worst case for the coupled system (see the curve labelled 'Wt' on Figure 6.6).

Remark 7 *In [74], the authors have proposed the following explanation for the unexpected behavior of the variance on the stress : with Brownian motions not depending on space (and accordingly initial random variables not depending on space), the initial equilibrium distribution may not be correctly sampled. We have performed the computation with initial random variables uncorrelated in space and Brownian motions not depending on space and observed the same large variance on the stress, which seems to indicate, at least in the simple case considered here, that the major role is played by the space correlation of the Brownian motions and not by the initial value of the random variables.*

6.3.3 Dependency of the variance in term of the correlation in space

6.3.3.1 Computation of the variances

In the following, we want to explicitly compute the variances of the velocity and the stress solutions of the system (6.14)-(6.16). In order to enable explicit computations, we make the following simplifications :
- we focus on the long-time behavior of the system (6.14)-(6.16),
- accordingly to the previous assumption, we take $\dfrac{\partial u}{\partial t} = 0$ in (6.14),
- we consider only the space and Monte Carlo discretized system (no discretization in time),
- we consider only one dumbbell (i.e. one realization : $R = 1$).

We have checked all the conclusions we draw on this simplified case by numerical experiments on the long-time behavior of the time-dependent problem, for both Hookean and FENE dumbbells (see Section 6.4 below).

Taking into account these simplifications, we consider, instead of (6.14)-(6.16), the following system of equations :

$$-\frac{\partial^2 u(t,y)}{\partial y^2} = \frac{\partial\, \mathbb{E}(Y_t X_t(y))}{\partial y}, \tag{6.22}$$

$$dX_t(y) = \left(\frac{\partial u(t,y)}{\partial y}Y_t - \frac{X_t(y)}{2}\right) dt + dW_t(y), \tag{6.23}$$

$$Y_t = e^{-\frac{t}{2}}Y_0 + \int_0^t e^{\frac{s-t}{2}}\, dV_s. \tag{6.24}$$

Accordingly to Section 6.3.2, we consider a $\mathbb{P}1$ discretization in space on a uniform grid with I intervals (the space step is $\delta y = 1/I$). Since we consider only one dumbbell, we obtain the following discretization of (6.22)-(6.24), written in an algebraic form :

$$-MU(t) = Y_t B X_t + b_1', \tag{6.25}$$

$$dX_t = \left(Y_t C U(t) + Y_t b_2' - \frac{X_t}{2} \right) dt + dW_t, \tag{6.26}$$

where Y is a process with value in $\mathbb{R}$ defined by (6.24), U is a vector of size $(I - 1)$ (because $u(y = 0)$ and $u(y = 1)$ are known) and X_t is now a $\mathbb{R}^I$-valued process (the $i - th$ components is the value of the discretization of X_t in cell (y_{i-1}, y_i)). Accordingly, W_t is now a process with value in $\mathbb{R}^I$. The matrices M, B and C are respectively of size $(I - 1) \times (I - 1)$, $(I - 1) \times I$ and $I \times (I - 1)$. One can easily check that, should the grid be uniform or not :

$$BC = M. \tag{6.27}$$

Here, we use a uniform grid in space and we obtain the finite differences matrices :

$$M = \frac{1}{\delta y^2} \begin{bmatrix} -2 & 1 & 0 & \ldots & 0 \\ 1 & -2 & 1 & \ldots & 0 \\ \vdots & \ddots & \ddots & \ddots & \vdots \\ 0 & \ldots & 1 & -2 & 1 \\ 0 & \ldots & 0 & 1 & -2 \end{bmatrix}, \qquad B = \frac{1}{\delta y} \begin{bmatrix} -1 & 1 & 0 & \ldots & 0 \\ 0 & -1 & 1 & \ldots & 0 \\ \vdots & \ddots & \ddots & \ddots & \vdots \\ 0 & \ldots & 0 & -1 & 1 \end{bmatrix},$$

$$C = -{}^t B = \frac{1}{\delta y} \begin{bmatrix} 1 & 0 & \ldots & 0 \\ -1 & 1 & \ldots & 0 \\ \vdots & \ddots & \ddots & \vdots \\ 0 & \ldots & -1 & 1 \\ 0 & \ldots & 0 & -1 \end{bmatrix}.$$

The vectors b_1' and b_2', of respective size $(I - 1)$ and I, depend on the boundary conditions on u : $b_1' = (v/\delta y^2, 0, \ldots, 0)$, $b_2' = (-v/\delta y, 0, \ldots, 0)$.

We therefore have :

$$U(t) = -Y_t M^{-1} B X_t + b_1, \tag{6.28}$$

$$dX_t = \left(-(Y_t)^2 C M^{-1} B X_t + Y_t b_2 - \frac{X_t}{2} \right) dt + dW_t, \tag{6.29}$$

where $b_1 = -M^{-1}b_1'$ and $b_2 = -CM^{-1}b_1' + b_2'$ are two vectors depending on the boundary conditions on u. What can be easily checked is that $Bb_2 = 0$.

The aim of the remaining of this section is to analyze the covariance of the random variables U (the velocity) and $Y_t X_t$ (the stress) in function of the covariance K in space of W_t (see Eq. 6.21). We first remark that the covariance of U can be expressed in function of the covariance of $Y_t X_t$:

$$\begin{aligned} \mathrm{Cov}(U(t)) &= \mathbb{E}(U(t) \otimes U(t)) - \mathbb{E}(U(t)) \otimes \mathbb{E}(U(t)), \\ &= (M^{-1}B) \, \mathrm{Cov}(Y_t X_t) \, {}^t(M^{-1}B). \end{aligned} \tag{6.30}$$

Let us explain how we can compute $\text{Cov}(Y_t X_t) = \mathbb{E}(Y_t X_t \otimes Y_t X_t) - \mathbb{E}(Y_t X_t) \otimes \mathbb{E}(Y_t X_t)$. First, from (6.29), one can compute the following expression of X :

$$
\begin{aligned}
X_t &= \exp\left(\int_0^t A(s)\,ds\right) X_0 + \int_0^t \exp\left(\int_s^t A(u)\,du\right) \text{b}_2 Y_s\,ds \\
&\quad + \int_0^t \exp\left(\int_s^t A(u)\,du\right) dW_s,
\end{aligned}
\tag{6.31}
$$

where

$$
A(s) = -CM^{-1}B(Y_s)^2 - \frac{1}{2}\text{Id}.
$$

Note that $A(t)$ is a random matrix, which is $(Y_0, (V_s)_{s \leq t})$-measurable. The last term in equation (6.31) makes sense since (Y_0, V) (and therefore Y) is independent from W.

The main Lemma that will be used in the sequel to compute the variances is the following :

Lemma 1 *The matrix $CM^{-1}B$ can be decomposed as follows :*

$$
CM^{-1}B = Id - P,
$$

where Id is the identity matrix of size $I \times I$ and P is the matrix of a projection on $\text{Ker}(B)$.

Proof. The proof uses the fact that $BC = M$ (see (6.27)). A simple computation shows that :
$$
(\text{Id} - CM^{-1}B)(\text{Id} - CM^{-1}B) = (\text{Id} - CM^{-1}B),
$$
and thus $P = \text{Id} - CM^{-1}B$ is a projector. Besides, it is clear that $\text{Ker}(B) \subset \{x,\, P(x) = x\}$. The converse inclusion is also easy to prove : if x is such that $P(x) = x$, then $CM^{-1}Bx = 0$ and therefore, by multiplying on the left by B, one obtains $Bx = 0$. In a uniform in space mesh setting, one obtains $P = \delta y J$ where J is the $I \times I$ matrix with all components equal to 1. $\qquad\square$

Using $A(s) = (Y_s)^2 P - \left(\frac{1}{2} + (Y_s)^2\right)\text{Id}$ and the fact that, by Lemma 1, $P^n = P$, one obtains the following expression of $\exp\left(\int_s^t A(u)\,du\right)$:

$$
\exp\left(\int_s^t A(u)\,du\right) = a(s,t)\text{Id} + b(s,t)P,
\tag{6.32}
$$

where

$$
a(s,t) = \exp\left(-\frac{t-s}{2}\right)\exp\left(-\int_s^t (Y_u)^2\,du\right),
$$

and

$$
b(s,t) = \exp\left(-\frac{t-s}{2}\right)\left(1 - \exp\left(-\int_s^t (Y_u)^2\,du\right)\right).
$$

This leads to the following expression of $Y_t X_t$ (using the fact that $P\mathrm{b}_2 = \mathrm{b}_2$) :

$$
\begin{aligned}
Y_t X_t &= Y_t \big(a(0,t)\mathrm{Id} + b(0,t)P \big) X_0 + Y_t \int_0^t \big(a(s,t) + b(s,t) \big) Y_s \, ds \, \mathrm{b}_2 \\
&\quad + Y_t \int_0^t \big(a(s,t)\mathrm{Id} + b(s,t)P \big) \, dW_s.
\end{aligned}
\tag{6.33}
$$

Remark 8 *These first computations allow us to explain the dependency of the variances upon the correlation in space of the Brownian motion as follows, at least in the particular case $K = Id$ or $K = J$. When the Brownian motions are completely uncorrelated in space ($K = Id$), one computes in the velocity equation (6.25) the difference between two independent random variables divided by the space step. It is therefore natural that this induces a variance much more important than in the case of a uniform in space Brownian motion ($K = J$). On the contrary, when we consider the equation (6.33) verified by X_t, we observe that the term $\int_0^t b(s,t)P \, dW_s$ (we recall that $P = \delta y J$) induces more variance in the case of a Brownian motion not depending on space for the same reason that, if G^i are i independent Gaussian random variables, $\mathrm{Var}\left(\sum_{i=1}^I G^i \right) < \mathrm{Var}\left(\sum_{i=1}^I G^1 \right)$. Indeed, in the case of completely uncorrelated Brownian motions in space, the term $P dW_s = \delta y J dW_s$ leads to a sum of independent random variables, whose variance is less than a sum of one single random variable.*

We now turn to the computation of $\mathrm{Cov}(Y_t X_t)$. Using the independence of X_0, $(Y_s)_{s \leq t}$, and $(W_s)_{s \leq t}$, we check that the covariance between any two different terms of the right-hand-side of (6.33) is null. Therefore, we obtain the following expression of $\mathrm{Cov}(Y_t X_t)$:

$$
\begin{aligned}
\mathrm{Cov}(Y_t X_t) &= \mathbb{E}(a(0,t)^2 Y_t^2) \, \mathbb{E}(X_0 \otimes X_0) + \mathbb{E}(b(0,t)^2 Y_t^2) P \, \mathbb{E}(X_0 \otimes X_0)^t P \\
&\quad + \mathbb{E}(a(0,t)b(0,t)Y_t^2) \left(P\mathbb{E}(X_0 \otimes X_0) + \mathbb{E}(X_0 \otimes X_0)^t P \right) \\
&\quad + \mathbb{E}\left(\int_0^t \exp\left(-\frac{t-s}{2} \right) (Y_s Y_t - \mathbb{E}(Y_s Y_t)) \, ds \right)^2 \mathrm{b}_2 \otimes \mathrm{b}_2 \\
&\quad + \int_0^t \mathbb{E}(a(s,t)^2 Y_t^2) \, ds \, K + \int_0^t \mathbb{E}(b(s,t)^2 Y_t^2) \, ds \, P K^t P \\
&\quad + \int_0^t \mathbb{E}(a(s,t)b(s,t)Y_t^2) \, ds \, (PK + K^t P).
\end{aligned}
\tag{6.34}
$$

We now want to take the limit $t \longrightarrow \infty$ in each of the terms of (6.34).

Using the fact that $a(0,t) \leq \exp\left(-\frac{t}{2} \right)$ and $b(0,t) \leq \exp\left(-\frac{t}{2} \right)$, one can see that the part of the covariance of $Y_t X_t$ which depends on the initial condition X_0 goes to zero in the limit $t \to \infty$.

One can exactly compute (using the fact that $\mathbb{E}(Y_t^2) = 1$ and $\mathbb{E}(Y_s Y_t) = e^{-\frac{|s-t|}{2}}$) the part of the covariance of $Y_t X_t$ which depends on b_2. We obtain :

$$
\begin{aligned}
&\mathbb{E}\left(\int_0^t \exp\left(-\frac{t-s}{2} \right) (Y_s Y_t - \mathbb{E}(Y_s Y_t)) \, ds \right)^2 \\
&= 4\exp(-2t) \left(-\exp(t)(1+t) + 4\exp(2t) - 4\exp(-3t/2) + 1 \right)
\end{aligned}
\tag{6.35}
$$

which tends to 16 when t goes to ∞.

One can also show that the other terms in the expression (6.34) of the covariance of $Y_t X_t$ have a limit when $t \to \infty$. Indeed, the sum of the three last terms of (6.34) writes :

$$I_t(K + PK^tP - PK - K^tP) + J_t(PK + K^tP - 2PK^tP) + (1 - \exp(-t))PK^tP$$

where

$$I_t = \int_0^t \exp(-t + s)\mathbb{E}\left(\exp\left(-2\int_s^t (Y_u)^2\, du\right) Y_t^2\right)\, ds$$

and

$$J_t = \int_0^t \exp(-t + s)\mathbb{E}\left(\exp\left(-\int_s^t (Y_u)^2\, du\right) Y_t^2\right)\, ds.$$

Clearly, I_t and J_t are smaller than $1 - \exp(-t)$. Hence, it is enough to check that these terms are increasing to conclude that they have finite limits as $t \to \infty$, respectively denoted by α and β.

To prove that I_t is increasing, one can compute the following expression of I_t (by using the change of variable $r = t - s$ and the fact that, by stationarity, $(Y_u)_{t-r \leq u \leq t}$ and $(Y_u)_{0 \leq u \leq r}$ have the same law) :

$$
\begin{aligned}
I_t &= \int_0^t \exp(-t + s)\mathbb{E}\left(\exp\left(-2\int_s^t Y_u^2\, du\right) Y_t^2\right)\, ds \\
&= \int_0^t \exp(-r)\mathbb{E}\left(\exp\left(-2\int_{t-r}^t Y_u^2\, du\right) Y_t^2\right)\, dr \\
&= \int_0^t \exp(-r)\psi(r)\, dr
\end{aligned}
$$

where $\psi(r) = \mathbb{E}\left(\exp\left(-2\int_0^r (Y_u)^2\, du\right) Y_r^2\right)$ is a positive function. Using the same arguments, we obtain for J_t :

$$J_t = \int_0^t \exp(-r)\mathbb{E}\left(\exp\left(-\int_0^r (Y_u)^2\, du\right) Y_r^2\right).$$

These expressions clearly demonstrate that I and J are increasing.

This shows that, in the limit $t \to \infty$, $\mathrm{Cov}(Y_t X_t) = 16\, b_2 \otimes b_2 + \alpha_1 K + \alpha_2(K^t P + PK) + \alpha_3 PK^tP$, and thus (since $P =^t P$),

$$\lim_{t \to \infty} \mathrm{Cov}(Y_t X_t) = 16\, b_2 \otimes b_2 + \alpha_1 K + \alpha_2(KP + PK) + \alpha_3 PKP, \qquad (6.36)$$

where $\alpha_1 = \alpha$, $\alpha_2 = \beta - \alpha$ and $\alpha_3 = 1 - 2\beta + \alpha$ are three positive constants.

Using (6.30) and the fact that $BP = 0$ et $Bb_2 = 0$, we obtain :

$$\lim_{t \to \infty} \mathrm{Cov}(U(t)) = \alpha_1\, M^{-1}B\, K\,{}^t(M^{-1}B). \qquad (6.37)$$

Remark 9 *One can compute numerically the values of α_i, $i = 1, 2, 3$. We have found $\alpha \simeq 0.26$ and $\beta \simeq 0.39$. Therefore $\alpha_1 \simeq 0.26$, $\alpha_2 \simeq 0.13$ and $\alpha_3 \simeq 0.48$. Notice also that $\alpha_1 + 2\alpha_2 + \alpha_3 = 1$, which will be used later on.*

$t \longrightarrow \infty$	$\mathrm{Cov}(Y_t X_t)$ (stress)	$\mathrm{Cov}(U(t))$ (velocity)
W_t	$16\mathrm{b}_2 \otimes \mathrm{b}_2 + J$	0
$W_t(y)$	$16\mathrm{b}_2 \otimes \mathrm{b}_2 + \alpha_1 \mathrm{Id} + (1-\alpha_1)\delta y J$	$-\alpha_1 M^{-1}$

FIG. 6.5 – Variances of u and τ (for long time) for a Brownian motion not depending on space (W_t) and for Brownian motions uncorrelated in space ($W_t(y)$). Notice that the covariance matrices of the stress (resp. of the velocity) are of size $I \times I$ (resp. $(I-1) \times (I-1)$) where $I = 1/\delta y$.

Remark 10 *All the computations we have made in this section can also be done with a mesh with non-constant space-steps. In particular, Lemma 1 holds with any mesh in space.*

Remark 11 *One can notice that the variance on the velocity is not influenced by the value of the boundary condition v on the velocity. This is not the case for the stress. In our simple case, since* b_2 *is a constant vector in space which is proportional to v, we observe that the variance on $Y_t X_t$ is uniformly in space influenced by v, and behaves like v^2 when $v \to \infty$. The boundary condition on the velocity therefore influences in the same manner the variance on the stress, at all points of the domain.*

6.3.3.2 Analysis of the cases $K = \mathbf{Id}$ and $K = J$

On the basis of the main two results of the previous section (namely (6.36) and (6.37)), we can explain the way the variances on U and YX vary when ones goes from completely uncorrelated Brownian motions in space ($K = \mathrm{Id}$) to a Brownian motion not depending on space ($K = J$).

In the case of a completely uncorrelated Brownian motion, we have $K = \mathrm{Id}$ and we obtain $\mathrm{Cov}(Y_t X_t) = 16\mathrm{b}_2 \otimes \mathrm{b}_2 + \alpha_1 \mathrm{Id} + (2\alpha_2 + \alpha_3)\delta y J = 16\mathrm{b}_2 \otimes \mathrm{b}_2 + \alpha_1 \mathrm{Id} + (1-\alpha_1)\delta y J$ and $\mathrm{Cov}(U(t)) = -\alpha_1 M^{-1}$.

In the case of a Brownian motion not depending on space, we have $K = J$ and we obtain $\mathrm{Cov}(Y_t X_t) = 16\mathrm{b}_2 \otimes \mathrm{b}_2 + (\alpha_1 + 2\alpha_2 + \alpha_3)J = 16\mathrm{b}_2 \otimes \mathrm{b}_2 + J$ and $\mathrm{Cov}(U(t)) = 0$ (since $BJ = 0$).

Table 6.5 summarizes the results we have obtained. These results corroborate the behavior of the numerical experiments and the observations of the authors in [15,74]. In particular, if one considers the variance of YX at a point in the middle of the flow, one obtains $C(b_2) + 1$ with Wt and $C(b_2) + \alpha_1 + (1-\alpha_1)\delta y \simeq C(b_2) + 0.26 + 0.74\delta y$ with Wt(y) (where $C(b_2)$ denotes a constant which depends on b_2) : the variance reduces with a Brownian which depends on space (since $\delta y < 1$). Note also (see off-diagonal terms) the strong correlation which is introduced between the variables, at different point in space, when one uses a Brownian motion not depending on space.

6.3.3.3 Analysis of other correlation matrices K

We now want to further investigate the dependency of the variances in terms of K. What is of interest is the traces of these covariance matrices (renormalized by

the number of cells), which measures the variance of the whole variable in space :

$$\delta y \, \text{tr}(\text{Cov}(Y_t X_t)) = \alpha_1 + 16\delta y \, ||\text{b}_2||^2 + (2\alpha_2 + \alpha_3)\delta y \, ||PN||^2,$$
$$= \alpha_1 + 16\delta y \, ||\text{b}_2||^2 + (1 - \alpha_1)\delta y \, ||PN||^2,$$

$$\delta y \, \text{tr}(\text{Cov}(U(t))) = \alpha_1 \delta y \, ||M^{-1}BN||^2,$$

where $||.||$ denotes the Frobenius or Euclidean norm and N is the matrix such that $K = N(^tN)$ (see Section 6.3.2 : N is a $I \times I$ matrix such that each line has a norm equal to one). We have obtained these expressions using some simple properties like $\text{tr}(EF) = \text{tr}(FE)$ for any matrices E and F, or $P^2 = P$. From these expressions of the variances, we can deduce the following :
   – The minimum of the variance on U is zero and is obtained if and only if the Brownian motion does not depend on space. Indeed, $||M^{-1}BN|| = 0$ implies $BN = 0$, which implies that each line of N is the same.
   – The minimum of the variance on $Y_t X_t$ is $\alpha_1 + 16\delta y \, ||\text{b}_2||^2$. It is attained if and only if $PN = 0$ (and this is *not* the case with a Brownian motion not depending on space). This is equivalent to the fact that the sum of the components within each column of the matrix N is zero.
   Let us now try to determine among all covariances matrices K such that the variance on $Y_t X_t$ is minimum, the one that leads to a variance on $U(t)$ that is minimum.
   Variance reduction using only one Brownian motion in space.
   In a first step, we solve this question in the case when we use only one Brownian motion in space to construct K, in order to keep the same computational cost as in the case of a Brownian motion not depending on space. In other words, we can only choose $+W_t$ or $-W_t$ in each cell of the mesh. We can then state the following result : in case I is even, using only one Brownian in space, the covariance matrix K defined by $K_{i,j} = (-1)^{i+j}$ is such that, among all K possible such that the variance on X_t is minimum, the variance on $U(t)$ is minimum. To prove this result, one has to notice that we obtain all the admissible covariance matrices $K = N(^tN)$ with the matrices N of the following form : the first column equal to $\epsilon = (\epsilon_1, ..., \epsilon_I)$ and zero elsewhere, with $\epsilon_i = \pm 1$, and $\sum_{i=1}^{I} \epsilon_i = 0$. The variance on U is then minimal if and only of the norm of $M^{-1}B\epsilon$ is minimal. But this vector $\nu = M^{-1}B\epsilon$ can also be interpreted as the solution in $\mathbb{P}1$ of the finite element discretization of the following problem : $\frac{\partial^2 r}{\partial y^2} = \frac{\partial \epsilon}{\partial y}$, where $y \in (0,1)$, with zero Dirichlet boundary conditions $r(0) = r(1) = 0$. Since the finite element solution is equal to the non-discretized solution, it is then obvious that the minimum of the norm of $\nu = M^{-1}B\epsilon$ is obtained, for example, with an oscillatory ϵ ($\epsilon = (1, -1, 1, -1, ...)$). We have plotted on Figure 6.6 the results obtained on the initial problem (6.14-6.16) in this case of an oscillatory-in-space Brownian motion (see the curves labelled '+/- Wt').
   This result is interesting since it shows that, if the aim is to reduce the variance on $Y_t X_t$, one can further reduce the variances on *both* $U(t)$ and $Y_t X_t$, compared with the case of an uncorrelated Brownian motion (compare the curves labelled '+/- Wt' and 'Wt(y)' on Figure 6.6), and this using only *one* Brownian motion in space.

Remark 12 *One could argue that the reduction of variance on the stress obtained by using Brownian motions uncorrelated in space is due to a kind of law of large*

numbers : we introduce more random numbers and therefore we reduce the variance, with of course more costly simulations. We have shown in this section that this argument does not hold, since the variance on YX can even be more reduced, using only one Brownian motion in space.

Remark 13 *This reduction of variance using an oscillatory Brownian motion in space reminds us of the antithetic variables method, classically used in Monte Carlo simulations to reduce the variance.*

Variance reduction using arbitrarily many Brownian motions.

In a second step, we allow for the use of an arbitrary number of Brownian motions. We can reformulate the minimization problem we consider in the following :
Minimize $\text{tr}(M^{-1}BK(^tB)(^tM^{-1}))$ among the matrices K such that :
  – K is a symmetric matrix of size $I \times I$,
  – K is positive,
  – $\forall i$, $K_{i,i} = 1$,
  – $\text{tr}(KP) = 0$ (we recall that P is the orthogonal projector on the vector of size $I : (1, ..., 1)$).
This problem has a solution, since we minimize a linear function on a bounded convex closed set. We have solved this problem with the function 'lmisolver' of Scilab (also available in the LMITOOL library for Matlab). This function makes use of interior point methods and has polynomial complexity (see [149]). The time required to compute the matrix K is less than one second for $I = 10$, which is negligeable compared with the resolution of the physical problem (6.17)-(6.20). We have used the covariance matrix obtained to construct a Brownian motion and perform a simulation on the initial time-dependent problem (6.14)-(6.16). The results plotted on Figure 6.6 show that we have indeed further reduced the variance on $U(t)$, with an optimal variance on $Y_t X_t$.

6.4   Numerical simulations

6.4.1   Hookean dumbbells

We here present some simple numerical experiments performed in the case of a pure shear flow with Hookean dumbbells on a uniform mesh (see Eq. (6.17)-(6.20)). The numerical parameters are : the number of cells I, the number of time step N, the number of realizations R, and the number of independent tests $NbTest$ we have performed in order to estimate the variances. The physical parameters in all the simulations are : $v = 1$ (velocity on the boundary), $T = 5$ (final time of the simulation), $\epsilon = 0.9$, Re $= 0.1$, We $= 0.5$.

We can observe that, replacing a Brownian motion not depending on y (see the curves labelled 'Wt' on Figure 6.6) by Brownian motions completely uncorrelated in space (see the curves labelled 'Wt(y)' on Figure 6.6) results into :
  – an increase of the variance of u (velocity) (the variance is multiplied by a factor of 250 for short times and 10^6 for long times : in fact, in case of a Brownian motion not depending on space, we have observed on our simple case that the variance on u seems to tend to zero as t goes to infinity),

– a decrease of the variance of τ (stress) (the variance is divided by about 5 for short times and 2 for long times).

We here observe, in our simple geometry, the same behaviour as other authors already noticed in more complex flows (see [15,74]) which legitimates a throughfull study of the 1D case.

We have also plotted on Figure 6.6 the results obtained with an oscillatory-in-space Brownian motion, and with the optimized covariance matrix.

6.4.2   FENE dumbbells

In the FENE case, the equations (6.14)-(6.16) become :

$$\frac{\partial u}{\partial t}(t,y) = \frac{\partial^2 u}{\partial y^2}(t,y) + \frac{\partial}{\partial y}\mathbb{E}\left(\frac{X_t(y)Y_t(y)}{1-(X_t(y)^2+Y_t(y)^2)/b}\right)\ , \tag{6.38}$$

$$dX_t(y) = \left(\frac{\partial u(t,y)}{\partial y}Y_t(y) - \frac{1}{2}\frac{X_t(y)}{1-(X_t(y)^2+Y_t(y)^2)/b}\right)dt + dW_t(y)\ , \tag{6.39}$$

$$dY_t(y) = -\frac{1}{2}\frac{Y_t(y)}{1-(X_t(y)^2+Y_t(y)^2)/b}dt + dV_t(y)\ , \tag{6.40}$$

One can notice that we may now let the Brownian motion V_t which acts on Y_t depends on space, since Y_t naturally depends on space.

Because of the nonlinear drift in the stochastic differential equations (6.39)-(6.40), we are not able to conduct the arguments of Section 6.3, even for this simple geometry. However, we have tested our three main correlations in space investigated in the Hookean dumbbell case, in the FENE framework (see Figure 6.7) : Brownian motion not depending on space, uncorrelated Brownian motions in space, and oscillatory Brownian motion in space. In our simulations, the parameter b is equal to 20. Let us make precise the oscillatory Brownian motion we consider : to be consistent with the Hookean dumbbell case, we have taken alternatively (W_t, V_t) and $(-W_t, V_t)$ from one cell to another. Note that according to numerical experiments, taking alternatively (W_t, V_t) and $(-W_t, -V_t)$ does not reduce the variance of the stress compared with the case of Brownian motions not depending on space. It seems that *the product* of the Brownian motions driving X_t and Y_t has to be alternating in space to reduce the variance of the stress.

For example (see Figure 6.7), if one uses an oscillatory Brownian motion in space instead of a Brownian motion not depending on space, for short time ($t = 0.12$), the variance on the velocity is only multiplied by 3 but the variance on the stress is divided by 6, and is even better than for uncorrelated Brownian motions in space, which yet corresponds to a more costly simulation. To enable comparisons between the FENE case and the Hookean dumbbell case, notice that for FENE dumbbells, the value of the stress at $t = 5$ is about -0.73, compared to -0.9 for Hookean dumbbells.

We can then draw the following conclusion : using only one Brownian motion in space (and therefore at a fixed computational cost), one can reduce the variance on τ compared to the case of a Brownian motion not depending on space, by using an oscillatory Brownian motion in space.

FIG. 6.6 – Variances of u and τ (versus time) for different correlations in space : solid-line=Wt : a Brownian motion not depending on space ; long-dashed-line=Wt(y) : completely uncorrelated Brownian motions in space ; short-dashed-line=+/-Wt : an oscillatory Brownian motion in space ; dotted-line=Wt optim : results obtained with an optimized correlation matrix.

8

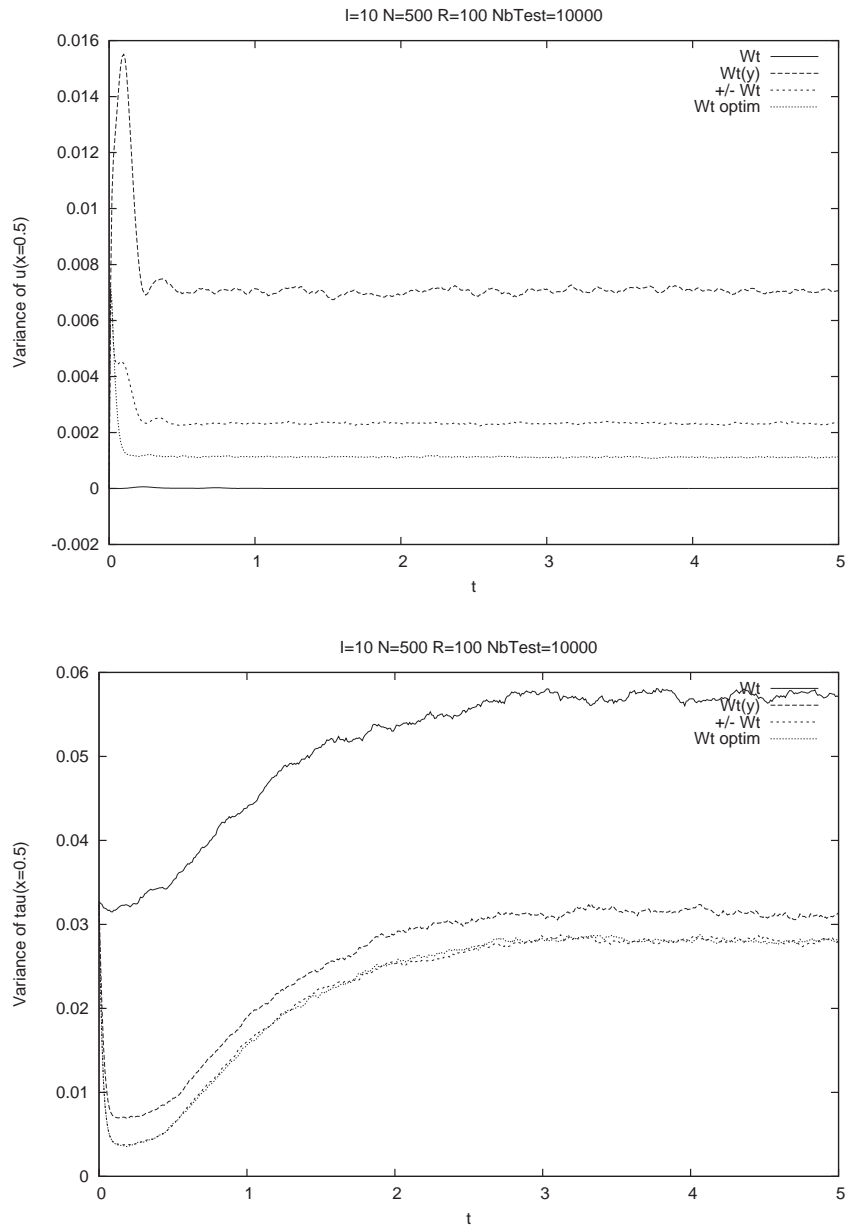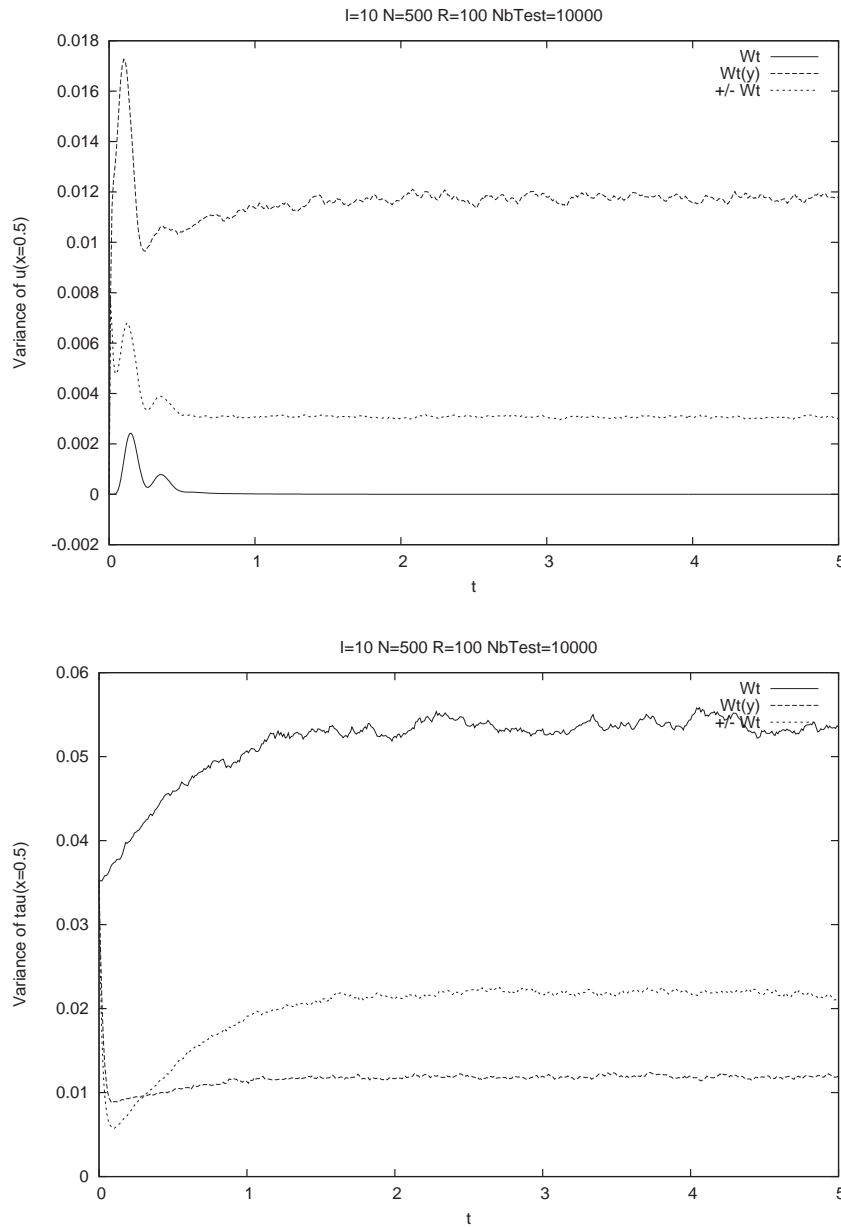FIG. 6.7 – In the case of FENE dumbbells : variances of u and τ versus time for different correlations in space : solid-line=Wt : a Brownian motion not depending on space ; long-dashed-line=Wt(y) : completely uncorrelated Brownian motions in space ; short-dashed-line=+/-Wt : an oscillatory Brownian motion in space.

$t \longrightarrow \infty$	$\delta y \operatorname{tr}(\operatorname{Cov}(Y_t X_t))$ (stress)	$\delta y \operatorname{tr}(\operatorname{Cov}(U(t)))$ (velocity)
W_t	$O(1)$	0
$W_t(y)$	$O(1)$	$O(\delta y)$

FIG. 6.8 – Dependency of the variances of u and τ (for long time) with respect to δy.

6.5 Related issues

6.5.1 Dependency of the variances with respect to the space step δy

In Table 6.8, we give the dependency of the variances of $Y_t X_t$ and $U(t)$ for long time in our simple case. To derive this results, we have used the fact that $b_2 = O(1)$ and $M^{-1} = O(\delta y)$. These last results can be numerically checked by observing that $b_2 = (-1, -1, ..., -1)$ and $(M^{-1})_{i,i} = -\frac{i(I-i)}{I^3}$.

Remark 14 *In case of uncorrelated Brownian motions in space, we observe that the velocity becomes deterministic in the limit $\delta y \to 0$. This can be formally explained in our simple case by the fact that the velocity is an integral over the space of $Y_t X_t$: therefore, a kind of law of large numbers occurs when $\delta y \to 0$.*

6.5.2 Some remarks concerning the bias

The problem we consider is non-linear in the Mc Kean sense, since all the dumb-bells are coupled through the velocity. Therefore, the law of each dumbbell depends on the total number of dumbbells R : to stress this dependency, we denote $(X_t^{j,R}, Y_t^{j,R})$ the end-to-end vector of the j-th dumbbell and $\overline{XY}_t^R = \frac{1}{R} \sum_{j=1}^R X_t^{j,R} Y_t^{j,R}$ the estimated stress. In general, this estimated stress is biased i.e. $\mathbb{E}(\overline{XY}_t^R) = \mathbb{E}(X_t^{j,R} Y_t^{j,R}) \neq \mathbb{E}(X_t Y_t)$, where (X_t, Y_t) is solution of (6.14)-(6.16). From a numerical point of view, one may compute the empirical mean of the estimated stress over NbTest independent experiments $\frac{1}{\text{NbTest}} \sum_{k=1}^{\text{NbTest}} \overline{XY}_t^{R,k}$, with the same number R of dumbbells.

The error induced on the stress can be decomposed as follows :

$$
\mathbb{E}(X_t Y_t) - \frac{1}{\text{NbTest}} \sum_{k=1}^{\text{NbTest}} \overline{XY}_t^{R,k} = \left(\mathbb{E}(X_t Y_t) - \mathbb{E}\left(\overline{XY}_t^R \right) \right)
$$
$$
+ \left(\mathbb{E}\left(\overline{XY}_t^R \right) - \frac{1}{\text{NbTest}} \sum_{k=1}^{\text{NbTest}} \overline{XY}_t^{R,k} \right).
$$

The second term is the statistical error induced by the Monte Carlo method. The first term is a deterministic error, called the bias, which comes from the fact that
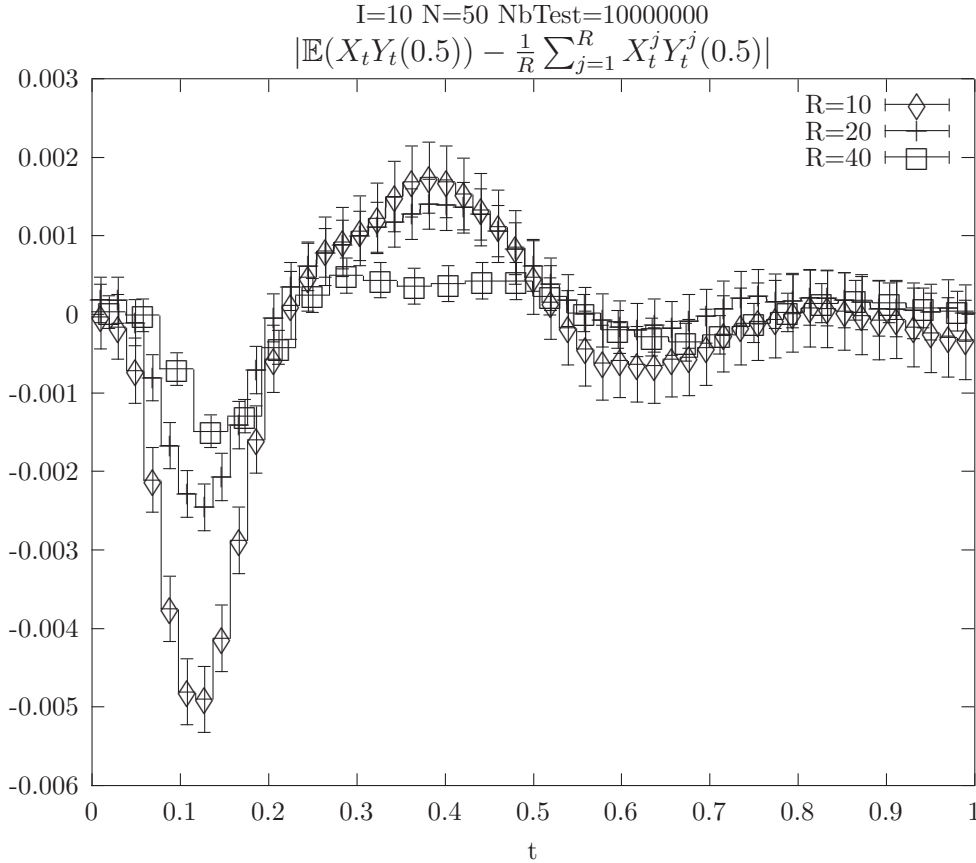
FIG. 6.9 – Error between the estimator of τ and its exact value, at $y = 0.5$, in the Hookean dumbbell case.

the random variables $X_t^{j,R}$ et $Y_t^{j,R}$ are coupled (through the velocity). We have numerically observed a bias which is $O\left(\frac{1}{R}\right)$ (see the values obtained for $t = 0.1$ on Figure 6.9), which seems to be usual for this kind of coupling. In order to underline this dependency, we have performed a huge number of independent tests (NbTest = 10 000 000) to distinguish between the bias (which is typically $O\left(\frac{1}{R}\right)$) and the statistical error (which is typically $O\left(\frac{1}{\sqrt{R}}\right)$ for one single test). We also observe that for long time, the bias vanishes.

From this numerical observation, one can give an answer to the following classical question : in order to reduce the variance on the result, is it preferable to increase the number of dumbbells (R) or the number of tests (NbTest) ? Since the bias is $O\left(\frac{1}{R}\right)$ and the statistical error is $O\left(\frac{1}{\sqrt{R\,\mathrm{NbTest}}}\right)$, it does not make sense to choose NbTest such that NbTest $>> R$. Note that this conclusion also holds when one takes into account the computational cost for it is linear in both R and NbTest, since there are no complex interactions between the dumbbells.

The fact that the statistical error dominates the bias also shows the importance of understanding the variance of the results.

6.6   Conclusions

In this paper, we have explained what kind of dependency in space of the Brownian motion is natural to adopt in the micro-macro modeling of polymeric fluids, namely some Brownian motions dependent in space through the Lagrangian trajectories of the flow.

We have then considered the pure shear flow for one single Hookean dumbbell in the long time limit and we have been able to prove on this simple case that :

a The variance on the velocity u is minimum when one considers a Brownian motion which is constant in space,

b The use of uncorrelated Brownian motions in space is not the best correlation in space to consider, if one wants to reduce the variance on the stress τ ; the use of an oscillatory-in-space Brownian motion is optimal as far as the variance on the stress is concerned,

c It is possible to reduce the variance on τ, compared to a Brownian motion which is constant in space, and this with the same computational cost.

On the simple case of a shear flow with Hookean dumbbells, we have checked by numerical experiments that point (c) above holds on the time-dependent problem, which validates our approach. We have also verified point (c) in the FENE case.

This analysis has shown the importance, for the variance of the results, of the interplay between the correlation matrix in space of the Brownian motions at the microscopic level and the matrices of the discretization of the differential operators at the macroscopic level.

As byproducts of our analysis, we have shown that :

– on our simple case and in the long time limit, the boundary condition does not influence the variance on the velocity but influences the variance on the stress, in the same manner at all points of the domain,

– on our simple case and in the long time limit, when one uses uncorrelated Brownian motions in space, the variance on the velocity goes to zero when the space-step δy goes to zero,

– since we have numerically observed that the bias is $O\left(\frac{1}{R}\right)$ and the statistical error is $O\left(\frac{1}{\sqrt{R\,\mathrm{NbTest}}}\right)$, where R denotes the number of dumbbells in each cell and NbTest the number of independent tests performed with R dumbbells, it does not make sense to choose NbTest such that NbTest $>> R$.

We have summarized these conclusions in Tables 6.10 and 6.11.

	Rigorously proved	Numerically checked	Admitted in the literature
The dependency in space of the Brownian motion does not influence the continuous solution.	Shear flow with Hookean dumbbells or any flow with regular solutions and trajectorial dependency.		Any geometry, any spring, [82].
The CONNFFESSIT method converges to a unique continuous solution whatever the dependency in space.	Shear flow with Hookean dumbbells.	Shear flow or 4 to 1 contraction or journal bearing, [74, 82, 98].	Any flow, any spring, but a question in [121].
A Brownian motion not depending on space reduces the variance on u, but increases the variance on τ.	Shear flow for long time and Hookean dumbbell, $R = 1$.	Shear flow or 4 to 1 contraction with Hookean and FENE dumbbells, [15, 74].	
One can reduce the variance on τ with *one single* Brownian motion.	Shear flow for long time and Hookean dumbbell, $R = 1$.	Shear flow with Hookean and FENE dumbbells.	

FIG. 6.10 – Summary of the principle results : part 1.

	Rigorously proved	Numerically checked	Admitted in the literature
The boundary conditions influence the variance on τ but not on u.	Shear flow for long time and Hookean dumbbell, $R = 1$.	Shear flow with Hookean and FENE dumbbells.	
The variance on u is $O(\delta y)$ with uncorrelated Brownian motions.	Shear flow for long time and Hookean dumbbell, $R = 1$.	Shear flow with Hookean and FENE dumbbells.	
The bias is $O(1/R)$.		Shear flow with Hookean dumbbells.	

FIG. 6.11 – Summary of the principle results : part 2.

Chapitre 7

Convergence d'une approximation particulaire pour FENE-P

Ce chapitre est une version étendue d'un article soumis à *Stochastic Processes and their Application.* Il s'agit de prouver la convergence de l'approximation particulaire du modèle FENE-P. On s'intéresse ici à l'équation différentielle stochastique dans un écoulement homogène.

Convergence of a stochastic particle approximation of the stress tensor for the FENE-P model

Benjamin Jourdain, Tony Lelièvre

We are interested in the FENE-P micro-macro model of polymeric fluid. This model couples a nonlinear stochastic differential equation ruling the evolution of the polymers at the microscopic level and a partial differential equation prescribing the evolution of the velocity and pressure at the macroscopic level. In this paper, we suppose that the velocity field is known and we analyse the nonlinear stochastic differential equation. We prove existence and convergence of a stochastic particle approximation and deduce the convergence of the approximate macroscopic stress tensor.

Keywords : FENE-P model, particle approximations, nonlinear stochastic differential equation, propagation of chaos.

7.1 Introduction

Some models of polymeric fluids are based on the coupling of a stochastic differential equation (SDE) which rules the evolution of a vector representing the polymer in the flow (a microscopic parameter), and a partial differential equation (typically Navier-Stokes equation with an additional term depending on the microscopic parameter) modelling the evolution of macroscopic quantities in the fluid (velocity, pressure) (see [13, 120]). In these so-called micro-macro models, the microscopic quantities influence the macroscopic ones through the stress tensor, and the macroscopic quantities intervene in the evolution of the microscopic unknowns through transport and friction.

The vector $\boldsymbol{X}$ representing the polymer in the flow at the microscopic level gives the orientation and the length of the polymer (see Figure 7.1) which is modelled by two beads linked by a spring. Three forces act on each bead : a drag force, an entropic force modelled by the spring, and a Brownian force due to the thermal agitation of the molecules of the solvent.

Writing down the Langevin equation on each bead in a given velocity field $\boldsymbol{u}(t, \boldsymbol{x})$, one obtains by difference the following stochastic partial differential equation on the vector $\boldsymbol{X}_t(\boldsymbol{x})$ (see [13, 120]) :

$$d\boldsymbol{X}_t(\boldsymbol{x}) + \boldsymbol{u}(t, \boldsymbol{x}).\nabla\boldsymbol{X}_t(\boldsymbol{x})\, dt = \left(\nabla\boldsymbol{u}(t, \boldsymbol{x})\boldsymbol{X}_t(\boldsymbol{x}) - \frac{1}{2\mathrm{We}}\boldsymbol{F}(\boldsymbol{X}_t(\boldsymbol{x})) \right)\, dt + \frac{1}{\sqrt{\mathrm{We}}}d\boldsymbol{W}_t \tag{7.1}$$

where $\boldsymbol{x}$ denotes the space variable, We the Weissenberg number, $\boldsymbol{W}$ a Brownian motion not depending on $\boldsymbol{x}$ and $\boldsymbol{F}$ the entropic force between the two beads. Here and in the following, we write all the equations in a non-dimensional form and we suppose that $\boldsymbol{X} \in \mathbb{R}^N$ with $N = 2$ or $N = 3$. The contribution $\boldsymbol{\tau}_p$ of the polymers to the stress tensor is then :

$$\boldsymbol{\tau}_p(t, \boldsymbol{x}) = \frac{\varepsilon}{\mathrm{We}}\left(\mathbb{E}\left(\boldsymbol{X}_t(\boldsymbol{x}) \otimes \boldsymbol{F}(\boldsymbol{X}_t(\boldsymbol{x})) \right) - \mathrm{Id} \right) \tag{7.2}$$
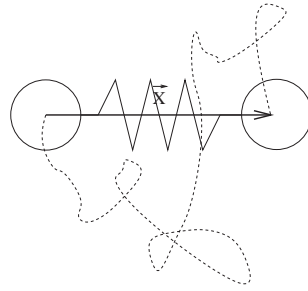
FIG. 7.1 – The polymer (in dashed line) is modelled by two beads linked by a spring, and the length and orientation of the polymer is given by the so-called end-to-end vector $\boldsymbol{X}$.

where ε denotes the ratio of the viscosity due to the polymer over the total viscosity of the liquid.

In the following, we consider that the velocity field $\boldsymbol{u}$ is regular enough (say $\mathcal{C}^1$) so that one can use the characteristic method (by integrating the vector field $\boldsymbol{u}$) to rewrite equation (7.1) in the following form, for each characteristic :

$$dX_t = \left(\boldsymbol{G}(t)\boldsymbol{X}_t - \frac{1}{2\mathrm{We}}\boldsymbol{F}(\boldsymbol{X}_t)\right) dt + \frac{1}{\sqrt{\mathrm{We}}}d\boldsymbol{W}_t \qquad (7.3)$$

where $\boldsymbol{G} : \mathbb{R}_+ \to \mathbb{R}^{N \times N}$. In the following, we suppose that

$$\boldsymbol{G} \text{ is a locally bounded fonction of time on } \mathbb{R}_+. \qquad (7.4)$$

Notice that the process $\boldsymbol{X}_t$ in (7.3) is labelled by the characteristic (see [83]). In the following, we therefore consider one process $\boldsymbol{X}_t$, on a fixed characteristic, for a fixed velocity field (see also Remark 21).

A typical example for the entropic force is a linear force, $\boldsymbol{F}(\boldsymbol{X}) = \boldsymbol{X}$: this leads to the the so-called Hookean dumbbell model. For an analysis of the coupling of the SDE in this case with a PDE on the velocity of the fluid $\boldsymbol{u}$, we refer to [85]. In order to take into account the finite extensibility of the polymer, Warner (see [151]) introduced the Finite Extensible Nonlinear Elastic (FENE) model which consists in choosing the following force law in the dumbbell :

$$\boldsymbol{F}(\boldsymbol{X}) = \frac{\boldsymbol{X}}{1 - ||\boldsymbol{X}||^2/b}. \qquad (7.5)$$

This model gives better results than the Hookean model compared to experimental results. In the case of the FENE model, the SDE for the end-to-end vector $\boldsymbol{X}_t$ of a dumbbell is then :

$$d\boldsymbol{X}_t = \left(\boldsymbol{G}(t)\boldsymbol{X}_t - \frac{1}{2\mathrm{We}}\frac{\boldsymbol{X}_t}{1 - ||\boldsymbol{X}_t||^2/b}\right) dt + \frac{1}{\sqrt{\mathrm{We}}}d\boldsymbol{W}_t \qquad (7.6)$$

where $\sqrt{b}$ denotes the maximal extensibility of the polymer. For an analysis of this SDE, we refer to [84].

The contribution $\boldsymbol{\tau}_p$ of the polymers to the stress tensor is then :

$$\boldsymbol{\tau}_p = \frac{\varepsilon}{\text{We}} \left(\mathbb{E}\left(\frac{\boldsymbol{X}_t \otimes \boldsymbol{X}_t}{1 - ||\boldsymbol{X}_t||^2/b} \right) - \text{Id} \right). \qquad (7.7)$$

To date, it is believed (see [13] p. 89) that it is not possible to obtain a closed consitutive equation for the FENE model. In other words, one cannot find a partial differential equation (PDE) on $\boldsymbol{\tau}_p$. This is a problem when one wants to compare these micro-macro models with classical macroscopic models (for example Oldroyd B, PTT or Giesekus models, see [12]) which are usually based on a PDE written on the stress tensor. From a numerical point of view, these macroscopic models are also interesting since the computational cost to simulate them is less than for models based on microscopic equations. Following the ideas of Peterlin (see [123]), Bird et al. (see [14]) then suggested to consider a force law with the square of the length of the polymer in the denominator of (7.5) replaced by its expectation :

$$\boldsymbol{F}(\boldsymbol{X}_t) = \frac{\boldsymbol{X}_t}{1 - \mathbb{E}(||\boldsymbol{X}_t||^2)/b}, \qquad (7.8)$$

where $\boldsymbol{X}_t$ is therefore solution of the following SDE :

$$d\boldsymbol{X}_t = \left(\boldsymbol{G}(t)\boldsymbol{X}_t - \frac{1}{2\text{We}} \frac{\boldsymbol{X}_t}{1 - \mathbb{E}(||\boldsymbol{X}_t||^2)/b} \right) dt + \frac{1}{\sqrt{\text{We}}} d\boldsymbol{W}_t. \qquad (7.9)$$

This is the so-called FENE-P model (see [14,43,89]). Notice that this SDE is nonlinear in the sense of Mc Kean because of the presence of the expectation of the square of the solution norm in the denominator of the drift coefficient. In Section 7.2, we prove existence of solution to (7.9).

With this closure approximation, one can thus show that the stress tensor $\boldsymbol{\tau}_p$ obtained by the following formula :

$$\boldsymbol{\tau}_p = \frac{\varepsilon}{\text{We}} \left(\frac{\mathbb{E}\left(\boldsymbol{X}_t \otimes \boldsymbol{X}_t\right)}{1 - \mathbb{E}\left(||\boldsymbol{X}_t||^2\right)/b} - \text{Id} \right) \qquad (7.10)$$

can be obtained equivalently by solving a nonlinear PDE. Indeed, one can easily show (at least formally) that $\boldsymbol{A}(t) = \mathbb{E}(\boldsymbol{X}_t \otimes \boldsymbol{X}_t)$ is solution of :

$$\frac{d\boldsymbol{A}(t)}{dt} = \boldsymbol{G}(t)\boldsymbol{A}(t) + \boldsymbol{A}(t)\boldsymbol{G}(t)^T - \frac{1}{\text{We}} \frac{\boldsymbol{A}(t)}{1 - \text{tr}(\boldsymbol{A}(t))/b} + \frac{1}{\text{We}}\text{Id} \qquad (7.11)$$

and then recover $\boldsymbol{\tau}_p = \dfrac{\varepsilon}{\text{We}} \left(\dfrac{\boldsymbol{A}}{1 - \text{tr}(\boldsymbol{A})/b} - \text{Id} \right).$

Remark 18 *This closure approximation does not yield valid results compared to the FENE model at zero shear rate. Bird (see [13] page 89) suggested to modify (7.10) by adding an isotropic constant tensor to preserve the right values at equilibrium. We will not go here into the details of the improvements of the FENE model (see also [29] and the FENE-CR model, or [104] and the FENE-L(S) model).*

For the computation of the FENE-P model, some authors (see for example [89]) have compared the PDE approach and the Monte-Carlo approach based on the following system of SDEs (see details about the CONNFFESSIT method in [97,98, 121] for example) : $\forall 1 \leq i \leq M$,

$$d\boldsymbol{X}_t^{i,M} = \left(\boldsymbol{G}(t)\boldsymbol{X}_t^{i,M} - \frac{1}{2\text{We}} \frac{\boldsymbol{X}_t^{i,M}}{1 - \frac{1}{M}\sum_{i=1}^{M} ||\boldsymbol{X}_t^{i,M}||^2/b} \right) dt + \frac{1}{\sqrt{\text{We}}} d\boldsymbol{W}_t^i \quad (7.12)$$

where $(\boldsymbol{W}^i)_{1 \leq i \leq M}$ denotes a collection of M independent Brownian motions. The stress tensor is then approximated by the empirical mean :

$$\boldsymbol{\tau}_p^M = \frac{\varepsilon}{\text{We}} \left(\frac{\frac{1}{M}\sum_{i=1}^{M} \left(\boldsymbol{X}_t^{i,M} \otimes \boldsymbol{X}_t^{i,M} \right)}{1 - \frac{1}{M}\sum_{i=1}^{M} ||\boldsymbol{X}_t^{i,M}||^2/b} - \text{Id} \right). \quad (7.13)$$

After studying (7.12) in Section 7.3, we prove our main result in Section 7.4 :

Theorem 8 *Assuming (7.4) and under suitable hypothesis on b and the initial conditions $\boldsymbol{X}_0$ and $\boldsymbol{X}_0^i$ (see (7.35) and (7.38)), we have, $\forall t \geq 0$,*

$$\lim_{M \to \infty} \mathbb{E} \left| \boldsymbol{\tau}_p^M(t) - \boldsymbol{\tau}_p(t) \right| = 0, \quad (7.14)$$

where $\boldsymbol{\tau}_p^M$ is defined by (7.13) and $\boldsymbol{\tau}_p$ is defined by (7.10).

Remark 19 *These kinds of mean-field interactions in the framework of fluid mechanics occur not only in the case of closure approximations, but can also be relevant from the physical point of view, for example in the case of liquid crystal polymers (cf. [120] p. 114 and 252-255, or chapter 10 of [39]). We intend to generalize the results obtained here for the FENE-P model also for these models.*

Remark 20 *Since for the FENE-P model, the stress tensor can be computed from the PDE it solves, the FENE-P particle approximation of the stress tensor can be used as a control variate for the computation of the stress tensor in the FENE model. Of course, one then takes the same driving Brownian motions for the FENE and the FENE-P SDEs (see [15] for the use of control variates in CONNFFESSIT simulations).*

Remark 21 (Homogeneous flows) *If $\boldsymbol{u}(t,\boldsymbol{x}) = \boldsymbol{\kappa}(t)\boldsymbol{x}$, together with a pressure $p(t,\boldsymbol{x})$, solve the original Navier-Stokes equations (without the term $\text{div}(\boldsymbol{\tau}_p)$), then $\nabla\boldsymbol{u}(t,\boldsymbol{x}) = \boldsymbol{\kappa}(t)$ does not depend on space. Therefore, (7.1) reduces to (7.3) with $\boldsymbol{G}(t) = \boldsymbol{\kappa}(t)$ and the tensor $\boldsymbol{\tau}_p$ does not depend on space. As $\text{div}(\boldsymbol{\tau}_p) = 0$, the momentum equation on $\boldsymbol{u}$ reduces to the original Navier-Stokes equations. Therefore, $(\boldsymbol{u}, p, \boldsymbol{X}_t)$ solves the micro-macro system (see formula (1.8) in [85]). In other words, in the homogeneous flow case, there is only a one-way coupling : the velocity field is not influenced by the microscopic variables.*

7.2 Continuous level : the nonlinear SDE

Definition 3 *A $(\mathcal{F}_t)$-adapted process $(\boldsymbol{X}_t)_{t\geq 0}$ is a global solution to (7.9) if, $\forall t \geq 0$,*

$$
\begin{cases}
\displaystyle\sup_{0\leq s\leq t} \mathbb{E}\left(||\boldsymbol{X}_s||^2\right) < b, \ \text{and, } \mathbb{P}\text{-a.s.,} \\[2mm]
\displaystyle\int_0^t \frac{||\boldsymbol{X}_s||}{1 - \mathbb{E}\left(||\boldsymbol{X}_s||^2\right)/b}\, ds < \infty, \\[2mm]
\displaystyle\boldsymbol{X}_t = \boldsymbol{X}_0 + \int_0^t \left(\boldsymbol{G}(s)\boldsymbol{X}_s - \frac{1}{2\mathrm{We}}\frac{\boldsymbol{X}_s}{1 - \mathbb{E}\left(||\boldsymbol{X}_s||^2\right)/b}\right) ds + \frac{1}{\sqrt{\mathrm{We}}}\boldsymbol{W}_t.
\end{cases}
\tag{7.15}
$$

We shall prove the following result :

Proposition 3 *Assume (7.4) and $\mathbb{E}(||\boldsymbol{X}_0||^2) < b$ then (7.9) admits a unique solution in the sense of Definition 3.*

Remark 22 *Going through the proof of this Proposition, one can notice that uniqueness for solutions such that $\mathbb{E}(||\boldsymbol{X}_0||^2) < b$ also holds when replacing the first requirement on $(\boldsymbol{X}_t)$ in (7.15) by the weaker requirement :*

$$
\sup_{0\leq s\leq t} \mathbb{E}\left(||\boldsymbol{X}_s||^2\right) < \infty.
$$

To prove Proposition 3, we proceed in two steps. First we prove an existence result on the equation verified by $\mathbb{E}(\boldsymbol{X}_t \otimes \boldsymbol{X}_t)$. Then we prove existence and uniqueness of solutions to (7.9).

Let us introduce the following ordinary differential equation, defined for a time-dependent $N \times N$ matrix $\boldsymbol{A}(t)$:

$$
\begin{cases}
\displaystyle\frac{d\boldsymbol{A}(t)}{dt} = \boldsymbol{G}(t)\boldsymbol{A}(t) + \boldsymbol{A}(t)\boldsymbol{G}(t)^T - \frac{1}{\mathrm{We}}\frac{\boldsymbol{A}(t)}{1 - \mathrm{tr}(\boldsymbol{A}(t))/b} + \frac{1}{\mathrm{We}}\mathrm{Id}, \\[2mm]
\boldsymbol{A}(0) = \mathbb{E}(\boldsymbol{X}_0 \otimes \boldsymbol{X}_0).
\end{cases}
\tag{7.16}
$$

Definition 4 *Let $\boldsymbol{X}_0$ be such that $\mathbb{E}(||\boldsymbol{X}_0||^2) < b$. A continuous $(\mathbb{R}^{N\times N})$-valued function $(\boldsymbol{A}(t))$ is a solution to (7.16) on $[0,T)$ if, $\forall 0 \leq t < T$,*

$$
\begin{cases}
\displaystyle\sup_{0\leq s\leq t} \mathrm{tr}(\boldsymbol{A}(s)) < b, \\[2mm]
\displaystyle\boldsymbol{A}(t) = \mathbb{E}(\boldsymbol{X}_0 \otimes \boldsymbol{X}_0) + \int_0^t \boldsymbol{G}(s)\boldsymbol{A}(s) + \boldsymbol{A}(s)\boldsymbol{G}(s)^T - \frac{1}{\mathrm{We}}\frac{\boldsymbol{A}(s)}{1 - \mathrm{tr}(\boldsymbol{A}(s))/b}\, ds + \frac{t}{\mathrm{We}}\mathrm{Id}.
\end{cases}
\tag{7.17}
$$

Proposition 4 *Assume (7.4) and $\mathbb{E}(||\boldsymbol{X}_0||^2) < b$. There exists a global-in-time solution $(\boldsymbol{A}(t))_{t\geq 0}$ to (7.16) such that, $\forall t \geq 0$, $\boldsymbol{A}(t)$ is a symmetric non-negative matrix. Moreover, any other solution on a time interval $[0,T)$ coincides with $\boldsymbol{A}(t)$ on $[0,T)$. In addition, $\boldsymbol{A}(t)$ is the unique solution of the following ordinary differential equation :*

$$
\overline{\boldsymbol{A}}(0) = \boldsymbol{A}(0)\, ; \, \frac{d\overline{\boldsymbol{A}}(t)}{dt} = \boldsymbol{G}(t)\overline{\boldsymbol{A}}(t) + \overline{\boldsymbol{A}}(t)\boldsymbol{G}(t)^T - \frac{1}{\mathrm{We}}\frac{\overline{\boldsymbol{A}}(t)}{1 - \mathrm{tr}(\boldsymbol{A}(t))/b} + \frac{1}{\mathrm{We}}\mathrm{Id}.
\tag{7.18}
$$

Proof. Let us consider the ordinary differential equation (7.16). Using hypothesis (7.4), it is clear that the application

$$(t, \boldsymbol{A}) \mapsto \boldsymbol{G}(t)\boldsymbol{A} + \boldsymbol{A}\boldsymbol{G}(t)^T - \frac{1}{\text{We}} \frac{\boldsymbol{A}}{1 - \text{tr}(\boldsymbol{A})/b} + \frac{1}{\text{We}}\text{Id}$$

is locally Lipschitz w.r.t. $\boldsymbol{A}$ on $\mathbb{R}_+ \times \left(\mathbb{R}^{N \times N} \setminus \{ \boldsymbol{M} \in \mathbb{R}^{N \times N}, \text{tr}(\boldsymbol{M}) = b \} \right)$. Therefore, by the Cauchy theorem, there exists a unique solution to (7.16) in the sense of Definition 4 on a maximum time interval $[0, T^*)$ such that :

$$\text{if } T^* < \infty, \text{ then } \lim_{t \to T^*} \text{tr}(\boldsymbol{A}(t)) = b. \tag{7.19}$$

By the uniqueness result of the Cauchy theorem, it is clear that this solution is symmetric ($\boldsymbol{A} = \boldsymbol{A}^T$) since if $\boldsymbol{A}(t)$ is solution of (7.16), $\boldsymbol{A}(t)^T$ is solution of the same equation, with the same initial condition.

We shall now prove that the solution $\boldsymbol{A}(t)$ to (7.16) is necessarily non negative.

Let us introduce the process $\boldsymbol{Y}_t$ such that $\boldsymbol{Y}_0 = \boldsymbol{X}_0$ and $\boldsymbol{Y}_t$ is solution to the following SDE :

$$d\boldsymbol{Y}_t = \left(\boldsymbol{G}(t)\boldsymbol{Y}_t - \frac{1}{2\text{We}} \frac{\boldsymbol{Y}_t}{1 - \text{tr}(\boldsymbol{A}(t))/b} \right) dt + \frac{1}{\sqrt{\text{We}}} d\boldsymbol{W}_t. \tag{7.20}$$

It is clear that there exists a solution to (7.20) on the time interval $[0, T^*)$ and that $t \mapsto \mathbb{E}(\|\boldsymbol{Y}_t\|^2)$ is locally bounded on $[0, T^*)$ since the application

$$(t, \boldsymbol{Y}) \mapsto \boldsymbol{G}(t)\boldsymbol{Y} - \frac{1}{2\text{We}} \frac{\boldsymbol{Y}}{1 - \text{tr}(\boldsymbol{A}(t))/b}$$

is Lipschitz and with linear growth w.r.t. $\boldsymbol{Y}$ locally in time on $[0, T^*)$. Let us now consider $\overline{\boldsymbol{A}}(t) = \mathbb{E}(\boldsymbol{Y}_t \otimes \boldsymbol{Y}_t)$. One can easily check by Itô's calculus that $\overline{\boldsymbol{A}}(t)$ is solution of (7.18) on $[0, T^*)$. As the right-hand side of (7.18) is affine w.r.t. $\overline{\boldsymbol{A}}$, with coefficients bounded locally in time on $[0, T^*)$, uniqueness of solution to (7.18) on $[0, T^*)$ holds and thus

$$\boldsymbol{A}(t) = \mathbb{E}(\boldsymbol{Y}_t \otimes \boldsymbol{Y}_t)$$

and therefore $\boldsymbol{A}(t)$ is a symmetric and non negative matrix on $[0, T^*)$.

We shall now prove that $T^* = +\infty$. Let us suppose that $T^* < \infty$ and obtain a contradiction. We notice that $\text{Tr}(t) = \text{tr}(\boldsymbol{A}(t))$ is solution of the following ODE :

$$\frac{d\text{Tr}(t)}{dt} = \text{tr}\left((\boldsymbol{G}(t) + \boldsymbol{G}(t)^T)\boldsymbol{A}(t) \right) - \frac{1}{\text{We}} \frac{\text{Tr}(t)}{1 - \text{Tr}(t)/b} + \frac{N}{\text{We}}. \tag{7.21}$$

One can check that there exists $C > 0$ such that, for any symmetric non negative matrix $\boldsymbol{A}$,

$$\text{tr}\left((\boldsymbol{G}(t) + \boldsymbol{G}(t)^T)\boldsymbol{A} \right) \leq C\|\boldsymbol{G}(t)\|\text{tr}(\boldsymbol{A}).$$

This can be proved using the fact that, for a symmetric non negative matrix $\boldsymbol{A}$, $\sqrt{\text{tr}(\boldsymbol{A}^2)} \leq \text{tr}(\boldsymbol{A})$. Therefore, we have :

$$\frac{d\text{Tr}(t)}{dt} \leq C\|\boldsymbol{G}(t)\|\text{Tr}(t) - \frac{1}{\text{We}} \frac{\text{Tr}(t)}{1 - \text{Tr}(t)/b} + \frac{N}{\text{We}}. \tag{7.22}$$

By (7.19), we have $\forall t \in [0, T^*)$, $\mathrm{Tr}(t) \in [0, b)$ and $\lim_{t \to T^*} \mathrm{Tr}(t) = b$ so that,

$$\lim_{t \to T^*} C\|\boldsymbol{G}(t)\|\mathrm{Tr}(t) - \frac{1}{\mathrm{We}}\frac{\mathrm{Tr}(t)}{1 - \mathrm{Tr}(t)/b} + \frac{N}{\mathrm{We}} = -\infty,$$

and therefore there exists $\epsilon > 0$ such that $\forall t \in (T^* - \epsilon, T^*)$, $\frac{d\mathrm{Tr}(t)}{dt} < 0$. This is the desired contradiction and shows that $T^* = \infty$.

One can finally easily show uniqueness of solution to (7.16) on any interval $[0, T)$ by the uniqueness result of the Cauchy theorem.

<div align="right">□</div>

The proof of Proposition 3 is now straightforward. One considers the solution $\boldsymbol{A}(t)$ to (7.16) we have built in Proposition 4. It is then easy to find a solution $\boldsymbol{Y}_t$ to (7.20) defined on $\mathbb{R}_+$. By uniqueness of solutions to (7.18), we obtain $\boldsymbol{A}(t) = \mathbb{E}(\boldsymbol{Y}_t \otimes \boldsymbol{Y}_t)$. This shows that $\boldsymbol{Y}_t$ is solution of (7.9) in the sense of Definition 3. Uniqueness can then be deduced from the fact that if $\boldsymbol{X}_t$ is solution to (7.9) in the sense of Definition 3, then, by Itô's calculus, $\mathbb{E}(\boldsymbol{X}_t \otimes \boldsymbol{X}_t)$ is solution to (7.16). Therefore, $\mathbb{E}(\boldsymbol{X}_t \otimes \boldsymbol{X}_t) = \boldsymbol{A}(t)$ where $\boldsymbol{A}(t)$ is the unique solution to (7.16). Uniqueness of the solution $\boldsymbol{X}_t$ to (7.9) therefore follows from uniqueness of solutions to (7.20).

7.3 Discrete level : the particle system

We prove existence of solutions to (7.12) and study some properties of these solutions, which will be useful for the proof of Theorem 8 in Section 7.4. Henceforth, $(\boldsymbol{W}_t^i)_{i \geq 1}$ denote a collection of independent Brownian motions, and $(\boldsymbol{X}_0^i)_{i \geq 1}$ an independent collection of initial random variables. Notice that the case $M = 1$ coincides with the FENE model, studied in [84, 86].

7.3.1 Existence of solutions to (7.12)

We consider the system of SDEs (7.12) and prove existence and uniqueness of solution.

Definition 5 *We shall say that the $(\mathcal{F}_t)$-adapted process $(\boldsymbol{X}_t^{i,M})_{1 \leq i \leq M}$ (with value in $\mathbb{R}^{N \times M}$) is solution to (7.12) if, $\mathbb{P} - a.s.$, $\forall t \geq 0$,*

$$\begin{cases} \displaystyle\int_0^t \left| \frac{\sum_{i=1}^M \|\boldsymbol{X}_s^{i,M}\|}{1 - \frac{1}{M}\sum_{i=1}^M \|\boldsymbol{X}_t^{i,M}\|^2/b} \right| ds < \infty \qquad and, \ \forall 1 \leq i \leq M, \\[4mm] \displaystyle\boldsymbol{X}_t^{i,M} = \boldsymbol{X}_0^i + \int_0^t \left(\boldsymbol{G}(s)\boldsymbol{X}_s^{i,M} - \frac{1}{2\mathrm{We}}\frac{\boldsymbol{X}_s^{i,M}}{1 - \frac{1}{M}\sum_{i=1}^M \|\boldsymbol{X}_s^{i,M}\|^2/b} \right) ds + \frac{1}{\sqrt{\mathrm{We}}}\boldsymbol{W}_t^i. \end{cases}$$

Proposition 5 *Assume (7.4), $Mb \geq 2$ and that, a.s., $\frac{1}{M}\sum_{i=1}^M \|\boldsymbol{X}_0^i\|^2 < b$. There exists a unique solution $(\boldsymbol{X}_t^{i,M})_{1 \leq i \leq M}$ to (7.12) in the sense of Definition 5. In*

addition, this solution is such that

$$\mathbb{P}\left(\exists t \geq 0, \frac{1}{M}\sum_{i=1}^{M}||\boldsymbol{X}_t^{i,M}||^2 = b\right) = 0.$$

Moreover, for any $r > 1$, if

$$b > 2(r+1) \quad and \quad \sup_{M \geq 1}\mathbb{E}\left(\frac{1}{1-\frac{1}{M}\sum_{i=1}^{M}||\boldsymbol{X}_0^i||^2/b}\right)^p < \infty, \text{ for some } p > r, \quad (7.23)$$

then

$$t \mapsto \sup_{M \geq 1}\mathbb{E}\left(\frac{1}{1-\frac{1}{M}\sum_{i=1}^{M}||\boldsymbol{X}_t^{i,M}||^2/b}\right)^r \text{ is locally bounded.} \quad (7.24)$$

Remark 23 *If moreover the initial conditions $(\boldsymbol{X}_0^i)_{i \geq 1}$ are i.i.d., then the particles $(\boldsymbol{X}_t^{i,M})_{1 \leq i \leq M}$ are exchangeable and, $\forall t \geq 0$,*

$$\mathbb{E}(||\boldsymbol{X}_t^{1,M}||^2) = \mathbb{E}\left(\frac{1}{M}\sum_{i=1}^{M}||\boldsymbol{X}_t^{i,M}||^2\right) \leq b. \quad (7.25)$$

Proof. Let us introduce the process $(\boldsymbol{X}_t^{i,M,n})_{1 \leq i \leq M}$ solution of

$$\boldsymbol{X}_t^{i,M,n} = \boldsymbol{X}_0^i + \int_0^t\left(\boldsymbol{G}(s)\boldsymbol{X}_s^{i,M,n} - \frac{1}{2\text{We}}\frac{\boldsymbol{X}_s^{i,M,n}}{\max\left(1-\frac{1}{M}\sum_{i=1}^{M}||\boldsymbol{X}_t^{i,M,n}||^2/b, \frac{1}{n}\right)}\right)ds + \frac{1}{\sqrt{\text{We}}}\boldsymbol{W}_t^i,$$

and the stopping time $\tau_n = \inf\left\{t, \frac{1}{M}\sum_{i=1}^{M}||\boldsymbol{X}_t^{i,M,n}||^2 \geq b(1-1/n)\right\}$. By continuation of the solutions $(\boldsymbol{X}_t^{i,M,n})_{1 \leq i \leq M}$ considered on $[0, \tau_n)$, one easily obtains a solution $(\boldsymbol{X}_t^{i,M})_{1 \leq i \leq M}$ to (7.12) on $[0, \lim_{n \to \infty}\tau_n)$.

Let us now introduce

$$R_t^M = \frac{1}{M}\sum_{i=1}^{M}||\boldsymbol{X}_t^{i,M}||^2. \quad (7.26)$$

By Itô's calculus, one obtains that R_t^M is solution of the following SDE on $[0, \lim_{n \to \infty}\tau_n)$:

$$\begin{aligned}R_t^M &= R_0^M + \int_0^t\left(\frac{2}{M}\sum_{i=1}^{M}\boldsymbol{X}_s^{i,M}.\left(\boldsymbol{G}(s)\boldsymbol{X}_s^{i,M}\right) - \frac{1}{\text{We}}\frac{R_s^M}{1-R_s^M/b} + \frac{N}{\text{We}}\right)ds \\ &\quad + \frac{2}{\sqrt{\text{We}\,M}}\int_0^t\sqrt{R_s^M}\,dB_s,\end{aligned} \quad (7.27)$$

with (B_t) a Brownian motion defined by

$$B_t = \int_0^t\frac{1_{\{\sum_{i=1}^{M}||\boldsymbol{X}_s^{i,M}||^2 > 0\}}}{\sqrt{\sum_{i=1}^{M}||\boldsymbol{X}_s^{i,M}||^2}}\sum_{i=1}^{M}\boldsymbol{X}_s^{i,M}d\boldsymbol{W}_s^i + \int_0^t 1_{\{\sum_{i=1}^{M}||\boldsymbol{X}_s^{i,M}||^2 = 0\}}d\boldsymbol{W}_s^1.$$

We will use the fact that $\forall \boldsymbol{X}, |\boldsymbol{X}.(\boldsymbol{G}(t)\boldsymbol{X})| \leq \frac{C}{2}||\boldsymbol{G}(t)||\,||\boldsymbol{X}||^2$, with $C > 0$ a constant, and we denote in the following $g(t) = C||\boldsymbol{G}(t)||$.

Let us now introduce ρ_t^M a stochastic process solution of the following SDE :

$$\rho_t^M = R_0^M + \int_0^t \left(g(s)\rho_s^M \, ds - \frac{1}{\mathrm{We}} \frac{\rho_s^M}{1 - \rho_s^M/b} + \frac{N}{\mathrm{We}} \right) ds + \frac{2}{\sqrt{\mathrm{We}\,M}} \int_0^t \sqrt{\rho_s^M} \, dB_s. \tag{7.28}$$

Notice that one can build a process ρ_t^M weak solution to (7.28) by considering the solution $(\boldsymbol{Y}_t^{i,M})_{1 \leq i \leq M}$ of the following system of SDEs :

$$\boldsymbol{Y}_t^{i,M} = \boldsymbol{X}_0^i + \int_0^t \left(g(s)\boldsymbol{Y}_s^{i,M} - \frac{1}{2\mathrm{We}} \frac{\boldsymbol{Y}_s^{i,M}}{1 - \frac{1}{M}\sum_{i=1}^{M} ||\boldsymbol{Y}_t^{i,M}||^2/b} \right) ds + \frac{1}{\sqrt{\mathrm{We}}} \boldsymbol{W}_t^i, \tag{7.29}$$

and then considering $\rho_t^M = \frac{1}{M}\sum_{i=1}^{M} ||\boldsymbol{Y}_t^{i,M}||^2$. By using the fact that $Mb \geq 2$ and that g is locally square integrable and by following exactly the lines of the proof of the existence of a solution for the FENE model (see Section 2 in [86]), it is easy to show that (7.29) admits a solution $(\boldsymbol{Y}_t^{i,M})_{1 \leq i \leq M}$ defined on $\mathbb{R}_+$, and such that

$$\mathbb{P}(\exists t \geq 0, \rho_t^M = b) = \mathbb{P}(\exists t \geq 0, \rho_t^M = 0) = 0.$$

Moreover, using (7.23) and following the proof in Section 2 of [86], we have

$$t \mapsto \mathbb{E}\left(\frac{1}{1-\rho_t^M/b} \right)^r \text{ is locally bounded, uniformly in } M.$$

Existence of a strong solution to (7.28) follows then from Yamada-Watanabe theorem since pathwise uniqueness holds for solutions with paths in $\mathcal{C}(\mathbb{R}^+, (0,b))$.

Let us prove this last point. Let us consider two solutions (ρ_t) and $(\tilde{\rho}_t)$ to (7.28) with same initial condition and same Brownian motion, and with paths in $\mathcal{C}(\mathbb{R}^+, (0,b))$. By Corollary 3.4 page 360 in [134], we know that $L^0(\rho - \tilde{\rho}) = 0$. Therefore, by Tanaka's formula (see Theorem 1.2 p. 207 in [134]) :

$$
\begin{aligned}
(\rho_t - \tilde{\rho}_t)^+ &= \int_0^t 1_{\rho_s \geq \tilde{\rho}_s} d(\rho - \tilde{\rho})_s \\
&\leq \int_0^t g(s)(\rho_s - \tilde{\rho}_s)^+ \, ds + \frac{2}{\sqrt{\mathrm{We}\,M}} \int_0^t 1_{\rho_s \geq \tilde{\rho}_s} (\sqrt{\rho_s} - \sqrt{\tilde{\rho}_s}) \, dB_s
\end{aligned}
$$

where we have used the fact that $r \mapsto \dfrac{r}{1 - r/b}$ is increasing on $(0,b)$. We know that ρ and $\tilde{\rho}$ are bounded so that :

$$\mathbb{E}(\rho_t - \tilde{\rho}_t)^+ \leq \int_0^t g(s)\mathbb{E}(\rho_s - \tilde{\rho}_s)^+ \, ds.$$

Using Gronwall Lemma and the fact that g is locally integrable, we therefore obtain that $\rho \leq \tilde{\rho}$. It is clear then that we also have $\tilde{\rho} \leq \rho$ and therefore pathwise uniqueness holds for (7.29).

Using exactly the same proof as above on $[0, \lim_{n\to\infty} \tau_n)$ with R^M and ρ^M replacing ρ and $\tilde{\rho}$, it is easy to show that $\forall t \in [0, \lim_{n\to\infty} \tau_n)$,

$$R_t^M \leq \rho_t^M. \tag{7.30}$$

Since a.s. $\rho^M \in \mathcal{C}(\mathbb{R}_+, (0, b))$, we deduce from (7.30) that a.s. :

$$\lim_{n\to\infty} \tau_n = \infty.$$

This also shows (7.24).

To conclude the proof, one needs to show pathwise uniqueness of solutions to (7.12), but this can be easily done using the same proof as in Lemma 1 of [86]. □

7.3.2   Properties of solutions to (7.12)

Let us now introduce ρ_t^∞ solution of the following ODE :

$$\rho_t^\infty = \mathbb{E}(||\boldsymbol{X}_0^1||^2) + \int_0^t \left(g(s)\rho_s^\infty \, ds - \frac{1}{\text{We}} \frac{\rho_s^\infty}{1 - \rho_s^\infty/b} + \frac{N}{\text{We}} \right) ds. \tag{7.31}$$

We suppose that $\mathbb{E}(||\boldsymbol{X}_0^1||^2) < b$. Using the fact that $t \mapsto g(t)$ is locally bounded and the fact that, $\forall t \geq 0$, uniformly in $s \in [0, t]$, $\rho \mapsto g(s)\rho - \dfrac{1}{\text{We}} \dfrac{\rho}{1 - \rho/b} + \dfrac{N}{\text{We}}$ goes to $-\infty$ when ρ tends to b^-, and to $\frac{N}{\text{We}} > 0$ when ρ tends to 0^+, it is easy to show that (7.31) admits a unique solution defined on $\mathbb{R}_+$ and with values in $(0, b)$. We will use the following lemma :

Lemma 19 *Let us suppose (7.4), $b \geq 2$, $\mathbb{E}(||\boldsymbol{X}_0^1||^2) < b$, $\mathbb{E}(||\boldsymbol{X}_0^1||^4) < \infty$ and that the initial conditions $\boldsymbol{X}_0^i$ are i.i.d.. We have, $\forall t > 0$,*

$$\mathbb{E}\left(\sup_{s \leq t} ((R_s^M - \rho_s^\infty)^+)^2 \right) \leq \frac{C(t)}{M}, \tag{7.32}$$

where $C(t)$ depends on b, $\text{Var}(||\boldsymbol{X}_0^1||^2)$ and $||\boldsymbol{G}||$.

Proof. By Itô's calculus, one obtains :

$$
\begin{aligned}
(\rho_t^M - \rho_t^\infty)^2 &= \left(\frac{1}{M} \sum_{i=1}^M ||\boldsymbol{X}_0^i||^2 - \mathbb{E}(||\boldsymbol{X}_0^1||^2) \right)^2 + 2 \int_0^t (\rho_s^M - \rho_s^\infty) \, d(\rho^M - \rho^\infty)_s \\
&\quad + \frac{4}{\text{We } M} \int_0^t \rho_s^M \, ds \\
&\leq \left(\frac{1}{M} \sum_{i=1}^M ||\boldsymbol{X}_0^i||^2 - \mathbb{E}(||\boldsymbol{X}_0^1||^2) \right)^2 + 2 \int_0^t g(s)(\rho_s^M - \rho_s^\infty)^2 \, ds \\
&\quad + \frac{4}{\text{We } M} \int_0^t \rho_s^M \, ds + \frac{4}{\sqrt{\text{We } M}} \int_0^t (\rho_s^M - \rho_s^\infty) \sqrt{\rho_s^M} \, dB_s.
\end{aligned}
$$

So that :

$$\mathbb{E}\left(\sup_{0 \le s \le t}(\rho_s^M - \rho_s^\infty)^2\right) \le \frac{\text{Var}(||\boldsymbol{X}_0^1||^2)}{M} + 2\int_0^t g(s)\mathbb{E}\left(\sup_{0 \le r \le s}(\rho_r^M - \rho_r^\infty)^2\right)\,ds + \frac{4b}{\text{We}\,M}t$$
$$+ \frac{4}{\sqrt{\text{We}\,M}}\mathbb{E}\left(\sup_{0 \le s \le t}\int_0^s(\rho_r^M - \rho_r^\infty)\sqrt{\rho_r^M}\,dBr\right).$$

Using Burkholder-Davis-Gundy inequality, we have :

$$\mathbb{E}\left(\sup_{0 \le s \le t}\int_0^s(\rho_r^M - \rho_r^\infty)\sqrt{\rho_r^M}\,dBr\right) \le C\mathbb{E}\left(\sqrt{\int_0^t(\rho_r^M - \rho_r^\infty)^2\rho_r^M\,dr}\right)$$

$$\le C\sqrt{b}\sqrt{\int_0^t\mathbb{E}\left(\sup_{0 \le r \le s}(\rho_r^M - \rho_r^\infty)^2\right)\,ds}$$

$$\le C\sqrt{b}\left(\frac{1}{\sqrt{M}} + \frac{\sqrt{M}}{4}\int_0^t\mathbb{E}\left(\sup_{0 \le r \le s}(\rho_r^M - \rho_r^\infty)^2\right)\,ds\right)$$

so that,

$$\mathbb{E}\left(\sup_{0 \le s \le t}(\rho_s^M - \rho_s^\infty)^2\right) \le \int_0^t\left(2g(s) + \frac{C\sqrt{b}}{\sqrt{\text{We}}}\right)\mathbb{E}\left(\sup_{0 \le r \le s}(\rho_r^M - \rho_r^\infty)^2\right)\,ds$$
$$+ \frac{1}{M}\left(\frac{4b}{\text{We}}t + \frac{4C\sqrt{b}}{\sqrt{\text{We}}} + \text{Var}(||\boldsymbol{X}_0^1||^2)\right).$$

Using the fact that g is locally integrable, we then obtain, by Gronwall Lemma,

$$\mathbb{E}\left(\sup_{s \le t}(\rho_s^M - \rho_s^\infty)^2\right) \le \frac{C(t)}{M}. \tag{7.33}$$

It is then easy to prove (7.32) using (7.30) :

$$(R_s^M - \rho_s^\infty)^+ \le (R_s^M - \rho_s^M)^+ + (\rho_s^M - \rho_s^\infty)^+ \le (\rho_s^M - \rho_s^\infty)^+.$$

$\square$

Let us now generalize (7.25) and control the moments of $\boldsymbol{X}_t^{1,M}$:

Lemma 20 *Let us assume (7.4). Let $p \ge 1$ and suppose that $\mathbb{E}(||\boldsymbol{X}_0^1||^{2p}) < b$. Then $\forall t \ge 0$,*
$$\sup_{M \ge 1}\sup_{s \le t}\mathbb{E}\left(||\boldsymbol{X}_s^{1,M}||^{2p}\right) \le C_p(t). \tag{7.34}$$

where $C_p(t)$ depends on $||\boldsymbol{G}||$ and b.

Proof. By Itô's calculus, we have :

$$
\begin{aligned}
||\boldsymbol{X}_t^{1,M}||^{2p} &= ||\boldsymbol{X}_0^{1,M}||^{2p} + \int_0^t 2p||\boldsymbol{X}_s^{1,M}||^{2p-2}\boldsymbol{X}_s^{1,M}.\boldsymbol{G}(s)\boldsymbol{X}_s^{1,M}\,ds \\
&\quad + \frac{1}{\text{We}}\int_0^t p(2p+N-2)||\boldsymbol{X}_s^{1,M}||^{2p-2}\,ds \\
&\quad - \frac{p}{\text{We}}\int_0^t \frac{||\boldsymbol{X}_s^{1,M}||^{2p}}{1-R_s^M/b}\,ds + \frac{1}{\sqrt{\text{We}}}\int_0^t 2p||\boldsymbol{X}_s^{1,M}||^{2p-2}\boldsymbol{X}_s^{1,M}.d\boldsymbol{W}_s
\end{aligned}
$$

We then obtain formally (using the fact that $\mathbb{E}(||\boldsymbol{X}_s^{1,M}||^{2p-2}) \leq C\left(1+\mathbb{E}(||\boldsymbol{X}_s^{1,M}||^{2p})\right))$:

$$
\begin{aligned}
\mathbb{E}(||\boldsymbol{X}_t^{1,M}||^{2p}) &\leq \mathbb{E}(||\boldsymbol{X}_0^{1,M}||^{2p}) + \int_0^t 2p||\boldsymbol{G}(s)||\mathbb{E}(||\boldsymbol{X}_s^{1,M}||^{2p})\,ds \\
&\quad + \frac{1}{\text{We}}\int_0^t p(2p+N-2)\mathbb{E}(||\boldsymbol{X}_s^{1,M}||^{2p-2})\,ds \\
&\leq \mathbb{E}(||\boldsymbol{X}_0^{1,M}||^{2p}) + \int_0^t C(s)\mathbb{E}(||\boldsymbol{X}_s^{1,M}||^{2p})\,ds + Ct
\end{aligned}
$$

where the constants depend on $||\boldsymbol{G}||$, p but not on M. One can then conclude by Gronwall Lemma. One uses a localization argument to complete the proof rigorously. □

7.4 Convergence of $\boldsymbol{\tau}_p^M$ towards $\boldsymbol{\tau}_p$

This section is devoted to the proof of Theorem 8. From now on, we suppose that (7.4) holds and that :

The initial variable $\boldsymbol{X}_0$ is such that
$$\mathbb{P}\text{-a.s. } ||\boldsymbol{X}_0||^2 < b \text{ and } \mathbb{E}\left(\frac{1}{1-||\boldsymbol{X}_0||^2/b}\right)^p < \infty \text{ for some } p > 2.$$
Moreover, initial conditions $\boldsymbol{X}_0^i$ are independent with the same distribution as $\boldsymbol{X}_0$. (7.35)

We consider the solutions $\boldsymbol{X}_t^{i,M}$ to (7.12), R_t^M defined by (7.26) for $M \geq 1$. We will also use ρ_t^∞ defined by (7.31). Notice that under these assumptions, the results stated in Lemma 19 and in Lemma 20 (for any p) hold. In particular, we have $\forall p \geq 1$, $\forall t \geq 0$,

$$\sup_{M \geq 1}\sup_{s \leq t}\mathbb{E}\left(||\boldsymbol{X}_s^{1,M}||^{2p}\right) \leq C_p(t). \tag{7.36}$$

Notice that for the exponent p defined in (7.35), by convexity of $x \in (0,b) \mapsto \left(\frac{1}{1-x/b}\right)^p$ and Jensen inequality, we also have :

$$
\begin{aligned}
\sup_{M \geq 1}\mathbb{E}\left(\frac{1}{1-\frac{1}{M}\sum_{i=1}^M ||\boldsymbol{X}_0^i||^2/b}\right)^p &\leq \sup_{M \geq 1}\mathbb{E}\left(\frac{1}{M}\sum_{i=1}^M\left(\frac{1}{1-||\boldsymbol{X}_0^i||^2/b}\right)^p\right) \\
&\leq \mathbb{E}\left(\frac{1}{1-||\boldsymbol{X}_0||^2/b}\right)^p < \infty. \tag{7.37}
\end{aligned}
$$

Moreover, we suppose in the following that :

$$b > 6. \tag{7.38}$$

Therefore, by (7.37) and (7.38), using (7.24) in Proposition 5, we know that $\exists r > 2$,

$$t \mapsto \sup_{M \geq 1} \mathbb{E} \left(\frac{1}{1 - \frac{1}{M} \sum_{i=1}^{M} ||\boldsymbol{X}_t^{i,M}||^2 / b} \right)^r \text{ is locally bounded.} \tag{7.39}$$

Remark 24 *The parameter b is in practice of the order of 100 (see [120] page 217). The hypothesis (7.38) is therefore not a constraint from the physical point of view.*

Let us consider the solution $(\boldsymbol{X}_t^{i,M})_{1 \leq i \leq M}$ to (7.12) and $\boldsymbol{\tau}_p^M$ defined by (7.13). We want to show that, in the limit $M \to \infty$, $\boldsymbol{\tau}_p^M$ converges towards $\boldsymbol{\tau}_p$ defined by (7.10) with $\boldsymbol{X}_t$ solution to (7.9).

We introduce the random variable μ_M with values in $\mathcal{P}(\mathcal{C}(\mathbb{R}_+, \mathbb{R}^N))$ defined by :

$$\mu_M = \frac{1}{M} \sum_{i=1}^{M} \delta_{\boldsymbol{X}^{i,M}}. \tag{7.40}$$

We denote $\Pi_M \in \mathcal{P}\left(\mathcal{P}(\mathcal{C}(\mathbb{R}_+, \mathbb{R}^N))\right)$ the law of μ_M.

We will prove the convergence of $\boldsymbol{\tau}_p^M$ towards $\boldsymbol{\tau}_p$ (Section 7.4.3) by proving first the convergence (in probability) of μ_M towards the law of $\boldsymbol{X}_t$, solution to (7.9) in the sense of Definition 3 (Section 7.4.2). To perform the proof, we need to characterize the law of $\boldsymbol{X}_t$ as the solution of a martingale problem (Section 7.4.1).

In the following, we denote $(\boldsymbol{Y}_t)_{t \geq 0}$ the canonical process on $\mathcal{C}(\mathbb{R}_+, \mathbb{R}^N)$ and Q the canonical variable on $\mathcal{P}(\mathcal{C}(\mathbb{R}_+, \mathbb{R}^N))$.

7.4.1 A nonlinear martingale problem

In order to prove the convergence of Π_M, we introduce the following martingale problem.

Definition 6 *We say that $Q \in \mathcal{P}(\mathcal{C}(\mathbb{R}_+, \mathbb{R}^N))$, with marginals $(Q_t)_{t \geq 0}$ defined in $\mathcal{P}(\mathbb{R}^N)$, is solution of the martingale problem (MP) if :*

$$Q_0 \text{ is the law of } \boldsymbol{X}_0, \tag{7.41}$$

$$\forall t > 0, \sup_{0 \leq s \leq t} \left(\int ||\boldsymbol{Y}_s||^2 Q(d\boldsymbol{Y}) \right) < b, \tag{7.42}$$

$$\left\{ \begin{array}{l} \forall \phi \in \mathcal{C}_0^2(\mathbb{R}^N), \\ M_t^\phi = \phi(\boldsymbol{Y}_t) - \phi(\boldsymbol{Y}_0) - \int_0^t \left(\boldsymbol{G}(s)\boldsymbol{Y}_s - \frac{1}{2\mathrm{We}} \frac{\boldsymbol{Y}_s}{1 - \int ||\boldsymbol{Y}_s||^2 Q(d\boldsymbol{Y})/b} \right) . \nabla \phi(\boldsymbol{Y}_s) \\ \qquad + \frac{1}{2\mathrm{We}} \Delta \phi(\boldsymbol{Y}_s) \, ds \\ \text{is a } Q\text{-martingale,} \end{array} \right. \tag{7.43}$$

where $\mathcal{C}_0^2(\mathbb{R}^N)$ denotes the set of twice continuously differentiable functions having compact support.

Remark 25 *Writing the constancy of the expectation of the martingale M_t^ϕ, one obtains that if Q verifies (7.43), then $t \mapsto Q_t$ is a weak solution of the Fokker-Planck equation associated to (7.9) :*

$$\partial_t \psi(t, \boldsymbol{\xi}) = -\text{div}\,_{\boldsymbol{\xi}} \left(\left(\boldsymbol{G}(t)\boldsymbol{\xi} - \frac{1}{2\text{We}} \frac{\boldsymbol{\xi}}{1 - \int ||\boldsymbol{\xi}||^2 \psi(t, \boldsymbol{\xi})\,d\boldsymbol{\xi}/b} \right) \psi(t, \boldsymbol{\xi}) \right) + \frac{1}{2\text{We}} \Delta_{\boldsymbol{\xi}} \psi(t, \boldsymbol{\xi}).$$

We have the following proposition :

Proposition 6 *The martingale problem (MP) admits a unique solution, which is the law of the process $\boldsymbol{X}_t$ solution to (7.9) in the sense of Definition 3.*

Proof. The fact that the law of the solution $\boldsymbol{X}_t$ to (7.9) solves the martingale problem (MP) is an easy consequence of Itô's formula. We refer to Proposition 3 for existence of the process $\boldsymbol{X}_t$.

Let us now consider uniqueness of solutions to (MP). We first notice that if Q is solution to (MP), then, according to Paul Lévy's characterization, the process $(\boldsymbol{B}_t)$ defined by :

$$\boldsymbol{B}_t = \sqrt{\text{We}} \left(\boldsymbol{Y}_t - \boldsymbol{Y}_0 - \int_0^t \left(\boldsymbol{G}(s)\boldsymbol{Y}_s - \frac{1}{2\text{We}} \frac{\boldsymbol{Y}_s}{1 - \int ||\boldsymbol{Y}_s||^2 Q(d\boldsymbol{Y})/b} \right) ds \right)$$

is a Brownian motion under Q. This can be proved by choosing $\phi(\boldsymbol{Y}) = \boldsymbol{Y}_i$ and $\phi(\boldsymbol{Y}) = \boldsymbol{Y}_i \boldsymbol{Y}_j$ in (7.43) and a localization argument (see for example Proposition 4.6 p. 315 in [87]). Therefore, $((\boldsymbol{Y}_t)_{t \geq 0}, (\boldsymbol{B}_t)_{t \geq 0}, Q)$ is a weak solution to (7.9).

Let us now consider two solutions Q^1 and Q^2 to (MP) and set $\boldsymbol{A}^1(t) = \int \boldsymbol{Y}_t \otimes \boldsymbol{Y}_t Q^1(d\boldsymbol{Y})$ and $\boldsymbol{A}^2(t) = \int \boldsymbol{Y}_t \otimes \boldsymbol{Y}_t Q^2(d\boldsymbol{Y})$. We know from (7.42) that these two quantities are well defined. Moreover, it is easy to check that $\boldsymbol{A}^1$ and $\boldsymbol{A}^2$ are solution to the ODE (7.16). By Proposition 4, we therefore obtain, $\forall t \geq 0$,

$$\boldsymbol{A}^1(t) = \boldsymbol{A}^2(t).$$

From this we deduce that

$$\int ||\boldsymbol{Y}_t||^2 Q^1(d\boldsymbol{Y}) = \int ||\boldsymbol{Y}_t||^2 Q^2(d\boldsymbol{Y}),$$

so that, by (7.41-7.42), Q^1 and Q^2 are solutions of a martingale problem with (locally in time) Lipschitz coefficients and therefore are weak solutions of a SDE with (locally in time) Lipschitz coefficients. By Yamada-Watanabe theorem, uniqueness in law holds for such SDEs and thus we have :

$$Q^1 = Q^2.$$

$\square$

7.4.2 Weak convergence of the empirical distribution

Theorem 9 *The sequence $(\mu_M)_{M \geq 1}$ converges in the probability sense on $\mathcal{P}\left(\mathcal{P}(\mathcal{C}(\mathbb{R}_+, \mathbb{R}^N))\right)$ towards the constant $P \in \mathcal{P}(\mathcal{C}(\mathbb{R}_+, \mathbb{R}^N))$ where P is the unique solution of the martingale problem (MP).*

We prove this theorem in three steps :

Step 1 : First we prove the tightness of the sequence $(\Pi_M)_{M \geq 1}$ on $\mathcal{P}\left(\mathcal{P}(\mathcal{C}(\mathbb{R}_+, \mathbb{R}^N))\right)$ so that (up to the extraction of a subsequence) $\lim_{M \to \infty} \Pi_M = \Pi_\infty$ (in the weak sense) (see Section 7.4.2.1 and Lemma 21),

Step 2 : Then we prove that $\Pi_\infty(dQ)$-a.s., Q verifies the properties (7.41) and (7.42) of the martingale problem (MP) (see Section 7.4.2.2 and Lemma 22).

Step 3 : Finally, we show that $\Pi_\infty(dQ)$-a.s., Q is solution of the martingale problem (MP) by showing that $\Pi_\infty(dQ)$-a.s., Q verifies (7.43) (see Section 7.4.2.3 and Lemma 23).

After these three steps, we have that $\Pi_\infty(dQ)$-a.s., Q is solution of the martingale problem (MP). From this and the fact that the martingale problem (MP) admits a unique solution P (see Proposition 6), we deduce that $\Pi_\infty = \delta_P$ and therefore that the convergence $\lim_{M \to \infty} \mu_M = P$ holds in probability. This concludes the proof of Theorem 9.

The next three sections give the proof of each steps.

7.4.2.1 Step 1

Lemma 21 *The sequence $(\Pi_M)_{M \geq 1}$ on $\mathcal{P}\left(\mathcal{P}(\mathcal{C}(\mathbb{R}_+, \mathbb{R}^N))\right)$ is tight. Therefore, there exists a subsequence of $(\Pi_M)_{M \geq 1}$, that we still denote $(\Pi_M)_{M \geq 1}$ for the sake of clarity, which converges in the weak sense towards $\Pi_\infty \in \mathcal{P}\left(\mathcal{P}(\mathcal{C}(\mathbb{R}_+, \mathbb{R}^N))\right)$.*

Proof.

Let us first notice that, since the initial conditions $\boldsymbol{X}_0^i$ are i.i.d., the random variables $(\boldsymbol{X}_t^{i,M})_{1 \leq i \leq M}$ on $\mathcal{C}(\mathbb{R}_+, \mathbb{R}^N)$ are exchangeable so that to prove the tightness of the sequence $(\Pi_M)_{M \geq 1}$ on $\mathcal{P}\left(\mathcal{P}(\mathcal{C}(\mathbb{R}_+, \mathbb{R}^N))\right)$, it suffices to prove the tightness of the sequence of laws of $(\boldsymbol{X}_t^{1,M})_{M \geq 1}$ in $\mathcal{P}(\mathcal{C}(\mathbb{R}_+, \mathbb{R}^N))$. This can be proved using Kolmogorov criterion (see Problem 4.11 p. 64 in [87]). Let us set $0 < \beta < r/2 - 1$,

where r is defined in (7.39), and $0 \leq u < v \leq t$. We have :

$$\mathbb{E}\left(||\boldsymbol{X}_v^{1,M} - \boldsymbol{X}_u^{1,M}||^{2(1+\beta)}\right)$$

$$\leq \quad 3^{(1+2\beta)}\mathbb{E}\left(\int_u^v ||\boldsymbol{G}(s)||\,||\boldsymbol{X}_s^{1,M}||\,ds\right)^{2(1+\beta)}$$

$$+\frac{3^{(1+2\beta)}}{(2\mathrm{We})^{2(1+\beta)}}\mathbb{E}\left(\int_u^v \frac{||\boldsymbol{X}_s^{1,M}||}{1 - R_s^M/b}\,ds\right)^{2(1+\beta)} + \frac{3^{(1+2\beta)}}{\mathrm{We}^{(1+\beta)}}\mathbb{E}||\boldsymbol{W}_v - \boldsymbol{W}_u||^{2(1+\beta)},$$

$$\leq \quad C\left(\int_u^v ||\boldsymbol{G}(s)||^{2(1+\beta)}\,\mathbb{E}\left(||\boldsymbol{X}_s^{1,M}||^{2(1+\beta)}\right)\,ds(v-u)^{1+2\beta}\right.$$

$$+\int_u^v \mathbb{E}\left(\frac{||\boldsymbol{X}_s^{1,M}||}{1 - R_s^M/b}\right)^{2(1+\beta)}\,ds\,(v-u)^{1+2\beta} + (v-u)^{(1+\beta)}\bigg),$$

$$\leq \quad C\left(||\boldsymbol{G}||_{L^\infty(0,t)}^{2(1+\beta)}C_{(1+\beta)}(t)(v-u)^{2(1+\beta)}\right.$$

$$+\sup_{s\leq t}\left(\mathbb{E}\left(\frac{1}{1-R_s^M/b}\right)^r\right)^{1/p}\sup_{s\leq t}\left(\mathbb{E}||\boldsymbol{X}_s^{1,M}||^{2q(1+\beta)}\right)^{1/q}(v-u)^{2(1+\beta)} + (v-u)^{(1+\beta)}\bigg),$$

$$\leq \quad C(t)(v-u)^{(1+\beta)},$$

where $p = \frac{r}{2(1+\beta)}$, $q = \frac{p}{1-p}$, $C(t)$ is a constant depending on b, r, $\boldsymbol{G}$ but not on M, and where we have used (7.36) and (7.39). $\qquad\square$

We now want to identify Π_∞ as δ_P, where P is the unique solution of the martingale problem (MP).

7.4.2.2   Step 2

As the initial variables are i.i.d. according to P_0, one easily obtains (7.41).

Let us now consider the second point (7.42) of (MP), namely the estimation of $\int ||\boldsymbol{Y}_t||^2 Q(d\boldsymbol{Y})$ under Π_∞. We prove the following lemma, which implies (7.42) :

Lemma 22 $\Pi_\infty(dQ)$-a.s., $\forall t \geq 0$, $\int ||\boldsymbol{Y}_t||^2 Q(d\boldsymbol{Y}) \leq \rho_t^\infty$.

Proof.

$$\mathbb{E}^{\Pi_\infty}\left(\left(\int ||\boldsymbol{Y}_t||^2 Q(d\boldsymbol{Y}) - \rho_t^\infty\right)^+\right)$$

$$= \quad \lim_{n\to\infty}\mathbb{E}^{\Pi_\infty}\left(\left(\int(||\boldsymbol{Y}_t||^2 \wedge n)Q(d\boldsymbol{Y}) - \rho_t^\infty\right)^+\right) \qquad (7.44)$$

$$= \quad \lim_{n\to\infty}\lim_{M\to\infty}\mathbb{E}^{\Pi_M}\left(\left(\int(||\boldsymbol{Y}_t||^2 \wedge n)Q(d\boldsymbol{Y}) - \rho_t^\infty\right)^+\right) \qquad (7.45)$$

$$\leq \quad \lim_{M\to\infty}\mathbb{E}\left(\left(R_t^M - \rho_t^\infty\right)^+\right) \leq \lim_{M\to\infty}\sqrt{\frac{C(t)}{M}} = 0. \qquad (7.46)$$

We have used the monotone convergence theorem for (7.44), the fact that $Q \mapsto \left(\int (||\boldsymbol{Y}_t||^2 \wedge n)Q(d\boldsymbol{Y}) - \rho_t^\infty\right)^+$ is continuous and bounded for (7.45), and estimation (7.32) for (7.46). This shows that $\forall t \geq 0$, $\Pi_\infty(dQ)$-a.s.,

$$\int ||\boldsymbol{Y}_t||^2 Q(d\boldsymbol{Y}) \leq \rho_t^\infty.$$

The lower semi-continuity of $t \mapsto \int ||\boldsymbol{Y}_t||^2 Q(d\boldsymbol{Y})$ (which follows from Fatou Lemma) and the continuity of ρ^∞ enable to conclude the proof. $\qquad\square$

7.4.2.3 Step 3

We now want to show the last point (7.43) of (MP), namely that :

Lemma 23 $\Pi_\infty(Q)$-a.s., $\forall \phi \in \mathcal{C}_0^2(\mathbb{R}^N)$, M_t^ϕ *is a Q-martingale.*

Proof. Let $p \in \mathbb{N}$, $p \geq 1$ and $0 \leq s_1 \leq ... \leq s_p \leq s \leq t$. Let us introduce $g \in \mathcal{C}_b(\mathbb{R}^{p \times N}, \mathbb{R})$ and $F_n : \mathcal{P}(\mathcal{C}(\mathbb{R}_+, \mathbb{R}^N)) \to \mathbb{R}$ defined by :

$$
\begin{aligned}
F_n(Q) &= \int \Bigg(\phi(\boldsymbol{Y}_t) - \phi(\boldsymbol{Y}_s) - \int_s^t \Bigg(\boldsymbol{G}(r)\boldsymbol{Y}_r - \frac{1}{2\mathrm{We}} \frac{\boldsymbol{Y}_r}{\max\left(1 - \int(||\boldsymbol{Y}_r||^2 \wedge n)Q(d\boldsymbol{Y})/b, \frac{1}{n}\right)} \Bigg) \\
&\quad .\nabla\phi(\boldsymbol{Y}_r) + \frac{1}{2\mathrm{We}}\Delta\phi(\boldsymbol{Y}_r)\, dr \Bigg) g(\boldsymbol{Y}_{s_1}, ..., \boldsymbol{Y}_{s_p})Q(d\boldsymbol{Y}).
\end{aligned}
\tag{7.47}
$$

Notice that $F_n : \mathcal{P}(\mathcal{C}(\mathbb{R}_+, \mathbb{R}^N)) \to \mathbb{R}$ is continuous and bounded. We also define $F_\infty : \mathcal{P}(\mathcal{C}(\mathbb{R}_+, \mathbb{R}^N)) \to \mathbb{R}$ by :

$$
\begin{aligned}
F_\infty(Q) &= \int \Bigg(\phi(\boldsymbol{Y}_t) - \phi(\boldsymbol{Y}_s) - \int_s^t \Bigg(\boldsymbol{G}(r)\boldsymbol{Y}_r - \frac{1}{2\mathrm{We}} \frac{\boldsymbol{Y}_r}{1 - \int ||\boldsymbol{Y}_r||^2 Q(d\boldsymbol{Y})/b} \Bigg).\nabla\phi(\boldsymbol{Y}_r) \\
&\quad + \frac{1}{2\mathrm{We}}\Delta\phi(\boldsymbol{Y}_r)\, dr \Bigg) g(\boldsymbol{Y}_{s_1}, ..., \boldsymbol{Y}_{s_p})Q(d\boldsymbol{Y}).
\end{aligned}
\tag{7.48}
$$

We want to show that :

$$\mathbb{E}^{\Pi_\infty} |F_\infty(Q)| = 0. \tag{7.49}$$

Notice that when (7.49) will be proved, the proof of Lemma 23 will be complete, since we can intervert "$\forall \phi \in \mathcal{C}_0^2(\mathbb{R}^N)$" and "$\Pi_\infty(dQ) - a.s.$" using a countable dense subset of $\mathcal{C}_0^2(\mathbb{R}^N)$. We can also intervert "$\forall p \in \mathbb{N}, p \geq 1, \forall 0 \leq s_1 \leq ... \leq s_p \leq s \leq t$" and "$\Pi_\infty(dQ) - a.s.$" by using a countable dense subset of $\mathbb{R}_+$.

Let us now consider (7.49). We have :

$$
\begin{aligned}
\mathbb{E}^{\Pi_\infty} |F_\infty(Q)| &\leq \mathbb{E}^{\Pi_\infty} |F_\infty(Q) - F_n(Q)| + \mathbb{E}^{\Pi_\infty} |F_n(Q)|, \\
&\leq \mathbb{E}^{\Pi_\infty} |F_\infty(Q) - F_n(Q)| + \lim_{M \to \infty} \mathbb{E}^{\Pi_M} |F_n(Q)|, \\
&\leq \mathbb{E}^{\Pi_\infty} |F_\infty(Q) - F_n(Q)| + \limsup_{M \to \infty} \mathbb{E}^{\Pi_M} |F_n(Q) - F_\infty(Q)| + \limsup_{M \to \infty} \mathbb{E}^{\Pi_M} |F_\infty(Q)|.
\end{aligned}
$$

The last term is null. Indeed,

$$
\begin{aligned}
\mathbb{E}^{\Pi_M}|F_\infty(Q)| &= \frac{1}{M}\mathbb{E}\left|\sum_{i=1}^{M}\left(\phi(\boldsymbol{X}_t^{i,M})-\phi(\boldsymbol{X}_s^{i,M})-\int_s^t\left(\boldsymbol{G}(r)\boldsymbol{X}_r^{i,M}-\frac{1}{2\mathrm{We}}\frac{\boldsymbol{X}_r^{i,M}}{1-R_r^M/b}\right)\right.\right. \\
&\qquad\left.\left..\nabla\phi(\boldsymbol{X}_r^{i,M})+\frac{1}{2\mathrm{We}}\Delta\phi(\boldsymbol{X}_r^{i,M})\,dr\right)g(\boldsymbol{X}_{s_1}^{i,M},...,\boldsymbol{X}_{s_p}^{i,M})\right|, \\
&= \frac{1}{\mathrm{We}\,M}\mathbb{E}\left|\sum_{i=1}^{M}\left(\int_s^t\nabla\phi(\boldsymbol{X}_r^{i,M}).d\boldsymbol{W}_r^i\right)g(\boldsymbol{X}_{s_1}^{i,M},...,\boldsymbol{X}_{s_p}^{i,M})\right|\leq\frac{C}{\sqrt{M}}.
\end{aligned}
$$

We have therefore :

$$
\mathbb{E}^{\Pi_\infty}|F_\infty(Q)|\leq\limsup_{n\to\infty}\mathbb{E}^{\Pi_\infty}|F_\infty(Q)-F_n(Q)|+\limsup_{n\to\infty}\limsup_{M\to\infty}\mathbb{E}^{\Pi_M}|F_n(Q)-F_\infty(Q)|.
\tag{7.50}
$$

We first analyse the term $|F_\infty(Q)-F_n(Q)|$. Since g is bounded and $\nabla\phi$ is bounded with compact support, we obtain :

$$
\begin{aligned}
&|F_\infty(Q)-F_n(Q)| \\
&\leq \frac{1}{2\mathrm{We}}\int\int_s^t\left|\left(\frac{1}{\max\left(1-\int(||\boldsymbol{Y}_r||^2\wedge n)Q(d\boldsymbol{Y})/b,\frac{1}{n}\right)}-\frac{1}{1-\int||\boldsymbol{Y}_r||^2Q(d\boldsymbol{Y})/b}\right)\right. \\
&\qquad\left.\boldsymbol{X}_r.\nabla\phi(\boldsymbol{X}_r)\,dr\right||g|(\boldsymbol{X}_{s_1},...,\boldsymbol{X}_{s_p})Q(d\boldsymbol{X}) \\
&\leq C\int_s^t\left|\frac{1}{1-\int||\boldsymbol{Y}_r||^2Q(d\boldsymbol{Y})/b}-\frac{1}{\max\left(1-\int(||\boldsymbol{Y}_r||^2\wedge n)Q(d\boldsymbol{Y})/b,\frac{1}{n}\right)}\right|dr,\tag{7.51}
\end{aligned}
$$

where C is a constant depending on the datas but not on Q. Notice that the term between the absolute value signs in (7.51) is (a.s.) non negative under $\Pi_\infty(dQ)$ or $\Pi_M(dQ)$, since in this case, $\int||\boldsymbol{Y}_r||^2Q(d\boldsymbol{Y})<b$.

Let us now consider the first term in the r.h.s. of (7.50). Using Lemma 22, we know that $\exists\epsilon>0,\forall s\leq r\leq t$, $\Pi_\infty(dQ)$-a.s.,

$$
\int||\boldsymbol{Y}_r||^2Q(d\boldsymbol{Y})\leq b(1-\epsilon).
$$

From this, one can deduce that $\exists n_0,\ \forall n\geq n_0,\ \forall s\leq r\leq t$, $\Pi_\infty(dQ)$-a.s.,

$$
\int||\boldsymbol{Y}_r||^2Q(d\boldsymbol{Y})\leq b(1-1/n).
$$

Therefore, we have : $\forall n\geq n_0$, $\Pi_\infty(dQ)$-a.s.,

$$
|F_\infty(Q)-F_n(Q)|\leq C\int_s^t\left(\frac{1}{1-\int||\boldsymbol{Y}_r||^2Q(d\boldsymbol{Y})/b}-\frac{1}{1-\int(||\boldsymbol{Y}_r||^2\wedge n)Q(d\boldsymbol{Y})/b}\right)dr.
$$

Moreover, by the monotone convergence theorem, $\Pi_\infty(dQ)$-a.s., $\forall r$,

$$\lim_{n\to\infty} \int (||\boldsymbol{Y}_r||^2 \wedge n)Q(d\boldsymbol{Y}) = \int ||\boldsymbol{Y}_r||^2 Q(d\boldsymbol{Y}).$$

Since we also have by Lemma 22, $\Pi_\infty(dQ)$-a.s.,

$$\left(\frac{1}{1 - \int ||\boldsymbol{Y}_r||^2 Q(d\boldsymbol{Y})/b} - \frac{1}{1 - \int (||\boldsymbol{Y}_r||^2 \wedge n)Q(d\boldsymbol{Y})/b}\right) \leq \frac{1}{1 - \rho_r^\infty/b}$$

by the Lebesgue's theorem, we obtain :

$$\limsup_{n\to\infty} \mathbb{E}^{\Pi_\infty} \int_s^t \left(\frac{1}{1 - \int ||\boldsymbol{Y}_r||^2 Q(d\boldsymbol{Y})/b} - \frac{1}{\max\left(1 - \int (||\boldsymbol{Y}_r||^2 \wedge n)Q(d\boldsymbol{Y})/b, \frac{1}{n}\right)}\right) dr = 0.$$
$$(7.52)$$

Equation (7.52) shows that the first term in the r.h.s. of (7.50) is zero.

Let us now consider the second term in the r.h.s. of (7.50). Using the bound (7.51) on $|F_n(Q) - F_\infty(Q)|$ and exchangeability of the random variables $(\boldsymbol{X}_t^{i,M})_{1\leq i\leq M}$, we have :

$$\mathbb{E}^{\Pi_M}|F_n(Q) - F_\infty(Q)|$$

$$\leq C \int_s^t \mathbb{E}\left(\frac{1}{1 - \frac{1}{M}\sum_{i=1}^M ||\boldsymbol{X}_r^{i,M}||^2/b} - \frac{1}{\max\left(1 - \frac{1}{M}\sum_{i=1}^M (||\boldsymbol{X}_r^{i,M}||^2 \wedge n)/b, \frac{1}{n}\right)}\right) dr$$

$$\leq C \int_s^t \mathbb{E}\left(\frac{1}{1 - R_r^M/b} - \frac{1}{\max\left(1 - R_r^M/b, \frac{1}{n}\right)}\right) dr \qquad (7.53)$$

$$+C \int_s^t \mathbb{E}\left(\frac{1}{\max\left(1 - R_r^M/b, \frac{1}{n}\right)} - \frac{1}{\max\left(1 - \frac{1}{M}\sum_{i=1}^M (||\boldsymbol{X}_r^{i,M}||^2 \wedge n)/b, \frac{1}{n}\right)}\right) dr (7.54)$$

For the first term (7.53), we have, using (7.39) :

$$\mathbb{E}\left(\frac{1}{1 - R_r^M/b} - \frac{1}{\max\left(1 - R_r^M/b, \frac{1}{n}\right)}\right)$$

$$\leq \mathbb{E}\left(\left(\frac{1}{1 - R_r^M/b}\right)^2 \left(\max\left(1 - R_r^M/b, \frac{1}{n}\right) - \left(1 - R_r^M/b\right)\right)\right)$$

$$\leq \frac{1}{n}\mathbb{E}\left(\frac{1}{1 - R_r^M/b}\right)^2 \leq \frac{C(t)}{n}$$

where $C(t)$ does not depend on M and r. Therefore, we obtain :

$$\limsup_{n\to\infty} \limsup_{M\to\infty} \int_s^t \mathbb{E}\left(\frac{1}{1 - R_r^M/b} - \frac{1}{\max\left(1 - R_r^M/b, \frac{1}{n}\right)}\right) = 0. \qquad (7.55)$$

For the second term (7.54), we have :

$$\frac{1}{\max\left(1 - \frac{1}{M}\sum_{i=1}^{M}||\boldsymbol{X}_r^{i,M}||^2/b, \frac{1}{n}\right)} - \frac{1}{\max\left(1 - \frac{1}{M}\sum_{i=1}^{M}(||\boldsymbol{X}_r^{i,M}||^2 \wedge n)/b, \frac{1}{n}\right)}$$

$$\leq \left(\frac{1}{1 - R_r^M/b}\right)^2$$

$$* \left(\max\left(1 - \frac{1}{M}\sum_{i=1}^{M}(||\boldsymbol{X}_r^{i,M}||^2 \wedge n)/b, \frac{1}{n}\right) - \max\left(1 - \frac{1}{M}\sum_{i=1}^{M}||\boldsymbol{X}_r^{i,M}||^2/b, \frac{1}{n}\right)\right)$$

$$\leq \left(\frac{1}{1 - R_r^M/b}\right)^2 \frac{1}{Mb}\sum_{i=1}^{M}\left(||\boldsymbol{X}_r^{i,M}||^2 - (||\boldsymbol{X}_r^{i,M}||^2 \wedge n)\right).$$

We have therefore :

$$\mathbb{E}\left(\frac{1}{\max\left(1 - \frac{1}{M}\sum_{i=1}^{M}||\boldsymbol{X}_r^{i,M}||^2/b, \frac{1}{n}\right)} - \frac{1}{\max\left(1 - \frac{1}{M}\sum_{i=1}^{M}(||\boldsymbol{X}_r^{i,M}||^2 \wedge n)/b, \frac{1}{n}\right)}\right)$$

$$\leq \mathbb{E}\left(\left(\frac{1}{1 - R_r^M/b}\right)^2 \frac{1}{Mb}\sum_{i=1}^{M}\left(||\boldsymbol{X}_r^{i,M}||^2 - (||\boldsymbol{X}_r^{i,M}||^2 \wedge n)\right)\right)$$

$$\leq \frac{1}{b}\mathbb{E}\left(\left(\frac{1}{1 - R_r^M/b}\right)^2 (||\boldsymbol{X}_r^{1,M}||^2 - (||\boldsymbol{X}_r^{1,M}||^2 \wedge n))\right)$$

$$\leq \frac{1}{b}\left(\mathbb{E}\left(\frac{1}{1 - R_r^M/b}\right)^r\right)^{1/p}\left(\mathbb{E}\left(||\boldsymbol{X}_r^{1,M}||^2 - (||\boldsymbol{X}_r^{1,M}||^2 \wedge n))^q\right)\right)^{1/q}$$

$$\leq \frac{1}{b}\left(\mathbb{E}\left(\frac{1}{1 - R_r^M/b}\right)^r\right)^{1/p}\left(\mathbb{E}\left(||\boldsymbol{X}_r^{1,M}||^{2q}\mathbb{1}_{||\boldsymbol{X}_r^{1,M}||^2 \geq n}\right)\right)^{1/q}$$

$$\leq \frac{1}{b}\left(\mathbb{E}\left(\frac{1}{1 - R_r^M/b}\right)^r\right)^{1/p}\left(\mathbb{E}\left(\frac{||\boldsymbol{X}_r^{1,M}||^{2(q+1)}}{n}\right)\right)^{1/q}$$

$$\leq \frac{1}{b\, n^{1/q}}\left(\mathbb{E}\left(\frac{1}{1 - R_r^M/b}\right)^r\right)^{1/p}\left(\mathbb{E}\left(||\boldsymbol{X}_r^{1,M}||^{2(q+1)}\right)\right)^{1/q},$$

where $p = r/2$ and $q = \frac{p}{p-1}$. Using (7.39) and (7.36), we therefore obtain :

$$\limsup_{n\to\infty}\limsup_{M\to\infty}\int_s^t \mathbb{E}\left(\frac{1}{\max\left(1 - R_r^M/b, \frac{1}{n}\right)} - \frac{1}{\max\left(1 - \frac{1}{M}\sum_{i=1}^{M}(||\boldsymbol{X}_r^{i,M}||^2 \wedge n)/b, \frac{1}{n}\right)}\right) = 0.$$

$$(7.56)$$

By (7.55) and (7.56), we have :

$$\limsup_{n\to\infty}\limsup_{M\to\infty}\mathbb{E}^{\Pi_M}|F_n(Q) - F_\infty(Q)| = 0. \tag{7.57}$$

Using (7.52, 7.57), we obtain (7.49) and this ends the proof of Lemma 23.

$\square$

7.4.3 Convergence of the stress tensor

We can now prove Theorem 8. For $t \geq 0$, we consider

$$\mathbb{E} \left| \boldsymbol{\tau}_p^M(t) - \boldsymbol{\tau}_p(t) \right| = \mathbb{E}^{\Pi^M} \left| \boldsymbol{T}_\infty(Q) \right|,$$

where $\boldsymbol{T}_\infty : \mathcal{P}(\mathcal{C}(\mathbb{R}^+, \mathbb{R}^N)) \to \mathbb{R}^{N \times N}$ is defined by :

$$\boldsymbol{T}_\infty(Q) = \frac{\varepsilon}{\text{We}} \left(\frac{\int (\boldsymbol{Y}_t \otimes \boldsymbol{Y}_t) \, Q(d\boldsymbol{Y})}{1 - \int ||\boldsymbol{Y}_t||^2 Q(d\boldsymbol{Y})/b} - \frac{\int (\boldsymbol{Y}_t \otimes \boldsymbol{Y}_t) \, P(d\boldsymbol{Y})}{1 - \int ||\boldsymbol{Y}_t||^2 P(d\boldsymbol{Y})/b} \right). \qquad (7.58)$$

Let us also introduce, for $n \in \mathbb{N}$, $n \geq 1$, $\boldsymbol{T}_n : \mathcal{P}(\mathcal{C}(\mathbb{R}^+, \mathbb{R}^N)) \to \mathbb{R}^{N \times N}$ defined by :

$$\boldsymbol{T}_n(Q) = \frac{\varepsilon}{\text{We}} \left(\frac{\int (\boldsymbol{Y}_t \otimes \boldsymbol{Y}_t) * \frac{||\boldsymbol{Y}_t||^2 \wedge n}{||\boldsymbol{Y}_t||^2} Q(d\boldsymbol{Y})}{\max(1 - \int (||\boldsymbol{Y}_t||^2 \wedge n) \, Q(d\boldsymbol{Y})/b, \frac{1}{n})} - \frac{\int (\boldsymbol{Y}_t \otimes \boldsymbol{Y}_t) \, P(d\boldsymbol{Y})}{1 - \int ||\boldsymbol{Y}_t||^2 P(d\boldsymbol{Y})/b} \right).$$
$$(7.59)$$

Notice that $\boldsymbol{T}_n$ is a bounded and continuous function. We want to show that

$$\lim_{M \to \infty} \mathbb{E}^{\Pi^M} \left| \boldsymbol{T}_\infty(Q) \right| = 0. \qquad (7.60)$$

Using that $\mathbb{E}^{\Pi^\infty} \left| \boldsymbol{T}_\infty(Q) \right| = 0$, we have :

$$
\begin{aligned}
\limsup_{M \to \infty} \mathbb{E}^{\Pi^M} \left| \boldsymbol{T}_\infty(Q) \right| &\leq \limsup_{M \to \infty} \mathbb{E}^{\Pi^M} \left| \boldsymbol{T}_\infty(Q) - \boldsymbol{T}_n(Q) \right| + \limsup_{M \to \infty} \mathbb{E}^{\Pi^M} \left| \boldsymbol{T}_n(Q) \right|, \\
&\leq \limsup_{M \to \infty} \mathbb{E}^{\Pi^M} \left| \boldsymbol{T}_\infty(Q) - \boldsymbol{T}_n(Q) \right| + \mathbb{E}^{\Pi^\infty} \left| \boldsymbol{T}_n(Q) \right|, \\
&\leq \limsup_{M \to \infty} \mathbb{E}^{\Pi^M} \left| \boldsymbol{T}_\infty(Q) - \boldsymbol{T}_n(Q) \right| + \mathbb{E}^{\Pi^\infty} \left| \boldsymbol{T}_n(Q) - \boldsymbol{T}_\infty(Q) \right|.
\end{aligned}
$$

Therefore, we obtain :

$$
\begin{aligned}
&\limsup_{M \to \infty} \mathbb{E}^{\Pi^M} \left| \boldsymbol{T}_\infty(Q) \right| \\
&\leq \limsup_{n \to \infty} \limsup_{M \to \infty} \mathbb{E}^{\Pi^M} \left| \boldsymbol{T}_\infty(Q) - \boldsymbol{T}_n(Q) \right| + \limsup_{n \to \infty} \mathbb{E}^{\Pi^\infty} \left| \boldsymbol{T}_n(Q) - \boldsymbol{T}_\infty(Q) \right| (7.61)
\end{aligned}
$$

Let us analyse the term $|\boldsymbol{T}_n(Q) - \boldsymbol{T}_\infty(Q)|$:

$$|\boldsymbol{T}_\infty(Q) - \boldsymbol{T}_n(Q)| = \frac{\varepsilon}{\text{We}} \left| \frac{\int (\boldsymbol{Y}_t \otimes \boldsymbol{Y}_t) \, Q(d\boldsymbol{Y})}{1 - \int ||\boldsymbol{Y}_t||^2 Q(d\boldsymbol{Y})/b} - \frac{\int (\boldsymbol{Y}_t \otimes \boldsymbol{Y}_t) * \frac{||\boldsymbol{Y}_t||^2 \wedge n}{||\boldsymbol{Y}_t||^2} Q(d\boldsymbol{Y})}{\max(1 - \int (||\boldsymbol{Y}_t||^2 \wedge n) \, Q(d\boldsymbol{Y})/b, \frac{1}{n})} \right|$$

$$\leq \frac{\varepsilon}{\text{We}} \left| \frac{\int (\boldsymbol{Y}_t \otimes \boldsymbol{Y}_t) \left(1 - \frac{||\boldsymbol{Y}_t||^2 \wedge n}{||\boldsymbol{Y}_t||^2} \right) Q(d\boldsymbol{Y})}{1 - \int ||\boldsymbol{Y}_t||^2 Q(d\boldsymbol{Y})/b} \right|$$

$$+ \frac{\varepsilon}{\text{We}} \left| \int (\boldsymbol{Y}_t \otimes \boldsymbol{Y}_t) * \frac{||\boldsymbol{Y}_t||^2 \wedge n}{||\boldsymbol{Y}_t||^2} Q(d\boldsymbol{Y}) \right.$$

$$\left. * \left(\frac{1}{1 - \int ||\boldsymbol{Y}_t||^2 Q(d\boldsymbol{Y})/b} - \frac{1}{\max(1 - \int (||\boldsymbol{Y}_t||^2 \wedge n) \, Q(d\boldsymbol{Y})/b, \frac{1}{n})} \right) \right|$$

$$\leq C \left(\frac{\int (||\boldsymbol{Y}_t||^2 - (||\boldsymbol{Y}_t||^2 \wedge n)) \, Q(d\boldsymbol{Y})}{1 - \int ||\boldsymbol{Y}_t||^2 Q(d\boldsymbol{Y})/b} \right) \qquad (7.62)$$

$$+ C \int ||\boldsymbol{Y}_t||^2 Q(d\boldsymbol{Y})$$

$$* \left| \frac{1}{1 - \int ||\boldsymbol{Y}_t||^2 Q(d\boldsymbol{Y})/b} - \frac{1}{\max(1 - \int (||\boldsymbol{Y}_t||^2 \wedge n) \, Q(d\boldsymbol{Y})/b, \frac{1}{n})} \right|. \quad (7.63)$$

Notice that the term between the absolute value signs in (7.63) is (a.s.) non negative under $\Pi_\infty(dQ)$ or $\Pi_M(dQ)$, since in this case, $\int ||\boldsymbol{Y}_r||^2 Q(d\boldsymbol{Y}) < b$.

We now divide the rest of the proof in two steps : we start by proving that the second term in (7.61) is zero, and then prove that the first term in (7.61) is zero.

7.4.3.1   Step 1

Let us consider the second term in (7.61).

We first consider the term (7.62). Using Lemma 22, we have, $\Pi_\infty(dQ)$-a.s. :

$$\frac{\int (||\boldsymbol{Y}_t||^2 - (||\boldsymbol{Y}_t||^2 \wedge n)) \, Q(d\boldsymbol{Y})}{1 - \int ||\boldsymbol{Y}_t||^2 Q(d\boldsymbol{Y})/b} \leq \frac{1}{1 - \rho_t^\infty/b} \int (||\boldsymbol{Y}_t||^2 - (||\boldsymbol{Y}_t||^2 \wedge n)) \, Q(d\boldsymbol{Y})$$

Moreover, by the monotone convergence theorem, $\Pi_\infty(dQ)$-a.s.,

$$\lim_{n \to \infty} \int (||\boldsymbol{Y}_t||^2 \wedge n) Q(d\boldsymbol{Y}) = \int ||\boldsymbol{Y}_t||^2 Q(d\boldsymbol{Y}).$$

We therefore obtain :

$$\limsup_{n \to \infty} \mathbb{E}^{\Pi^\infty} \left| \frac{\int (||\boldsymbol{Y}_t||^2 - (||\boldsymbol{Y}_t||^2 \wedge n)) \, Q(d\boldsymbol{Y})}{1 - \int ||\boldsymbol{Y}_t||^2 Q(d\boldsymbol{Y})/b} \right| = 0. \qquad (7.64)$$

Let us now consider the second term (7.63). Using Lemma 22, we know that $\exists n_0$, $\forall n \geq n_0$, $\Pi_\infty(dQ)$-a.s.,

$$\int ||\boldsymbol{Y}_t||^2 Q(d\boldsymbol{Y}) \leq b(1 - 1/n),$$

and therefore

$$\max \left(1 - \int (||\boldsymbol{Y}_t||^2 \wedge n) Q(d\boldsymbol{Y})/b, \frac{1}{n} \right) = 1 - \int (||\boldsymbol{Y}_t||^2 \wedge n) Q(d\boldsymbol{Y})/b.$$

Using again the monotone convergence theorem, we have :

$$\limsup_{n \to \infty} \mathbb{E}^{\Pi^\infty} \left| \int ||\boldsymbol{Y}_t||^2 Q(d\boldsymbol{Y}) \left(\frac{1}{1 - \int ||\boldsymbol{Y}_t||^2 Q(d\boldsymbol{Y})/b} \right. \right.$$

$$\left. \left. - \frac{1}{\max(1 - \int (||\boldsymbol{Y}_t||^2 \wedge n) Q(d\boldsymbol{Y})/b, \frac{1}{n})} \right) \right| = 0. \tag{7.65}$$

From (7.64) and (7.65), we deduce :

$$\limsup_{n \to \infty} \mathbb{E}^{\Pi^\infty} |\boldsymbol{T}_n(Q) - \boldsymbol{T}_\infty(Q)| = 0. \tag{7.66}$$

7.4.3.2   Step 2

Let us now consider the first term in (7.61). Using the bound (7.62,7.63) and exchangeability of the random variables $(\boldsymbol{X}_t^{i,M})_{1 \leq i \leq M}$, we have :

$$\mathbb{E}^{\Pi^M} |\boldsymbol{T}_\infty(Q) - \boldsymbol{T}_n(Q)|$$

$$\leq \ C\mathbb{E}\left(\left(||\boldsymbol{X}_t^{1,M}||^2 - (||\boldsymbol{X}_t^{1,M}||^2 \wedge n) \right) \frac{1}{1 - R_t^M/b} \right)$$

$$+ C\mathbb{E}\left(||\boldsymbol{X}_t^{1,M}||^2 \left(\frac{1}{1 - R_t^M/b} - \frac{1}{\max\left(1 - \frac{1}{M} \sum_{i=1}^M \left(||\boldsymbol{X}_t^{i,M}||^2 \wedge n \right) /b, \frac{1}{n} \right)} \right) \right)$$

$$\leq \ C\mathbb{E}\left(\left(||\boldsymbol{X}_t^{1,M}||^2 - (||\boldsymbol{X}_t^{1,M}||^2 \wedge n) \right) \frac{1}{1 - R_t^M/b} \right) \tag{7.67}$$

$$+ C\mathbb{E}\left(||\boldsymbol{X}_t^{1,M}||^2 \left(\frac{1}{1 - R_t^M/b} - \frac{1}{\max\left(1 - R_t^M/b, \frac{1}{n} \right)} \right) \right) \tag{7.68}$$

$$+ C\mathbb{E}\left(||\boldsymbol{X}_t^{1,M}||^2 \left(\frac{1}{\max\left(1 - R_t^M/b, \frac{1}{n} \right)} - \frac{1}{\max\left(1 - \frac{1}{M} \sum_{i=1}^M \left(||\boldsymbol{X}_t^{i,M}||^2 \wedge n \right) /b, \frac{1}{n} \right)} \right) \right) \tag{7.69}$$

We first consider the term (7.67). Using (7.39) and (7.36), we have :

$$\mathbb{E}\left(\left(||\boldsymbol{X}_t^{1,M}||^2 - (||\boldsymbol{X}_t^{1,M}||^2 \wedge n) \right) \frac{1}{1 - R_t^M/b} \right)$$

$$\leq \ \sqrt{\mathbb{E}\left(||\boldsymbol{X}_t^{1,M}||^2 - (||\boldsymbol{X}_t^{1,M}||^2 \wedge n) \right)^2} \sqrt{\mathbb{E}\left(\frac{1}{1 - R_t^M/b} \right)^2}$$

$$\leq \ C\sqrt{\mathbb{E}\left(||\boldsymbol{X}_t^{1,M}||^4 \mathbb{1}_{||\boldsymbol{X}_t^{1,M}||^2 \geq n} \right)} \leq \frac{C}{\sqrt{n}} \sqrt{\mathbb{E}\left(||\boldsymbol{X}_t^{1,M}||^6 \right)} \leq \frac{C}{\sqrt{n}},$$

where C does not depend on M. Therefore, we obtain :

$$\limsup_{n\to\infty}\limsup_{M\to\infty} \mathbb{E}\left(\left(||\boldsymbol{X}_t^{1,M}||^2 - (||\boldsymbol{X}_t^{1,M}||^2 \wedge n)\right)\frac{1}{1-R_t^M/b}\right) = 0. \qquad (7.70)$$

Let us now consider the term (7.68). We have, using (7.36) :

$$\mathbb{E}\left(||\boldsymbol{X}_t^{1,M}||^2\left(\frac{1}{1-R_t^M/b} - \frac{1}{\max\left(1-R_t^M/b,\frac{1}{n}\right)}\right)\right)$$

$$\leq \left(\mathbb{E}||\boldsymbol{X}_t^{1,M}||^{2p}\right)^{1/p}\left(\mathbb{E}\left(\frac{1}{1-R_t^M/b} - \frac{1}{\max\left(1-R_t^M/b,\frac{1}{n}\right)}\right)^{r/2}\right)^{1/q}$$

$$\leq C_p(t)^{1/p}\left(\mathbb{E}\left(\frac{1}{1-R_t^M/b} - \frac{1}{\max\left(1-R_t^M/b,\frac{1}{n}\right)}\right)^{r/2}\right)^{1/q}$$

with $q = r/2$ and $p = \frac{q}{q-1}$, where r is defined in (7.39). Arguing like in the proof of (7.55), we easily obtain :

$$\mathbb{E}\left(\frac{1}{1-R_t^M/b} - \frac{1}{\max\left(1-R_t^M/b,\frac{1}{n}\right)}\right)^{r/2} \leq \frac{C}{n^{r/2}},$$

where C does not depend on M. Therefore, we obtain :

$$\limsup_{n\to\infty}\limsup_{M\to\infty}\mathbb{E}\left(||\boldsymbol{X}_t^{1,M}||^2\left(\frac{1}{1-R_t^M/b} - \frac{1}{\max\left(1-R_t^M/b,\frac{1}{n}\right)}\right)\right) = 0. \qquad (7.71)$$

Let us now consider the term (7.69). We have, using (7.36) :

$$\mathbb{E}\left(||\boldsymbol{X}_t^{1,M}||^2\left(\frac{1}{\max\left(1-R_t^M/b,\frac{1}{n}\right)} - \frac{1}{\max\left(1-\frac{1}{M}\sum_{i=1}^M\left(||\boldsymbol{X}_t^{i,M}||^2\wedge n\right)/b,\frac{1}{n}\right)}\right)\right)$$

$$\leq C_p(t)^{1/p}\left(\mathbb{E}\left(\frac{1}{\max\left(1-R_t^M/b,\frac{1}{n}\right)} - \frac{1}{\max\left(1-\frac{1}{M}\sum_{i=1}^M\left(||\boldsymbol{X}_t^{i,M}||^2\wedge n\right)/b,\frac{1}{n}\right)}\right)^q\right)^{1/q}$$

with $1 < q < r/2$ and $p = \frac{q}{q-1}$, where r is defined in (7.39). Using (7.39), we have :

$$
\mathbb{E} \left(\frac{1}{\max\left(1 - R_t^M/b, \frac{1}{n}\right)} - \frac{1}{\max\left(1 - \frac{1}{M}\sum_{i=1}^{M}\left(||\boldsymbol{X}_t^{i,M}||^2 \wedge n\right)/b, \frac{1}{n}\right)} \right)^q
$$

$$
\leq \quad \mathbb{E}\left(\left(\frac{1}{1 - R_t^M/b} \right)^{2q} \left(\frac{1}{Mb}\sum_{i=1}^{M}\left(||\boldsymbol{X}_t^{i,M}||^2 - ||\boldsymbol{X}_t^{i,M}||^2 \wedge n \right) \right)^q \right)
$$

$$
\leq \quad \left(\mathbb{E}\left(\frac{1}{1 - R_t^M/b} \right)^r \right)^{1/p'} \left(\mathbb{E}\left(\frac{1}{Mb}\sum_{i=1}^{M}\left(||\boldsymbol{X}_t^{i,M}||^2 - ||\boldsymbol{X}_t^{i,M}||^2 \wedge n \right) \right)^{qq'} \right)^{1/q'}
$$

$$
\leq \quad C\left(\mathbb{E}\left(\frac{1}{Mb}\sum_{i=1}^{M}\left(||\boldsymbol{X}_t^{i,M}||^2 - ||\boldsymbol{X}_t^{i,M}||^2 \wedge n \right) \right)^{qq'} \right)^{1/q'}
$$

with $p' = \frac{r}{2q}$, $q' = \frac{p'}{p'-1}$, and C is a constant not depending on M. Finally, we observe that, using (7.36) and arguing as in the proof of (7.70) :

$$
\mathbb{E}\left(\frac{1}{Mb}\sum_{i=1}^{M}\left(||\boldsymbol{X}_t^{i,M}||^2 - ||\boldsymbol{X}_t^{i,M}||^2 \wedge n \right) \right)^{qq'}
$$

$$
\leq \quad \left(\frac{1}{Mb} \right)^{qq'} \sum_{i=1}^{M} \mathbb{E}\left(||\boldsymbol{X}_t^{i,M}||^2 - ||\boldsymbol{X}_t^{i,M}||^2 \wedge n \right)^{qq'} M^{qq'-1}
$$

$$
\leq \quad \left(\frac{1}{b} \right)^{qq'} \mathbb{E}\left(||\boldsymbol{X}_t^{1,M}||^2 - ||\boldsymbol{X}_t^{1,M}||^2 \wedge n \right)^{qq'}
$$

$$
\leq \quad \left(\frac{1}{b} \right)^{qq'} \mathbb{E}\left(||\boldsymbol{X}_t^{1,M}||^2 \mathbb{1}_{||\boldsymbol{X}_t^{1,M}||^2 \geq n} \right)^{qq'}
$$

$$
\leq \quad \left(\frac{1}{bn} \right)^{qq'} \mathbb{E}\left(||\boldsymbol{X}_t^{1,M}||^{4qq'} \right) \leq \left(\frac{1}{bn} \right)^{qq'} C_{2qq'}(t).
$$

Therefore we obtain :

$$
\mathbb{E}\left(||\boldsymbol{X}_t^{1,M}||^2 \left(\frac{1}{\max\left(1 - R_t^M/b, \frac{1}{n}\right)} - \frac{1}{\max\left(1 - \frac{1}{M}\sum_{i=1}^{M}\left(||\boldsymbol{X}_t^{i,M}||^2 \wedge n\right)/b, \frac{1}{n}\right)} \right) \right) \leq \frac{C}{n},
$$

where C does not depend on M. And thus,

$$
\limsup_{n\to\infty} \limsup_{M\to\infty} \mathbb{E}\left(||\boldsymbol{X}_t^{1,M}||^2 \right.
$$

$$
\left. \left(\frac{1}{\max\left(1 - R_t^M/b, \frac{1}{n}\right)} - \frac{1}{\max\left(1 - \frac{1}{M}\sum_{i=1}^{M}\left(||\boldsymbol{X}_t^{i,M}||^2 \wedge n\right)/b, \frac{1}{n}\right)} \right) \right) = 0. \quad (7.72)
$$

By (7.70), (7.71) and (7.72), we have :

$$\limsup_{n\to\infty} \limsup_{M\to\infty} \mathbb{E}^{\Pi^M} \left| \boldsymbol{T}_\infty(Q) - \boldsymbol{T}_n(Q) \right| = 0. \tag{7.73}$$

7.4.3.3 End of the proof of Theorem 8

By (7.66) and (7.73), we have (7.60) which is equivalent to (7.14). Notice that the convergence in Theorem 8 is uniform in $t \in [0, T]$.

7.5 Conclusion

We have analyzed the SDE arising in the FENE-P model of polymeric fluids. We have shown that both the nonlinear SDE at the continuous level and the particle system at the discrete level admit a solution, and that the stress tensor obtained with the particle system converges towards the stress tensor obtained with the nonlinear SDE, in the limit of an infinite number of particles. This theoretical result confirms numerical experiments performed in [89].

From a mathematical point of view, we can summarize the results obtained by the following : the solutions to the FENE-P model behave like Hookean dumbbells (see [85]) with a time-variable spring constant at the continuous level (they can reach infinite extensibility), and rather like FENE dumbbells (see [84, 86]) at the discrete level, once the problem is discretized in a particle system (since they cannot reach infinite extensibility).

Chapitre 8

Comportement en temps long

On présente ici des résultats préliminaires sur le comportement en temps long du système micro-macro. Dans ce chapitre, on ne se restreint pas au cas d'un écoulement cisaillé. Nous montrons en particulier que l'énergie libre est une quantité bien adaptée à l'étude du système couplé.

<div align="center">

**Entropy estimates and longtime behaviour
for some micro-macro models of polymeric fluids**

Benjamin Jourdain, Claude Le Bris, Tony Lelièvre

</div>

8.1   Introduction

We are interested in the longtime behavior of a micro-macro model for dilute solutions of polymers. We present some *formal* computations : we suppose that there exists global-in-time solutions to the problems we consider, and that these solutions are regular enough so that the formal computations are justified. With this limitation in mind, our aim is to prove the convergence to a stationary state under adequate assumptions.

We consider the following system of (non-dimensional) PDEs :

$$
\left\{
\begin{aligned}
&\mathrm{Re}\left(\frac{\partial \boldsymbol{u}}{\partial t}(t,\boldsymbol{x}) + \boldsymbol{u}(t,\boldsymbol{x}).\nabla \boldsymbol{u}(t,\boldsymbol{x})\right) = (1-\epsilon)\Delta \boldsymbol{u}(t,\boldsymbol{x}) - \nabla p(t,\boldsymbol{x}) + \mathrm{div}\,\boldsymbol{\tau}(t,\boldsymbol{x}), \\
&\mathrm{div}\,(\boldsymbol{u}(t,\boldsymbol{x})) = 0, \\
&\boldsymbol{\tau}(t,\boldsymbol{x}) = \frac{\epsilon}{\mathrm{We}}\left(\int_{\mathbb{R}^d}(\boldsymbol{X}\otimes\nabla\Pi(\boldsymbol{X}))\psi(t,\boldsymbol{x},\boldsymbol{X})\,d\boldsymbol{X} - \mathrm{Id}\right), \\
&\frac{\partial\psi}{\partial t}(t,\boldsymbol{x},\boldsymbol{X}) + \boldsymbol{u}(t,\boldsymbol{x}).\nabla_{\boldsymbol{x}}\psi(t,\boldsymbol{x},\boldsymbol{X}) \\
&\quad = -\mathrm{div}_{\boldsymbol{X}}\left(\left(\nabla_{\boldsymbol{x}}\boldsymbol{u}(t,\boldsymbol{x})\boldsymbol{X} - \frac{1}{2\mathrm{We}}\nabla\Pi(\boldsymbol{X})\right)\psi(t,\boldsymbol{x},\boldsymbol{X})\right) + \frac{1}{2\mathrm{We}\,M}\Delta_{\boldsymbol{X}}\psi(t,\boldsymbol{x},\boldsymbol{X}),
\end{aligned}
\right.
$$

where the Reynolds number $\mathrm{Re} > 0$, the Weissenberg number $\mathrm{We} > 0$, $\epsilon \in (0,1)$ and $M > 0$ are the non-dimensional numbers in the system. We suppose that the space variable $\boldsymbol{x}$ lies in *a bounded domain* $\mathcal{D}$ of $\mathbb{R}^d$. On the other hand, the Fokker-Planck equation is set on the whole space $\mathbb{R}^d$. This system is complemented with initial conditions on the velocity $\boldsymbol{u}$ and on the distribution ψ, and also with boundary conditions on the velocity $\boldsymbol{u}$.

The potential Π of the entropic force within the dumbbells can be :
– Hookean dumbbell :
$$
\Pi(\boldsymbol{X}) = \frac{||\boldsymbol{X}||^2}{2}, \tag{8.1}
$$

– FENE dumbbell :
$$
\Pi(\boldsymbol{X}) = -\frac{bM}{2}\ln\left(1 - \frac{||\boldsymbol{X}||^2}{bM}\right), \tag{8.2}
$$

– more generally, any potential which is a α-convex function and which can be expressed as a function of the norm of $\boldsymbol{X}$:
$$
\Pi(\boldsymbol{X}) = \pi(||\boldsymbol{X}||). \tag{8.3}
$$

Remark 26 *One can show that the α-convexity of Π is equivalent to the α-convexity of π together with $\pi'(0) \geq 0$. These properties on π can be easily checked for the case of Hookean and FENE dumbbell.*

Henceforth, in order to simplify notations, we take the following values for the non-dimensional parameters : $\text{Re} = \frac{1}{2}$, $\text{We} = 1$, $\epsilon = \frac{1}{2}$ and $M = 1$. We are thus interested in the following system :

$$
\left\{
\begin{array}{ll}
\dfrac{\partial \boldsymbol{u}}{\partial t}(t, \boldsymbol{x}) + \boldsymbol{u}(t, \boldsymbol{x}).\nabla \boldsymbol{u}(t, \boldsymbol{x}) = \Delta \boldsymbol{u}(t, \boldsymbol{x}) - \nabla p(t, \boldsymbol{x}) + \text{div } \boldsymbol{\tau}(t, \boldsymbol{x}), & (8.4) \\[2mm]
\text{div } (\boldsymbol{u}(t, \boldsymbol{x})) = 0, & (8.5) \\[2mm]
\boldsymbol{\tau}(t, \boldsymbol{x}) = \displaystyle\int_{\mathbb{R}^d} (\boldsymbol{X} \otimes \nabla \Pi(\boldsymbol{X}))\psi(t, \boldsymbol{x}, \boldsymbol{X}) \, d\boldsymbol{X}, & (8.6) \\[2mm]
\dfrac{\partial \psi}{\partial t}(t, \boldsymbol{x}, \boldsymbol{X}) + \boldsymbol{u}(t, \boldsymbol{x}).\nabla_{\boldsymbol{x}} \psi(t, \boldsymbol{x}, \boldsymbol{X}) \\[2mm]
\qquad = -\text{div }_{\boldsymbol{X}} \left((\nabla_{\boldsymbol{x}} \boldsymbol{u}(t, \boldsymbol{x})\boldsymbol{X} - \frac{1}{2}\nabla \Pi(\boldsymbol{X}))\psi(t, \boldsymbol{x}, \boldsymbol{X}) \right) + \frac{1}{2}\Delta_{\boldsymbol{X}} \psi(t, \boldsymbol{x}, \boldsymbol{X}). & (8.7)
\end{array}
\right.
$$

We recall that we can alternatively consider a coupled PDE-SDE system by replacing (8.6)–(8.7) by :

$$
\left\{
\begin{array}{ll}
\boldsymbol{\tau}(t, \boldsymbol{x}) = \mathbb{E}\left(\boldsymbol{X}_t(\boldsymbol{x}) \otimes \nabla\Pi(\boldsymbol{X}_t(\boldsymbol{x})) \right), & (8.8) \\[2mm]
d\boldsymbol{X}_t(\boldsymbol{x}) + \boldsymbol{u}(t, \boldsymbol{x}).\nabla_{\boldsymbol{x}} \boldsymbol{X}_t(\boldsymbol{x}) \, dt \\[2mm]
\qquad = \left(\nabla_{\boldsymbol{x}} \boldsymbol{u}(t, \boldsymbol{x})\boldsymbol{X}_t(\boldsymbol{x}) - \frac{1}{2}\nabla\Pi(\boldsymbol{X}_t(\boldsymbol{x})) \right) dt + d\boldsymbol{W}_t, & (8.9)
\end{array}
\right.
$$

where $\boldsymbol{W}_t$ denotes a d-dimensional standard Brownian motion. When the limit exists, we denote $\boldsymbol{u}_\infty$ the limit of the velocity field $\boldsymbol{u}$ when $t \to \infty$.

In the following, we refer to the special stationary state corresponding to $\boldsymbol{u}_\infty = 0$ as the *equilibrium* state. Such a state can of course only be reached in the case of homogeneous (or vanishing) boundary conditions on the velocity. In case of equilibrium, the stationary solution of the Fokker-Planck equation is ψ_∞ defined by :

$$
\psi_\infty(\boldsymbol{X}) = \frac{\exp(-\Pi(\boldsymbol{X}))}{\int_{\mathbb{R}^d} \exp(-\Pi(\boldsymbol{X}))}. \tag{8.10}
$$

Notice that $(\boldsymbol{u}_\infty, \psi_\infty)$ is then a stationary solution to the system (8.4)–(8.5)–(8.6)–(8.7)

As a simpler problem, we will also consider the coupled system in the special geometry of a plane shear flow in dimension $d = 2$. In this case, $\boldsymbol{u}(t, \boldsymbol{x}) = (u(t, y), 0)$, where $\boldsymbol{x} = (0, y)$ and all the variables only depend on y. We suppose that $y \in \mathcal{D} =$

$(0, 1)$. In this case, the system (8.4)–(8.5)–(8.6)–(8.7) becomes :

$$
\begin{cases}
\dfrac{\partial u}{\partial t}(t, y) &= \partial_{y,y} u(t, y) + \partial_y \tau(t, y), & (8.11) \\[2ex]
\tau(t, y) &= \displaystyle\int_{\mathbb{R}^2} (X \partial_Y \Pi(\boldsymbol{X})) \psi(t, y, \boldsymbol{X}) \, d\boldsymbol{X}, & (8.12) \\[2ex]
\dfrac{\partial \psi}{\partial t}(t, y, \boldsymbol{X}) &= -\partial_X \left((\partial_y u(t, y) Y - \dfrac{1}{2} \partial_X \Pi(\boldsymbol{X})) \psi(t, y, \boldsymbol{X}) \right) \\[2ex]
& \quad -\partial_Y \left(-\dfrac{1}{2} \partial_Y \Pi(\boldsymbol{X}) \psi(t, y, \boldsymbol{X}) \right) + \dfrac{1}{2} \Delta_{\boldsymbol{X}} \psi(t, y, \boldsymbol{X}), & (8.13)
\end{cases}
$$

where $\boldsymbol{X} = (X, Y)$ and τ denotes the (X, Y) component of the stress tensor $\boldsymbol{\tau}$. The SDE version of (8.12)–(8.13) is :

$$
\begin{cases}
\tau(t, y) &= \mathbb{E}\left(X_t(y) \partial_Y \Pi(X_t(y), Y_t(y)) \right), & (8.14) \\[2ex]
dX_t(y) &= \left(\partial_y u(t, y) Y_t(y) - \dfrac{1}{2} \partial_X \Pi(X_t(y), Y_t(y)) \right) dt + dV_t, & (8.15) \\[2ex]
dY_t(y) &= -\dfrac{1}{2} \partial_Y \Pi(X_t(y), Y_t(y)) \, dt + dW_t, & (8.16)
\end{cases}
$$

where $\boldsymbol{X}_t(\boldsymbol{x}) = (X_t(y), Y_t(y))$ and $\boldsymbol{W}_t = (V_t, W_t)$.

Remark 27 *In the following, t, $\boldsymbol{x}$ and ω denote respectively the variable in time, space and probability. For example, $\boldsymbol{X}_t(\boldsymbol{x}) \in L_t^2(L_{\boldsymbol{x}}^2(L_\omega^2))$ means that $\int_{\mathbb{R}_+} \int_{\mathcal{D}} \mathbb{E}(||\boldsymbol{X}_t(\boldsymbol{x})||^2) \, d\boldsymbol{x} \, dt < \infty$.*

8.2 Analysis of the Hookean dumbbell model in a shear flow

In this section, we consider the coupled system (8.11)–(8.14)–(8.15)–(8.16) for Hookean dumbbells (8.1). In this case, the process $Y_t(y)$ is defined independently from $(u(t, y)), X_t(y))$, and there is only a coupling between $u(t, y)$ and $X_t(y)$. We consider any initial conditions : $u(0, y) = u_0(y)$ and $(X_0(y), Y_0(y))$, where $X_0(y)$ and $Y_0(y)$ lie in $L_y^2(L_\omega^2)$ and are independent and independent of the Brownian motion (V_t, W_t). We also complement this system with Dirichlet boundary conditions on u : $u(t, 0) = f_0(t)$ and $u(t, 1) = f_1(t)$. We suppose that

$$
\lim_{t \to \infty} f_0(t) = a_0 \qquad \lim_{t \to \infty} f_1(t) = a_1, \tag{8.17}
$$

so that the expected asymptotic state for the velocity is

$$
u_\infty(y) = a_0 + y(a_1 - a_0).
$$

Accordingly, we introduce the expected "limit processes" (X_t^∞, Y_t^∞) as solution of the following SDE :

$$
\begin{cases}
dX_t^\infty &= \left((a_1 - a_0) Y_t^\infty - \dfrac{1}{2} X_t^\infty \right) dt + dV_t \\[2ex]
dY_t^\infty &= -\dfrac{1}{2} Y_t^\infty \, dt + dW_t
\end{cases}
$$

with initial condition such that (X_t^∞, Y_t^∞) is a stationary Gaussian process not depending on y :

$$(X_0^\infty, Y_0^\infty) \sim \mathcal{N}\left(\begin{pmatrix} 0 \\ 0 \end{pmatrix}, \begin{bmatrix} 1 + 2(a_1 - a_0)^2 & (a_1 - a_0) \\ (a_1 - a_0) & 1 \end{bmatrix} \right).$$

Moreover, we suppose that $(Y_0(y), Y_0^\infty)$ are such that,

either $\forall y$, $Y_0(y)$ is independent from Y_0^∞ **or** $Y_0(y)$ does not depend on y. (8.18)

The triple $(u_\infty, X^\infty, Y^\infty)$ is solution of the following system :

$$\begin{cases} 0 & = & \partial_{y,y} u_\infty(y) + \partial_y \tau_\infty, \\ \tau_\infty & = & \mathbb{E}\left(X_t^\infty Y_t^\infty \right), \\ dX_t^\infty & = & (\partial_y u_\infty(y) Y_t^\infty - \dfrac{1}{2} X_t^\infty \, dt + dV_t, \\ dY_t^\infty & = & -\dfrac{1}{2} Y_t^\infty \, dt + dW_t, \end{cases}$$

where τ_∞ does not depend on time and space, since (X^∞, Y^∞) is a stationary process not depending on space. In this special case, we are able to prove convergence to the stationary state $(u_\infty, X^\infty, Y^\infty)$:

Lemma 24 *We assume (8.17)–(8.18), that $f_0, f_1 \in W^{1,1}_{\text{loc}}(\mathbb{R}_+)$ and*

$$\lim_{t \to \infty} \dot{f}_0(t) = \lim_{t \to \infty} \dot{f}_1(t) = 0, \tag{8.19}$$

where $\dot{f}$ denotes the derivative of f with respect to time. Then, the triple (u, X, Y) converges towards $(u_\infty, X^\infty, Y^\infty)$ as $t \longrightarrow \infty$ in the following sense :

$$\lim_{t \to \infty} ||u(t,y) - u_\infty(y)||_{L^2_y} = 0,$$

$$\lim_{t \to \infty} ||X_t(y) - X_t^\infty||_{L^2_y(L^2_\omega)} = 0,$$

$$\lim_{t \to \infty} ||Y_t(y) - Y_t^\infty||_{L^2_y(L^2_\omega)} = 0.$$

In particular, the stress $\mathbb{E}(X_t(y) Y_t(y))$ converges towards $\mathbb{E}(X_t^\infty Y_t^\infty) = a_1 - a_0$ in L^1_y.

Proof. In this proof, C denotes a universal positive constant, which may change from one occurence to another. We introduce

$$\tilde{u}(t,y) = f_0(t) + y(f_1(t) - f_0(t))$$

and $\tilde{X}_t$ defined by :

$$\tilde{X}_t = X_0^\infty + \int_0^t \left((f_1(s) - f_0(s)) Y_s^\infty - \frac{1}{2} \tilde{X}_s \right) ds + V_t.$$

By using the analytical expressions of $Y_t(y)$ and Y_t^∞, one can first check that

$$||Y_t(y) - Y_t^\infty||_{L_y^2(L_\omega^2)} = ||Y_0(y) - Y_0^\infty||_{L_y^2(L_\omega^2)} e^{-t/2}. \tag{8.20}$$

Moreover, we also have :

$$||\tilde{u} - u_\infty||_{L_y^2} \leq C \left(|f_0(t) - a_0| + |f_1(t) - a_1| \right). \tag{8.21}$$

Moreover, it is easy to show that :

$$\frac{d}{dt}||\tilde{X} - X^\infty||_{L_\omega^2}^2 \leq C \left((|f_0(t) - a_0| + |f_1(t) - a_1|)||\tilde{X} - X^\infty||_{L_\omega^2} - ||\tilde{X} - X^\infty||_{L_\omega^2}^2 \right),$$

so that,

$$\frac{d}{dt}||\tilde{X} - X^\infty||_{L_\omega^2} \leq C \left((|f_0(t) - a_0| + |f_1(t) - a_1|) - ||\tilde{X} - X^\infty||_{L_\omega^2} \right),$$

and

$$||\tilde{X} - X^\infty||_{L_\omega^2} \leq C \int_0^t (|f_0(s) - a_0| + |f_1(s) - a_1|) \exp(-C(t-s)) \, ds. \tag{8.22}$$

By Lemma 25-(ii), we therefore obtain :

$$\lim_{t \to \infty} ||\tilde{X} - X^\infty||_{L_\omega^2} = 0. \tag{8.23}$$

It remains now to compare X with $\tilde{X}$ and u with $\tilde{u}$. Notice that, since $\tilde{X}$ and Y^∞ do not depend on space, $(u - \tilde{u})$ and $(X - \tilde{X})$ are solution of :

$$\begin{cases} \dfrac{\partial(u - \tilde{u})}{\partial t}(t, y) &= \partial_{y,y}(u - \tilde{u})(t, y) + \partial_y(\tau - \tilde{\tau})(t, y) - (\dot{f}_0(t) + y(\dot{f}_1(t) - \dot{f}_0(t))), \\ \tau(t, y) &= \mathbb{E}\left(X_t(y)Y_t(y)\right), \\ \tilde{\tau}(t) &= \mathbb{E}\left(\tilde{X}_t Y_t^\infty\right), \\ \dfrac{\partial(X_t(y) - \tilde{X}_t)}{\partial t} &= (\partial_y u(t, y)Y_t(y) - \partial_y \tilde{u}(t)Y_t^\infty) - \dfrac{1}{2}(X_t(y) - \tilde{X}_t). \end{cases}$$

By multiplying the equation on $(u - \tilde{u})$ by $(u - \tilde{u})$ and the equation on $(X - \tilde{X})$ by $(X - \tilde{X})$, using the fact that $(u - \tilde{u})$ is zero for $y = 0$ and $y = 1$ and the fact that f_0 and f_1 are bounded functions, one can check that :

$$\frac{1}{2}\frac{d}{dt}\left(||u - \tilde{u}||_{L_y^2}^2 + ||X_t - \tilde{X}_t||_{L_y^2(L_\omega^2)}^2 \right)$$

$$= -||\partial_y(u - \tilde{u})||_{L_y^2}^2 - \frac{1}{2}||X_t - \tilde{X}_t||_{L_y^2(L_\omega^2)}^2 - \int (\dot{f}_0(t) + y(\dot{f}_1(t) - \dot{f}_0(t)))(u - \tilde{u})$$

$$- \int \mathbb{E}\left(X_t(y)Y_t(y) - \tilde{X}_t Y_t^\infty \right) \partial_y(u - \tilde{u}) + \int \mathbb{E}\left((\partial_y u(t, y)Y_t(y) - \partial_y \tilde{u}(t)Y_t^\infty)(X_t(y) - \tilde{X}_t) \right)$$

$$\leq C \left(-||u - \tilde{u}||_{L_y^2}^2 - ||X_t - \tilde{X}_t||_{L_y^2(L_\omega^2)}^2 + (|\dot{f}_0| + |\dot{f}_1|)||u - \tilde{u}||_{L_y^2} \right)$$

$$+ \int \mathbb{E}\left((X_t(y) - \tilde{X}_t)(Y_t(y) - Y_t^\infty) \right) \partial_y \tilde{u}(t) + \int \mathbb{E}\left(\tilde{X}_t(Y_t(y) - Y_t^\infty) \right) \partial_y(\tilde{u} - u)(t, y)$$

$$\leq C \left(-||u - \tilde{u}||_{L_y^2}^2 - ||X_t - \tilde{X}_t||_{L_y^2(L_\omega^2)}^2 + (|\dot{f}_0| + |\dot{f}_1|)||u - \tilde{u}||_{L_y^2} + e^{-t/2}||X_t - \tilde{X}_t||_{L_y^2(L_\omega^2)} \right),$$

where we have used the fact that, by (8.18) and using the analytical expressions of Y_t, Y_t^∞ and $\tilde{X}_t$, $\mathbb{E}\left(\tilde{X}_t(Y_t(y) - Y_t^\infty)\right)$ does not depend on y and therefore,

$$\int \mathbb{E}\left(\tilde{X}_t(Y_t(y) - Y_t^\infty)\right) \partial_y(\tilde{u} - u)(t, y) = 0.$$

Therefore,

$$\frac{d}{dt}\left(||u - \tilde{u}||^2_{L^2_y} + ||X_t - \tilde{X}_t||^2_{L^2_y(L^2_\omega)}\right)$$
$$\leq C\Big(-||u - \tilde{u}||^2_{L^2_y} - ||X_t - \tilde{X}_t||^2_{L^2_y(L^2_\omega)}$$
$$+ (|\dot{f}_0| + |\dot{f}_1| + e^{-t/2})(||u - \tilde{u}||_{L^2_y} + ||X_t - \tilde{X}_t||_{L^2_y(L^2_\omega)})\Big)$$
$$\leq C\Big(-||u - \tilde{u}||^2_{L^2_y} - ||X_t - \tilde{X}_t||^2_{L^2_y(L^2_\omega)}$$
$$+ \sqrt{2}(|\dot{f}_0| + |\dot{f}_1| + e^{-t/2})\sqrt{||u - \tilde{u}||^2_{L^2_y} + ||X_t - \tilde{X}_t||^2_{L^2_y(L^2_\omega)}}\Big).$$

We then obtain that :

$$\sqrt{||u - \tilde{u}||^2_{L^2_y} + ||X_t - \tilde{X}_t||^2_{L^2_y(L^2_\omega)}} \leq C\int_0^t (|\dot{f}_0| + |\dot{f}_1| + e^{-s/2})\exp(-C(t-s))\,ds. \quad (8.24)$$

By Lemma 25, we therefore obtain :

$$\lim_{t \to \infty} ||u - \tilde{u}||_{L^2_y} + ||X_t - \tilde{X}_t||_{L^2_y(L^2_\omega)} = 0. \quad (8.25)$$

$\square$

Lemma 25 *Let $k \in L^1_{\text{loc}}(\mathbb{R}_+)$ be a positive function, $\alpha > 0$, and h a function defined by :*

$$h(t) = \int_0^t \exp(-\alpha(t - s))k(s)\,ds.$$

(i) If we assume that $k \in L^p(\mathbb{R}_+)$, with $1 \leq p < \infty$, then $h \in W^{1,p}(\mathbb{R}_+)$ and therefore $\lim_{t \to \infty} h(t) = 0$.
(ii) If we assume that $\lim_{t \to \infty} k(t) = 0$, then $\lim_{t \to \infty} h(t) = 0$.
(iii) If we suppose that $0 \leq k(t) \leq Ce^{-\beta t}$, with $\beta > 0$ and $\alpha \neq \beta$, then $h(t) \leq \dfrac{C}{|\alpha - \beta|}e^{-\alpha \wedge \beta\, t}$.

Proof. To prove the first assertion, one can check (by using Hölder inequality and Fubini theorem) that if $k \in L^p(\mathbb{R}_+)$, then $h \in L^p(\mathbb{R}_+)$. Therefore, $\dot{h}(t) = -\alpha h(t) + k(t)$ is in $L^p(\mathbb{R}_+)$. The fact that $h \in W^{1,p}(\mathbb{R}_+)$ then implies that $\lim_{t \to \infty} h(t) = 0$. For the second assertion, let us introduce a $\epsilon > 0$. There exists $T > 0$ such that $\forall t > T$, $0 \leq k(t) \leq \epsilon$. One can then conclude by considering the integral on $(0, T)$ and (T, t) and by letting $t \to \infty$. The last assertion is obtained by a simple computation. $\square$

By using Lemma 25 and the estimates (8.20)–(8.21)–(8.22)–(8.24), one can also consider the following hypothesis in Lemma 24 alternatively to (8.17)–(8.19) :

- if $(f_0(t) - a_0) \in W^{1,p}(\mathbb{R}_+)$ and $(f_1(t) - a_1) \in W^{1,p}(\mathbb{R}_+)$, for a $1 \le p < \infty$, then the results of Lemma 24 still hold,
- if , that $f_0, f_1 \in W^{1,1}_{\text{loc}}(\mathbb{R}_+)$ and $(f_0(t) - a_0)$, $(f_1(t) - a_1)$, $\dot{f}_0(t)$ and $\dot{f}_1(t)$ converge exponentially fast to 0, then the convergences stated in Lemma 24 are also exponential.

We are not able to extend the above arguments as such in order to settle the case when the force is not linear (for FENE dumbbell for example) or the geometry is not a shear flow. In the next section, we present a more general approach, which requires to introduce the probability density function ψ of the process (X, Y).

8.3 Convergence to equilibrium by the entropy method

In this section, we are interested in convergence to *equilibrium* ($\boldsymbol{u}_\infty = 0$, $\psi_\infty(\boldsymbol{X}) \propto \exp(-\Pi(\boldsymbol{X}))$) in a more general setting than in Section 8.2. More precisely, we consider the problem (8.4)–(8.5)–(8.6)–(8.7) on a general geometry $\mathcal{D}$, for any radial α-convex potential Π (8.3), but we restric ourselves to *homogeneous boundary conditions on the velocity* : $\boldsymbol{u} = 0$ on $\partial\mathcal{D}$.

8.3.1 A first energy estimate

The energy estimate we have used to study the coupled PDE-SDE system in the case of one-dimensional shear flow (see [85, 86]) can be established formally for any flows in any geometry. Multiplying (8.4) by $\boldsymbol{u}$,

$$\frac{1}{2}\frac{d}{dt}\int_{\mathcal{D}}|\boldsymbol{u}|^2 = -\int_{\mathcal{D}}|\nabla\boldsymbol{u}|^2 - \int_{\mathcal{D}}\mathbb{E}(\boldsymbol{X}_t \otimes \nabla\Pi(\boldsymbol{X}_t)) : \nabla\boldsymbol{u}, \qquad (8.26)$$

while, by Itô's calculus,

$$\frac{d}{dt}\mathbb{E}(\Pi(\boldsymbol{X}_t)) = \mathbb{E}(\nabla\Pi(\boldsymbol{X}_t).\nabla\boldsymbol{u}\boldsymbol{X}_t) - \frac{1}{2}\mathbb{E}(||\nabla\Pi(\boldsymbol{X}_t)||^2) + \frac{1}{2}\mathbb{E}(\Delta\Pi(\boldsymbol{X}_t)), \quad (8.27)$$

we obtain the following energy estimate for the system :

$$\frac{1}{2}\frac{d}{dt}\int_{\mathcal{D}}|\boldsymbol{u}|^2 + \frac{d}{dt}\int_{\mathcal{D}}\mathbb{E}(\Pi(\boldsymbol{X}_t)) + \int_{\mathcal{D}}|\nabla\boldsymbol{u}|^2 + \frac{1}{2}\int_{\mathcal{D}}\mathbb{E}(||\nabla\Pi(\boldsymbol{X}_t)||^2) = \frac{1}{2}\int_{\mathcal{D}}\mathbb{E}(\Delta\Pi(\boldsymbol{X}_t)).$$
$$(8.28)$$

Notice that we have supposed that $\forall t \ge 0$, $\int_0^t \mathbb{E}(||\nabla\Pi(\boldsymbol{X}_s)||^2)\,ds < \infty$ and that we have used the following equality :

$$\mathbb{E}(\boldsymbol{X}_t \otimes \nabla\Pi(\boldsymbol{X}_t)) : \nabla\boldsymbol{u} = \mathbb{E}(\nabla\Pi(\boldsymbol{X}).\nabla\boldsymbol{u}\boldsymbol{X}) \qquad (8.29)$$

which holds since $\boldsymbol{X} \otimes \nabla\Pi(\boldsymbol{X}) = \nabla\Pi(\boldsymbol{X}) \otimes \boldsymbol{X}$. The latter relation is related to the fact that the stress tensor must be symmetric (which is a physical requirement), which holds for a radial potential Π, since in this case, $\nabla\Pi(\boldsymbol{X}) = \pi'(||\boldsymbol{X}||)\dfrac{\boldsymbol{X}}{||\boldsymbol{X}||}$.

We have checked that these formal computations can be rigorously justified in the case of shear flow for Hookean dumbbells (see Section 3.2 in [85]) and for FENE dumbbells (see Lemma 4 in [86]).

The main difficulty in the *a priori* estimate (8.28) is due to the presence of the non negative term $\dfrac{1}{2}\displaystyle\int_{\mathcal{D}}\mathbb{E}(\Delta\Pi(\boldsymbol{X}_t))$ on the right hand side : this term, stemming from Itô's calculus and non negative by the convexity of Π, "brings energy" into the system, so that it is not clear how to use this estimate to study the longtime behaviour. The aim of this note is to show that the use of an entropy equality (see (8.34) below) in lieu of (8.27) allows to study the convergence of the system to equilibrium. However, contrary to the energy inequality that can be stated either in the stochastic form (see (8.27)), or using the probability density function ψ, the entropy inequality seems to be restricted to the analysis of the system in the Fokker-Planck form (8.4)–(8.5)–(8.6)–(8.7) since we introduce an entropy of the probability density function ψ, which cannot be simply expressed in term of the stochastic process $\boldsymbol{X}_t$.

8.3.2 Entropy and convergence to equilibrium

Let us first introduce the kinetic energy E :

$$E(t) = \frac{1}{2}\int_{\mathcal{D}}|\boldsymbol{u}|^2. \tag{8.30}$$

As we have already mentioned, we have (see (8.26)) :

$$\frac{dE}{dt} = -\int_{\mathcal{D}}|\nabla\boldsymbol{u}|^2 - \int_{\mathcal{D}}\int_{\mathbb{R}^d}(\boldsymbol{X}\otimes\nabla\Pi(\boldsymbol{X})):\nabla\boldsymbol{u}\,\psi(t,\boldsymbol{x},\boldsymbol{X}). \tag{8.31}$$

We now introduce the entropy of the system (in fact the entropy relative to ψ_∞), namely :

$$
\begin{aligned}
H(t) &= \int_{\mathcal{D}}\int_{\mathbb{R}^d}\psi(t,\boldsymbol{x},\boldsymbol{X})\ln\left(\frac{\psi(t,\boldsymbol{x},\boldsymbol{X})}{\psi_\infty(\boldsymbol{X})}\right) \\
&= \int_{\mathcal{D}}\int_{\mathbb{R}^d}\Pi(\boldsymbol{X})\psi(t,\boldsymbol{x},\boldsymbol{X}) + \int_{\mathcal{D}}\int_{\mathbb{R}^d}\psi(t,\boldsymbol{x},\boldsymbol{X})\ln(\psi(t,\boldsymbol{x},\boldsymbol{X})) + C
\end{aligned}
\tag{8.32}
$$

with

$$\psi_\infty(\boldsymbol{X}) = \frac{\exp(-\Pi(\boldsymbol{X}))}{\int_{\mathbb{R}^d}\exp(-\Pi(\boldsymbol{X}))}, \tag{8.33}$$

and $C = \ln(\int_{\mathbb{R}^d}\exp(-\Pi(\boldsymbol{X})))|\mathcal{D}|$. Note that ψ_∞ is the stationary solution to the Fokker-Planck equation (8.7) for $\boldsymbol{u} = \boldsymbol{u}_\infty = 0$. Function H is the relative entropy of ψ with respect to ψ_∞. It is non negative since $x\ln(x) - x + 1 \geq 0$ for all $x \geq 0$.

After some computations (which will be done with more details below in a more general case, see Section 8.4.1), we obtain :

$$\frac{dH}{dt} = -\frac{1}{2}\int_{\mathcal{D}}\int_{\mathbb{R}^d}\psi\left|\nabla\ln\left(\frac{\psi}{\psi_\infty}\right)\right|^2 + \int_{\mathcal{D}}\int_{\mathbb{R}^d}(\boldsymbol{X}\otimes\nabla\Pi(\boldsymbol{X})):\nabla\boldsymbol{u}\,\psi(t,\boldsymbol{x},\boldsymbol{X}). \tag{8.34}$$

Therefore, if we consider the free energy of the system $F(t) = E(t) + H(t)$, we have :

$$\frac{dF}{dt} + \int_{\mathcal{D}} |\nabla \boldsymbol{u}|^2 + \frac{1}{2} \int_{\mathcal{D}} \int_{\mathbb{R}^d} \psi \left| \nabla \ln \left(\frac{\psi}{\psi_\infty} \right) \right|^2 = 0. \qquad (8.35)$$

The comparison of (8.35) with (8.28) reflects the physical fact that the model is intrisically of entropic nature, and therefore that the energy is not the thermodynamic quantity to consider.

On the basis of the free energy estimate (8.34), we can proceed further. First, we are able to identify the stationary state :

Proposition 7 *The unique stationary solution of the coupled problem for homogeneous Dirichlet boundary conditions on the velocity is :*

$$\boldsymbol{u} = \boldsymbol{u}_\infty = 0 \text{ and } \psi = \psi_\infty = \frac{\exp(-\Pi(\boldsymbol{X}))}{\int_{\mathbb{R}^d} \exp(-\Pi(\boldsymbol{X}))}.$$

Proof. It is easy to check that $(\boldsymbol{u}_\infty, \psi_\infty)$ is a stationary solution to the coupled problem for homogeneous Dirichlet boundary conditions. The proof is then a straightforward application of (8.35) to time-independent fields. $\qquad\square$

In addition, we may prove the convergence to equilibrium :

Proposition 8 *If one considers a regular global solution of the coupled system in the case of homogeneous Dirichlet boundary conditions on the velocity, then we have the following convergences :* $\boldsymbol{u}$ *converges exponentially fast towards* $\boldsymbol{u}_\infty = 0$ *in* $L_{\boldsymbol{x}}^2$ *norm and* ψ *converges exponentially fast towards* $\psi_\infty = \dfrac{\exp(-\Pi(\boldsymbol{X}))}{\int_{\mathbb{R}^d} \exp(-\Pi(\boldsymbol{X}))}$ *in* $L_{\boldsymbol{x}}^2(L_{\boldsymbol{X}}^1)$ *norm.*

Proof. Let us simply give an outline of the proof. Using the following inequalities in (8.34) :
- Poincaré inequality :

$$\int_{\mathcal{D}} |\boldsymbol{u}|^2 \leq C \int_{\mathcal{D}} |\nabla \boldsymbol{u}|^2,$$

- Sobolev logarithmic inequality for ψ_∞, which holds for example if the potential Π is α-convex (see [1, 2]) :

$$\int_{\mathbb{R}^d} \psi \ln \left(\frac{\psi}{\psi_\infty} \right) \leq C \int_{\mathbb{R}^d} \psi \left| \nabla \ln \left(\frac{\psi}{\psi_\infty} \right) \right|^2,$$

we obtain an inequality of the type $\dfrac{dF}{dt} \leq -CF$ and therefore exponential convergence of F to 0. This implies the exponential convergence of $\boldsymbol{u}$ to 0.

One finally uses the Csiszar-Kullback inequality :

$$\left(\int_{\mathbb{R}^d} |\psi - \psi_\infty| \right)^2 \leq 4 \int_{\mathbb{R}^d} \psi \ln \left(\frac{\psi}{\psi_\infty} \right) \qquad (8.36)$$

to obtain exponential convergence of ψ towards ψ_∞ in $L_{\boldsymbol{x}}^2(L_{\boldsymbol{X}}^1)$-norm. $\qquad\square$

8.4 The case of non homogeneous conditions

The entropy method we have used in Section 8.3 is well suited for the convergence to equilibrium ($\boldsymbol{u}_\infty = 0$), i.e. when we consider homogeneous boundary conditions on the velocity $\boldsymbol{u}$. On the other hand, the generalization to non homogeneous boundary conditions, and therefore to non zero stationary state, is unclear to date. In the following, we suppose that $\boldsymbol{u} \neq 0$ on $\partial\mathcal{D}$. More precisely, we assume that $\boldsymbol{u} = g$ on $\partial\mathcal{D}$, where g is a function defined on $\partial\mathcal{D}$ and *not depending on time t*.

8.4.1 Calculus in a general geometry

Stationary solutions are defined in this case as some solutions of the following equations :

$$
\begin{cases}
\boldsymbol{u}_\infty(\boldsymbol{x}).\nabla\boldsymbol{u}_\infty(\boldsymbol{x}) &= \Delta\boldsymbol{u}_\infty(\boldsymbol{x}) - \nabla p_\infty(\boldsymbol{x}) + \operatorname{div}\boldsymbol{\tau}_\infty(\boldsymbol{x}), \\[4pt]
\operatorname{div}(\boldsymbol{u}_\infty) &= 0, \\[4pt]
\boldsymbol{\tau}_\infty(\boldsymbol{x}) &= \displaystyle\int_{\mathbb{R}^d}(\boldsymbol{X}\otimes\nabla\Pi(\boldsymbol{X}))\psi_\infty(\boldsymbol{x},\boldsymbol{X})\,d\boldsymbol{X}, \\[8pt]
\boldsymbol{u}_\infty(\boldsymbol{x}).\nabla_{\boldsymbol{x}}\psi_\infty(\boldsymbol{x},\boldsymbol{X}) &= -\operatorname{div}_{\boldsymbol{X}}\left((\nabla_{\boldsymbol{x}}\boldsymbol{u}_\infty(\boldsymbol{x}).\boldsymbol{X} - \frac{1}{2}\nabla\Pi(\boldsymbol{X}))\psi_\infty(\boldsymbol{x},\boldsymbol{X})\right) \\[8pt]
& \quad + \frac{1}{2}\Delta_{\boldsymbol{X}}\psi_\infty(\boldsymbol{x},\boldsymbol{X}),
\end{cases}
$$

with $\boldsymbol{u}_\infty = g$ on $\partial\mathcal{D}$. One can rewrite the equation on ψ_∞ in the following manner :

$$
\begin{aligned}
2\boldsymbol{u}_\infty&(\boldsymbol{x}).\nabla_{\boldsymbol{x}}(\ln\psi_\infty(\boldsymbol{x},\boldsymbol{X})) + 2\nabla_{\boldsymbol{x}}\boldsymbol{u}_\infty(\boldsymbol{x})\boldsymbol{X}.\nabla_{\boldsymbol{X}}\ln(\psi_\infty(\boldsymbol{x},\boldsymbol{X})) \\
&= \Delta_{\boldsymbol{X}}\Pi(\boldsymbol{X}) + \nabla_{\boldsymbol{X}}\Pi(\boldsymbol{X}).\nabla_{\boldsymbol{X}}(\ln\psi_\infty(\boldsymbol{x},\boldsymbol{X})) + \Delta_{\boldsymbol{X}}(\ln\psi_\infty(\boldsymbol{x},\boldsymbol{X})) \\
&\quad + |\nabla_{\boldsymbol{X}}(\ln\psi_\infty(\boldsymbol{x},\boldsymbol{X}))|^2.
\end{aligned}
\tag{8.37}
$$

In the following, we set $\overline{\boldsymbol{u}}(t,\boldsymbol{x}) = \boldsymbol{u}(t,\boldsymbol{x}) - \boldsymbol{u}_\infty(\boldsymbol{x})$ and $\overline{\psi}(t,\boldsymbol{x},\boldsymbol{X}) = \psi(t,\boldsymbol{x},\boldsymbol{X}) - \psi_\infty(\boldsymbol{x},\boldsymbol{X})$.

We also introduce the following quantities :

$$
\overline{E}(t) = \frac{1}{2}\int_{\mathcal{D}}|\overline{\boldsymbol{u}}|^2(\boldsymbol{x},t)
\tag{8.38}
$$

$$
H(t) = \int_{\mathcal{D}}\int_{\mathbb{R}^d}\psi(t,\boldsymbol{x},\boldsymbol{X})\ln\left(\frac{\psi(t,\boldsymbol{x},\boldsymbol{X})}{\psi_\infty(\boldsymbol{x},\boldsymbol{X})}\right)
\tag{8.39}
$$

$$
\overline{F}(t) = \overline{E}(t) + H(t)
\tag{8.40}
$$

For the velocity, we easily obtain :

$$
\begin{aligned}
\frac{d\overline{E}}{dt} &= -\int_{\mathcal{D}}|\nabla\overline{\boldsymbol{u}}|^2 - \int_{\mathcal{D}}\int_{\mathbb{R}^d}(\boldsymbol{X}\otimes\nabla\Pi(\boldsymbol{X})):\nabla\overline{\boldsymbol{u}}(\boldsymbol{x},t)\overline{\psi}(t,\boldsymbol{x},\boldsymbol{X}) \\
&\quad - \int_{\mathcal{D}}\overline{\boldsymbol{u}}.\nabla\boldsymbol{u}_\infty\overline{\boldsymbol{u}}.
\end{aligned}
\tag{8.41}
$$

Compared to the case of homogeneous boundary condition, the supplementary term comes from the nonlinearity of the advection term in the Navier-Stokes equations. Using again the equality (8.29), we have :

$$\frac{d}{dt} \int_{\mathcal{D}} \int_{\mathbb{R}^d} \psi \ln\left(\frac{\psi}{\psi_\infty}\right) = -\frac{1}{2} \int_{\mathcal{D}} \int_{\mathbb{R}^d} \frac{|\nabla\psi|^2}{\psi} - \int_{\mathcal{D}} \int_{\mathbb{R}^d} \nabla(\ln\psi_\infty).\nabla\boldsymbol{u}\boldsymbol{X}\psi$$

$$+ \int_{\mathcal{D}} \int_{\mathbb{R}^d} \frac{1}{2} \left(\Delta\Pi + \nabla(\ln\psi_\infty).\nabla\Pi - \Delta(\ln\psi_\infty)\right)\psi - \int_{\mathcal{D}} \int_{\mathbb{R}^d} \boldsymbol{u}.\nabla_{\boldsymbol{x}}(\ln\psi_\infty)\psi,$$

$$= -\frac{1}{2} \int_{\mathcal{D}} \int_{\mathbb{R}^d} |\nabla\ln\psi|^2\psi - \int_{\mathcal{D}} \int_{\mathbb{R}^d} \nabla(\ln\psi_\infty)\nabla\overline{\boldsymbol{u}}\boldsymbol{X}\psi$$

$$+ \int_{\mathcal{D}} \int_{\mathbb{R}^d} \left(-\frac{1}{2}|\nabla(\ln\psi_\infty)|^2 - \Delta(\ln\psi_\infty)\right)\psi - \int_{\mathcal{D}} \int_{\mathbb{R}^d} \overline{\boldsymbol{u}}.\nabla_{\boldsymbol{x}}(\ln\psi_\infty)\psi,$$

$$= -\frac{1}{2} \int_{\mathcal{D}} \int_{\mathbb{R}^d} \psi \left|\nabla\ln\left(\frac{\psi}{\psi_\infty}\right)\right|^2 - \int_{\mathcal{D}} \int_{\mathbb{R}^d} \nabla(\ln\psi_\infty)\nabla\overline{\boldsymbol{u}}\boldsymbol{X}\psi - \int_{\mathcal{D}} \int_{\mathbb{R}^d} \overline{\boldsymbol{u}}.\nabla_{\boldsymbol{x}}(\ln\psi_\infty)\psi.$$

Therefore, we obtain the following equality on the free energy $\overline{F}$:

$$\frac{d\overline{F}}{dt} = -\int_{\mathcal{D}} |\nabla\overline{\boldsymbol{u}}|^2 - \frac{1}{2} \int_{\mathcal{D}} \int_{\mathbb{R}^d} \psi \left|\nabla_{\boldsymbol{X}} \ln\left(\frac{\psi}{\psi_\infty}\right)\right|^2 - \int_{\mathbb{R}^d} \overline{\boldsymbol{u}}.\nabla\boldsymbol{u}_\infty\overline{\boldsymbol{u}} - \int_{\mathcal{D}} \int_{\mathbb{R}^d} \overline{\boldsymbol{u}}.\nabla_{\boldsymbol{x}}(\ln\psi_\infty)\psi$$

$$- \int_{\mathcal{D}} \int_{\mathbb{R}^d} \nabla_{\boldsymbol{X}}(\ln\psi_\infty).\nabla\overline{\boldsymbol{u}}\boldsymbol{X}\psi - \int_{\mathcal{D}} \int_{\mathbb{R}^d} \nabla\overline{\boldsymbol{u}}(\boldsymbol{x},t)\boldsymbol{X}.\nabla\Pi(\boldsymbol{X})\overline{\psi}$$

$$= -\int_{\mathcal{D}} |\nabla\overline{\boldsymbol{u}}|^2 - \frac{1}{2} \int_{\mathcal{D}} \int_{\mathbb{R}^d} \psi \left|\nabla_{\boldsymbol{X}} \ln\left(\frac{\psi}{\psi_\infty}\right)\right|^2 - \int_{\mathcal{D}} \overline{\boldsymbol{u}}.\nabla\boldsymbol{u}_\infty\overline{\boldsymbol{u}} - \int_{\mathcal{D}} \int_{\mathbb{R}^d} \overline{\boldsymbol{u}}.\nabla_{\boldsymbol{x}}(\ln\psi_\infty)\psi$$

$$- \int_{\mathcal{D}} \int_{\mathbb{R}^d} \left(\nabla_{\boldsymbol{X}}(\ln\psi_\infty) + \nabla\Pi(\boldsymbol{X})\right).\nabla\overline{\boldsymbol{u}}\boldsymbol{X}\psi + \int_{\mathcal{D}} \int_{\mathbb{R}^d} \nabla\Pi(\boldsymbol{X}).\nabla\overline{\boldsymbol{u}}(\boldsymbol{x},t)\boldsymbol{X}\psi_\infty$$

We thus obtain four supplementary terms compared to the case $\boldsymbol{u}_\infty = 0$ contained in (8.35) :

— two terms coming from the advection :

$$-\int \overline{\boldsymbol{u}}.\nabla\boldsymbol{u}_\infty\overline{\boldsymbol{u}} - \int\int \overline{\boldsymbol{u}}.\nabla_{\boldsymbol{x}}(\ln\psi_\infty)\psi, \tag{8.42}$$

— one term involving $\ln(\psi_\infty)$ and Π :

$$-\int\int \left(\nabla_{\boldsymbol{X}}(\ln\psi_\infty) + \nabla\Pi(\boldsymbol{X})\right).\nabla\overline{\boldsymbol{u}}\boldsymbol{X}\psi = -\int\int \nabla_{\boldsymbol{X}}\left(\ln\left(\frac{\psi_\infty}{\exp(-\Pi)}\right)\right).\nabla\overline{\boldsymbol{u}}\boldsymbol{X}\psi, \tag{8.43}$$

— and one term involving $\boldsymbol{\tau}_\infty$:

$$\int\int \nabla\Pi(\boldsymbol{X}).\nabla\overline{\boldsymbol{u}}(\boldsymbol{x},t)\boldsymbol{X}\psi_\infty = \int \boldsymbol{\tau}_\infty : \nabla\overline{\boldsymbol{u}}. \tag{8.44}$$

Remark 28 *If one considers the following free energy :* $\overline{F}(t) = \overline{E}(t) + \lambda H(t)$, *where* $\lambda > 0$, *the term (8.43) becomes :*

$$\int \int \nabla_{\boldsymbol{X}} \left(\ln \left(\frac{(\psi_\infty)^\lambda}{C \exp(-\Pi)} \right) \right) . \nabla \overline{\boldsymbol{u}} \boldsymbol{X} \psi,$$

where λ *and* C *are two constants which can be arbitrarily chosen.*

Notice that if $\boldsymbol{u}_\infty$ is a homogeneous flow $(\boldsymbol{u}_\infty(\boldsymbol{x}) = \boldsymbol{\kappa}\boldsymbol{x})$, then ψ_∞ does not depend on space, so that the second term in (8.42) and the term (8.44) vanish.

We have not been able to use these estimates to derive the convergence of the solution to the stationary state. Moreover, the fact that there exists a Sobolev logarithmic inequality for ψ_∞ in this case does not seem straightforward.

8.4.2 The case of a shear flow

We would like to perform the same computation in the special case of the shear flow, and for the special boundary conditions : $u(t, 0) = 0$, $u(t, 1) = V$ (which corresponds to $a_0(t) = 0$ and $a_1(t) = V$ in section 8.2). The "natural" stationary state is then

$$u_\infty(y) = Vy$$

and therefore, we expect ψ_∞ not to depend on y. The function ψ_∞ is defined as the solution of :

$$-\partial_X (VY\psi_\infty) - \text{div }_{X,Y} \left(-\frac{1}{2}\psi_\infty \nabla\Pi \right) + \frac{1}{2}\Delta_{X,Y}\psi_\infty = 0 \qquad (8.45)$$

Notice that the couple (u_∞, ψ_∞) is then a solution of the coupled problem, since the stress τ_∞ does not depend on space.

Following the computations of the last paragraph, we obtain :

$$\begin{aligned} \frac{d\overline{F}}{dt} &= -\int_{\mathcal{D}} |\partial_y \overline{u}|^2 - \frac{1}{2}\int_{\mathcal{D}} \int_{\mathbb{R}^2} \psi \left| \nabla_{\boldsymbol{X}} \ln \left(\frac{\psi}{\psi_\infty} \right) \right|^2 \\ &\quad - \int_{\mathcal{D}} \int_{\mathbb{R}^2} (\partial_X (\ln(\psi_\infty)) + \partial_X \Pi(X, Y)) (\partial_y \overline{u}) Y\psi. \end{aligned}$$

Due to the particular geometry, both terms in (8.42) vanish and so does the term (8.44) since τ_∞ does not depend on y. Therefore, only the term (8.43) remains, which can be (by changing the free energy to $\overline{E}(t) + \lambda H(t)$) rewritten in the following form (see Remark 28) :

$$\int_{\mathcal{D}} \int_{\mathbb{R}^2} \partial_X \left(\ln \left(\frac{(\psi_\infty)^\lambda}{C \exp(-\Pi)} \right) \right) \partial_y \overline{u} Y\psi,$$

where λ and C are two arbitrarily constants.

Remark 29 *In the case of Hookean dumbbells (see Section 8.2), the explicit expression of ψ_∞ :*

$$\psi_\infty(X, Y) \propto \exp\left(-\frac{1}{2(1+V^2)}\left((1+2V^2)Y^2 - 2VXY + X^2\right)\right)$$

can be used, which provides an alternative proof of convergence to that of Section 8.2. Notice that, contrary to the case of homogeneous boundary conditions, ψ_∞ does not satisfy the detailed balance in the sense that ψ_∞ is solution of :

$$-\text{div}_{\boldsymbol{X}}\left((\nabla_{\boldsymbol{x}}\boldsymbol{u}_\infty(\boldsymbol{x}).\boldsymbol{X} - \frac{1}{2}\nabla\Pi(\boldsymbol{X}))\psi_\infty(\boldsymbol{x}, \boldsymbol{X}) - \frac{1}{2}\nabla_{\boldsymbol{X}}\psi_\infty(\boldsymbol{x}, \boldsymbol{X})\right) = 0$$

but not of :

$$(\nabla_{\boldsymbol{x}}\boldsymbol{u}_\infty(\boldsymbol{x}).\boldsymbol{X} - \frac{1}{2}\nabla\Pi(\boldsymbol{X}))\psi_\infty(\boldsymbol{x}, \boldsymbol{X}) - \frac{1}{2}\nabla_{\boldsymbol{X}}\psi_\infty(\boldsymbol{x}, \boldsymbol{X}) = 0.$$

8.4.3   Other entropy functions

One can also generalize these computations with other entropy functions than $x \ln(x)$. More precisely, let $h : \mathbb{R} \to \mathbb{R}_+^*$ be a $\mathcal{C}^2$ function, such that $h(1) = 0$ (see [2]). These are typical examples of entropy functions :
  – $h(x) = x \ln(x) - (x - 1)$
  – $h(x) = x^p - 1 - p(x - 1)$ with $1 < p \le 2$
We here consider the same situation as in the previous paragraph (a shear flow with $u_\infty \ne 0$), but the following computations can be generalize to any geometry.
We set :

$$\overline{E}(t) = \frac{1}{2}\int_{\mathcal{D}} |\overline{u}|^2(y, t)\, dy \tag{8.46}$$

$$H(t) = \int_{\mathcal{D}}\int_{\mathbb{R}^2} h\left(\frac{\psi(t, y, \boldsymbol{X})}{\psi_\infty(\boldsymbol{X})}\right)\psi_\infty(\boldsymbol{X})\, dy\, d\boldsymbol{X} \tag{8.47}$$

$$\overline{F}(t) = \overline{E}(t) + H(t) \tag{8.48}$$

where ψ_∞ is independant of y and is defined as a solution of (8.45). As above, we have :

$$\frac{d\overline{E}}{dt} = -\int_{\mathcal{D}} |\partial_y\overline{u}|^2 - \int_{\mathcal{D}}\int_{\mathbb{R}^2} Y\left(\partial_X\Pi\right)\psi\left(\partial_y\overline{u}\right) \tag{8.49}$$

Using integrations by part, the equation (8.37) and the fact that $\partial_X\psi = \psi_\infty\partial_X\left(\frac{\psi}{\psi_\infty}\right) + \psi\partial_X(\ln\psi_\infty)$, we obtain after some tedious computations :

$$\begin{aligned}
\frac{dH}{dt} = &-\frac{1}{2}\int_{\mathcal{D}}\int_{\mathbb{R}^2}\left|\nabla\left(\frac{\psi}{\psi_\infty}\right)\right|^2 h''\left(\frac{\psi}{\psi_\infty}\right)\psi_\infty \\
&-\int_{\mathcal{D}}\int_{\mathbb{R}^2} Y\partial_X(\ln\psi_\infty)\psi\partial_y\overline{u}\left(h'\left(\frac{\psi}{\psi_\infty}\right) - h\left(\frac{\psi}{\psi_\infty}\right)\frac{\psi_\infty}{\psi}\right). \tag{8.50}
\end{aligned}$$

Therefore, we have :

$$
\begin{aligned}
\frac{d\overline{F}}{dt} \;=\;& -\int_{\mathcal{D}} |\partial_y \overline{u}|^2 - \frac{1}{2}\int_{\mathcal{D}}\int_{\mathbb{R}^2} \left|\nabla\left(\frac{\psi}{\psi_\infty}\right)\right|^2 h''\left(\frac{\psi}{\psi_\infty}\right)\psi_\infty \\
& -\int_{\mathcal{D}}\int_{\mathbb{R}^2} Y\psi\partial_y\overline{u}\left(\partial_X\Pi + \partial_X(\ln\psi_\infty)\left(h'\left(\frac{\psi}{\psi_\infty}\right) - h\left(\frac{\psi}{\psi_\infty}\right)\frac{\psi_\infty}{\psi}\right)\right)
\end{aligned} \tag{8.51}
$$

Remark 30 *In the special case of homogeneous boundary conditions ($u_\infty = 0$ and $\partial_X(\ln\psi_\infty) = -\partial_X\Pi$), we see that a sufficient condition to obtain the energy equality is that : $h'(x) - h(x)/x = 1$, which yields $h(x) = x\ln(x)$. Therefore, it seems that the "adapted" entropy function for the coupled system is indeed $x\ln(x)$. Notice that one can on the contrary use many others entropy functions to study the convergence to equilibrium of the Fokker-Planck equation alone (see [2]).*

The last term in (8.51) can also be rewritten in the following form :

$$
\begin{aligned}
-\int_{\mathcal{D}}\int_{\mathbb{R}^2} Y\psi\partial_y\overline{u}&\left(\partial_X\Pi + \partial_X(\ln\psi_\infty)\left(h'\left(\frac{\psi}{\psi_\infty}\right) - h\left(\frac{\psi}{\psi_\infty}\right)\frac{\psi_\infty}{\psi}\right)\right) \\
&= \int_{\mathcal{D}}\int_{\mathbb{R}^2} Y\psi\partial_y\overline{u}\left(-\partial_X\Pi + \partial_X\left(h'\left(\frac{\psi}{\psi_\infty}\right)\right)\right).
\end{aligned}
$$

8.5   Conclusion and perspectives

In this short paper, we have derived some *a priori* entropy and energy estimates to study the longtime behaviour of a coupled system arising in the micro-macro modelling of polymeric fluids. We have shown that unless in the special case of Hookean dumbbells in a shear flow, the quantity to be considered need to account for an entropy term. Moreover, we have checked that the "adapted entropy function" to study the coupled system is the "physical entropy" $h(x) = x\ln(x)$. With this entropy function, we have been able to prove formally exponential convergence to equilibrium in the case of homogeneous Dirichlet boundary conditions on the velocity $\boldsymbol{u}$.

But the computations made in this paper leave a lot of questions unsolved :

– In the case of homogeneous Dirichlet boundary conditions on the velocity $\boldsymbol{u}$, how to perform these computations using the stochastic process $\boldsymbol{X}_t$ (and not the density function ψ) ? Is it possible to perform these computations on the discretized system ?

– In the case of homogeneous Dirichlet boundary conditions on $\boldsymbol{u}$, are these new energy estimates useful to obtain global-in-time existence results ? How to show the convergence of the stress tensor, from the convergence of the density ψ ?

– How to generalize the computations made with homogeneous Dirichlet boundary conditions on the velocity to non homogeneous boundary conditions ?

Deuxième partie

Magnétohydrodynamique et modélisation des cuves d'électrolyse d'aluminium

Chapitre 9

Présentation générale du procédé et des méthodes numériques

Ce chapitre reproduit un article paru dans *Computers and Fluids*. Il permet notamment de présenter le contexte industriel des problématiques traitées dans cette partie ainsi que les méthodes numériques utilisées.

Modeling and simulation of the industrial production of aluminium : the nonlinear approach[a]

J.-F. Gerbeau, T. Lelièvre, and C. Le Bris

We report on the numerical simulation of the industrial production of aluminium. The motion of the two non miscible conducting fluids is modeled through the incompressible Navier-Stokes equations coupled with the (parabolic) Maxwell equations. Stabilized finite elements techniques and an Arbitrary Lagrangian Eulerian formulation (for the motion of the interface separating the two fuids) are used in the numerical simulation. The industrial problem and the modeling strategy are presented in details. An outline of the numerical analysis of the problem, with a special emphasis on conservation and stability properties is provided. Examples of numerical simulations of the industrial case are eventually presented.

Keywords : industrial problem ; aluminium production ; magnetohydrodynamic ; free interface ; two-fluids flow ; surface tension ; geometric conservation law ; ALE formulation.

---

[a]This article has been presented by the third author (CLB) as a plenary lecture at the AMIF conference, April 2002, Lisbon.

9.1 Introduction

We report here on a long-term work on the modeling and the numerical simulation of an electrolysis cell used for the industrial production of aluminium. We shall first present the challenging issues raised by this problem. Next, we isolate some modelling difficulties, which are of general interest. We show how we solved or circumvented them. In one sentence, our approach can be summarized as follows : we conduct a deep mathematical analysis of the models, then we focus on the nonlinearities on the problem, and simulate their consequences on the behaviour of the system, thereby complementing linear approaches that are more commonly developed in the literature.

For the sake of brevity, we shall not go here into the details neither on the mathematical analysis of the models, nor on the numerical analysis of the methods. We shall only give an outline of the techniques we have adopted or developed, and present significant simulations we have performed. For more details, we refer the interested reader to other publications of us : [37, 51, 53–63]. In particular, a companion article [61] presents a thorough account of the numerical analysis.

9.1.1 The industrial problem

The industrial production of aluminium is a problem of outstanding difficulty. The aluminium is produced from an aluminium oxyde Al_2O_3, itself coming from a native form, bauxite. In presence of Carbon, the aluminium oxyde Al_2O_3 is reduced into pure aluminium. Thermodynamically, the reduction can only occur around 1000 degrees Celsius, a temperature at which Aluminium is a liquid. Let us briefly indicate that a schematic picture of the functioning of the electrolysis cell is as follows (*see* [95]) : an electric current of the order of 10^5 A runs through two horizontal layers of conducting incompressible fluids, namely a bath of the aluminium oxyde above, and a layer of liquid aluminium below, which is the aluminium produced "so far" (*see* Figure 9.1). The oxydoreduction reaction takes place both at the interface between the two fluids

$$Al_2O_3 + 6\,e^- \longrightarrow 2\,Al^{3+} + 3\,O^{2-} + 6\,e^- \longrightarrow 2\,Al + 3\,O^{2-} \tag{9.1}$$

and at the surface of anods, which provide the bath with the Carbon needed for the reaction :

$$3\,O^{2-} + 3/2\,C \longrightarrow 3/2\,C0_2(\text{gas}) + 6\,e^- . \tag{9.2}$$

The global balance reads

$$2\,Al_2O_3 + 3\,C \longrightarrow 4\,Al + 3\,CO_2 \tag{9.3}$$
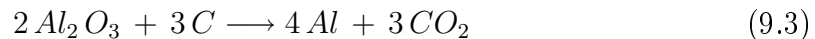
The difference of electric potential needed for the oxydoreduction is small (around a few Volts) but the intensity of the current is so large that the electric power spent in the cell is huge. The reason why the intensity of the electric current is taken so large is of course that the quantity of aluminium produced in the cell is proportional to the intensity (accordingly to (9.1)). For an intensity such as 10^5 A, the production is typically of a few tons of aluminium per cell and per day. A plant of production of aluminium consists in one (or many) line(s) of, say, 250 cells connected in series.

The electric power needed for the whole plant is typically of the order of magnitude of that produced by one unit of a contemporary nuclear plant.

With a view to reducing the power waste, the distance between the carbon anods covering the top of the cell and the surface of the aluminium layer (a perfectly conducting fluid directly connected to the cathode at the bottom of the cell) is to be kept as small as possible. Indeed, as the intensity needs to be kept as large as possible, diminishing the power amounts to diminishing the difference of potential. The latter, which is bounded from below by the potential needed for the oxydoreduction to occur, is also due to the potential drop in the (badly conducting) upper fluid of the cell. The goal is therefore to keep the thickness of the upper fluid layer as small as possible. This thickness is called the *anod-metal distance* which is a self explanatory term. Typically, the order of magnitude of the anod-metal distance is of a few centimeters vertically, which is a very tiny distance with respect to the horizontal sizes of the cell which are of the order of many meters, say 4 by 10 to fix the ideas. In addition to this penalizing aspect ratio, the main difficulty in trying to diminish the anod-metal distance lies in the fact that, due to the presence of the electric current, the conducting fluids experience strong Lorentz forces (the induced magnetic field is of the order of 0.01 T) and therefore move (the typical flow velocity in the cell is 0.2 m/s). This causes movement of the interface, which separates the two fluids. This movement may lead to instabilities. The anod-metal ditance should be small to reduce the cost ; however, this distance should be sufficiently large to avoid short-circuits : this optimization is an experimental challenge. Let us indeed emphasize that if the interface between the two fluids ever touches the anod, the consequences may be dramatic, as is easily understandable when a short-circuit occurs at such huge powers. There is even the possibility of destroying the series of cells. The challenge is all the more difficult as the intensity used in the cell becomes larger and larger, which is indeed the case with the endless seek for financial profit. As is often the case for industrial processes, the maximum pay-off that is dreamed of will be obtained by adopting risky strategies, on the borderline of instabilities.
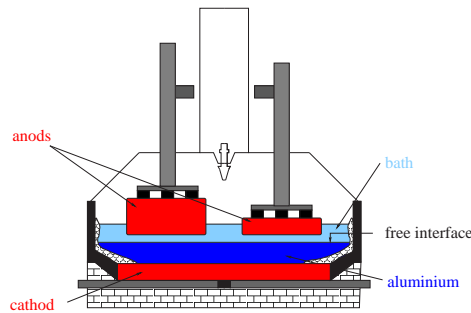

Fig. 9.1 – An aluminium cell : vertical cut.

9.1.2   A need for numerical simulations

The stage is now set. It is understandable that controlling and optimizing such an industrial process is not an easy task. An electrolysis cell is kind of a wicked

environment, where precise experimental observations are difficult to make. Even monitoring the phenomena at play inside the cell is a challenge : high temperature, corrosive medium,.... Controlling and optimizing is one step further. In such a framework, numerical simulation can efficiently complement the experimental strategy, and advantageously compensate for its weaknesses.

We intend to address in further research the optimal control problem, say : how to stabilize the position of the interface ? Which parameter should be used ? is it possible in practice ? In such industrial problems, it should indeed be born in mind that the practical constraints are of enormous impact : some actual control parameters are the height of anods, the intensity, the shape of the conducting wires bringing the current to and from the cell. These parameters cannot be tuned in real time. This is a feature that must be accounted for, one way or another, when posing the optimization problem.

But for the time being, as a preliminary and necessary step before attacking the optimization problem, and also as a step which has its own interest, we have concentrated our efforts on the direct simulation problem. It was expected that the results of careful numerical simulations could give a valuable insight into the understanding of the phenomena inside the cell, and therefore implicitly help to optimize it. It is indeed the case. But before we describe the modeling strategy we have employed, two comments are in order.

First, the fact that experimental observations are difficult, and therefore rather incomplete, to the least, has another consequence than that of giving full value to the strategy of numerical simulation. It also precisely renders this strategy difficult, because of the lack of complete reliable measurements. As only a few measures are available, the question is indeed how to obtain definite conclusions about the validity of the numerical simulations. In order to overcome, as far as possible, this difficulty, we have chosen both (a) to validate our algorithms on academic test problems, and (b) to try and recover in "real" simulations phenomena well known in the engineering world, or recipes well known by engineers of the field. This has proven to be a reasonable strategy in such a context, so far.

Second, it is useful to mention at this point the possible numerical approaches for this problem. Simplifying assumptions have to be done, due to the overwhelming number of physical phenomena involved in the functioning of the cell, namely (i) magnetohydrodynamics (MHD), (ii) moving interface, (iii) ferromagnetism (the material the boundaries are made of is ferromagnetic), (iv) electrochemistry (the concentration of the chemical species is not homogeneous throughout the bath, which has some impact on the global behaviour of the cell), (v) three-phase flows (bubbles of carbon oxydes at the surface of anods (see (9.2)), solidification process at the boundaries), (vi) temperature effects (which influences the value of the physical parameters, in particular). Usually, a continuum, purely fluid, description is chosen. Items (iv), (v) and (vi) are neglected, or postponed to specifically dedicated studies, item (iii) is accounted for in establishing the boundary condition for the magnetic field. Apart from the present work, the existing approaches are essentially based upon the use of mechanical/physical arguments to guess recipes for stability, possibly together with a strategy of numerical simulation based upon a linearization procedure applied to the equations at the vicinity of the equilibrium state, followed by a linear stability analysis. Instances of such works are [31,35,36,117,118,138,140].

9.2 The modeling strategy

Our strategy has been to adopt a genuine nonlinear approach, where no linearization at all is made (at the continuous level). As taught to us by analysis on test situations (even in radically different contexts), a nonlinear stability analysis, as the one needed here to study the stability of the interface between the two fluids, can only come out from direct numerical simulations. This has been our bottom line. Of course, we only have succeeded in our program at the price of doing other simplifying assumptions, none of them related to nonlinearity issues.

Therefore, we start with the very complete system consisting of the Maxwell equations coupled to the multifluid Navier-Stokes equations, and then try to reduce the complexity by carefully imposing simplifying assumptions we have total control upon. The system we start from therefore reads

$$\partial_t \rho + \operatorname{div}(\rho \boldsymbol{u}) = 0, \tag{9.4}$$

$$\begin{cases} \partial_t(\rho \boldsymbol{u}) + \operatorname{div}(\rho \boldsymbol{u} \otimes \boldsymbol{u}) - \operatorname{div}(2\eta \epsilon(\boldsymbol{u})) + \boldsymbol{\nabla} p &= \rho \boldsymbol{f} + \dfrac{1}{\mu} \operatorname{\mathbf{curl}} \boldsymbol{B} \times \boldsymbol{B} \\ \operatorname{div} \boldsymbol{u} &= 0 \end{cases} \tag{9.5}$$

$$\begin{cases} \partial_t \boldsymbol{B} + \operatorname{\mathbf{curl}} \boldsymbol{E} &= 0 \\ \operatorname{div} \boldsymbol{B} &= 0 \\ -\partial_t(\varepsilon \boldsymbol{E}) + \operatorname{\mathbf{curl}} \dfrac{\boldsymbol{B}}{\mu} &= \boldsymbol{j} \end{cases} \tag{9.6}$$

$$\boldsymbol{j} = \sigma(\boldsymbol{E} + \boldsymbol{u} \times \boldsymbol{B}), \tag{9.7}$$

where one recognizes (from (9.4) to (9.7)) the mass conservation equation, the incompressible two-fluids Navier-Stokes equations, the Maxwell equations and Ohm's law. We introduce ρ to denote the density of the fluids (it is a piecewise constant function), $\boldsymbol{u}$ the velocity field, $\boldsymbol{B}$ the magnetic field, $\boldsymbol{E}$ the electric field, $\boldsymbol{j}$ the current, $\boldsymbol{f}$ the body force (gravity), p the pressure field, and $\boldsymbol{\epsilon}(\boldsymbol{u})$ the deformation gradient $(\boldsymbol{\nabla}\boldsymbol{u} + \boldsymbol{\nabla}\boldsymbol{u}^T)/2$. The electrical conductivity σ and the viscosity η are assumed to be known functions of ρ.

It turns out that, as such, system (9.4)-(9.5)-(9.6)-(9.7) cannot be studied mathematically, due to the hyperbolic nature of the Maxwell equations, and is not tractable numerically either. As a matter of fact, this system is likely to be not necessary for the situation at hand. We indeed believe, that a simpler system, both well-posed mathematically and tractable numerically, suffices to correctly reproduce the behaviour of the cell. It is obtained from the full system (9.4)-(9.5)-(9.6)-(9.7) by neglecting the $\partial_t(\varepsilon \boldsymbol{E})$ term (low frequency hypothesis), and, less important, by setting $\mu = \mu_0$. This allows one to eliminate the unknown $\boldsymbol{E}$, and to obtain a system with the only unknowns $\boldsymbol{u}$, p, ρ, $\boldsymbol{B}$.

The governing equations we shall use are thus the time-dependent incompressible Navier-Stokes equations for two viscous immiscible fluids (9.4)-(9.5) coupled with the Maxwell equations in their parabolic form (*see* [81] for example) :

$$\partial_t \boldsymbol{B} + \operatorname{\mathbf{curl}}\left(\dfrac{1}{\mu_0 \sigma} \operatorname{\mathbf{curl}} \boldsymbol{B}\right) = \operatorname{\mathbf{curl}}(\boldsymbol{u} \times \boldsymbol{B}), \tag{9.8}$$

$$\operatorname{div} \boldsymbol{B} = 0. \tag{9.9}$$

These equations are set on a fixed bounded domain Ω of $\mathbb{R}^d$ (with $d = 2$ or 3), and complemented with the magnetic boundary conditions

$$(\boldsymbol{B} \cdot \boldsymbol{n})|_{\partial\Omega} = \text{given}, \qquad (\mathbf{curl}\, \boldsymbol{B} \times \boldsymbol{n})|_{\partial\Omega} = \text{given}, \qquad (9.10)$$

and for the hydrodynamic boundary conditions, pure slip on the side walls and no-slip elsewhere. The initial conditions read : $\rho|_{t=0} = \rho^0$, $\quad \boldsymbol{u}|_{t=0} = \boldsymbol{u}^0 \quad$ and $\quad \boldsymbol{B}|_{t=0} = \boldsymbol{B}^0$, where $\boldsymbol{u}^0$ and $\boldsymbol{B}^0$ are divergence free vector fields. The density of each fluid is assumed to be constant at $t = 0$, a property which is propagated in time by (9.4), the volume of each fluid being then preserved.

Let us emphasize again that no additional simplification will be made on these equations and that we shall therefore deal with all the nonlinearities of this strongly coupled system of PDEs. The mathematical analysis of this system, as well as the foundation of it on the basis of a whole hierarchy of possible models, is an issue that has already been dealt with in a series of previous works : existence of solution to (9.4)-(9.5)-(9.8)-(9.9) in [54], regularity of the flow and of the interface in [37], long-time behaviour of the hydrodynamics two fluid system in [56], regularity of the Navier-Stokes equation in [57].

In particular, it is to be emphasized that the system we shall employ cannot be simplified further naively, for instance by considering that the electromagnetic phenomena are so more rapid than the hydrodynamic ones that they can be considered as stationary (which is indeed a tempting assumption). It would lead (even in the one-fluid case, see the details in [55, 59]) to an ill-posed mathematical system consisting of a coupling between the time dependent Navier Stokes equations and the stationary Maxwell equations, i.e. the static form of (9.8). Consequently, if one wants to use the stationary Maxwell equation, then one needs also to consider the stationary Navier-Stokes equations, i.e. the static version of (9.4)-(9.5). From the theoretical viewpoint, studying mathematically this purely static system requires to answer the open mathematical question : can one prove existence of a solution to the steady-state two-fluids Navier-Stokes equations ? In spite of the fact that the existence of solution is an open question, we shall nevertheless try in our computations to reach the infinite time limit of (9.4)-(9.5)-(9.6)-(9.7) and thus the steady state version of our time dependent equations. It indeed is of primary interest to determine the steady state in practice. Let us emphasize the crucial message : the choice of system (9.4)-(9.5)-(9.8)-(9.9) is supported by a rigorous mathematical analysis (in the limit of course of the capabilities of the current mathematical techniques, see [54]).

From the numerical viewpoint, the simulation of system (9.4)-(9.5)-(9.8)-(9.9) requires to understand the following issues
  – how to conveniently discretize the MHD coupling,
  – what type of finite elements should be used,
  – how to deal with the motion of the interface, and to ensure, when necessary, the motion of the mesh,
  – how to ensure the conservation of the mass of each fluid and the energy stability in the time dependent simulation.
Let us briefly say here that we use an Arbitray Lagrangian Eulerian formulation to move the interface and the mesh, that we take care of having a discrete energy inequality and a conservation of mass using a discretization scheme that ensures a

geometric conservation law. Apart from the above issues, we have also examined (in [61]) the numerical strategy to properly account for the surface tension term when such a term is added to the right-hand side of (9.4), either for physical reasons or as a numerical artefact. For the sake of brevity, we however leave this question aside here.

We concentrate in the remainder of this article on the numerical strategies we used to answer to the above questions, together with a rapid exposition of the results we obtained.

For computational purposes, it proves convenient after a rewriting of the preceeding equations in non-dimensional form (for which we refer to [61]), to eliminate the body force in one fluid, in the spirit of the method described in [60]. This trick greatly improves the robustness of the numerical computations. As far as the non-dimensional numbers are concerned, let us only mention that they are seven of them : the Reynolds numbers $Re_i = \dfrac{\rho_i U L}{\eta_i}$ (of the order of 10^5 in our application), the magnetic Reynolds numbers $Rm_i = \mu_0 \sigma_i L U$ (10^{-1} in one fluid, 10^{-5} in the other one), the coupling parameter $S = \dfrac{B^2}{\mu_0 \rho_1 U^2}$ (of the order of 1), the Froude number $F = \dfrac{U^2}{gL}$, the density ratio $M = \dfrac{\rho_2}{\rho_1}$. The simulations we shall present in Section 9.4 make use of non-dimensional numbers that are one or two orders of magnitude smaller than in reality. In particular, the Reynolds number will be taken 100 times as small as the real one, which can be interpreted as a somewhat vague way to account for turbulence effects. It is a concern of us to perform computations with the physically relevant non-dimensional numbers within a near future.

To begin with, we concentrate, in Subsection 9.3.1, on the difficulties in the numerical simulation of the coupled MHD problem in the case of one single fluid, postponing the specific difficulties due to the presence of two fluids to Subsection 9.3.2. The numerical computations of (9.4)-(9.5)-(9.8)-(9.9) we show in Section 9.4 are obtained by a combination of all the techniques of Section 9.3.

9.3 Numerical strategies

9.3.1 The one-fluid MHD equations

With a view to focusing on the MHD coupling, we come back as announced to the one-fluid case, and therefore consider the system

$$
\begin{cases}
\rho \partial_t \boldsymbol{u} + \rho \boldsymbol{u} \cdot \boldsymbol{\nabla} \boldsymbol{u} - \operatorname{div}(2\eta\epsilon(\boldsymbol{u})) + \boldsymbol{\nabla} p = \rho \boldsymbol{f} + \dfrac{1}{\mu_0} \operatorname{\mathbf{curl}} \boldsymbol{B} \times \boldsymbol{B} \\[2mm]
\operatorname{div} \boldsymbol{u} = 0 \\[2mm]
\partial_t \boldsymbol{B} + \operatorname{\mathbf{curl}}\left(\dfrac{1}{\mu_0 \sigma} \operatorname{\mathbf{curl}} \boldsymbol{B}\right) = \operatorname{\mathbf{curl}}(\boldsymbol{u} \times \boldsymbol{B}) \\[2mm]
\operatorname{div} \boldsymbol{B} = 0
\end{cases}
$$

where ρ is a constant throughout the domain. The system is supplied with *ad hoc* boundary and initial conditions. It is straightforward to show that, due to a cancellation of terms in the right-hand side, the solution satisfies the energy equality

$$\frac{1}{2}\frac{d}{dt}\int_\Omega \left(\rho|\boldsymbol{u}|^2 + \frac{|\boldsymbol{B}|^2}{\mu_0}\right) + \int_\Omega \left(\frac{1}{\sigma}\frac{|\mathbf{curl}\,\boldsymbol{B}|^2}{\mu_0^2} + \eta|\boldsymbol{\nabla}\boldsymbol{u}|^2\right) = \int_\Omega \rho\boldsymbol{f}\cdot\boldsymbol{u} \qquad (9.11)$$

The fact that this estimate of energy is to be reproduced at the discrete level will be a guide for our discretization strategy. For the sake of simplicity, let us detail how we iterate inside the coupling terms in the case of the stationary version of the above equations, written in non-dimensional form :

$$\left\{\begin{array}{rcl} -\dfrac{1}{Re}\triangle\,\boldsymbol{u} + \boldsymbol{u}\cdot\boldsymbol{\nabla}\boldsymbol{u} + \boldsymbol{\nabla}p &=& S\,\mathbf{curl}\,\boldsymbol{B}\times\boldsymbol{B} + \frac{1}{F}\boldsymbol{f} \\[2mm] \dfrac{1}{Rm}\mathbf{curl}\,(\mathbf{curl}\,\boldsymbol{B}) &=& \mathbf{curl}\,(\boldsymbol{u}\times\boldsymbol{B}) \end{array}\right.$$

Basically, one can at first think of a segregated algorithm of the following type

$$-\frac{1}{Re}\triangle\,\boldsymbol{u}^{n+1} + \boldsymbol{u}^n.\boldsymbol{\nabla}\boldsymbol{u}^{n+1} + \boldsymbol{\nabla}p^{n+1} = S\,\mathbf{curl}\,\boldsymbol{B}^n\times\boldsymbol{B}^n + \frac{1}{F}\boldsymbol{f}$$
$$\frac{1}{Rm}\mathbf{curl}\,(\mathbf{curl}\,\boldsymbol{B}^{n+1}) = \mathbf{curl}\,(\boldsymbol{u}^{n+1}\times\boldsymbol{B}^{n+1}) \qquad (9.12)$$

It may be proven that the above algorithm needs a good amount of damping, and is only conditionally stable. On the other hand, a more efficient strategy is to design a fully coupled algorithm in the following way

$$\left\{\begin{array}{rcl} \boldsymbol{u}^n\cdot\boldsymbol{\nabla}\boldsymbol{u}^{n+1} - \dfrac{1}{Re}\triangle\,\boldsymbol{u}^{n+1} + \boldsymbol{\nabla}p^{n+1} + S\,\boldsymbol{B}^n\times\mathbf{curl}\,\boldsymbol{B}^{n+1} &=& \frac{1}{F}\boldsymbol{f} \\[2mm] \dfrac{1}{Rm}\mathbf{curl}\,(\mathbf{curl}\,\boldsymbol{B}^{n+1}) - \mathbf{curl}\,(\boldsymbol{u}^{n+1}\times\boldsymbol{B}^n) &=& 0, \end{array}\right. \qquad (9.13)$$

(Both systems (9.12) and (9.13) are complemented by the divergence free constraints $\mathrm{div}\,\boldsymbol{u}^{n+1} = 0$, $\mathrm{div}\,\boldsymbol{B}^{n+1} = 0$), where it should be noted that the special discretization of the coupling terms allows one to recover an energy estimate of the form (9.11) at the discrete level. In addition, the above algorithm is unconditionally stable (provided that the continuous solution is unique).

When implementing algorithm (9.13) in a finite element type method, a specific feature appears, that we now wish to underline. Even if the magnetic equation (second line of (9.13)) is diffusion dominated, it is actually necessary to use a stabilization technique for it. A stabilization method for the fully coupled MHD equation has thus been developed (see [53]).

Let us also briefly mention that various methods for solving the magnetic equation (second line of (9.13)) have been tested in [51, 58]. We also refer to the latter work for the description of some numerical methods to impose the boundary conditions (9.10).

The consideration of classical benchmarks of the MHD literature such as the Hartmann flow ("magnetic version" of the hydrodynamic Poiseuille flow) has allowed

us to validate the above numerical strategy, see [61]. Incidentally, let us mention that such numerical experiments also indicate that turbulence effects are very specific in a MHD framework which convinced us to deliberately forget them, in the absence of any deep understanding of turbulence for such MHD flows.

In addition, a simple one-fluid model for the real electrolysis cell has been designed and the influence of the shape of the wires and the distribution of the external current upon the behaviour of the hydrodynamic flow inside the cell has been investigated. Again, this has been found to be in good qualitative agreement with well known behaviours.

9.3.2 The two-fluids MHD equations

We now come back to the two-fluid MHD problem. With respect to the previous section, the extension is now to simulate the motion of the free interface between the two fluids. As no topological change of the interface is expected (it is reasonable to assume that it remains the graph of a function), and as a great accuracy is needed in the determination of its position (as the anod-metal distance is the central issue that heavily influences the behaviour of the cell, as explained above), we have chosen to explicitly track the interface and therefore have adapted an Arbitrary Lagrangian Eulerian formulation to the present context of a MHD flow. The ALE formulation for *one* fluid with a free surface has been used by several authors, for example [5, 24, 77, 79, 112, 141, 142]. In the case of two fluids, see for example [128], and in the framework of MHD, see [20].

As for the computation of the domain velocity field $\boldsymbol{w}$, we have chosen a special form for it, namely $\boldsymbol{w}^n = (0, 0, w)$, at each time step t_n, and define it as the solution of

$$\begin{cases} -\triangle w &= 0 & \text{on } \Omega_i^n, i = 1, 2, \\ w &= \dfrac{\boldsymbol{u}^n \cdot \boldsymbol{n}}{n_z} & \text{on } \Sigma^n, \\ \dfrac{\partial w}{\partial n} &= 0 & \text{on } \partial\Omega. \end{cases} \tag{9.14}$$

This special determination allows us to ensure the following Geometric Conservation Law (in the spirit of [70, 103, 119] in the framework of the finite volume method, [48] in the framework of finite element methods, and [101] for fluid structure interaction problems) :

$$\begin{aligned} \int_{\Omega_i^{n+1}} \psi(x)\,dx - \int_{\Omega_i^n} \psi \circ \mathcal{A}_{n,n+1}(y)\,dy &= \delta t \int_{\Omega_i^n} \psi \circ \mathcal{A}_{n,n+1}(y)\mathrm{div}_y \boldsymbol{w}^n\,dy \\ &= \delta t \int_{\Omega_i^{n+1}} \psi(x)\mathrm{div}_x \boldsymbol{w}^n \circ \mathcal{A}_{n,n+1}^{-1}(x)\,dx \end{aligned} \tag{9.15}$$

for any ψ defined on Ω_i^{n+1}, where $\mathcal{A}_{n,n+1}$ is the discretization in time of the function that maps the reference domain onto the current one.

Relation (9.15) is the discrete analogue of the continuous formula

$$\frac{d}{dt} \int_{\Omega(t)} \psi(x, t)\,dx = \int_{\Omega(t)} \frac{\partial \psi}{\partial t}\Big|_{\hat{x}}\,dx + \int_{\Omega(t)} \psi(x, t)\,\mathrm{div}\,\boldsymbol{w}\,dx.$$

This being done, we are in position to ensure two key properties for our global algorithm : first, the conservation of the mass of each fluid, and second, the stability in the energy norm. Both of these properties are easy to fulfill on a fixed mesh, but have seemed to us not so trivial to ensure in the ALE setting. The above GCL is one ingredient to ensure both these properties. More explicitely, when (i) the normal vectors at the nodes of the free interface $\Sigma(t)$ are computed so as to have (see also [42]) $\int_{\Sigma} \boldsymbol{u}_h \cdot \boldsymbol{n}_h \, d\sigma = \int_{\Omega_1} \operatorname{div} \boldsymbol{u}_h \, dx$, (ii) the condition $\int_{\Omega_1} \operatorname{div} \boldsymbol{u}_h \, dx = 0$ holds, and (iii) GCL is satisfied, then we can first prove that the mass of each fluid is conserved at the discrete level. Second, denoting by $E^n = \int_{\Omega^n} \frac{\rho |\boldsymbol{u}^n|^2}{2} \, dy + \int_{\Omega^n} \frac{|\boldsymbol{B}^n|^2}{2\mu_0} \, dy$ the total energy of the system, we may show, again because of the above three properties (i)-(ii)-(iii), that the discrete analogue of (9.11) holds (for convenient simple data), namely (see [61])

$$\frac{E^{n+1} - E^n}{\delta t} + \int_{\Omega^{n+1}} 2\eta |\boldsymbol{\epsilon}(\boldsymbol{u}^{n+1})|^2 \, dx + \int_{\Omega^{n+1}} \frac{1}{\mu_0 \sigma} |\operatorname{\mathbf{curl}} \boldsymbol{B}^{n+1}|^2 \, dx \leq 0.$$

As was the case for the issues examined in the previous subsection, we also have tested the above numerical methodology on classical benchmarks. In addition, we have checked that the properties (i)-(ii)-(iii) are in some sense optimal in order to obtain the conservation of the mass of each fluid. For instance, test cases have shown that when the displacement field for the mesh $\boldsymbol{w}$ is assumed to be the solution of

$$\left\{ \begin{array}{rcll} -\triangle \boldsymbol{w} & = & 0 & \text{on } \Omega_i^n, i = 1, 2, \\ \boldsymbol{w} & = & \boldsymbol{u} & \text{on } \Sigma^n, \\ \dfrac{\partial \boldsymbol{w}}{\partial n} & = & 0 & \text{on } \partial\Omega, \end{array} \right. \tag{9.16}$$

instead of (9.14), so that the GCL property does not hold anymore, then the mesh is distorsed as time evolves, and a modification of the mass is indeed observed, thus condition (iii) is "necessary". Likewise, we have shown through test cases, that condition (ii) is also instrumental : it can be ensured using discontinuous finite elements for the discretization of the pressure (for example with the mixed elements Q2/P1), or using continuous finite elements while imposing with a Lagrange multiplier that the numerical flux $\int_{\Sigma^n} \boldsymbol{u}_h^n \cdot \boldsymbol{n}_h \, d\sigma$ through the interface vanishes (see [47]). Then, the conservation of mass holds. It has been experimentally checked that it does not hold otherwise in the context of continuous finite elements for the pressure.

9.4 Numerical simulations

9.4.1 The steady state of the cell

We have performed computations on realistic cells, however on a simplified geometry (but a real aspect ratio), with a viscosity two orders of magnitude as large as the real one (for both transient and steady-state calculations) and boundary

conditions on the magnetic field divided by 10 (for transient calculations). The boundary conditions on the magnetic fields are taken either from experimental measures or from independent numerical simulations of the magnetic field created by the conductors around the cell. The aim of our simulations is to recover some well known phenomenological parameters (e.g. the number of vortices : *see* [53]) and to have an insight into some parameters that are difficult to measure (e.g. the shape of the interface between the bath and the metal).

In this article, we present in Figure 9.2 the result of a computation on a cell with a simplified (nevertheless relevant) circuit of conductors. The electric current in the cell is 90 kA and the dimensions of the cell are about $3 \times 9 \times 1.5$ m. For Biot and Savart computations (giving the boundary conditions on the magnetic field), we use either linear or parallelepipedic conductors. This interface has been obtained by computing the solution of the time-dependent system after a long time. On Figure 9.3, we show the result of a steady state calculation for a typical cell (the position of the interface is assumed to be known from a previous computation). The four swirls shown are effectively observed in reality and the magnitude of the velocities is rather close to the experimentally measured one.

Despite the fact we have artificially decreased the Reynolds number (for transient and steady-state calculations) and the magnetic field on the boundary (transient calculations), our results turn out to be in good qualitative agreement (shape of the interface, number of swirls) and even quantitative agreement (magnitudes of velocity in the steady-state calculation) with the experimental observations.
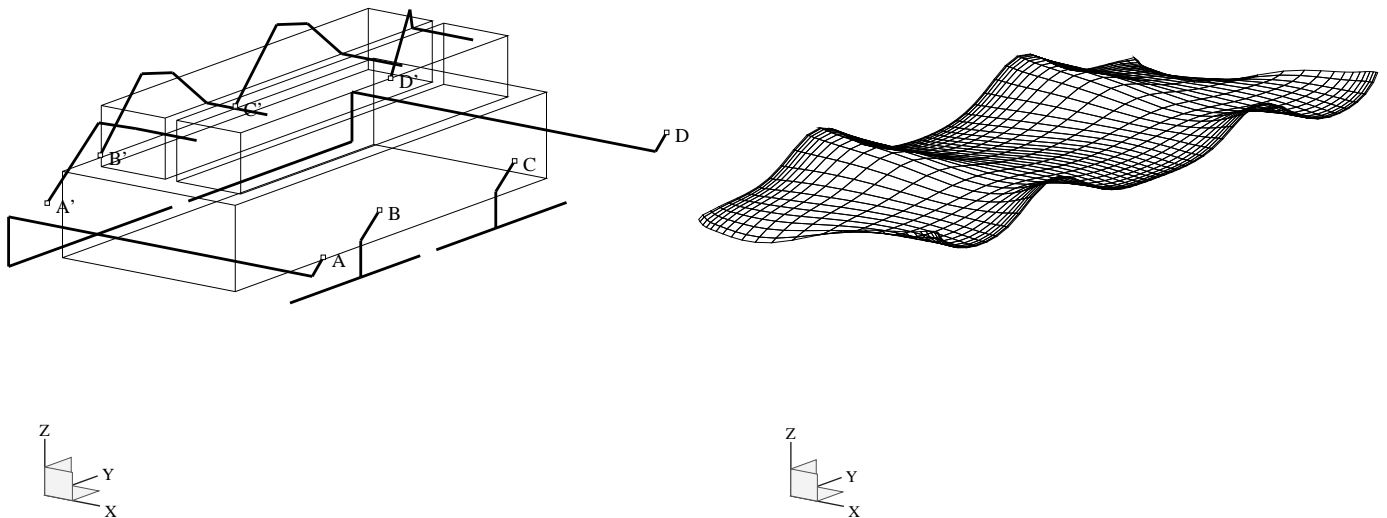
FIG. 9.2 – On the right, the shape of the interface at large time. The circuit of conductors is represented on the left.

9.4.2 The rolling phenomenon

One of the phenomena which is observed in industrial cells and which has been thoroughly investigated with a view to understanding it, forecasting it and avoiding it, is *metal pad rolling*. It is an oscillation of the cryolite / aluminium interface
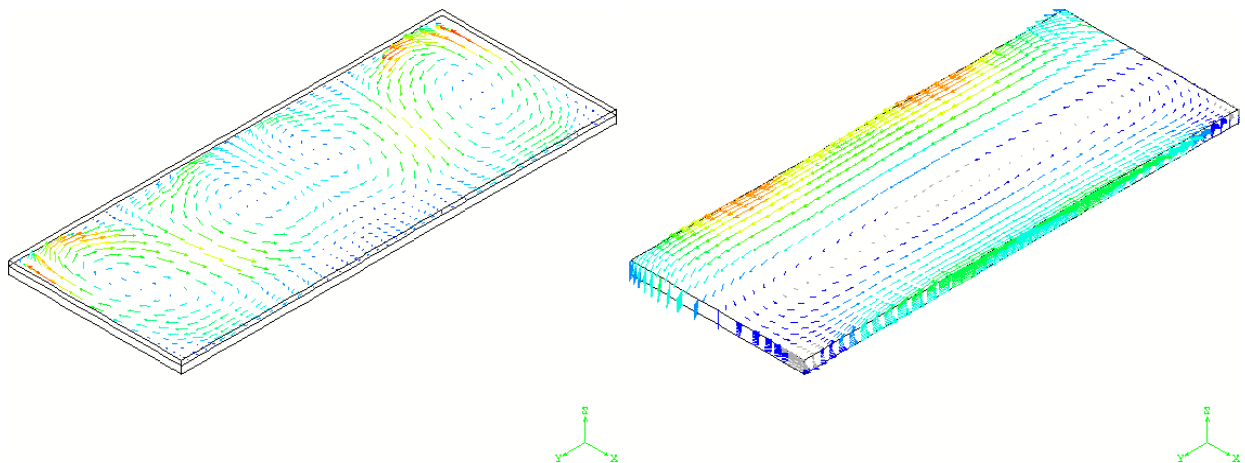
FIG. 9.3 – Left : velocity profile in the cell in a plane situated 5 cm under the interface. Velocity is between 1 cm.s^{-1} and 9 cm.s^{-1}. Right : magnetic field on the boundary of the cell.

with a period ranging from five seconds up to more than one minute (see [95]). The physical origin of the phenomenon is a "constructive" interaction between the vertical component B_z of the magnetic field and a possible horizontal perturbed electric current, which results in a possibly instable rotating motion of the interface. It has been reported on that the metal can even get out of the cell in some cases! Most studies, in the vein of [31, 139], are based upon a linearization procedure that leads to a definite criterion on the stability or unstability of a given cell, depending on its geometry, parameters,... In [31], the authors assert that a cylindrical cell becomes instable whatever the vertical field B_z. With a view to test this strong result of instability, we have developped a numerical simulation (see [61,63]) that has shown that actually the situation is not truly described by the linearized system. For large B_z, our time dependent simulations show an interface that is indeed unstable, in accordance to the conclusions of the linearized study. But, there exists some B_z, small enough and not ridiculously small, for which the same time dependent simulation shows a stable motion of the interface. Of course, one could argue that, for times larger than those reached in our numerical simulations, the motion of the interface indeed becomes unstable, as predicted by the linearization study. But we wish then to make the following point. From a practical viewpoint, the goal is to understand what happens when the nominal functioning of the cell is unfortunately perturbed by an exterior event (say a change of anod in the cell, or in the cell nearby, or ...), which generally happens over a definite time window. Thus the perturbation is turned off after a while. This is exactly the conditions we have imposed for our time dependent simulation. The pertinent issue is then to know whether this "bounded in time" perturbation will durably unstabilize the interface, or if the instability will vanish after a while. Typically, this type of transient external conditions are out of reach of the linearization studies, which are more binary, in some sense, but also more predictive in the infinite time limit. This explains why there is room for both approaches.

Of course, definite conclusions about this comparison between the two approaches

are yet to be obtained, but this test case demonstrates the capability of our nonlinear approach to simulate complex MHD phenomena. In the past, these phenomena were analyzed with models based on many simplifications of the original equations providing excellent qualitative results, most of the time. But the influences of such simplifications need in any case to be tested and may become not negligible when precise results are desired. We have demonstrated that we can reproduce qualitatively the results predicted by simplified models, but that we are also able to give *quantitative* informations on the transient evolution of the system. This capability should have practical implications in the study of the instabilities of industrial cells.

FIG. 9.4 – The phenomenon of metal pad rolling in a circular cell. Visualization of the interface and the lower fluid (the upper fluid is not represented for the sake of clarity). This is a case with B_z large. Reprinted from [61], with permission from Elsevier Science.

Chapitre 10

Le "metal pad rolling"

Ce chapitre reproduit un proceeding paru dans *proceeding of the 2002 TMS Annual Meeting and Exhibition*. On y présente en détail le cas-test du "metal pad rolling".

<div align="center">

Metal pad roll instabilities

</div>

Jean-Frédéric Gerbeau, Tony Lelièvre, Claude Le Bris, Nicolas Ligonesche

We present some numerical results obtained with a code developed in order to better take into account the coupling between the magnetic field and the velocity in magnetohydrodynamic phenomena. We compare our simulations with some results obtained on linearized equations. We show that the nonlinear approach may usefully complement the linear one and even correct its conclusions in some situations.

10.1   Introduction

The magnetohydrodynamic (MHD) phenomena which dominate the motions of fluids (cryolite and aluminium) in Hall-Héroult cells are extremely complicated. Indeed, the hydrodynamic and magnetic equations are deeply coupled, through the Lorentz force ($F = J \times B$) and induced currents ($J = \sigma(E + u \times B)$). This coupling is responsible for instabilities in the cells, which result from interaction between the velocity profile, the magnetic field and the shape of the metal/bath interface.

To avoid these instabilities is one of the most important aims of some current research. Indeed, important displacements of the interface reduce the efficiency of the cell.

One of the phenomena which is observed in industrial cells and which has been investigated a lot over the past few years is the metal pad rolling. It is an oscillation of the bath / metal interface with period ranging from five seconds up to more than one minute. The aim of most of the theoretical and applied studies of MHD cells has been to understand, forecast and avoid this phenomenon. See [95] and the references therein for a survey on the main approaches until 1992.

This phenomenon has been explored through analytical studies on simplified systems or through numerical experiments on linearized systems. The originality of our approach is to solve the initial physical equations in a real 3d geometry, without any simplifying assumptions. In particular, we take into account the background motion, the viscosity, the deformation of the interface, the induced currents, the induced magnetic fields and the surface tension. Using the whole system, we have obtained a result on the instability of circular cells, that we can compare to some previous analytical studies (see [31]).

10.2   The physical phenomenon

One of the explanation of the metal pad rolling is the presence of a vertical field. The famous Sele's criterion is part of this theory (see [139]). T. Sele has been the first one to provide a physical reason of the rotation by the interaction of the vertical magnetic field with horizontal perturbed currents. More recently, Davidson

and Lindsay (see [31]) have derived a more general linearized system. Their analysis leads to quantitative results for the instability of standing and travelling waves in rectangular and circular cells. They also suggest a mechanical analogue which provides a good physical insight into the phenomenon.

The physical phenomenon is explained on Figure 10.1. An initial tilting (or a long-wavelength disturbance) creates a perturbed current flow $j = J - J_0$ (J_0 is the unperturbed -or background- current and J the total current in the cell) which is largely vertical in the cryolite and horizontal in the aluminium. The interaction of this current with the vertical magnetic field results in a horizontal Lorentz force $F = j \times B_z$, in the direction perpendicular to j. It finally induces a rotating motion of the interface.
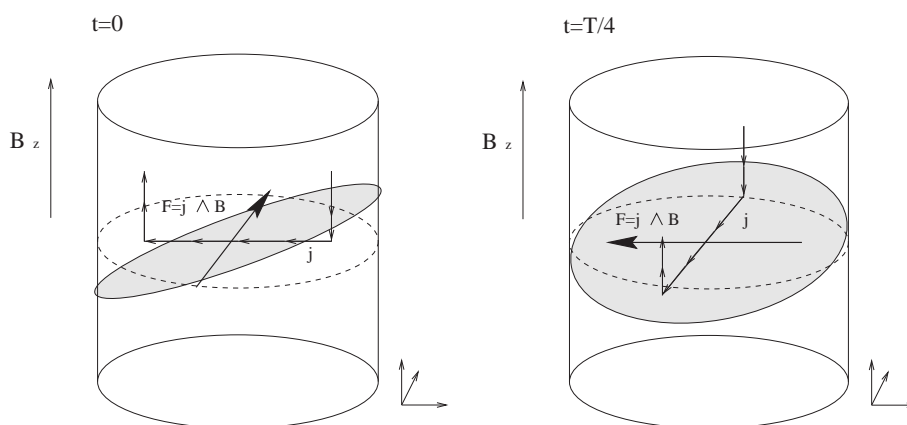
FIG. 10.1 – Schematic representation of the rolling phenomenon.

In some cases, this phenomenon can lead to an instability : when the vertical field is too large, the amplitude of the oscillation may grow with time. It has been reported on that some metal may even escape from the cell in some cases !

10.3   Numerical choices of our code

In this section, we want to briefly present the principal features of the code we have developed to simulate aluminium electrolysis cells, and the metal pad rolling in particular. We refer to [52] and [61] for more details.

251

10.3.1   The equations of MHD

The equations we solve are deduced from three physical equations : the Navier-Stokes equations, the Maxwell equations and the Ohm's law.

$$
\begin{cases}
\zeta \dfrac{\partial u}{\partial t} + \zeta(u.\nabla)u + \nabla p - \operatorname{div}\left(\dfrac{\zeta}{Re}\nabla u\right) &= \dfrac{\zeta}{Fr}g + S\,\mathbf{curl}\,B \times B \\[2mm]
\dfrac{\partial B}{\partial t} + \mathbf{curl}\left(\dfrac{1}{Rm}\mathbf{curl}\,(B)\right) &= \mathbf{curl}\,(u \times B)
\end{cases}
$$

$$
\operatorname{div}(u) = \operatorname{div}(B) = 0
$$

The unknowns are (u, B, p) (5 scalar unknowns in 2d, 7 scalar unknowns in 3d). Our code also gives the possibility to add a surface tension term. For a stationary computation, we just set $\partial_t = 0$ and $g = 0$ in the above equations. In practice, these equations are separately written in the two liquids : cryolite and aluminium. The non-dimensional numbers are :

- the Reynolds number : $Re = \dfrac{\rho U L}{\eta}$
- the magnetic Reynolds number : $Rm = \mu \sigma L U$
- the coupling parameter : $S = \dfrac{B^2}{\mu U^2}$
- the Froude number : $Fr = \dfrac{U^2}{gL}$

The numbers U, L and B are respectively the characteristic velocity, length and magnetic field. The density of the fluid is denoted by ρ, the viscosity is denoted by η, and the conductivity is denoted by σ. The parameter ζ is a non-dimensional density ($\zeta = 1$ in the aluminium and $\zeta = \dfrac{\rho_{\mathrm{cryo}}}{\rho_{\mathrm{alu}}}$ in the cryolite). The values of the parameter ζ, of the Reynolds number Re and of the magnetic Reynolds number Rm depend on the fluid.

The boundary conditions on the velocity u can be :
- tangential velocity : $u.n = 0$
- zero velocity (no-slip boundary condition) : $u = 0$

The boundary conditions on the magnetic flux B can be :
- either tangential[a] :
$$
\begin{cases}
\left(\dfrac{1}{Rm}\mathbf{curl}\,(B) - u \times B\right) \times n = \left(\dfrac{1}{Rm}\mathbf{curl}\,(B_0) - u \times B_0\right) \times n \\
B.n = B_0.n
\end{cases}
$$
- or normal[b] : $\begin{cases} B \times n &= B_0 \times n \\ \operatorname{div}(B) &= 0 \end{cases}$

---

[a]Notice that $\left(\frac{1}{Rm}\mathbf{curl}\,(B) - u \times B\right)$ is the electric field. In practice, we use this type of boundary condition where a no-slip boundary condition holds on u. The first condition is therefore reduced to : $\mathbf{curl}\,(B) \times n = \mathbf{curl}\,(B_0) \times n$.

[b]The condition $\operatorname{div}(B) = 0$ derives in fact from the variational formulation.

The field B_0 is a given magnetic field which can come from some measures or from a previous magnetostatic computation. In practice, we have observed that tangential boundary conditions give better results.

These equations are then discretized using quadrilateral finite elements. The three unknowns are Q1 fields, and we use some stabilisation methods (streamline upwinding) to bypass the inf-sup condition and solve advection problems (see [53]).

The position of the interface is updated at each time step, using an Arbitrary Lagrangian Eulerian (ALE) technique. The mesh at the interface is moved along the velocity at the interface. The rest of the mesh is then moved arbitrarily. We have chosen this method since the interface does not encounter big motions nor topological changes.

10.3.2 Numerical assets and drawbacks of our scheme

In this section, we present the main advantages of our choices of discretization. These choices have also a few drawbacks. All the assertions of this section are detailed in [61].

10.3.2.1 Coupling of magnetic fields and velocity

Our discretization couples the degrees of freedom (u, B, p) : the linear system we directly solve give us the three unknowns. When the problem becomes stiff, this is more robust than segregated schemes which decouple the unknowns.

The main drawback of this choice is that it leads to large systems to be solved. However, these systems are sparse and well conditioned (thanks to the stabilisation method we use). We solve them using iterative methods (GMRES) and the incomplete LU factorisation as preconditioner (ILU). In the time-dependent problem, the initial guess is the result of the last time step and we obtain the desired precision in about ten iterations. The principal limitation is finally the construction of the matrix at each time step, and the upper bound on this time step.

10.3.2.2 Motion of the interface

The ALE scheme we have chosen has a lot of advantages. Apart from good energetic properties (see below), it satisfies the geometric conservation law (GCL). The GCL is a property which ensures the conservation of the mass of each liquid from one time-step to the next.

10.3.2.3 Time discretization and stability

We use an implicit Euler time discretization. The main advantage of this scheme is that it ensures energetic conservation : the only additional energetic term which stems from time discretization (and which cannot be avoided) is a negative term of order δt. This means that, at worst, we lose an energy of size δt in the system. In particular, the energetic compensation between the Laplace force in the momentum

equation and the term of induced currents in the equation on B is preserved in the discretized formulation.

This property of energetic conservation is definitely important in computations dealing with stability results : the instability can therefore not stem from a numerical *artefact*.

10.4 Numerical simulations

We present in this section a result of computation on an unstable system : a circular cell submitted to a uniform vertical field.

10.4.1 Choice of the test case

In [31], it is shown that it is the interaction between the different gravitational modes which causes instable rolling waves. In particular, the authors assert that a circular cell becomes unstable whenever a vertical field B_z is applied.

We have chosen to reproduce this simple experiment of a circular cell. The following assumptions are made in [31] in order to derive this result (actually, these assumptions are made in order to obtain an analytically solvable linear system) :
  – No background motion, which implies a uniform vertical magnetic field.
  – No induced currents.
  – No surface tension.
  – The undisturbed surface is taken to be flat.
  – The fluid is inviscid.
  – Shallow water approximations (which leads to vertical j in the cryolite for instance).
The advantage of a circular cell is also that the magnetic field at the boundary is easily computed (by Biot and Savart law). The idea is to numerically test the influence of some parameters which are neglected in this linear approach. We also want to check if induced currents have a stabilizing effect, as it is often reported on in the literature. The linearized approach may well reproduce qualitatively the metal pad rolling, but some of the assumptions may be questionable as far as quantitative results are concerned.

The test case cell is a circular cell of radius equal to 1 and height equal to 2. The interface aluminium / cryolite is situated at the mean height. In order to create an initial disturbance, we have chosen to slightly tilt the cell, and then put it straight again and apply the current J and the vertical field B_z.

10.4.2 Some results

We have indeed observed the metal pad rolling on this test case. We show an example in Figure 10.2. The physical explanation of the phenomenon can be checked by computing the disturbed currents in the cryolite. In Figure 10.3, we show the

disturbance of the currents created by the tilting of the interface. In order to compute this disturbance, we have subtracted from **curl** (B) the initial current **curl** (B_0), with B_0 calculated with a flat horizontal interface.
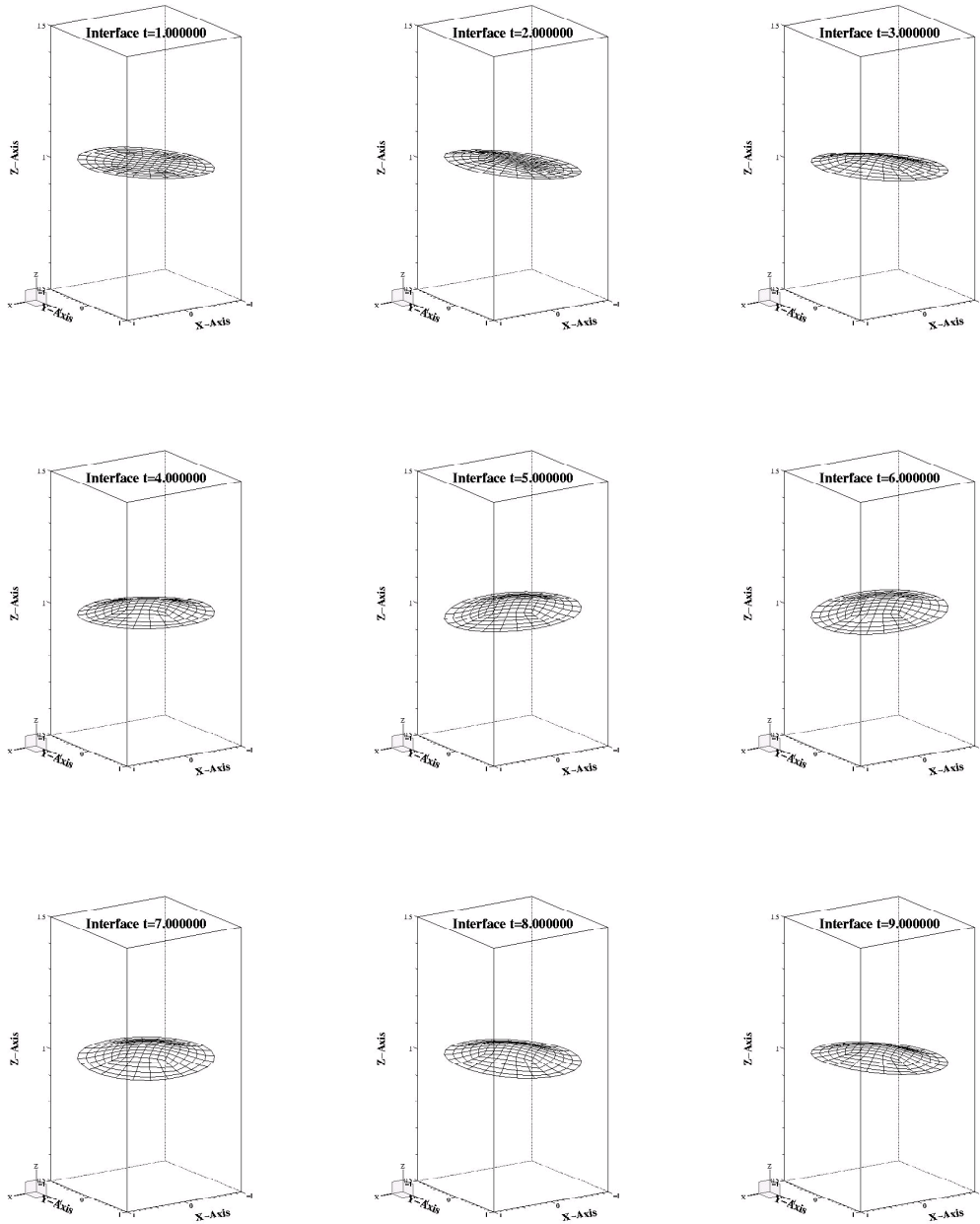

FIG. 10.2 – The phenomenon of metal pad rolling in a circular cell. Visualization of the interface. This is a case with $B_z > 0$ and no instabilities.
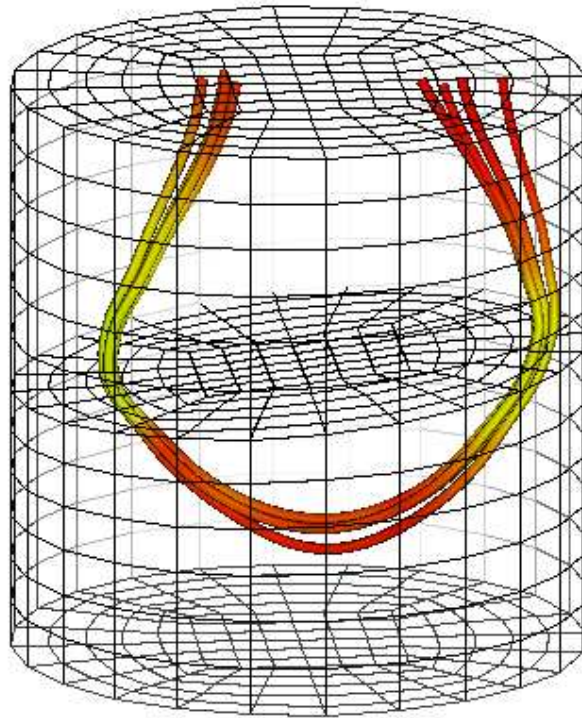
FIG. 10.3 – Loops of currents in cryolite while metal pad rolling. We show here some streamlines of the field j (the pertubed current). The pertubed current goes from the right-hand side (where the elevation is the highest) to the left-hand side.

In our simulation, we have also observed that small disturbances of the initial state do not lead to instability (for example in the case of Figure 10.2). In the same way, a small positive B_z does not induce instability. This is in contradiction with the results of the linear approach which claim the instability of the cell. At least our results show that if instability occurs, it will occur only across a large time frame, and therefore may not be relevant from a practical viewpoint. The result of our computation indeed shows that the amplitude of the rolling does not grow during 5 or 6 periods. Of course, definite conclusions about this comparison between the two approaches are yet to be determined.

10.5   Conclusion

This test case demonstrates the ability of our code to simulate complex MHD phenomena, which are usually numerically reproduced after many simplifications of the original equations. The impact of these simplifications on the result is certainly not negligible. Taking all the real physical parameters and equations into account, we hope to predict more *quantitatively* the instability of industrial cells.

This case shows that it is possible to deal with the original initial physical system and that this approach complements the linear one and helps to understand qualitatively and quantitatively the behavior of electrolysis cells.

Chapitre 11

Simulations MHD avec interface mobile

Les résultats présentés dans ce chapitre ont fait l'objet d'un article paru dans *Journal of Computational Physics*. On démontre et complète ici les résultats théoriques et numériques présentés dans les deux chapitres précédents.

Simulations of MHD flows with moving interfaces

J.-F. Gerbeau, T. Lelièvre and C. Le Bris

We report on the numerical simulation of a two-fluid magnetohydrodyna-mics problem arising in the industrial production of aluminium. The motion of the two non miscible fluids is modeled through the incompressible Navier-Stokes equations coupled with the Maxwell equations. Stabilized finite elements techniques and an Arbitrary Lagrangian Eulerian formulation (for the motion of the interface separating the two fuids) are used in the numerical simulation. With a view to justifying our strategy, details on the numerical analysis of the problem, with a special emphasis on conservation and stability properties and on the surface tension discretization, as well as results on tests cases are provided. Examples of numerical simulations of the industrial case are eventually presented.

Keywords : magnetohydrodynamic ; free interface ; two-fluids flow ; surface tension ; geometric conservation law ; ALE formulation.

11.1 Introduction

The numerical simulation of the electrolysis cell for the industrial production of aluminium is a problem of outstanding difficulty. Let us briefly indicate that a schematic picture of the cell is as follows (*see* e.g. A.F. Lacamera *et al.* [95]) : an electric current of the order of 10^5 A runs through two horizontal layers of conducting incompressible fluids, namely a bath of an aluminium oxyde above, and a layer of liquid aluminium below (*see* Figure 11.1). With a view to reducing the energy cost, the distance between the carbon anode covering the top of the cell and the surface of the aluminium layer (a perfectly conducting fluid directly connected to the cathode at the bottom of the cell) is to be kept as small as possible. However, due to the presence of the electric current, the conducting fluids experience strong Lorentz forces and therefore move. This causes the interface separating the two fluids to also move, which may lead to instabilities. Ensuring a compromise between these two contradictory needs to have a small anode-aluminium distance in order to reduce the cost, and a large enough one in order to prevent short-circuits is the experimental challenge. Additional (substantial) difficulties (that will not be dealt with hereafter) come from the presence of a gas phase (carbon oxydes), from ferromagnetic effects on the boundary of the cell, and from solidification processes taking place on the edges of the cell.

The numerical simulation can efficiently complement the experiments in giving some insight into the working of the cell. There is indeed a large body of literature devoted to such numerical simulations (*see* P.A. Davidson and R.I. Lindsay [31], J. Descloux *et al.* [35,36] R. Moreau *et al.* [117,118], M. Segatz and C. Droste [138], A.D. Sneyd and A. Wang [140]). Of course, in view of the large number of physical phenomena interacting with each other, a direct complete simulation of the cell
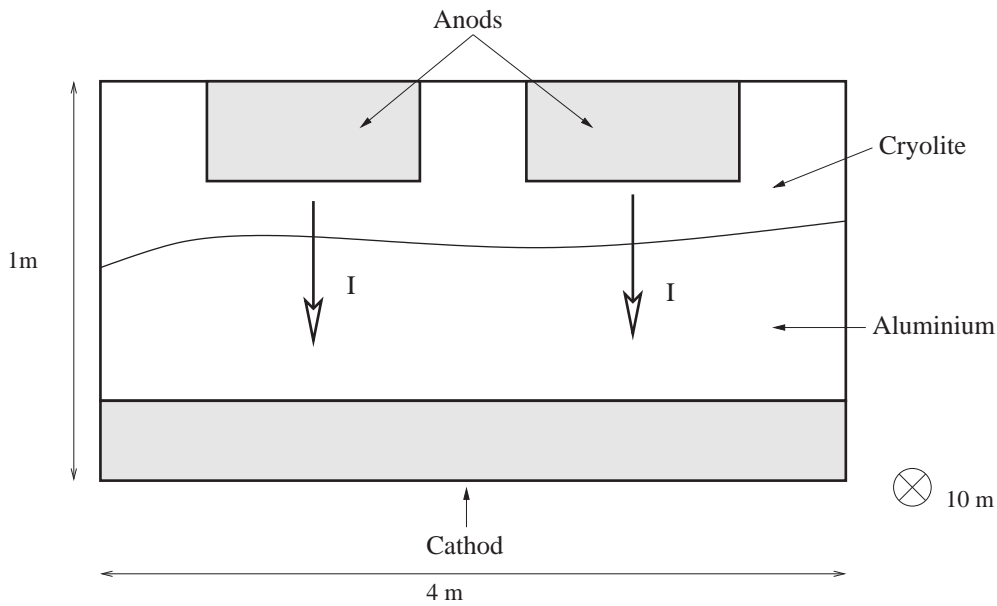
FIG. 11.1 – Schematic represention of an aluminium cell

cannot be achieved. At present, only partial simulations are available. Simplifying assumptions must be made. With a view to drawing a comparison with the numerous strategies based upon the linearization of the governing equations at the vicinity of a stationary solution (*see* e.g. [31]), we have decided to adopt a fully nonlinear strategy where no linearization is made.

The governing equations we shall discretize are the time-dependent incompressible Navier-Stokes equations for two viscous immiscible fluids coupled through Ohm's law with the Maxwell equations in their parabolic form (see equations (11.1)-(11.5) below). Let us emphasize that no additional simplification will be made on these equations and that we shall therefore deal with all the nonlinearities of this strongly coupled system of PDEs. The mathematical analysis of this system, as well as the foundation of it on the basis of a whole hierarchy of possible models, is an issue that has already been dealt with by two of us in a series of previous works (*see* [51, 54–56, 58]). Finally, let us also mention that in the absence of a convenient turbulence model for the MHD flows, we prefer to concentrate our efforts on the (laminar) Navier-Stokes equations.

From the numerical viewpoint, the simulation of such a system requires to understand the following issues
- what type of finite elements should be used,
- how to ensure the conservation of the mass of each fluid and the energy stability in the time dependent simulation,
- how to deal with the motion of the interface, and to ensure, when necessary, the motion of the mesh,
- how to account properly for the surface tension effects when needed.

In the sequel, we shall detail how we have answered to these questions, but let us

briefly say in this introduction that we use an Arbitray Lagrangian Eulerian formulation to move the interface and the mesh, and a discretization scheme such that a geometric conservation law holds. We are aware of the fact that some of these ingredients are now commonly used in the finite element community. Nevertheless, we believe that one of the originalities of the present work lies in the careful combination of those techniques in the framework of MHD in such a way that the crucial properties of conservation of mass and of energy stability is ensured at the discrete level. Moreover, we have checked the validity of our approach on some non-trivial benchmark tests, which are new in the finite element framework, to the best of our knowledge.

The article is organized as follows. Section 2 presents the governing equations in their dimensional and next adimensional form. In Section 3, we give details on the ALE formulation we use. Section 4 is devoted to the presentation of the global numerical algorithm. The conservation and stability properties of the discretization we have chosen are investigated in Section 5. A special attention is paid to the discretization of the surface tension term in Section 6. Finally, Section 7 presents numerical tests on academic as well as industrial situations.

Let us mention that an abridged version of this paper focusing on more practical aspects appears in [63].

11.2   The MHD equations for two fluids

11.2.1   Notations

As announced in the introduction, we consider a system consisting of two viscous incompressible non-miscible fluids in the presence of a magnetic field. The fluids fill in a fixed bounded domain Ω of $\mathbb{R}^d$ (with $d = 2$ or 3). The governing equations are the so-called incompressible MHD equations (*see* W.F. Hughes and F.J. Young [81] for example). We denote by ρ the density of the fluids, $\boldsymbol{u}$ the velocity field, $\boldsymbol{B}$ the magnetic field and p the pressure field. The electrical conductivity σ and the viscosity η are assumed to be known functions of ρ. Then, the following equations are satisfied in Ω :

$$\delta t\rho + \operatorname{div}(\rho\boldsymbol{u}) = 0, \tag{11.1}$$

$$\rho\delta t\boldsymbol{u} + \rho\boldsymbol{u}\cdot\boldsymbol{\nabla}\boldsymbol{u} - \operatorname{div}(2\eta\boldsymbol{\epsilon}(\boldsymbol{u})) + \boldsymbol{\nabla}p = \rho\boldsymbol{f} + \frac{1}{\mu}\operatorname{\mathbf{curl}}\boldsymbol{B}\times\boldsymbol{B}, \tag{11.2}$$

$$\operatorname{div}\boldsymbol{u} = 0, \tag{11.3}$$

$$\delta t\boldsymbol{B} + \operatorname{\mathbf{curl}}(\frac{1}{\mu\sigma}\operatorname{\mathbf{curl}}\boldsymbol{B}) = \operatorname{\mathbf{curl}}(\boldsymbol{u}\times\boldsymbol{B}) \tag{11.4}$$

$$\operatorname{div}\boldsymbol{B} = 0, \tag{11.5}$$

where $\boldsymbol{\epsilon}(\boldsymbol{u}) = (\boldsymbol{\nabla}\boldsymbol{u} + \boldsymbol{\nabla}\boldsymbol{u}^T)/2$. For the sake of simplicity, we assume that

$$(\boldsymbol{B}\cdot\boldsymbol{n})|_{\partial\Omega} = \text{given}, \tag{11.6}$$

$$(\operatorname{\mathbf{curl}}\boldsymbol{B}\times\boldsymbol{n})|_{\partial\Omega} = \text{given}. \tag{11.7}$$

For the sake of simplicity, we assume in the following theoretical analysis zero magnetic boundary conditions. The results can be extended by standard technics to more realistic cases when $\boldsymbol{B} \cdot \boldsymbol{n}|_{\partial\Omega}$, $\mathbf{curl}\,\boldsymbol{B} \times \boldsymbol{n}|_{\partial\Omega}$ are non zero. Of course, in our numerical experiments (see Section 11.7), the magnetic boundary conditions are non zero. As for the hydrodynamic boundary conditions, pure slip will be assumed on the side walls and no-slip elsewhere. We complement this system with the initial conditions :

$$\rho|_{t=0} = \rho^0, \quad \boldsymbol{u}|_{t=0} = \boldsymbol{u}^0 \quad \text{and} \quad \boldsymbol{B}|_{t=0} = \boldsymbol{B}^0, \tag{11.8}$$

where $\boldsymbol{u}^0$ and $\boldsymbol{B}^0$ are divergence free vector fields. The density of each fluid is assumed to be constant at $t = 0$: if x is in the domain occupied by the fluid i then $\rho^0(x) = \rho_i$, where ρ_i is a given constant, for $i = 1, 2$. Note that equation (11.1) implies that

$$\rho(x,t) = \rho_i \text{ for } x \text{ located in the fluid } i \text{ at time } t \quad (i = 1, 2). \tag{11.9}$$

We shall denote the jump of density through the interface by

$$\delta\rho = \rho_2 - \rho_1.$$

The viscosity and the electrical conductivity of each fluid are also assumed to be constant :

$$\eta(\rho_i) = \eta_i \quad \text{and} \quad \sigma(\rho_i) = \sigma_i \quad (i = 1, 2). \tag{11.10}$$

We refer the interested reader to [54] for an existence result of a weak solution to the system (11.1)-(11.5), and to [58] for the description of some numerical methods to impose the boundary conditions (11.6)-(11.7).

11.2.2   Non-dimensional form and body force correction

For computational purposes, it proves convenient to rewrite the preceeding equations in non-dimensional form and to eliminate the body force in one fluid, in the spirit of the method described in [60]. In practice, the body force $\boldsymbol{f}$ will be the gravity. Thus, it is sufficient to restrict oneself to the case when the body force is potential

$$\boldsymbol{f} = \boldsymbol{\nabla}\Phi.$$

Characteristic values of the magnetic field B, of the velocity U and of the length L are introduced. Time and pressure characteristic values are then defined by $T = L/U$, $P = \rho_1 U^2$. The MHD system rewritten in terms of the non-dimensional variables x/L, t/T (still denoted by x and t) and $\tilde{\boldsymbol{u}} = \boldsymbol{u}/U$, $\tilde{\boldsymbol{B}} = \boldsymbol{B}/B$, and $\tilde{p} = p/P$, involves seven non-dimensional numbers :

$$
\begin{aligned}
Re_i &= \frac{\rho_i U L}{\eta_i},\ i = 1, 2, &&\text{(Reynolds numbers)}, \\
Rm_i &= \mu\sigma_i L U,\ i = 1, 2, &&\text{(magnetic Reynolds numbers)}, \\
S &= \frac{B^2}{\mu\rho_1 U^2}, &&\text{(coupling parameter)}, \\
Fr &= \frac{U^2}{gL}, &&\text{(Froude number)}, \\
M &= \frac{\rho_2}{\rho_1}, &&\text{(density ratio)}.
\end{aligned}
$$

The non-dimensional potential of the body force is defined by $\tilde{\Phi} = \Phi/(gL)$ where g is the gravitational field strength. A "corrected pressure" $\tilde{P}$ is introduced :

$$\tilde{P} = \tilde{p} - \frac{M}{Fr}\tilde{\Phi}.$$

This allows to eliminate the body force in fluid 2. Although this trick does not change anything at the continuous level, it greatly improves the robustness of the numerical computations.

In fluid 1 (lower fluid, *i.e.* aluminium), the equations read

$$\delta t\tilde{\boldsymbol{u}} + \tilde{\boldsymbol{u}}.\boldsymbol{\nabla}\tilde{\boldsymbol{u}} + \boldsymbol{\nabla}\tilde{P} - \mathrm{div}\left(\frac{2}{Re_1}\,\boldsymbol{\epsilon}(\tilde{\boldsymbol{u}})\right) \;=\; \frac{1-M}{Fr}\boldsymbol{\nabla}\tilde{\Phi} + S\,\mathbf{curl}\,\tilde{\boldsymbol{B}} \times \tilde{\boldsymbol{B}},$$

$$\delta t\tilde{\boldsymbol{B}} + \mathbf{curl}\left(\frac{1}{Rm_1}\mathbf{curl}\,\tilde{\boldsymbol{B}}\right) \;=\; \mathbf{curl}\,(\tilde{\boldsymbol{u}} \times \tilde{\boldsymbol{B}}),$$

and in fluid 2 (upper fluid, *i.e.* cryolite),

$$M\delta t\tilde{\boldsymbol{u}} + M\tilde{\boldsymbol{u}}.\boldsymbol{\nabla}\tilde{\boldsymbol{u}} + \boldsymbol{\nabla}\tilde{P} - \mathrm{div}\left(\frac{M}{Re_2}\,\boldsymbol{\epsilon}(\tilde{\boldsymbol{u}})\right) \;=\; S\,\mathbf{curl}\,\tilde{\boldsymbol{B}} \times \tilde{\boldsymbol{B}},$$

$$\delta t\tilde{\boldsymbol{B}} + \mathbf{curl}\left(\frac{1}{Rm_2}\mathbf{curl}\,\tilde{\boldsymbol{B}}\right) \;=\; \mathbf{curl}\,(\tilde{\boldsymbol{u}} \times \tilde{\boldsymbol{B}}).$$

11.3   Weak ALE formulation for two-fluid MHD flows
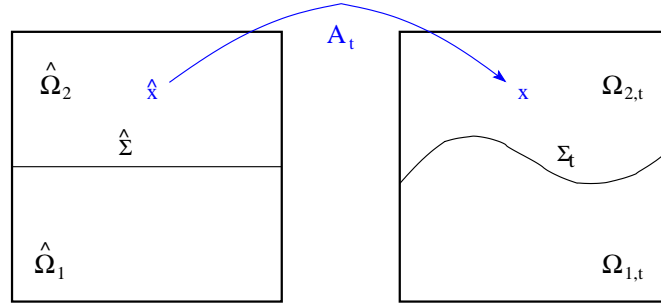

FIG. 11.2 – The partition of the domain Ω.

We tackle the problem of two fluids simulations with the so-called *Arbitrary Lagrangian Eulerian* (ALE) approach. Our computational grid therefore follows the physical interface. Although other methods have been investigated and have proven to be efficient in the past to simulate two-fluid flows, in particular on fixed grids (*see* for example R. Glowinski *et al.* [65]), the choice of the ALE approach is motivated here by two arguments : first, strong topological changes of the interface are not expected in our problem ; second, a high precision on the position of the interface is of major interest in aluminium electrolysis simulations and we believe that such a

precision can be obtained at a lower cost with ALE methods rather than with purely Eulerian ones. The ALE formulation, first introduced by C.W. Hirt, A.A. Amsden and J.L. Cook [76] has been used by several authors. In the case of *one* fluid with a free surface, *see* for example A. Soulaïmani *et al.* [141,142], B. Maury [112], A. Huerta and W.K. Liu [79], R.A. Cairncross *et al.* [5, 24], L.W. Ho [77]. In the case of two fluids, *see* for example H.K. Rasmussen *et al.* [128]. In the context of MHD, the ALE method has been used in 2D simulations of compressible flows in the pioneer works by J.U. Brackbill and W.E. Pracht [20] and J.U. Brackbill [18], using finite difference methods.

We now introduce some notations. For $t > 0$, we denote the physical domain occupied by the fluid i by $\Omega_{i,t}$, for $i = 1, 2$. The domain Ω is the union of $\Omega_{1,t}$ and $\Omega_{2,t}$. The interface between $\Omega_{1,t}$ and $\Omega_{2,t}$ is denoted by Σ_t. The normal to Σ_t oriented from $\Omega_{1,t}$ to $\Omega_{2,t}$ is denoted by $\boldsymbol{n}$ and we set $\boldsymbol{n}_1 = \boldsymbol{n}$ and $\boldsymbol{n}_2 = -\boldsymbol{n}$. We define a reference configuration $\hat{\Omega} = \hat{\Omega}_1 \cup \hat{\Omega}_2$, $\hat{\Omega}_i$ being $\Omega_{i,t=0}$, and we consider a mapping $\hat{\mathcal{A}}_t$ which associates to a point $\hat{x} \in \hat{\Omega}$ a point $x \in \Omega$. Throughout, the mapping $\hat{\mathcal{A}}_t$ will be assumed to be smooth enough in $\hat{x}$, invertible with a smooth inverse, and differentiable with respect to t. For a function $\psi(\cdot, t)$ defined on Ω, we denote by $\hat{\psi}(\cdot, t)$ the function defined on $\hat{\Omega}$ satisfying $\hat{\psi}(\hat{x}, t) = \psi(x, t)$, with $x = \hat{\mathcal{A}}_t(\hat{x})$. By a classical abuse of notation, we will denote $\frac{\partial \psi}{\partial t}|_{\hat{x}}$ the time derivative on the ALE frame :

$$\frac{\partial \psi}{\partial t}\Big|_{\hat{x}}(x, t) = \frac{\partial \hat{\psi}}{\partial t}(\hat{x}, t), \qquad \text{with } \hat{x} = \hat{\mathcal{A}}_t^{-1}(x).$$

The domain velocity is defined by

$$\boldsymbol{w}(x, t) = \hat{\boldsymbol{w}}(\hat{x}, t) = \frac{\partial \hat{\mathcal{A}}_t}{\partial t}(\hat{x}), \text{ with } \hat{x} = \hat{\mathcal{A}}_t^{-1}(x).$$

If $\boldsymbol{\nu}$ is the normal to $\partial\Omega$, the mapping $\hat{\mathcal{A}}_t$ is supposed to be such that

$$\boldsymbol{w} \cdot \boldsymbol{\nu} = 0 \qquad \text{on } \partial\Omega, \tag{11.11}$$

which means that the domain Ω is fixed in $\mathbb{R}^d$ and

$$\boldsymbol{u} \cdot \boldsymbol{n} = \boldsymbol{w} \cdot \boldsymbol{n} \qquad \text{on } \Sigma_t, \tag{11.12}$$

which means that the domains $\Omega_{1,t}$ and $\Omega_{2,t}$ follow the free interface. Thus,

$$\text{for } \hat{x} \in \hat{\Omega}_i, \quad x = \hat{\mathcal{A}}_t(\hat{x}) \in \Omega_{i,t}, \qquad i = 1, 2. \tag{11.13}$$

Although the domains Ω and $\hat{\Omega}$ are in fact the same domain of $\mathbb{R}^d$, we will keep both notations for the sake of clarity.

We now recall some standard formulae which will be useful in the sequel. Otherwise explicitly mentioned, all the differential operators ($\boldsymbol{\nabla}$, div, **curl**, ...) will be taken with respect to the eulerian variable x. We have

$$\frac{\partial \psi}{\partial t}\Big|_{\hat{x}}(x, t) = \frac{\partial \hat{\psi}}{\partial t}(\hat{x}, t) = \frac{\partial \psi}{\partial t}(x, t) + \boldsymbol{w} \cdot \boldsymbol{\nabla}\psi(x, t). \tag{11.14}$$

We denote by $\hat{\mathbf{J}}_t$ the Jacobian matrix of $\hat{\mathcal{A}}_t$,

$$\hat{\mathbf{J}}_t = \left[\frac{\partial \hat{\mathcal{A}}_t}{\partial \hat{x}_j} \right],$$

and by $\hat{J}_t$ its determinant. Then, we have the Euler formula,

$$\frac{\partial \hat{J}_t}{\partial t}(\hat{\mathcal{A}}_t^{-1}(x), t) = \hat{J}_t(\hat{\mathcal{A}}_t^{-1}(x), t) \operatorname{div} \boldsymbol{w}(x, t). \tag{11.15}$$

Using this relation we get in particular,

$$\begin{aligned}
\frac{d}{dt} \int_\Omega \psi(x, t) \, dx &= \frac{d}{dt} \int_{\hat{\Omega}} \hat{\psi}(\hat{x}, t) \, \hat{J}_t \, d\hat{x} \\
&= \int_{\hat{\Omega}} \frac{\partial}{\partial t} (\hat{\psi}(\hat{x}, t) \hat{J}_t) \, d\hat{x} \\
&= \int_{\hat{\Omega}} \left(\frac{\partial \hat{\psi}}{\partial t}(\hat{x}, t) \, \hat{J}_t + \hat{\psi}(\hat{x}, t) \hat{J}_t \operatorname{div} \boldsymbol{w} \right) d\hat{x}
\end{aligned}$$

and thus

$$\frac{d}{dt} \int_\Omega \psi(x, t) \, dx = \int_\Omega \frac{\partial \psi}{\partial t} \Big|_{\hat{x}} \, dx + \int_\Omega \psi(x, t) \operatorname{div} \boldsymbol{w} \, dx \tag{11.16}$$

We now propose a weak formulation of equations (11.1)-(11.5). The following functional spaces will be needed :

$$\mathbb{H}_0^1(\Omega) = \{ \boldsymbol{v} \in (H^1(\Omega))^d, \boldsymbol{v} = 0 \text{ on } \partial\Omega \},$$

$$\mathbb{H}_n^1(\Omega) = \{ \mathbb{C} \in (H^1(\Omega))^d, \mathbb{C} \cdot \boldsymbol{n} = 0 \text{ on } \partial\Omega \},$$

and $L_0^2(\Omega)$, the space of $L^2(\Omega)$ functions whose integral over Ω vanishes. We define

$$V = L^2(0, T; \mathbb{H}_0^1(\Omega)), \quad W = L^2(0, T; \mathbb{H}_n^1(\Omega)), \quad M = L^2(0, T; L_0^2(\Omega))$$

We will denote by $(\cdot, \cdot)$ the $(L^2(\Omega))^d$ scalar product

$$(\boldsymbol{u}, \boldsymbol{v}) = \int_\Omega \boldsymbol{u} \cdot \boldsymbol{v} \, dx,$$

and we introduce the following bilinear and trilinear forms :

$$a_1(\boldsymbol{v}_1, \boldsymbol{v}_2) = \int_\Omega 2\eta \boldsymbol{\epsilon}(\boldsymbol{v}_1) \cdot \boldsymbol{\epsilon}(\boldsymbol{v}_2) \, dx,$$

$$a_2(\mathbb{C}_1, \mathbb{C}_2) = \int_\Omega \left(\frac{1}{\mu\sigma} \mathbf{curl}\, \mathbb{C}_1 \cdot \mathbf{curl}\, \mathbb{C}_2 + \alpha \operatorname{div} \mathbb{C}_1 \operatorname{div} \mathbb{C}_2 \right) dx,$$

α being a given positive constant,

$$b(\boldsymbol{v}, q) = \int_{\Omega} q \operatorname{div} \boldsymbol{v} \, dx,$$

$$c(\boldsymbol{v}_1, \boldsymbol{v}_2, \boldsymbol{v}_3) = \int_{\Omega} \boldsymbol{v}_1 \cdot \boldsymbol{\nabla} \boldsymbol{v}_2 \cdot \boldsymbol{v}_3 \, dx,$$

$$c_{\boldsymbol{w}}(\boldsymbol{v}_1, \boldsymbol{v}_2, \boldsymbol{v}_3) = \int_{\Omega} \rho \, (\boldsymbol{v}_1 - \boldsymbol{w}) \cdot \boldsymbol{\nabla} \boldsymbol{v}_2 \cdot \boldsymbol{v}_3 \, dx,$$

$$d(\boldsymbol{v}_1, \boldsymbol{v}_2, \boldsymbol{v}_3) = \int_{\Omega} \boldsymbol{v}_2 \cdot \boldsymbol{v}_3 \operatorname{div} \boldsymbol{v}_1 \, dx,$$

$$l(\boldsymbol{v}, \mathbb{C}_1, \mathbb{C}_2) = \int_{\Omega} \boldsymbol{v} \times \mathbb{C}_1 \cdot \mathbf{curl} \, \mathbb{C}_2 \, dx.$$

We introduce the test function spaces on the reference domain

$$\hat{V} = \mathbb{H}_0^1(\hat{\Omega}), \qquad \hat{W} = \mathbb{H}_n^1(\hat{\Omega}), \qquad \hat{M} = L_0^2(\hat{\Omega}).$$

On the current domain, the test function spaces are defined by

$$V_0 = \{\boldsymbol{v} : \Omega \times [0, T] \to \mathbb{R}^d, \; \boldsymbol{v}(x, t) = \hat{\boldsymbol{v}}(\hat{\mathcal{A}}_t^{-1}(x)), \hat{\boldsymbol{v}} \in \hat{V}\},$$

$$W_0 = \{\mathbb{C} : \Omega \times [0, T] \to \mathbb{R}^d, \; \mathbb{C}(x, t) = \hat{\mathbb{C}}(\hat{\mathcal{A}}_t^{-1}(x)), \hat{\mathbb{C}} \in \hat{W}\},$$

$$M_0 = \{q : \Omega \times [0, T] \to \mathbb{R}, \; q(x, t) = \hat{q}(\hat{\mathcal{A}}_t^{-1}(x)), \hat{q} \in \hat{M}\}.$$

It is worth noticing that the test functions do not depend on t on the reference frame whereas they do on the current one. More precisely, denoting by $(v_i)_{i=1,..,d}$ the components of $\boldsymbol{v} \in V_0$, we have

$$\left. \frac{\partial v_i}{\partial t} \right|_{\hat{x}} = \frac{\partial v_i}{\partial t} + \boldsymbol{w} \cdot \boldsymbol{\nabla} v_i = 0. \tag{11.17}$$

Of course, similar relations hold for the functions of W_0 and M_0. We now give the formulation that will be used in the numerical simulations.

Weak ALE formulation : Suppose that the domain is moving as described above (in particular relations (11.11) and (11.12) are satisfied). We compute the density ρ simply by

$$\rho(x, t) = \rho^0(\hat{x}) = \rho_i \qquad \text{for } x \in \Omega_{i,t} \tag{11.18}$$

and we look for $(\boldsymbol{u}, \boldsymbol{B}, p)$ in $V \times W \times M$ such that, for all $(\boldsymbol{v}, \mathbb{C}, q)$ in $V_0 \times W_0 \times M_0$:

$$\frac{d}{dt}(\rho\boldsymbol{u}, \boldsymbol{v}) + a_1(\boldsymbol{u}, \boldsymbol{v}) + c_{\boldsymbol{w}}(\boldsymbol{u}, \boldsymbol{u}, \boldsymbol{v}) - d(\boldsymbol{w}, \rho\boldsymbol{u}, \boldsymbol{v})$$

$$+ b(\boldsymbol{v}, p) + \frac{1}{\mu} l(\boldsymbol{v}, \boldsymbol{B}, \boldsymbol{B}) = (\rho\boldsymbol{f}, \boldsymbol{v}), \tag{11.19}$$

$$b(\boldsymbol{u}, q) = 0, \tag{11.20}$$

$$\frac{d}{dt}(\boldsymbol{B}, \mathbb{C}) + a_2(\boldsymbol{B}, \mathbb{C}) - c(\boldsymbol{w}, \boldsymbol{B}, \mathbb{C}) - d(\boldsymbol{w}, \boldsymbol{B}, \mathbb{C}) = l(\boldsymbol{u}, \boldsymbol{B}, \mathbb{C}). \tag{11.21}$$

Proposition 1 *System (11.1)-(11.5) is formally equivalent to the weak ALE formulation (11.18)-(11.21).*

Proof. Let $(\rho, \boldsymbol{u}, \boldsymbol{B}, p)$ be a solution to (11.1)-(11.5). Equation (11.1) clearly yields (11.18). As for the momentum equation (11.19), using formula (11.14), we have from (11.2)

$$\rho \delta t \boldsymbol{u}|_{\hat{x}} + \rho(\boldsymbol{u} - \boldsymbol{w}) \cdot \boldsymbol{\nabla} \boldsymbol{u} = \mathbf{g},$$

with $\mathbf{g} = \rho \boldsymbol{f} - \boldsymbol{\nabla} p + \operatorname{div}(2\eta \boldsymbol{\epsilon}(\boldsymbol{u})) + \frac{1}{\mu} \mathbf{curl}\, \boldsymbol{B} \times \boldsymbol{B}$. We multiply this equation by $\boldsymbol{v} \in V_0$ and we integrate on Ω :

$$\int_\Omega \rho \frac{\partial \boldsymbol{u}}{\partial t}\bigg|_{\hat{x}} \cdot \boldsymbol{v}\, dx + \int_\Omega \rho(\boldsymbol{u} - \boldsymbol{w}) \cdot \boldsymbol{\nabla} \boldsymbol{u} \cdot \boldsymbol{v}\, dx = \int_\Omega \mathbf{g} \cdot \boldsymbol{v}\, dx.$$

Using (11.16), (11.17) and (11.18), we can write the first term as follows

$$\int_\Omega \rho \frac{\partial \boldsymbol{u}}{\partial t}\bigg|_{\hat{x}} \cdot \boldsymbol{v}\, dx = \int_\Omega \frac{\partial}{\partial t}\bigg|_{\hat{x}} (\rho\, \boldsymbol{u} \cdot \boldsymbol{v})\, dx = \frac{d}{dt} \int_\Omega \rho\, \boldsymbol{u} \cdot \boldsymbol{v}\, dx - \int_\Omega \rho \boldsymbol{u} \cdot \boldsymbol{v} \operatorname{div} \boldsymbol{w}\, dx.$$

Thus the momentum equation reads

$$\frac{d}{dt} \int_\Omega \rho \boldsymbol{u} \cdot \boldsymbol{v}\, dx + \int_\Omega \rho(\boldsymbol{u} - \boldsymbol{w}) \cdot \boldsymbol{\nabla} \boldsymbol{u} \cdot \boldsymbol{v}\, dx - \int_\Omega \rho \boldsymbol{u} \cdot \boldsymbol{v} \operatorname{div} \boldsymbol{w}\, dx = \int_\Omega \mathbf{g} \cdot \boldsymbol{v}\, dx.$$

Then, classical integration by parts on the right-hand side of this equation gives (11.19).

Analogous computations give the left-hand side of equation (11.21) and its right-hand side is a straightforward consequence of the formula

$$\int_\Omega \mathbf{curl}\, \boldsymbol{B} \cdot \mathbb{C}\, dx = \int_\Omega \boldsymbol{B} \cdot \mathbf{curl}\, \mathbb{C}\, dx + \int_{\partial\Omega} \boldsymbol{n} \times \boldsymbol{B} \cdot \mathbb{C}\, dx.$$

and the boundary condition (11.7).

Conversely, suppose that $(\rho, \boldsymbol{u}, \boldsymbol{B}, p)$ is a solution to the weak ALE formulation (11.18)-(11.21). With (11.18), it is clear that

$$\frac{\partial \rho}{\partial t}\bigg|_{\hat{x}} = 0. \tag{11.22}$$

Moreover, using (11.12),

$$(\boldsymbol{u} - \boldsymbol{w}) \cdot \boldsymbol{\nabla} \rho = \delta \rho\, \boldsymbol{n} \cdot (\boldsymbol{u} - \boldsymbol{w})|_{\Sigma_t} = 0.$$

Therefore, with (11.14),

$$\delta t \rho + \operatorname{div}(\rho \boldsymbol{u}) = \delta t \rho + \boldsymbol{u} \cdot \boldsymbol{\nabla} \rho = \delta t \rho|_{\hat{x}} + (\boldsymbol{u} - \boldsymbol{w}) \cdot \boldsymbol{\nabla} \rho = 0,$$

which proves (at least formally) that (11.1) holds. The same manipulations as above show that (11.2) and (11.4) hold, and the continuity relation (11.3) is a clear consequence of (11.20).

We now turn to relation (11.5). Let $\hat{\phi} \in H^2(\hat{\Omega})$, with $\frac{\partial \phi}{\partial \boldsymbol{n}} = 0$ on $\partial\Omega$. Taking $\boldsymbol{\nabla}\phi$ as a test function in (11.21), using (11.14) and (11.16) , we obtain

$$\int_\Omega \delta t \boldsymbol{B} \cdot \boldsymbol{\nabla}\phi \, dx + \alpha \int_\Omega \operatorname{div}(\boldsymbol{\nabla}\phi) \operatorname{div}\boldsymbol{B} = 0.$$

Using $\frac{\partial \phi}{\partial \boldsymbol{n}} = 0$ and $\boldsymbol{B} \cdot \boldsymbol{n} = 0$ on $\partial\Omega$, this gives

$$\int_\Omega (\delta t \operatorname{div}\boldsymbol{B} - \alpha\triangle(\operatorname{div}\boldsymbol{B}))\phi \, dx = -\alpha \int_{\partial\Omega} \frac{\partial(\operatorname{div}\boldsymbol{B})}{\partial \boldsymbol{n}}\phi \, d\sigma.$$

Thus

$$\left\{ \begin{array}{rcll} \delta t \operatorname{div}\boldsymbol{B} - \alpha\triangle(\operatorname{div}\boldsymbol{B}) & = & 0 & \text{in } \Omega, \\ \dfrac{\partial(\operatorname{div}\boldsymbol{B})}{\partial \boldsymbol{n}} & = & 0 & \text{on } \partial\Omega, \end{array} \right.$$

Using $\operatorname{div}\boldsymbol{B}^0 = 0$, this implies (11.5). $\diamond$

11.4 Discretization

The goal of this section is to present the space and time discretizations that are used to solve the system (11.19)-(11.21). For this purpose, we introduce a new trilinear form $\tilde{c}_{\boldsymbol{w}}$ which is a slight modification of $c_{\boldsymbol{w}}$:

$$\begin{aligned} \tilde{c}_{\boldsymbol{w}}(\boldsymbol{v}_1, \boldsymbol{v}_2, \boldsymbol{v}_3) &= c_{\boldsymbol{w}}(\boldsymbol{v}_1, \boldsymbol{v}_2, \boldsymbol{v}_3) + \frac{1}{2}\int_\Omega \rho \operatorname{div}\boldsymbol{v}_1 \, \boldsymbol{v}_2 \cdot \boldsymbol{v}_3 \, dx \\ &\quad + \frac{\delta\rho}{2}\int_{\Sigma_t} (\boldsymbol{v}_1 - \boldsymbol{w}) \cdot \boldsymbol{n} \, \boldsymbol{v}_2 \cdot \boldsymbol{v}_3 \, d\sigma \end{aligned} \tag{11.23}$$

Note that at the continuous level, relations (11.3) and (11.12) yield

$$c_{\boldsymbol{w}}(\boldsymbol{u}, \boldsymbol{u}, \boldsymbol{v}) = \tilde{c}_{\boldsymbol{w}}(\boldsymbol{u}, \boldsymbol{u}, \boldsymbol{v}).$$

The first integral in (11.23) is analogous to the well-known Temam's term that allows to recover at the discrete level, when the density is constant, the skew-symmetry property of the advection term. The second integral is less standard. Its introduction will be motivated in Section 11.5.3 (see equation (11.39)). Note that the normal vectors $\boldsymbol{n}$ introduced here are not the approximated node normals defined below (Section 11.5.2, formula (11.29)) but rather the "real" normals defined almost everywhere on the interface, and in particular on the Gauss-Legendre integration points located inside the elements.

11.4.1 Space discretization

We consider a finite element discretization of the current domain Ω. The finite element spaces for the velocity, the magnetic field and the pressure are respectively denoted by

$$V_h \subset (H_0^1(\Omega))^d, \qquad W_h \subset (H_n^1(\Omega))^d, \qquad M_h \subset L_0^2(\Omega).$$

In our numerical tests, V_h and W_h are always based on the same same Lagrangian finite element. We use either stable or stabilized spaces. By "stable spaces", we mean a pair (V_h, M_h) of spaces satisfying the following standard inf-sup condition

$$\inf_{p \in M_h} \sup_{\boldsymbol{v}_h \in V_h} \frac{b(\boldsymbol{v}_h, q)}{\|\boldsymbol{v}_h\|_{\mathbb{H}^1} \|q\|_{L^2}} \geq \beta > 0.$$

We refer the reader to M.D. Gunzburger *et al.* [73] for a complete analysis of the stable spaces for the stationary MHD equations and also to N. Ben Salah *et al.* [7] for an alternative formulation. In the computations with stable elements, we used Q2 elements for the velocity and the magnetic field and, either discontinuous piecewise P1 or continuous piecewise Q1 elements for the pressure. On the other hand, the stabilized finite elements spaces that we use are based on the formulation proposed in [53]. This choice allows us to use equal order finite elements for the three unknown fields (typically Lagrangian Q1 finite elements) and improves the stability at high Reynolds numbers.

11.4.2   Time discretization and linearization

We denote by Ω_i^n the domain occupied by the fluid i at time t_n and by $\boldsymbol{w}_n$ the approximated domain velocity at time t_n. We introduce the application $\mathcal{A}_{n,n+1}$: $\Omega \longrightarrow \Omega$, such that $\mathcal{A}_{n,n+1}$ maps Ω_i^n onto Ω_i^{n+1}, for $i = 1, 2$:

$$x = \mathcal{A}_{n,n+1}(y) = y + \delta t \boldsymbol{w}^n(y), \quad \text{for } y \in \Omega_i^n.$$

Whenever it improves the clarity, y will denote the points in Ω_i^n and x the points in Ω_i^{n+1}. We denote by $\mathbf{J}_{n,n+1}$ the Jacobian matrix of $\mathcal{A}_{n,n+1}$,

$$\mathbf{J}_{n,n+1} = \left[\frac{\partial \mathcal{A}_{n,n+1}}{\partial y_j} \right],$$

and by $J_{n,n+1}$ the absolute value of its determinant.

We use the following semi-implicit Euler scheme :

$$
\begin{cases}
\begin{aligned}
\frac{1}{\delta t}(\rho \boldsymbol{u}^{n+1}, \boldsymbol{v})^{n+1} + a_1^{n+1}(\boldsymbol{u}^{n+1}, \boldsymbol{v}) + \tilde{c}_{\boldsymbol{w}^n}^{n+1}(\boldsymbol{u}^n, \boldsymbol{u}^{n+1}, \boldsymbol{v}) & \\
-d^{n+1}(\boldsymbol{w}^n, \rho \boldsymbol{u}^{n+1}, \boldsymbol{v}) + b^{n+1}(\boldsymbol{v}, p^{n+1}) + \frac{1}{\mu} l^{n+1}(\boldsymbol{v}, \boldsymbol{B}^n, \boldsymbol{B}^{n+1}) &= (\rho \boldsymbol{f}^{n+1}, \boldsymbol{v})^{n+1} \\
&\quad + \frac{1}{\delta t}(\rho \boldsymbol{u}^n, \boldsymbol{v})^n, \\
b^{n+1}(\boldsymbol{u}^{n+1}, q) &= 0, \\
\frac{1}{\delta t}(\boldsymbol{B}^{n+1}, \mathbb{C})^{n+1} + a_2^{n+1}(\boldsymbol{B}^{n+1}, \mathbb{C}) - c^{n+1}(\boldsymbol{w}^n, \boldsymbol{B}^{n+1}, \mathbb{C}) & \\
-d^{n+1}(\boldsymbol{w}^n, \boldsymbol{B}^{n+1}, \mathbb{C}) - l^{n+1}(\boldsymbol{u}^{n+1}, \boldsymbol{B}^n, \mathbb{C}) &= \frac{1}{\delta t}(\boldsymbol{B}^n, \mathbb{C})^n.
\end{aligned}
\end{cases}
\tag{11.24}
$$

The superscripts on the forms $(\cdot, \cdot)$, a_1, a_2, b, c, d and l indicate the configuration on which the space integrals are performed. For example :

$$(\rho \boldsymbol{u}^{n+1}, \boldsymbol{v})^{n+1} = \int_{\Omega^{n+1}} \rho \boldsymbol{u}^{n+1} \cdot \boldsymbol{v} \, dx = \sum_{i=1,2} \rho_i \int_{\Omega_i^{n+1}} \boldsymbol{u}^{n+1} \cdot \boldsymbol{v} \, dx,$$

$$(\rho \boldsymbol{u}^n, \boldsymbol{v})^n = \int_{\Omega^n} \rho \boldsymbol{u}^n \cdot \boldsymbol{v} \, dx = \sum_{i=1,2} \rho_i \int_{\Omega_i^n} \boldsymbol{u}^n \cdot \boldsymbol{v} \, dy,$$

$$a_1^{n+1}(\boldsymbol{u}^{n+1}, \boldsymbol{v}) = \int_{\Omega^{n+1}} 2\eta \, \boldsymbol{\epsilon}(\boldsymbol{u}^{n+1}) \cdot \boldsymbol{\epsilon}(\boldsymbol{v}) \, dx = \sum_{i=1,2} 2\eta_i \int_{\Omega_i^{n+1}} \boldsymbol{\epsilon}(\boldsymbol{u}^{n+1}) \cdot \boldsymbol{\epsilon}(\boldsymbol{v}) \, dx,$$

$$\tilde{c}_{\boldsymbol{w}^n}^{n+1}(\boldsymbol{u}^n, \boldsymbol{u}^{n+1}, \boldsymbol{v}) = \sum_{i=1,2} \rho_i \int_{\Omega_i^{n+1}} \left[(\boldsymbol{u}^n - \boldsymbol{w}^n) \cdot \boldsymbol{\nabla} \boldsymbol{u}^{n+1} \cdot \boldsymbol{v} + \frac{1}{2} \operatorname{div} \boldsymbol{u}^n \boldsymbol{u}^{n+1} \cdot \boldsymbol{v} \right] dx$$

$$+ \frac{\delta \rho}{2} \int_{\Sigma^{n+1}} (\boldsymbol{u}^n - \boldsymbol{w}^n) \cdot \boldsymbol{n} \, \boldsymbol{u}^{n+1} \cdot \boldsymbol{v} \, d\sigma.$$

$$(11.25)$$

Note that in the latter formula, $\boldsymbol{u}^n$ is a shortcut for $\boldsymbol{u}^n \circ \mathcal{A}_{n,n+1}^{-1}(x)$. The other definitions for l, b, d, a_2 can be deduced straightforwardly.

We emphasize that the system to be solved at each time step is now linear but that the hydrodynamic and magnetic equations are still coupled through the terms $l^{n+1}(\boldsymbol{v}, \boldsymbol{B}^n, \boldsymbol{B}^{n+1})$ and $l^{n+1}(\boldsymbol{u}^{n+1}, \boldsymbol{B}^n, \mathbb{C})$. As will be shown in Section 11.5.3, this choice is one of the ingredients of the stability property of the scheme.

11.4.3 Global algorithm

In order to describe the global algorithm, we still have to define precisely the mesh motion. The basic requirements are to satisfy the kinematic conditions (11.11) and (11.12). Next, we have to choose how to move the points inside the domain. Many solutions have been proposed in the literature. For example, we refer to R.A. Cairncross *et al.* [24] for a presentation of a method adapted to the cases when the mesh experiences large strains. In the practical problem we are interested in, it seems sufficient to adopt the very standard method that consists in solving a simple Poisson problem to compute the velocity of the mesh (*see* e.g. A. Soulaimani and Y. Saad [142]). Moreover, we choose to constrain the displacement to be purely vertical. This choice, which is definitely reasonable in the physical situation that we consider, has important consequences on the quality of the algorithm. This point will be made precise in the next section.

We may now write the global algorithm. Let us be given Ω^n and $(\boldsymbol{u}^n, \boldsymbol{B}^n, p^n)$, Ω^{n+1} and $(\boldsymbol{u}^{n+1}, \boldsymbol{B}^{n+1}, p^{n+1})$ are computed as follows :

(i) Compute the terms on Ω_n (namely $\frac{1}{\delta t} \int_{\Omega^n} \rho^n \boldsymbol{u}^n \cdot \boldsymbol{v} \, dx$ and $\frac{1}{\delta t} \int_{\Omega^n} \boldsymbol{B}^n \cdot \mathbb{C} \, dx)$).

(ii) Compute $\boldsymbol{w}^n = (0, 0, w)$ with w such that

$$\begin{cases} -\triangle w = 0, & \text{on } \Omega_i^n, i = 1, 2 \\ w = \boldsymbol{u}^n \cdot \boldsymbol{n}/n_z, & \text{on } \Sigma^n, \\ \dfrac{\partial w}{\partial n} = 0 & \text{on } \partial \Omega, \end{cases} \quad (11.26)$$

(iii) Move the mesh : $\Omega^{n+1} = \Omega^n + \delta t \, \boldsymbol{w}^n$. The matrix corresponding to system (11.24) is computed on this new domain.

(iv) Solve (11.24) to determine $(\boldsymbol{u}^{n+1}, \boldsymbol{B}^{n+1}, p^{n+1})$. The resolution is performed by a GMRES iterative procedure with an ILU preconditioner and $(\boldsymbol{u}^n, \boldsymbol{B}^n, p^n)$ as the initial guess.

11.5   Conservation and stability properties

In this section, two important properties of the above algorithm are proved : the mass conservation, and the energy stability.

11.5.1   Geometric conservation law

Lemma 1 *Suppose that the domain velocity $\boldsymbol{w}^n$ has the form $(0,0,w)$. Let ψ be a function defined on Ω_i^{n+1}, for $i = 1$ or 2. Then*

$$\int_{\Omega_i^{n+1}} \psi(x)\,dx - \int_{\Omega_i^n} \psi \circ \mathcal{A}_{n,n+1}(y)\,dy \;=\; \delta t \int_{\Omega_i^n} \psi \circ \mathcal{A}_{n,n+1}(y)\,div_y \boldsymbol{w}^n\,dy \qquad (11.27)$$

$$= \;\delta t \int_{\Omega_i^{n+1}} \psi(x)\,div_x \boldsymbol{w}^n \circ \mathcal{A}_{n,n+1}^{-1}(x)\,dx \qquad (11.28)$$

Proof. The change of variable defined by $x = \mathcal{A}_{n,n+1}(y)$ gives in the first integral :

$$\int_{\Omega_i^{n+1}} \psi(x)\,dx = \int_{\Omega_i^n} \psi \circ \mathcal{A}_{n,n+1}(y) J_{n,n+1}\,dy.$$

With the assumption on the mesh velocity, the Jacobian matrix has the following form

$$\mathbf{J}_{n,n+1} = \begin{bmatrix} 1 & 0 & 0 \\ 0 & 1 & 0 \\ \delta t \frac{\partial w}{\partial y_1} & \delta t \frac{\partial w}{\partial y_2} & 1 + \delta t \frac{\partial w}{\partial y_3} \end{bmatrix},$$

and therefore

$$J_{n,n+1} = 1 + \delta t\,\mathrm{div}_y \boldsymbol{w}^n,$$

which concludes the proof of the first relation (11.27).

For relation (11.28), we perform in the second integral of the left-hand side the change of variable defined by $y = \mathcal{A}_{n,n+1}^{-1}(x)$. Noticing that $y = x - \delta t \boldsymbol{w}^n \circ \mathcal{A}_{n,n+1}^{-1}(x)$, analogous computations as with the proof of (11.27) give :

$$\int_{\Omega_i^n} \psi(\mathcal{A}_{n,n+1}(y))\,dy = \int_{\Omega_i^{n+1}} \psi(x)(1 - \delta t\,\mathrm{div}_x \boldsymbol{w}^n \circ \mathcal{A}_{n,n+1}^{-1}(x))\,dx,$$

which is (11.28). $\diamond$

Relations (11.27) and (11.28) can be viewed as discrete counterparts of relation (11.16). There are related to the so-called *geometric conservation law* (hereafter abbreviated as GCL).

The notion of GCL has been much investigated in the framework of the finite volume method, *see* in particular H. Guillard and C. Farhat [70], M. Lesoinne and

C. Farhat [103], B. Nkonga and H. Guillard [119]. H. Guillard and C. Farhat prove in [70] that the GCL is a sufficient condition for a numerical scheme to be first-order time-accurate on a moving grid, independently of the grid motion. More generally, these authors claim that a higher accuracy is obtained with schemes satisfying the GCL compared to the schemes that violate it and that the schemes satisfying the GCL generally allow for a larger time step. In the framework of finite element methods, F. Nobile and L. Formaggia prove in [48] that the GCL is a sufficient condition to ensure the unconditional stability of a backward Euler scheme applied to an advection diffusion equation on a moving domain. Let us also cite the work by P. Le Tallec and J. Mouro [101] where implications of the GCL in the framework of fluid structure interaction problems are discussed.

In the sequel, we will show that (11.27) and (11.28) are key properties to ensure discrete mass conservation and global energy inequality.

11.5.2   Discrete mass conservation

We now present the ingredients that allows us to obtain an exact mass conservation of each fluid after time and space discretization.

The first ingredient is the computation of the normals. It is convenient, in view of enforcing Dirichlet boundary conditions in (11.26), to compute approximated discrete normals at the *nodes* of the interface. But these approximation must be done carefully. More precisely, let i be a node on the interface Σ^n and let φ_i be the basis function associated to this node. Following M.S. Engelman, R.L. Sani and P.M. Gresho [42], we define $\boldsymbol{n}_{1,i}$ by

$$\boldsymbol{n}_{1,i} = \frac{1}{\int_{\Sigma^n} \varphi_i \, d\sigma} \int_{\Omega_1^n} \boldsymbol{\nabla} \varphi_i \, dx \tag{11.29}$$

Note that, if we define $\boldsymbol{n}_{2,i}$ by substituting Ω_1^n by Ω_2^n in (11.29), it is straightforward to check that $\boldsymbol{n}_{1,i} = -\boldsymbol{n}_{2,i}$. We then define $\boldsymbol{n}_i = \boldsymbol{n}_{1,i}$ the approximated normal, on node i, oriented from Ω_1^n to Ω_2^n. The component of $\boldsymbol{n}_i$ are denoted by $(n_i^{(1)}, n_i^{(2)}, n_i^{(3)})$. Let $\boldsymbol{v}_h$ be an element of V_h whose components are $(v^{(1)}, v^{(2)}, v^{(3)})$. By convention, we denote

$$\boldsymbol{v}_h \cdot \boldsymbol{n}_h = \sum_i (v_i^{(1)} n_i^{(1)} + v_i^{(2)} n_i^{(2)} + v_i^{(3)} n_i^{(3)}) \varphi_i.$$

Then, formula (11.29) yields the following key property : let $\boldsymbol{v}_h^1$ (resp. $\boldsymbol{v}_h^2$) be a function of V_h whose support is included in Ω_1^n (resp. Ω_2^n), then

$$\int_{\Omega_1^n} \operatorname{div} \boldsymbol{v}_h^1 \, dx = \int_{\Sigma^n} \boldsymbol{v}_h^1 \cdot \boldsymbol{n}_h \, d\sigma, \quad \text{and} \quad \int_{\Omega_2^n} \operatorname{div} \boldsymbol{v}_h^2 \, dx = -\int_{\Sigma^n} \boldsymbol{v}_h^2 \cdot \boldsymbol{n}_h \, d\sigma. \tag{11.30}$$

The second ingredient to ensure mass conservation is to satisfy the following property :

$$\int_{\Omega_i^n} \operatorname{div} \boldsymbol{u}_h^n \, dx = 0, \qquad \text{for } i = 1, 2. \tag{11.31}$$

This can be achieved either by using a space of *discontinuous* finite elements for the discretization of the pressure (for example with the mixed elements Q2/P1), or by imposing with a Lagrange multiplier that the numerical flux through the interface vanishes :

$$\int_{\Sigma^n} \boldsymbol{u}_h^n \cdot \boldsymbol{n}_h \, d\sigma = 0. \tag{11.32}$$

For more details on this latter strategy, we refer the interested reader to L. Formaggia *et al.* [47]. We have tested the two approaches, and they both give the expected results. Another interesting possibility that we have however not investigated is to use continuous finite element for the pressure on each fluid, but discontinuous on the interface.

On a fixed domain, the two relations (11.30) and (11.31) would be sufficient to ensure the mass conservation. But the GCL property of Lemma 1 will be needed to extend it to the case of moving domains.

Proposition 2 *If the discrete normals to the interface and the discrete velocity are computed in such a way that formula (11.30) and (11.31) are true, and if the motion of the mesh is such that (11.27) is satisfied, then the mass of each fluid is preserved :*

$$\rho_i |\Omega_i^n| = \rho_i |\Omega_i^{n+1}|, \ \textit{for } i = 1, 2,$$

where $|\Omega_i^n|$ *denotes the measure of* Ω_i^n.

Proof. Relation (11.27) gives with $\psi = \rho_i$

$$\rho_i |\Omega_i^{n+1}| - \rho_i |\Omega_i^n| = \delta t \rho_i \int_{\Omega_i^n} \mathrm{div}_y \boldsymbol{w}_h^n \, dy.$$

Thus, using successively (11.30), (11.12) and (11.31), we have

$$
\begin{aligned}
\rho_i |\Omega_i^{n+1}| - \rho_i |\Omega_i^n| &= \delta t \rho_i \int_{\Sigma^n} \boldsymbol{w}_h^n \cdot \boldsymbol{n}_i \, d\sigma \\
&= \delta t \rho_i \int_{\Sigma^n} \boldsymbol{u}_h^n \cdot \boldsymbol{n}_i \, d\sigma \\
&= \delta t \rho_i \int_{\Omega_i^n} \mathrm{div}_y \boldsymbol{u}_h^n \, dy = 0.
\end{aligned}
\tag{11.33}
$$

$$\diamondsuit$$

11.5.3 Discrete energy inequality

It is assumed throughout this section that stable finite element spaces are used.

Proposition 3 *We denote by*

$$E^n = \int_{\Omega^n} \frac{\rho |\boldsymbol{u}^n|^2}{2} \, dy + \int_{\Omega^n} \frac{|\boldsymbol{B}^n|^2}{2\mu} \, dy \tag{11.34}$$

the total energy of the system at time t^n. If the body force $\boldsymbol{f}$ vanishes, the solution computed by the algorithm of Section 11.4.3 satisfies the energy inequality

$$\frac{E^{n+1} - E^n}{\delta t} + \int_{\Omega^{n+1}} 2\eta |\boldsymbol{\epsilon}(\boldsymbol{u}^{n+1})|^2 \, dx + \int_{\Omega^{n+1}} \frac{1}{\mu\sigma} |\mathbf{curl}\, \boldsymbol{B}^{n+1}|^2 \, dx \leq 0.$$

Proof. We take $\boldsymbol{v} = \boldsymbol{u}^{n+1}$ in the hydrodynamic equation and $C = \frac{1}{\mu}\boldsymbol{B}^{n+1}$ in the magnetic equation.

The first argument of the proof is once again based on the GCL. Elementary manipulations give

$$\frac{1}{\delta t} \int_{\Omega^{n+1}} \rho |\boldsymbol{u}^{n+1}|^2 \, dx - \frac{1}{\delta t} \int_{\Omega^n} \rho \boldsymbol{u}^n \cdot \boldsymbol{u}^{n+1} \, dy = \frac{1}{\delta t} \int_{\Omega^{n+1}} \rho |\boldsymbol{u}^{n+1}|^2 \, dx$$
$$- \frac{1}{2\delta t} \int_{\Omega^n} \rho |\boldsymbol{u}^{n+1}|^2 \, dy - \frac{1}{2\delta t} \int_{\Omega^n} \rho |\boldsymbol{u}^n|^2 \, dy + \frac{1}{2\delta t} \int_{\Omega^n} \rho |\boldsymbol{u}^{n+1} - \boldsymbol{u}^n|^2 \, dy. \tag{11.35}$$

Then, using Lemma 1, we obtain

$$\frac{1}{\delta t} \int_{\Omega^{n+1}} \rho |\boldsymbol{u}^{n+1}|^2 \, dx - \frac{1}{\delta t} \int_{\Omega^n} \rho |\boldsymbol{u}^{n+1}|^2 \, dy = \int_{\Omega^{n+1}} \rho |\boldsymbol{u}^{n+1}|^2 \mathrm{div}\, \boldsymbol{w}^n \, dx,$$

and therefore

$$\frac{1}{\delta t} \int_{\Omega^{n+1}} \rho |\boldsymbol{u}^{n+1}|^2 \, dx - \frac{1}{\delta t} \int_{\Omega^n} \rho \boldsymbol{u}^{n+1} \cdot \boldsymbol{u}^n \, dy =$$
$$\frac{1}{2\delta t} \int_{\Omega^{n+1}} \rho |\boldsymbol{u}^{n+1}|^2 \, dx - \frac{1}{2\delta t} \int_{\Omega^n} \rho |\boldsymbol{u}^n|^2 \, dy \tag{11.36}$$
$$+ \frac{1}{2\delta t} \int_{\Omega^n} \rho |\boldsymbol{u}^{n+1} - \boldsymbol{u}^n|^2 \, dy + \frac{1}{2} \int_{\Omega^{n+1}} \rho |\boldsymbol{u}^{n+1}|^2 \mathrm{div}\, \boldsymbol{w}^n \, dx.$$

Following the same idea, a similar relation can be straightforwardly obtained for the magnetic field.

The second argument is to use the "correction" that we have performed on the advection term. Definition (11.23) gives

$$\tilde{c}_{\boldsymbol{w}^n}^{n+1}(\boldsymbol{u}^n, \boldsymbol{u}^{n+1}, \boldsymbol{u}^{n+1}) = \int_{\Omega^{n+1}} \rho(\boldsymbol{u}^n - \boldsymbol{w}^n) \cdot \boldsymbol{\nabla} \left(\frac{|\boldsymbol{u}^{n+1}|^2}{2} \right) \, dx$$
$$+ \frac{1}{2} \int_{\Omega^{n+1}} \rho |\boldsymbol{u}^{n+1}|^2 \mathrm{div}\, \boldsymbol{u}^n \, dx + \frac{\delta\rho}{2} \int_{\Sigma^{n+1}} (\boldsymbol{u}^n - \boldsymbol{w}^n) \cdot \boldsymbol{n} |\boldsymbol{u}^{n+1}|^2 \, d\sigma \tag{11.37}$$

The first integral reads

$$\int_{\Omega^{n+1}} \rho(\boldsymbol{u}^n - \boldsymbol{w}^n) \cdot \boldsymbol{\nabla} \left(\frac{|\boldsymbol{u}^{n+1}|^2}{2} \right) \, dx = -\frac{1}{2} \int_{\Omega^{n+1}} |\boldsymbol{u}^{n+1}|^2 \mathrm{div}\, (\rho(\boldsymbol{u}^n - \boldsymbol{w}^n)) \, dx$$
$$= -\frac{1}{2} \int_{\Omega^{n+1}} \rho |\boldsymbol{u}^{n+1}|^2 \mathrm{div}\, (\boldsymbol{u}^n - \boldsymbol{w}^n) \, dx - \frac{\delta\rho}{2} \int_{\Sigma^{n+1}} (\boldsymbol{u}^n - \boldsymbol{w}^n) \cdot \boldsymbol{n} |\boldsymbol{u}^{n+1}|^2 \, d\sigma. \tag{11.38}$$

Thus,

$$\tilde{c}_{\boldsymbol{w}^n}^{n+1}(\boldsymbol{u}^n, \boldsymbol{u}^{n+1}, \boldsymbol{u}^{n+1}) = \frac{1}{2} \int_{\Omega^{n+1}} \rho |\boldsymbol{u}^{n+1}|^2 \mathrm{div}\, \boldsymbol{w}^n \, dx. \qquad (11.39)$$

This term added to the last one of (11.36) exactly compensates for the quantity $-d^{n+1}(\boldsymbol{w}^n, \rho \boldsymbol{u}^{n+1}, \boldsymbol{u}^{n+1})$.

Finally, the third argument of the proof consists in noticing that the term coming from the Lorentz force $\frac{1}{\mu} l^{n+1}(\boldsymbol{u}^{n+1}, \boldsymbol{B}^n, \boldsymbol{B}^{n+1})$ exactly balances the coupling term in the magnetic equation. This fact comes from the way we linearize the equation in the Euler scheme (11.24).

Then, after some standard integrations by parts, we readily obtain (11.34). $\diamondsuit$

11.6   Surface tension

Surface tension is a force appearing at the interface between the aluminium and the cryolite. This force tends to minimize the area of the interface. It is generally admitted that surface tension does not play a major role in aluminium electrolysis. Nevertheless, it might be not completely negligible, especially when physical instabilities appear. Moreover, it may also have a smoothing effect on the numerical instabilities of the interface. Therefore, it is useful to allow our computation to take it into account.

There is a large body of literature reporting on numerical results accounting for surface tension effects. However, to the best of our knowledge, not so much literature has been devoted to the detailed explanation of the numerical treatment of surface tension terms. In order to compensate for this lack and also for the sake of consistency, we now give the lines of our strategy, emphasizing that we do not claim any originality. The reader familiar with this kind of problem may easily skip this part.

The classical Laplace formulation of the surface tension correlates the normal force with the main curvature of the surface (*see* L. Landau and E. Lifschitz [96] for example) :

$$\mathrm{TS} = \gamma H \mathbf{n} \qquad (11.40)$$

The parameter γ is the surface tension coefficient (in N/m) and H is the mean curvature positively counted with respect to the normal $\mathbf{n}$. The surface tension coefficient at the interface aluminium / cryolite is 0.5 N/m (in comparison of 0.07 N/m for water / air interface). In the non-dimensional formulation of Section 11.2.2, the following quantity must be added to the right-hand side of the equations :

$$\frac{1}{We} \tilde{H} \boldsymbol{n}$$

where $We = \rho_1 U^2 L / \gamma$ is the Weber number.

For a 1D surface (a curve) $H = \frac{1}{R}$, with R the radius of curvature positively counted along the normal. For a 2D surface, $H = \frac{1}{R1} + \frac{1}{R_2}$, with $R1$ and $R2$ the principal radiuses of curvature positively counted along the normal. The main difficulty to compute the surface tension is that it requires, at least in principle, the mean curvature of the surface, which is not trivial to evaluate on a discretized surface.

In order to discretize the surface tension, we multiply (11.40) by a test function Φ and integrate over the interface Σ :

$$\int_\Sigma \mathrm{TS}\Phi\, d\sigma = \int_\Sigma \gamma H\Phi.\mathbf{n}\, d\sigma \qquad (11.41)$$

The mean curvature H can be expressed as the opposite of the trace of the derivative of the Gauss application which is the application associating to each point of the surface the normal of this surface. This can be written in the following way (see for example J.U. Brackbill, D.B. Kothe and C. Zemach [19]) :

$$H = -\mathrm{tr}(\nabla_s\mathbf{n})$$

with ∇_s the gradient along the surface (more precisely, the orthogonal projection of the gradient onto the tangential space).

The generalization of the well-known divergence theorem to surfaces of non-zero curvature is the following :

$$\int_\Sigma \mathrm{tr}(\nabla_s\mathbf{n})\Phi.\mathbf{n}\, d\sigma = \int_\Sigma \mathrm{tr}(\nabla_s\Phi)\, d\sigma - \int_{\partial\Sigma} \Phi.\mathbf{m}\, dl. \qquad (11.42)$$

The vector $\mathbf{m}$ is the normal vector to $\partial\Sigma$ (in the tangential space of Σ). The weak formulation of the surface tension is then :

$$\int_\Sigma \mathrm{TS}\Phi\, d\sigma = -\gamma \int_\Sigma \mathrm{tr}(\nabla_s\Phi)\, d\sigma + \gamma \int_{\partial\Sigma} \Phi.\mathbf{m}\, dl \qquad (11.43)$$

The vector $\mathbf{m}$ is the contact angle between the interface and the wall, it is a data of the problem. In practice, we have chosen a contact angle equal to zero. We now have to express the derivative $\mathrm{tr}(\nabla_s\Phi)$ on the discretized surface Σ.

In one dimension, it is easy to evaluate $\mathrm{tr}(\nabla_s\Phi)$ using the formula :

$$\mathrm{tr}(\nabla_s\Phi) = \frac{< d\Phi(e_u), e_u >}{||e_u||^2}$$

with $d\Phi(e_u) = \frac{d\Phi}{du}$. In this formula, e_u is a vector in the tangent space : $e_u = \frac{\partial f}{\partial u}$ with f a parameterization of the curve. In practice, this parameterization is given by the application which sends the element of reference $[0,1]$ onto the finite element. The derivative $\frac{d\Phi}{du}$ is then evaluated by finite differences. We are now going to generalize this approach in two dimensions.

In order to evaluate the divergence along the surface $\mathrm{tr}(\nabla_s\Phi)$ in two dimensions, we need a local parameterization $f : U \subset \mathbb{R}^2 \to \mathbb{R}^3$. From a discrete point of view, this parameterization is given by the finite element test functions (we suppose that we use Lagrangian finite element) :

$$f : \begin{cases} [0,1]^2 & \to & \mathbb{R}^3 \\ (u,v) & \mapsto & \displaystyle\sum_{P\in\mathcal{P}(\mathcal{E})} \phi_P X_P \end{cases}$$

where $\phi_P : [0,1]^2 \to \mathbb{R}$ is the shape function related to the point P, X_P is the coordinate vector of P and $\mathcal{P}(\mathcal{E})$ is the set of the points of the element $\mathcal{E}$. A basis of the tangential space is given by (e_u, e_v) with $e_u = \frac{\partial f}{\partial u}$ and $e_v = \frac{\partial f}{\partial v}$. The metric tensor M is the matrix $\begin{bmatrix} E & F \\ F & G \end{bmatrix}$ with $E = ||e_u||^2$, $F = < e_u, e_v >$ and $G = ||e_v||^2$. The element of area is $da = \sqrt{EG - F^2}\, du\, dv$. We want to evaluate the trace of the derivative $d\Phi$ along the surface. We define : $e = < d\Phi(e_u), e_u >$, $f_1 = < d\Phi(e_u), e_v >$, $f_2 = < d\Phi(e_v), e_u >$ and $g = < d\Phi(e_v), e_v >$. Of course, we have $d\Phi(e_u) = \frac{\partial \Phi}{\partial u}$ and $d\Phi(e_v) = \frac{\partial \Phi}{\partial v}$. We have the following equality :

$$\begin{bmatrix} e & f_1 \\ f_2 & g \end{bmatrix} = \begin{bmatrix} a_{1,1} & a_{1,2} \\ a_{2,1} & a_{2,2} \end{bmatrix} \begin{bmatrix} E & F \\ F & G \end{bmatrix}$$

with $A = [a_{i,j}]$ the matrix of the derivative $d\Phi$ in the basis (e_u, e_v). A simple computation gives the following expression of $\text{tr}(\nabla_s \Phi) = -(a_{1,1} + a_{2,2})$:

$$\text{tr}(\nabla_s \Phi) = -\frac{eG + Eg - F(f_1 + f_2)}{EG - F^2}$$

Let us now explain the way we evaluate e, $f1$, $f2$ and g for a $Q1$ discretization (see
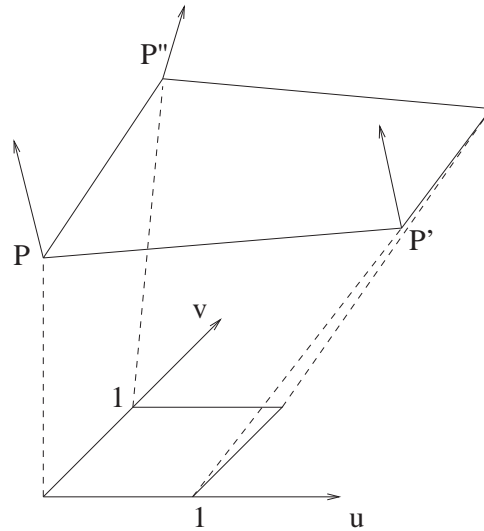
FIG. 11.3 – A $Q1$ element parameterized by $[0,1]^2$.

Figure 11.3). Let P be the point $(0,0)$, P', the point $(1,0)$ and P'' the point $(0,1)$. The application $f_0(t) = f(t, 0)$ is a parameterization of $[PP']$. Then, we have :

$$\begin{aligned} d\Phi(P)(e_u) &= \frac{d}{dt}(\Phi(\gamma(t))|_{t=0} \\ &\sim \Phi(\gamma(1)) - \Phi(\gamma(0)) \\ &\sim \Phi(P') - \Phi(P) \end{aligned}$$

In the same manner, we derive :

$$d\Phi(P)(e_v) \sim \Phi(P'') - \Phi(P)$$

and therefore :

$$
\begin{aligned}
e &\sim\ <\Phi(P') - \Phi(P), e_u> \\
f_1 &\sim\ <\Phi(P') - \Phi(P), e_v> \\
f_2 &\sim\ <\Phi(P'') - \Phi(P), e_u> \\
g &\sim\ <\Phi(P'') - \Phi(P), e_v>
\end{aligned}
$$

We can therefore implement a weak formulation of the term of surface tension.

11.7 Numerical experiments

All the results shown in this section are presented in the non-dimensional form detailed in Section 11.2.2.

11.7.1 On the mass conservation

We described precisely in Section 11.5.2 the three key arguments that allow us to ensure mass conservation in the two-fluids problems. We give in this section a few examples of mass loss if some of the above requirements are not fulfilled. The aim of this section is therefore to illustrate by numerical experiments that the second and third ingredients (namely the mass conservation of each fluid at each time step, see formula (11.31) and the GCL, see formula (11.27)) seem indeed to be necessary in order to ensure mass conservation, at least for general cases.

For this purpose, we consider the case when the two fluids are only subjected to an oscillating gravity. The computational domain is $\Omega = [-2, 2] \times [0, 2]$, the lower (resp. upper) fluid occupies at $t = 0$ the subdomain $\Omega_{1,t=0} = [-2, 2] \times [0, 1]$ (resp. $\Omega_{2,t=0} = [-2, 2] \times [1, 2]$). The potential of the body force is given by :

$$\tilde{\Phi}(x, y, t) = Ax \sin(2\pi\nu t) - y$$

We choose the following non-dimensional parameters : $Re_1 = Re_2 = 100$, $M = 0.91$, $\nu = 0.0625$, $A = 0.05$. Figure 11.4 shows the evolution in time of the elevation of a point on the interface.

In Figure 11.5, we show the evolution in time of the mass of fluid 1 with three finite element spaces : Q2/Q1 (with a continuous pressure), Q2/P1 (with a discontionuous pressure), and Q2/Q1 with the flux constraint (11.32). The pair Q2/Q1 does not satisfy (11.31) which explains the non conservation of mass.

We now illustrate the role of the GCL in mass conservation. We use the Q1/Q1 stabilized finite element with flux constraint (11.32). Thus (11.30) is now satisfied. If the displacement of the mesh is purely vertical, the GCL property (11.27) is satisfied,
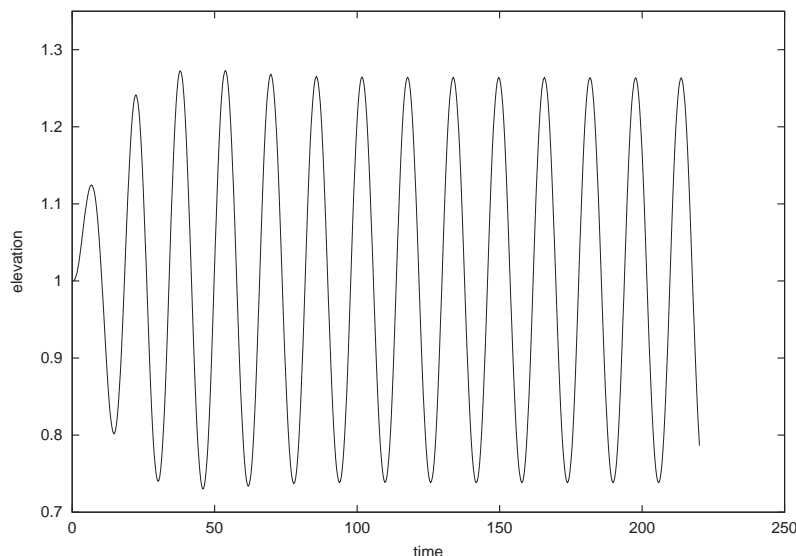
FIG. 11.4 – The time history of the elevation of a point of the interface.

and the mass is preserved. But, if we replace system (11.26) by

$$
\begin{cases}
-\triangle\, \boldsymbol{w} = 0, & \text{on } \Omega_i^n, \\
\boldsymbol{w} = \boldsymbol{u}, & \text{on } \Sigma^n, \\
\dfrac{\partial \boldsymbol{w}}{\partial n} = 0 & \text{on } \partial\Omega,
\end{cases}
\tag{11.44}
$$

the displacement of the mesh is now arbitrary, and relation (11.27) is no more true (an additional term appears in the development of the jacobian determinant). We show on the left-hand side of Figure 11.6, the mesh obtained with (11.26) and on the right-hand side, the one obtained with (11.44). Of course, it seems not very natural to allow for a mesh displacement along to x axis for this test case, but it is just for illustration. We see on Figure 11.7 that the mass is not preserved when the displacement is along x and y. The fact that relation (11.31) is not sufficient on a moving mesh to ensure mass conservation is striking.

11.7.2 A MHD experiment with a free surface and a free interface

We present here the numerical simulation of a laboratory MHD experiment (described by R. Moreau [115, 116]). A uniform vertical electrical current flows in a cylindrical tank through two layers of fluid subjected to the gravity. The interface between the fluid and the upper surface are both free (see Figure 11.8). The above formulation must be slightly modified to treat this case due to the presence of two free surfaces, but the modifications are straightforward and we do not detail them here. Let us just mention that, because of the presence of the upper free surface, we do not perform the "pressure correction" presented in Section 11.2.2. This test
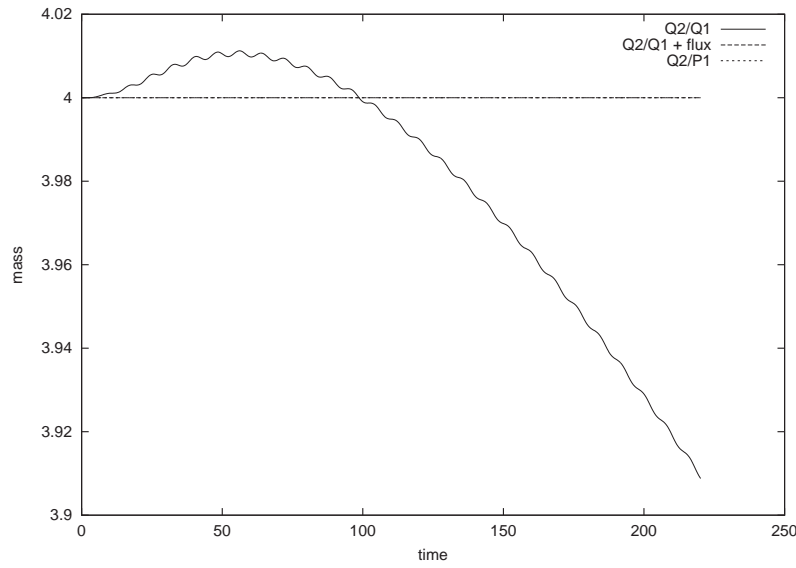
FIG. 11.5 – Mass conservation is ensured with Q2/P1 or Q2/Q1 with a flux constraint (the two curves are the same), but it fails with Q2/Q1 elements.

case is of interest for two reasons : first, the physical system is not too far from the aluminium electrolysis, and second, an analytical steady state solution is known.

We denote by $\tilde{J}_0$ the intensity of the non-dimensional homogeneous density of current and by R the radius of the cylinder. Working with the natural cylindrical coordinates $(\boldsymbol{e}_r, \boldsymbol{e}_\theta, \boldsymbol{e}_z)$ associated with the cylindrical tank, we have :

$$\tilde{\boldsymbol{B}} = \tilde{B}(r)\boldsymbol{e}_\theta, \qquad \text{with } \tilde{B}(r) = -\frac{J_0}{2}r \quad (\text{for } r \leq R),$$

and the magnetic force is

$$S\,\mathbf{curl}\,\tilde{\boldsymbol{B}} \times \tilde{\boldsymbol{B}} = -\frac{SJ_0^2}{2}r\,\boldsymbol{e}_r.$$
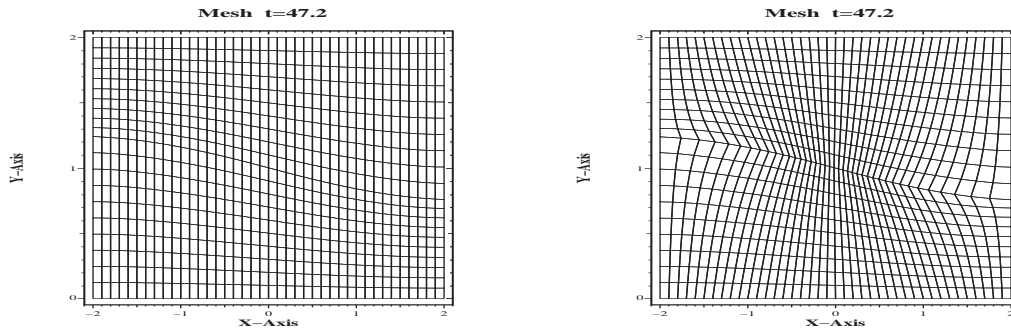
FIG. 11.6 – The velocity of the mesh is computed with (11.26) on the left-hand side, and with (11.44) on the right-hand side.
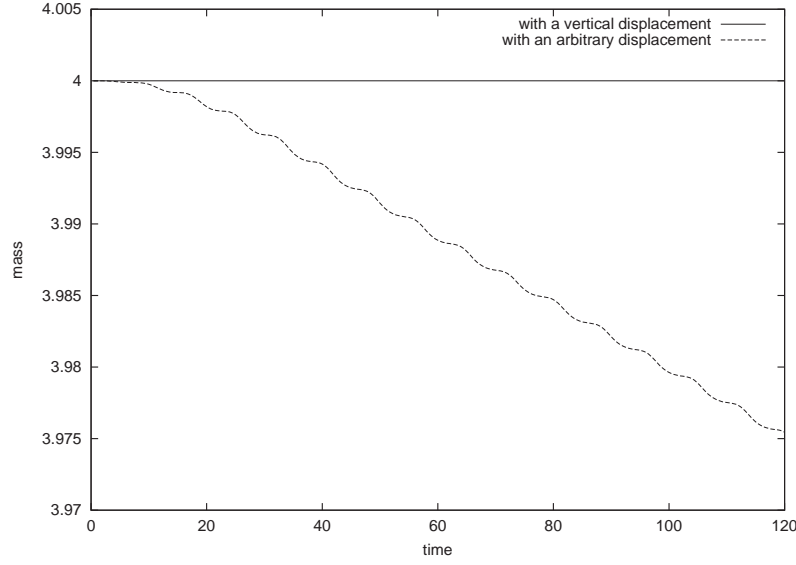
FIG. 11.7 – Both curves are obtained with Q1/Q1 finite element with flux constraint (11.32). When the displacement of the mesh is arbitrary, Lemma 1 does not apply and we observe a mass loss, contrarily to the case when the displacement is purely vertical.

The only body force being the gravity, we have $\tilde{\Phi} = -z$. Looking for a solution with $\boldsymbol{u} = 0$, we have

$$\boldsymbol{\nabla}\tilde{p} = -\frac{m}{Fr}\boldsymbol{e}_z - \frac{SJ_0^2}{2}r\,\boldsymbol{e}_r, \tag{11.45}$$

with $m = M$ in the upper fluid and $m = 1$ in the lower one. Thus

$$\tilde{p}(r, z) = -\frac{m}{Fr}z - \frac{SJ_0^2}{4}r^2 + C,$$

where C is a constant. We denote by h_1^0 (resp. h_2^0) the elevation of the free interface (resp. surface) before the application of the electrical current, and by $h_1(r)$ (resp. $h_2(r)$) their steady state elevation, in the presence of the electrical current. The pressure above the free surface is supposed to be constant and equal to zero. Thus, we have :

$$0 = \tilde{p}(r, h_2(r)) = -\frac{M}{Fr}h_2(r) - \frac{SJ_0^2}{4}r^2 + C$$

The constant C is then determined by writing the conservation of the volume of the upper fluid, and we finally obtain :

$$h_2(r) = h_2^0 + \frac{S\,Fr\,J_0^2 R^2}{8M}\left(1 - \frac{2r^2}{R^2}\right) \tag{11.46}$$

Next, taking the **curl** of equation (11.45), we have :

$$0 = \mathbf{curl}\left(\frac{m}{Fr}\boldsymbol{e}_z\right) = \boldsymbol{\nabla}\left(\frac{m}{Fr}\right) \times \boldsymbol{e}_z = \frac{M-1}{Fr}\boldsymbol{n} \times \boldsymbol{e}_z,$$

where $\boldsymbol{n}$ is the normal to the interface. Therefore, $\boldsymbol{n} = \boldsymbol{e}_z$, which proves that the steady state interface is horizontal :

$$h_1(r) = h_1^0.$$
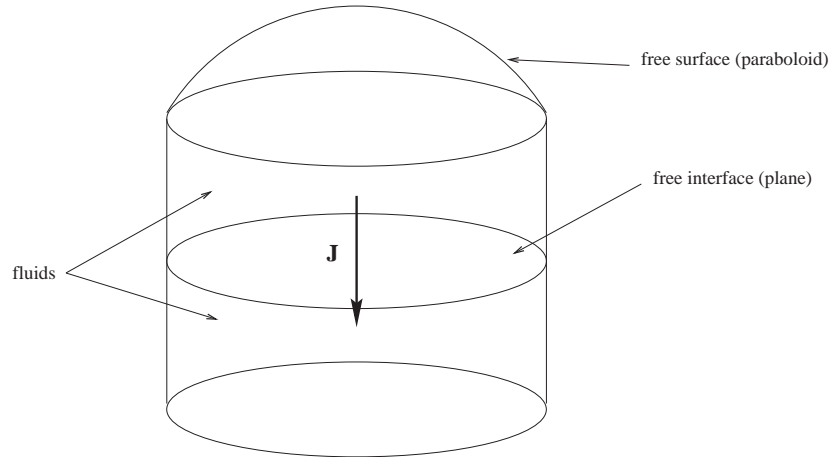
FIG. 11.8 – Schematic representation of the experiment of Section 11.7.2.

We use the following numerical values : $Re_1 = Re_2 = 200$, $S = 1$, $Rm_1 = Rm_2 = 1$, $Fr = 8$, $J_0 = 0.3$, $M = 0.5$, $We = 10^2$. Figure 11.9 shows a comparison between the elevation of the upper surface and the analytical solution (11.46) along the plane $y = 0$. Figure 11.10 shows the steady-state upper surface and the interface. Figure 11.11 shows the time evolution of the elevation of the center of the upper surface (left-hand side) and of the interface (right-hand side).

11.7.3   Aluminium electrolysis cells simulations

We have also performed numerical simulations on real cells. The geometry of the domain of calculus is that of the industrial cell. The boundary conditions on the magnetic fields stem either from experimental measures in the factory or from independent numerical simulation of the magnetic field created by the conductors around the cell.

The aim of our simulations is to recover some well known phenomenological parameters (e.g. the number of vortices : see [53]) and to have an insight into some parameters that are difficult to measure (e.g. the shape of the interface between the bath and the metal).

We only present here the result of a computation on a cell with an over simplified circuit of conductors (see Figure 11.12). However, this circuit is enough to give a good idea of the real problem. The electric current in the cell is 90 kA and the dimensions of the cell are about $3 \times 9 \times 1.5$ m. For Biot and Savart computations (giving the boundary conditions on the magnetic field), we use either linear or parallelepipedic conductors. This interface has been obtained after a long time computation.
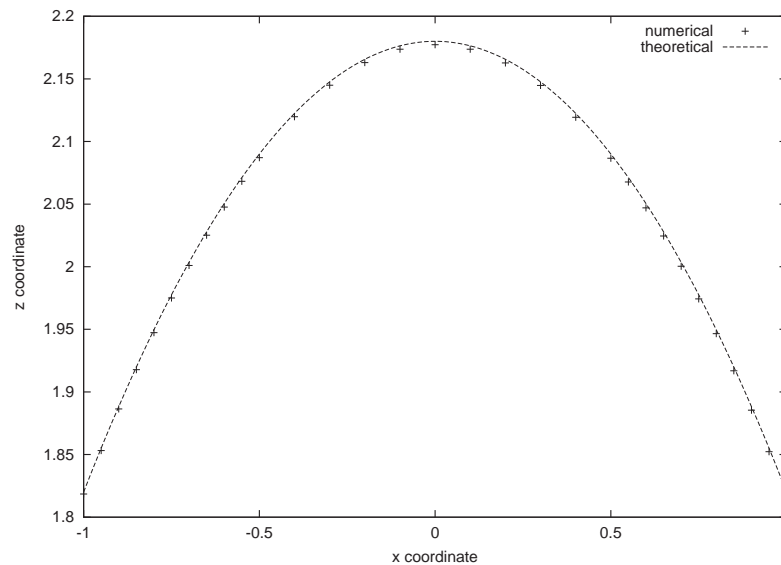
F<small>IG</small>. 11.9 – Elevation of the steady state top surface in the simulation of Section 11.7.2. Comparison between theoretical and numerical results.

11.7.4   Metal pad roll instabilities

One of the phenomena which is observed in industrial cells and which has been a lot investigated over the past few years is metal pad rolling. It is an oscillation of the cryolite / aluminium interface with a period ranging from five seconds up to more than one minute. The aim of most of the theoretical and experimental studies of MHD cells has been to understand, forecast and avoid this phenomenon. See A.F. LaCamera, D.P. Ziegler and R.L. Kozarek [95] and the references herein for a survey on the main approaches until 1992.

One of the explanation of the metal pad rolling is the presence of a vertical field. The famous Sele's criterion belongs to this theory (*see* T. Sele [139]). T. Sele has been the first one to give a physical reason of the rotation by the interaction of the vertical magnetic field with horizontal perturbed currents. More recently, P.A. Davidson and R.I. Lindsay [31] have derived a more general linearized system. Their analysis leads to quantitative results for the instability of standing and travelling waves in rectangular and circular cells. They also give a mechanical analogue which provides a good physical insight into the phenomenon.

The physical phenomenon is explained on Figure 11.13. An initial tilting (or a long-wavelength disturbance) creates a perturbed current flow $\boldsymbol{j} = \boldsymbol{J} - \boldsymbol{J}_0$ ($\boldsymbol{J}_0$ denotes the unperturbed – or background – current and $\boldsymbol{J}$ the total current in the cell) which is mainly vertical in the cryolite and horizontal in the aluminium (because of the strong difference of electrical conductivity). The interaction of this current with the vertical magnetic field results in a horizontal Lorentz force $\boldsymbol{F} = \boldsymbol{j} \times \boldsymbol{B}$, in the direction perpendicular to $\boldsymbol{j}$. It consequently induces a rotating motion of the interface.

In some cases, this phenomenon can lead to an instability : when the vertical
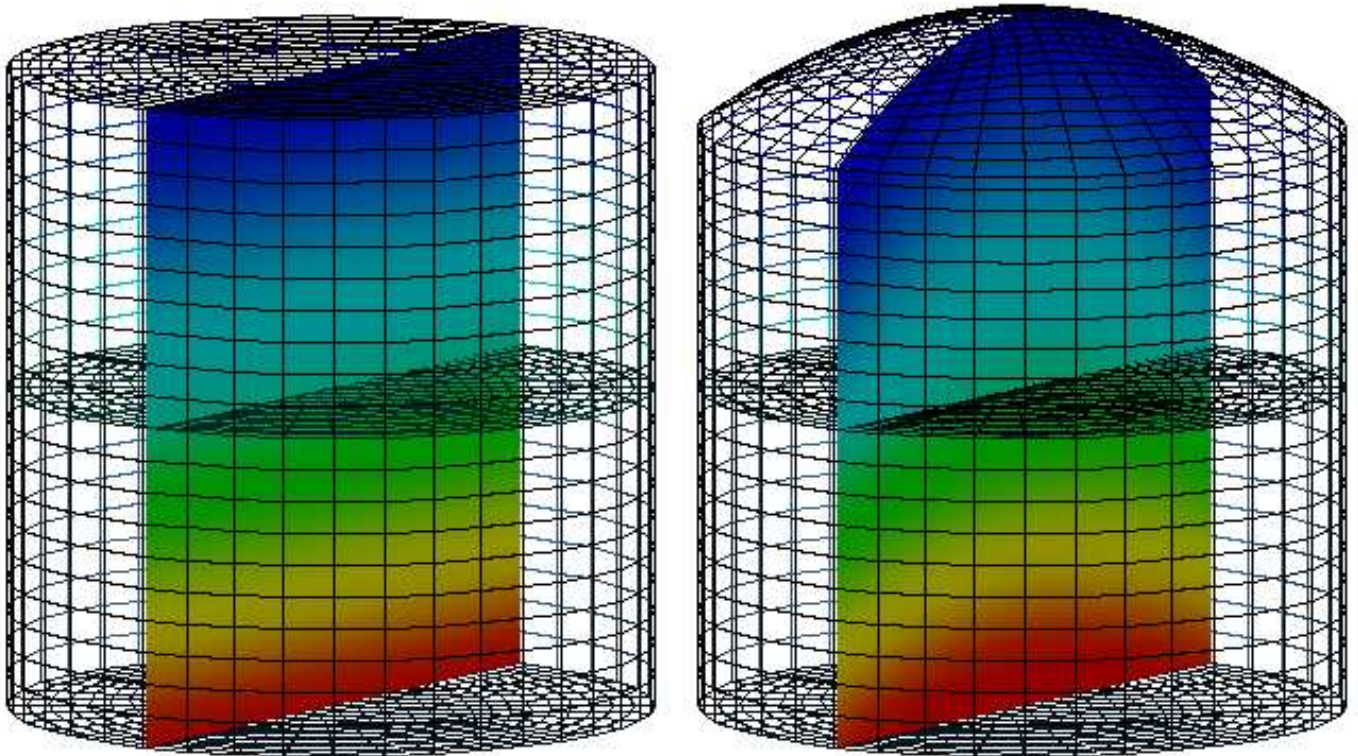
FIG. 11.10 – Mesh and Isovalues of pressure on a portion of the mesh, in presence of gravity (left), after the application of an electrical current (right)
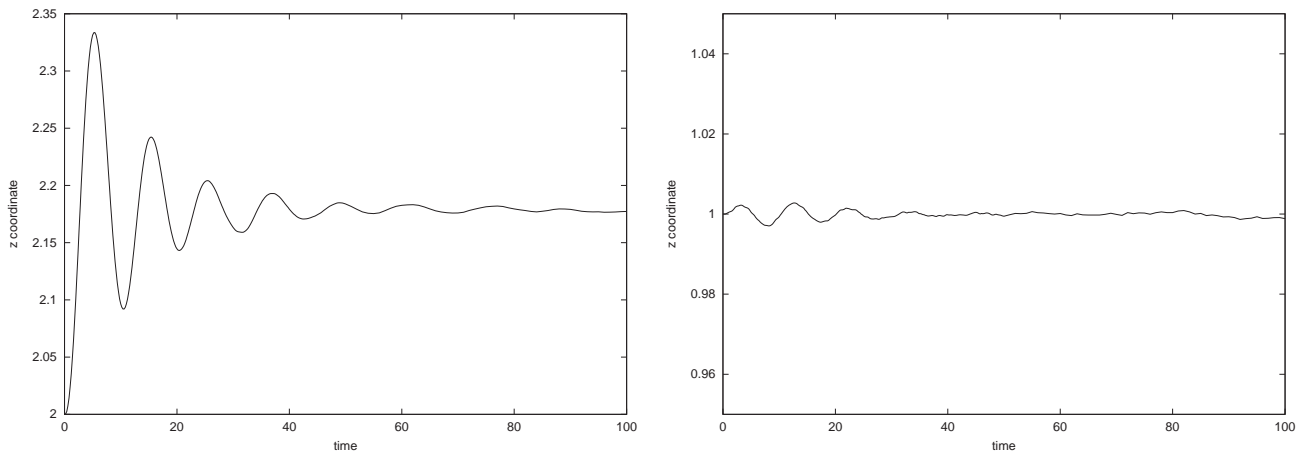

FIG. 11.11 – Evolution in time of the elevation of centers of the top surface (left) and of the interface (right) in the simulation of Section 11.7.2.
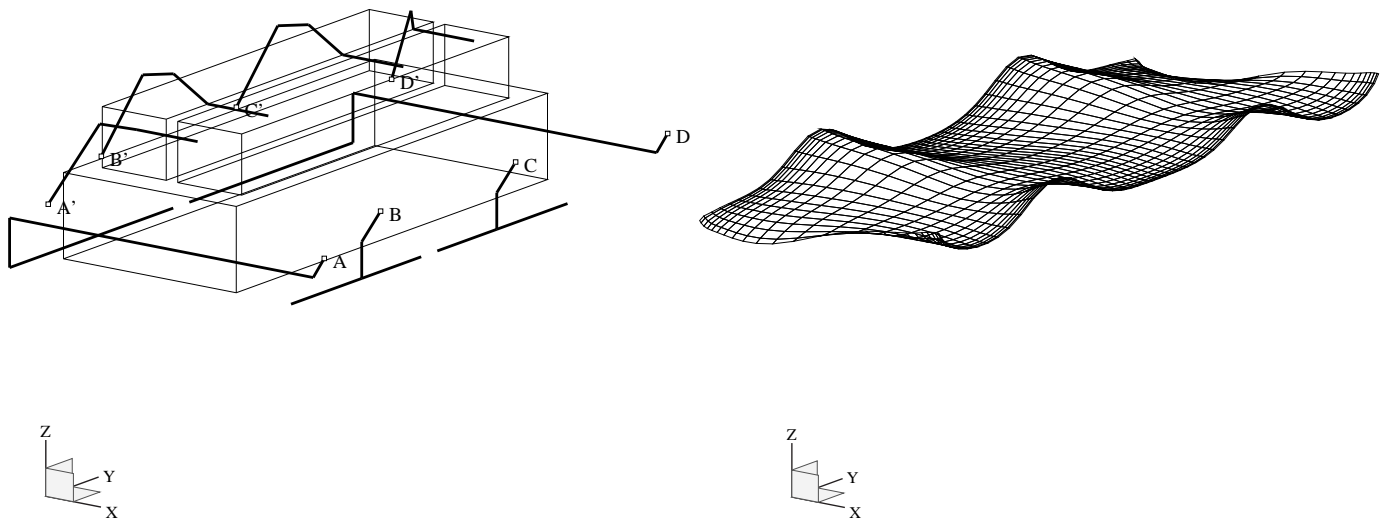
FIG. 11.12 – On the right, the shape of the interface at large time. The circuit of conductors is represented on the left. In the factories, the cells are in series, so that the points A (resp. B, C and D) are linked to the points A' (resp. B',C' and D') of the next cell. The cell is represented by the lower parallelepiped, while the two smaller parallelepipeds above model the anods.

field is too large, the amplitude of the oscillation may grow with time. It has been reported on that the metal can even get out of the cell in some cases !

In [31], it is shown that it is the interaction between gravitational modes which leads to instable rolling waves. In particular, the authors assert that a circular cell becomes instable whenever a vertical field B_z is applied. We have chosen to reproduce this simple experiment of a circular cell to check this strong result of instability, which is obtained after many assumptions and linearization (*see* [31]). The linearized approach may well reproduced qualitatively the metal pad rolling, but a few of the assumptions are quite questionable as far as quantitative results are concerned.

The test case cell is a circular cell of radius equals to 1 and height equals to 2. Initially, the fluids are at rest, the interface is situated at the mean height and is flat and horizontal. On the wall, we impose during the whole simulation the magnetic boundary conditions corresponding to a uniform vertical electrical current $J_0\boldsymbol{e}_z$ (when the fluids are at rest and the interface is horizontal). For $0 \leq t \leq 1$, the fluids are subjected to a gravity having an angle of 5 degree with the vertical. This slightly "tilts" the cell and creates an initial disturbance. For $1 < t \leq 25$, the gravity is put straight again, and a vertical magnetic field B_z is superimposed to the magnetic field created by the electrical current. This actually induces the metal rolling phenomenon. For $t > 25$, the vertical magnetic field is removed, and the system can therefore retrieve its initial configuration, at least when it does not explode before. The non-dimensional parameters are the following : $Re_1 = Re_2 = 1000$, $M = 0.935$, $Fr = 0.1$, $Rm_1 = 10^{-4}$, $Rm_2 = 1.$, $S = 1.$, $We = 50$, $J_0 = 2$. We perform the simulations for various values of B_z. Figure 11.14 shows the lower fluid and the interface when $B_z = 0.2$. Figure 11.15 shows the evolution in time of the elevation of the point of the interface initially situated at $(1., 0., 1.)$ for $B_z =$
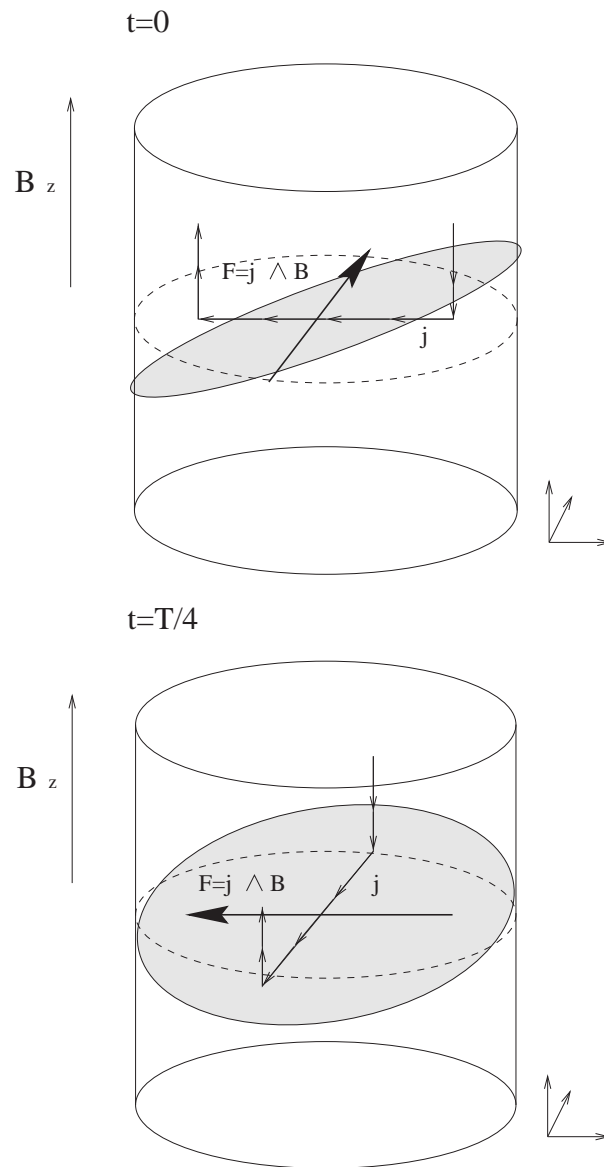
t=0

t=T/4

FIG. 11.13 – Rolling phenomenon.

$0.1, 0.2, 0.3$ and 0.5. The three last values lead to an "explosion" of the interface. The physical explanation of the phenomenon proposed on Figure 11.13 can be checked by computing the disturbed currents. In order to compute this disturbance, the initial current $\mathbf{curl}\,\boldsymbol{B}_0$ is substracted from $\mathbf{curl}\,\boldsymbol{B}$. A few streamlines of the perturbated current are represented on Figure 11.16 : there is indeed a "loop of current" as predicted in the theoretical explanation of the phenomenon.

In other simulations, we have also observed that small disturbances of the initial state do not lead to instability, at least on a reasonable time scale. In the same way, a small positive B_z does not induce instability. This is in apparent contradiction with the results of the linear approach which claim the instability of the cell. At least our results show that, should the instability occur, it will occur only in the large time limit, and therefore may not be relevant from the practical viewpoint. Of course, definite conclusions about this comparison between the two approaches are yet to be obtained.

This test case demonstrates the capability of our nonlinear approach to simulate complex MHD phenomena. In the past, these phenomena were analyzed with models based on many simplifications of the original equations providing excellent qualitative results most of the time. But the influences of such simplifications need in any case to be tested and may become not negligible when precise results are desired. We have demonstrated that we can reproduce qualitatively the results predicted by simplified models, but that we are also able to give *quantitative* informations on the transient evolution of the system. This capability should have practical implications in the study of the instabilities of industrial cells.
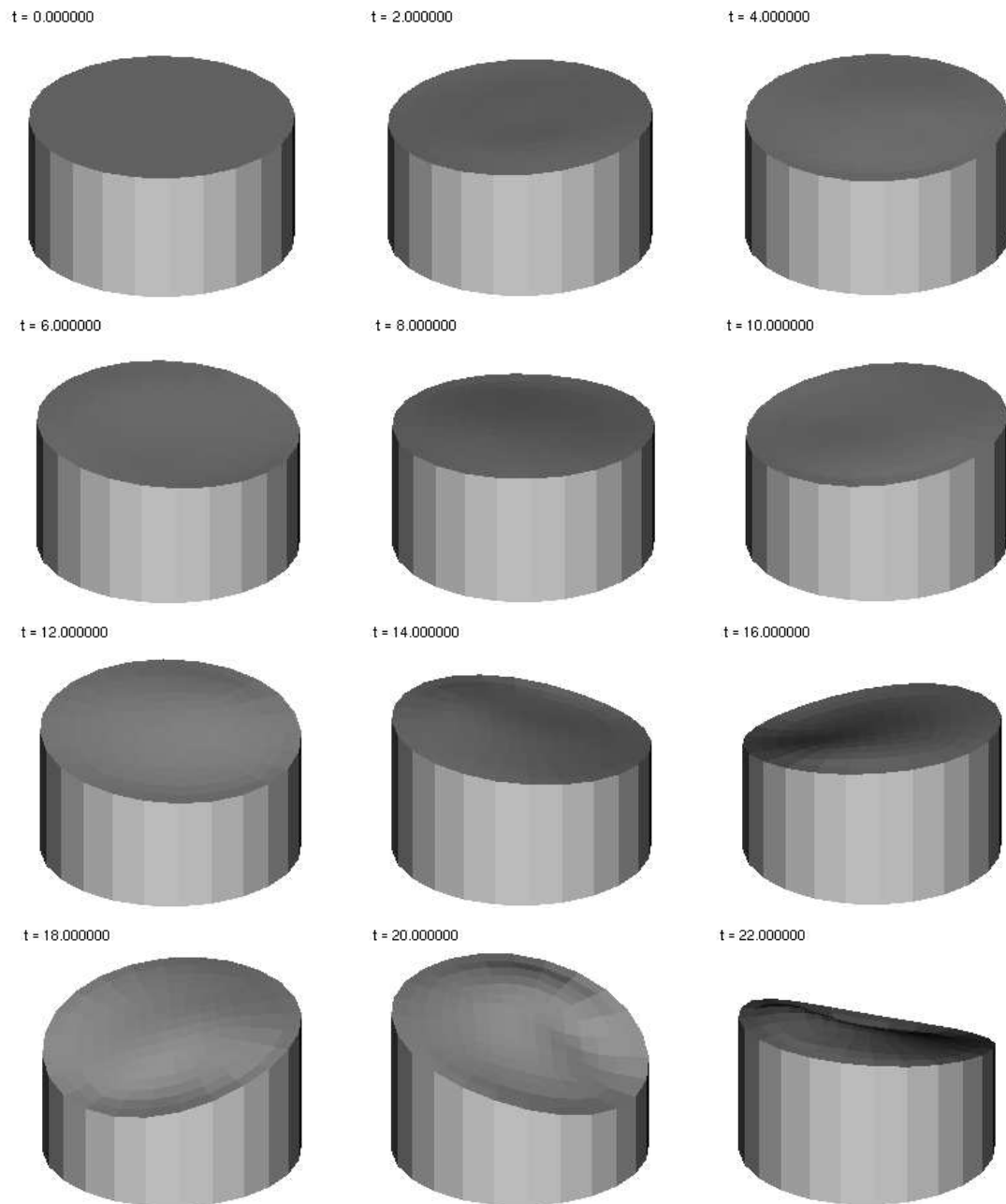
FIG. 11.14 – The phenomenon of metal pad rolling in a circular cell. Visualization of the interface and the lower fluid (the upper fluid is not represented for the sake of clarity). This is a case with $B_z = 0.2$.
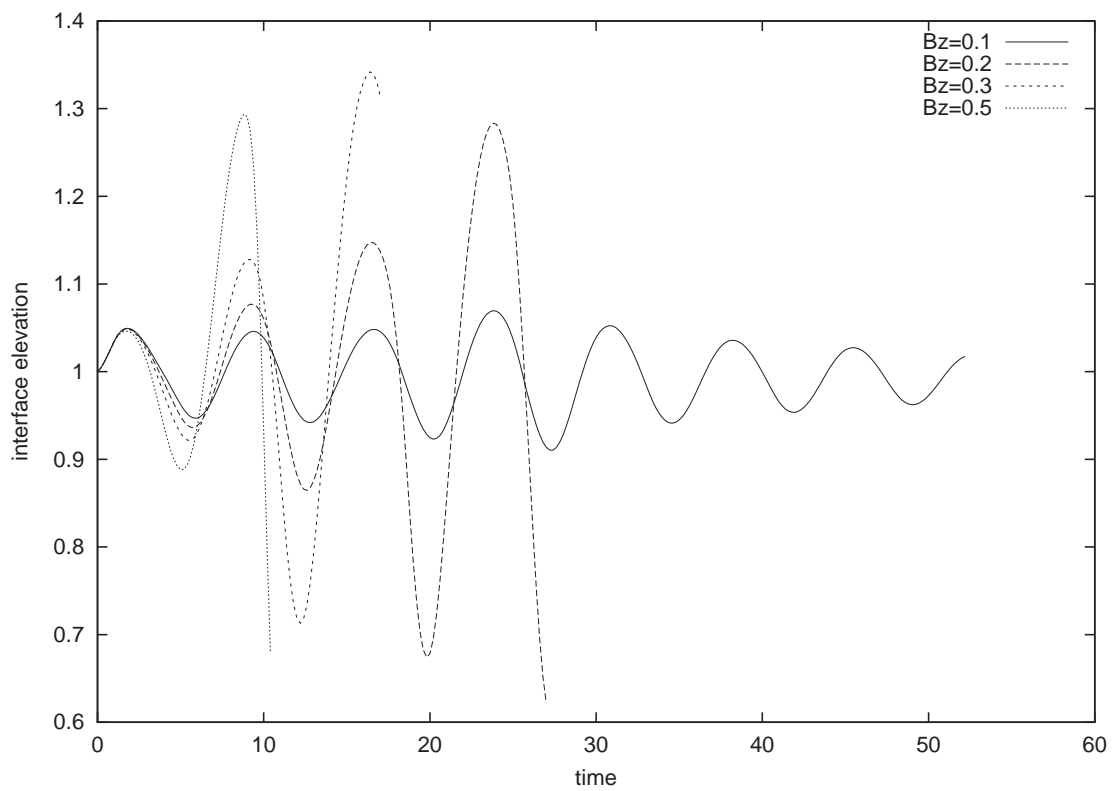
FIG. 11.15 – Time evolution of the elevation of a point of the interface in the "metal pad roll" experiment for various values of B_z. The only stable simulation is obtained with $B_z = 0.1$.
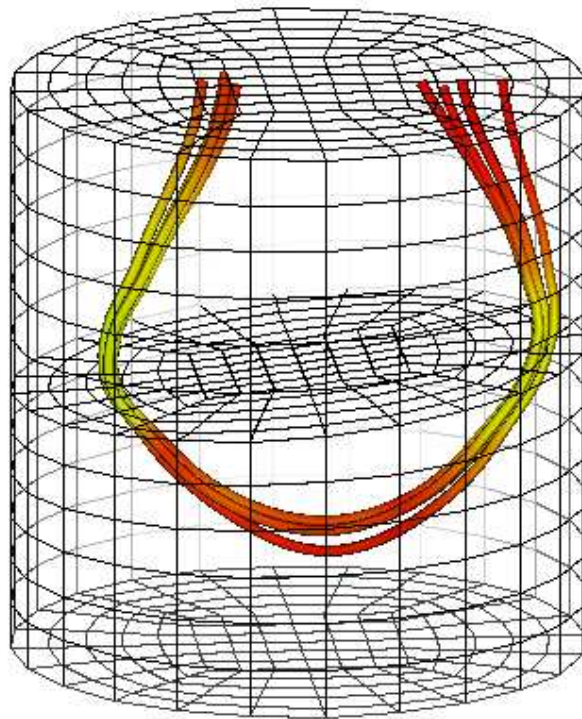
FIG. 11.16 – Loops of currents in cryolite during metal pad roll. We show here some streamlines of the field j (the perturbed current). The perturbed current goes here from the right-hand side of the Figure (where the elevation of the interface is the highest) to the left-hand side.

Bibliographie

[1] C. Ané, S. Blachère, D. Chafaï, P. Fougères, I. Gentil, F. Malrieu, C. Roberto, and G. Scheffer. *Sur les inégalités de Sobolev logarithmiques*. SMF, 2000.

[2] A. Arnold, P. Markowich, G. Toscani, and A. Unterreiter. On convex Sobolev inequalities and the rate of convergence to equilibrium for Fokker-Planck type equations. *Comm. Part. Diff. Eq.*, 26 :43–100, 2001.

[3] K. Atalik and R. Keunings. Non-linear stability analysis of viscoelastic plane channel flows using a fully-spectral method. *J. Non-Newtonian Fluid Mech.*, 102 :299–319, 2002.

[4] F.P.T. Baaijens. Mixed finite element methods for viscoelastic flow analysis : a review. *J. Non-Newtonian Fluid Mech.*, 79 :361–385, 1998.

[5] T.A. Baer, R.A. Cairncross, P.R. Schunk, P.A. Sackinger, and R.R. Rao. A finite element method for free surface flows of incompressible fluids in three dimensions. Part II : dynamic wetting line. *Int. Jour. Num. Meth. Fluids*, 33 :405–427, 2000.

[6] H.A. Barnes, J.F. Hutton, and K. Walters. *An introduction to rheology*. Elsevier, 1989.

[7] N. Ben Salah, A. Soulaimani, and W. G. Habashi. A finite element method for magnetohydrodynamics. *Comp. Methods Appl. Mech. Engrg.*, 190(43-44) :5867–5892, 2001.

[8] A. Bensoussan, J.L. Lions, and G.C. Papanicolaou. *Asymptotic analysis for periodic structures*. North-Holland, 1978.

[9] A.N. Beris and B.J. Edwards. *Thermodynamics of flowing systems with internal microstructure*. Oxford University Press, 1994.

[10] D. Bernardin. Introduction à la dynamique des milieux continus, 2003. Ecole de printemps, G.D.R. Matériaux vitreux.

[11] D. Bernardin. Introduction à la rhéologie des fluides : approche macroscopique, 2003. Ecole de printemps, G.D.R. Matériaux vitreux.

[12] R.B. Bird, R.C. Armstrong, and O. Hassager. *Dynamics of polymeric liquids*, volume 1. Wiley Interscience, 1987.

[13] R.B. Bird, C.F. Curtiss, R.C. Armstrong, and O. Hassager. *Dynamics of polymeric liquids*, volume 2. Wiley Interscience, 1987.

[14] R.B. Bird, P.J. Dotson, and N.L. Johnson. Polymer solution rheology based on a finitely extensible bead-spring chain model. *J. Non-Newtonian Fluid Mech.*, 7 :213–235, 1980. Errata : J. Non-Newtonian Fluid Mech., 8 (1981) 193.

[15] J. Bonvin and M. Picasso. Variance reduction methods for CONNFFESSIT-like simulations. *J. Non-Newtonian Fluid Mech.*, 84 :191–215, 1999.

[16] J.C. Bonvin. *Numerical simulation of viscoelastic fluids with mesoscopic models*. PhD thesis, Ecole Polytechique Fédérale de Lausanne, 2000.

[17] M. Bossy, M. Picasso, and D. Talay. Probabilistic numerical methods for physical and financial problems. *Computer in Physics*, 11(4) :325–330, 1997.

[18] J.U. Brackbill. Numerical magnetohydrodynamics for high-beta plasmas. *Meth. Comput. Phys.*, 16 :1–41, 1976.

[19] J.U. Brackbill, D.B. Kothe, and C. Zemach. A continuum method for modeling surface tension. *J. Comput. Phys.*, 100(2) :335–354, 1992.

[20] J.U. Brackbill and W.E. Pracht. An implicit, almost lagrangian algorithm for magnetohydrodynamics. *J. Comput. Phys.*, 13 :455–482, 1973.

[21] F. Brezzi, D. Marini, and A. Russo. Pseudo residual-free bubbles and stabilized methods. In *Computational method in Applied sciences*. ECCOMAS, Wiley, 1996.

[22] F. Brezzi and A. Russo. Choosing bubbles for advection-diffusion problems. *Math. Mod. Meth. Appl. Sci.*, 4 :571–587, 1994.

[23] A.N. Brooks and T.J.R. Hughes. Streamline upwind/Petrov-Galerkin formulations for convection dominated flows with particular emphasis on the incompressible Navier-Stokes equations. *Comp. Meth. App. Mech. Eng.*, 32 :199–259, 1982.

[24] R.A. Cairncross, P.R. Schunk, T.A. Baer, R. Rao, and P.A. Sackinger. A finite element method for free surface flows of incompressible fluids in three dimensions. Part I : Boundary fitted mesh motion. *Int. Jour. Num. Meth. Fluids*, 33 :375–403, 2000.

[25] E. Cépa. *Équations différentielles stochastiques multivoques*. Thèse, Université d'Orléans, 1994.

[26] E. Cépa. Equations différentielles stochastiques multivoques. *Sem. Prob.*, XXIX :86–107, 1995.

[27] E. Cépa and D. Lépingle. Diffusing particles with electrostatic repulsion. *Probab. Theory Relat. Fields*, 107 :429–449, 1997.

[28] C. Chauvière. A new method for micro-macro simulations of viscoelastic flows. *SIAM J. Sci. Comput.*, 23(6) :2123–2140, 2002.

[29] M.D. Chilcott and J.M. Rallison. Creeping flow of dilute polymer solutions past cylinders and spheres. *J. Non-Newtonian Fluid Mech.*, 29 :381–432, 1988.

[30] R. Codina. Comparison of some finite element methods for solving the diffusion-convection-reaction equation. *Comp. Meth. Appl. Mech. Engrg.*, 156 :185–210, 1998.

[31] P.A Davidson and R.I. Lindsay. Stability of interfacial waves in aluminium reduction cells. *J. Fluid Mech.*, 362 :273–295, 1998.

[32] P.G. de Gennes. Concept de reptation pour une chaîne polymérique. *J. Chem. Phys.*, 55 :572–579, 1971.

[33] P.G. de Gennes. *Scaling concepts in polymer physics*. Cornell University Press, 1979.

[34] P. Degond, M. Lemou, and M. Picasso. Viscoelastic fluid models derived from kinetic equations for polymers. to appear in SIAM J. Appl. Math.

[35] J. Descloux, M. Flueck, and M.V. Romerio. Modelling for instabilities in hall-heroult cells : mathematical and numerical aspects. *Magnetohydrodynamics in Process Metallurgy*, pages 107–110, 1991.

[36] J. Descloux, M. Flueck, and M.V. Romerio. Stability in aluminium reduction cells : a spectral problem solved by an iterative procedure. *Light Metal*, pages 275–281, 1994.

[37] B. Desjardins. Regularity results for the two dimensional multiphase viscous flows. *Arch. Rat. Mech. Anal.*, 137 :135–158, 1997.

[38] M. Doi. *Introduction to Polymer Physics*. International Series of Monographs on Physics. Oxford University Press, 1996.

[39] M. Doi and S.F. Edwards. *The Theory of Polymer Dynamics*. International Series of Monographs on Physics. Oxford University Press, 1988.

[40] M. Duflo. *Random iterative models*. Springer, 1997.

[41] W. E, T.J. Li, and P.W. Zhang. Convergence of a stochastic method for the modeling of polymeric fluids. *Acta Mathematicae Applicatae Sinica, English Series*, 18(4) :529–536, 2002.

[42] M.S. Engelman, R.L. Sani, and P.M. Gresho. The implementation of normal and/or tangential velocity boundary conditions in finite element codes for incompressible fluid flow. *Int. J. Num. Meth. Fluids*, 2(3) :225–238, 1982.

[43] X.J. Fan. Viscosity, first normal-stress coefficient, and molecular stretching in dilute polymer solutions. *J. Non-Newtonian Fluid Mech.*, 17 :125–144, 1985.

[44] X.J. Fan, R.B. Bird, and M. Renardy. Configuration-dependent friction coefficients and elastic dumbbell rheology. *J. Non-Newtonian Fluid Mech.*, 18 :255–272, 1985.

[45] E. Fernández-Cara, F. Guillén, and R.R. Ortega. *Handbook of numerical analysis. Vol. 8 : Solution of equations in $\mathbb{R}^n$ (Part 4). Techniques of scientific computing (Part 4). Numerical methods of fluids (Part 2).*, chapter Mathematical modeling and analysis of viscoelastic fluids of the Oldroyd kind, pages 543–661. Amsterdam : North Holland/ Elsevier, 2002.

[46] P.J. Flory. *Statistical Mechanics of Chain Molecules*. John Wiley and Sons, New York, 1969.

[47] L. Formaggia, J.-F. Gerbeau, F. Nobile, and A. Quarteroni. Numerical treatment of defective boundary conditions for the navier-stokes equations. *SIAM Journal on Numerical Analysis*, 40 :376–401, 2002.

[48] L. Formaggia and F. Nobile. A stability analysis for the arbitrary Lagrangian Eulerian formulation with finite elements. *East-West J. Numer. Math.*, 7(2) :105–131, 1999.

[49] M. Fortin and A. Fortin. A new approach for the FEM simulation of viscoelastic flows. *J. Non-Newtonian Fluid Mech.*, 32 :295–310, 1989.

[50] L.P. Franca, S.L. Frey, and T.J.R. Hughes. Stabilized finite element methods : I. Application to the advective-diffusive model. *Comp. Meth. Appl. Mech. Eng.*, 95 :253–276, 1992.

[51] J.-F. Gerbeau. Comparison of numerical methods for solving a magnetostatic problem. application to the magnetohydrodynamic equations. In *Proceedings of the Fourth European Computational Fluid Dynamics, ECCOMAS 98*, pages 821–825. Wiley, 1998.

[52] J.-F. Gerbeau. *Problèmes mathématiques et numériques posés par la modélisation de l'électrolyse de l'aluminium.* Thèse, Ecole Nationale des Ponts et Chaussées, 1998.

[53] J.-F. Gerbeau. A stabilized finite element method for the incompressible magnetohydrodynamic equations. *Numerische Mathematik*, 87(1) :83–111, 2000.

[54] J.-F. Gerbeau and C. Le Bris. Existence of solution for a density-dependent magnetohydrodynamic equation. *Advances in Differential Equations*, 2(3) :427–452, May 1997.

[55] J.-F. Gerbeau and C. Le Bris. On a coupled system arising in magnetohydrodynamics. *Appl. Math. Lett.*, 12 :53–57, 1999.

[56] J.-F. Gerbeau and C. Le Bris. On the long time behaviour of the solution to the two-fluids incompressible navier-stokes equations. *Differential Integral Equations*, 12(5) :691–740, 1999.

[57] J.-F. Gerbeau and C. Le Bris. A basic remark on some Navier-Stokes equations with body forces. *Appl. Math. Lett.*, 13(3) :107–112, 2000.

[58] J.-F. Gerbeau and C. Le Bris. Comparison between two numerical methods for a magnetostatic problem. *Calcolo*, 37(1) :1–20, 2000.

[59] J.-F. Gerbeau and C. Le Bris. *Mathematical study of a coupled system arising in Magnetohydrodynamics*, volume 215 of *Lecture Notes in Pure and Applied Mathematics*, pages 355–367. Marcel Dekker Inc., 2000.

[60] J.-F. Gerbeau, C. Le Bris, and M. Bercovier. Spurious velocities in the steady flow of an incompressible fluid subjected to external forces. *Int. Jour. Num. Meth. Fluids*, 25 :679–695, October 1997.

[61] J.-F. Gerbeau, C. Le Bris, and T. Lelièvre. Simulations of MHD flows with moving interfaces. *Journal of Computational Physics*, 184 :163–191, 2003.

[62] J.-F. Gerbeau, T. Lelièvre, and C. Le Bris. Numerical simulations of two-fluids MHD flows. In *Fundamental and Applied MHD. Proceedings of the Fifth international PAMIR Conference*, pages I.101–I.105, 2002.

[63] J.-F. Gerbeau, T. Lelièvre, C. Le Bris, and N. Ligonesche. Metal pad roll instabilities. *Light Metal*, pages 483–487, 2002. proceeding of the 2002 TMS Annual Meeting and Exhibition.

[64] H. Giesekus. A simple constitutive equation for polymeric fluids based on the concept of deformation-dependent tensorial mobility. *J. Non-Newtonian Fluid Mech.*, 11 :69–109, 1982.

[65] R. Glowinski, P. Le Tallec, M. Ravachol, and V. Tsikkinis. Numerical solution of the Navier-Stokes equations modeling the flow of two incompressible non-miscible viscous fluids. In *Finite elements in fluids, Vol. 8 (Huntsville, AL, 1989)*, pages 137–163. Hemisphere, Washington, DC, 1992.

[66] M. Grmela and H.C. Öttinger. Dynamics and thermodynamics of complex fluids. I. development of a general formalism. *Phys. Rev. E*, 56 :6620–6632, 1997.

[67] M. Grmela and H.C. Öttinger. Dynamics and thermodynamics of complex fluids. II. illustrations of a general formalism. *Phys. Rev. E*, 56 :6633–6655, 1997.

[68] R. Guénette and M. Fortin. A new mixed finite element method for computing viscoelastic flows. *J. Non-Newtonian Fluid Mech.*, 60 :27–52, 1999.

[69] J.L. Guermond. Stabilization of galerkin approximations of transport equations by subgrid modeling. *Math. Model. Numer. Anal.*, 33(6) :1293–1316, 1999.

[70] H. Guillard and C. Farhat. On the significance of the geometric conservation law for flow computations on moving meshes. *Comput. Methods Appl. Mech. Engrg.*, 190(11-12) :1467–1482, 2000.

[71] C. Guillopé and J.C. Saut. Existence results for the flow of viscoelastic fluids with a differential constitutive law. *Nonlinear Analysis, Theory, Methods & Appl.*, 15(9) :849–869, 1990.

[72] C. Guillopé and J.C. Saut. Global existence and one-dimensional nonlinear stability of shearing motions of viscoelastic fluids of Oldroyd type. *RAIRO Math. Model. Num. Anal.*, 24(3) :369–401, 1990.

[73] M.D. Gunzburger, A.J. Meir, and J.S. Peterson. On the existence, uniqueness, and finite element approximation of solutions of the equations of stationary, incompressible magnetohydrodynamics. *Mathematics of Computation*, 56(194) :523–563, April 1991.

[74] P. Halin, G. Lielens, R. Keunings, and V. Legat. The Lagrangian particle method for macroscopic and micro-macro viscoelastic flow computations. *J. Non-Newtonian Fluid Mech.*, 79 :387–403, 1998.

[75] P. Hébraud and F. Lequeux. Mode-coupling theory for the pasty rheology of soft glassy materials. *Phys. Rev. Lett.*, 81 :2934–2937, 1998.

[76] C.W. Hirt, A.A. Amsden, and J.L. Cook. An arbitrary lagrangian-eulerian computing method for all flow speeds. *J. Comput. Phys.*, 14(3) :227–253, 1974.

[77] L.W. Ho. *A legendre spectral element method for simulation of incompressible unsteady viscous free-surface flows.* PhD thesis, Massachussets Institute of Technology, 1989.

[78] J. Honerkamp and H.C. Öttinger. The Schwinger-Dyson approximation in elastic dumbbell models for flexible polymers. *J. Non-Newtonian Fluid Mech.*, 21 :157–165, 1986.

[79] A. Huerta and W. K. Liu. Viscous flow with large surface motion. *Comp. Meth. Appl. Mech. Engng.*, 69 :277–324, 1988.

[80] T.J.R. Hughes. Multiscale phenomena : Green's functions, the dirichlet-to-neumann formulation, subgrid scale models, bubbles and the origin of stabilized methods. *Comp. Meth. App. Mech. Eng.*, 127 :387–401, 1995.

[81] W.F. Hughes and F.J. Young. *The electromagnetodynamics of fluids*. Wiley, 1966.

[82] M.A. Hulsen, A.P.G. van Heel, and B.H.A.A. van den Brule. Simulation of viscoelastic flows using Brownian configuration fields. *J. Non-Newtonian Fluid Mech.*, 70 :79–101, 1997.

[83] B. Jourdain, C. Le Bris, and T. Lelièvre. On a variance reduction technique for micro-macro simulations of polymeric fluids. *J. Non-Newtonian Fluid Mech.*, 2003. To appear.

[84] B. Jourdain and T. Lelièvre. Mathematical analysis of a stochastic differential equation arising in the micro-macro modelling of polymeric fluids. In I.M. Davies, N. Jacob, A. Truman, O. Hassan, K. Morgan, and N.P. Weatherill, editors, *Probabilisitic Methods in Fluids Proceedings of the Swansea 2002 Workshop*, pages 205–223. World Scientific, 2003.

[85] B. Jourdain, T. Lelièvre, and C. Le Bris. Numerical analysis of micro-macro simulations of polymeric fluid flows : a simple case. *Math. Models and Methods in Applied Sciences*, 12(9) :1205–1243, 2002.

[86] B. Jourdain, T. Lelièvre, and C. Le Bris. Existence of solution for a micro-macro model of polymeric fluid : the FENE model. *Journal of Functional Analysis*, 209 :162–193, 2004.

[87] I. Karatzas and S.E. Shreve. *Brownian motion and stochastic calculus*. Springer-Verlag, 1988.

[88] R. Keunings. *Fundamentals of Computer Modeling for Polymer Processing*, chapter Simulation of viscoelastic fluid flow, pages 402–470. Hanser, 1989.

[89] R. Keunings. On the Peterlin approximation for finitely extensible dumbbells. *J. Non-Newtonian Fluid Mech.*, 68 :85–100, 1997.

[90] R. Keunings. A survey of computational rheology. In D.M. Binding et al., editor, *Proc. 13th Int. Congr. on Rheology*, pages 7–14. British Society of Rheology, 2000.

[91] R. Keunings. Advances in the computer modeling of the flow of polymeric liquids. *Comp. Fluid Dyn. J.*, 9 :449–458, 2001.

[92] R. Keunings, 2003. Personal communication.

[93] R. Keunings. Micro-macro methods for the multiscale simulation of viscoelastic flows using molecular models of kinetic theory. In D.M. Binding and K. Walters, editors, *Rheology Reviews 2004*. British Society of Rheology, 2004.

[94] P.E. Kloeden and E. Platen. *Numerical Solution of Stochastic Differential Equations*, volume 23 of *Applications of Mathematics*. Springer, 1992.

[95] A.F. LaCamera, D.P. Ziegler, and R.L. Kozarek. Magnetohydrodynamics in the Hall-Héroult process, an overview. *Light Metals*, pages 1179–1186, 1992.

[96] L. Landau and E. Lifchitz. *Course of Theoretical Physics, volume 6*. Pergamon Press, 1984.

[97] M. Laso and H.C. Öttinger. Calculation of viscoelastic flow using molecular models : The CONNFFESSIT approach. *J. Non-Newtonian Fluid Mech.*, 47 :1–20, 1993.

[98] M. Laso, M. Picasso, and H.C. Öttinger. Two-dimensional, time-dependent viscoelastic flow calculations using CONNFFESSIT. *AIChE J.*, 43 :877–892, 1997.

[99] C. Le Bris. Systèmes multi-échelles : modélisation et simulation, 2004. Cours de l'Ecole Polytechnique.

[100] C. Le Bris and P.L. Lions. Renormalized solutions to some transport equations with partially $W^{1,1}$ velocities and applications. *Annali di Matematica pura ed applicata*, 183 :97–130, 2004.

[101] P. Le Tallec and J. Mouro. Fluid structure interaction with large structural displacements. *Comput. Meth. Appl. Mech. Engrg.*, 190 :3039–3067, 2001.

[102] T. Lelièvre. Optimal error estimate for the CONNFFESSIT approach in a simple case. *Computers and Fluids*, 33 :815–820, 2004.

[103] M. Lesoinne and C. Farhat. Geometric conservation laws for flow problems with moving boundaries and deformable meshes and their impact on aeroelastic computations. *Computer Methods in Applied Mechanics and Engineering*, 134 :71–90, 1996.

[104] G. Lielens, R. Keunings, and V. Legat. The FENE-L and FENE-LS closure approximations to the kinetic theory of finitely extensible dumbbells. *J. Non-Newtonian Fluid Mech.*, 87 :179–196, 1999.

[105] J.L. Lions. *Quelques méthodes de résolution de problèmes aux limites non linéaires.* Dunod, Paris, 1969.

[106] P.L. Lions and N. Masmoudi. Global solutions for some Oldroyd models of non-newtonian flows. *Chin. Ann. Math., Ser. B*, 21(2) :131–146, 2000.

[107] A.S. Lodge. *Elastic Liquids.* Academic Press, 1964.

[108] A. Lozinski. *Spectral methods for kinetic theory models of viscoelastic fluids.* PhD thesis, Ecole Polytechnique Fédérale de Lausanne, 2003.

[109] F. Malrieu. *Inégalités de Sobolev logarithmiques pour des problèmes d'évolution non linéaires.* PhD thesis, Université Paul Sabatier, 2001.

[110] J.M. Marchal and M.J. Crochet. A new mixed finite element for calculating viscoelastic flows. *J. Non-Newtonian Fluid Mech.*, 26 :77–114, 1987.

[111] A-M. Matache and C. Schwab. Two-scale fem for homogenization problems. *Mathematical Modelling and Numerical Analysis*, 36(4) :537–572, 2002.

[112] B. Maury. Characteristics ALE methods for the unsteady 3D Navier-Stokes equations with a free surface. *Comp. Fluid. Dyn.*, 6 :175–188, 1996.

[113] M. Melchior and H.C. Öttinger. Variance reduced simulations of polymer dynamics. *J. Chem. Phys.*, 105(8) :3316–3331, 1996.

[114] T. Min, J.Y. Yoo, and H. Choi. Effect of spatial discretization schemes on numerical solutions of viscoelastic fluid flows. *J. Non-Newtonian Fluid Mech.*, 100 :27–47, 2001.

[115] R. Moreau. *Magnetohydrodynamics.* Kluwer Academic Publishers, 1990.

[116] R. Moreau. Ecoulement d'un métal liquide en présence d'un champ magnétique. In *Traité de Génie électrique*, volume D4, pages D2950–3 – D2950–30. Editions Techniques de l'ingénieur, 1992.

[117] R. Moreau and J.W. Evans. An analysis of the hydrodynamics of aluminium in reduction cells. *J. Electrochem. Soc. : Electrochem. Sci. Tech.*, 131(10) :2251–2259, 1984.

[118] R. Moreau and D. Ziegler. The moreau-evans hydrodynamic model applied to actual hall-héroult cells. *Metal. Trans. B.*, 19B :737–744, 1988.

[119] B. Nkonga and H. Guillard. Godunov type method on nonstructured meshes for three-dimensional moving boundary problems. *Comput. Methods Appl. Mech. Engrg.*, 113(1-2) :183–204, 1994.

[120] H.C. Öttinger. *Stochastic Processes in Polymeric Fluids*. Springer, 1995.

[121] H.C. Öttinger, B.H.A.A. van den Brule, and M.A. Hulsen. Brownian configuration fields and variance reduced CONNFFESSIT. *J. Non-Newtonian Fluid Mech.*, 70 :255–261, 1997.

[122] R.G. Owens and T.N. Phillips. *Computational rheology*. Imperial College Press / World Scientific, 2002.

[123] A. Peterlin. Hydrodynamics of macromolecules in a velocity field with longitudinal gradient. *J. Polym. Sci. B*, 4 :287–291, 1966.

[124] N. Phan-Thien and R.I. Tanner. A new constitutive equation derived from network theory. *J. Non-Newtonian Fluid Mech.*, 2 :353–365, 1977.

[125] M. Picasso, 2003. Personal communication.

[126] E. Platen. An introduction to numerical methods for stochastic differential equations. *Acta Numerica*, pages 197–246, 1999.

[127] A. Quarteroni and A. Valli. *Numerical Approximation of Partial Differential Equations*. Springer, 1997.

[128] H.K. Rasmussen, O. Hassager, and A. Saasen. Viscous flow with large fluid-fluid interface displacement. *Int. Jour. Num. Meth. Fluids*, 28 :859–881, 1998.

[129] M. Renardy. Local existence theorems for the first and second initial-boundary value problems for a weakly non-newtonian fluid. *Arch. Rat. Mech. Anal.*, 83 :229–244, 1983.

[130] M. Renardy. Local existence of solutions of the Dirichlet initial-boundary value problem for incompressible hypoelastic materials. *SIAM J. Math. Anal.*, 21(6) :1369–1385, 1990.

[131] M. Renardy. An existence theorem for model equations resulting from kinetic theories of polymer solutions. *SIAM J. Math. Anal.*, 22 :313–327, 1991.

[132] M. Renardy. Initial value problems with inflow boundaries for Maxwell fluids. *SIAM J. Math. Anal.*, 27 :914–931, 1996.

[133] M. Renardy. *Mathematical analysis of viscoelastic flows*. SIAM, 2000.

[134] D. Revuz and M. Yor. *Continuous martingales and Brownian motion*. Springer-Verlag, 1994.

[135] L.C.G. Rogers. Smooth transition densities for one-dimensional diffusions. *Bull. London Math. Soc.*, 17 :157–161, 1985.

[136] D. Sandri. Non integrable extra stress tensor solution for a flow in a bounded domain of an Oldroyd fluid. *Acta Mech.*, 135(1-2) :95–99, 1999.

[137] W.R. Schowalter. *Mechanics of Non-Newtonian Fluids*. Pergamon Press, New York, 1978.

[138] M. Segatz and C. Droste. Analysis of magnetohydrodynamic instabilities in aluminium reduction cells. *Light Metals*, pages 313–322, 1994.

[139] T. Sele. Instabilities of the metal surface in electrolytic cells. *Light Metal*, pages 7–24, 1977.

[140] A.D. Sneyd and A. Wang. Interfacial instability due to mhd mode coupling in aluminium reduction cells. *J. Fluid Mech.*, 263 :343–359, 1994.

[141] A. Soulaïmani, M. Fortin, G. Dhatt, and Y. Ouellet. Finite element simulation of two- and three dimensional free surface flows. *Comp. Meth. Appl. Mech. Engng*, 86 :265–296, 1991.

[142] A. Soulaïmani and Y. Saad. An arbitrary Lagrangian-Eulerian finite element method for solving three-dimensional free surface flows. *Comput. Meth Appl. Mech Engrg.*, 162 :79–106, 1998.

[143] J.K.C. Suen, Y.L. Joo, and R.C. Armstrong. Molecular orientation effects in viscoelasticity. *Annu. Rev. Fluid Mech.*, 34 :417–444, 2002.

[144] E.B. Tadmor, M. Ortiz, and R. Phillips. Quasicontinuum analysis of defects in solids. *Phil. Mag. A*, 73 :1529–1563, 1996.

[145] R. Temam. *Navier-Stokes Equations*. North-Holland, 1979. Revised edition.

[146] V. Thomée. *Galerkin finite element methods for parabolic problems*. Springer, 1997.

[147] L.R.G. Treloar. *The physics of rubber elasticity*. Oxford University Press, 1949.

[148] A.P.G. Van Heel. *Simulation of viscoelastic fluids : from microscopic models to macroscopic complex flows*. PhD thesis, Delft University of Technology, 2000.

[149] L. Vandenberghe and S. Boyd. Semidefinite programming. *SIAM Review*, 38(1) :49–95, 1996.

[150] P. Wapperom, R. Keunings, and V. Legat. The backward-tracking lagrangian particle method for transient viscoelastic flows. *J. Non-Newtonian Fluid Mech.*, 91 :273–295, 2000.

[151] H.R. Warner. Kinetic theory and rheology of dilute suspensions of finitely extensible dumbbells. *Ind. Eng. Chem. Fundam.*, 11 :379–387, 1972.